FINITE ELEMENT ANALYSIS OF SOIL CUTTING AND TRACTION

by

Alfred W. Hanna

FINITE ELEMENT ANALYSIS OF SOIL CUTTING AND TRACTION

by

Alfred W. Hanna

A thesis submitted to the Faculty of Graduate Studies and Research in partial fulfilment of the requirements of the Degree of Doctor of Philosophy

Department of Civil Engineering and Applied Mechanics
McGill University
Montreal

May 1975

ABSTRACT

FINITE ELEMENT ANALYSIS OF SOIL CUTTING AND TRACTION

A thesis presented by A.W. Hanna in partial fulfilment for the degree of Doctor of Philosophy

Department of Civil Engineering and Applied Mechanics
McGill University
Montreal May 1975

The purpose of this study is to provide a rational analytical means for predicting the performance of a cutting or a traction tool, using parameters that describe the soil response due to interaction with the tool. The analytical techniques examined have the objective of deriving statically possible stresses compatible with kinematically possible strains while satisfying the boundary conditions.

Due to the extent of the overall problem, the study is limited in scope to the verification of the validity of the application of the finite element technique to the analysis of simplified cutting and traction elements interacting with cohesive soils under plane-strain conditions. The solution provides detailed stress and deformation fields within the loaded soils, as well as contact stresses at the soil tool interface, for various tool positions. Consequently, a relatively complete description of the load-deformation behavior, as the tool advances in the soil, is obtained.

The applicability of the proposed analytical model is verified by the successful prediction of tool developed forces and soil deformation

fields. In addition, through the application of the principle of conservation of energy to the cutting and traction element-soil systems, the energy dissipated in the soil deformation process is calculated, using the visioplasticity method. The energy values obtained are shown to provide reasonably good correlations with the experimentally measured and the finite element calculated energy components.

PRECIS

L'ANALYSE DE LA TRACTION ET DE LA TRANCHEE DES SOLS PAR LA METHODE DES ELEMENTS FINIS

Thèse présentée par Alfred W. Hanna faisant
partie des conditions requises pour le titre
de Docteur de Philosophie

Département de Génie Civil et Mécanique Appliquée
Université McGill
Montréal

Mai 1975

Le but de cette étude est de pourvoir un moyen analytique rationnel qui puisse prédire la performance d'un outil de tranchée ou de traction, et ceci en utilisant des paramètres qui décrivent la réaction des sols due à l'interaction avec l'outil. Les techniques examinées ont pour objectif de dériver des forces statiques compatibles avec des déformations cinématiques possibles, tout en satisfaisant les conditions de limite.

Etant donné l'étendue du problème global, l'étude est limitée à la vérification de la validité de l'application de la technique des éléments finis, à l'analyse des éléments simplifiés de traction et de tranchée et leur interaction avec des sols cohésifs sous les effets de déformations à surface plane. La solution donne des forces et des champs de déformation détaillés à l'intérieur des sols chargés, ainsi que des forces de contact à la surface commune de l'outil avec le sol, et ceci pour diverses positions de l'outil. Conséquemment, on obtient, durant

l'avancement de l'outil dans le sol, une description relativement complète des caractéristiques forces-déformations.

La validité du modèle analytique proposé est vérifiée par la bonne prédiction des forces développées par l'outil et des déformations du sol. En plus, en appliquant le principe de la conservation de l'énergie au problème et en utilisant la méthode de la plasticité visuelle, on peut calculer l'énergie dissipée dans le processus de déformation du sol. Les valeurs de l'énergie ainsi obtenues, donnent de bonnes corrélations avec celles mesurées expérimentalement ainsi qu'avec les valeurs obtenues par la méthode des éléments finis.

ACKNOWLEDGEMENTS

The author expresses his sincere appreciation to:

1. Dr. R.N. Yong, William Scott Professor of Civil Engineering and Applied Mechanics, for his constant encouragement and sustained guidance he so readily extended throughout this investigation.
2. Mr. E. Fattah, for the stimulating discussions and help.
3. Dr. C.K. Chen and Dr. R. Sylvestre-Williams for their help in developing the test facility and the experimental technique.
4. Mr. L. Vroomen, Department of Mechanical Engineering, for his assistance in data reduction.
5. Mr. B. Cockayne, Chief Laboratory Technician, for technical help.
6. Mr. S. Selim and Mr. A. Paz for their assistance in the preparation of diagrams.
7. Mrs. M. Powell and Miss J.M. Richards for typing this dissertation.
8. The National Research Council of Canada, for financial assistance during the course of this study.

TABLE OF CONTENTS

CHAPTER | Page

APPENDICES

LIST OF FIGURES

LIST OF FIGURES (continued)

LIST OF FIGURES (continued)

LIST OF FIGURES (continued)

LIST OF FIGURES (continued)

LIST OF FIGURES (continued)

LIST OF FIGURES (continued)

LIST OF FIGURES (continued)

LIST OF FIGURES (continued)

LIST OF FIGURES (continued)

LIST OF FIGURES (continued)

LIST OF FIGURES (continued)

LIST OF PLATES

LIST OF TABLES

LIST OF TABLES (continued)

NOTATION

The symbols adopted in this thesis are defined as they are first used. The principal ones are listed below.

A_i	area of i^{th} quadrilateral of inscribed grid
a,b	empirical coefficients representing the intercept and the slope of the shear stress-displacement curve
b	grouser or blade width
c	soil cohesion
c_a	soil-metal adhesion
D	deformation energy loss
E	elastic modulus
E_o	initial elastic modulus
E_T	slope of the deviator stress, $(\sigma_1 - \sigma_3)$, versus principal strain, ε_1, curve
$\underline{f}$	lumped nodal point forces
F_i	body force field
h	grouser depth
I	strain rate invariant
K	element stiffness matrix
k	von Mises yield function
k_n	element stiffness per unit length in the normal direction
k_s	element stiffness per unit length in the tangential direction
k_{si}	initial tangent stiffness modulus for joint element
l	grouser or blade length

NOTATION (continued)

P_p	total lateral pressure
P_h	lateral pressure at depth h below the soil surface
q	surcharge pressure
T_i	surface force field
U, V	velocity components
$\underset{\sim}{U}$	displacement field
u, v	displacement or velocity components
W	work done
Y	strain energy
Z	sinkage
α	blade inclination angle with vertical
γ	soil density
γ_{xy}	shear strain
δ	soil-metal friction angle
Δ_n	average relative normal displacement across joint element
Δ_s	average relative shear displacement across joint element
$\varepsilon_i (i=1,2,3)$	major, intermediate and minor principal strains, respectively
$\bar{\varepsilon}$	effective stress
$\varepsilon_x, \varepsilon_y$	normal strains
λ	plasticity modulus
ρ	specific mass
ϕ	friction angle
Φ	coordinate matrix of the nodal points

NOTATION (continued)

σ	normal stresses on failure plane
$\bar{\sigma}$	effective stress
$\sigma_i(i=1,2,3)$	major, intermediate and minor principal stresses, respectively
σ_x, σ_y	normal stresses
τ	shear stress
τ_i	stress tensor
τ_{xy}	shear stress component
ν	Poisson's ratio
ω	relative displacement vector for joint elements

ABBREVIATIONS

in(s).	inch(es)
ft.	feet
lb(s).	pound(s)
sec.	second
min.	minute
pcf.	pounds per cubic foot
psi	pounds per square inch
W.E.S.	U.S. Army Waterways Experiment Station, Vicksburg, Missippi
%	percent
R.A.P.G.	Right Angle Plate Grouser (figure 3-1)
S.E.W.G.	Straight-Edge Wedge Grouser (figure 3-1)
C.E.W.G.	Curved-Edge Wedge Grouser (figure 3-1)
CST(element)	Constant Strain Triangular (element)

CHAPTER 1

INTRODUCTION

1.1 SUMMARY OF THE GENERAL PROBLEM

Cutting and traction tools are mechanical devices used to apply forces to the soil to cause some desired effect such as cutting, movement of soil, or the production of adequate traction for suitable trafficability. For purposes of definition, a tool will be considered a single soil-working element whereas an implement or machine will be considered a group of soil working elements. Although tillage and traction are nearly always affected with a machine, the emphasis here will be on the performance of a single tool rather than implements and tracked vehicles.

A partial statement of the overall soil-machine interaction problem is shown in Fig. 1.1. It is appreciated that this description centers on the manipulation of soil by mechanical forces, and the results of the final soil condition and the reaction of soil to forces are of primary importance. Thus, primary emphasis is placed on the soil response to an imposed set of loading parameters.

Traditionally, implement and track designers relied on empirical rules to develop earth-moving equipment and off-road vehicles. These empirical methods are trial and error attempts; the tool or track element [grouser] is varied in some manner, and acceptable designs are identified when the results are judged to be satisfactory. Quantitative descriptions or representations of the final soil conditions are seldom

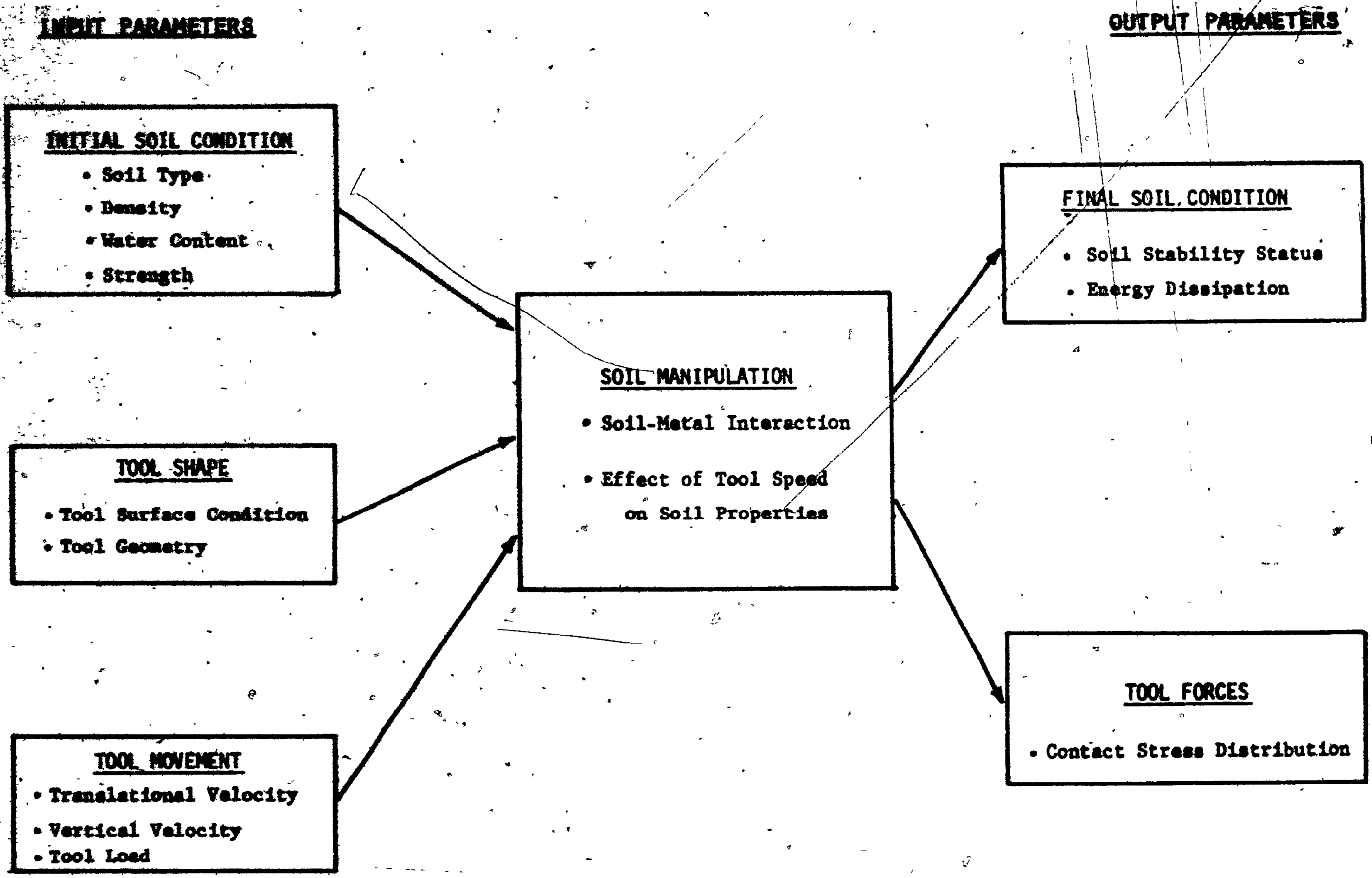

FIG. 1-1 - OVERALL SOIL-MACHINE INTERACTION PROBLEM used and, in addition, the forces required to move the tools or grousers are frequently not quantitatively assessed. Generally, no effort is made to describe the reactions of the soil. Gill and Vanden Berg (1969) present an excellent review of the empirical methods being used at the present time for design purposes. The following is a brief summary of the developments as well as the problems encountered in soil-cutting and soil-grouser interaction analyses.

1.1.1 Soil Cutting

The knowledge of soil mechanics has only been recently applied to the study of the problem of soil cutting. In the early part of the century, research in the United Kingdom and the U.S.A. was confined to the investigation of the draft of tillage implements. The inability of researchers to isolate the relevant soil parameters made it difficult for them to visualize the possibility of a theoretical analysis in terms of classical soil mechanics.

The history of the development of a quantitative analysis of the action of cutting tools in soil has been described by Hettiaratchi (1965). Following the work of Payne (1956) on the action of agricultural tines and Bekker's (1956) success with the study of vehicle performance, Osman (1964) showed that the retaining wall theory developed by Ode (1938) could accurately predict the forces required to cut a wide range of soils. Reece (1965) put forth an equation, which was similar in form to Terzaghi's bearing capacity equation, to predict the force acting on a blade. This equation was later modified by Hettiaratchi et. al. (1966). A summary of the reported investigations in soil cutting is presented in Appendix C.

In reviewing the literature, the various methods attempted to provide a solution for the blade problem appear to fall in four groups; methods relying on dimensional analysis [Wismer and Forth (1969) and Wismer and Luth (1970)], rigid body statical techniques [Osman (1964)], plasticity techniques such as those using a form of the Prandtl solution, specialized for bearing stability [Osman (1964) and Reece (1965)], and methods relying on the principle of limit equilibrium of the soil [Yong et al. (1969) and Yong and Chen (1970)].

It must be realized that in employing dimensional analysis techniques, using laboratory model tests, a required assumption is that soil properties can be adequately scaled. The difficulties surrounding the scaling of soil, or the derivation of appropriate scaling laws for soils, are most complex [Yong et al. (1967)]. In addition to the problems of separate examination of component parts, one must recognize that the problem of a moving rigid blade in soil is an interacting phenomenon and, therefore, should be considered as an interdependent system. The behavior of the soil mass in front of the moving blade is conditioned not only by the geometry of the blade itself, but also by the driving forces associated with the blade. In turn, the progress of the blade in the soil is controlled or influenced by the manner in which the soil will deform, the boundary conditions, and the constitutive makeup of the soil itself.

1.1.2 Soil-Grouser Interaction

In the past decade, a number of research groups have begun intensive investigations into the problems associated with soil-wheel interaction [e.g. Reece (1965), Freitag (1965), Yong (1969-1970) among others]. The same cannot be said for those problems associated with soil-grouser interaction. Some attempts have been made at examining the geometry of the failure surface beneath a moving rigid grouser [e.g. Bekker (1960) and Haythornthwaite (1961)] but apparently investigations into the mode and mechanisms of failure have been limited. Intensive research efforts are necessary in order to define the influence of such parameters as track type, grouser spacing, grouser geometry and grouser size on the magnitude of the forces exerted on the grouser plate by the soil.

As a consequence of the fact that the locomotive ability of any vehicle is dependent on the soil response, it would seem logical that in any attempt to describe the overall behavior of a tracked vehicle in soil, a clear understanding of the fundamental interaction process between grouser and soil is necessary. The little research which has been done on the problem has been oriented towards the prediction of macroscopic effects and has been directed more towards vehicular response than towards soil response.

Previous to the second world war, the design of tracked vehicles was largely an empirical process. Some research must undoubtedly have been carried out before this, but apparently was not reported in the available literature. The first systematic attempt at providing a solution to the overall problem was made by Micklewait (1944). He reported an empirical equation describing the tractive effort developed by a tracked vehicle moving on soft soils, an equation which formed the basis of design until Bekker (1956, 1960, 1969) examined the problem from a more rigorous point of view.

With the assumptions that the grouser plate could be approximated by a strip footing, and an elastic stress distribution in the soil, Bekker was able to derive a theoretical expression relating the horizontal thrust on the grouser to the grouser parameters. By optimizing the grouser spacing and summing the horizontal forces operative on each grouser plate in the track, he was then able to predict the horizontal thrust exerted on a tracked vehicle by the soil. The equations for the horizontal and vertical forces on a grouser are given as:

$$H = b(\eta_c \, lc + \gamma \, \eta_q \, lz + \gamma \, \eta_\gamma \, l^2) \sin \theta \qquad (1.1)$$

$$W = b(\eta_c \, lc + \gamma \, \eta_q \, lz + \gamma \, \eta_\gamma \, l^2) \cos \theta \qquad (1.2)$$

where

b = grouser width, in inches.

η_c, η_q, η_γ = dimensionless trafficability factors which are dependent on ϕ, θ [shown in Fig. 1-2] and the ratio l/h.

l = grouser length, in inches.

h = grouser depth, in inches.

c = cohesion, in psi.

z = sinkage, in inches.

The geometry of the forces is as shown in Fig. 1-2 in which the imaginary strip footing is represented by line AB sloped to the horizontal at an angle of:

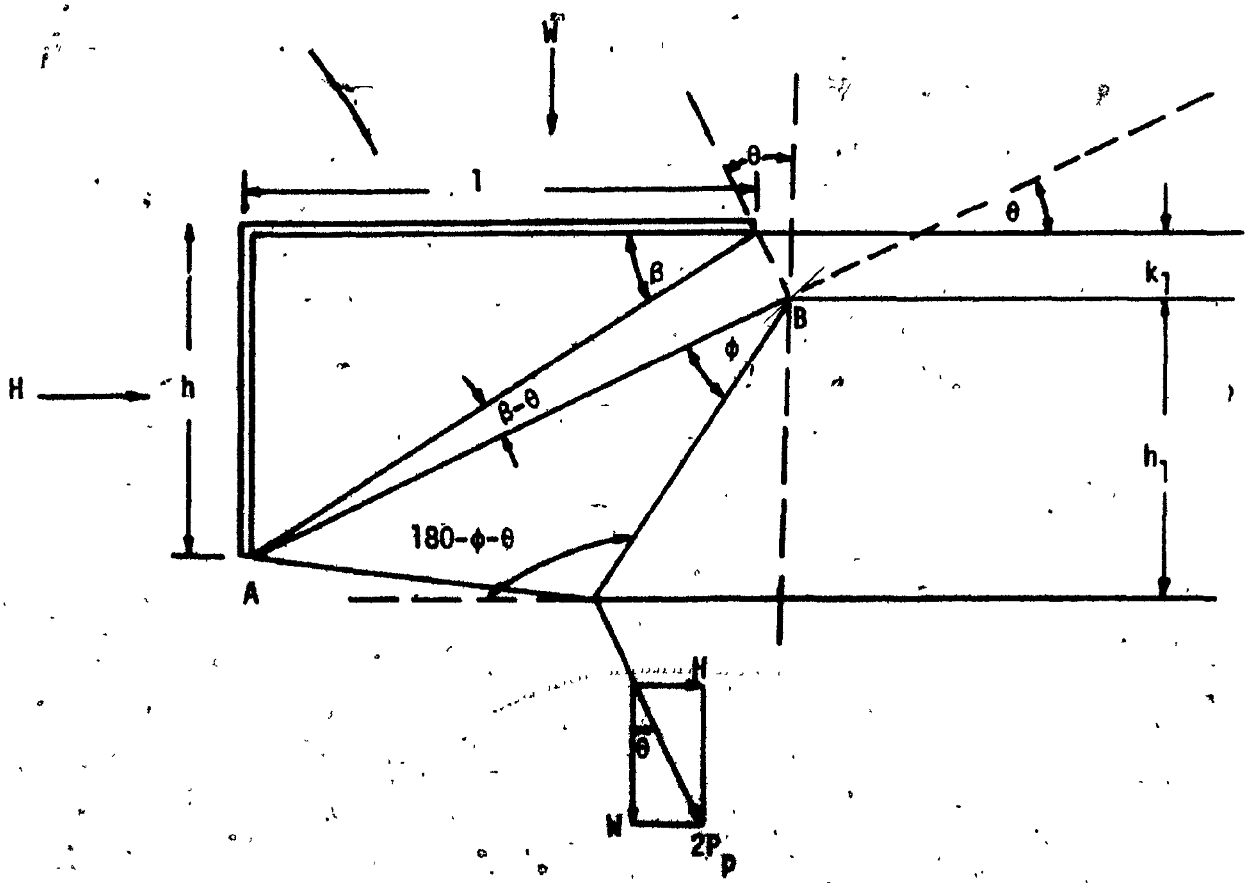

FIGURE 1-2 FORCE DIAGRAM OF A SINGLE GROUSER

[After BEKKER (1960)]

$$\theta = \arctan (H/W)$$

and the bearing capacity of the soil under the footing is given as P_p.

Despite the fact that no experimental evidence was cited in support of his theoretical conclusions, Bekker's equations formed the basis for the design of tracked vehicles until very recently, at which time an extensive research programme was entered into by the U.S. Army Waterways Experiment Station at Vicksburg. The results to date of this programme have dealt primarily with the response of soils to the action of rigid wheels [e.g. Freitag (1965),(1965a),(1965b),(1968)], and an absence of reported data on the response of soils to grouser action is still evident on an examination of the available literature. A summary of the reported investigations has been given in Appendix C.

1.2 PURPOSE OF STUDY

Most of the soil cutting and traction research conducted to date have been based on empirical approaches using the results of a large amount of experimental data obtained from tests to develop methods of analysis and design. While such approaches may have been necessary in the past, the advent of digital computers and the development of modern methods of numerical analysis now provide the necessary tools to obtain analytical solutions which can replace much of the empirical testing carried out in the past. However, such analytical solutions must be checked by a selected, but smaller number of experimental tests to verify their accuracy.

The problem of soil-machine interaction has been the subject of a rigorous study under a research programme in operation at the

Soil Mechanics Laboratory of McGill University since 1963. This programme can be divided into two distinct phases. Investigation of the behavior of soil under driven rigid wheels [Yong and Webb (1969), Yong and Windisch (1970) and Windisch and Yong (1970)], and the study of the performance of an isolated element [tractive or cutting] moving through soil [Yong and Chen (1970), Yong et al. (1969) and Yong and Sylvestre-Williams (1969)].

The present study is a continuation of the second phase of the overall McGill programme. Its purpose is to provide a rational analytical means for predicting the performance of a cutting or a tractive tool, using parameters that describe the soil response due to interaction with the tool. It is to be appreciated that an accurate prediction of machine-soil response behavior would provide a sound basis for the evaluation of the efficiency and economy of soil cutting and mobility. Consequently, the computer solution technique developed herein can be used to aid in the designing of the tool or the interacting unit, since the various machine and soil parameters input to the computer code can be varied and the resultant output evaluated. This philosophy is demonstrated in schematic form in Fig. 1-3.

1.3 SCOPE OF STUDY

The factors considered pertinent in soil cutting and traction experiments relate to:

(a) Soil - Type, density, and shear resistance parameters.

(b) Cutting or traction tool - Geometry, depth of cut, speed of travel and interfacial characteristics.

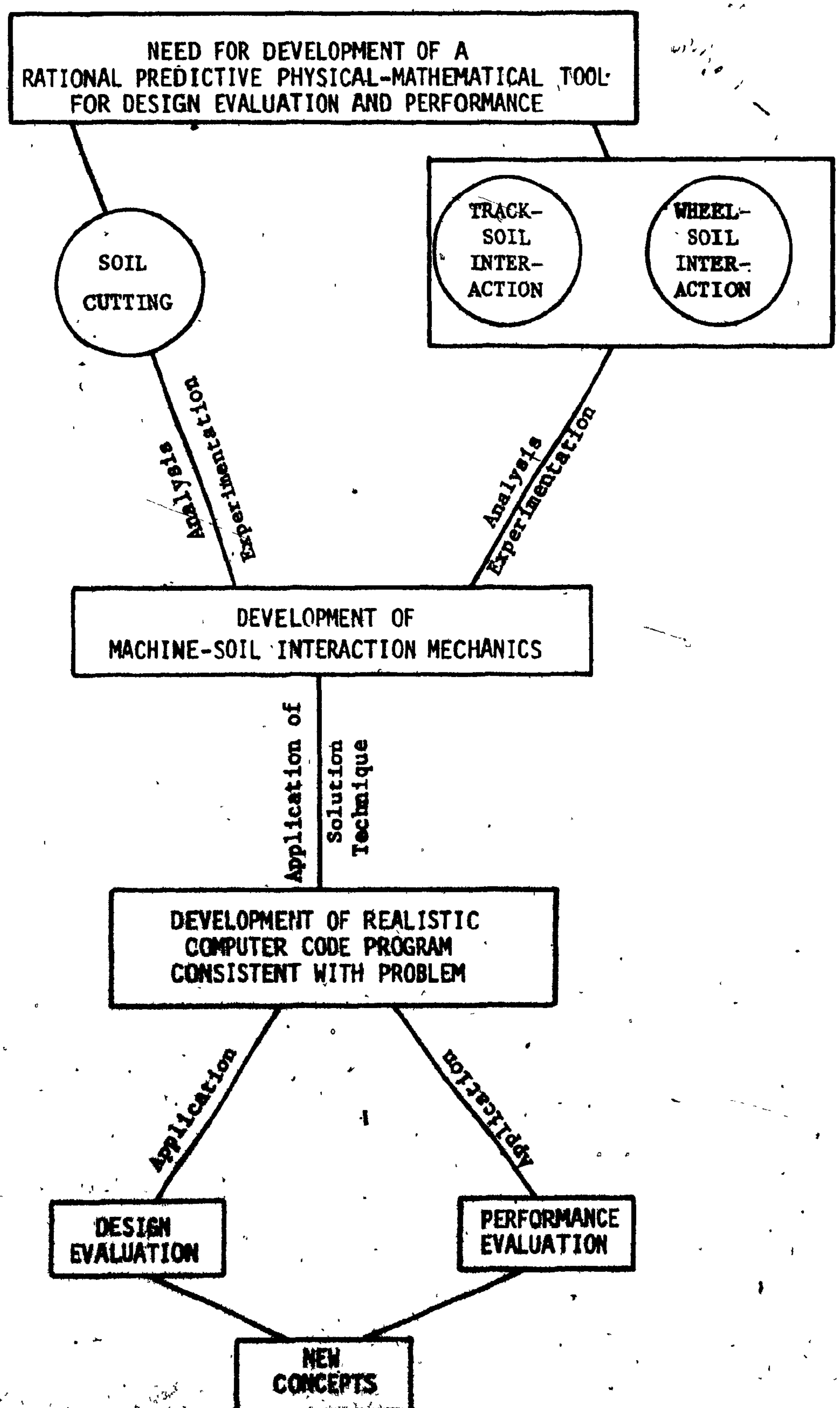

FIG. 1-3 - SCHEMATIC REPRESENTATION OF MACHINE-INTERACTION STUDY PURPOSE

(c) Forces - Developed forces [horizontal and vertical].

In general, the variations with regard to the above are concerned with the specification of the desired condition, i.e.:

(1) Specified constant speed and constant depth of cut. This will yield developed forces on the tool, which may subsequently be decomposed into horizontal and vertical components.

(2) Specified constant horizontal force and constant depth of cut. The measured variables in this instance are speed and developed vertical forces.

(3) Specified constant horizontal and vertical forces. In this particular case, both speed and depth of cut are the measured variables.

To allow for a rational approach in the analysis of results, the experiments performed in the course of this study are limited to the first condition [i.e. specified constant speed and constant depth of cut]. The procedure employed accounts for measurement of developed forces [both horizontal and vertical], accompanied by photographic recording of soil distortion.

The scope of this study is limited to verifying the validity of the application of the finite element technique to the analysis of simple problems of soil-machine interaction in nearly-saturated kaolinite clay under plane strain conditions. Comparisons between theoretical and experimental results are made to assess the validity of the assumed model. The approach adopted can be easily extended to field problems where the soil-machine interaction is more complex.

1.4 ANALYSIS OF THE PROBLEM

Within the broad definition of the problem, there are numerous paths that can be followed according to emphasis and assumptions made. Figure 1-4 shows a schematic diagram of a number of available solution procedures.

If soil deformation is neglected, rigid body forces and theories of classical soil mechanics can be used in attempting to calculate the developed reactions. Forces are evaluated by studying the static equilibrium of an assumed failure surface which is chosen to satisfy the limiting stress condition of a Coulomb material. These theories, however, neglect the soil deformation and therefore are not sufficiently accurate to be acceptable.

If the soil is assumed to be perfectly plastic with a Coulomb, or any other yield surface, there would be no difficulty, in principle, in computing reactions. The theorems of limit analysis [upper and lower bound theorems] will give bound on the answer. Yong et al. (1969) and Yong and Chen (1970), have successfully used the method of limit equilibrium to predict the force required to move a blade through a frictional material. Yong and Sylvestre-Williams (1969) adopted the same approach to study the traction of grousers. Limit equilibrium analysis uses a statically admissible stress field, giving lower bounds.

A lower bound solution requires an assumption of a statically

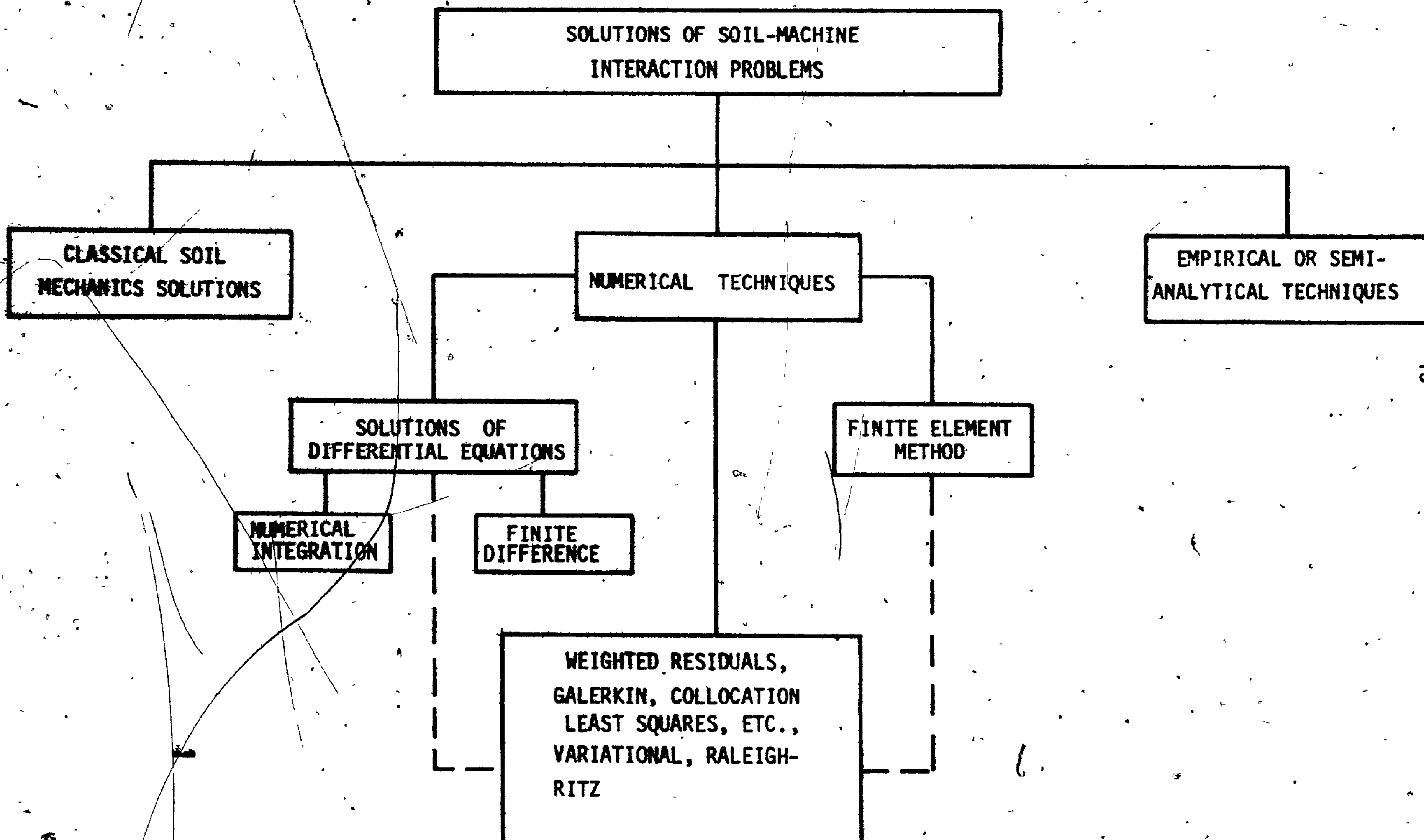

FIG. 1-4 - A SCHEMATIC DIAGRAM OF A NUMBER OF SOLUTION PROCEDURES FOR SOIL-MACHINE INTERACTION PROBLEMS admissible stress field, while an upper bound solution requires a kinematically admissible displacement or velocity field. In a mixed boundary-value problem, there is no apparent independence between the two fields, and compatibility between the two fields is the essential final justification that the solution obtained is, in fact, the correct one.

Until quite recently, an important defect in the theory of earth pressure lay in its development without reference to stress-strain relations, the theory being based upon the concept of limiting equilibrium satisfying Coulomb's law of soil failure in conjunction with an extremum principle. This procedure neglects the important fact that stress-strain relations are an essential constituent of a complete theory of any branch of the continuum mechanics of deformable solids [Morgenstern and Eisenstein (1970)].

Semi-analytical techniques such as the visioplasticity method were investigated at McGill University. Yong and Webb (1969) used this method for determining the useful output energy for a rigid moving wheel. Yong and Windisch (1970) used it for determining the interfacial and subsoil stresses under a towed rigid wheel. In the visioplasticity method, the displacement field is recorded experimentally, from which a stress field is determined using a constitutive relationship. This method is only applicable to small scale testing [assuming steady-state conditions] and cannot be used to predict field conditions.

Based on the above discussion, it was concluded that a numerical method which can predict both the stress distribution and the soil deformation resulting from a cutting or a tractive tool would have a place in soil-machine mechanics. Such a method should take into account the non-linear behavior of soil and the effect of large deformation due to the implement movement.

1.5 PROCEDURE FOR DEVELOPING A RELIABLE NUMERICAL TECHNIQUE

For a given problem, development of a reliable numerical technique involves various steps as depicted in Fig. 1-5. These steps essentially represent a trial and error procedure which requires the examination of factors such as idealization of the problem as a discretized body, numerical characteristics and constitutive laws. In the Figure, the first two factors are indicated by dashed lines, whereas the trial and error procedure for constitutive laws is shown by solid lines [Desai (1972)].

A numerical technique for solving soil-machine problems can be developed in progressive stages. The purpose of the technique is to quantitatively describe the action of the machine on the soil. In the initial recognition phase, the action is observed and noted to be repetitive. The recognition phase is gradually supplanted by an "equivalent" model. For complicated problems, the idealization stage can be difficult and would require a number of trials before a model of acceptable accuracy can be evolved. The final model may be arrived at after a number of trials.

The second step of developing a solution technique is arriving at a representative constitutive law. A constitutive law for soil is

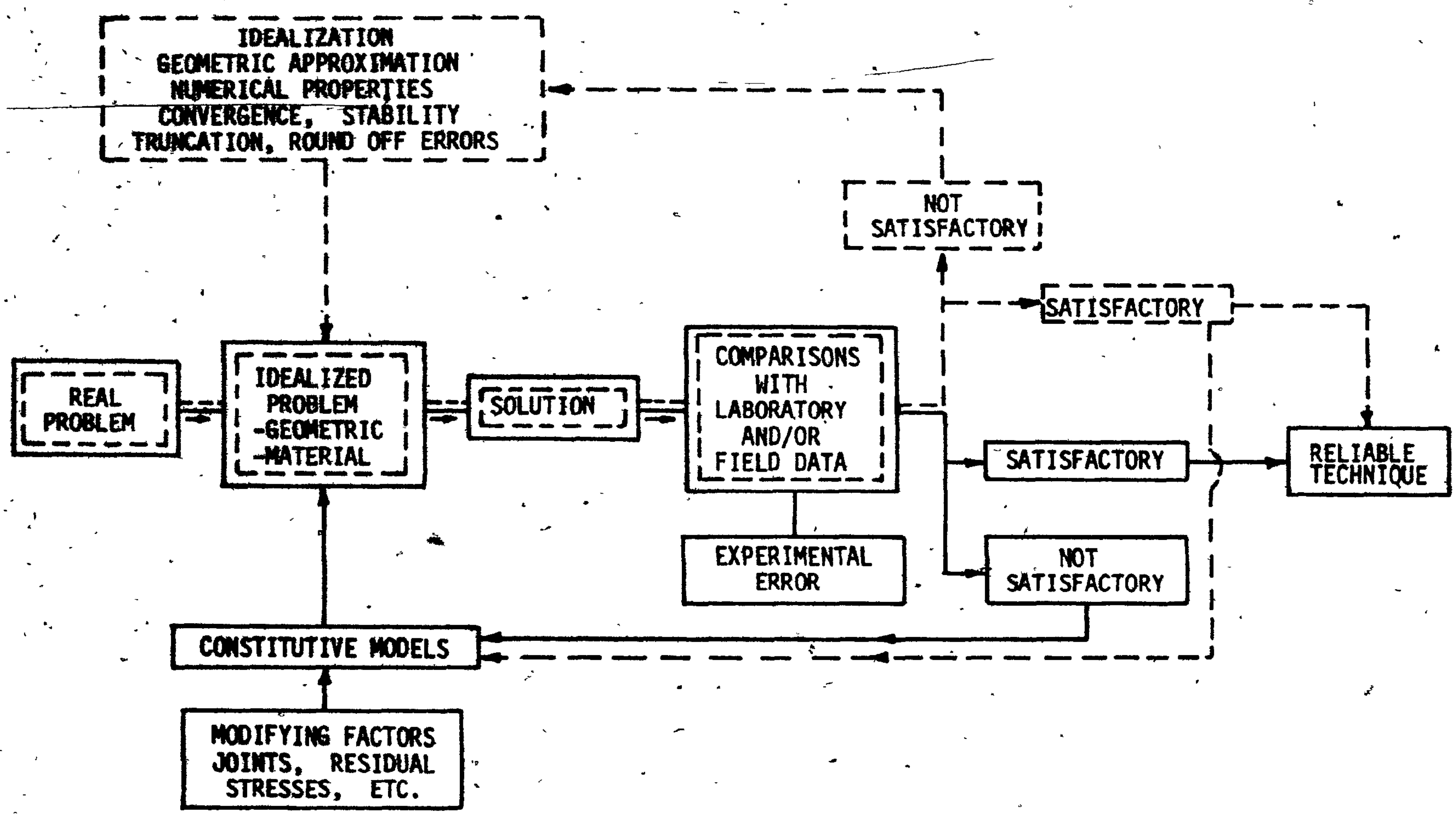

FIG. 1-5 - DEVELOPMENT OF A RELIABLE NUMERICAL TECHNIQUE AFTER DESAI (1972) usually dependent on a number of factors such as density, stress history, water content, and existence of discontinuities. The constitutive relation can be established through the application of several distinct phases of study. First, some specific behavior is observed and studied. Second, having noted the behavior, factors involved in the behavior are identified and their relation ascertained in a cause-and-effect manner. Mathematical equations are required to quantitatively describe the cause-and-effect relation and, hence, the behavior. Resorting to mathematical equations is possible only when both input and output quantities can be expressed in some form of numerical description.

With reasonably accurate constitutive equations, a complete analytical technique can be developed to describe machine actions. A specific machine tool has a fixed geometrical shape that can be expressed by appropriate equations. An overall coordinate framework can be established in which the direction of travel and the path of tool motion, the orientation of the tool, and the continuous nature and profile of the soil can be described. Specifying the path of motion of the tool in the reference framework thus produces the boundary conditions necessary to define the problem. Simultaneous solution of the system of governing equations utilizing the boundary conditions provides a quantitative solution to the problem.

Many numerical techniques can be attempted in developing a solution for a particular soil-machine interaction problem; among them are the limit equilibrium [classical soil mechanics solution], the finite difference, and the finite element method [Figure 1-4].

Adopting the limit equilibrium approach, Sokolovski (1960) developed the mathematical methods that made it possible to solve numerically the equations of equilibrium to obtain the force required to fail soil by loading an interface. In a plane problem, there are three unknown stresses and two equations of equilibrium. If the soil is assumed to be in a state of failure, the Coulomb relationship could therefore be introduced as the third equation. In three-dimensional problems there are six unknown stresses and only four equations; a solution is therefore impossible - without the introduction of stress-strain and compatibility relationships. It must be pointed out that if the problem is statically determined [i.e., boundary conditions are only given in terms of stresses], the equilibrium equations and the Coulomb failure condition are sufficient to give the stress distribution without any reference to the stress-strain relations. However, if displacements or velocities are specified over part or all of the boundary, then the stress-strain relations must be used to relate the stresses to the strains and the problem becomes much more complicated and must usually be solved by trial and error. A stress field satisfying all stress boundary conditions is assumed. The velocities are then computed and a check made to see if the velocity boundary conditions are satisfied. If not, the stress field is modified and the procedure is repeated as often as necessary. In addition to all these difficulties, the solution obtained is valid only for the case of incipient plastic flow; once plastic flow progresses, the shape of the boundaries changes considerably and it becomes necessary to satisfy the boundary conditions on the deformed boundary. This makes it virtually impossible to obtain the load-deformation history of a continuously deforming soil.

The basic difference between the finite difference and the finite element methods lies in the approaches used in arriving at the node point [or discrete mass] equilibrium equations. In the usual finite difference techniques, the governing system of differential equations is approximated by difference equations, which in essence require an assumption of the displacement form between neighboring node points. The restriction applied by this approach is the relative uniformity of node point spacing which yields solutions at only a fixed number of points in the domain of interest, and may require additional interpolation for solutions at other points. Also, the finite difference method can be cumbersome for handling irregular boundaries and nonhomogeneities. In the finite element technique, on the other hand, the soil mass is divided into various small elements, with each element connected to its neighboring elements at their node points. Over each element, approximate displacement functions are defined. In this manner, the finite element method recognizes the continuity of masses, and does not require separate interpolations for extension to other points. The use of separate approximating models for each finite element permits greater flexibility in tackling masses with extensive nonhomogeneities, complex realistic geometries and mixed boundary conditions. Since the main advantage of the finite element method lies in its capacity of handling relatively complex problems, the method was chosen in this study to investigate the subject of simple cases of soil-machine interactions.

1.6 ORGANIZATION OF THE THESIS

The Thesis is divided into two separate parts:

1. The first part deals with the development of the analytical model used in this study, together with the results of the experimental program. In addition, comparisons between theoretical, experimental and analytical results are presented to assess the validity of the assumed model.

2. The second part of the thesis, which consists of five appendices, concerns itself mainly with providing the pertinent information necessary for a complete appreciation of the computational and experimental techniques.

The first part, which deals mainly with the introduction, appreciation, application, and verification of the proposed analytical model, is subdivided into eight chapters [see Fig. 1-6].

Chapter 1, of which this Section is a part, is an introductory chapter in which a statement of the problem is presented.

Chapter 2 describes the finite element technique and the proposed model adopted in this study.

Chapter 3 provides a brief description of the experimental facilities and techniques used, together with some initial experimental data.

Chapter 4 contains results of the cutting and traction experiments performed, and results of the strength tests. In addition, this

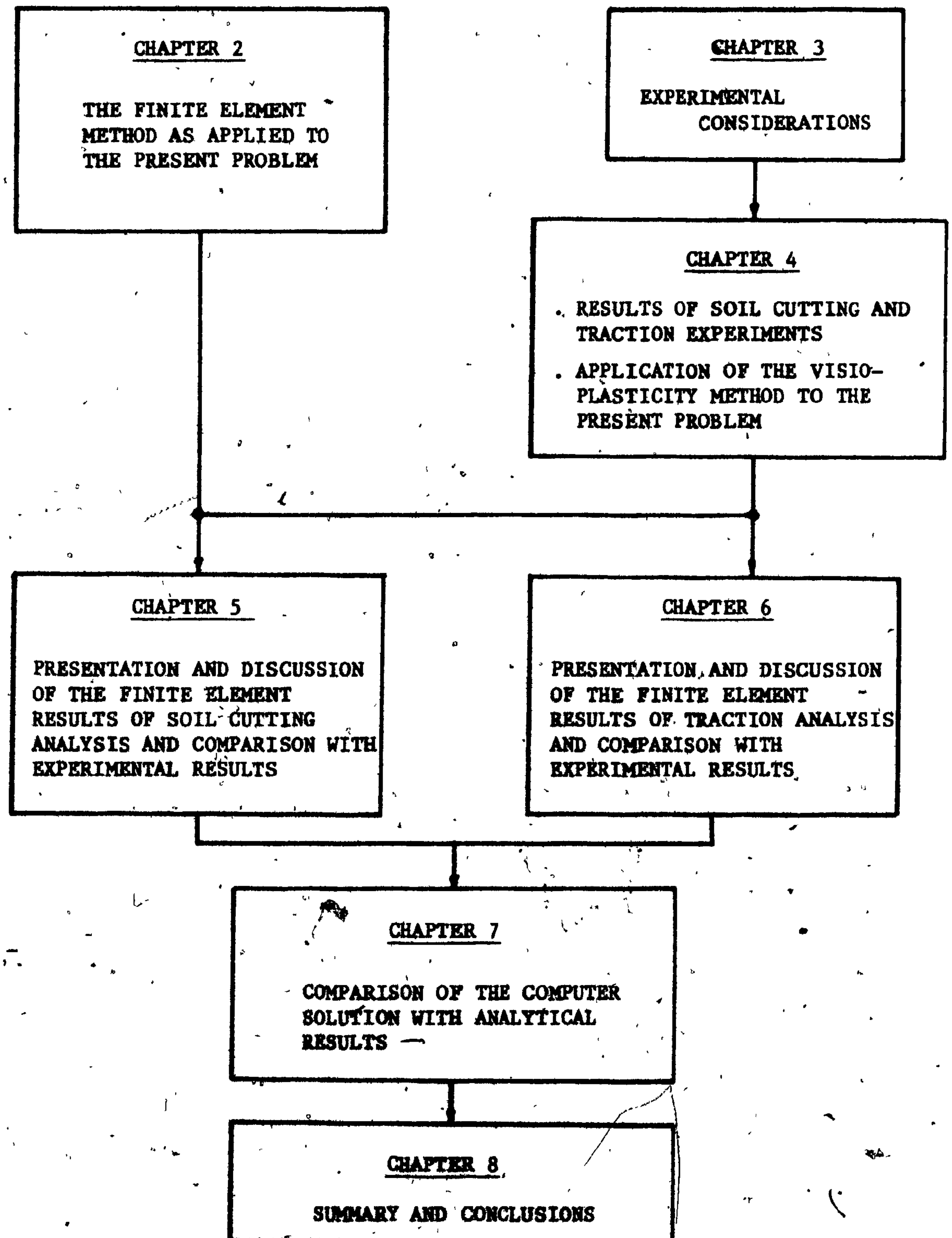

FIGURE (1-6) ORGANIZATION OF THE MAIN BODY OF THE THESIS

Chapter provides a development of the visioplasticity method as applied to the present study, together with an appreciation of its applicability to the problem by means of the invoked assumptions.

Chapter 5 is concerned with the presentation and discussion of the finite element results of soil cutting analysis, and comparisons with the experimental results.

Chapter 6 presents the finite element results of soil traction analysis accompanied by comparisons with the experimental results.

Chapter 7 discusses the applicability of the proposed analytical solution by examining the significance of implied conditions and requirements in relation to observations and results. This is accomplished by dividing this Chapter into two main Sections:

1. finite element analysis, employing the proposed model, of a long vertical wall retaining clay, and comparisons with a closed-form solution scheme, and
2. comparisons of soil cutting and traction analytical and experimental results, obtained in this study, with results computed from existing theories.

Chapter 8 contains the summary and conclusions.

The second part of the thesis is composed of the experimental and data reduction techniques, as well as computer program descriptions and other pertinent material required to provide the input for the experimental-theoretical study presented in the first part of the thesis. This part consists of:

<u>Appendix A</u> - experimental considerations.

<u>Appendix B</u> - data reduction techniques.

<u>Appendix C</u> - review of previous work.

<u>Appendix D</u> - solution of linear equations by direct Gaussian elimination method.

<u>Appendix E</u> - computer program listings.

CHAPTER 2

FINITE ELEMENT METHOD
AS APPLIED TO THE PRESENT PROBLEM

2.1 INTRODUCTION

Analyses of soil-structure interaction problems are of considerable importance in investigations concerned with soil-implement and soil-vehicle mechanics. The calculation of earth pressures on structures has been given detailed attention by researchers, and there now exists a wealth of both theoretical and experimental knowledge on this subject. These sources are continuously being investigated with a view to possible adaptation and improvement to meet the more specialized requirements of soil-machine problems. As an example of this approach, the familiar cases of two-dimensional soil response encountered in long retaining walls and strip footings bear a close parallel to wide cutting blades and track-laying tractor running gear, respectively. This analogy is not limited to the actual physical similarity between these structures but extends to the more significant factors associated with the problem boundary conditions, the soil mode of deformation and the actual failure surface geometry involved.

It must be emphasized, however, that the mechanics of soil cutting and traction is much more complex than that of the soil-structure interaction, as there is more than one process in operation. The resistance of soil to the forward motion of a tool is caused by shearing action, friction and adhesion between the soil and the tool, raising and accelerating the soil, and cracking if the tensile strength is exceeded.

The problem at hand is so complex that an acceptable general solution technique capable of handling a wide variety of soil-machine interaction problems is not anticipated for some time to come due to:

1] The difference in soil response to the action of an implement. This can range from shear failure for cohesionless soils to brittle behavior for a nonplastic soil to flow in the case of wet cohesive soils.

2] The different functions which determine the shape of the implements, their manner of movement [such as depth and speed], orientation and path of motion.

Within these limits the problem can range from investigating a case of a simple tool moving in a homogeneous soil with controlled properties to evaluating performance of complicated machinery designed to perform in different soils. With this in mind, the scope of this study as stated in Chapter 1 is to investigate a specific simplified problem under certain established conditions. While these conditions and hence the approach adopted may seem to be restrictive as to render a solution technique too specialized to be of immediate practical use, it is believed that a proposed technique that possesses a potential for extension to similar and more difficult problems with some or little modifications will ultimately have practical usefulness. Furthermore, such a technique can be very instrumental in investigating and understanding the fundamental mechanisms involved in the case of simplified cutting and tractive tools moving through soils.

In the specific problem of a soil-tool interaction, an accurate analytical determination of soil reactions as well as the internal stress and deformation fields in the soil mass throughout the loading sequence is complicated by a number of factors. Some of these factors are:

1] The system is composed of two materials, soil and metal, having in most instances complex interface geometries.

2] The system has a continuously changing topology caused by the movement of the tool in the soil. This will have the effect of introducing cracks or discontinuities in a brittle or frictional soil or flow in a plastic soil.

3] The stress-strain relationship for soil is nonlinear and is a function of many variables. Constitutive relationships and failure criteria for soils under combined stress states are difficult to obtain.

4] Soil behavior is dependent on loading rate and sequence.

5] The characteristics of the soil-metal interface in terms of the degree of soil slip and the nonlinearity in the relationship between interface shear stresses and shear displacements add to the complexity of the problem.

One of the factors that requires special consideration in the construction of a realistic analytical model for soil cutting and traction is the effect of the progressive cutting of the soil at the tool tip with the possible development of failure surfaces wherever the shear strength of the soil is exceeded. Figure 2-1 illustrates the general mechanisms operating in cases of soil cutting [constant depth of cut] and soil-grouser systems [constant depth of embedment].

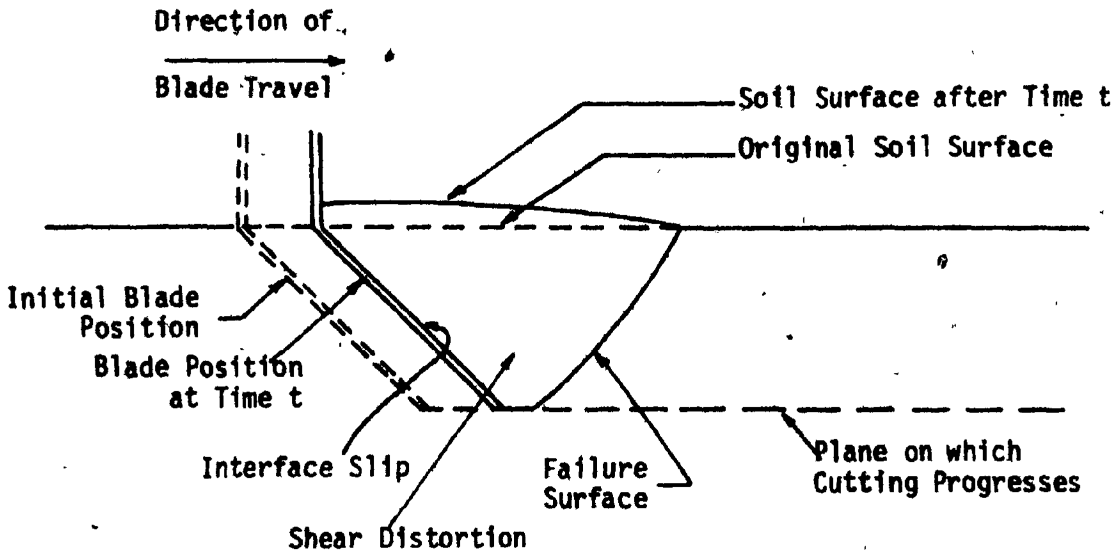

(A) BLADE-SOIL SYSTEM AT CONSTANT DEPTH OF CUT

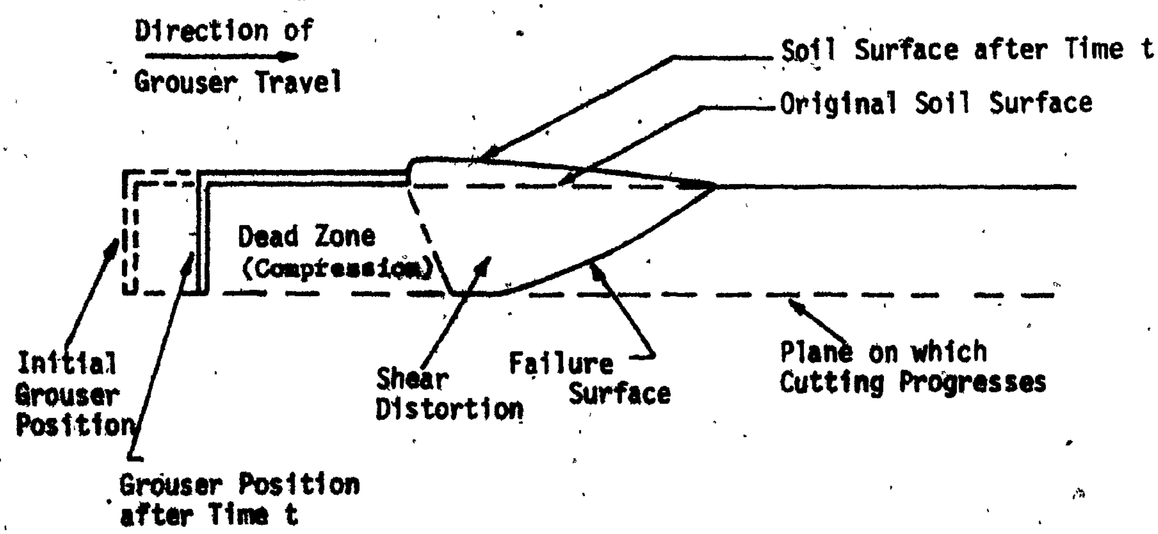

(B) GROUSER-SOIL SYSTEM

FIGURE 2-1 MECHANISMS OPERATING IN CASES OF SOIL CUTTING AND SOIL GROUSER SYSTEMS

In view of the great complexities mentioned above, the problem can be classified from the continuum mechanics point of view as an inelastic, nonlinear analysis of a nonhomogeneous anisotropic system. An analysis to determine stresses and deformations throughout the soil medium by a direct application of the classical theories of continuum mechanics can be extremely difficult. However, if by an adoption of a numerical technique such as the finite element method, detailed stress and deformation fields could be determined for various tool positions, studies or the basic interaction behavior would be immeasurably aided.

2.2 IDEALIZATION

In developing an analytical model for problems of soil machine mechanics, it is essential that proper appreciation be given to the material performance and boundary conditions. The appropriate framework defined by using realistic similarities between physical and mathematical boundary conditions will ensure a higher order of predictability with the developed analytical model. The observation of soils deformation and failure patterns during a loading process often provides the basis for the development of valid models leading to solutions of forces and stress fields.

Classical soil mechanics idealizes soils as a rigid plastic frictional material [Chapter 1]. That is a material which supports loads without any deformation until a certain shear stress is reached, whereupon total failure occurs. This maximum stress is described by Coulomb's equation:

$$\tau_{max} = C + \sigma \tan \phi$$

and where the shearing occurs against a rigid interface by

$$\tau_{max} = C_a + \sigma \tan \delta$$

The strength properties of the soil model are defined by the three parameters, cohesion C, angle of internal friction ϕ, and density γ. δ is the angle of soil interface friction and C_a soil interface adhesion. As previously mentioned in Chapter 1, this model as well as the theory of limit equilibrium has been taken to a proper logical conclusion by Sokolovski (1960). Failure patterns predicted by this approach are shown in Fig. 2-2a for a cutting blade and in Fig. 2-2b for a grouser.

It should be pointed out that the limit equilibrium model leads to a solution by predicting the shape of the regions of soil sheared off from the main body. In practice, however, the soil in the failure zone does not shear all at the same time. Due to the gradual increase in the stresses with increasing strain, the conditions for the transition into the passive state are not realized. In this event, shear failure occurs locally and the slip lines do not propagate to the surface. This type of failure is termed progressive failure. Furthermore, the limit equilibrium model provides a solution for the forces up to the formation of the first shear plane or failure surface with no provisions for extending the solution beyond this stage. Another limitation in the application of this approach is that an assumption has to be made regarding the degree of mobilization of the soil-rigid interface friction and adhesion.

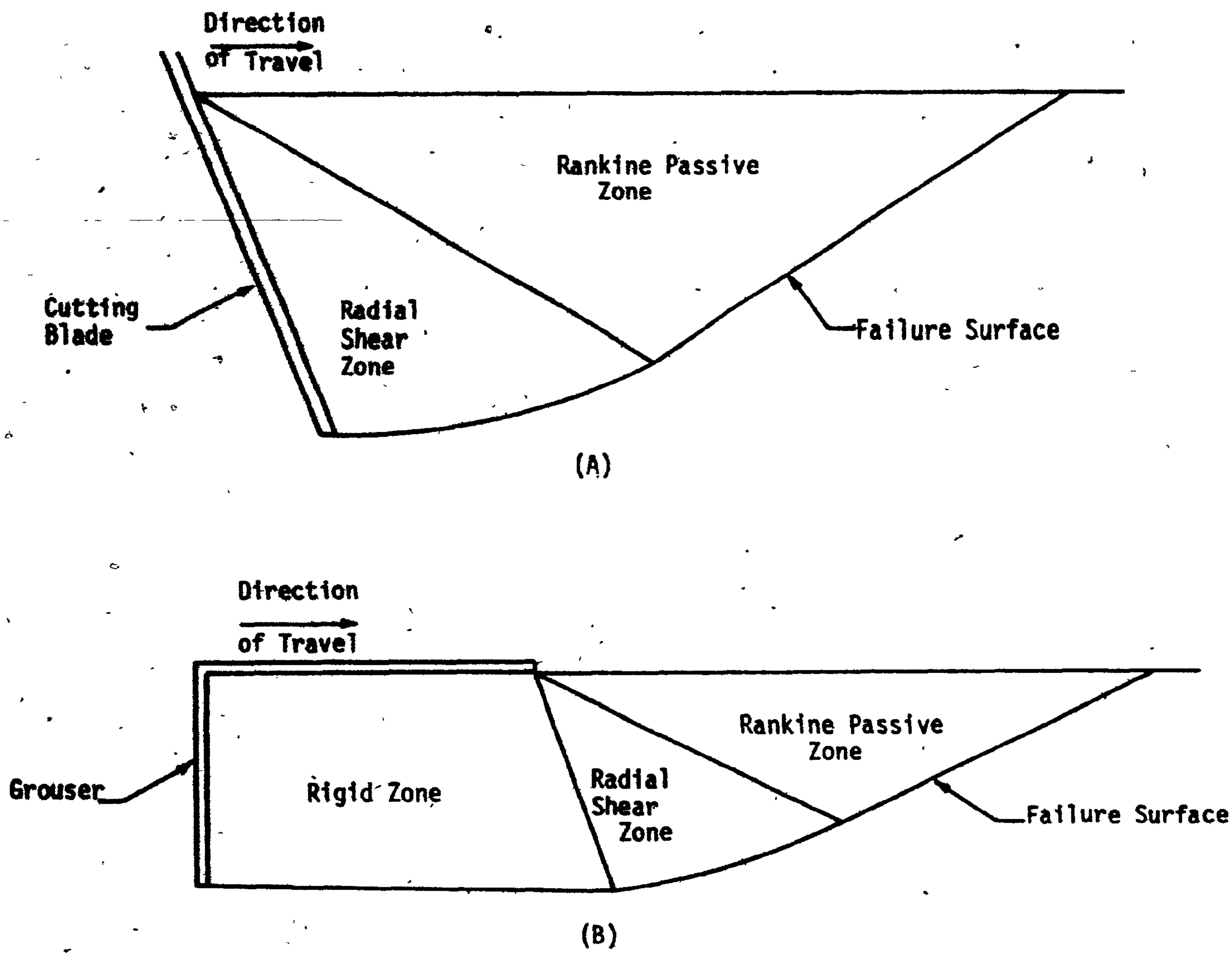

FIGURE 2-2 SOIL FAILURE PATTERNS IN FRONT OF A CUTTING BLADE AND A GROUSER AS PREDICTED FROM LIMIT EQUILIBRIUM THEOREM

While the limit equilibrium approach was utilized successfully for predictions of forces on cutting blades [Yong et al. (1969)], and grousers [Yong and Sylvestre-Williams (1969)], it is argued that a development of a finite element model to handle some of the cutting and traction problems can quite easily overcome most of the above limitations.

With this background, it is now possible to examine the deformation mechanism operative in a tool-soil system. Figure 2-3 divides the loaded soil into three distinct regions for ease of analytical treatment. These regions are typified by elements A, B and C. The first of these represents an interfacial element in which sliding of the soil on the rigid interface does occur. The second element [B] is a cutting element in which large shear distortions caused by the tool cutting action develop. Finally, element [C] represents a region in which plastic deformation takes place with possibilities of development of localized or general shear failures. While this representation may seem to oversimplify the soil response behavior, such philosophy does, in fact, take into account all the operative factors in the deformation process. It now remains to idealize these three elements to arrive at a viable finite element model for the problem at hand.

The initial step in developing an analytical model using the finite element approach consists of idealization of the problem by drawing a finite element mesh which simulates the presence of the soil mass and the tool. The construction of the finite element mesh requires that the type and number of elements included should be adequate to attain the correct flexibility of the continuum.

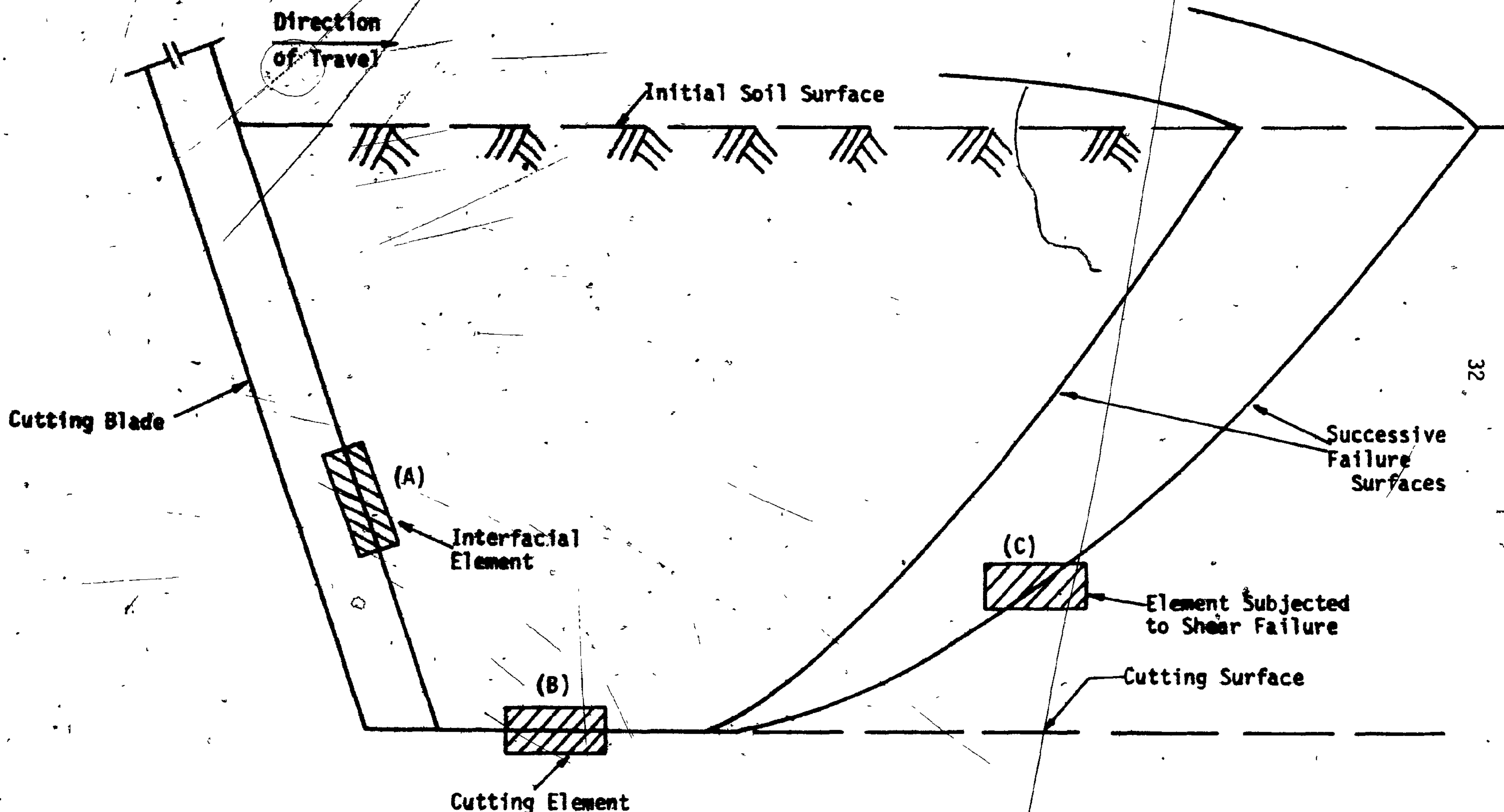

FIGURE 2-3 LOCATION OF ELEMENTS FOR DEVELOPMENT OF IDEALIZED MODEL (PROBLEM OF A CUTTING BLADE AT A FIXED DEPTH OF CUT)

To idealize a simple soil-tool interaction problem by a finite element model, certain characteristics must be incorporated in such a model so that it can represent the various elements shown in Fig. 2-3. Some of these characteristics are:

1] Relative displacements occur across a thin discontinuity at the tool tip level, for tool fixed depth of embedment, due to the cutting action caused by the tool movement in the soil mass. Above this discontinuity the soil is displaced by the tool while below it very little deformation occurs.

2] On the interface between soil and tool, relative displacements do occur and play an important role in the interaction between the two materials. The nature of the interface behavior depends upon the roughness of the tool and the friction and adhesion of the soil. Most finite element analyses have been performed using one of the two following limiting assumptions concerning the characteristics of a soil-rigid interface interaction:

(i) that the interface is perfectly rough, with no possibility for slip between the rigid interface and the soil, or

(ii) that the interface is perfectly smooth, with no possibility for shear stresses which would retard relative movements between the rigid interface and the soil.

Experimental and actual field evidence show that these assumptions are not realistic.

For a realistic analysis of the problem, it is essential that any relative displacement or discontinuity in the deformation field should be taken into consideration. It is obvious from the above discussions that the plane strain continuum elements used in the finite element analysis [constant strain triangular element, for example] cannot satisfactorily model the soil deformation behavior in a case where discontinuities may develop. These elements are assumed to be connected at the nodes preventing any slip or separation behavior. However, if an idealized material element that can transmit shear stress parallel to its direction - providing this does not exceed the frictional resistance - is incorporated in the overall model, one will be able to adequately include such behavior features as failing in shear and development of discontinuity surfaces.

Previous attempts have been made to develop discrete elements to represent discontinuities embedded in a continuous system [Goodman et al. (1968) and Zienkiewicz et al. (1970)]. In the following section a review of the research that has been done to simulate a discontinuity in the finite element analysis is presented, followed by the approach adopted in the present study to deal with such behavior.

2.2.1 Idealization of Discontinuities

Researchers in the fields of reinforced concrete and rock mechanics have investigated the possibility of modelling discontinuities in the deformation field by the finite element method. In reinforced concrete, the combination of steel and concrete, by itself, presents no difficulty in the analysis. However, the means of modelling the behavior at the interface between the two materials require special attention. In the first application of the finite element method to reinforced concrete, Ngo and Scordelis (1967) developed a linkage element consisting of two orthogonal springs to which stiffness was ascribed to represent other than a perfectly rigid connection between two nodes of adjacent elements. This element, shown in Fig. 2-4, has been used by many investigators, such as Ngo et al. (1967) and Nilson (1968), to simulate the bond-slip relationship between a reinforcing bar and the surrounding concrete.

With respect to cracking, Ngo and Scordelis (1967) studied the stress distribution in singly reinforced, simply supported beams into which they had incorporated predefined crack patterns. Nilson (1968) extended the work by allowing cracking to take place along the common edge between the elements where the principal tensile stresses exceeded the modulus of rupture of concrete. The crack was represented by altering the topology of the discretization by disconnecting cracked elements at their common nodes. In addition, Nilson introduced nonlinearities in the material properties and in the relationship between bond stress and bond slip. The loading was applied incrementally and the behavior studied up to the ultimate load.

In rock mechanics, a number of approximate models [or theories] have been proposed to represent the behavior of jointed media. These theories incorporate analyses of intact material, pre-existing or in situ joints or fractures, closing-opening and propagation of cracks, and sliding behavior of joints interpreted in terms of contact and interlocking of asperities.

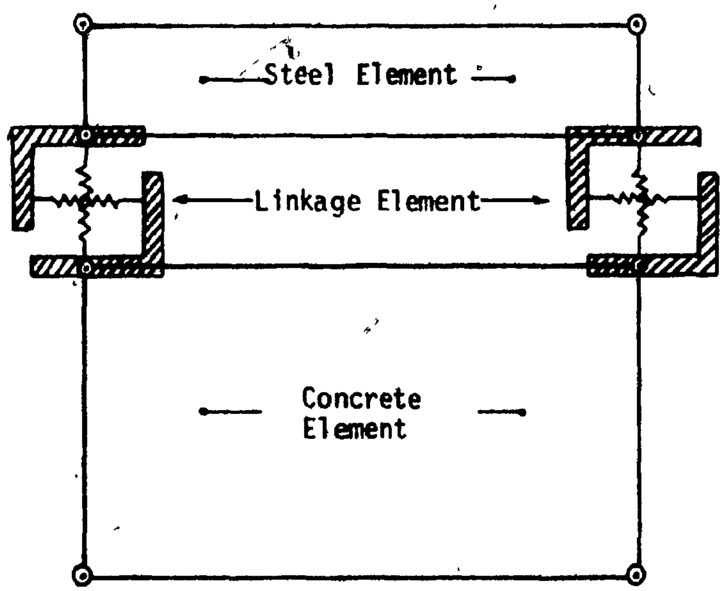

FIGURE 2-4 SCHEMATIC REPRESENTATION OF LINKAGE ELEMENT AS USED IN REINFORCED CONCRETE ANALYSIS.

In order to account for a fault, Anderson and Dodd (1966) used a pin-ended one-dimensional element, Fig. 2-5. This element can allow transfer of compressive stresses across a fault, but cannot sustain shear or tensile normal stresses. Duncan and Goodman (1968) proposed three different procedures:- ubiquitous joint, orthotropic continuum and single joint analysis, shown in Fig. 2-5. The ubiquitous joint analysis is based on the continuum approach in which the induced shear stresses are computed on a large number of plane orientation. Then the likelihood of slip or opening of joints that really exist is evaluated. The orthotropic continuum approach is based on linear elastic theory in which equivalent elastic parameters are computed for the parent mass influenced by three orthogonal joint sets. In the single joint analysis, Figs. 2-5d and 2-5e, stiffness formulation is obtained by considering the joint as either one- or two-dimensional. The stiffness of a joint is defined in terms of its normal and tangential stiffnesses. This approach is a modification of the concept proposed by Ngo and Scordelis (1967) for cracking in concrete elements.

The one-dimensional single joint proposed by Goodman et al (1968) and Heuze et al. (1971) is defined by four nodal points, Fig. 2-5d; with its thickness in the normal direction assumed as zero. This joint element, when inserted between two portions of the parent mass, can permit large relative displacements. Zienkiewicz et al. (1970) have formulated single joint analysis by using isoparametric element concept.

In application to soil-structure interaction problems, Clough and Duncan (1971) performed analyses of retaining walls using the one-dimensional finite elements to simulate the interface between the wall

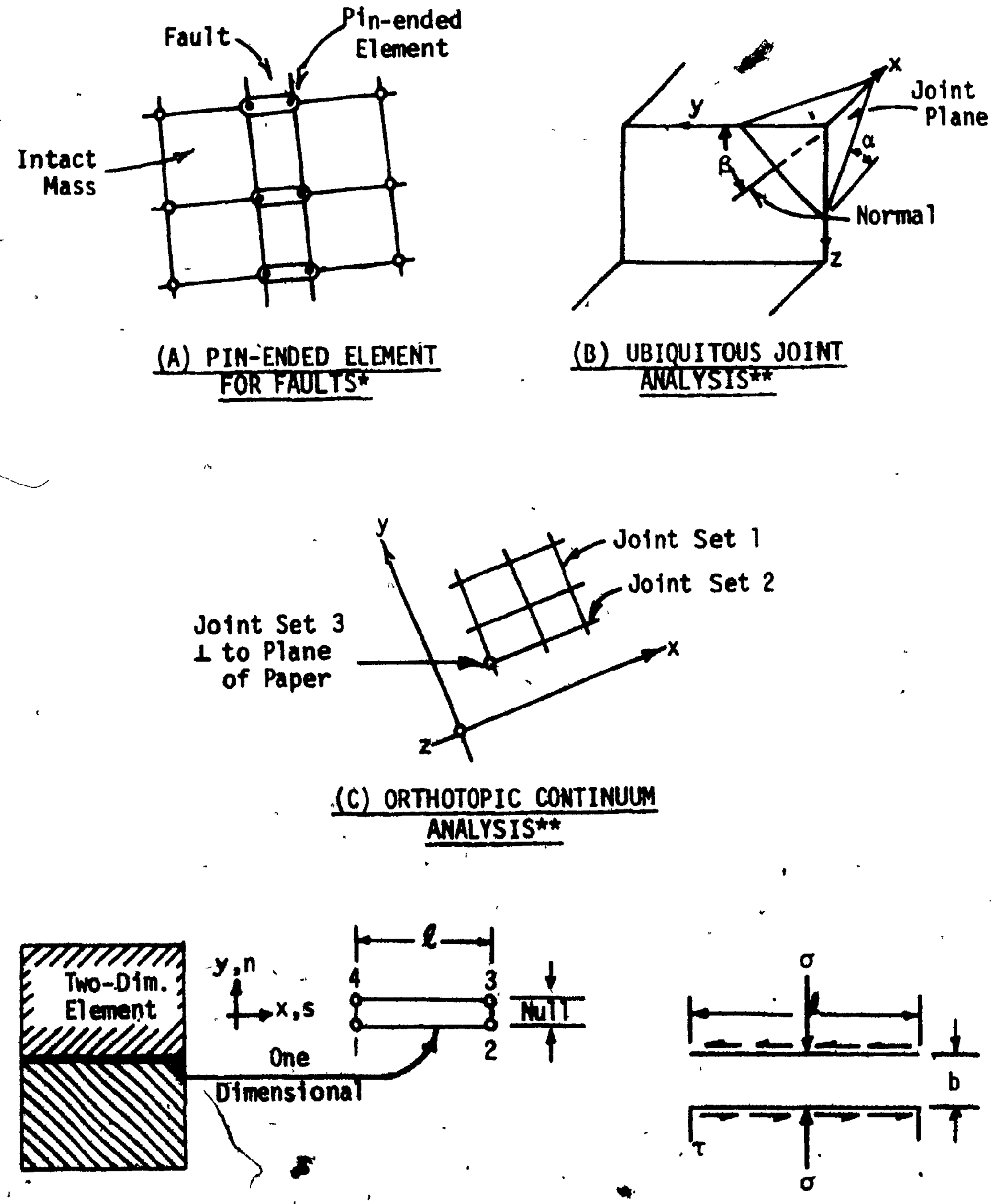

(A) PIN-ENDED ELEMENT FOR FAULTS*

(B) UBIQUITOUS JOINT ANALYSIS**

(C) ORTHOTOPIC CONTINUUM ANALYSIS**

(D) SINGLE JOINT: ONE-DIMENSIONAL ELEMENT**

(E) SINGLE JOINT: TWO-DIMENSIONAL ELEMENT**

* From Anderson and Dodd (1966)
**From Duncan and Goodman (1968)

FIGURE 2-5 VARIOUS MODELS FOR DISCONTINUITIES (JOINTS)

[After C. S. Desai (1972)]

and the backfill. The analyses were performed in a series of increments, adjusting the properties of the interface and the backfill in accordance with the stresses for each increment to approximate nonlinear behavior.

2.2.2 Idealization Adopted in the Present Study

The model adopted in the present study incorporates a predefined discontinuity at the level of the tool tip. This discontinuity is positioned on the cutting surface shown in Fig. 2-3. The purpose of including the cutting plane discontinuity in the finite element model is to represent the action of the cutting element, shown as element B in Fig. 2-3, where severe relative displacements and separation of soil blocks take place. Such discontinuity can be visualized as a thin soil layer on which the soil above slides on the soil mass below. This sliding behavior is governed by the soil constitutive shear stress-relative displacement relationship. It must be emphasized here that it is essential to consider such sliding action if an investigation is to be made of a continuous soil deformation process.

The discontinuity location was predetermined in this study due to the fact that the tool is assumed to be moving at a constant elevation. Such a predefined discontinuity plane is not to be confused with a failure plane which can initiate at the tool tip at any angle with respect to the horizontal depending on the direction of the maximum shear stress.

The horizontal movement of a cutting or a traction tool often produces a series of failures in the soil which are usually induced from the level of the tool tip to the soil surface. While these failure surfaces could be modelled also as discontinuities, a prior specification of failure surfaces will limit the usefulness of the proposed model. Location of the failure zones or surfaces in the soil medium is determined in this study, by examining the maximum shear stress induced in each finite element after each increment of tool displacement. If the stress is found equal to or greater than the shear strength of the soil at that location, the stiffness values for this element are reduced to small magnitudes, and this element is considered to have failed in shear. It becomes essential now to point out that such an approach for determination of failure zones or surfaces does not allow cracking to take place, and hence, sliding along a series of failure surfaces is not possible. Such behavior was not included in the proposed model partly because it did not take place in the experimentally observed deformation field, as will be shown later, and partly because of the large amount of computer memory and time required for such an analysis. However, in case sliding along a failure surface is found to be of importance in describing the soil behavior, an approach similar to that of Nilson (1968) could be adopted in which the topology of the discretization is altered by disconnecting cracked elements at their common nodes and inserting a form of a joint element, similar to those described in the previous section, along the cracked elements' common edge. By allowing these joint elements to transfer compressive stresses but not shear or tensile normal stresses, one will be able to represent the propagation of failure surfaces, and subsequently sliding along these surfaces.

As previously stated, in conventional finite element theory the displacements along the boundary between adjacent finite elements are required to be compatible, i.e., no gaps may open or relative displacements may occur between adjacent elements. It has also been pointed out that during the soil deformation process, relative displacements do occur on the interface between the soil and the tool representing a discontinuity in the finite element displacement field. Such discontinuity is presented in Fig. 2-3 as element A. Since the relative displacements occur in the tangential direction at the interface, the joint element, presented by Goodman et al. (1968), can be inserted between the tool surface and the soil mass, Fig. 2-6, to allow for soil slipping along the metal interface.

A similar approach is employed to model the cutting plane discontinuity in view of the fact that the deformation mechanism of this plane, presented in Fig. 2-3, by element B, is similar to that of a rock joint in that relative displacements occur across a thin discontinuity. Thus the simulation of the assumed discontinuity can be the same as that employed for rock joints where the joint elements are placed to model the separation of the two blocks of continuum adjacent to the discontinuity surface which were initially in contact.

Summarizing all of the above points, the finite element idealization adopted in this study, shown in Fig. 2-6, for a blade-soil system, consists of:

1] Continuum elements [constant strain triangles] representing the soil mass.

2] Interface discontinuity employing joint [interface] elements to represent the soil-tool interface characteristics.

3] Cutting discontinuity modelled by joint [cutting] elements inserted between the continuum elements to represent the

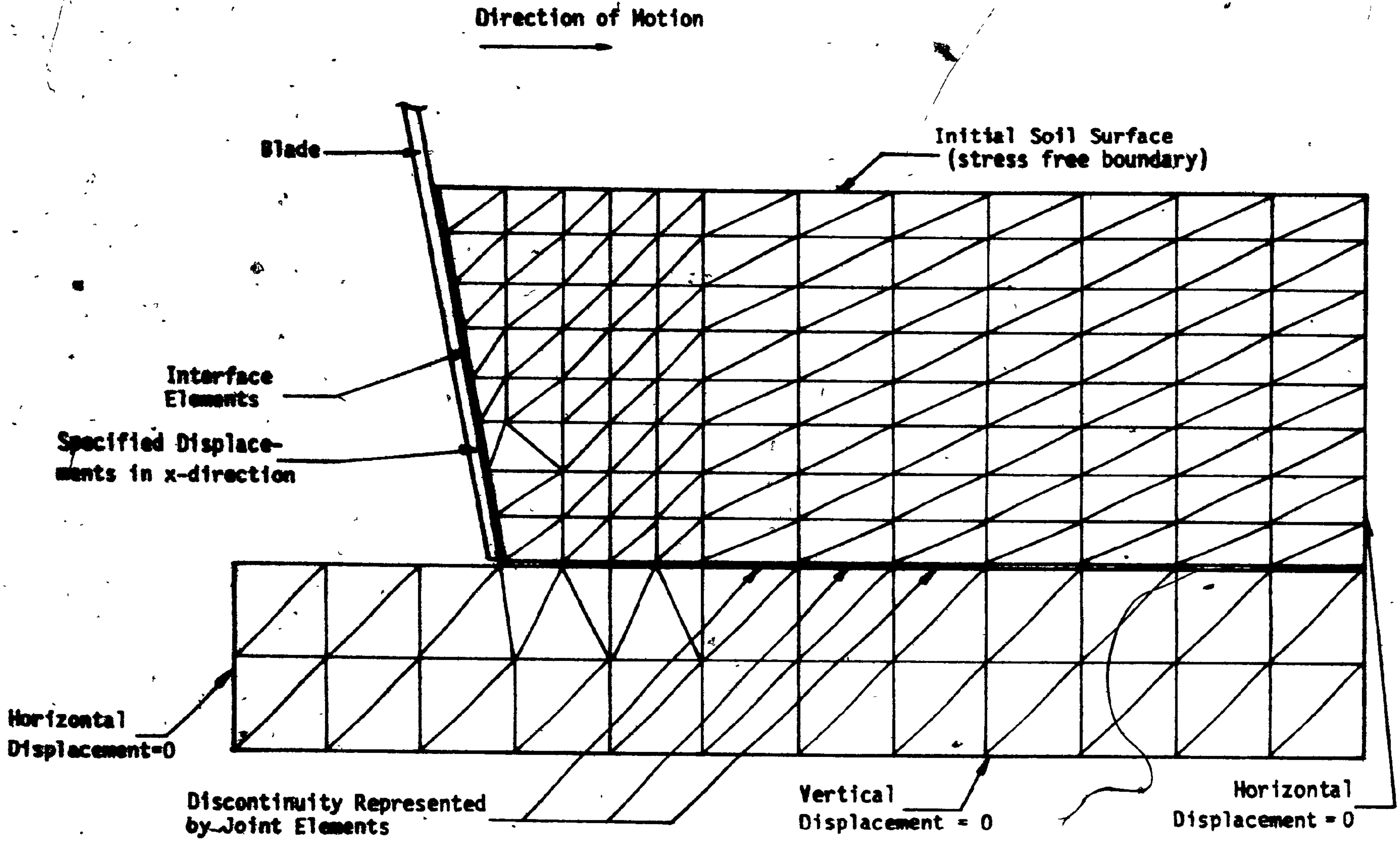

FIGURE 2-6 FINITE ELEMENT IDEALIZATION OF A BLADE-SOIL SYSTEM

shearing or cutting of the soil caused by the tool movement.

2.3 FORMULATION OF THE PROBLEM

The analysis of plane strain problems by the finite element method has been fully described in many publications [Zienkiewicz (1971)]. The derivations will not be presented here, only the general formulation and the essential features of the procedure required for the analysis of the present problem will be discussed.

From basic energy principles, for a body to be in equilibrium, its potential energy expressed as a functional Π should assume a stationary value in a class of admissable variations (δU_i) of the displacements U_i of the equilibrium state. The functional Π is given by:

$$\Pi(U_i) = Y - W$$

where

Y = strain energy, and

W = work done.

In a detailed form the above equation can be written as:

$$\Pi(U_i) = \int_V \tfrac{1}{2}\tau_i \varepsilon_i dV - \int_V F_i U_i dV - \int_B T_i U_i dB \tag{2.1}$$

where

τ_i = stress tensor.

ε_i = strain tensor.

F_i = body force field

T_i = surface force field, and

B, V represents the body boundary and volume, respectively.

In a matrix notation Eq. (2.1) becomes:

$$\Pi(U_i) = \int_V \tfrac{1}{2}\,\underset{\sim}{\tau}^T \underset{\sim}{\varepsilon}\, dV - \int_V \underset{\sim}{U}^T \underset{\sim}{F}\, dV - \int_B \underset{\sim}{U}^T \underset{\sim}{T}\, dB \tag{2.2}$$

Using a stress-strain relationship of the form:

$$\underset{\sim}{\tau} = \underset{\sim}{C}^i \cdot \underset{\sim}{\varepsilon}$$

Where C^i is a stress-strain matrix at stress level i, Eq. (2.2) can now be written as:

$$\Pi(U_i) = \int_V \tfrac{1}{2}\underset{\sim}{\varepsilon}^T \underset{\sim}{C}^i \underset{\sim}{\varepsilon}\, dV - \int_V \underset{\sim}{U}^T \underset{\sim}{F}\, dV - \int_B \underset{\sim}{U}^T \underset{\sim}{T}\, dB \tag{2.3}$$

Assuming a displacement field given by:

$$\underset{\sim}{U} = \underset{\sim}{\Phi}\, \underset{\sim}{\alpha} \tag{2.4}$$

where $\underset{\sim}{\Phi}$ is the coordinate matrix of the nodal points, and $\underset{\sim}{\alpha}$ are generalized coordinates.

It is possible to represent $\underset{\sim}{\alpha}$ in terms of $\underset{\sim}{\Phi}$ and $\underset{\sim}{U}$ by premultiplying both sides of Eq. (2.4) by $\underset{\sim}{\Phi}^{-1}$, giving:

$$\underset{\sim}{\alpha} = \underset{\sim}{h}\, \underset{\sim}{U}$$

where

$$\underset{\sim}{h} = \underset{\sim}{\Phi}^{-1}$$

The strain vector can now be obtained by differentiating the displacement vector $\underset{\sim}{U}$ with respect to $\underset{\sim}{\Phi}$ and can be expressed as:

$$\underset{\sim}{\varepsilon} = \underset{\sim}{\Phi}'\, \underset{\sim}{h}\, \underset{\sim}{U} \tag{2.5}$$

where $\underset{\sim}{\Phi}'$ is the $\underset{\sim}{\Phi}$ matrix after the necessary differentiation.

Substituting Eq. (2.5) into Eq. (2.3) yields:

$$\Pi(U_i) = \frac{1}{2} \int_V \underset{\sim}{U}^T \underset{\sim}{h}^T \underset{\sim}{\Phi}'^T \underset{\sim}{C}^i \underset{\sim}{\Phi}' \underset{\sim}{h} \underset{\sim}{U} \, dV - \int_V \underset{\sim}{U}^T \underset{\sim}{F} \, dV - \int_B \underset{\sim}{U}^T \underset{\sim}{T} \, dB \qquad (2.6)$$

After proper integration and conversion of the body forces $\underset{\sim}{F}$ and surface tractions $\underset{\sim}{T}$ to nodal forces, Eq. (2.6) can be written as:

$$\Pi(\underset{\sim}{U_i}) = \frac{1}{2} \underset{\sim}{U}^T \underset{\sim}{K} \underset{\sim}{U} - \underset{\sim}{U}^T \underset{\sim}{f} \qquad (2.7)$$

where $\underset{\sim}{f}$ are the lumped nodal point forces.

From the theorem of minimum potential energy, in an equilibrium state the variation of the functional Π vanishes, i.e.

$$\delta\Pi(U_i) = \frac{\partial \Pi (U_i)}{\partial U_i} = 0 \qquad (2.8)$$

Applying the condition set by Eq. (2.8) to Eq. (2.7), yields

$$\delta\Pi(U_i) = \underset{\sim}{K} \underset{\sim}{U} - \underset{\sim}{f} = 0$$

or $$\underset{\sim}{K} \underset{\sim}{U} = \underset{\sim}{f} \qquad (2.9)$$

where $\underset{\sim}{K}$ is the element stiffness matrix.

Solving Eq. (2.9), subject to the boundary conditions, provides both the stress and deformation fields.

2.3.1 Joint Element Stiffness Formulation.

A joint element was developed by Goodman, Taylor and Brekke (1968) and applied to several rock mechanics problems: sliding of joint with a tooth, behavior of joint intersections, tunnel in a system of staggered rocks. Héuze and Goodman (1967) also used it to simulate the behavior of mine roofs.

The following is a derivation of the stiffness properties of a joint element as presented by Goodman et al. (1968). This element, shown in Fig. 2.7 in a local coordinate system with the x-axis along the length, has a length, L, but very small width. The origin is at the center.

The stored energy, Φ, in such an element is due to the applied forces per unit length acting through the displacements and must be summed through the element. Thus,

$$\Phi = \frac{1}{2}\int_{-L/2}^{L/2} \omega_i \, P_i \, dx \tag{2.10}$$

in matrix notation

$$\Phi = \frac{1}{2}\int_{-L/2}^{L/2} (\omega)^T \, (P) \, dx \tag{2.11}$$

in which (ω) = the relative displacement vector given by

$$(\omega) = \begin{bmatrix} \omega_s^{Top} - \omega_s^{Bottom} \\ \\ \omega_n^{Top} - \omega_n^{Bottom} \end{bmatrix} \tag{2.12}$$

$$\text{and } (P) = \begin{bmatrix} P_s \\ \\ P_n \end{bmatrix} = \text{the vector of force per unit length} \tag{2.13}$$

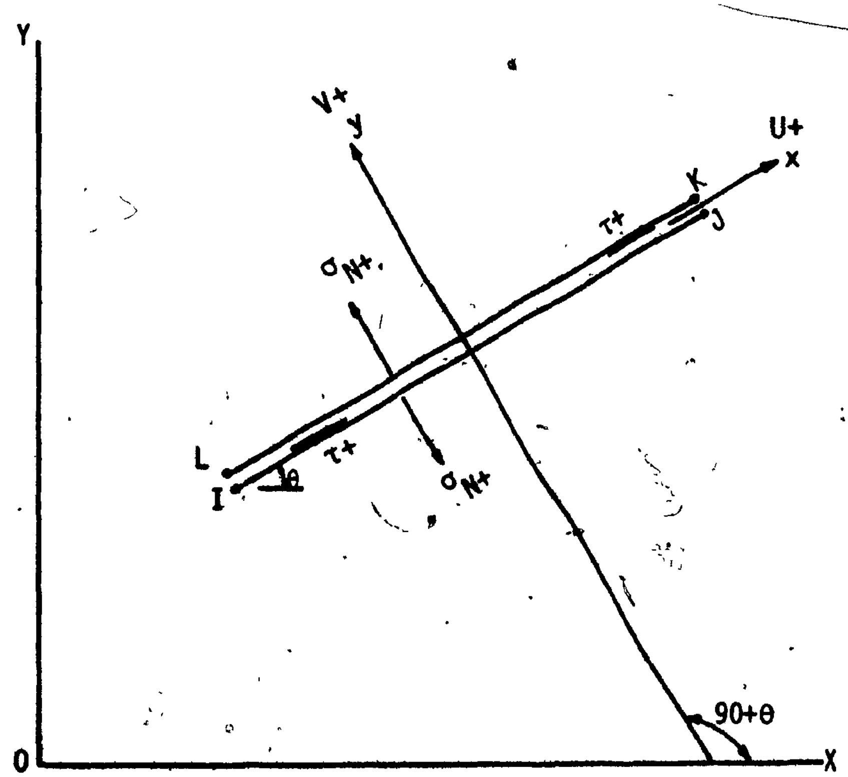

FIGURE 2-7 INTERFACE OR CUTTING ELEMENT WITH ITS LOCAL COORDINATE SYSTEM, x, y, IN TERMS OF GLOBAL SYSTEM, X, Y.

THE SIGN CONVENTION ON STRESSES AND DISPLACEMENTS IS INDICATED

The vector, (P), may be expressed in terms of a product of unit joint stiffness and displacement

$$(P) = (k)\ (\omega) \tag{2-14}$$

in which (k) = a diagonal material property matrix expressing the element stiffness per unit length in the normal and tangential directions,

$$(k) = \begin{bmatrix} k_s & 0 \\ & \\ 0 & k_n \end{bmatrix} \tag{2-15}$$

Substituting Eq. (2-15) in Eq. (2-14), gives

$$\phi = \tfrac{1}{2} \int_{-L/2}^{L/2} (\omega)^T\ (k)\ (\omega)\ dx \tag{2-16}$$

The displacement (ω) may be expressed in terms of the nodal point displacements (U) through a linear interpolation formula. Let U_i and V_i be displacements in the tangential and normal directions, respectively, at nodal point i along the bottom of the element

$$\begin{bmatrix} \omega_s^{bottom} \\ \\ \omega_n^{bottom} \end{bmatrix} = \tfrac{1}{2} \begin{bmatrix} 1 - \frac{2x}{L} & 0 & 1 + \frac{2x}{L} & 0 \\ & & & \\ 0 & 1 - \frac{2x}{L} & 0 & 1 + \frac{2x}{L} \end{bmatrix} \begin{bmatrix} U_1 \\ V_1 \\ U_2 \\ V_2 \end{bmatrix} \tag{2-17}$$

and along the top of the element.

$$\begin{bmatrix} \omega_s^{Top} \\ \\ \omega_n^{Top} \end{bmatrix} = \frac{1}{2} \begin{bmatrix} 1+\frac{2x}{L} & 0 & 1-\frac{2x}{L} & 0 \\ \\ 0 & 1+\frac{2x}{L} & 0 & 1-\frac{2x}{L} \end{bmatrix} \begin{bmatrix} U_3 \\ V_3 \\ U_4 \\ V_4 \end{bmatrix} \quad (2\text{-}18)$$

Thus the relative displacement in the element is

$$(\omega) = \begin{bmatrix} \omega_s^{Top} - \omega_s^{Bottom} \\ \\ \omega_n^{Top} - \omega_n^{Bottom} \end{bmatrix} = \frac{1}{2} \begin{bmatrix} -A & 0 & -B & 0 & B & 0 & A & 0 \\ \\ 0 & -A & 0 & -B & 0 & B & 0 & A \end{bmatrix} \begin{bmatrix} U_1 \\ V_1 \\ U_2 \\ V_2 \\ U3 \\ V_3 \\ U_4 \\ V_4 \end{bmatrix} \quad (2\text{-}19)$$

Where

$$A = 1 - \frac{2x}{L}, \quad \text{and } B = 1 + \frac{2x}{L}$$

Symbolically

$$(\omega) = \frac{1}{2}\,(D)\,(U) \quad (2\text{-}20)$$

in which (D) and (U) are defined by Eq. (2-19). Substitution of Eq. (2-20) in Eq. (2-16) yields:

$$\phi = \frac{1}{2}\int_{-L/2}^{L/2} \frac{1}{4}\,(U)^T\,(D)^T\,(k)\,(D)\,(U)\,dx \quad (2\text{-}21)$$

Substituting and simplifying, the expansion of Eq. (2.21) gives

$$\Phi = \tfrac{1}{2} L\,(U)^T\,(K)\,(U) \tag{2.22}$$

in which

$$(K) = \frac{1}{6}\begin{bmatrix} 2k_s & 0 & k_s & 0 & -k_s & 0 & -2k_s & 0 \\ 0 & 2k_n & 0 & k_n & 0 & -k_n & 0 & -2k_n \\ k_s & 0 & 2k_s & 0 & -2k_s & 0 & -k_s & 0 \\ 0 & k_n & 0 & 2k_n & 0 & -2k_n & 0 & -k_n \\ -k_s & 0 & -2k_s & 0 & 2k_s & 0 & k_s & 0 \\ 0 & -k_n & 0 & -2k_n & 0 & 2k_n & 0 & k_n \\ -2k_s & 0 & -k_s & 0 & k_s & 0 & 2k_s & 0 \\ 0 & -2k_n & 0 & -k_n & 0 & k_n & 0 & 2k_n \end{bmatrix} \tag{2.23}$$

K = the joint element stiffness per unit length

The element stiffness matrix has 32 nonzero terms but it depends on only two quantities, the unit joint stiffness in the normal and tangential directions.

The last step in the derivation is to place the element in a coordinate system for the entire structure. Adopting a global coordinate system X, Y as shown in Fig. 2-5, the transformation takes the following form:

$$\begin{bmatrix} x \\ y \end{bmatrix} = \begin{bmatrix} \cos\theta & \sin\theta \\ \sin\theta & \cos\theta \end{bmatrix} \begin{bmatrix} X \\ Y \end{bmatrix} \tag{2.24}$$

where

x and y = local coordinates in the tangential and normal directions, respectively.

2.3.2 Boundary Conditions

In the two-dimensional problem considered in this study, the boundary conditions can be either specified forces, specified displacements or both. Assuming direction of tool motion to be horizontal, the boundary conditions at the tool surface are specified horizontal displacements. The top soil surface is considered a stress-free boundary unless there is a vertical load distributed uniformly on a grouser [tool (a) - Fig. 3-1 for example]. At a reasonable distance from the tool, the bottom boundary is assumed to move only in the x-direction, while the sides are smooth in the y-direction but fixed in the x-direction. The assumed boundary conditions are shown in Fig.2-6.

If the boundary condition is that of an applied load, the value of the load is simply added to the appropriate components of the vector $\underset{\sim}{f}$ in Eq. (2.9). Equivalent nodal point forces due to body forces and surface tractions are calculated and assembled concurrently with the element stiffnesses. The body forces in a triangular element due to gravity are lumped as one-third values at each nodal point comprising the triangle.

In case displacement or kinematic boundary conditions are specified, as in the present study, the stiffness matrix $\underset{\sim}{K}$ has to be suitably altered to account for the specified displacements. If the i^{th} element of the deflection vector $\underset{\sim}{U}$ is specified to be Δ, the corresponding row of the stiffness matrix is made zero and the diagonal term is made unity, i.e.,

$$\begin{aligned} k_{ii} &= 1 \\ k_{ij} &= 0 \text{ for } i \neq j, \; j = 1, \ldots\ldots, n \end{aligned} \tag{2.25}$$

The corresponding force element, f_i, is then set equal to the prescribed displacement value Δ. One major disadvantage of this procedure is that the altered stiffness matrix, $\underset{\sim}{K}$ is no longer symmetrical leading to added storage requirements while solving for the unknown displacements. An additional modification, however, will restore the symmetry of the $\underset{\sim}{K}$ matrix as outlined below.

In addition to satisfying Eq. (2.25), all elements in the i^{th} column, except the diagonal element k_{ii}, are set equal to zero as in Eq.(2.26)the symmetrical nature of the $\underset{\sim}{K}$ matrix is retrieved.

$$\begin{aligned} &k_{ii} = 1 \\ &k_{ji} = 0 \quad \text{for} \quad i \neq j, \quad j = 1, \ldots\ldots n \end{aligned} \tag{2.26}$$

The force vector $\underset{\sim}{f}$ on the righthandside of Eq. (2.9) now has to be altered as:

$$\begin{aligned} &f_i = \Delta \\ &f_j = f_j - k_{ji}\,\Delta, \quad \text{for } i \neq j, \quad j = 1, \ldots\ldots n \end{aligned} \tag{2.27}$$

Thus, Eqs.(2.25), (2.26) and (2.27) can be used together to achieve the desired purpose. The method is discussed in more detail in Zienkiewicz' book (1971); it is very easy to program and is adopted in the computer program developed in this work.

2.3.3 Solution Method

Equation (2-9) after being modified for necessary boundary conditions represents a set of linear simultaneous equations. Various solution schemes that utilize certain special characteristics of the coefficient matrix have been used successfully in computer programs for the finite element. The banded nature of the matrix has led to the use of iterative methods of solution with over-relaxation factors [Fox (1965)]. The coefficient matrix has been decomposed into block tri-diagonal form and subsequently solved by elimination procedure, [McCormick (1963)]. Recursive techniques have also been used [Girijavallabhan (1967)]. The direct Gaussian elimination is simple and effective to program [Zienkiewicz (1971)]. It has been adopted in the program developed in the present study. A detailed discussion of the technique is presented in Appendix D.

2.4 CONSTITUTIVE RELATIONSHIP FOR SOILS AND FINITE ELEMENT NONLINEAR ANALYSIS

In the previous section, the finite element formulations were derived assuming that the stress-strain behavior of the material is known. A set of equations that defines the stress-strain behavior of a material represents the constitutive law for the material. Constitutive relations for soils are derived, based on some simplified assumptions for the behavior of the material. The number of variables occurring in the law would depend upon the complexity of the model chosen to simulate soil behavior. Nonlinear analysis by the finite element method or other numerical techniques will be influenced by the nature of the model chosen. In general, the more complex the model, the more the number of variables to be taken into account and the more involved the nonlinear analysis. Moreover, for a realistic analysis, it must be possible to obtain values for the constants involved in the constitutive law from laboratory experiments.

2.4.1 Remarks on Constitutive Relations

The simplest constitutive law will be the one that assumes that soil behavior can be represented by a linear, elastic material. This linear, elastic model has been used by many research workers in their investigations. Other workers have considered soil to be elasto-plastic or nonlinearily elastic.

The elasto-plastic approach idealizes the stress-strain curve for the soil, and uses the equations of elasticity in the elastic range and the equations of plasticity in the plastic range. The nonlinear elastic approach, on the other hand, does not idealize the stress-strain curve, but uses the equations of elasticity to solve for the stress state even after yielding has occurred in the soil. Any degree of nonlinearity can be accounted for in this approach. The elasto-plastic approach appears sound from a theoretical standpoint, but the practical problems involved in defining a yield limit and a flow law are quite a handicap. In as much as the nonlinear elastic analysis represents the actual stress-strain relation obtained from tests, it seems reasonable to expect fairly good results from this type of analysis.

It is to be recognized that anisotropy in materials can be of two types. Material anisotropy represents different elastic properties in different directions. In nonlinear materials, stress-induced anisotropy always exists and this may be coupled with material anisotropy. The principal stresses under a loaded condition will seldom be the same, and this will result in different elastic values in different directions depending on the stress level. This causes stress-induced anisotropy. It is generally difficult to take this type of anisotropy into account without elaborate testing or simplifying assumptions.

2.4.2 Solid Elements Constitutive Behavior

In the computer program developed in this study, the stress-strain relations obtained from laboratory plane-strain tests were used in the finite element analysis to predict the load deformation behavior of the continuum.

The nonlinear analysis in the finite element method is conducted as a series of linear analyses by an iterative or a step-by-step procedure, or a combination of both. Methods developed to obtain such solutions are described in the next section. However, both methods require procedures to compute values of E and ν, elastic modulus and Poisson's ratio, for the soil during any state of loading. The procedure that is used to obtain these values from plane-strain test results will be first outlined.

Evaluation of E and ν from plane-strain triaxial test results:

Hooke's law for an isotropic, linear, elastic material in a principal plane can be written as:

$$\varepsilon_1 = \frac{\sigma_1}{E} - \frac{\nu}{E}(\sigma_2 + \sigma_3)$$

$$\varepsilon_2 = \frac{\sigma_2}{E} - \frac{\nu}{E}(\sigma_1 + \sigma_3) \qquad (2.28)$$

$$\varepsilon_3 = \frac{\sigma_3}{E} - \frac{\nu}{E}(\sigma_1 + \sigma_2)$$

where

σ_i $(i = 1,2,3)$ are the major, intermediate and minor principal stresses, respectively.

ε_i $(i = 1,2,3)$ are the major, intermediate and minor principal strains, respectively.

For the case of plane strain

$$\varepsilon_2 = 0$$

and the second equation in Eq. (2.28) reduces to

$$\sigma_2 = \nu(\sigma_1 + \sigma_3)$$

for an incompressible material $\nu = 0.5$, and from the first equation of (2.28) it can be shown that

$$\varepsilon_1 = \frac{3}{4E}(\sigma_1 - \sigma_3)$$

or

$$E = \frac{3}{4}\frac{\sigma_1 - \sigma_3}{\varepsilon_1} \qquad (2.29)$$

The $\dfrac{\sigma_1 - \sigma_3}{\varepsilon_1}$ term in Eq. (2.29) represents the slope E_T of the deviator stress, $(\sigma_1 - \sigma_3)$, versus principal strain, ε_1, curve. Thus in the plane strain case

$$E = \frac{3}{4}E_T \qquad (2.30)$$

2.4.3 Joint Elements Constitutive Relationship

As mentioned earlier, the cutting phenomenon caused by the tool movement in the soil mass is idealized by inserting joint elements between the solid elements. In evaluating the stiffness of these elements, it is assumed that both normal and shear displacements vary linearly along the length of the element, which is compatible with the external boundary displacements of the continuum elements used herein.

The properties of these elements consist of a normal stiffness, k_n, and a shear stiffness, k_s, which are related to the normal and shear stresses acting on the element by

$$k_n \ \Delta_n = \sigma_n$$

and $$k_s \ \Delta_s = \tau \qquad (2.31)$$

where Δ_n = average relative normal displacement across the element,

and Δ_s = average relative shear displacement along the element.

The values assigned to k_s can be determined from the results of direct shear tests. The nonlinear tangential stress-displacement curves shown in Fig. 2-8 may be approximated by hyperbolae having equation of the form

$$\tau = \frac{\Delta_s}{a + b\Delta_s} \qquad (2.32)$$

where

τ = cutting stress,

Δ_s = shear displacement,

and a, b = empirical coefficients whose values are determined experimentally.

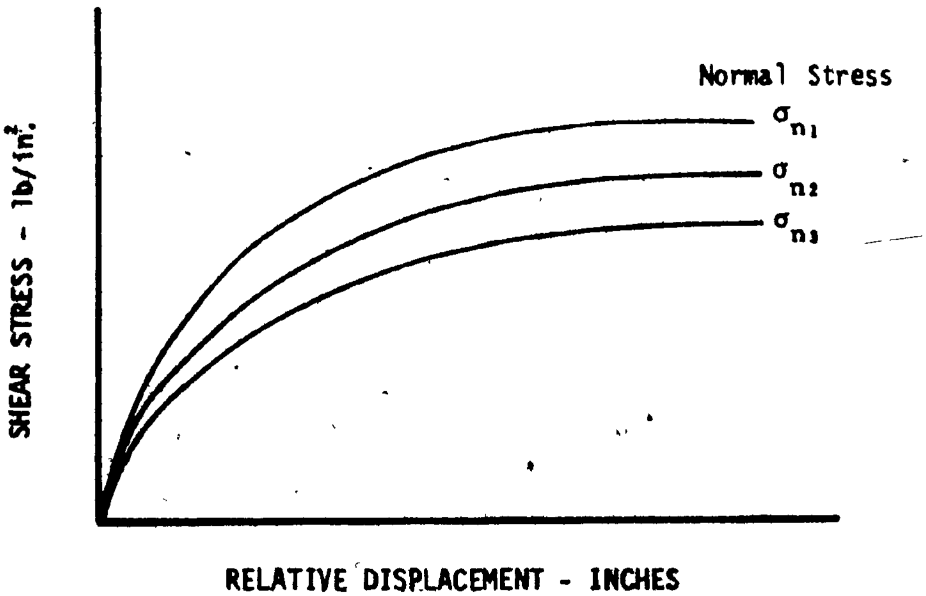

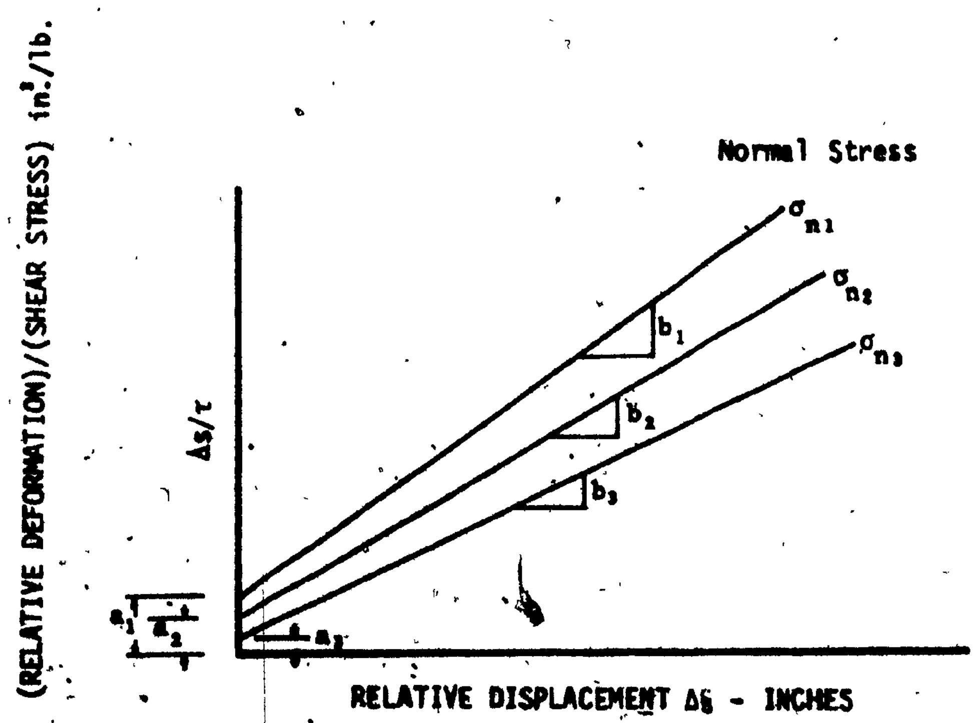

FIGURE 2-8 TRANSFORMED LINEAR HYPERBOLIC PLOTS FOR CUTTING AND INTERFACE TESTS

The values of the coefficients (a) and (b) may be determined most easily if the stress-displacement data are transformed to another set of axes, on which the hyperbolae plot as straight lines. By transposing Eq. (2.32), the following relationship may be obtained

$$\frac{\Delta_s}{\tau} = a + b\,\Delta_s \qquad (2.33)$$

If values of Δ_s/τ are plotted against values of Δ_s, as shown in Fig. 2-8, the resulting variation will be a straight line if the shear stress varies hyperbolically with displacement. It may be shown from the form of Eq. (2.33) that coefficient (a) is the intercept, and coefficient (b) is the slope of the straight line on this transformed plot.

The reciprocal of coefficient (a) is the initial slope of the shear stress displacement curve, and is analogous to the initial tangent modulus of a stress-strain curve. The quantity called herein the initial shear stiffness, K_{si}, has units of force per cubic length, or pounds per cubic inch for the curves shown in Fig. 2-8. The reciprocal of coefficient (b) is the asymptote approached by the shear stress displacement curve at very large values of displacement.

Tangent stiffness values, representing the slope of a tangent to the shear stress displacement curve, may be readily found by differentiating Eq. (2.33) with respect to Δ_s, and, eliminating Δ_s from the resulting equation, the tangent stiffness value may be expressed as

$$K_{st} = \frac{1}{a}(1 - \tau b)^2 \qquad (2\text{-}34)$$

Possible modes of behavior for the joint element are shown in Fig. 2-9. It can be seen that in the compression and combined modes the adjacent continuum elements tend to overlap, a condition which occurs because compressive stresses require compressive relative displacements across the element, which, for purposes of analysis, is assumed to have very small thickness.

The stiffness values assigned to these elements varied depending on the mode of behavior and the element stresses. For compression, the value of k_n was made equal to the initial elastic modulus of the continuum elements, and the value of k_s was calculated using Eq. (2.34). After an element had failed in shear, with the element still in compression, k_s was reduced to a negligible value but the value of k_n was kept constant.

Both the shear stiffness, k_s, and the shear strength of the cutting zone depend on the value of the normal stress existing on this layer. The tangential stiffness values assigned to these elements varied depending on the element normal stress. This was done by considering the values of the coefficients (a) and (b) as a function of the normal stress existing in the element.

In a similar fashion, the properties assigned to the interface elements are determined from the results of direct shear tests consisting partly of soil and partly of tool material. Equation (2.34) is again used to predict the tangent stiffness modulus provided that (a) and (b) coefficients are obtained from a soil-metal interaction test.

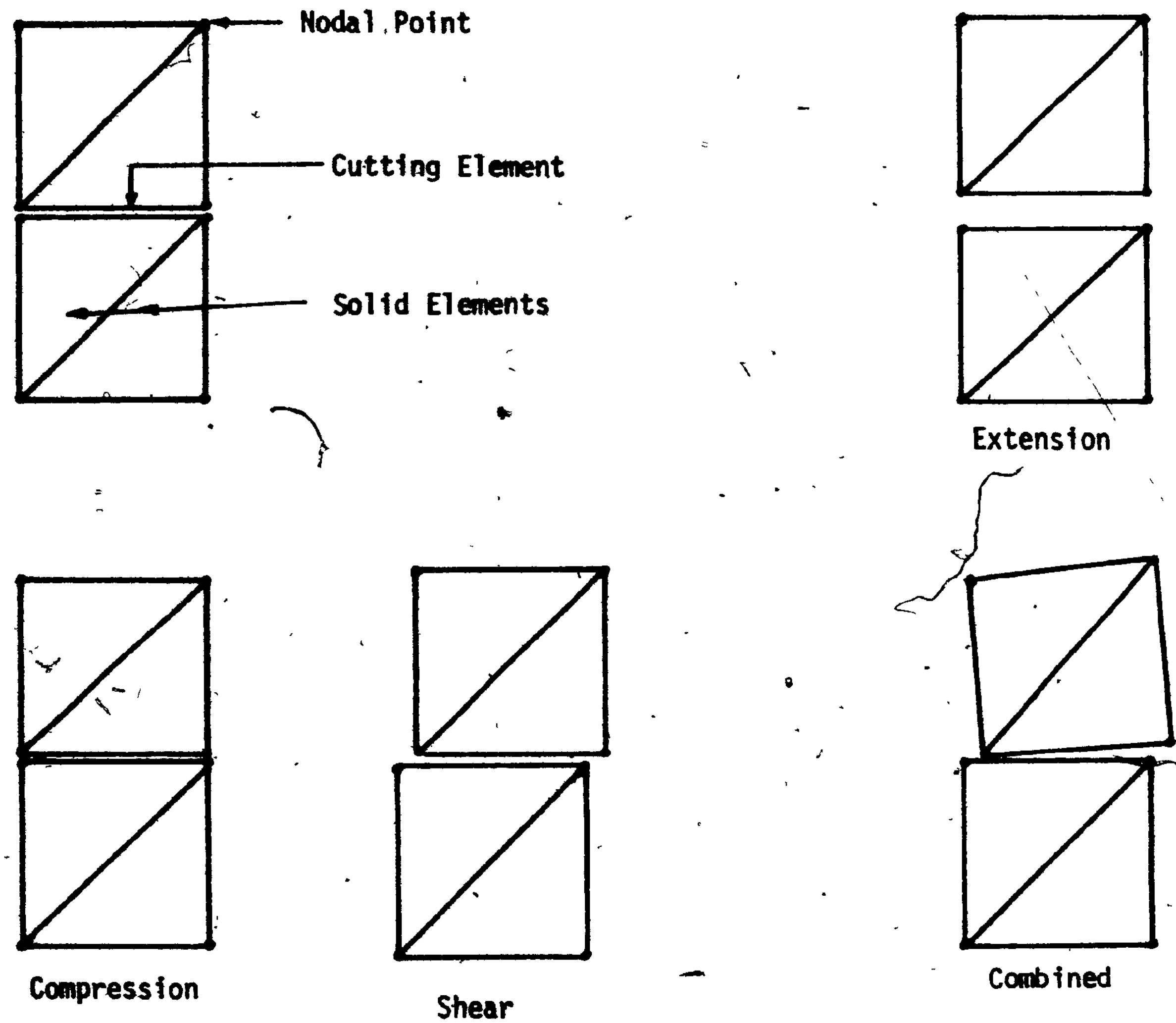

FIGURE 2-9 MODES OF BEHAVIOR OF CUTTING ELEMENT

[Modified after Duncan and Goodman (1968)]

2.5 METHOD OF ANALYSIS

In this particular study, nonlinearities occur in two different forms. The first is material or physical nonlinearity, which results from nonlinear constitutive laws [Section 2-4]. The second is geometric nonlinearity, which derives from finite changes in the geometry of the deforming body [Desai and Abel (1972)].

Material nonlinearity alone encompasses problems in which the stresses are not linearily proportional to the strains, but in which small displacements and small strains are considered. Displacements refer to the changes in the overall geometry of the soil body, whereas strains are related to internal deformations. Because of the small displacements encountered in some cases, local distortions of an element can be ignored and the areas of the original, undeformed element can be used in computing stresses. In this case the linear strain-displacement equations written for plane strain problems as:

$$\varepsilon_x = \frac{\partial u}{\partial x} \qquad \varepsilon_y = \frac{\partial v}{\partial y} \tag{2·35}$$

$$\gamma_{xy} = \frac{\partial v}{\partial x} + \frac{\partial u}{\partial y}$$

where ε_x and ε_y are the normal components of strain,

γ_{xy} is the component of shear strain,

u and v are the displacement components in the x- and y-directions,

are used.

Problems involving geometric nonlinearity arise both from non-linear strain-displacement relations, written for a plane strain case as:

$$\varepsilon_x = \frac{\partial u}{\partial x} + \tfrac{1}{2}\left[\left(\frac{\partial u}{\partial x}\right)^2 + \left(\frac{\partial v}{\partial x}\right)^2\right]$$

$$\varepsilon_y = \frac{\partial v}{\partial y} + \tfrac{1}{2}\left[\left(\frac{\partial u}{\partial y}\right)^2 + \left(\frac{\partial v}{\partial y}\right)^2\right] \qquad (2\cdot 36)$$

$$\gamma_{xy} = \frac{\partial v}{\partial x} + \frac{\partial u}{\partial y} + \frac{\partial u}{\partial x}\frac{\partial u}{\partial y} + \frac{\partial v}{\partial x}\frac{\partial v}{\partial y}$$

and from finite changes in geometry. In other words, this category encompasses large strain and large displacements.

The most general category of nonlinear problems is the combination of the material and geometric nonlinearities. It involves nonlinear constitutive behavior as well as large strains and finite displacements. This Section begins with the explanation of the computational procedure adopted to treat material nonlinearity, followed by a brief discussion on geometric nonlinearity.

2.5.1 Material Nonlinearity

Nonlinear stress-strain behavior may be approximated in finite element analyses by assigning different modulus values to each of the elements into which the soil is subdivided for purposes of analysis, as shown in Fig. 2-6. The modulus value assigned to each element is selected on the basis of the stress or strain in each element. Because the modulus values depend on the stresses, and the stresses in turn depend on the modulus values, it is necessary to make repeated analyses to insure that the modulus values correspond to the stress conditions for each element in the system.

Two techniques for approximate nonlinear analyses by the finite element method have been tried [Desai and Abel (1972)]. These are:

1] Direct iteration method, shown in Fig. 2-10. By this method, the same change in soil external loading is analyzed repeatedly. After each analysis, the values of stress and strain within each element are examined to determine if they satisfy the appropriate nonlinear stress-strain relationship. If the values of stress and strain do not correspond, a new value of modulus is selected for that element for the next analysis. The main advantage of this technique is the capability of the procedure to represent stress-strain relationships in which the stress decreases with increasing strain after reaching a peak value. The shortcoming of the iterative procedure is that it can only give the solution for the final level of applied load, and cannot consider the load and deformation history of the soil.

2] Incremental method, shown in Fig. 2-11. In this procedure, on the other hand, the soil loading is considered to be applied in small increments. If the state of stress and strain at the start of an increment is known in each element, the state at the end of the increment can be found by an addition of incremental changes. The constitutive relationship to be used for each element may be determined at the beginning of each interval. Thus the nonlinear stress-strain relationship is approxi-

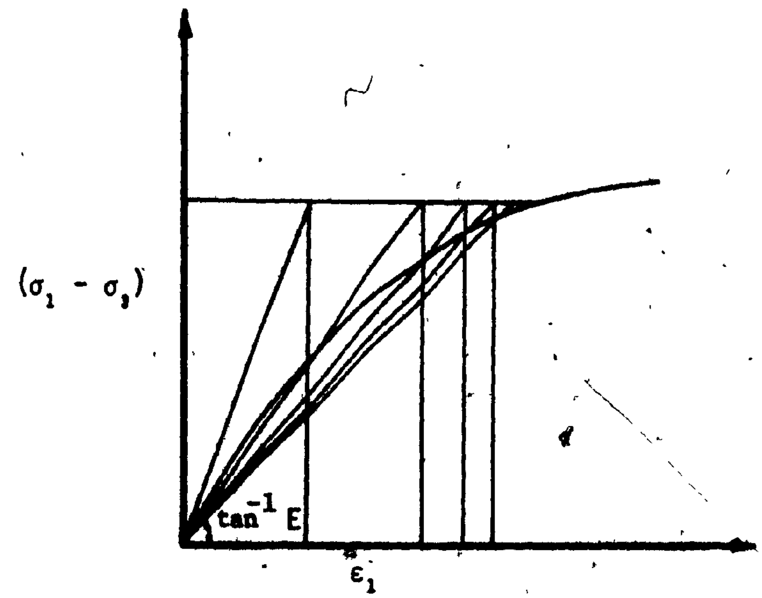

FIGURE 2-10 DIRECT ITERATION PROCEDURE

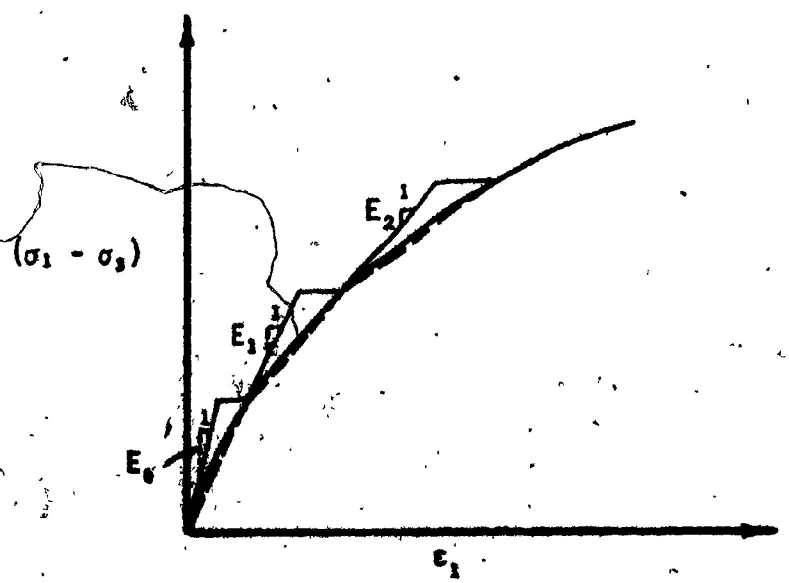

FIGURE 2-11 INCREMENTAL PROCEDURE

mated by a series of straight lines. The principal advantage of this procedure is that it provides a relatively complete description of the load-deformation behavior, as results are obtained for each of the intermediate states corresponding to an increment of loading.

In the present study, it is essential that the soil deformation and stress fields are obtained and examined as the tool advances in the soil. For this purpose the incremental procedure was employed.

The incremental technique adopted in the analysis makes use of the plane-strain triaxial stress-strain curves to compute the value of the elastic modulus, E, during each increment. The value of Poisson's ratio ν is kept constant in the analysis.

The starting value of the modulus, E_o, is taken as the initial slope of the plane-strain triaxial stress-strain curves at zero confining pressure. With the assumed value of Poisson's ratio, the stresses or strains in each element due to the first increment of displacement is computed using the elastic analysis. A new value of the modulus to be used in the second increment is computed by using the nonlinear curves. Either the stresses or strains computed in the elements can be used in the nonlinear curves to obtain the E values. The modified constitutive relation is used in the next increment of deformation. The process is continued until the desired total deformation is obtained.

The modulus value, E, is calculated in each increment as:

$$E = \frac{\frac{1}{2}(\sigma_1 - \sigma_3)_i - \frac{1}{2}(\sigma_1 - \sigma_3)_{i-1}}{(\varepsilon_1)_i - (\varepsilon_1)_{i-1}} \qquad (2.37)$$

where i represents the current increment state, and $i - 1$ represents the previous increment stage. Figure 2-11 illustrates the incremental procedure.

There are several possible ways by which the solutions obtained by the incremental method can be improved. Since for every increment the elastic constants used are from the previous increment, it is necessary that the increments be quite small to obtain good results. Further, if there are abrupt slope changes in the stress-strain diagram, the method is likely to give unsatisfactory results. One of the ways to reduce some of these errors is to iterate a few times after each increment to bring the assumed E values close to the actual values. This procedure would also allow taking larger load increments in the analysis. The incremental-iterative method suggested is used in the computer program developed in this study.

In most problems, it is found sufficient to iterate two to three times at each increment to obtain compatible stresses and strains. The number of iterations at each increment may be reduced by predicting the value of E for a load increment based on the stresses or strains attained in the previous increment, and by using this value of E as a first trial in the computations. Linear and parabolic predictions were programmed in this study and gave very satisfactory performance for a few idealized example problems. For soil stress-strain curves, it is felt that the parabolic prediction will work much better than the linear one. Figure 2-12 diagrammatically illustrates the working of the linear prediction method.

2.5.2 Geometric Nonlinearity

In the previous subsection [2.5.1], the material or physical nonlinearity arising from material properties was considered. It is recalled that in the case of material nonlinearity, both strains and displacements are assumed to be small, but stresses are not proportional to strains. In this particular study, in addition to material nonlinearity, geometric nonlinearity occurs due to the finite changes in the geometry of the deforming soil in front of the cutting or traction tool. Combination of both nonlinearities is particularly simple if an incremental procedure is adopted.

If a full load-deformation study is required it is common practice to proceed with small loading increments and treat for each such increment the problem as a piece-wise linear one with the tangential stiffness matrix evaluated at the start of the increment. If the nodal coordinates are continuously updated the calculation follows precisely the same pattern as used in small displacements-infinitesimal strain analysis. Updating for a plane strain case takes the form:

$$\bar{x}_i = x_i + u_i \qquad \bar{y}_i = y_i + v_i$$

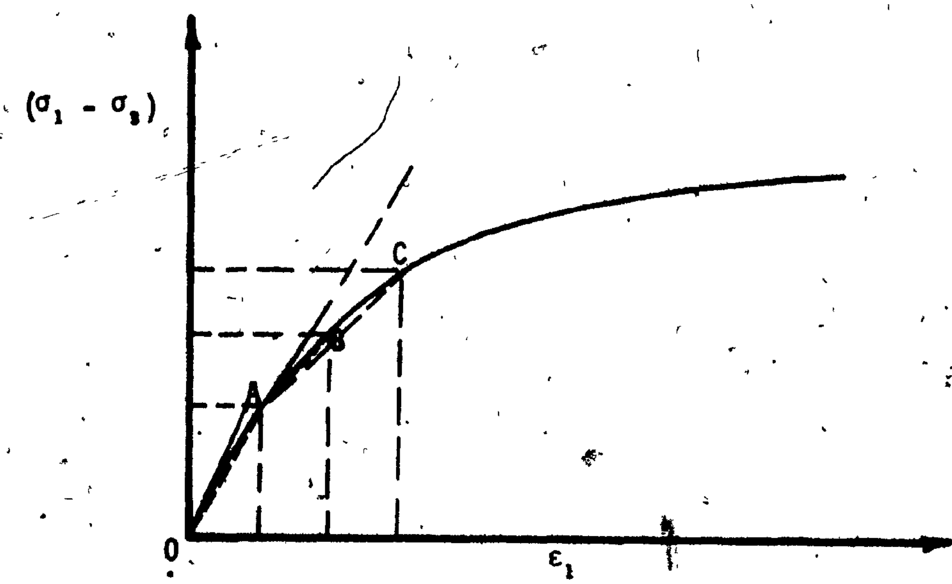

Slope of OA - first trial value for E without prediction for second increment.
Slope of AB - first trial value for E with linear prediction for second increment.
Slope of AC - actual E value for second increment after iterations.

FIGURE 2-12 INCREMENTAL-ITERATIVE METHOD WITH PREDICTION

where

$\bar{x}_i$, $\bar{y}_i$ are the updated nodal coordinates at the end of the i^{th} increment.

x_i, y_i are the nodal coordinates at the beginning of the i^{th} increment.

u_i, v_i are the i^{th} displacements in the x- and y-directions, respectively, associated with the nodes.

Strains are now determined by the derivatives of displacements with respect to the updated coordinates.

It is possible to use the general definition of strains, known as the Green's strain tensor, which is valid whether displacements or strains are large or small. For plane strain case the Green strain is defined by Eq. (2.36). If displacements are small the general first-order linear strain approximation is obtained by neglecting the quadratic terms [Eq. (2.35)]. Because the loading increments are small, it is assumed that the strain increments may be regarded as infinitesimal in the usual sense. In such case, the linear strain approximation [Eq. (2.35)] can be used. It is recognized, however, that the same may not be true of the accumulated values. In the limit of infinitesimal increments of loading, it may be shown that this procedure gives the so-called logarithmic strains; rather than simple displacement gradients [Fong (1965)]. While this is admittedly an approximation to the more formal definition of large strains, Eq. (2.36), the degree of approximation appears to be consistent with that of the overall method.

CHAPTER 3

EXPERIMENTATION

3.1 INTRODUCTION

The analysis described in the previous Chapter solves approximately the problem of a simplified cutting or traction element interacting with soils. Two kinds of unavoidable approximations were introduced into the analysis, namely the insertion of the cutting [joint] elements in the finite element model to represent the tool cutting effect, and the adoption of a numerical solution [incremental finite element] technique. The combined effect of all approximations can be investigated by comparing the results of the analysis with experimental measurements. Therefore, the purpose of the experimental programme carried out during the course of this study was to provide data on the interaction of the chosen cutting and traction elements with cohesive soils under plane strain conditions, which could be compared with the analytical results. Mainly the following facts were investigated:

(1) The load-displacement response of the soil.

(2) The soil deformation fields.

(3) Failure mechanisms.

In simulating traverse motion of a cutting or tractive element, it is common practice in laboratory experimentation to control:

(a) Depth of element travel - i.e. variable vertical force resulting therefrom.

(b) Applied vertical force - i.e. variable depth of element motion.

The resultant forces developed for situation (a) are obviously different from those of (b) - due to the different boundary conditions developed. The actual field problem however involves neither situation (a) nor situation (b), i.e. neither vertical loads nor elevations are controlled.

While in traction analysis the constant pressure approach [situation (b)] intends to simulate a portion of the vehicle weight applied to the top of the grouser and maintained throughout the entire test, it could be argued that this is not the case in reality as the vertical pressure on the grouser changes in magnitude while the track is moving. And since the actual field situation in traction involves multiple grousers on a link or a belt system, the prediction of mobility for track systems based on single grouser analysis must suitably account for multiplicity of grouser action. Track analysis however constitutes a separate problem and is not covered within the scope of this study.

Most of the work done up to the present time on the analysis of the problem of soil cutting assumes a constant depth of cut [Osman (1964), Reece (1965), Hettiaratchi et al. (1966) and Yong et al. (1969)]. This condition was maintained in both the cutting and traction test series conducted in this study. The reason for adopting such a condition in the traction series was to apply similar boundary conditions as those assumed for the soil cutting case, thus obtaining a unified method of analysis.

The tests performed in the course of the investigation may be divided into two categories:

(a) Cutting tests, in which a series of straight blades with different angles of inclination were moved through the soil. Vertical movements of blades were not permitted so as to produce a constant depth of cut condition.

(b) Traction tests, in which grousers with different geometries were moved in the soil at a constant height relative to the initial soil surface.

In both cases, the measured parameters were: the horizontal and vertical forces, and the tool horizontal displacement. All measurements were made on a time base which allowed for the determination of the horizontal carriage velocity. A complete description of the experimental facility and procedures used in the experimental phase of the study is provided as Appendix A.

Briefly, the experimental facility consisted of a tool-carriage assembly moving through a soil sample contained in a bin with transparent lucite side walls. Two soil types were employed during the course of investigation. These were kaolinite clay, with a specific gravity of 2.62 and a liquid limit and plastic limit of 54.5 and 37.5 per cent, respectively, and an artificial, oil base, clay [trade name "Plasticine"]. In all cases, the dimensions of the test specimens were such as to permit full development of the failure zones without interference occurring between the deforming zones and the ends of the sample holder.

As a means of specifying the deformation history during the deformation process, a network of lines was inscribed on the side surface of the test specimens. The inscribed lines provided a grid of one-half-inch squares and photographs of the deforming grid were taken every five seconds of tool motion. Subsequent plotting and superposition of the sequential photographs provided the history of the deformation process over a range of tool movement of three inches.

3.2 CUTTING AND TRACTION TOOL GEOMETRIES

The intent of this study is not to compare different tool geometries for the purpose of establishing suitability, efficiency or performance, but rather to develop an analytical method capable of predicting the interaction behavior of a wide spectrum of cutting and traction element geometries. Therefore, a number of tool geometries were chosen and tested to evaluate the applicability of the proposed method of analysis.

In case of the cutting experiments, four aluminum blades each measuring four inches wide by four inches long were utilized. The blades were set at angles of 10°, 20°, 40° and 50° with regard to the vertical.

As for the traction experiments, the groupings were separated in terms of the shape of the traction element and consisted of:

(1) Right Angle Plate Grousers [R.A.P.G.], [Fig. 3-1a] with aspect ratios h/l of 0.5 and 0.833. The length l was maintained constant at 3.0 inches, while h was varied to provide the differences in h/l.

(2) Straight-Edge Wedge Grousers [S.E.W.G.]. Only one tool was utilized with a height of 2.32 inches and tip angle of 45°, Fig. 3-1b.

(3) Curved-Edge Wedge Grousers [C.E.W.G.]. Two geometries were utilized to provide different boundary conditions. The dimensions of the C.E.W.G. are shown in Fig. Nos. 3-1c and 3-1d.

These grouser shapes simulate the most common boundary conditions of individual grousers which can arise in practice, and the results obtained from their analysis should therefore be representative of the behavior of the soil mass under typical loading systems.

3.3 EXPERIMENTAL PROGRAMME

The experimental research programme can be subdivided into two main phases, namely, cutting and tractive elements testing, and soil strength testing.

3.3.1 Cutting and Tractive Elements Testing

This phase consisted of two distinct groups. The groupings were separated in terms of the type of experiment, whether cutting or traction. In addition, two soils were used: an artificial, oil based,

FIGURE 3-1 GROUSER GEOMETRIES

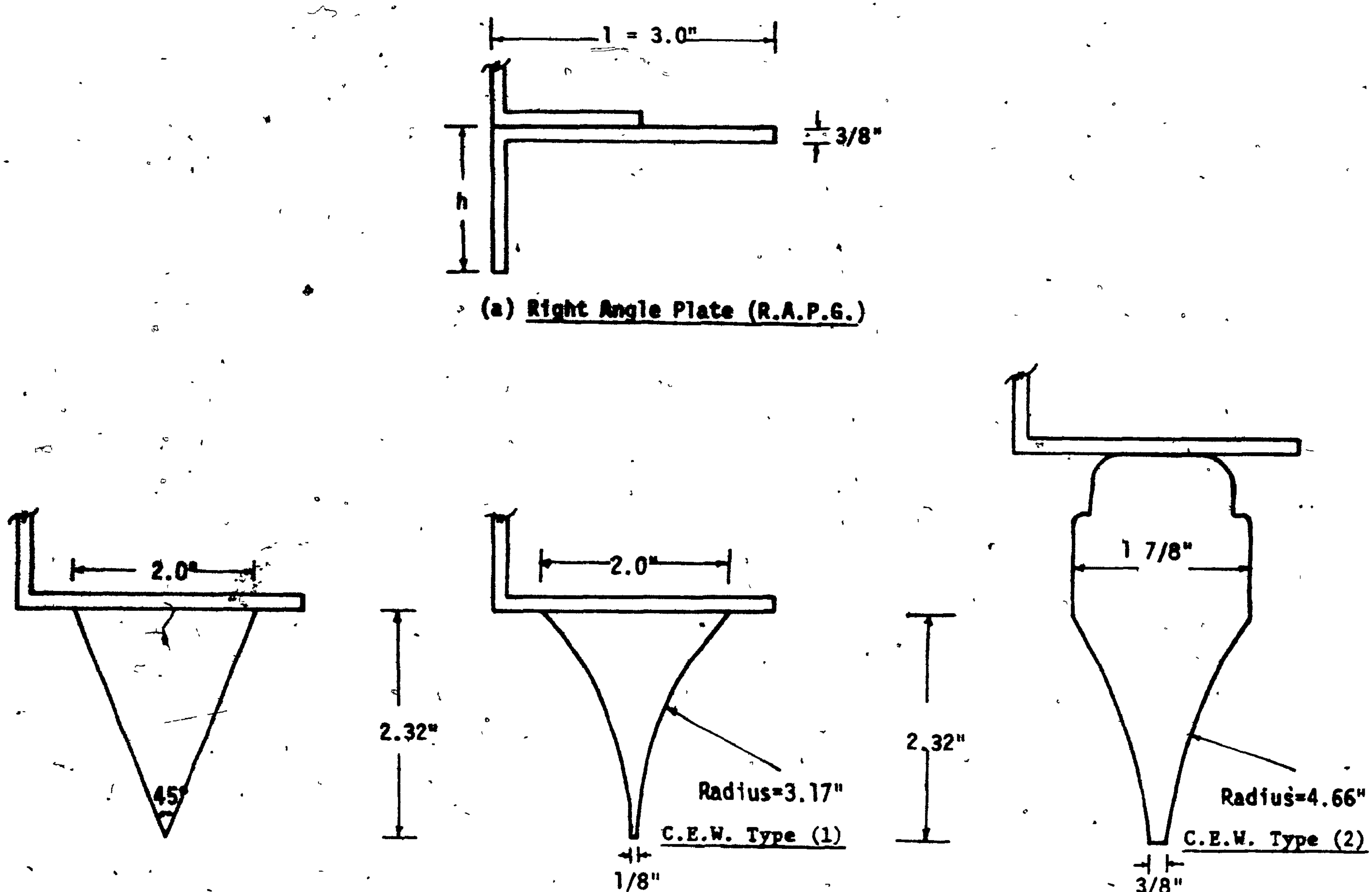

(a) Right Angle Plate (R.A.P.G.)

(b) Straight Edge Wedge Grouser (S.E.W.G.)

(c)

(d)

Curved Edge Wedge Grousers (C.E.W.G.)

clay and a kaolinite clay soil. The artificial clay was preferred in the initial test series due to the fact that preparation of the samples did not require water content control as they merely required moulding in the test bin and subsequent compaction. This permitted the development and debugging of test equipment and experimental techniques. The tests were continued to provide information regarding the interaction behavior of a cutting or tractive element with a plastic material. The conventional engineering properties of the kaolinite soil tested may be found in Appendix A, together with a description of the artificial, oil based, clay.

To minimize the number of experimental variables, the tools were tested at constant rate of horizontal movement of about 1.0 inch/minute. The various experiments performed are listed in Table 3-1 for soil cutting tests, and in Table 3-2 for traction tests. It will be noted here that the horizontal speed fluctuated between 0.85 and 1.05 inches/minute. The torque output produced by the varying speed DC-motor, utilized in the experimental facility, was found to be very sensitive to the input current at low speeds, making it difficult to reproduce any desired torque. This resulted in difficulties in maintaining the same horizontal speed throughout the duration of the experimental program. However, the speed was constant during any one test.

Included in Table 3-1 and Table 3-2 is a listing of the applicable bulk densities and water contents for each of the reported experiments. Examination of these values will show that both were very reproducible over the entire experimental series. Finally, Fig. 3-2 shows the density variations encountered in both the cutting and traction test series for the kaolinite clay, reported in terms of dry

TABLE 3-1

INITIAL DATA FOR SOIL CUTTING EXPERIMENTS

TEST NUMBER	ANGLE OF BLADE WITH VERTICAL	HORIZONTAL SPEED inch/min.	DENSITY PCF	WATER CONTENT %
ARTIFICIAL CLAY TESTS				
8	10°	0.85	110.0	-
9	10°	1.084	110.90	-
21	10°	0.98	108.0	-
3	20°	1.0	109	-
4	20°	0.95	109.5	-
12	20°	0.98	111.0	-
10	40°	1.05	110.2	-
23	40°	0.95	109.0	-
6	50°	1.0	108.5	-
7	50°	0.97	110.0	-
22	50°	1.03	109.3	-
NATURAL [KAOLINITE] CLAY TESTS				
27	10°	1.05	101.00	53.75
30	10°	0.90	102.80	52.15
28	20°	1.0	101.80	51.49
35	20°	1.05	102.40	52.50
26	40°	0.98	102.25	50.90
36	40°	1.03	99.96	51.30
29	50°	1.0	100.80	53.20
31	50°	1.0	101.75	53.60

TABLE 3-2

INITIAL DATA FOR TRACTION EXPERIMENTS

Test No.	Tractive Tool	Horizontal Speed inch/min	Density PCF	Water Content %
ARTIFICIAL CLAY TESTS				
18	R.A.P.G.	1.05	109.31	-
19	R.A.P.G.	0.97	110.0	-
20	R.A.P.G.	0.85	110.7	-
40	C.E.W. Type (1)	1.0	109.5	-
41	C.E.W. Type (1)	1.05	111.0	-
13	C.E.W. Type (2)	0.95	108.92	-
14	C.E.W. Type (2)	1.0	109.57	-
25	C.E.W. Type (2)	1.0	110.0	-
16	S.E.W.	1.0	110.35	-
17	S.E.W.	1.05	111.21	-
24	S.E.W.	1.03	109.65	-
NATURAL (KAOLINITE) CLAY TESTS				
34	R.A.P.G.	1.05	102.40	52.80
39	R.A.P.G.	0.95	103.00	53.20
42	C.E.W. Type (1)	1.05	102.2	52.6
43	C.E.W. Type (1)	1.0	100.0	51.2
33	C.E.W. Type (2)	1.0	102.80	53.35
38	C.E.W. Type (2)	1.0	100.10	50.95
32	S.E.W.	1.0	101.22	52.57
37	S.E.W.	1.05	103.10	51.79

Notes: Traction tools indicated by the letters -

R.A.P.G. - denote Right Angle Plate-Grouser

C.E.W. - denote Curved-Edge Wedge Grouser

S.E.W. - denote Straight-Edge Wedge Grouser density. In addition, it is observed that the kaolinite soil samples used in these experiments generally achieved a degree of saturation of the order of 95 per cent.

3.3.2 Soil Strength Tests

In addition to the cutting and traction experiments, strength tests were performed on compacted soil samples to obtain the stress-strain relationships required for the analytical solution. The results of these tests will be presented in the following Chapter, and complete descriptions of the techniques and apparatus are given in Appendix A. Briefly, however, two types of tests were performed.

(a) Tests to determine the stress-strain relationships for the soil represented by continuum elements in the analytical solution

After the cutting and traction tests were completed, undisturbed blocks of the soil were taken from the test bin at various locations away from the region of loading. These samples were subjected to two loading conditions, the first being testing of prismatic samples under plane-strain conditions in a modified triaxial chamber. The second consisted of the application of axisymmetric loading to a cylindrical soil sample placed in a standard triaxial cell. Some preliminary studies were conducted with a view to finding the effect of the rate of strain on the strength properties of the soil. Triaxial tests at three different rates of speed [0.1, 0.5 and 1.0 inch/minute], and three different confining pressures [0, 2.5 and 5.0 psi] were run on duplicate samples. The results showed some gain in strength with speed, Fig. A-5, Appendix A.

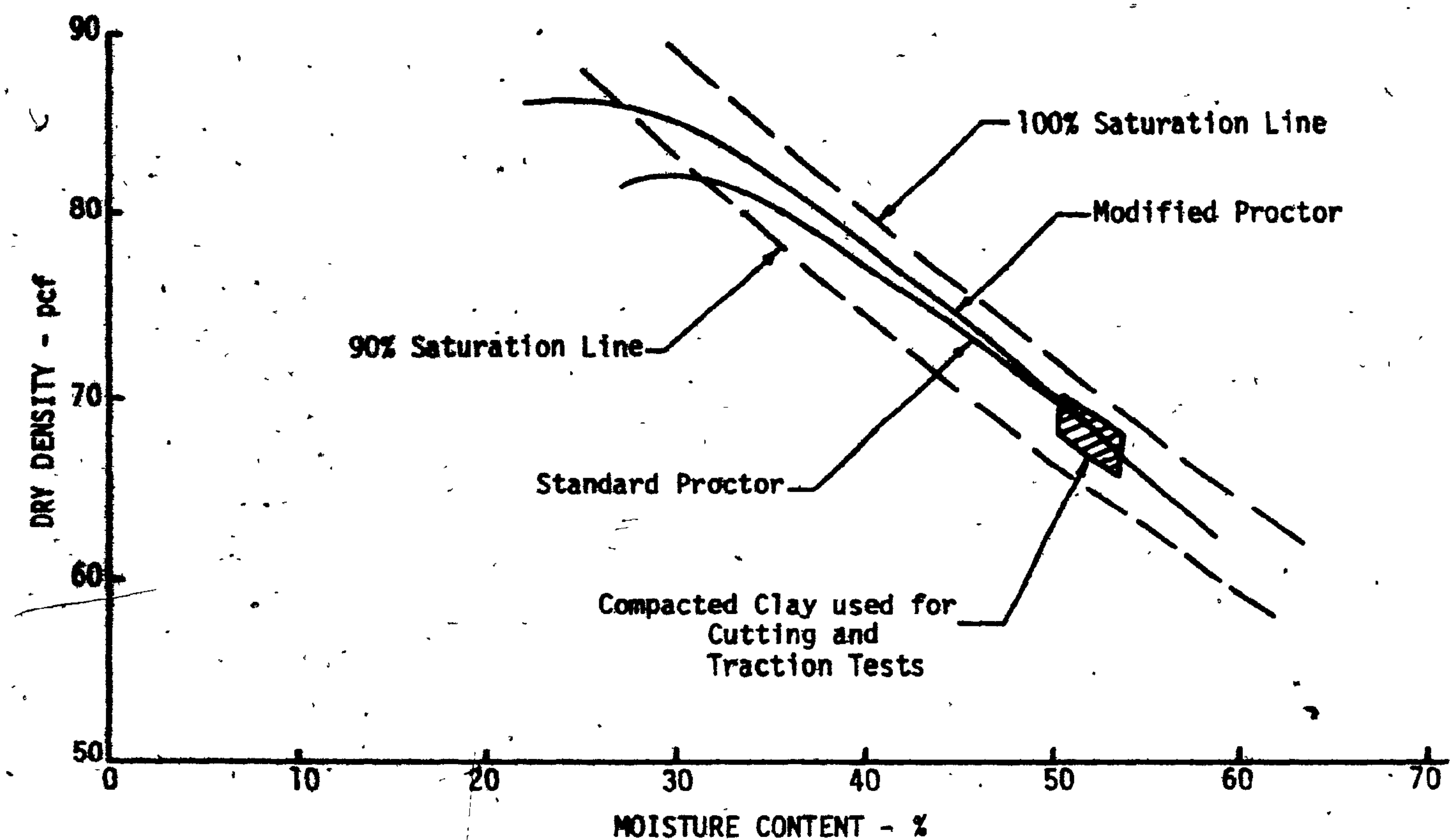

FIGURE 3-2 DRY DENSITY-WATER CONTENT CURVES FOR COMPACTED S-187 ENGLISH CLAY [After Sylvestre-Williams (1973)]

It was therefore decided to use the triaxial test results obtained at the same speed at which the cutting or traction element is loaded in the model test.

(b) Tests to determine the properties of the joint elements used in idealizing the cutting and interface behavior

As mentioned previously [Chapter 2] joint elements are utilized in the analytical solution to simulate the discontinuities in the finite element model proposed in this study. The properties of the joint elements consist of a shear stiffness, k_s, and a normal stiffness, k_n. These coefficients (K_s and K_n) express the rate of change of shear stress with shear deformation and of normal stress with normal deformation. The nonlinear, stress dependent, joint behavior may be conveniently obtained by performing direct shear tests due to the fact that the relative displacement in this test occurs along a predetermined plane which can be visualized as a discontinuity reflecting the behavior of a joint element. Two types of direct shear tests were performed.

(i) Cutting tests The soil was tested in a direct shear machine to obtain the stiffness values assigned to the joint elements inserted between the continuum elements to simulate the tool cutting action.

(ii) Interface tests In these tests, the lower part of the direct shear box consisted of a specimen of aluminum, the same material used in the fabrication of the cutting and traction tools, and the soil was compacted in the upper part of the shear box. The gap between the upper half of the shear box and the aluminum base was kept as small as possible, and the tests were interpreted assuming that the relative displacements between the upper and the lower parts of the box were due entirely to interface movements.

Furthermore, to account for the dependence of the shear stiffness modulus, k_s, on the normal stresses, the normal load, in both test series, was varied through the values 0, 2.5 and 5.0 lb.

CHAPTER 4

EXPERIMENTAL RESULTS AND ANALYSIS

SECTION A - EXPERIMENTAL RESULTS

4.A.1 GENERAL CONSIDERATIONS

A soil-tool interaction prediction must be based on quantitative descriptions of the forces applied by the tool and the resulting behavior of the soil. The actions recognized as being present in soil cutting and traction must be separated into simple behavior, which can be studied. Simple behaviors include, for example, stress-strain relations, soil-metal friction and adhesion, and yield by shear.

As previously stated, descriptions of behavior can be established through the application of several distinct phases of study. First, some specific behavior is observed and studied. Second, having noted the behavior, factors involved are identified and their relation ascertained in a cause-and-effect manner. Analytical techniques are required to quantitatively describe the cause-and-effect relation, and, hence, the behavior. The sequence adopted in the presentation of the test results and the methods of analyses in the present, and the following Chapters are shown in Fig. 4-1. In this Figure, the separation of the distinct phases of the study is clearly evident.

One of the difficulties in understanding a soil-tool action is that every behavior is not always operative. A behavior may appear

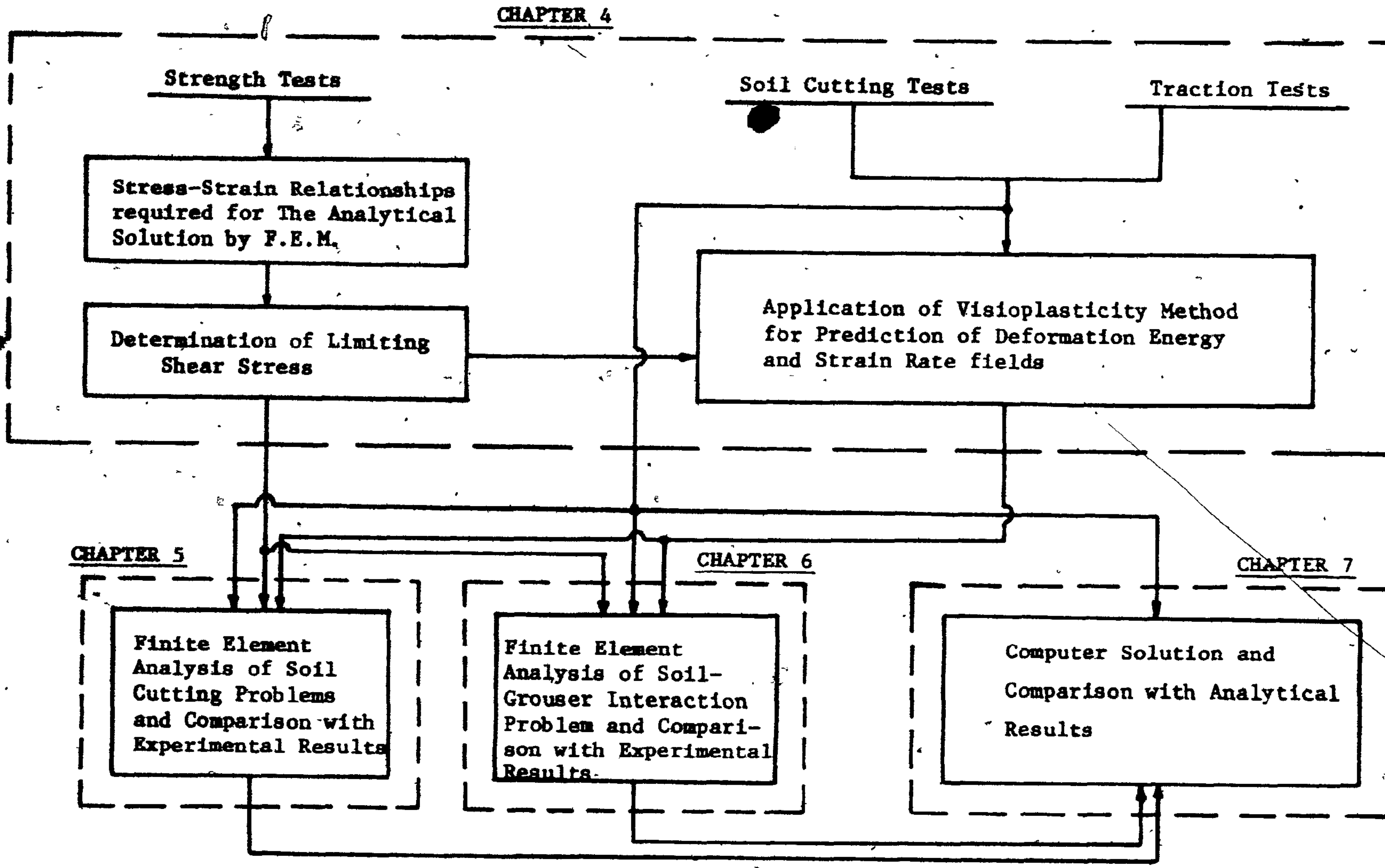

FIGURE (4-1) SCHEMATIC REPRESENTATION OF THE METHOD OF REPRESENTATION OF EXPERIMENTAL RESULTS AND ANALYTICAL SOLUTION intermittently, and its presence may be difficult to detect or assess. For example, a dry cemented soil does not exhibit plastic flow behavior or even compression failure to any great extent. Similarly, a wet saturated soil may exhibit great plastic flow but little shear failure. Elijah and Weber (1968) identified four distinct types of soil failure for flat cutting blades. They were designated as "shear plane", "flow", "bending", and "tensile" failures. This terminology was created by the authors as the most descriptive of the patterns involved. They have stated that "Predicting the type of failure in a given soil with a given tool will require some new soil parameters, ones that will distinguish quantitatively some of the soil characteristics that are now expressed in qualitative terms".

The results and associated discussions presented in this study deal mainly with plastic soils interacting with a number of tool geometries. The soil deformation behavior observed during the experimental investigation is of a plastic flow nature. The solution technique, in turn, is oriented towards analyzing interaction problems involving the plastic flow soil failure, and therefore cannot be considered a general solution technique covering the wide soil behavior spectrum. However, in the analytical approach adopted it is essential that proper appreciation of the constitutive performance of the material and boundary conditions be obtained and subsequently applied. Such rigorous requirements should provide for more general behavior predictions by the analytical method.

4.A.2. TYPICAL EXPERIMENTAL RESULTS

4.A.2.1 Soil Cutting Results

The soil cutting tests which were carried out in the course of the experimental programme are listed in Table 3-1. Prior to presentation and examination of test results some points should be discussed in order to arrive at a better insight and evaluation of these results.

The entire test series was performed at a constant rate of blade motion [about 1.0 inch/minute]. Although many studies have shown that the forces acting on soil-engaging tools increase with the increase in speed [Rowe and Barnes (1961), Olsen and Weber (1966) and others], no satisfactory explanation of this phenomenon has been reported. This increase in force has been attributed to acceleration of the soil, increased shear strength, and increase in length of the failure path [Siemens (1963), Shöne (1956)]. Rowe and Barnes (1961) and Olsen and Weber (1966) studied the effects of speed on the draft of an inclined flat blade and concluded that increase in draft with increase in speed was primarily due to increased soil shearing strength. Some of the conclusions reached by Olsen and Weber were:

1. acceleration of the loaded soil segment was not a significant contributing factor to the increase in tool force with increase in speed,
2. there was no significant change in length of the failure path or angle of inclination of the failure plane with change of speed for the soil tested, and

3. the shape of the stress-strain curve of a soil seems to be a determining factor in the magnitude of the increase in tool force with increase in speed.

In view of the above findings, it was argued that there was no need for examining the effect of speed on the developed forces since such effect is already included in relating the stress to the strain for the soil used in the experimental investigation. It will be recalled that the stress-strain relations obtained from laboratory plane-strain tests, performed at the same speed at which the cutting or traction element moved in the soil, are used in the finite element analysis to predict the load-deformation behavior of the soil. While realizing that the strain-rate dependence of a certain soil may vary with the test constraints [i.e., the difference between the boundary conditions of a plane-strain triaxial test and the model tests] which may lead to some error in prediction, such error should not diminish the effectiveness of the above technique, since by adopting a more appropriate framework defined by using more similarities in boundary conditions ensures a higher order of predictability.

The draft force is usually taken as the maximum force produced during the cutting operation. It is easy to determine the draft force if the material fails in shear and the draft-displacement curves exhibit peak values at small displacements. However, if the draft force gradually increases with tool displacement, the cutting forces should be computed at a specified value of displacement. Contrary to most of the previous research which was directed towards the measurement and prediction of the maximum draft forces regardless of the displacements at which these forces were attained, the present study is concerned with the prediction of the force-displacement history. For this purpose, the tool was moved in the soil for a distance of 3.0 inches, and the forces and displacements were recorded.

It has been previously mentioned that the model tests were performed for the purpose of checking the validity of the analytical approach. With this in mind, the experimental results should be viewed not as a study of the various factors influencing soil cutting, but rather as data gathered for the purpose of verifying the applicability of the predictive technique adopted.

A sample of the results showing measured horizontal and vertical forces for blades with inclination angles of 10°, 20°. 40° and 50° with the vertical are shown in Figs. 4-2 and 4-3 for the kaolinite clay, and in Appendix A for the artificial, oil based, clay. It should be noted here that the blades employed in this study were of a constant length of 4.0 inches which resulted in a depth of cut varying with the blade inclination angle. Such variation in the depth of cut makes it difficult to compare the forces developed by the various blades. It is argued that a normalization of the results by comparing the forces per unit depth of cut is not a viable approach since interaction forces cannot be assumed, without experimental evidence, to be directly proportional to the depth of cut for a particular blade. Any conclusion derived from a normalization technique employing such an assumption, without experimental verification, can be greatly misleading.

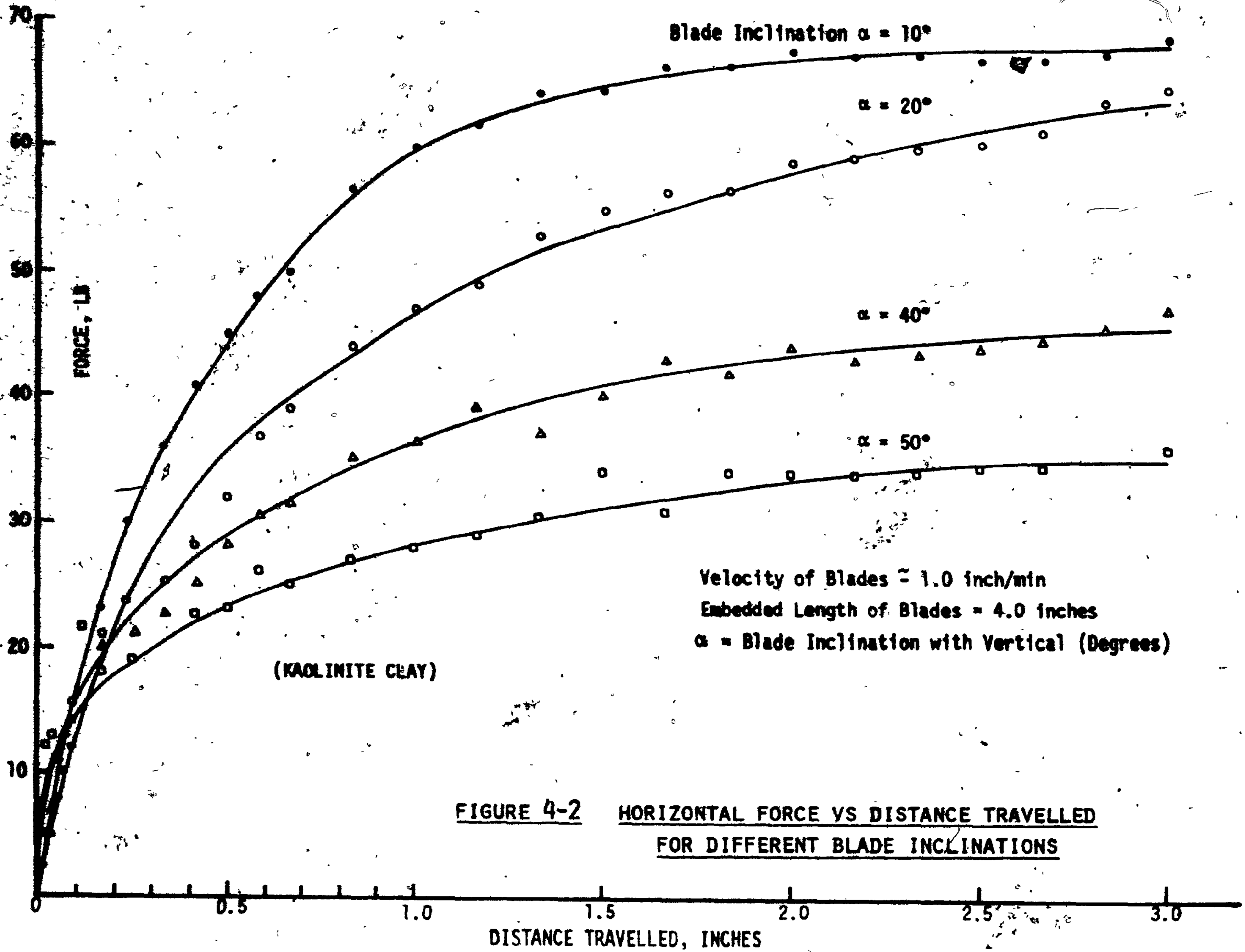

FIGURE 4-2 HORIZONTAL FORCE VS DISTANCE TRAVELLED FOR DIFFERENT BLADE INCLINATIONS

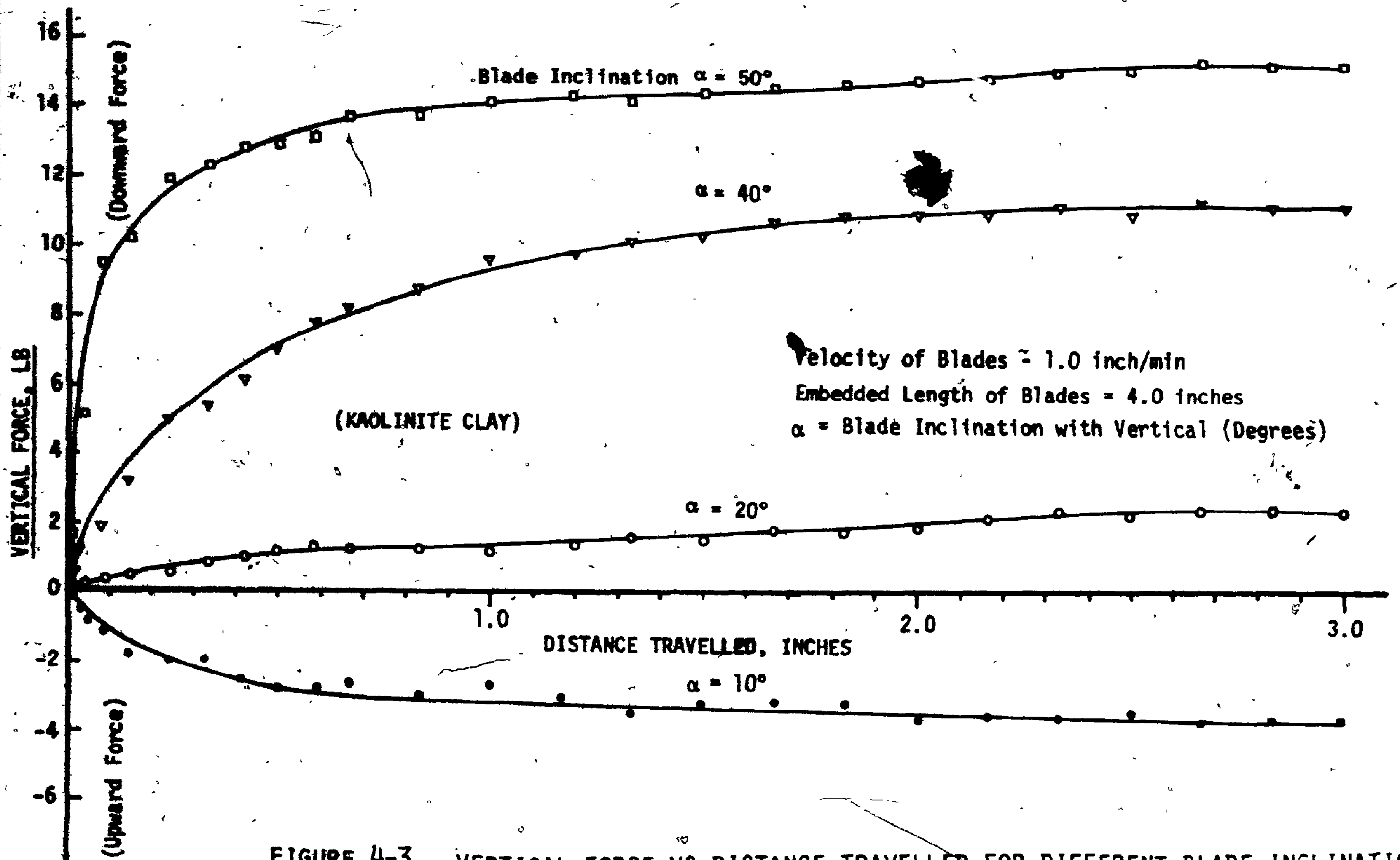

FIGURE 4-3 VERTICAL FORCE VS DISTANCE TRAVELLED FOR DIFFERENT BLADE INCLINATIONS

It has been mentioned in Section 2.2.2. [Chapter 2] that during the cutting process no distinct failure planes were developed in the loaded soil; instead continuous failures took the form of bulging. Such behavior was observed during the deformation process using the glass-sided soil bin [Chapter 3], and is confirmed from the plots of draft forces versus displacement, Fig. 4-2, for the various blades employed in this investigation. These plots show a nonlinear load-displacement relationship exhibiting no peaks that can indicate the formation of shear or failure planes. Yong and Chen (1970) observed in their investigation that the force-displacement plots for cutting blades in sand and $C - \Phi$ soils exhibited a first peak representing the major or maximum force development at first failure and subsequent perturbations which generally show higher values, corresponding to the subsequent development of secondary shear planes. In the case of clay soils tested in this study, no such peaks were recorded and the draft values are shown to keep on increasing with blade movement, an indication of the surcharge accumulation effect in front of the moving blade.

The development of the vertical forces, presented in Fig. 4-3, shows that the sense of the vertical force changes from downward [positive] on the blades with inclination angles greater than 10° to upward [negative] for the 10° inclined blade. Such behavior is consistent with the concept put forward by Osman (1964) stating that in the absence of much blade friction [or adhesion] the vertical force acts downwards for small blade rake angles, changing to upwards at a certain point as the rake angle increases. The friction [or adhesion] force always acts upwards along the blade because this is the direction of relative soil movement. The effect of friction [or adhesion] is therefore to diminish the downward force on low rake blades, increase the upward force on near vertical blades.

The influence of the angle of blade inclination on the developed horizontal and vertical forces at 1.0 inch displacement is illustrated in Fig. 4-4, for both kaolinite and artificial soils. Discussion relative to the above and also the following results will be developed in Chapters 5, 6 and 7. For continuity, the material presented at this point will relate primarily to the presentation of results, in a form which is amenable for examination and evaluation.

4.A.2.2 Traction Results

Regarding the traction test results, while the intent of the experiments is similar to that of blade testing, the results [in terms of developed forces and soil deformation] must be viewed from a different perspective. The purpose of using lugs or grousers on traction devices is to cause deformation of soil in a certain manner as to develop adequate traction capacity for a grouser. The deformation of a particular soil plays a very important role in the production of adequate traction for a single grouser. The deformation characteristics could be manipulated by changing the geometry of the traction tool in order to produce enough interaction for efficient performance. To this end, the purpose of performing the traction experiments was to investigate the influence of the tool boundary conditions on the interaction process in order to arrive at desirable developed forces for efficient

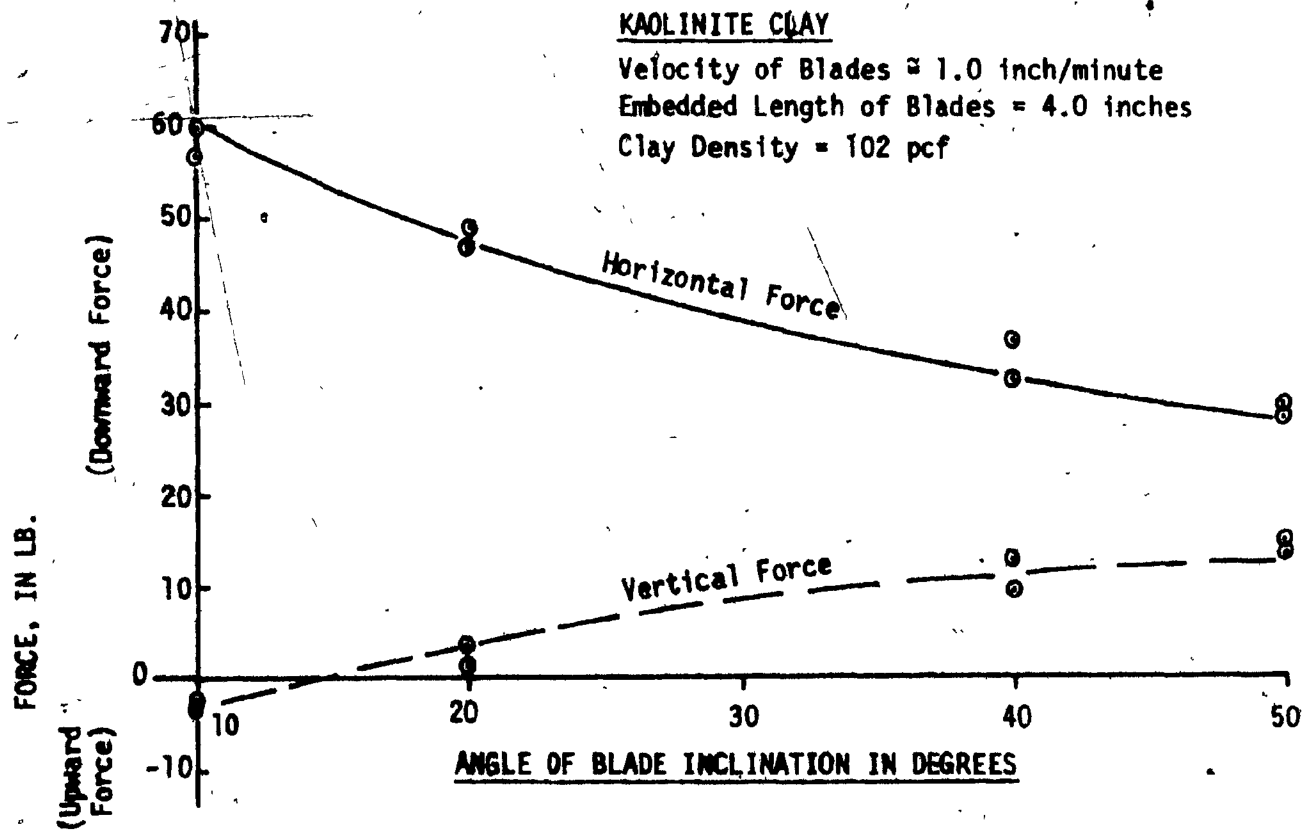

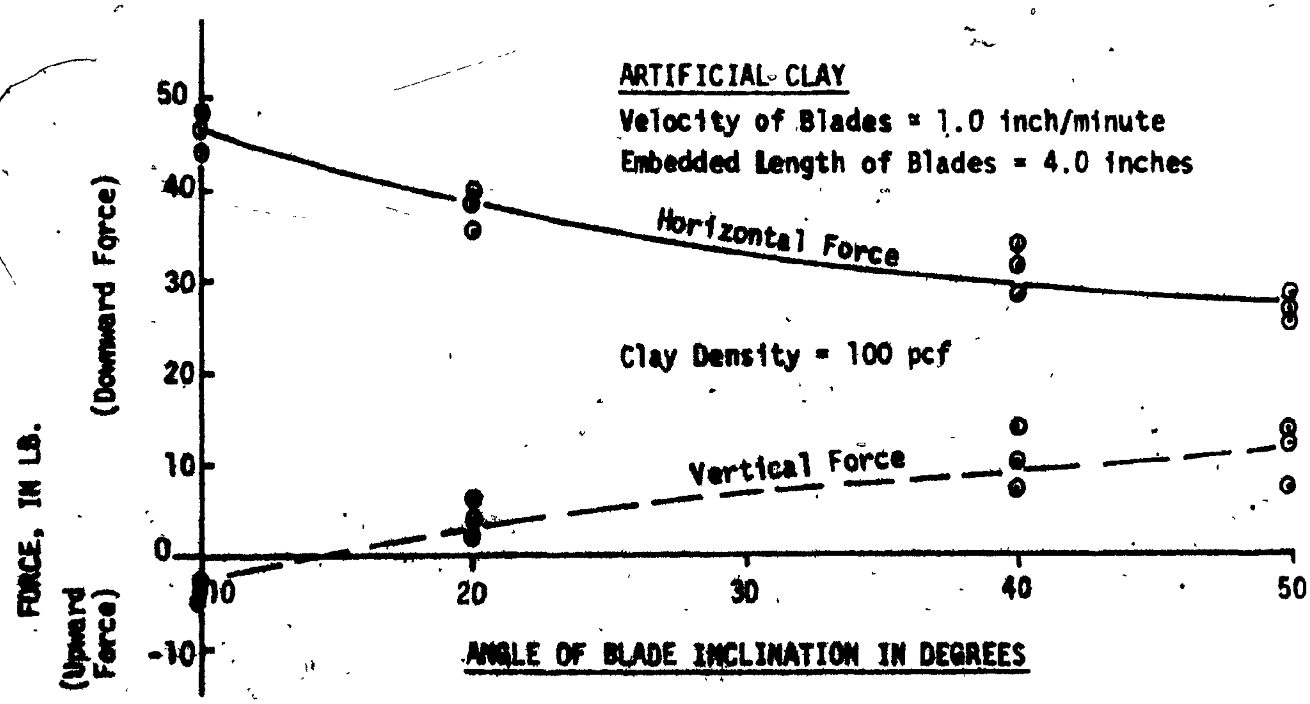

FIGURE 4-4 PLOTS OF HORIZONTAL AND VERTICAL FORCES AT 1.0 INCH DISPLACEMENT VS. ANGLE OF BLADE INCLINATION

conversion of traction into pull.

This study is concerned with the mechanics of a single grouser acting on clay soils as a phase of the study of track-soil interaction. Again, the intent here is to provide information on the physical behavior of the action of the moving grouser in order to formulate the necessary mathematical model and boundary conditions. Grouser action is defined in this study as the motion of the grouser in the soil to create a failure condition in the soil. Thus, the limits of the magnitudes of the horizontal and vertical forces defined for the action of the grouser serve to identify the maximum forces that can be applied to provide for forward motion of the tracked vehicle. Having established the viability of a certain predictive technique, further studies on multiple grousers can be initiated. The end purpose of multiple grouser study is to determine optimum spacing to achieve best total aggressive grouser motion.

With this appreciation of the problem, it will be recalled that grouser tests may be divided into two categories [Chapter 3], viz:

1. Constant vertical load tests

   In this type of test a constant vertical load intended to simulate a portion of the vehicle weight is applied to the top of the grouser and maintained throughout the entire test. Since the grouser is mounted on a carriage, it is free to translate both vertically and horizontally but is restrained against rotation. The measurable response parameters during this type of test are the horizontal displacement, the horizontal force and the vertical displacement.

2. Constant elevation tests

In this type of test, the grouser is restrained in the vertical direction and is only free to translate horizontally. The method of restraint is to keep the grouser at a constant height in relation to the initial surface throughout the duration of the test.

These two types of tests simulate most situations which arise in practice and the results obtained therefrom should be representative of the behavior of the soil mass under the most common loading systems which can be applied to a grouser. As previously mentioned, in this study the latter condition was chosen for simplicity in specifying the boundary conditions.

Typical results from the traction experiments listed in Table 3-2 are shown in Figs. 4-5 and 4-6. In Fig. 4-5 both the horizontal and vertical forces developed on the plate grousers [R.A.P.G.] are plotted as a function of the distance travelled. In this Figure the results are shown for two grousers with aspect ratios (h/l) of 0.5 and 0.833, tested in the kaolinite clay. Similar results are shown for the artificial clay in Appendix A. It must be noted that while the number of grousers tested does not permit a good comparison of the developed forces based on the aspect ratio (h/l), the results shown indicate that there seems to be no linear correlation between the grouser aspect ratio (h/l) and the developed forces. In Fig. 4-6

FIGURE 4-5 DEVELOPED FORCES VS DISTANCE TRAVELLED FOR PLATE GROUSERS (R.A.P.G.) WITH DIFFERENT ASPECT RATIOS

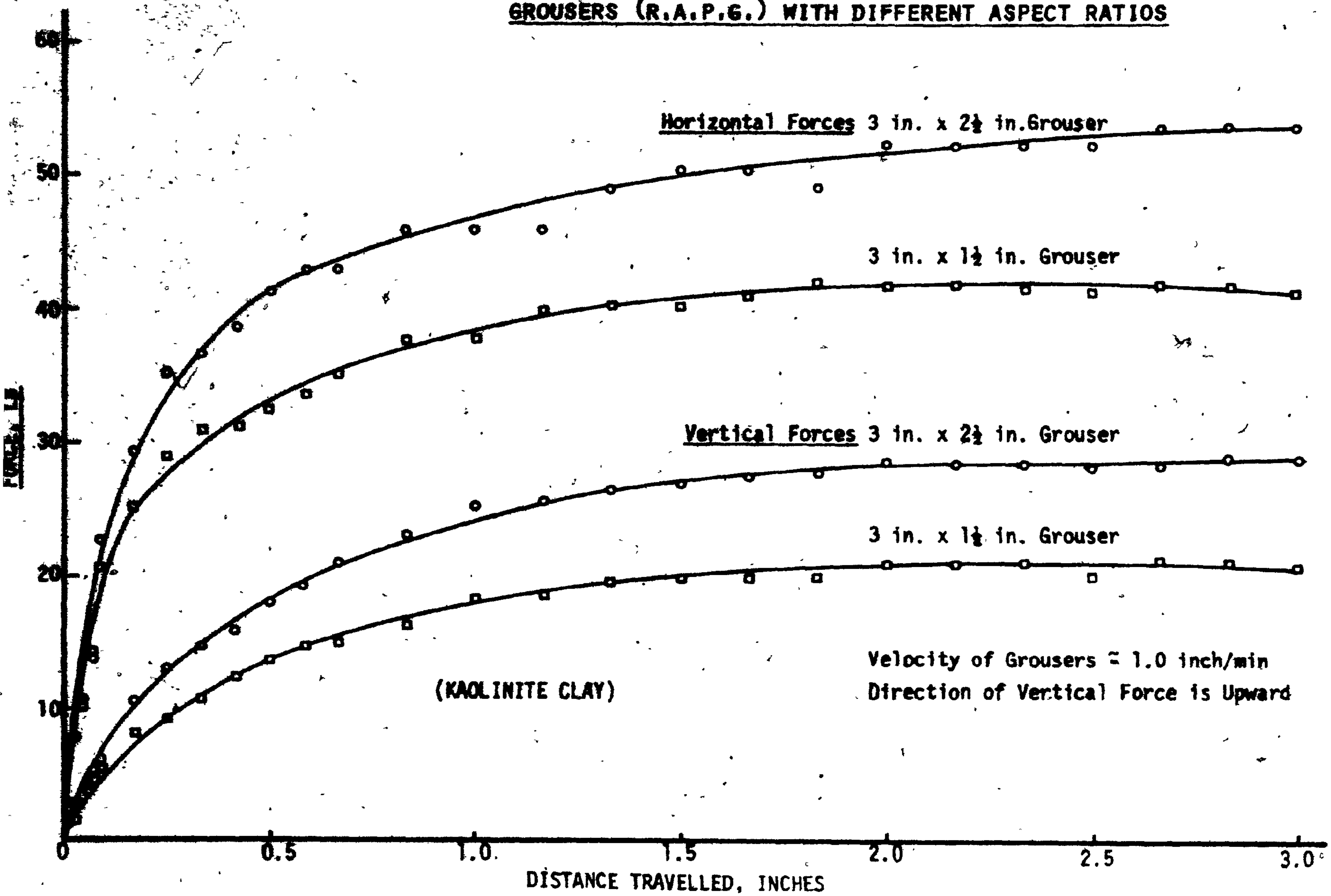

FIGURE 4-6 DEVELOPED FORCES VS DISTANCE TRAVELLED FOR WEDGE GROUSERS

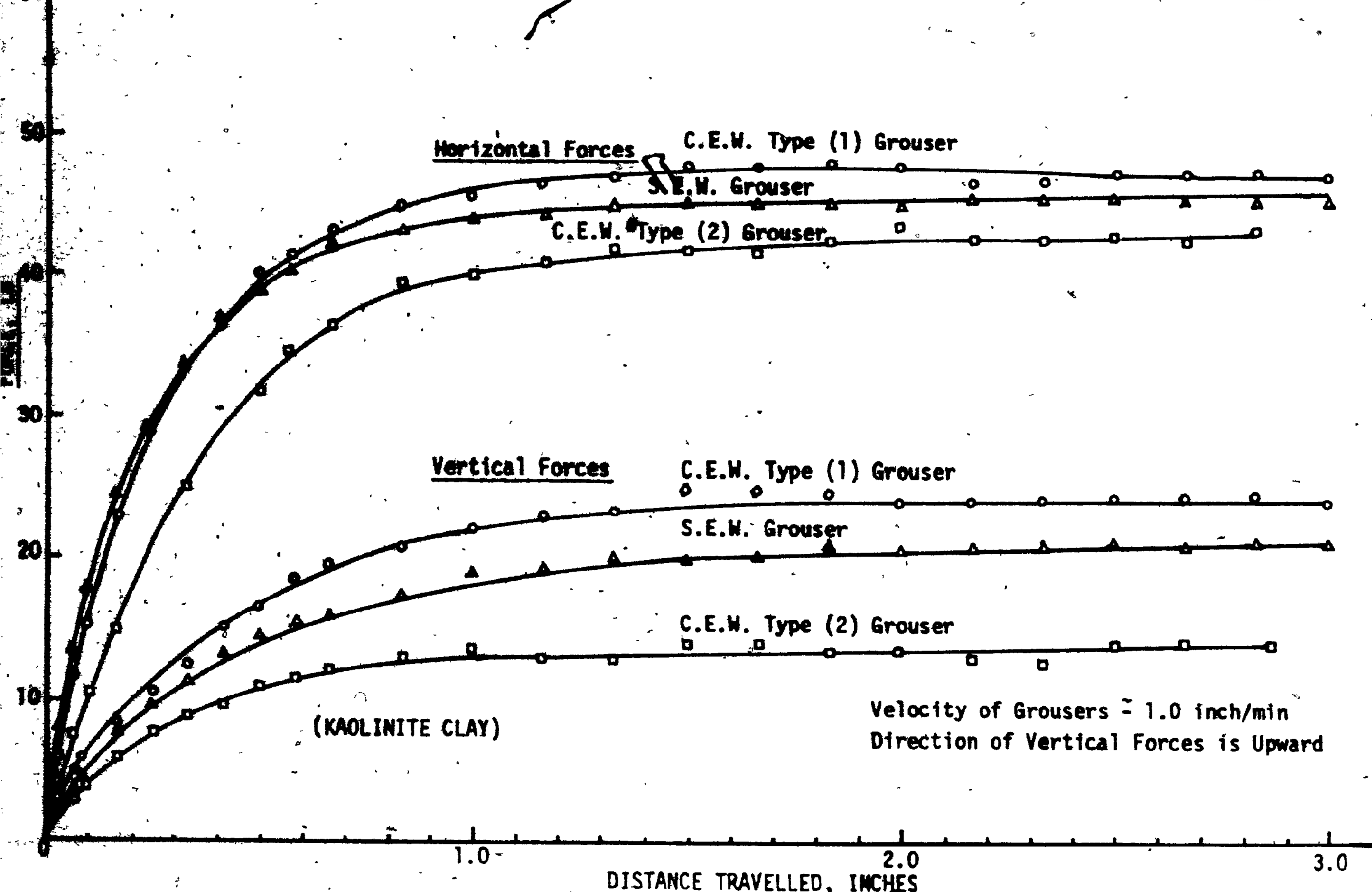

similar plots are shown for the C.E.W. and the S.E.W. grousers tested in the kaolin clay. The corresponding plots for the artificial clay are shown in Appendix A.

Table 4-1 presents a comparison of typical forces developed on the various grousers employed after a travel distance of 1.0 inch.

TABLE 4-1

Typical Developed Forces (in lb) for Various Grousers Tested at 1.0 inch Displacement (Constant Elevation Tests)

Grouser Type	Kaolin Clay		Artificial Clay	
	Horizontal Force	Vertical Force	Horizontal Force	Vertical Force
R.A.P.G.(h/l) = 0.5	38.5	18	30	11.5
R.A.P.G.(h/l) = 0.833	47.0	25.5	40	18.2
C.E.W. type (1)	45.5	22	38.2	17.5
S.E.W.	44.0	19	35.5	14.9
C.E.W. type (2)	40.0	13.5	33.6	11.0

With the exception of the R.A.P.G. with an aspect ratio (h/l) of 0.5 [h=1.5", l=3.0"], the rest of the grousers employed in this investigation have approximately the same depth of cut [2.5 inches for the R.A.P.G. with h/l of 0.833 and 2.32 inches for the wedge grousers]. Consequently, direct comparison of the developed forces as a function of grouser geometry is possible. It is shown from Figs. 4-5 and 4-6 and Table 4-1 that the plate grouser [h/l = 0.833] develops maximum traction, i.e., horizontal as well as vertical forces. The development of the large forces may be attributed to the soil deformation behavior in front of this grouser. From an examination of the displacement patterns as well as the velocity fields of the grid nodes [shown in a later section of this dissertation], it was noted that the soil confined by the plate grouser moves coherently with the grouser, leading to differential deformation between this and the surrounding soil. This effect is similar to the "dead" zone postulated by Terzaghi (1944) in his analysis of bearing capacity, and to the "dead" zone postulated by Yong and Sylvestre-Williams (1969) in studying grouser thrust on sand, see Fig. 2-1(t). It is believed that the existence of a similar "dead" zone in the present investigation extended the region of influence of the grouser resulting in larger developed forces. On the other hand, the wedge grousers' deformation fields indicated very small or no "dead" zones, and the regions of influence of such grousers were found to be smaller than those of the plate grousers.

Comparing the forces developed on the wedge grousers, it is noted that the C.E.W. type (1) grouser produces the largest forces [both horizontal and vertical]. While the depth of embedment is the same for all the wedge grousers, the contact surface area is larger for the C.E.W. type (1) grouser due to the wedge curvature and also due to the contact of the top horizontal plate with the soil, see Fig. 3-1, resulting in more soil interacting with the tool.

The effect of the curvature of the grouser interface on the developed forces can be seen from a comparison of the C.E.W. type (1) grouser results with those of the S.E.W. grouser. Both systems are similar in dimensions except for the curvature of the C.E.W. type (1) grouser surface. This curvature results in an increase in developed forces.

It seems, however, that the effect of the grouser top horizontal plate being in contact with the soil on the developed forces is much more pronounced. The C.E.W. type (2) grouser shown in Fig. 3-1(d) has a curved interface but the top horizontal plate does not touch the soil surface. This grouser produces the lowest forces.

Finally, from examination of the displacements of the surface grid, the geometry of the deformed soil mass subjected to the aggressive action of the different grousers showed no development of distinct failure surfaces in the initial three inches of grouser travel. This behavior resembles the deformation observed in the cutting tests which is attributed to the plasticity of the soils tested.

4.A.3 STRENGTH TEST RESULTS

For many soil-structure interaction problems, it is necessary to know, or to predict with a reasonable degree of accuracy, the strength and deformation characteristics of soil under load. The acceptability of a theory for predicting the stress-strain relationship for soil depends on the accuracy of the assumptions and the approximations made regarding the actual behavior of the soil. The simplest assumption that can be made is that a given soil can be classified as linear elastic, rigid plastic, or elasto-plastic. However, soil behavior is a function of mineral composition, stress level, density, strain conditions, etc., and, unlike most engineering materials, can neither be linear nor compatible with elastic, plastic, or elasto-plastic classification.

(a) Plane-strain and axisymmetric triaxial test results

It was felt that the best way to incorporate a constitutive behavior was to perform tests that reproduce as much as possible the assumed conditions during the cutting and traction tests. For this purpose, prismatic samples of nearly saturated remolded clay were prepared, and triaxial tests were conducted under plane-strain conditions. A given sample was installed into a modified triaxial cell between two polished and lubricated brass plates. The axial [vertical] load was applied through a lubricated rectangular platen of the same dimensions as the initial sample section. The apparatus used, together with the procedures, is described in Appendix A. The testing was conducted under different confining pressures of 0, 2.5 and 5.0 lb/in^2, and at axial strain-rates of 0.1, 0.5 and 1.0 inch/minute. Typical test results are shown in Fig. 4-7 for kaolinite clay and in Appendix A for the artificial clay. Analogous axisymmetric triaxial tests were performed on cylindrical samples 1.4 inches in diameter. These tests were performed in order to verify the fact that the nonexistence of a well defined failure condition i.e., absence of strain softening behavior, is not a result of the plane strain, "True Triaxial", test restraints (Fig. 4-8).

It may be noticed that the stress-strain curves do not exhibit a definite peak to define failure, but instead the stress difference ($\sigma_1 - \sigma_3$) keeps on increasing with axial strain for both soils tested. The finite element analysis in this investigation is performed by an incremental procedure, and in such a

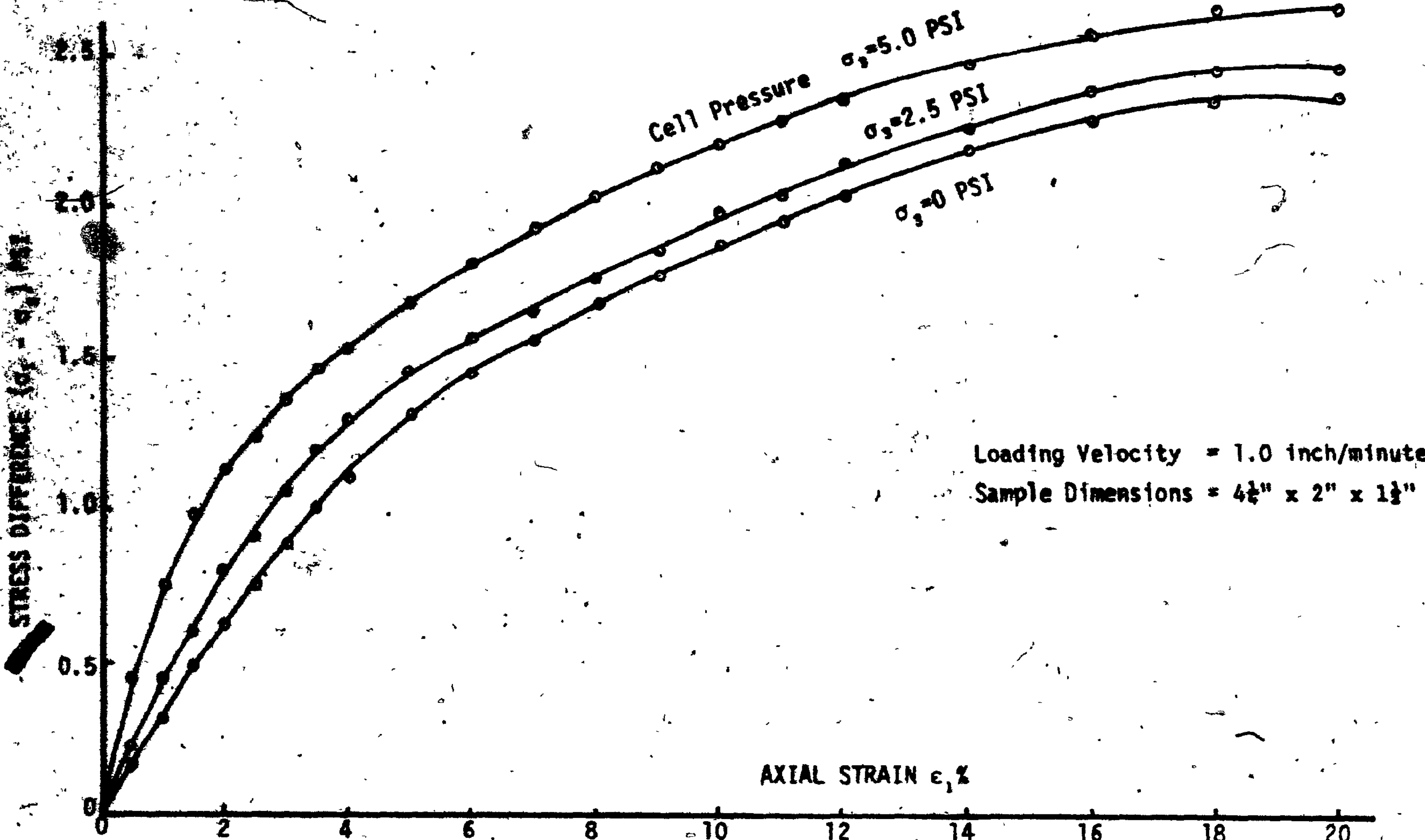

FIGURE 4-7 TYPICAL STRESS-STRAIN CURVES FOR PLANE STRAIN TRIAXIAL TESTS (KAOLINITE CLAY)

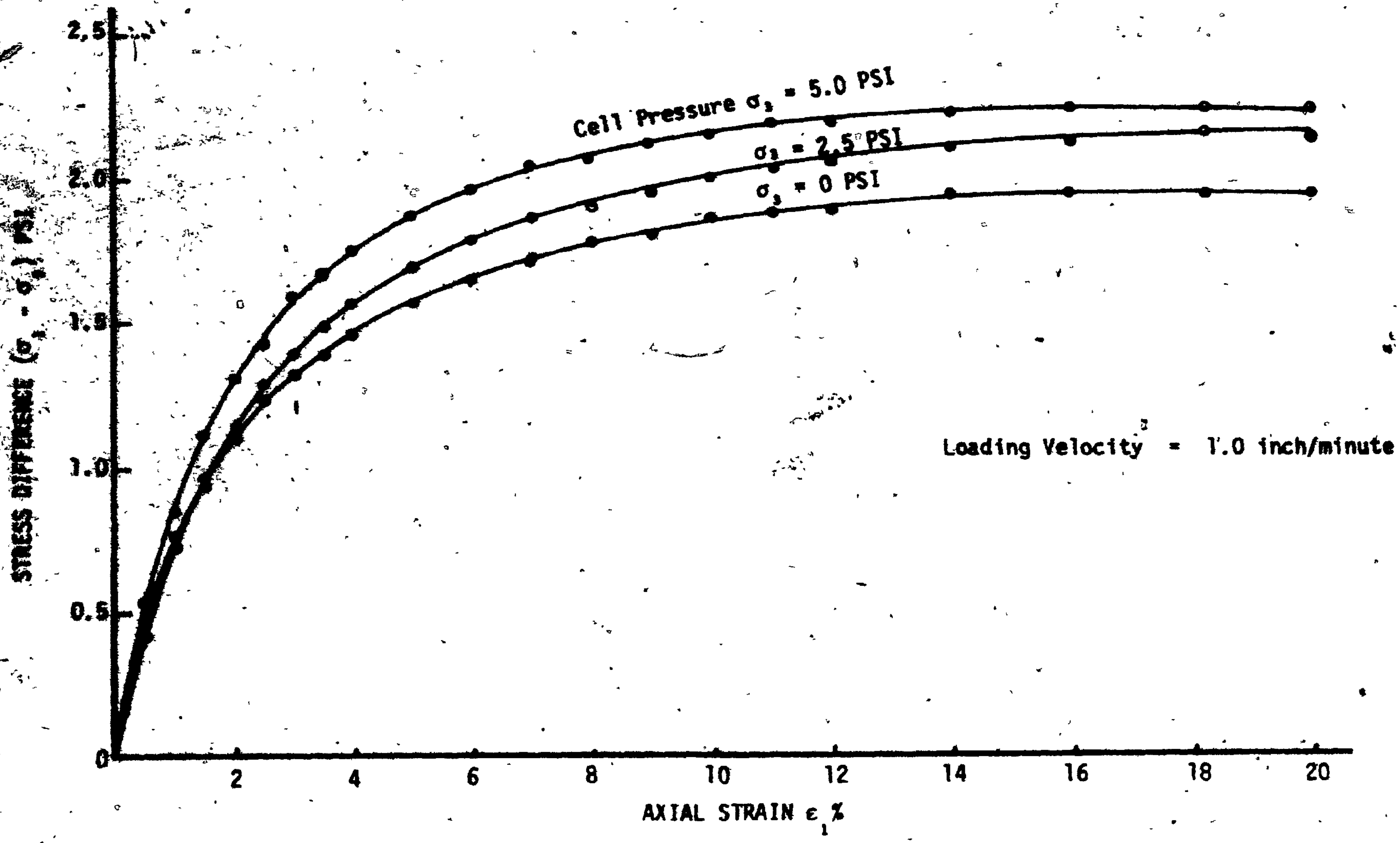

FIGURE 4-8 TYPICAL STRESS-STRAIN CURVES FOR STANDARD TRIAXIAL TESTS (KAOLINITE CLAY)

case, it is difficult to account for a drooping stress-strain curve. The observed rising of the stress-strain curves eliminated the need for an approximation to the stress-strain curves to avoid the numerical difficulties arising from strain softening behavior. Since no definite peak was evidenced, an axial strain of 20% was chosen to define failure.

There are two common procedures for incorporating a nonlinear stress-strain law into a finite element formulation for digital computations. The stress-strain law derived from a laboratory test can be used directly in a tabular or digital form. Several points on the curve are selected and are input in the form of number pairs denoting stress and strain at those points. The variable material parameters such as E and ν are obtained from such curves by suitable interpolation. If the behavior is represented by a single stress-strain curve, stresses are obtained by interpolation for a calculated state of strain. If the behavior is represented by several curves, interpolation must also be done between two curves for different confining pressures.

In the alternative procedure, the laboratory stress-strain relationship is expressed in the form of a suitable mathematical function. The material parameters for the nonlinear analysis are again obtained on the basis of the state of stress or strain.

The tabular or digital procedure was utilized in this study to represent the constitutive behavior of the soil modelled by continuum [triangular] elements in the analytical solution. To start the analysis, initial values of the modulus of elasticity, E_0, and Poisson's ratio ν, are required. The clays used can be considered to be fairly incompressible as they were nearly saturated. Therefore, it would be reasonable to choose the value of the Poisson's ratio of the soils close to 0.50. In the present study. ν, was assumed to be 0.48 for both the kaolinite and artificial clays. Furthermore, the value of ν was assumed to remain constant throughout the entire deformation process. Similar assumptions have been made by others earlier [Clough and Woodward (1967), Girijavallabhan and Reese (1968)]. The non-linear analysis was based directly on the plane-strain triaxial curves. The starting value of the modulus, E_0, was taken as the initial slope of the stress-strain curve at zero confining pressure. This value, obtained from Fig. 4-7, is 90 lb/in^2. for the kaolinite clay.

In an axisymmetric triaxial stress condition, the intermediate and minor principal stresses are the same, and the confining pressure for the sample is equal to the minor principal stress, σ_3. In the actual problem, however, these conditions are not strictly valid as, in general, the magnitudes of the intermediate and minor principal stresses in an element will be different. This is particularly true in a plane-strain condition where the intermediate principal stress is given by the relation:

$$\sigma_2 = \nu(\sigma_1 + \sigma_3) \quad (4.1)$$

For special cases only will Eq. (4.1) yield $\sigma_2 = \sigma_3$.

However, it seems reasonable to express the confinement in an element, for the sake of computations, as the average of the magnitudes of the intermediate, σ_2, and minor, σ_3, principal stresses induced at the centroid of the element. The analysis developed in this study adopts this approximation.

The finite element analysis first computes the values of the stresses, strains, and confining pressures in each element. In a general case, three interpolations are required to compute the state of stress $(\sigma_1 - \sigma_3)$ corresponding to a state of strain, ϵ_1, in an element from a set of nonlinear curves. Interpolations are performed to compute intermediate values in a curve and also between curves at different confining pressures. In the computer program "MAIN-2" developed in this study, stress values were computed from strain values obtained in the analysis. The details of the computer proram are given in Appendix E.

(b) <u>Direct shear test results</u>

As previously mentioned in Chapter 3, two types of direct shear tests were performed to determine the properties of the joint elements used in idealizing the cutting and the interface behavior. The first type was a conventional direct shear test which is referred to as a soil-to-soil shear mode, while the second test type was conducted with the lower part of the shear box consisting of an aluminum plate representing a soil-to-metal shear mode.

The shear stress-displacement curves for the soil-to-soil mode are shown in Fig. 4-9, and for the soil-to-metal mode in Fig. 4-10 for the kaolinite clay. In both Figures, it is seen that the shear stress values increase with increasing displacement reaching maximum values for relative displacements of approximately 0.2 inch, after which the shear stresses remain nearly constant. It may also be noted that both the steepness of the stress-displacement curves and the maximum values of shear stresses increase with increasing normal stress for both the soil-to-soil and soil-to-metal modes, Fig. 4-11.

The ratio of the peak stress in the soil-to-metal mode to the peak stress reached in the soil-to-soil mode is plotted in Fig. 4-12 as a function of the applied normal load. The relationship indicates that the ratio approaches unity at zero normal load, and decreases with increasing normal load up to a point after which it remains constant. While the reason for such behavior is not obvious, it appears that at low normal stresses the shearing does not occur at the soil-metal interface where the angle of metal friction is operative, but rather in the soil itself. This results in a condition approaching that of the soil-to-soil shearing mode, accounting for the high ratio. Increasing the normal load forced the soil to slide on the metal surface and a constant ratio of peak stresses is achieved.

The nonlinear shear stress-displacement behavior shown in Figs. 4-9 and 4-10 may be conveniently represented by a rectangular hyperbola, Eq. (2.32), repeated here for convenience:

FIGURE 4-9 SHEAR STRESS (τ) VS SHEAR DISPLACEMENT (Δ_s) PLOTS OF THE KAOLINITE CLAY DIRECT SHEAR TESTS

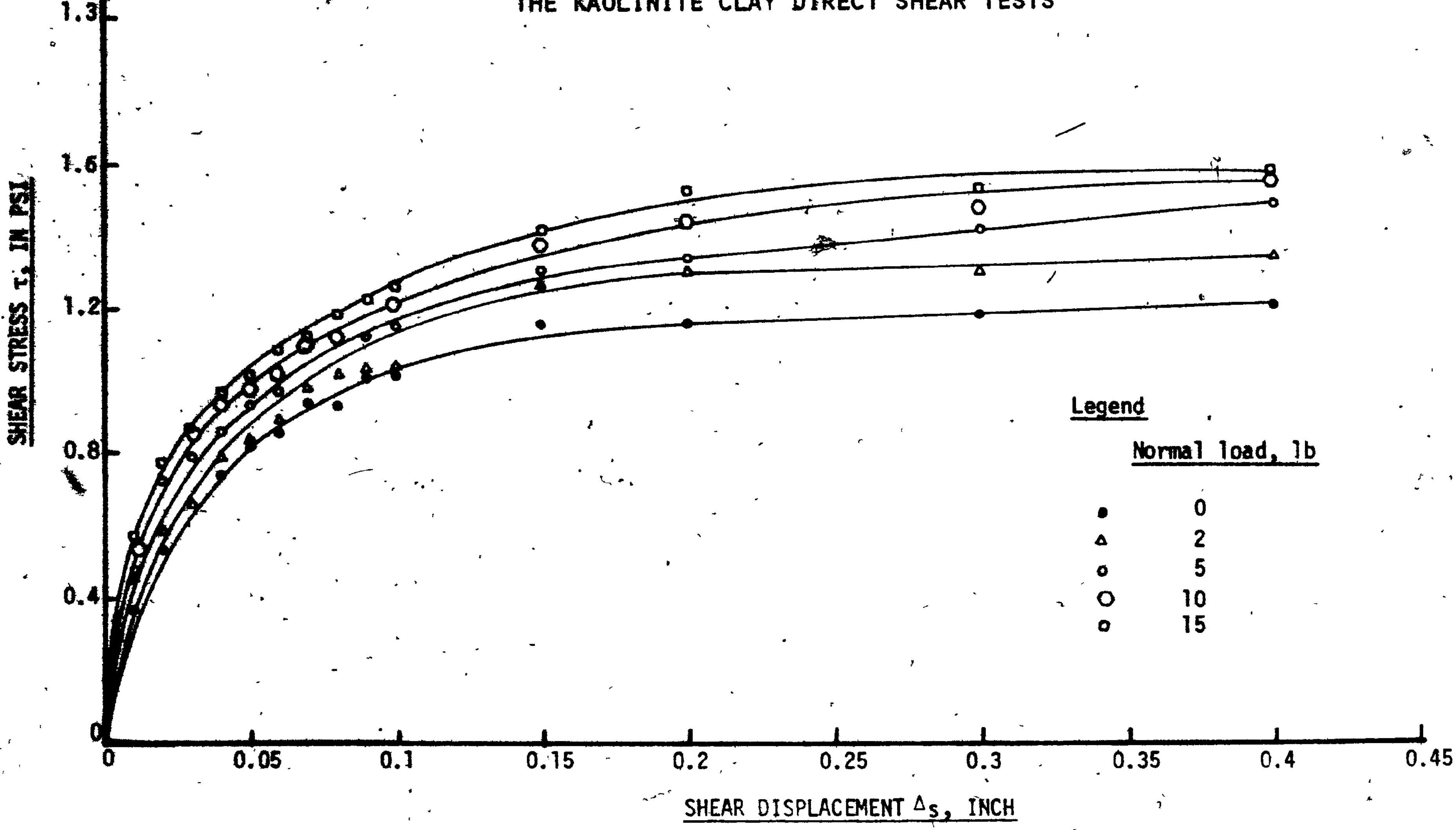

FIGURE 4-10 SHEAR STRESS (τ) VS SHEAR DISPLACEMENT (Δ_s) PLOTS OF THE KAOLINITE-METAL INTERFACE TESTS

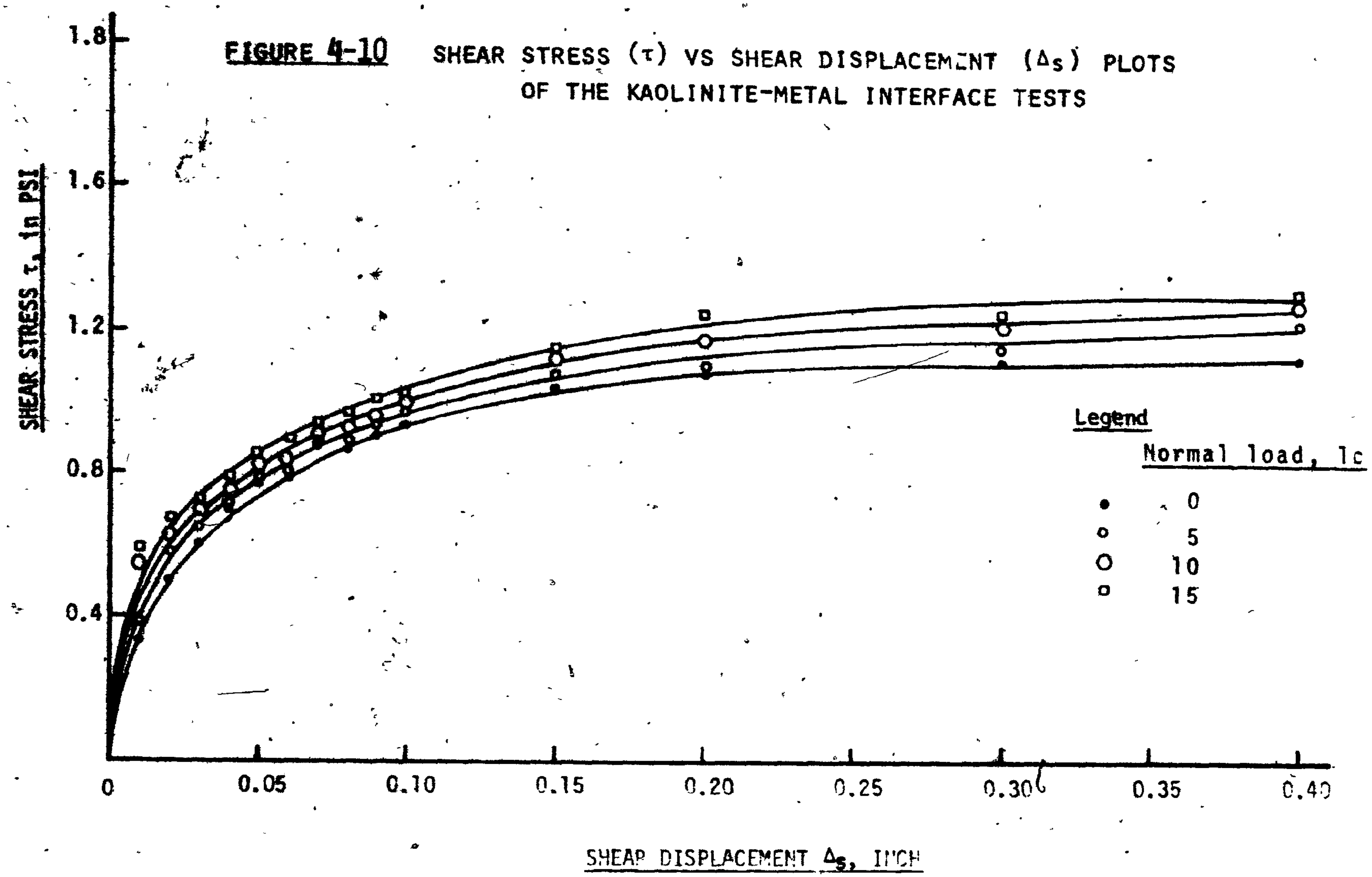

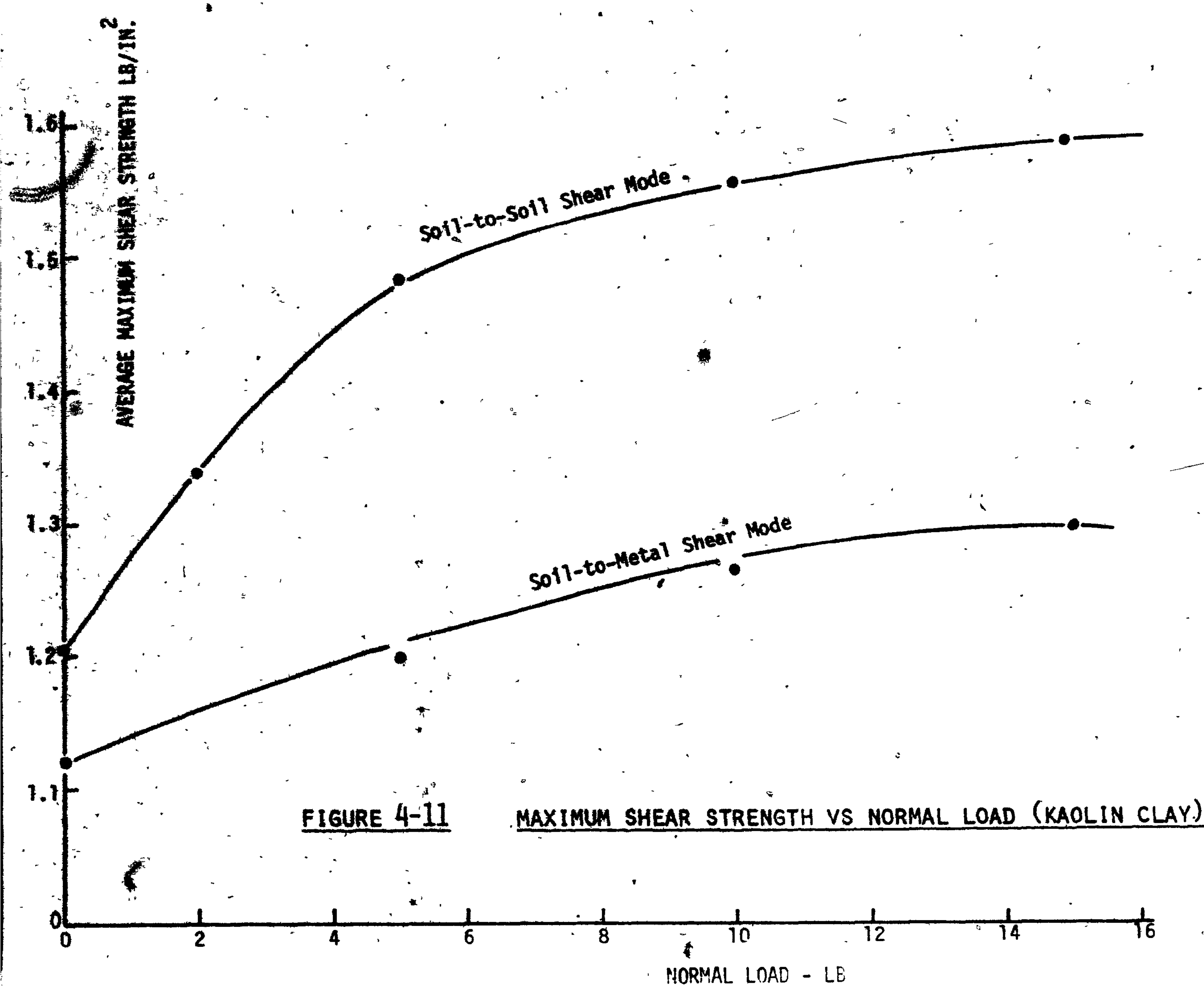

FIGURE 4-11 MAXIMUM SHEAR STRENGTH VS NORMAL LOAD (KAOLIN CLAY)

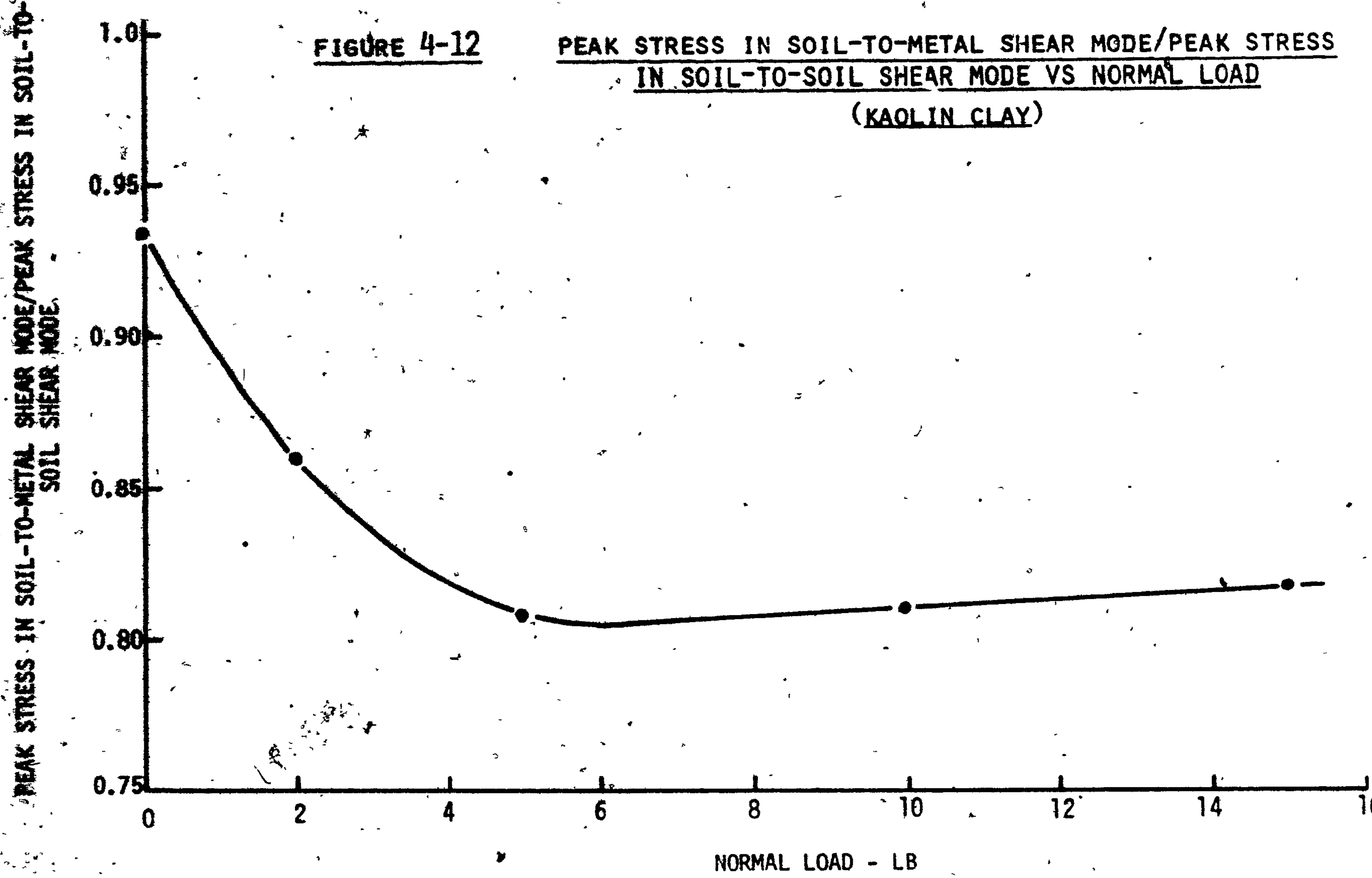

FIGURE 4-12
PEAK STRESS IN SOIL-TO-METAL SHEAR MODE/PEAK STRESS IN SOIL-TO-SOIL SHEAR MODE VS NORMAL LOAD
(KAOLIN CLAY)
PEAK STRESS IN SOIL-TO-METAL SHEAR MODE/PEAK STRESS IN SOIL-TO-SOIL SHEAR MODE
1.0
0.95
0.90
0.85
0.80
0.75
0
2
4
6
8
10
12
14
16
NORMAL LOAD - LB

$$\tau = \frac{\Delta_s}{a + b\Delta_s}$$

where (a) and (b) are parameters whose values depend on the material tested and the normal stresses applied (the symbols in the above equation are defined in Chapter 2). As explained earlier, the above equation can be simplified by expressing Δ_s/τ as a linear function of Δ_s, which would enable direct evaluation of the parameters (a) and (b) as depicted in Fig. 2-8. The linear form of Eq. (2.32) is given as Eq. (2.33) and repeated here:

$$\frac{\Delta_s}{\tau} = a + b\Delta_s$$

where (a) is the intercept and (b) is the slope of the line. Thus by plotting the experimental data in the transformed form, the corresponding values of (a) and (b) are easily obtained. The results of Figs. 4-9 and 4-10 plotted in the transformed form are shown in Fig. 4-13 for the soil-to-soil mode, and in Fig. 4-14 for the soil-to-metal mode. As can be seen, the observed points can be approximated by a straight line for any applied normal load and, therefore, the assumption of a hyperbolic shear stress-displacement relationship throughout the entire displacement range is valid. Table 4-2 lists the values of the intercept (a) and the slope (b) of the straight line in the transformed plot as obtained from Figs. 4-13 and 4-14

FIGURE 4-13 TRANSFORMED LINEAR HYPERBOLIC PLOTS FOR DIRECT SHEAR TESTS OF THE SOIL-TO-SOIL MODE (Δ_s/τ VS Δ_s FOR KAOLINITE CLAY)

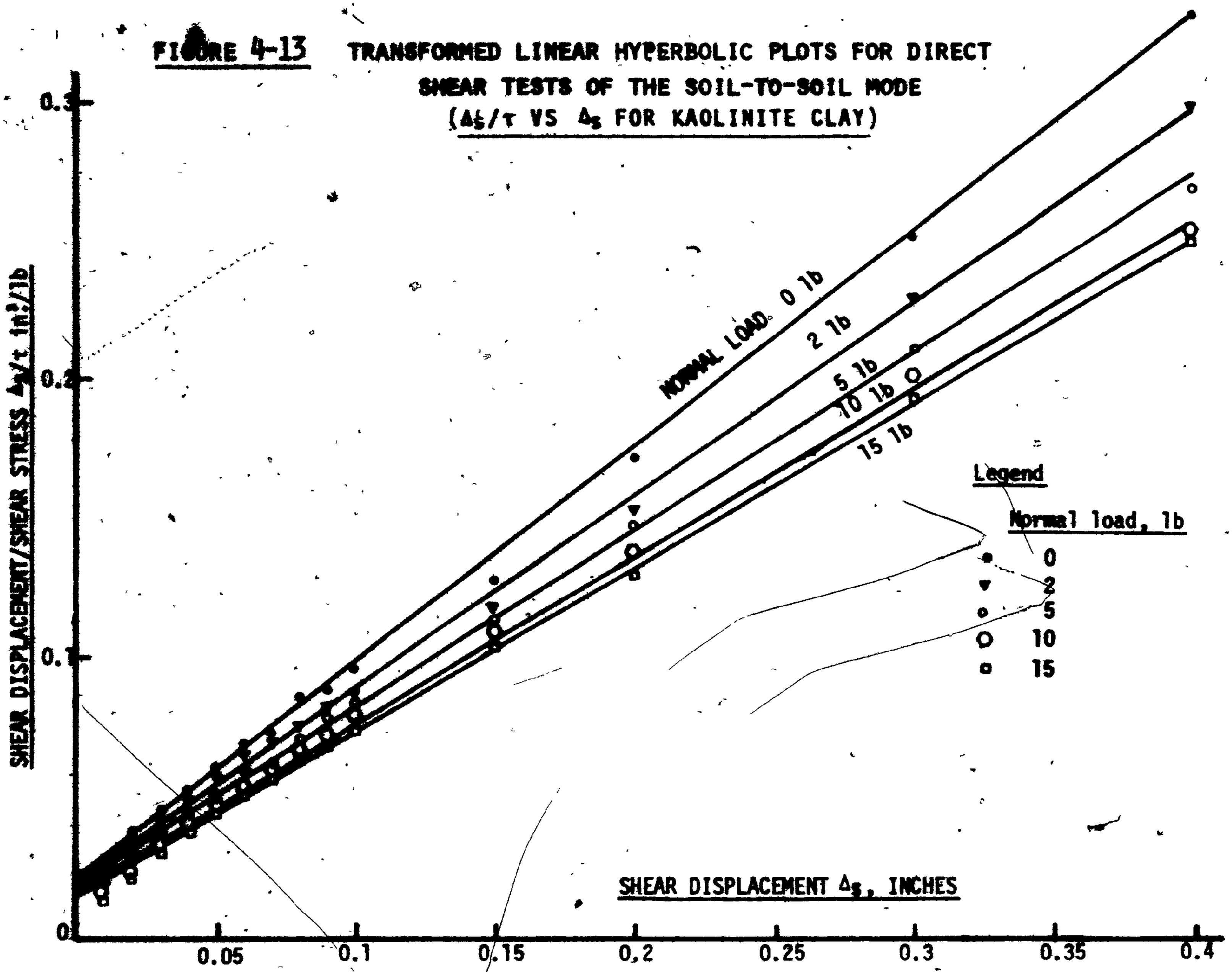

FIGURE 4-14 TRANSFORMED LINEAR HYPERBOLIC PLOTS FOR DIRECT SHEAR TESTS OF THE SOIL-TO-METAL MODE (Δ_s/τ VS Δ_s FOR KAOLINITE-METAL INTERFACE)

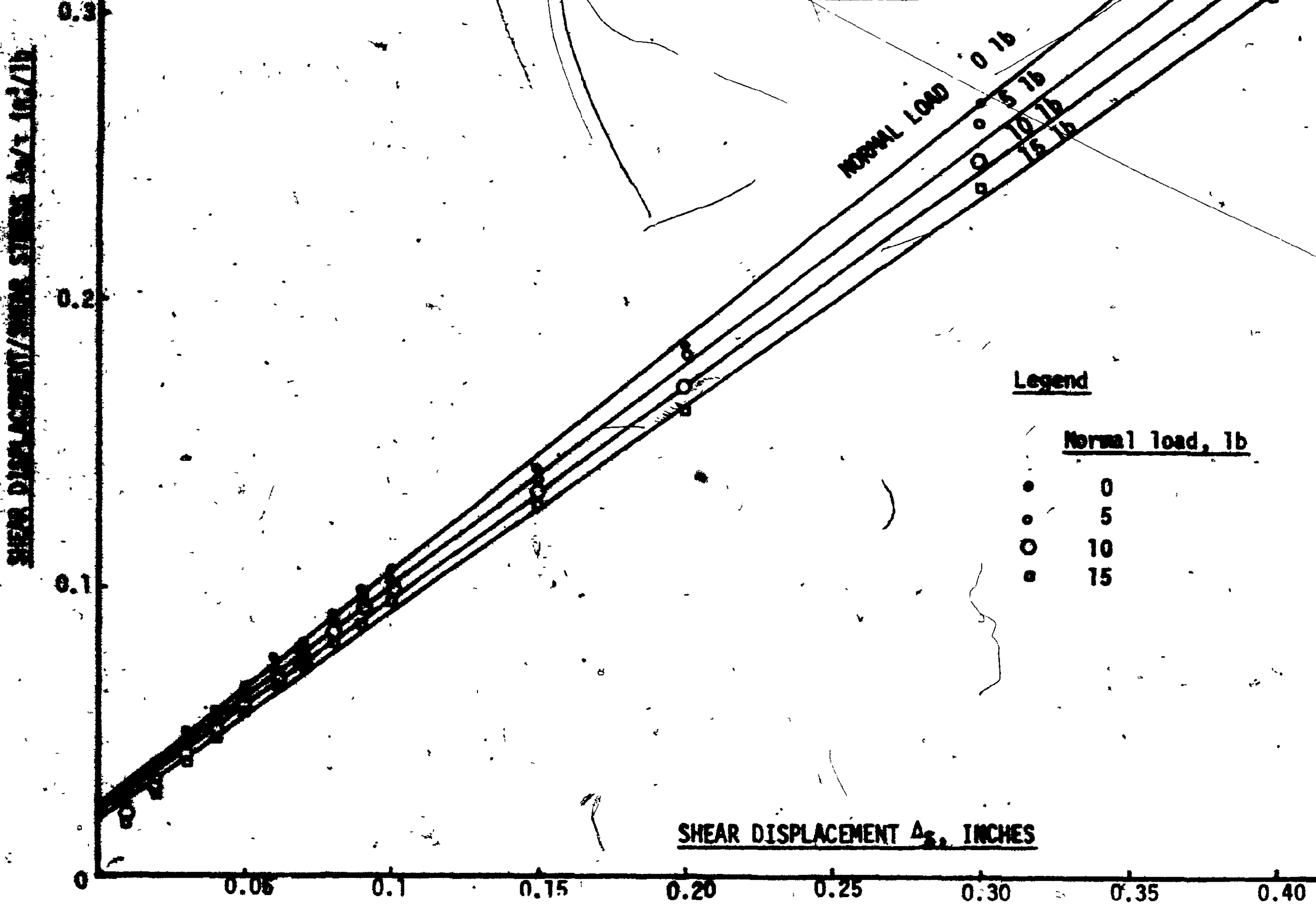

TABLE 4-2

PARAMETERS (a) AND (b) FOR THE CASES OF SOIL-TO-SOIL AND SOIL-TO-METAL SHEAR MODES

NORMAL LOAD	0 lb	2.0 lb	5.0 lb	10 lb	15 lb
Soil-to-soil mode	a = 0.022 b = 0.78	0.02 0.695	0.0185 0.64	0.017 0.60	0.015 0.59
Soil-to-Metal mode	a = 0.025 b = 0.81	- -	0.024 0.77	0.023 0.75	0.02 0.72

SECTION B - EXPERIMENTAL ANALYSIS

4.B.1 APPLICATION OF THE METHOD OF VISIOPLASTICITY TO THE PRESENT PROBLEM

In an interaction study, it is reasoned that the forcing function [i.e. blade or grouser load pattern] and the response function [i.e. soil response behavior] are suitably related and modified through some correlating function. Thus, if one can describe or evaluate the response function characteristics, and if the correlation functions are known, it becomes obvious that the surficial load parameters will be identified and accounted for.

In view of the differences in the deformation processes occurring in the faces of various cutting and traction tools, a solution must be sought in terms of a common parameter which will be relatively unaffected by the geometrical changes in the deformation fields and boundary conditions. The energy fields existing in these deformation processes represent a parameter common to all systems. Moreover, this parameter is a scalar quantity and as such the work output of two dissimilar systems, exhibiting differences in their stress fields and boundary conditions, can be compared without explicit account being taken of these differences.

Experience has shown that the soil response to an imposed loading can be described in terms of the conservation of energy of the system. Results reported by Yong and Webb (1969) indicate that the application of this principle to the rigid wheel-soil system allows for good predictions of the useful work output or drawbar-pull. A similar philosophy can be adopted for the tool-soil system. In this case, the statement of the conservation of energy will be of the form:

$$\int_s F\,ds = D + I \qquad (4.2)$$

or Work Input = Deformation energy loss + Interfacial energy loss

where

F = applied load or developed force

s = distance travelled.

Unlike the wheel-soil interaction problem, there appears to be very little slip energy [interfacial energy] loss vis-a-vis tool-soil interfacial performance [slip loss in a track system however still exists]. Thus, in terms of analytic modelling, the prime requirement is in regard to a proper description of the deformation energy loss.

In order to describe the dissipation process associated with the plastic deformation of the soil in the face of a cutting or a traction tool, the following field equations are necessary:

(a) a yield criterion describing the stress state existing in the soil at yield,

(b) a constitutive relationship between the stress and associated strain in the loaded soil, and

(c) continuity conditions.

The lack of an applicable load-deformation relationship relating the stresses and strains in the soil necessitates the use of empirical relationships in order to calculate the operative stress and energy fields.

Moreover, with the knowledge that clays undergo or sustain irrecoverable deformation under very small applied loads, and according to the definition of yield [i.e. onset of irrecoverable deformation], yielding therefore may be considered to begin virtually at the onset of shear stressing and continues throughout the loading process [Yong and Warkentin (1966)]. For the above two reasons, it may not be unreasonable to assume the material to follow a rigid perfectly-plastic model. This model was adopted by Yong and Webb (1969) in studying the plastic deformation of clay soil under the action of a moving rigid wheel, and by Sylvestre-Williams (1973) in analyzing the energy dissipation in indenter-soil systems. This model demands the following conditions:

(a) the application of a yield criterion,

(b) the measurement of a deformation field from experiments and calculations of the resultant strain rate fields within the loaded soil, and

(c) selection of plasticity flow rules consistent with the choice of the yield criterion.

An examination of these requirements suggests that the method of visio-plasticity is directly applicable to the present problem. The method, as developed by Yang and Thomsen (1953) and reported by Thomsen et al. (1965), is described in Fig. 4-15. It is apparent that the theoretical development permits the calculation of the plastic work rate, and hence the deformation energy, either directly or by means of a prior determination of the stress distribution within the soil. These two paths are denoted as (1) and (2) in Fig. 4-15. The subsequent theoretical development follows the former path.

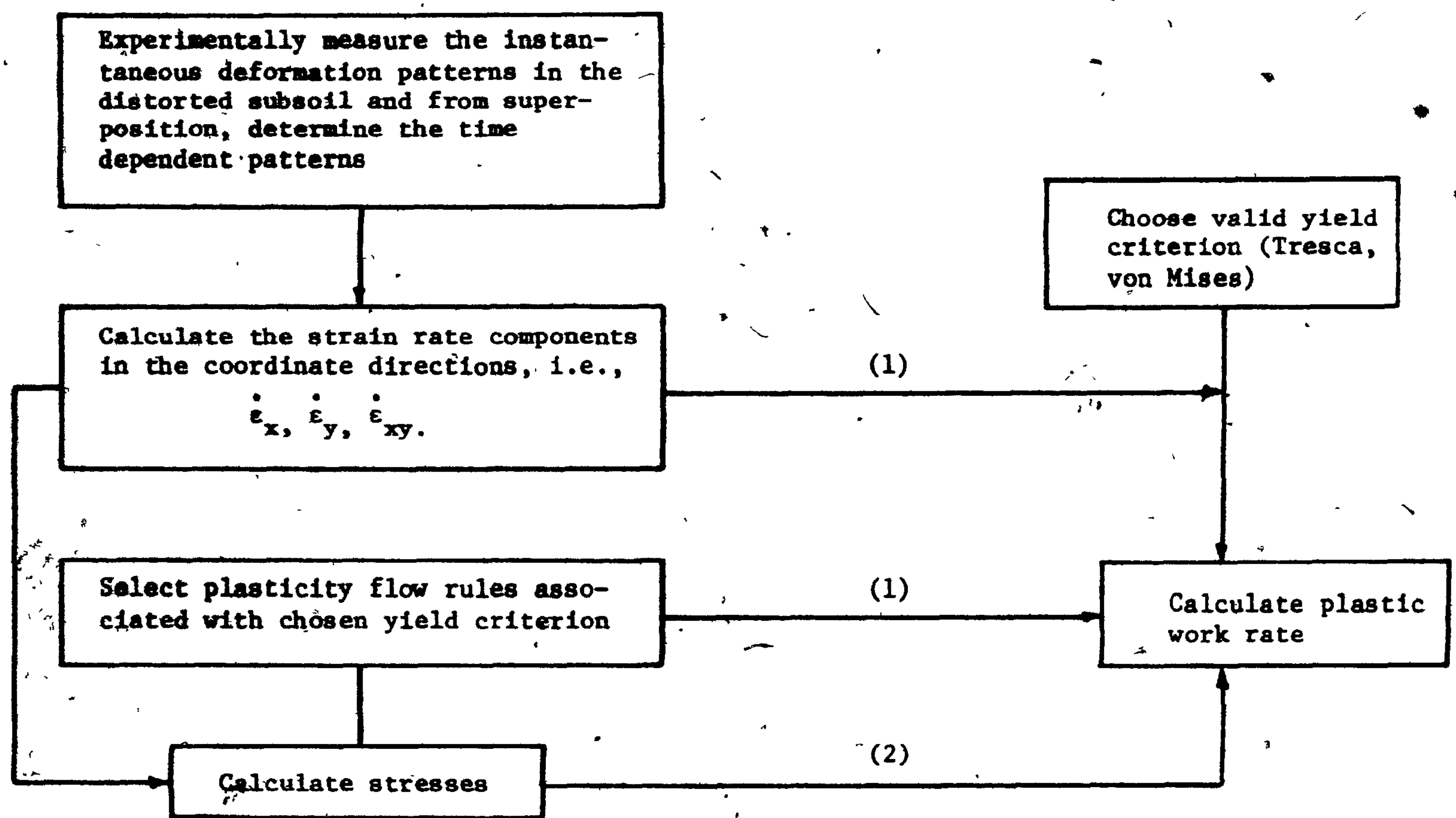

FIGURE (4-15) FLOW DIAGRAM OF METHOD OF VISIOPLASTICITY

In the next several subsections, the various elements shown in Fig. 4-15 will be developed separately.

4.B.1.1 Definition of Strain Rate Components

In order to follow the deformation history of a given point, one of two coordinate systems may be used. The first of these, the Lagrangian space, describes the instantaneous particle location in terms of its original position. The second system, known as the Eulerian description, specifies the particle position in terms of its current coordinates. Thus, for a point with initial coordinates $[a_1, a_2, a_3]$ moving to new coordinates $[x_1, x_2, x_3]$ in time t, a Lagrangian description would be of the form:

$$x_i = \overline{x}_i(a_1, a_2, a_3, t)$$

where $\overline{x}_i$ are single-valued continuous functions. The Eulerian description would use $[x_1, x_2, x_3]$ and the time, t, as independent variables [Fung (1965)].

In the present instance, the incremental velocities and strain rates are more readily determined if expressed in terms of the original coordinates of any given point rather than as a function of the instantaneous position of that point. As a result, a Lagrangian space is selected, in preference to an Eulerian space, as a means of following the deformation history of a selected point.

In terms of Cartesian coordinates within this space, the strain rate components are written as:

$$\dot{\varepsilon}_x = \frac{\partial u}{\partial x} + \tfrac{1}{2}\left[\left(\frac{\partial u}{\partial x}\right)^2 + \left(\frac{\partial v}{\partial y}\right)^2\right]$$

$$\dot{\varepsilon}_y = \frac{\partial v}{\partial y} + \tfrac{1}{2}\left[\left(\frac{\partial u}{\partial x}\right)^2 + \left(\frac{\partial v}{\partial y}\right)^2\right] \qquad (4.3)$$

$$\dot{\varepsilon}_{xy} = \tfrac{1}{2}\left(\frac{\partial u}{\partial y} + \frac{\partial v}{\partial x}\right) + \tfrac{1}{2}\left(\frac{\partial u}{\partial x} \cdot \frac{\partial u}{\partial y} + \frac{\partial v}{\partial x} \cdot \frac{\partial v}{\partial y}\right)$$

where

$u = \frac{dx}{dt}$ = instantaneous particle velocity in the X-coordinate direction.

$v = \frac{dy}{dt}$ = instantaneous particle velocity in the Y-coordinate direction.

It has been noted [Thomsen et al. (1965), Mendelson (1968)] that if the derivatives of the velocity components shown in Eqs. (4.3) are small, the strain rate components may be approximated by Cauchy's infinitesimal strain rate tensor, given in plane strain as :

$$\dot{\varepsilon}_x = \frac{\partial u}{\partial x}$$

$$\dot{\varepsilon}_y = \frac{\partial v}{\partial y} \qquad (4.4)$$

$$\dot{\varepsilon}_{xy} = \tfrac{1}{2}\left(\frac{\partial u}{\partial y} + \frac{\partial v}{\partial x}\right)$$

Thomsen et al. (1965) have shown that the possible error of estimate involved in neglecting the quadratic terms of Eqs. (4.3) is of the order of 0.5% per 1% increase of strain rate. The strain rates encountered in the present study are sufficiently small to ensure that the errors involved in the estimation of the strain rate fields are of acceptable magnitude [of the order of 1%]. As a result, Eqs. (4.4) are used in preference to Eqs. (4.3). By means of these relations the strain rate distributions within the loaded soil mass can be obtained from the experimentally measured deformation patterns.

4.B.1.2 Selection of a Yield Criterion

In the present study, the soil is assumed to form a part of an undrained system, in the light of the rapid load application. As a consequence, the loaded soil, assumed to be saturated, will show no dependence on the mean normal stress [Yong and Warkentin (1966)] and it can further be assumed that the behavior will be entirely cohesive with $\phi = 0$, i.e. a total stress analysis is valid.

Invoking these assumptions requires that the material exhibit no permanent volume change effects on load application. The similarity between this type of soil behavior and the behavior of ductile metals has been pointed out by several investigators [Haythornthwaite (1963), Bishop and Henkel (1957) and Abbott (1966)]. Consequently, in view of the widely successful application of the von Mises yield criterion in the field of metal plasticity, it is reasonable to assume that the stress state in the loaded soil, at yield, is adequately described by this condition.

The von Mises theory [also associated with Hencky] assumes that yielding occurs when the distortion energy equals the distortion energy at yield in simple tension and is expressed as:

$$\tfrac{1}{2}[(\sigma_1 - \sigma_2)^2 + (\sigma_2 - \sigma_3)^2 + (\sigma_3 - \sigma_1)^2] = \sigma_o^2 \qquad (4.5)$$

where

σ_o = yield stress in simple tension.

Owing to the difficulty of conducting simple tension tests on soils, σ_o has generally been defined as the yield stress in compoession, in soil mechanics [Webb (1969)]. Equation (4.5) may then be rewritten as:

$$\frac{1}{6}[(\sigma_1 - \sigma_2)^2 + (\sigma_2 - \sigma_3)^2 + (\sigma_3 - \sigma_1)^2] = \frac{1}{3}\sigma_o^2 \qquad (4.6)$$

Equation (4.6) can be also written as:

$$J_2 = \frac{1}{3}\sigma_o^2$$

$$= k^2 \qquad (4.7)$$

where J_2 is the second invariant of the stress deviator tensor and the scalar constant k may be identified as the yield stress in pure shear [Mendelson (1968)].

The magnitudes of the actual volume changes encountered in the test programme are presented in Section [4.B.3]. It will then be apparent that they are small enough so as not to invalidate the assumptions.

4.B.1.3 Selection of Associated Plasticity Relations

The Lévy-Mises equations of plasticity have been shown to be valid for ductile materials where the elastic component of the strain increment vector is of negligible magnitude [Hill (1950) and Mendelson (1968)]. The equations are given as:

$$d\epsilon_{ij} = d\lambda\, \sigma_{ij} \tag{4.8}$$

where $d\lambda$ is a non-negative scalar constant which may vary throughout the loading history and which relates the strain increment vector to the gradient of the loading surface defined by the yield function:

$$f(J_2, J_3) = 0 \tag{4.9}$$

Similar equations may be derived from the relationship between the strain rate vector and the instantaneous value of the stress deviation, viz:

$$\dot{\epsilon}_{ij} = \dot{\lambda}\, \sigma'_{ij}$$

In unabridged notation, under conditions of plane strain, the Lévy-Mises equations are written as:

$$\begin{aligned} \dot{\epsilon}_x &= \dot{\lambda}\, \sigma'_x \\ \dot{\epsilon}_y &= \dot{\lambda}\, \sigma'_y \\ \dot{\gamma}_{xy} &= 2\, \dot{\lambda}\, \tau_{xy} \end{aligned} \tag{4.10}$$

where

$$\dot{\gamma}_{xy} = 2\, \dot{\epsilon}_{xy} = \left(\frac{\partial u}{\partial y} + \frac{\partial v}{\partial x}\right)$$

represents the total shear distortion experienced by any point within the deforming sample.

It can be readily shown [Mendelson (1968)] that the compliance $\dot{\lambda}$ is given by:

$$\dot{\lambda} = \frac{3}{2} \cdot \frac{\bar{\dot{\epsilon}}}{\bar{\sigma}} \tag{4.11}$$

where $\bar{\dot{\varepsilon}}$ and $\bar{\sigma}$ are Hencky effective stress and strain rate parameters given as:

$$\bar{\sigma} = \frac{1}{\sqrt{2}}\left[(\sigma_x - \sigma_y)^2 + (\sigma_y - \sigma_z)^2 + (\sigma_z - \sigma_x)^2 + 6(\tau_{xy}^2 + \tau_{xz}^2 + \tau_{yz}^2)\right]^{\frac{1}{2}}$$

$$= \sqrt{3J_2}$$

$$\bar{\dot{\varepsilon}} = \frac{\sqrt{2}}{3}\left[(\dot{\varepsilon}_x - \dot{\varepsilon}_y)^2 + (\dot{\varepsilon}_y - \dot{\varepsilon}_z)^2 + (\dot{\varepsilon}_z - \dot{\varepsilon}_x)^2 + 6(\dot{\varepsilon}_{xy}^2 + \dot{\varepsilon}_{yz}^2 + \dot{\varepsilon}_{zx}^2)\right]^{\frac{1}{2}}$$

$$= \sqrt{\frac{4}{3} I_2}$$

J_2 and I_2 are the second invariant of the stress deviator tensor and the second invariant of the strain rate tensor, respectively. Combining Eqs. (4.11), (4.10) and (4.7) yields:

$$\begin{aligned} \dot{\varepsilon}_x &= \frac{\sqrt{I_2}}{K}\,\sigma'_x \\ \dot{\varepsilon}_y &= \frac{\sqrt{I_2}}{K}\,\sigma'_y \\ \dot{\gamma}_{xy} &= \frac{2\sqrt{I_2}}{K}\,\tau_{xy} \end{aligned} \qquad (4.12)$$

If reference is made to Fig. 4-15, it can be seen that the theoretical means of specifying the strain rate distributions have now been provided. In addition, a valid yield function, as well as the plasticity equations associated with this yield function, has now been specified. With these elements, it is now possible to develop the equations necessary for the calculation of the plastic work rate and hence of the deformation energy.

4.B.1.4 Plastic Work Rate Determination

The rate at which stresses do work in connection with the plastic distortion of an incompressible material is given as:

$$\dot{W} = \sigma'_{ij}\, \dot{\varepsilon}_{ij} \tag{4.13}$$

The rate of total energy dissipation with the soil is then:

$$\begin{aligned} \dot{D} &= \int_V \dot{W}\, dV \\ &= b \int_{x_1}^{x_2} \int_{y_1}^{y_2} (\sigma'_x \dot{\varepsilon}_x + \sigma'_y\, \dot{\varepsilon}_y + \tau_{xy}\, \dot{\gamma}_{xy})\, dx\, dy \end{aligned} \tag{4.14}$$

in plane strain, where b is the width of the sample under test.

Substituting Eqs. (4.12) into Eqs. (4.14) yields:

$$\begin{aligned} \dot{W} &= [\sigma_x'^2 \sqrt{I_2} + \sigma_y'^2 \sqrt{I_2} + 2\tau_{xy}^2 \sqrt{I_2}]\, \frac{1}{K} \\ &= \frac{\sqrt{I_2}}{k} [\sigma_x'^2 + \sigma_y'^2 + 2\tau_{xy}^2] \end{aligned} \tag{4.15}$$

The second invariant of the stress deviator tensor J_2 can be written for the case of plane strain as:

$$J_2 = \tfrac{1}{2}(\sigma_x'^2 + \sigma_y'^2) + \tau_{xy}^2$$

Equation (4.15) can now be written as:

$$\dot{W} = 2k\sqrt{I_2} \tag{4.16}$$

and by integration in time, the total work done, and hence the energy dissipated in accomplishing plastic deformation, is found to be:

$$D = 2b\int_{t_1}^{t_2}\int_{x_1}^{x_2}\int_{y_1}^{y_2} k\sqrt{I_2}\,dx\,dy\,dt \tag{4.17}$$

Equation (4.17) is sufficient to calculate the deformation energy component of the total energy in the tool-soil system, provided that the deformation fields within the loaded soil sample are experimentally specified.

4.B.2. DATA REDUCTION TECHNIQUE

Accepting that the proposed visioplasticity solution is a valid one, it becomes necessary to obtain data in an expedient and accurate manner in order to satisfy the theoretical requirements. The system of data retrieval used to reduce the experimental results of the soil cutting and traction tests required the manual plotting of the sequential positions of a number of grid nodes from projected 35 mm negative slides. Figure 4 -16 shows particle path trajectories [translation patterns] for a R.A.P.G. - soil interaction process. The coordinate pairs corresponding to each of the plotted points were then obtained with the aid of an x-y recorder and a process control computer. The resulting data were input to a computer routine, listed in Appendix E as program "FIT". With this routine, the corrected particle

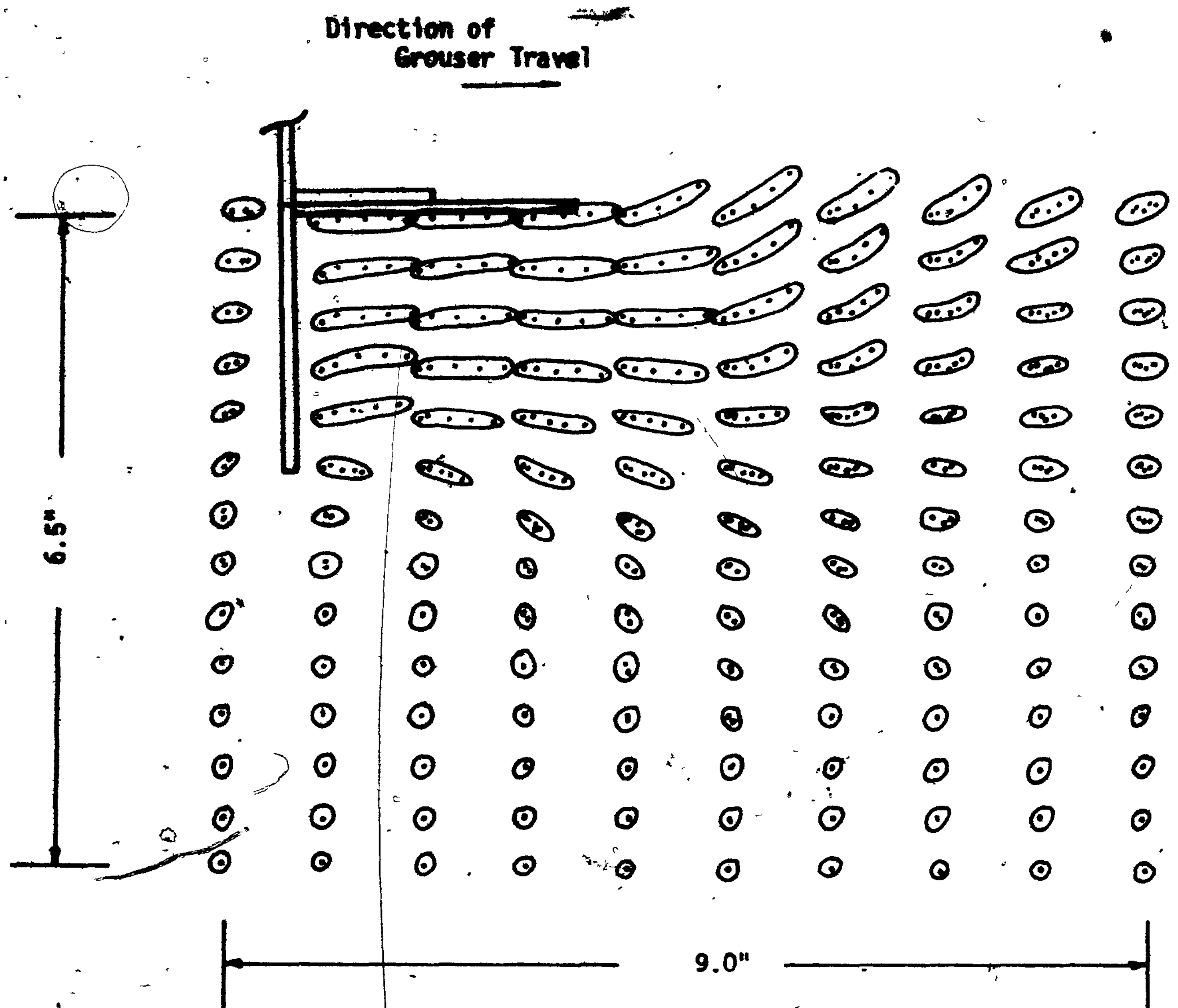

FIGURE 4-16 SUPERPOSED POSITIONS OF GRID NODES OF PLATE GROUSER (R.A.P.G.) TEST

coordinates, the incremental particle velocities, the instantaneous strain rate components and the rate of plastic energy dissipation were calculated. A schematic of the procedure used in the calculation is shown in Fig. 4-17.

An examination of Fig. 4-17 will show that the developed procedure provides a rapid and expedient means of obtaining data from the measured experimental results. A more comprehensive account of the data reduction technique is provided in Appendix B.

4.B.3. NO VOLUME CHANGE ASSUMPTION

The assumptions and constraints inherent in the visioplasticity technique have been discussed in Section 4.B.1. It was noted that an essential requirement of the theory is that the soil exhibits no permanent volume change characteristics when loaded. As a means of verifying the validity of this assumption, the actual volume changes occurring during the tests were obtained from the experimentally measured tool-soil deformation fields. In order to obtain the required data, the principle of conservation of mass was applied to elemental areas within the deforming field. These elements were each defined by four adjacent node points of the inscribed grid and were followed throughout the deformation history of the four relevant points. The method is shown schematically in Fig. 4-18.

Application of the principle of conservation of mass to these areas results in:

$$\rho_1 A_1 = \rho_2 A_2 = \rho_3 A_3 \qquad (4.18)$$

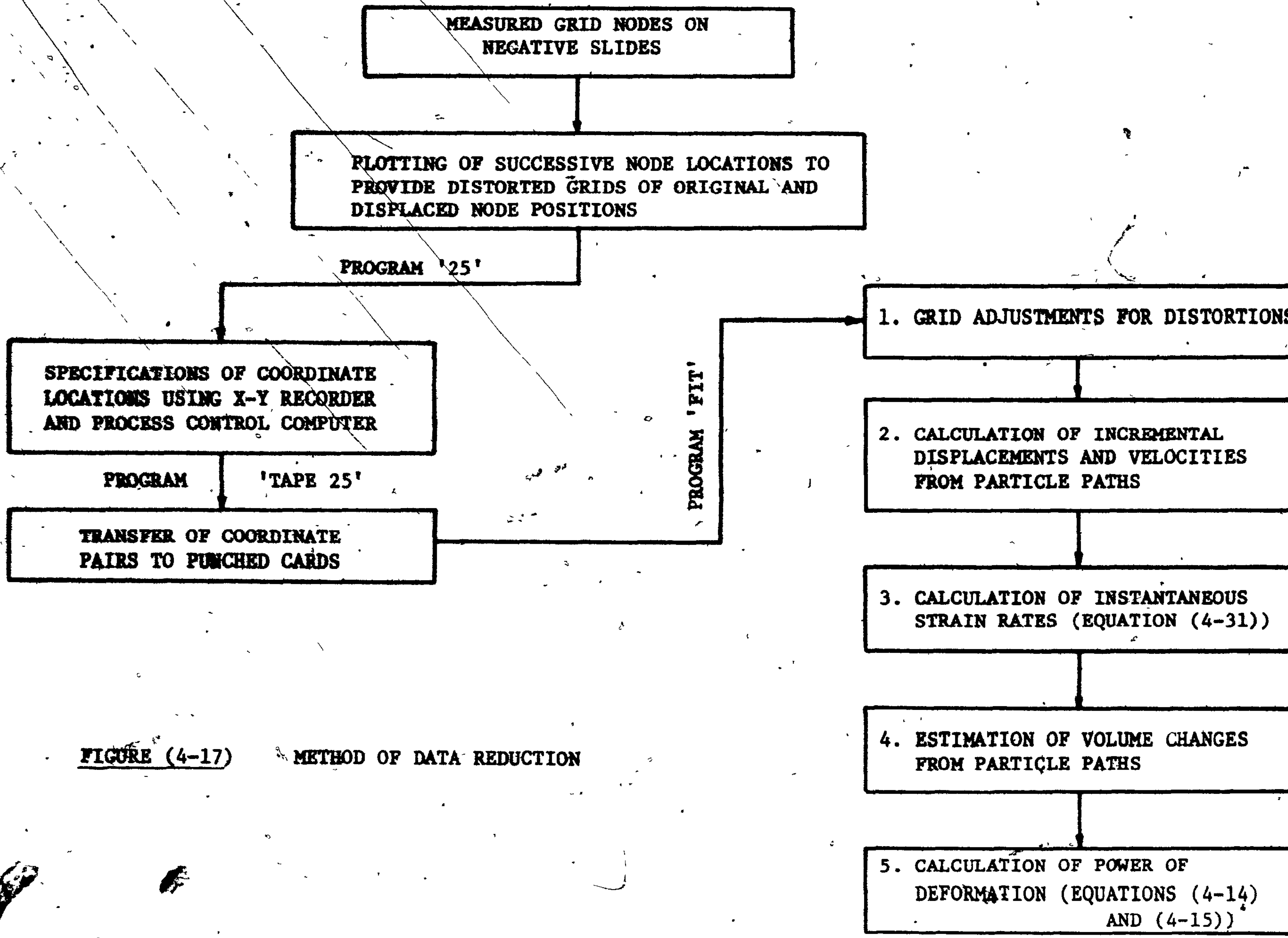

FIGURE (4-17) METHOD OF DATA REDUCTION

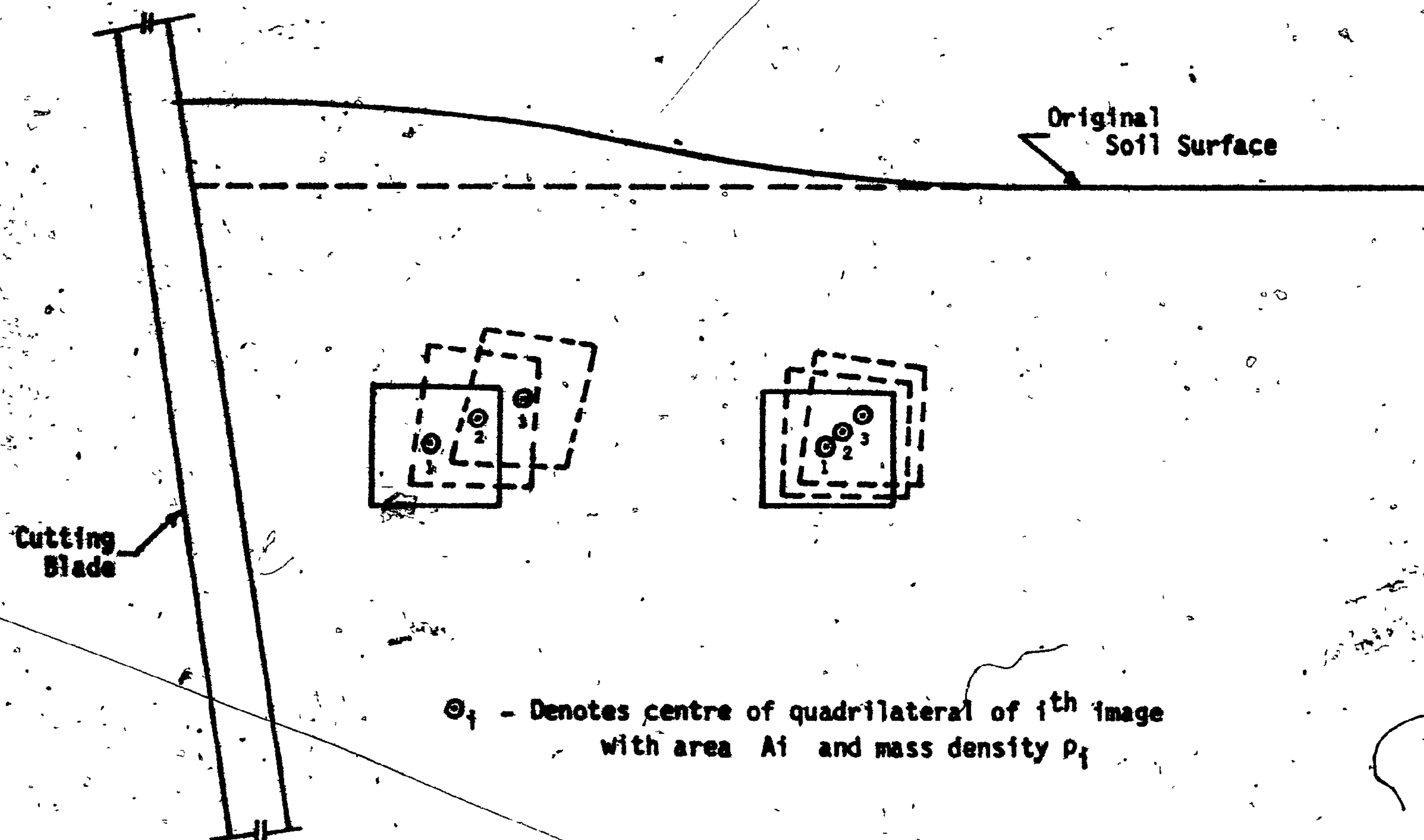

$\odot_i$ - Denotes centre of quadrilateral of i^{th} image with area A_i and mass density ρ_i

FIGURE 4-18 CALCULATION OF DENSITIES AT SUCCESSIVE IMAGE POSITIONS FOR A CUTTING BLADE

Equation (4.18) can also be written as:

$$\frac{\rho_i}{\rho_j} = \frac{A_j}{A_i} \tag{4.19}$$

where

ρ_i = mass density or specific mass of the ith elemental area.

A_i = area of the ith element.

Machine computation of the areas, carried out by program "FIT" shown in Appendix E, allowed for a comparison of the mass densities of the deforming soil through successive grid positions. The results of these computations are shown in Table 4-3 for the various kaolinite clay tests performed.

The permanent volume distortions reported are in terms of the average value over the entire deforming field, throughout the deformation process. Evidently, the average values do not necessarily reflect the magnitude of the peak local values since positive and negative values may tend to compensate each other. In Fig. 4-19, the volume changes computed indicate local volume changes up to five per cent. In the final analysis, however, the overall influence of the volume change on the exhibited behavior of the tool-soil system is a function of the entire deforming field and, consequently, the average values reported in Table 4-3 should be representative of this influence. In view of this, the small values reported here - of the order of two per cent - imply that the constant volume assumption invoked in the theoretical development is a justifiable one.

TABLE 4-3

VOLUME CHANGES
Natural (Kaolinite) Clay

Tool	Test No.	Average Volume Change %
10° Blade	27	- 0.57
	30	0.45
20° Blade	28	0.89
	35	1.05
40° Blade	26	- 0.69
	36	1.25
50° Blade	29	0.78
	31	0.90
Plate Grouser (R.A.P.G.)	32	2.01
	37	- 0.99
S.E.W. Grouser	33	0.77
	38	0.91
C.E.W. Grouser Type (2)	34	1.52
	39	- 0.71

Notes:
(1) Positive volume changes denote dilation.
(2) Negative volume changes denote compression.
(3) Average values represent the algebraic average over four images.

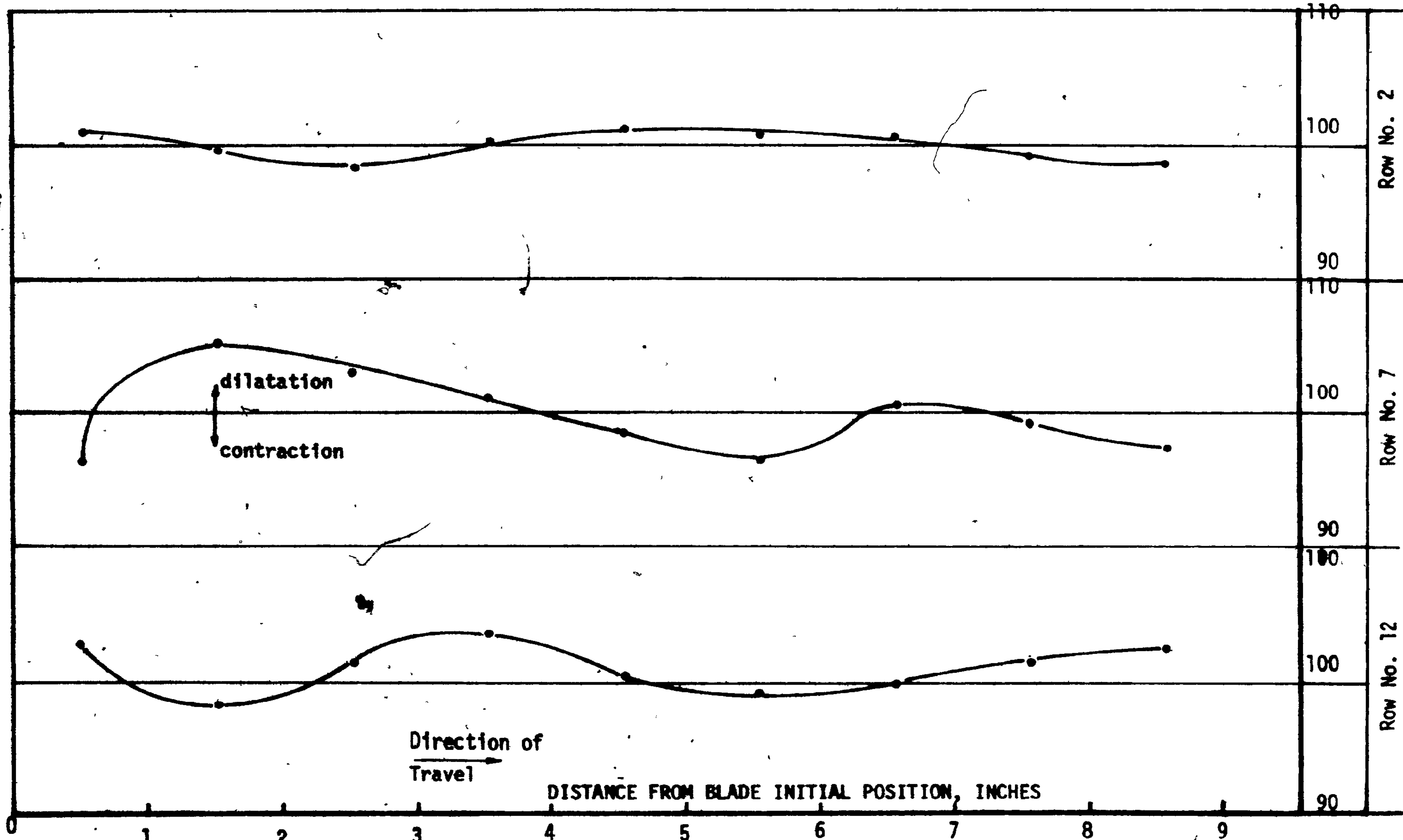

FIGURE 4-19 VOLUME CHANGE CALCULATED FROM GRID POSITIONS IN A CUTTING TEST FOR BLADE DISPLACEMENT OF 0.50 INCH. (CURRENT VOLUME IN PERCENTAGE OF ORIGINAL)

4.B.4. DETERMINATION OF THE LIMITING SHEAR STRESSES

The strength parameter, k, is defined in Eq. (4.7), viz:

$$J_2 = k^2$$

Here J_2 is the second invariant of the stress deviator tensor and the above equation can be written in detail as:

$$J_2 = \frac{1}{6}[(\sigma_1 - \sigma_2)^2 + (\sigma_2 - \sigma_3)^2 + (\sigma_3 - \sigma_1)^2] = k^2$$

For the case of plane strain deformation, with no permanent volume change occurring, the intermediate principal stress is given by [Mendelson (1968)]:

$$\sigma_2 = \frac{\sigma_1 + \sigma_3}{2}$$

Use of these two equations, together with the experimentally measured stress-strain curves, permits the calculation of k. An axial strain of 20% was chosen to define failure since no definite peaks were evidenced in the measured stress-strain curves, Figs. 4-7 and 4-8.

4.B.5. PREDICTION OF THE DEFORMATION ENERGY BY VISIOPLASTICITY

The influence of the tool geometry on the energy required for motion is shown in Fig. 4-20 for the cutting blades and in Figs. 4-21 and 4-22 for the R.A.P.G. and the wedge grousers, respectively. The curves represented by solid lines indicate measured values obtained from the integration of the areas beneath the experimentally measured force-displacement curves. In addition, the theoretically calculated values of the dissipation energy are shown for comparative purposes by broken lines. These values were obtained by means of the application of Eq. (4.17) together with the appropriate values of k obtained from the results of the plane-strain triaxial tests as outlined in the previous section. Comparisons of these results with those obtained from the measured force-displacement curves are also shown in Table 4-4 for cutting tests, and in Table 4-5 for traction tests. The comparisons are made in terms of measured and calculated values, referring to those results obtained from experimental curves and by means of Eq. (4.17), respectively, and are reported at 0.25 inch intervals over a displacement of 1.0 inch. The deviations between the two sets of values, expressed as a percentage of the applicable experimental values, are also shown in these Tables.

Examination of these data indicates that the analytical solution, as expressed by Eq. (4.17), provides reasonable estimate of the energy dissipated in the soil for tool displacement in excess of 0.25 inch. For displacements in excess of 0.25 inch, the average error in energy prediction is of the order of ten per cent, while the maximum error is of the order of 20 per cent. However, at 0.25 inch displacement the error of estimate is significant, with an average of 36.5 per cent, while the maximum error is some 75 per cent. These differences can be attributed to errors due to the assumptions made in the determination of the limiting shear stresses. Since no definite peaks were evidenced in the measured stress-strain curves, Figs. 4-7 and 4-8, an axial strain of 20 per cent was chosen to define failure. The stress values corresponding to the failure strain were used to calculate the value of the von Mises yield function, k. While this procedure implies a rigid plastic material, the stress-strain curves, Figs. 4-7 and 4-8, show a

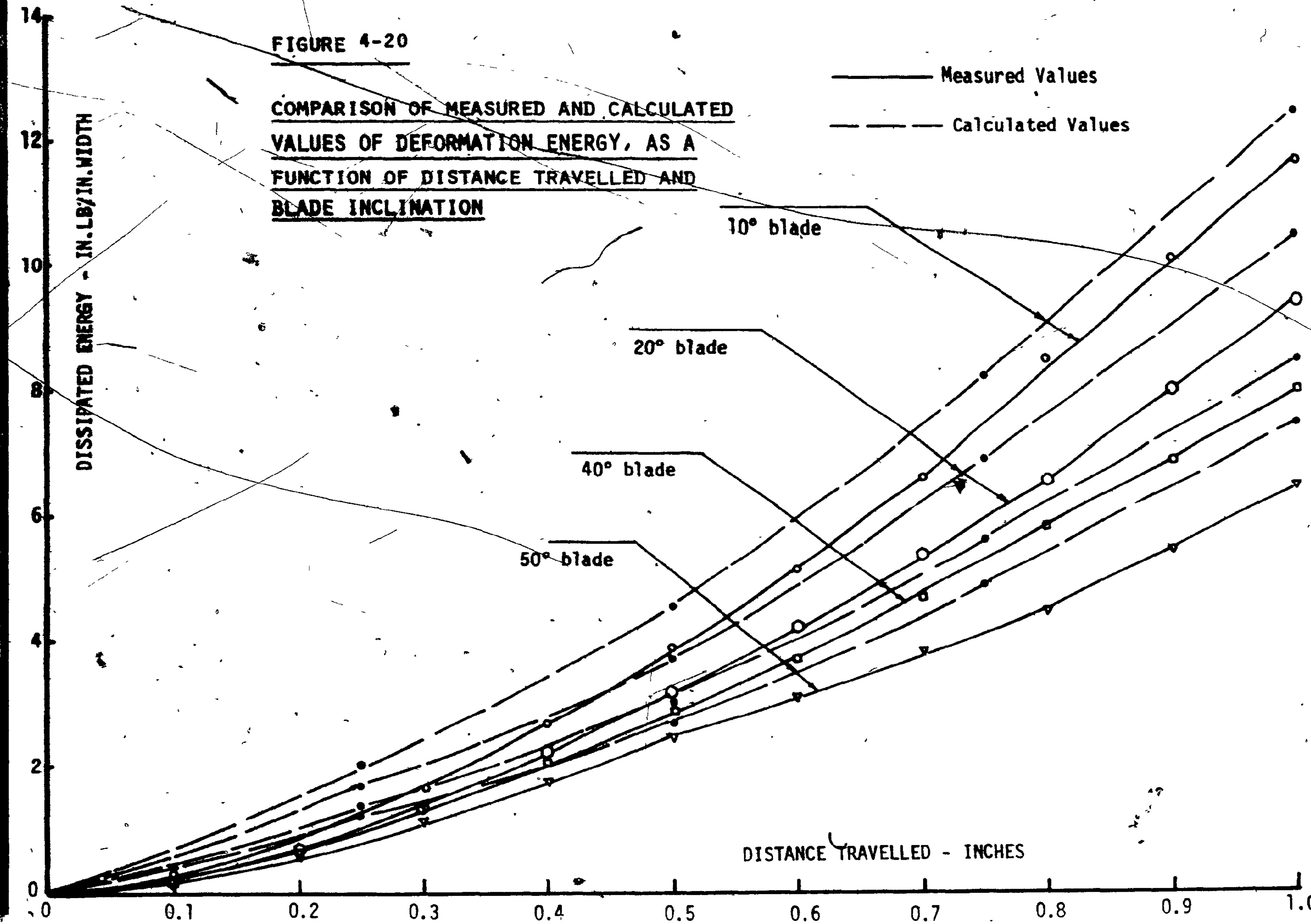

FIGURE 4-20

COMPARISON OF MEASURED AND CALCULATED VALUES OF DEFORMATION ENERGY, AS A FUNCTION OF DISTANCE TRAVELLED AND BLADE INCLINATION

FIGURE 4-21 COMPARISON OF MEASURED AND CALCULATED VALUES OF DEFORMATION ENERGY, AS A FUNCTION OF DISTANCE TRAVELLED AND R.A.P.G. GEOMETRY

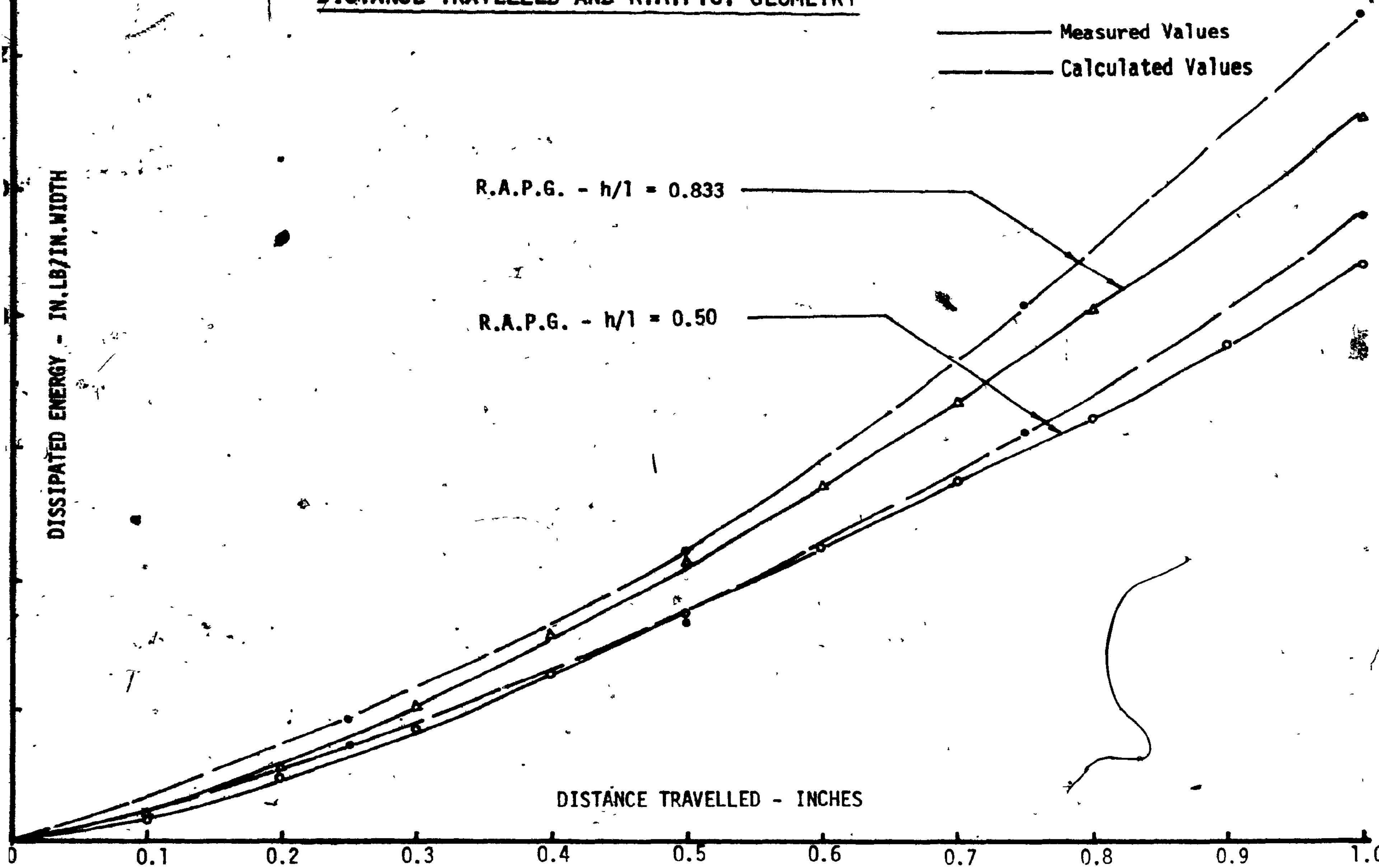

FIGURE 4-22 COMPARISON OF MEASURED AND CALCULATED VALUES OF DEFORMATION ENERGY, AS A FUNCTION OF DISTANCE TRAVELLED AND GROUSER GEOMETRY

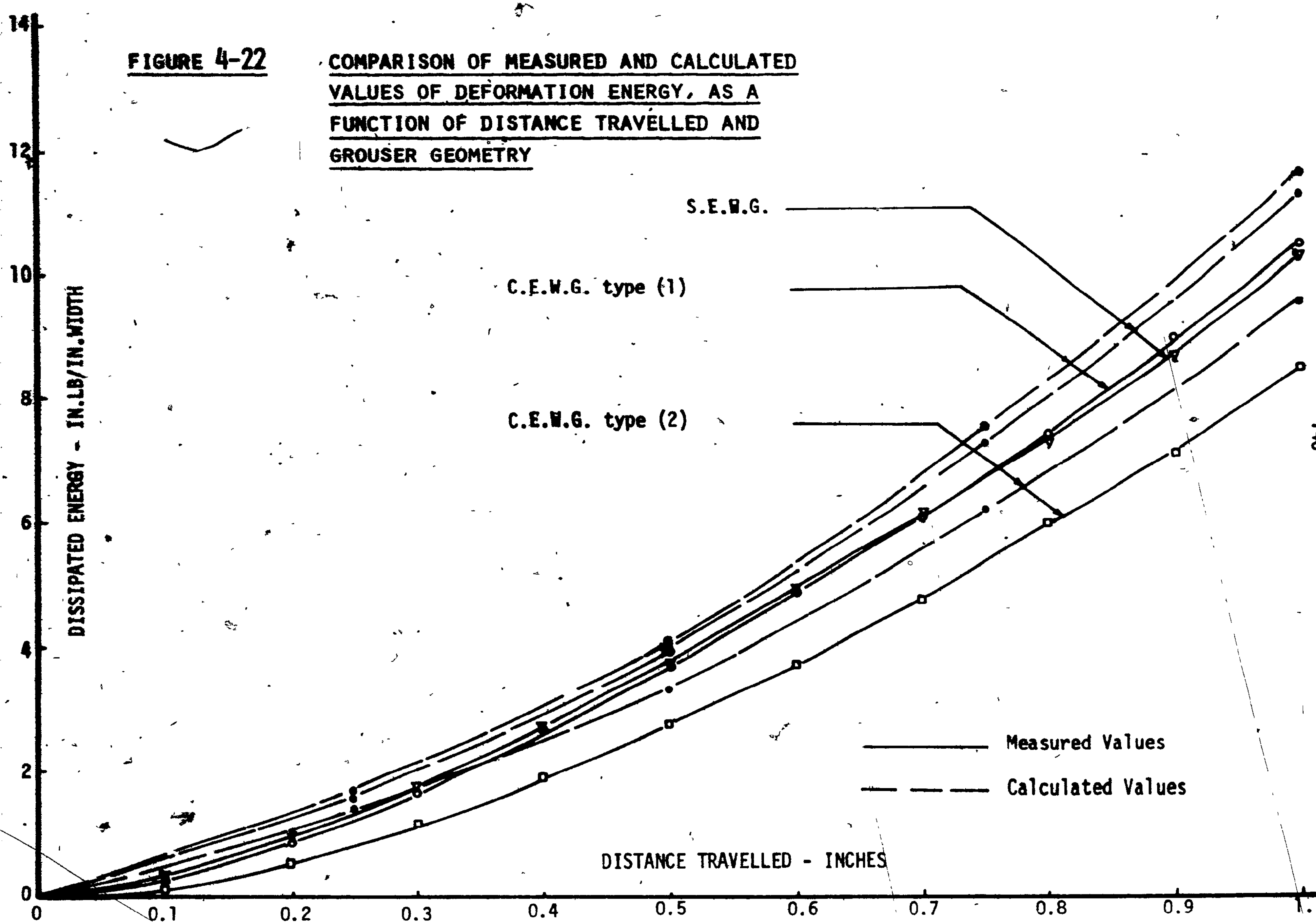

TABLE 4-4

COMPARISON OF MEASURED AND CALCULATED VALUES OF DEFORMATION ENERGY FOR CUTTING TESTS

TEST No.	ANGLE OF BLADE WITH VERTICAL	DEFORMATION ENERGY IN.LB/IN.WIDTH											
		Measured	Calculated	Difference %	Measured	Calculated	Difference %	Measured	Calculated	Difference %	Measured	Calculated	Difference %
		Tool Displacement: d=0.25 inch			d = 0.50 inch			d = 0.75 inch			d = 1.0 inch		
Artificial Clay Tests													
21	10°	1.47	1.90	+29.2	4.05	4.45	+ 9.87	7.03	7.90	+12.3	10.24	11.32	+10.5
12	20°	1.42	1.80	+26.7	3.81	4.1	+ 7.61	6.28	6.68	+ 6.36	9.14	9.816	+ 7.39
23	40°	1.10	1.40	+27.2	2.91	3.2	+ 9.96	5.02	5.48	+ 9.16	7.36	7.99	+ 8.55
22	50°	1.05	1.30	+23.8	2.6	2.9	+11.53	4.3	4.85	+12.7	6.16	6.899	+ 7.39
Natural (Kaolinite) Clay													
27	10°	1.32	1.95	+47.7	3.92	4.60	+17.3	7.65	8.35	+ 9.10	12.05	12.62	+ 4.7
30	10°	1.2	2.05	+70.8	3.86	4.56	+18.1	7.40	8.25	+11.48	11.71	12.50	+ 6.7
28	20°	1.01	1.72	+70.2	3.194	2.83	-11.3	6.0	6.93	+15.5	9.42	10.5	+11.4
35	20°	1.15	1.60	+39.1	3.33	3.61	+ 8.4	6.31	7.00	+10.9	9.55	10.7	+11.4
26	40°	1.061	1.39	+31.0	2.90	3.10	+ 6.9	5.12	5.61	+ 9.57	8.0	8.5	+ 6.25
36	40°	0.97	1.20	+23.71	2.96	3.27	+10.4	5.00	5.60	+12.0	8.3	8.7	+ 4.81
29	50°	0.92	1.23	+33.6	2.436	2.737	+12.3	4.3	4.95	+15.1	6.57	7.50	+14.1
31	50°	0.88	1.17	+32.9	2.65	2.91	+ 9.81	4.1	4.65	+13.4	6.90	7.55	+ 9.42

Notes: (1) Measured values denote values obtained from the experimental force-displacement curves.
(2) Calculated values denote theoretically calculated values obtained from Equation (4.17).
(3) Difference expressed in percentage of measured values.

TABLE 4-5

COMPARISON OF MEASURED AND CALCULATED VALUES OF DEFORMATION ENERGY FOR TRACTION TESTS

TEST No.	GROUSER	DEFORMATION ENERGY IN.LB/IN.WIDTH											
		Measured	Calculated	Difference %	Measured	Calculated	Difference %	Measured	Calculated	Difference %	Measured	Calculated	Difference %
		Tool Displacement: d=0.25 inch			d=0.50 inch			d=0.75 inch			d=1.0 inch		
Artificial Clay Tests													
18	R.A.P.G.h/1=0.83	1.7	2.11	+24.1	4.42	4.67	+10.6	7.21	7.79	+ 8.04	10.03	11.13	+10.9
19	R.A.P.G.h/1=0.5	1.29	1.56	+20.9	3.17	3.12	- 1.5	5.18	5.45	+ 5.2	7.29	7.79	+ 6.85
40	C.E.W.type(1)	0.94	1.33	+41.4	2.99	3.14	+ 5.0	5.5	5.84	+ 6.18	8.2	8.99	+ 9.6
14	C.E.W.type(2)	0.69	1.02	+47.8	2.33	2.56	+ 9.87	4.48	4.76	+ 6.25	6.85	7.33	+ 7.0
16	S.E.W.	0.83	1.15	+38.5	2.69	2.80	+ 4.0	5.02	5.25	+ 4.58	7.55	8.02	+ 6.22
Natural (Kaolinite) Clay													
34	R.A.P.G.h/1=0.83	1.56	1.90	+22.06	4.26	4.445	+ 4.34	7.343	8.255	+12.41	11.14	12.70	+14.00
39	R.A.P.G.h/1=0.5	1.33	1.44	+ 8.27	3.51	3.36	- 4.27	6.015	6.24	+ 3.70	8.85	9.60	+ 8.47
42	C.E.W.type(1)	1.22	1.74	+42.6	3.75	4.07	+ 8.53	6.79	7.56	+11.31	10.57	11.63	+10.0
43	C.E.W.type(1)	1.31	1.8	+37.4	3.65	4.15	+13.6	6.5	7.32	+12.6	10.7	11.33	+ 5.60
33	C.E.W.type(2)	0.821	1.44	+75.3	2.76	3.36	+21.7	5.278	6.24	+18.22	8.57	9.6	+12.0
38	C.E.W.type(2)	0.95	1.34	+41.0	3.1	3.4	+ 9.6	5.91	6.35	+ 7.45	8.70	9.4	+ 8.04
32	S.E.W.	1.31	1.70	+29.8	3.79	3.97	+ 4.74	6.72	7.38	+ 9.82	10.29	11.35	+10.3
37	S.E.W.	1.42	1.79	+26.0	3.4	3.9	+14.7	6.51	7.12	+ 9.37	10.6	11.71	+10.4

<u>Notes</u>: (1) Measured values denote values obtained from the experimental force-displacement curves.
(2) Calculated values denote theoretically calculated values obtained from Equaltion (4.17).
(3) Difference expressed in percentage of measured values.

nonlinear behavior which could be idealized by a work-hardening material. With the adoption of the stress values corresponding to 20 per cent strain, an overprediction of the dissipated energy would be expected. This explains the higher values obtained from the analytical solution in almost all the calculations performed.

Finally, Fig. 4-23 shows the distribution of the deformation energy as a function of depth for the various blade inclinations adopted in the experimental investigation. These distributions are instantaneous quantities in that they represent the deformation energy distributions at the specified instantaneous blade positions. In Chapters 5 and 6, the soil deformation energy results obtained by the method of visioplasticity as outlined in this Section, are compared to the work input computed from the integration of the areas under the experimentally measured load-displacement curves as well as the work output as determined from the finite element model proposed in this study.

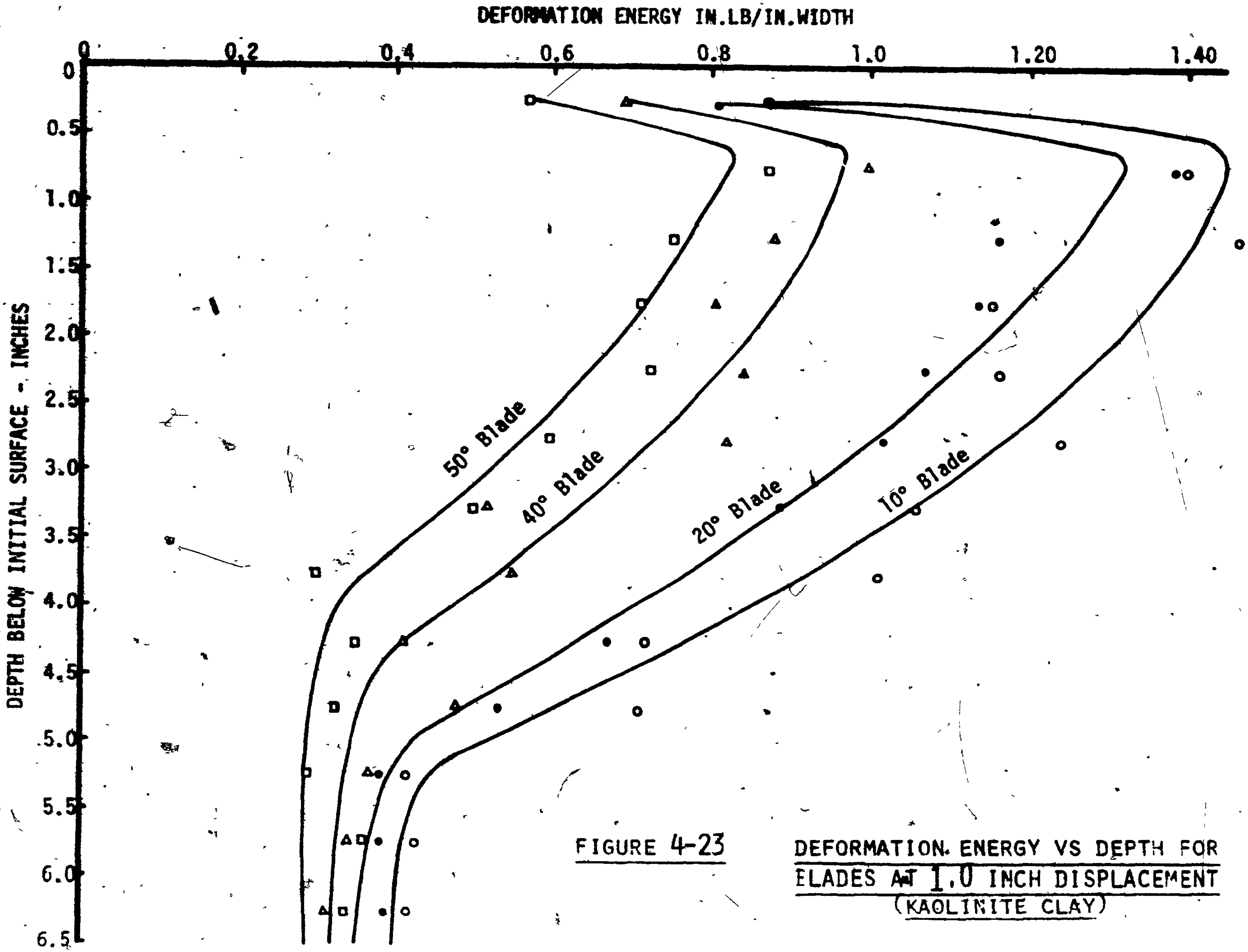

FIGURE 4-23 DEFORMATION ENERGY VS DEPTH FOR BLADES AT 1.0 INCH DISPLACEMENT (KAOLINITE CLAY)

CHAPTER 5

FINITE ELEMENT ANALYSIS OF SOIL CUTTING PROBLEM

Following from Fig. 4-1, this Chapter provides the development and presentation of the results of the finite element model used for solution of the stated problem, and a discussion of these results. In addition, comparisons between the finite element results of the soil cutting problem and the experimental results previously reported in Chapter 4 will be made. Further appreciation of the solution technique is achieved in Chapter 7 through a parametric study of the familiar case of two-dimensional soil response encountered in long retaining walls, when yielding in a passive sense. Recognizing that the retaining wall problem bears a close parallel to wide cutting blades moving in soils, it is believed that by comparing the results obtained from the analysis with the classical earth pressure theory, a better insight into the rationality of the solution technique will be accomplished. In the second part of Chapter 7, soil cutting and traction analytical and experimental results reported in this thesis are compared with the results computed from existing theories.

5.1 MESHES AND BOUNDARIES

The cutting tests described in the previous Chapters were modelled by the finite element method for solution in the digital computer [Chapter 2]. The boundary conditions for the problem are easily fixed since the laboratory tests were done in a box of known dimensions.

The meshes adopted for the 10° and 50° inclined blade problems are shown in Figs. 5-1 and 5-2. In the idealization of the 10° blade problem, 266 elements and 176 nodal points were used, while 199 elements and 136 nodal points were used for modelling the 50° blade problem. The mesh patterns were so arranged that smaller elements were employed near the blades and larger elements in regions away from them.

As mentioned earlier, constant strain triangle elements were employed in these models to represent the soil mass with joint [interface] elements inserted between the soil and the blades to simulate the interface characteristics. In addition, joint [cutting] elements were placed on the plane on which cutting progresses, as shown in Fig. 2-6.

Since the sides and the bottom of the box containing the soil were greased, it is reasonable to assume that these boundaries are smooth. In the finite element idealization, the boundaries were placed on rollers so that the horizontal movement was restrained on the sides and the vertical movement on the bottom boundary. The load setup in the laboratory was so designed as to insure uniform blade movement in the soil. In the analysis, the blades were considered rigid. Uniform horizontal rigid displacements were applied at all nodal points. The displacements were increased in 10 equal increments of 0.10 inch for a total displacement of 1.0 inch. The self weight of the soil was considered in all the analyses made.

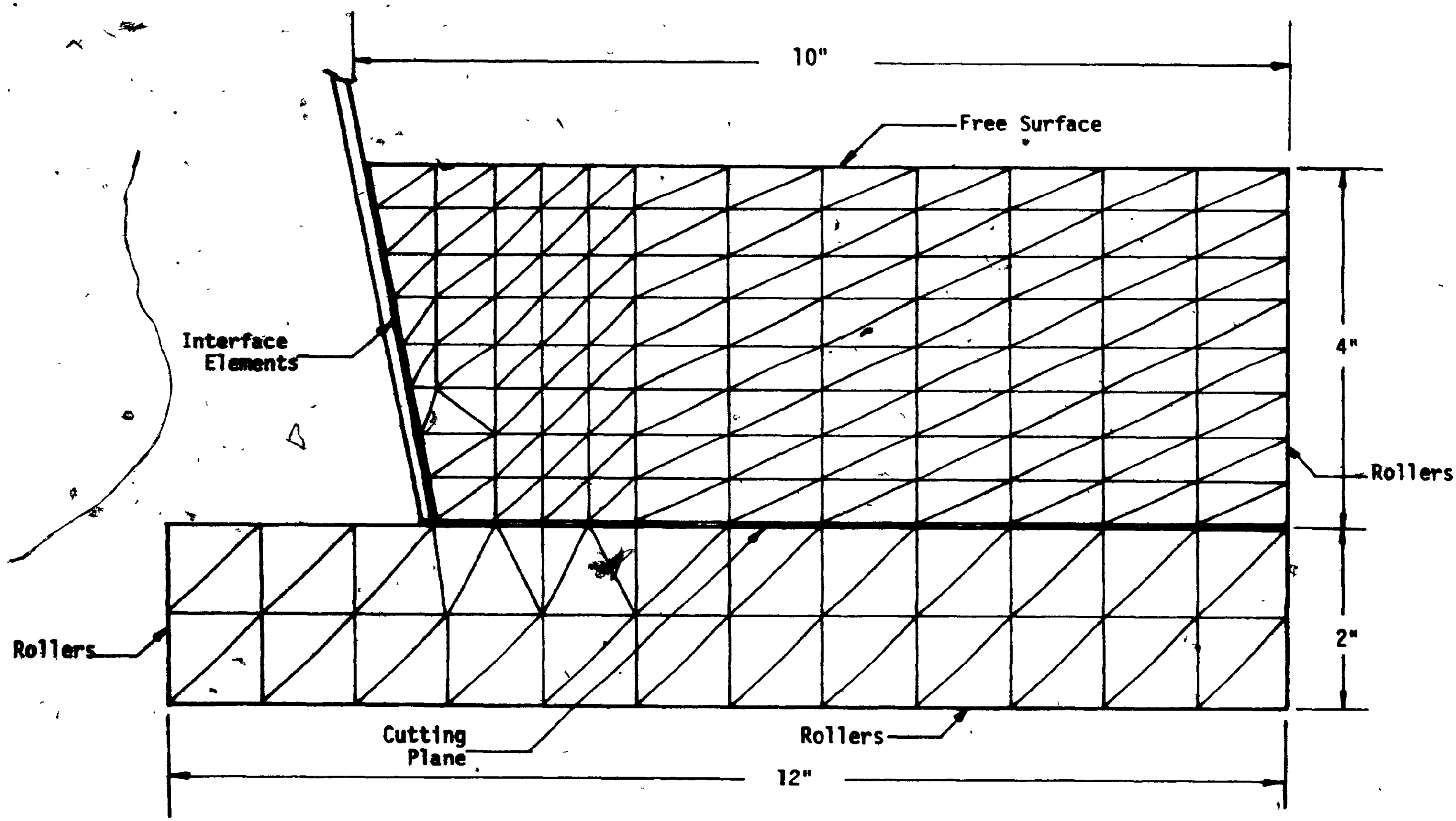

FIGURE 5-1 MESH LAYOUT FOR THE 10° INCLINED BLADE-SOIL SYSTEM

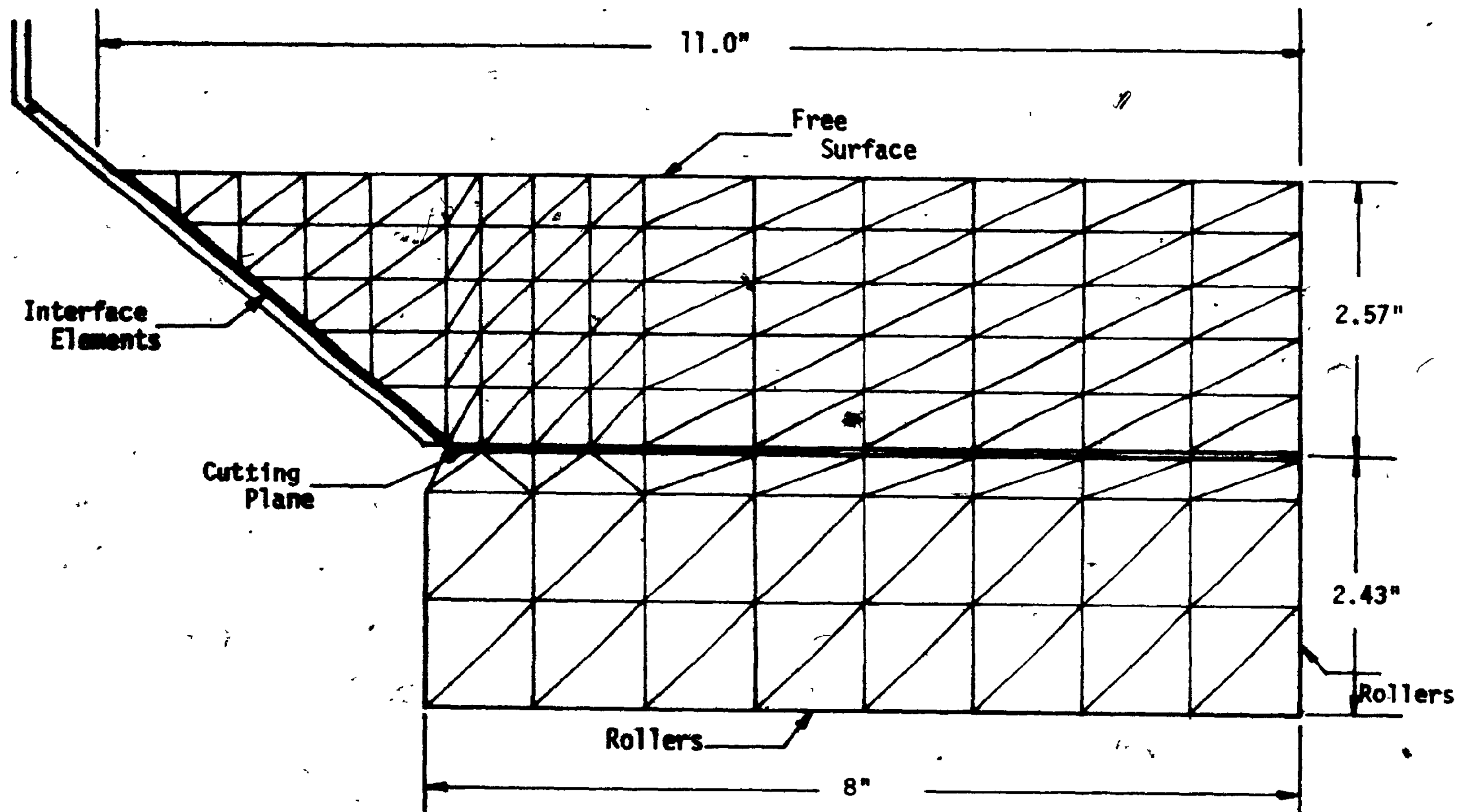

FIGURE 5-2 MESH LAYOUT FOR THE 50° INCLINED BLADE-SOIL SYSTEM

5.2 DISPLACEMENT AND VELOCITY PATTERNS

The displacement fields in the soil mass are computed from the magnitudes and directions of the vertical and horizontal displacements at the nodal points. Figures 5-3 and 5-4 show the displacement fields for the 10° and 50° inclined blades, respectively, at a displacement of 0.50 inch.

The displacement patterns indicate the existence of two zones. In the zone above the cutting plane, the soil undergoes large deformations resulting from the blade motion. In this region, the soil is moved forward and upward relative to the original blade position. These motions indicate that shear distortions occurred throughout the zone. On the other hand, the region below the cutting plane is shown to experience very little deformation. The discontinuity in the deformation field is shown to occur on the cutting plane, discontinuity that results from the relative displacements between the top and the bottom surfaces of the cutting [joint] elements. It must be noted, however, that according to the assumed model, the soil is displaced by continuous deformation rather than by sliding along a series of specific failure surfaces. Furthermore, it is seen that such a model allows for a build up of a surcharge as the blades progress in the soil.

The deformation patterns for the 10° and 50° inclined blades are generally the same. However, the zone of shearing deformation adjacent to the blade is found to be larger for the 10° inclined blade by approximately the volume of the soil enclosed within the projection of the blade face.

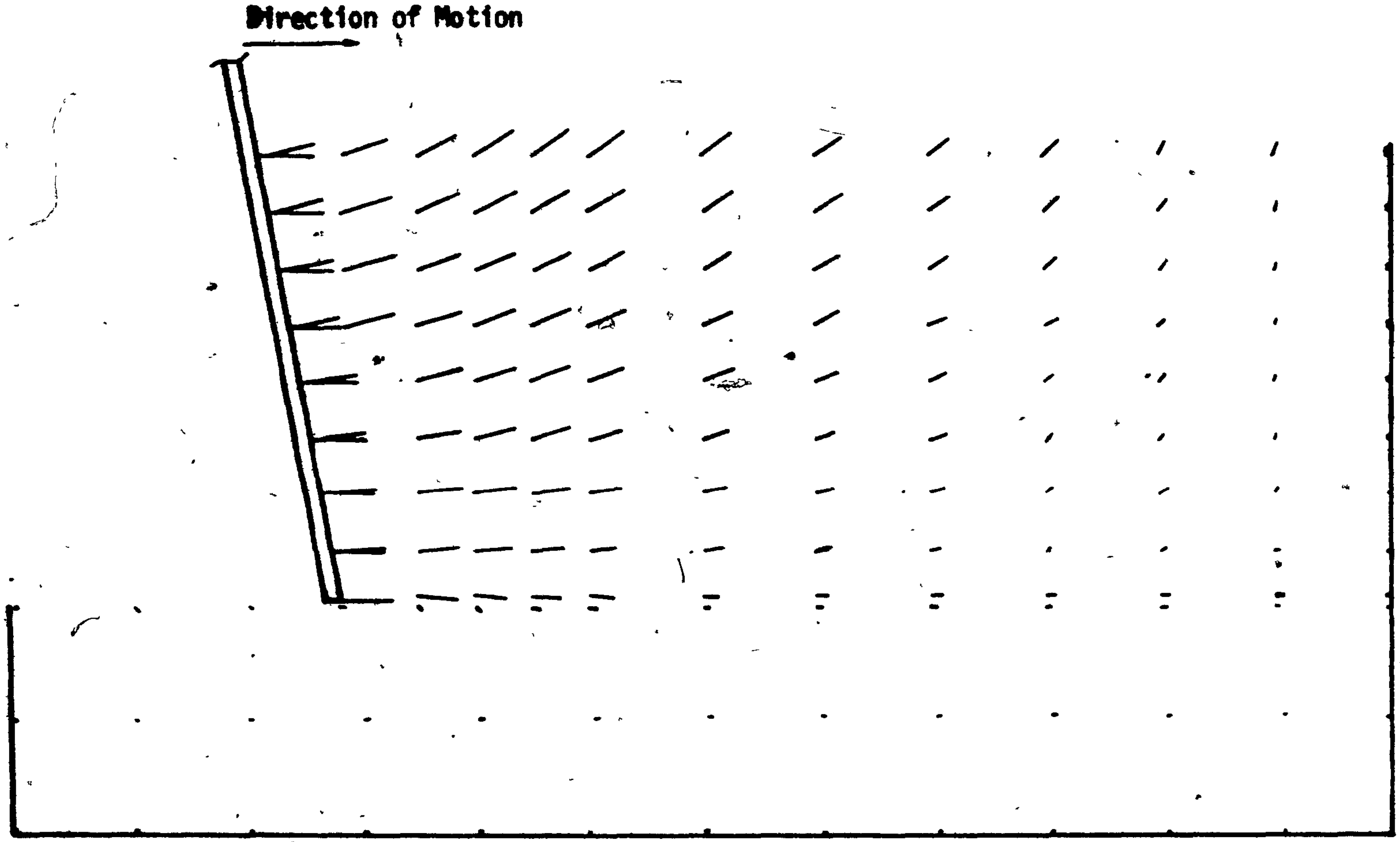

FIGURE 5-3 DISPLACEMENT FIELD FOR THE 10° INCLINED BLADE-SOIL SYSTEM

(BLADE DISPLACEMENT = 0.50 inch)

Scale: 1 inch = 0.65 inch

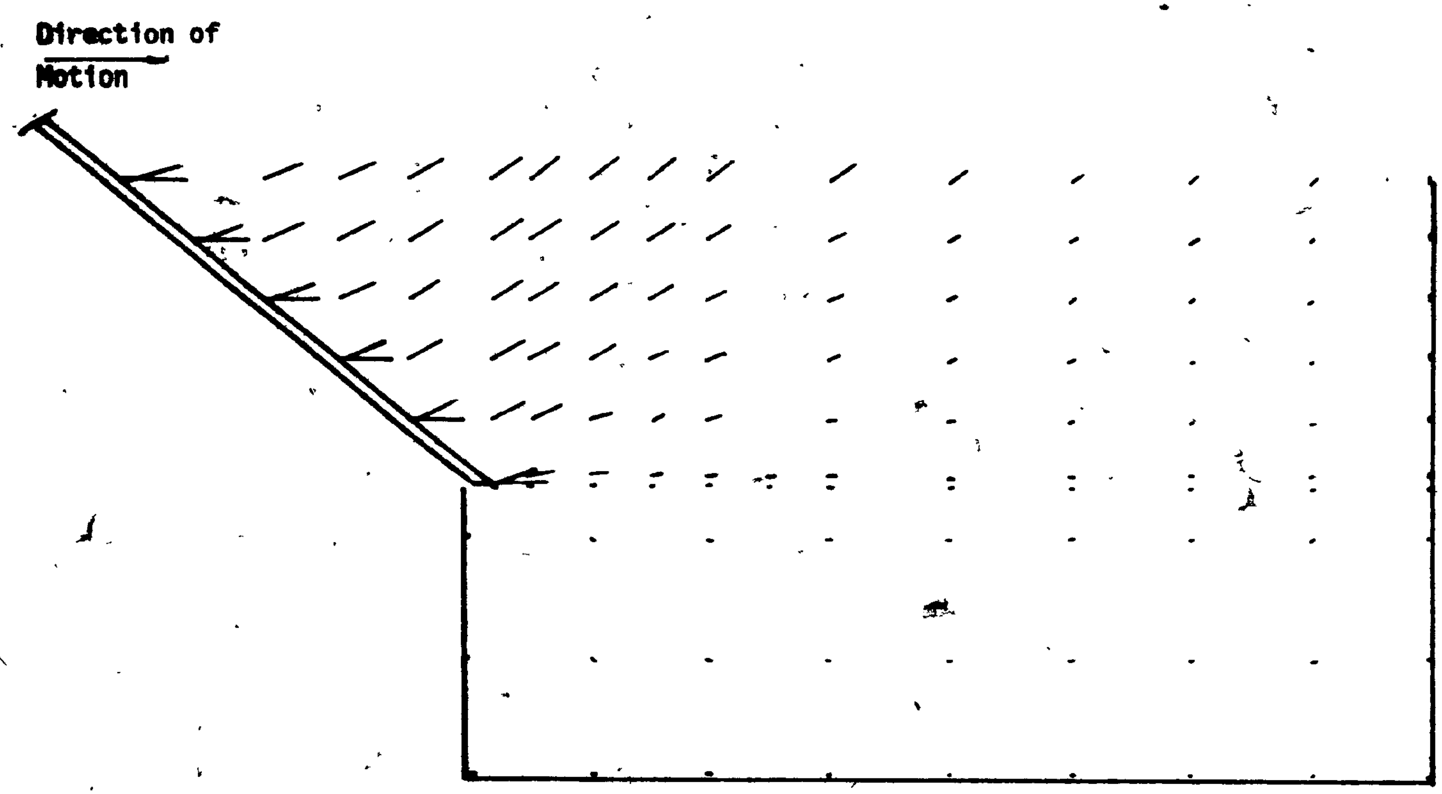

FIGURE 5-4 DISPLACEMENT FIELD FOR THE 50° INCLINED BLADE-SOIL SYSTEM

(BLADE DISPLACEMENT = 0.50 inch)

Scale: 1 inch = 0.65 inch

Regarding the interface displacements, it is shown in Figs. 5-3 and 5-4 that a certain degree of slip occurs between the blade surface and the adjacent soil. At 0.50 inch of blade displacement, the interface element nodal points attached to the triangular elements move upward relative to the nodal points fixed to the blade surface. In the case of the 10° blade deformation field, the magnitude of the soil slip is smaller near the blade tip and increases along the surface of the blade, reaching a maximum at the intersection of the soil surface with the blade. On the other hand, the magnitude of the soil slip along the 50° blade surface appears to be more uniform. Such difference in the slip behavior is attributed to the difference in the tangential stress distributions developed in the interface elements along both the 10° and 50° inclined blades. The contact stresses will be presented in a later section with a discussion on the observed differences.

Finally, the plots of the horizontal and vertical components of the nodal point velocities are shown in Fig. 5-5 for the 10° inclined blade and in Fig. 5-6 for the 50° inclined blade-soil system. These iso-velocity contours serve to show the effect of the insertion of the cutting elements on the development of discontinuities in the velocity fields. In Section [5.6.2] the displacement fields obtained by means of the finite element model proposed will be compared to those obtained from the experimental analysis described in Chapter 4, in order to establish the similarity between the corresponding fields.

5.3 STRAIN RATE DIRECTIONS

The directions of the principal strain rates are obtained on

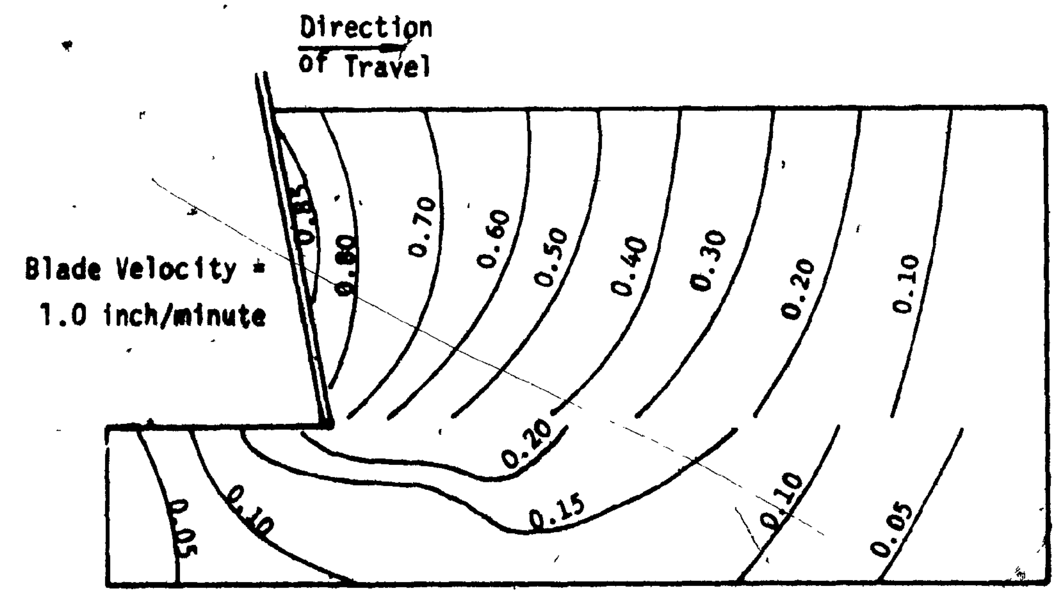

(A) HORIZONTAL VELOCITY FIELD

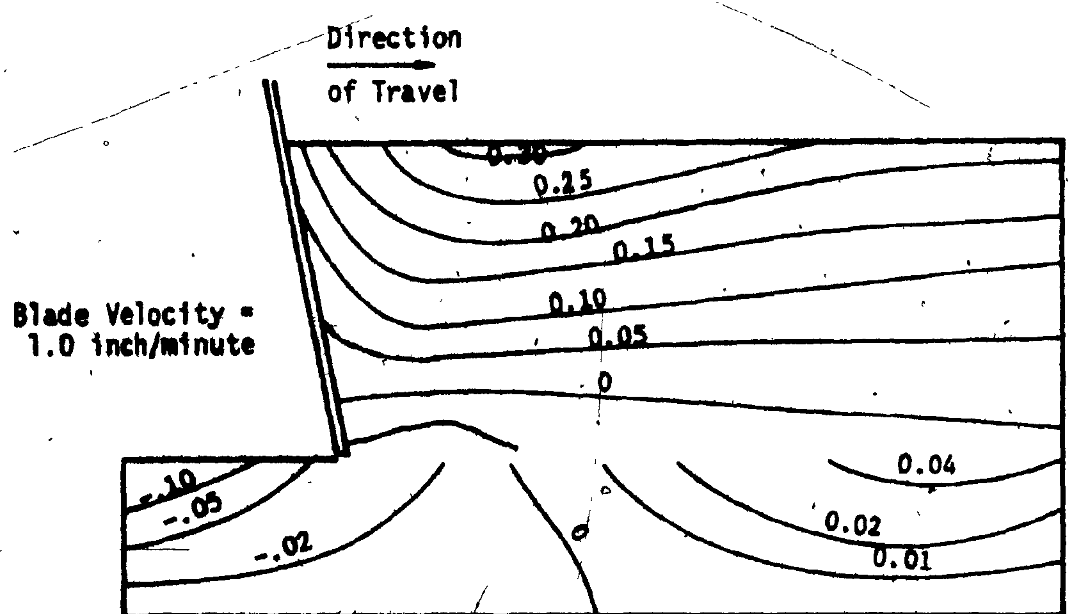

(B) VERTICAL VELOCITY FIELD

FIGURE 5-5 VELOCITY FIELDS FOR THE 10° INCLINED BLADE-SOIL SYSTEM DURING THE FIRST DISPLACEMENT INCREMENT OF 0.20 INCH

[CONTOUR VALUES ARE IN INCHES/MINUTE]

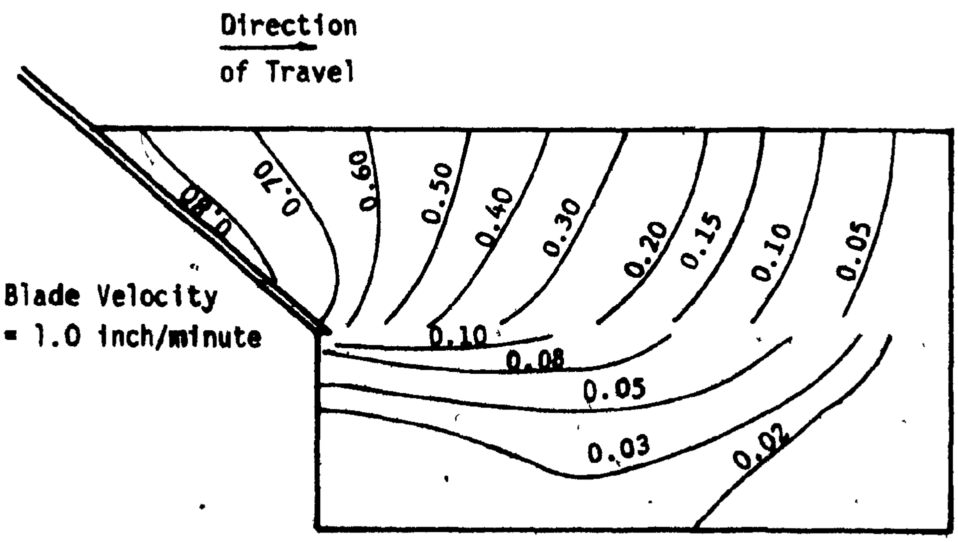

(A) _ HORIZONTAL VELOCITY FIELD

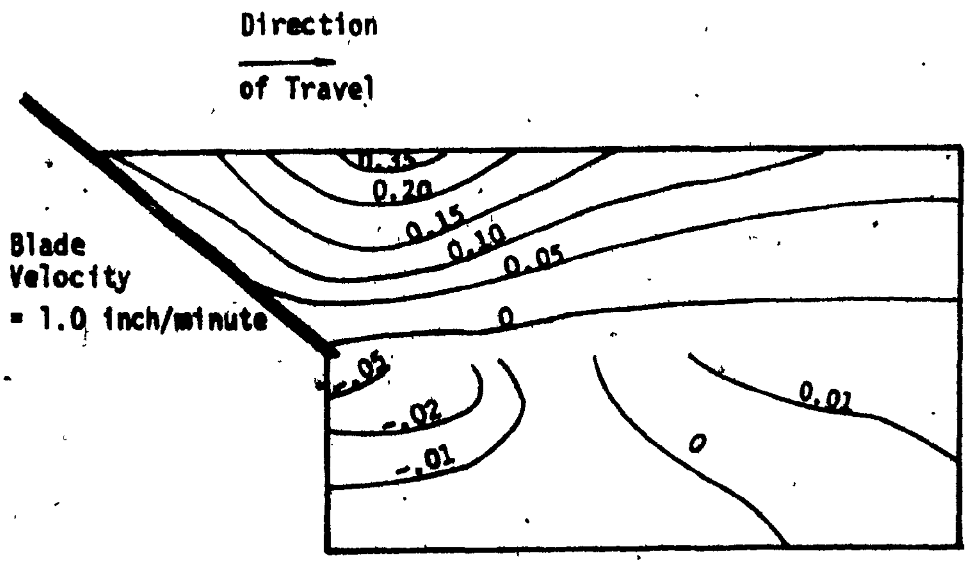

(B) VERTICAL VELOCITY FIELD

FIGURE 5-6 VELOCITY FIELDS FOR THE 50° INCLINED BLADE-SOIL SYSTEM DURING THE FIRST DISPLACEMENT INCREMENT OF 0.10 INCH

[CONTOUR VALUES ARE IN INCHES/MINUTE]

the basis of the strain rate components, calculated by dividing the incremental strain components $\delta\varepsilon_x$, $\delta\varepsilon_y$ and $\delta\varepsilon_{xy}$ by the time increment δt, or

$$\dot{\varepsilon}_x = \frac{\delta\varepsilon_x}{\delta t} \qquad \dot{\varepsilon}_y = \frac{\delta\varepsilon_y}{\delta t} \qquad \text{and} \qquad \dot{\varepsilon}_{xy} = \frac{\delta\varepsilon_{xy}}{\delta t} \tag{5.1}$$

However, due to the approximations involved in the formulation of the constant strain triangle elements employed in this study, it is logical to use some average value of strain [or stress] as representative for the element. The most common method of averaging is to use the strain at the centroid of the element, since the strains [or stresses] are constant over the element. For better averaging, an alternative procedure is admissible. Instead of averaging the strain [or stress] over the element to obtain a centroidal value, the strain at a particular node may be taken as the average value at that node among all the adjacent elements. This procedure has the double advantage of:

1] avoiding unacceptable discontinuities in the stress, velocity and strain rate fields: most elements currently in use exhibit discontinuities in stresses from one element to another, although the stresses in two adjacent elements often straddle the true stress curve [Zienkiewicz (1971)], and

2] simplifying data interpretations and presentations, as it is easier to visualize the results at the nodal points rather than at the elements' centroids.

In the present study all the stresses, strains, strain rates and velocities are averaged at the nodal points. The averaging procedure is carried out by subroutine "AVER" in program "MAIN -2", in Appendix E.

At every nodal point the strain rate components are calculated by Eq. (5.1), and the directions of the principal strain rate components as well as those of the maximum shear strain rates are determined as shown in Fig. 5-7. The network of the principal strain rate and the maximum shear strain rate directions are shown in Figs. 5-8 and 5-9 for the 10° and 50° blade problems, respectively.

Since the soil undergoing deformation in front of a moving blade constitutes essentially a closed system as far as water content is concerned, the loading being characterized by its short duration, it is relevant, as discussed previously, to base the analysis on a total stress approach with the friction parameter ϕ taken as zero. This reasoning indicates that the similarity in mechanical behavior of clay in front of a moving tool and ductile metals has a rational basis. According to these considerations, Saint Venant's postulate, already accepted to be valid for ductile metals can also be accepted for clays subjected to short duration loading conditions. The postulate states that: "In a plastic material, the principle directions of strain rate coincide with the principal directions of stress". The directions obtained in Figs. 5-8 and 5-9 can therefore be assumed to coincide with those of the principal stresses and maximum shear stresses.

5.4 STRESS ANALYSIS

The distributions of the horizontal, vertical and shear soil

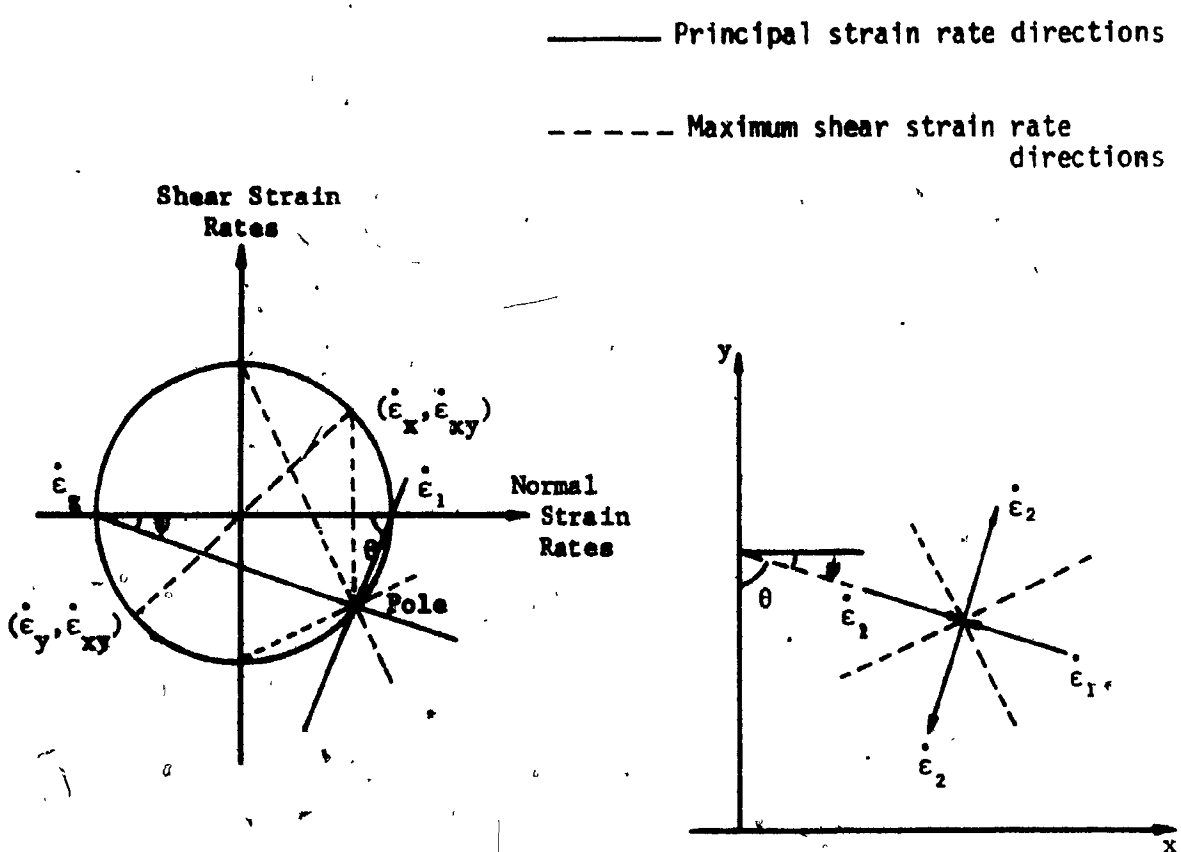

MOHR PLANE

PHYSICAL PLANE

FIGURE 5-7 DIRECTIONS OF PRINCIPAL STRAIN RATES AND MAXIMUM SHEAR STRAIN RATES

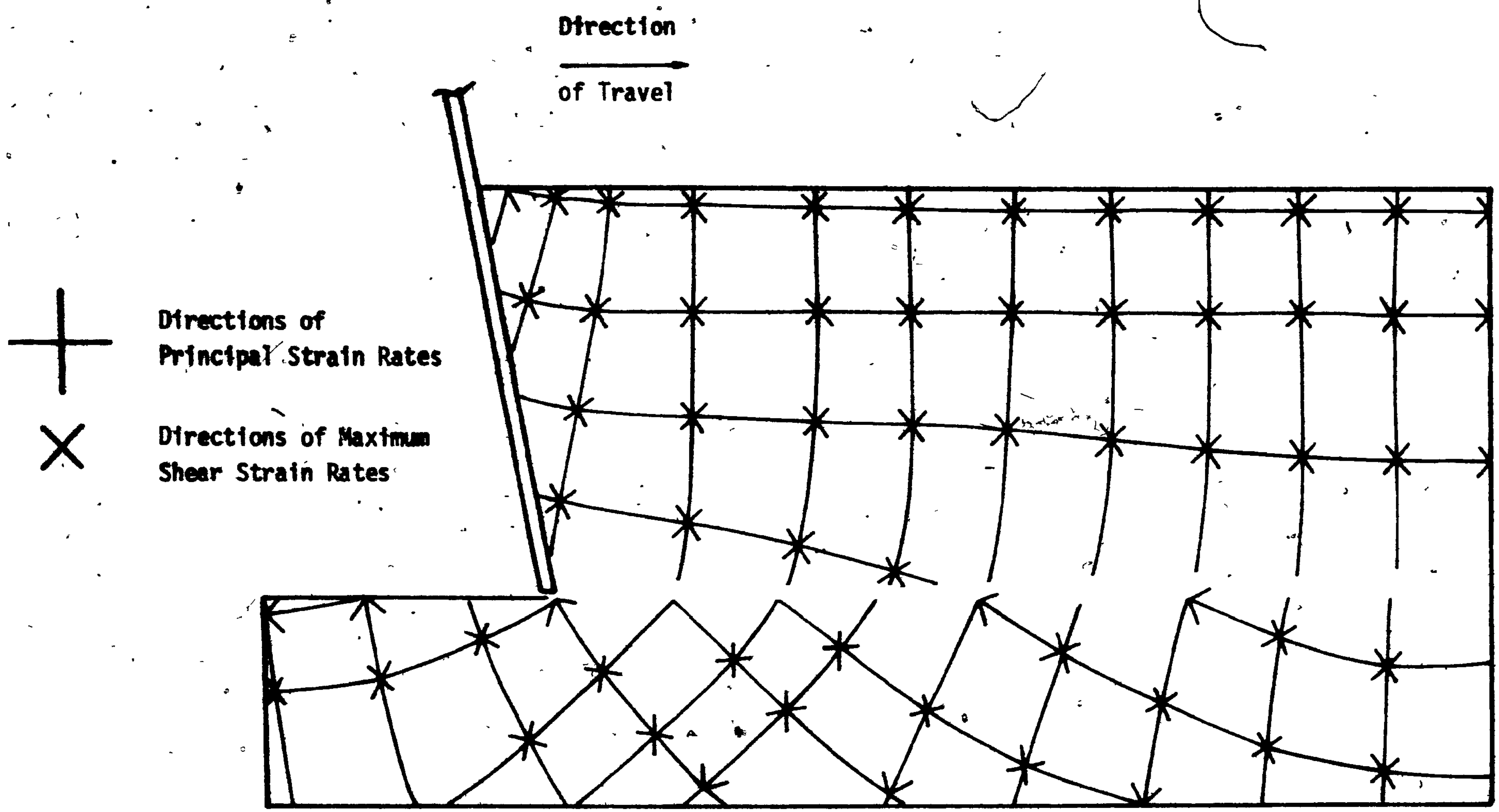

FIGURE 5-8 DIRECTIONS OF PRINCIPAL STRAIN RATES AND MAXIMUM SHEAR STRAIN RATES FOR THE 10° INCLINED BLADE-SOIL SYSTEM (BLADE DISPLACEMENT = 0.10 INCH)

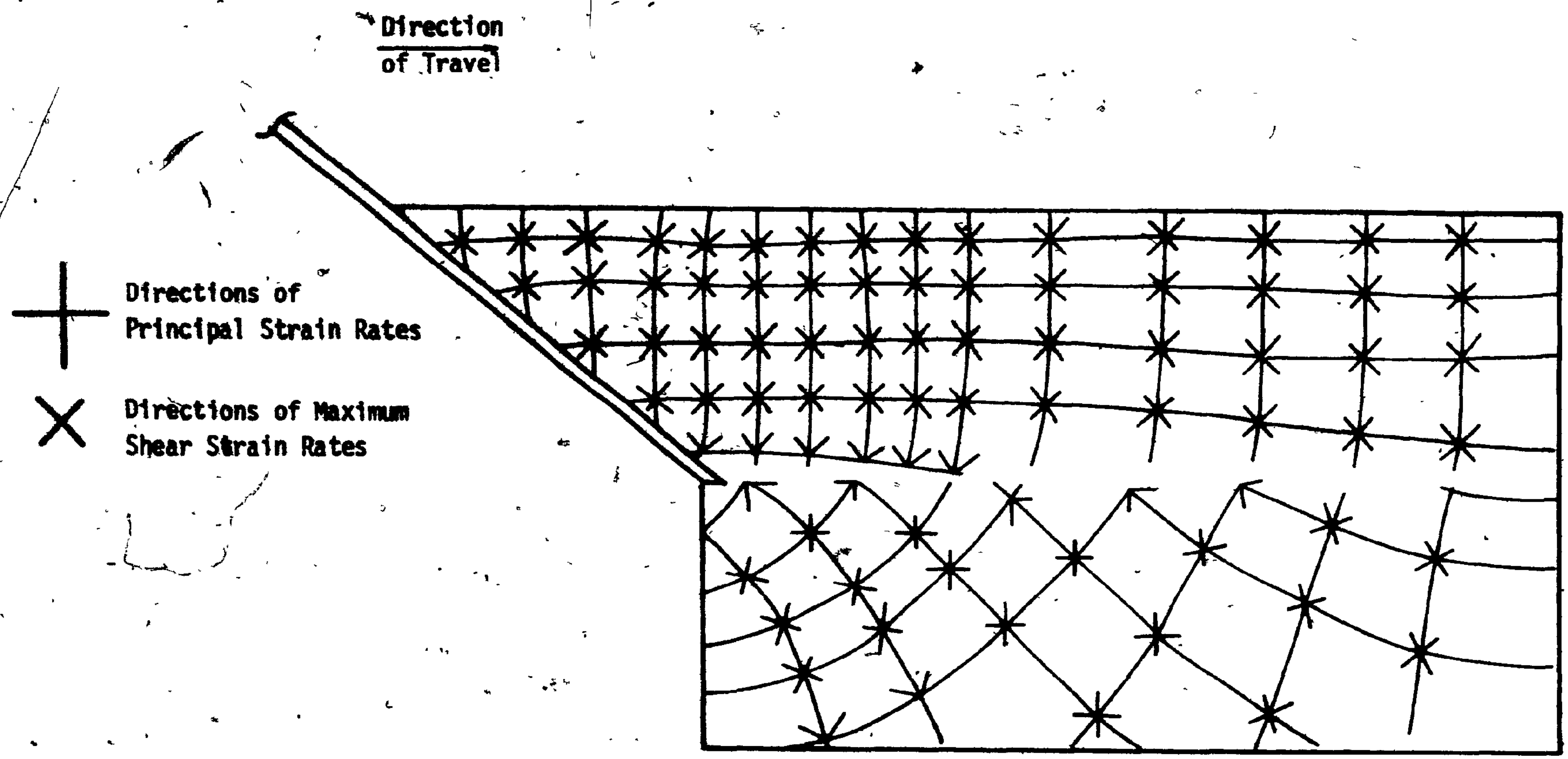

FIGURE 5-9 DIRECTIONS OF PRINCIPAL STRAIN RATES AND MAXIMUM SHEAR STRAIN RATES FOR THE 50° INCLINED BLADE-SOIL SYSTEM

(BLADE DISPLACEMENT = 0.10 INCH)

stresses in front of a moving cutting blade are presented in this Section. The stress contours for the 10° and 50° inclined blade problems are plotted at displacements of 0.1 and 0.50 inch. The stress contours for the 10° blade problem are shown in Figs. 5-10 and 5-11. For the 50° blade case, the contours are plotted in Figs. 5-12 and 5-13. The 0.1 inch blade displacement is typical of stress distributions in the elastic range, while the 0.5 inch plots are considered to indicate the distributions in the plastic range in the vicinity of the ultimate stresses.

The contours shown in these Figures seem to maintain the same general shapes with increasing blade displacement. Furthermore, the results clearly indicate the discontinuity in the stress distribution within the soil mass due to the effect of the cutting [joint] elements inserted at the level of the blades' tips. It must be kept in mind, however, that these elements were inserted, in the first place, to produce discontinuities in the stress and deformation fields similar to those occuring in the physical situation. Correlations between the analytical and experimental results are the final justification that the assumed analytical model with its assumed discontinuities can be employed with reasonable accuracy to predict the physical response. Correlations between analytical results and the experimental results obtained from the model tests performed are attempted in Section 5.6.

Examination of Figs. 5-10 through 5-13 leads to the following observations:

1] Stress concentrations at the tip of the blades are indicated in all cases. Horizontal, σ_x, vertical, σ_y,

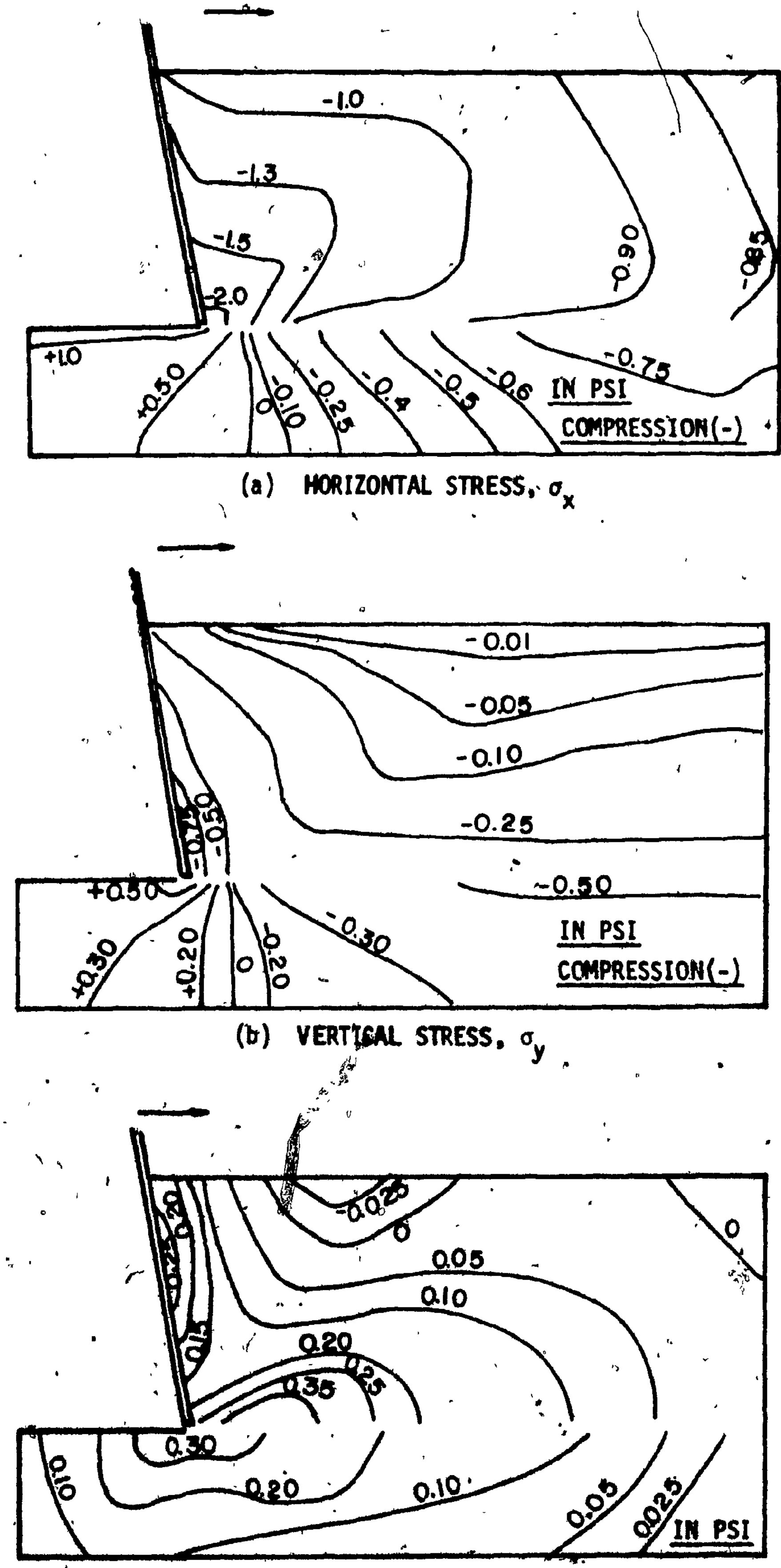

(a) HORIZONTAL STRESS, σ_x

(b) VERTICAL STRESS, σ_y

(c) SHEAR STRESS, τ_{xy}

FIGURE 5-10 STRESS FIELDS FOR THE 10° INCLINED BLADE-SOIL SYSTEM AT 0.10 INCH DISPLACEMENT

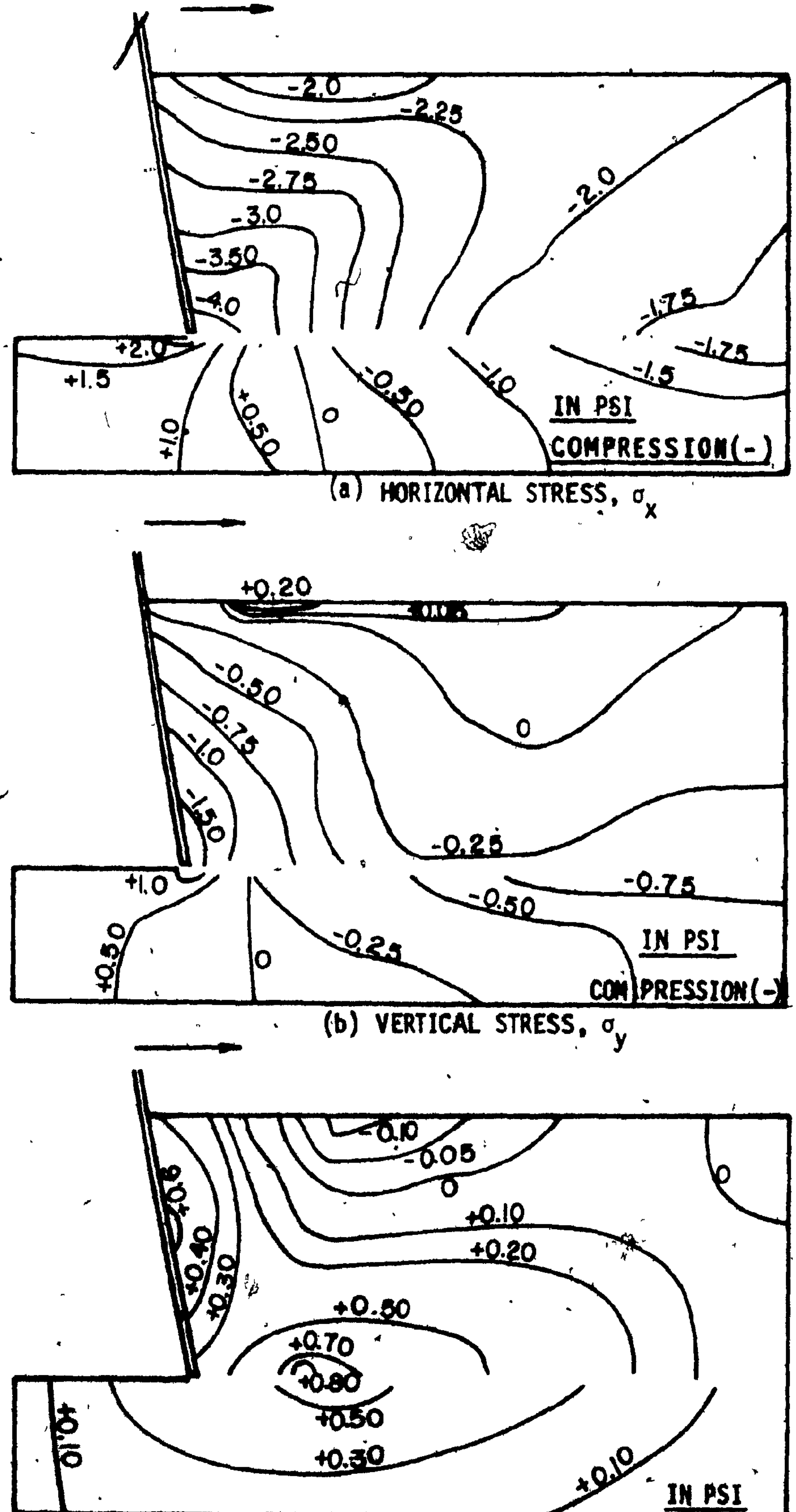

(a) HORIZONTAL STRESS, σ_x

(b) VERTICAL STRESS, σ_y

(c) SHEAR STRESS, τ_{xy}

FIGURE 5-11 STRESS FIELDS FOR THE 10° INCLINED BLADE-SOIL SYSTEM AT 0.50 INCH DISPLACEMENT

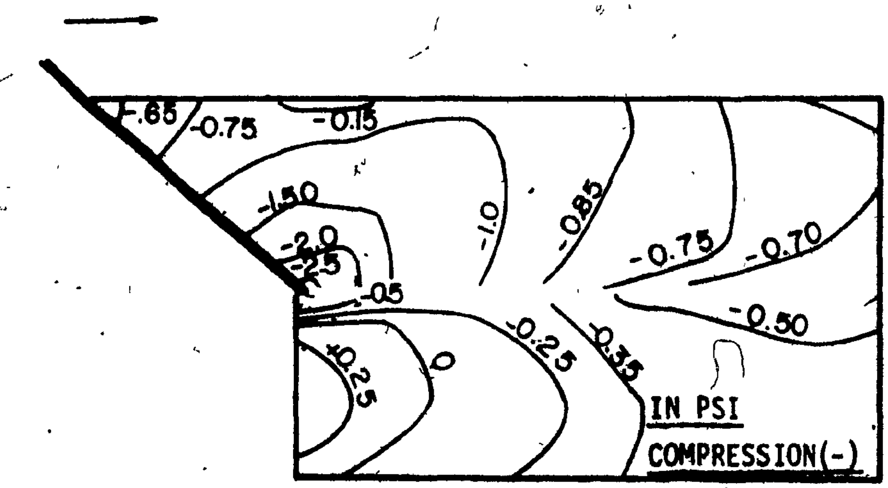

(a) HORIZONTAL STRESS, σ_x

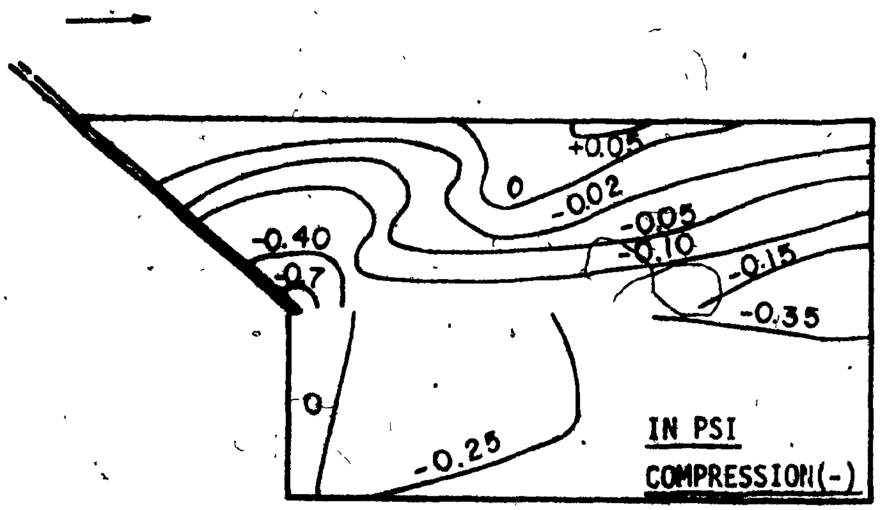

(b) VERTICAL STRESS, σ_y

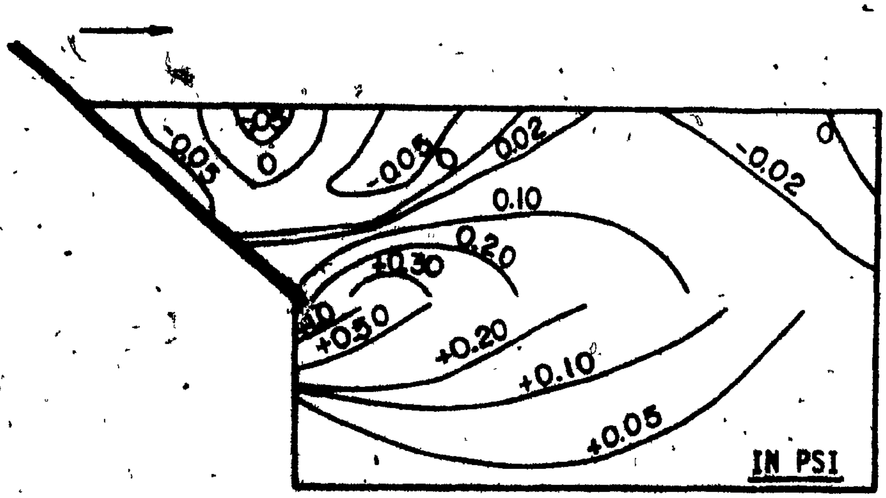

(c) SHEAR STRESS, τ_{xy}

FIGURE 5-12 STRESS FIELDS FOR THE 50° INCLINED BLADE-SOIL SYSTEM AT 0.10 INCH DISPLACEMENT

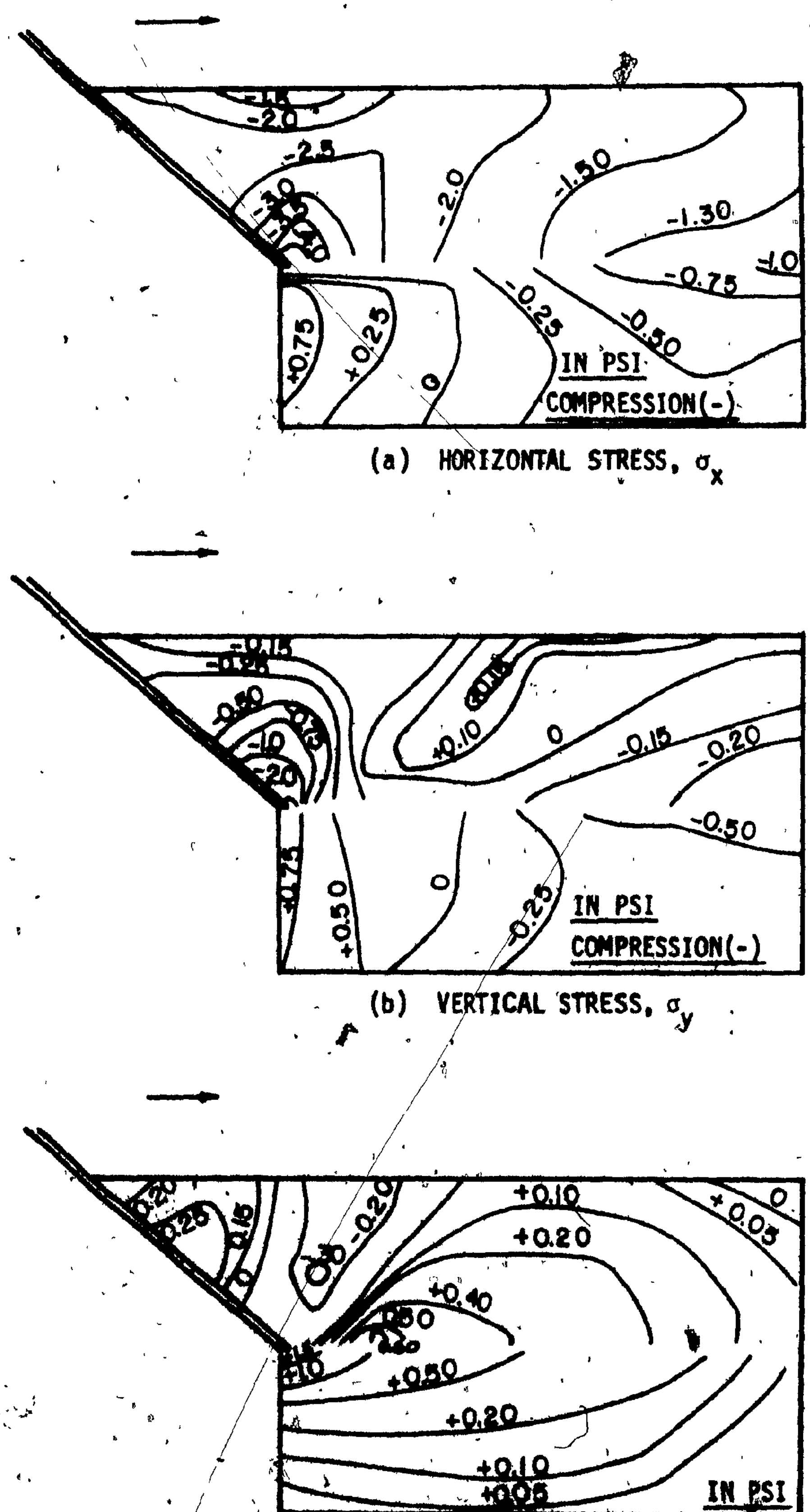

(a) HORIZONTAL STRESS, σ_x

(b) VERTICAL STRESS, σ_y

(c) SHEAR STRESS, τ_{xy}

FIGURE 5-13 STRESS FIELDS FOR THE 50° INCLINED BLADE-SOIL SYSTEM AT 0.50 INCH DISPLACEMENT

and shear, τ_{xy}, stress values are highest in the vicinity of the blade tip. Such concentrations are also characterized by a singular behavior where a change in the magnitudes and, in some instances, in the directions of the stresses above and below the blade tip-point result.

2] Comparison of the patterns of the horizontal stress, σ_x distribution in front of the 10° and 50° inclined blades shows no significant differences. However, while the stress values in the vicinity of the blades are similar in the two cases, it may be noted that, distant from the blade, the soil is subjected to higher horizontal stresses in the case of the 10° blade than in the case of the 50° inclined blade.

3] The effect of the plane of cutting elements on the horizontal stress distribution is to divide the stress field into two differently stressed regions:

(a) The upper field, where the compressive stresses are high near the blade surface and decrease with distance from that surface;

(b) The lower field, where lower stresses, partly tensile and partly compressive, are developed. The compressive stresses increase with distance from the blades, while a zone of tensile horizontal stresses develops in the soil below the blade tip in the two cases studied.

4] The vertical normal stress, σ_y, distributions, show the existence of a zero vertical stress contour in the upper part of the soil mass in both the 10° and 50° blade distributions. With the blade progressing in the soil, this contour shifts downward, resulting in larger zones of vertical tensile stresses. This behavior is attributed to the restraining influence of the fixed vertical end boundary which induces action that results in larger zones of tensile stresses. As in the case of the horizontal stress field, the lower part of the soil mass [below the cutting plane] experiences a change from tensile stress below the blade tip to compressive stress away from the blade.

5] The shear stress contours, indicate a zone in front of the blade tip experiencing high shear stresses. The shear stresses in this zone are positive, thus the shearing is a clockwise shearing action as would be expected. These zones could be termed the "active" shear zones as the shear stresses keep on increasing with blade movement. Above the "active" shear zones, there exists zero shear stress contours with zones of negative shear stresses, i.e., shearing is anticlockwise above the zero contour. These zones are found to expand with larger negative values in the 0.5 inch plots, indicating an upward action that explains the formation of the surcharge.

Figures 5-14 through 5-19 demonstrate the behavior of the joint elements placed on the cutting plane at 0.1, 0.3, 0.6 and 1.0 inch of blade displacement for the 10° and 50° inclined blade models, respectively. Figures 5-15 and 5-18 show how the average relative shear displacements at the centroids of the cutting elements vary as a function of the horizontal distance from the blade leading edges. The variation of the tangential stress, τ, as obtained from the hyperbolic Eq. (2.32) with the coefficients (a) and (b) obtained from Fig. 4-13, is plotted in Figs. 5-14 and 5-17. The variation of the tangential stiffness values, k_s, is presented in Figs. 5-16 and 5-19.

As indicated in Chapter 2, the relationship between shear stress and relative displacement on the interface between blade and soil is nonlinear and dependent upon the developed normal stress. In other words, the constitutive relationship for the yield point in soil shear at the blade-soil interface is assumed to take the form $\tau_s(P, \Delta_s)$. P is the normal pressure acting on the interface and Δ_s is the relative displacement between the soil and the blade surface. The tangential stress, τ, can then be defined in the following manner:

$$|\tau| \le \tau_s(P, \Delta_s) \qquad (5.2)$$

This follows because the shear stress of a point in the thin surface layer of soil adjacent to the blade surface is less than on a slipping surface at this point. The equality holds if the surface of contact is a slip surface, that is, the maximum value of the tangential stress is given by the relation:

$$|\tau| = \tau_s(P, \Delta_s) \qquad (5.3)$$

FIGURE 5-14 DISTRIBUTION OF TANGENTIAL STRESSES IN ELEMENTS ALONG CUTTING PLANE FOR THE 10° BLADE-KAOLIN CLAY MODEL

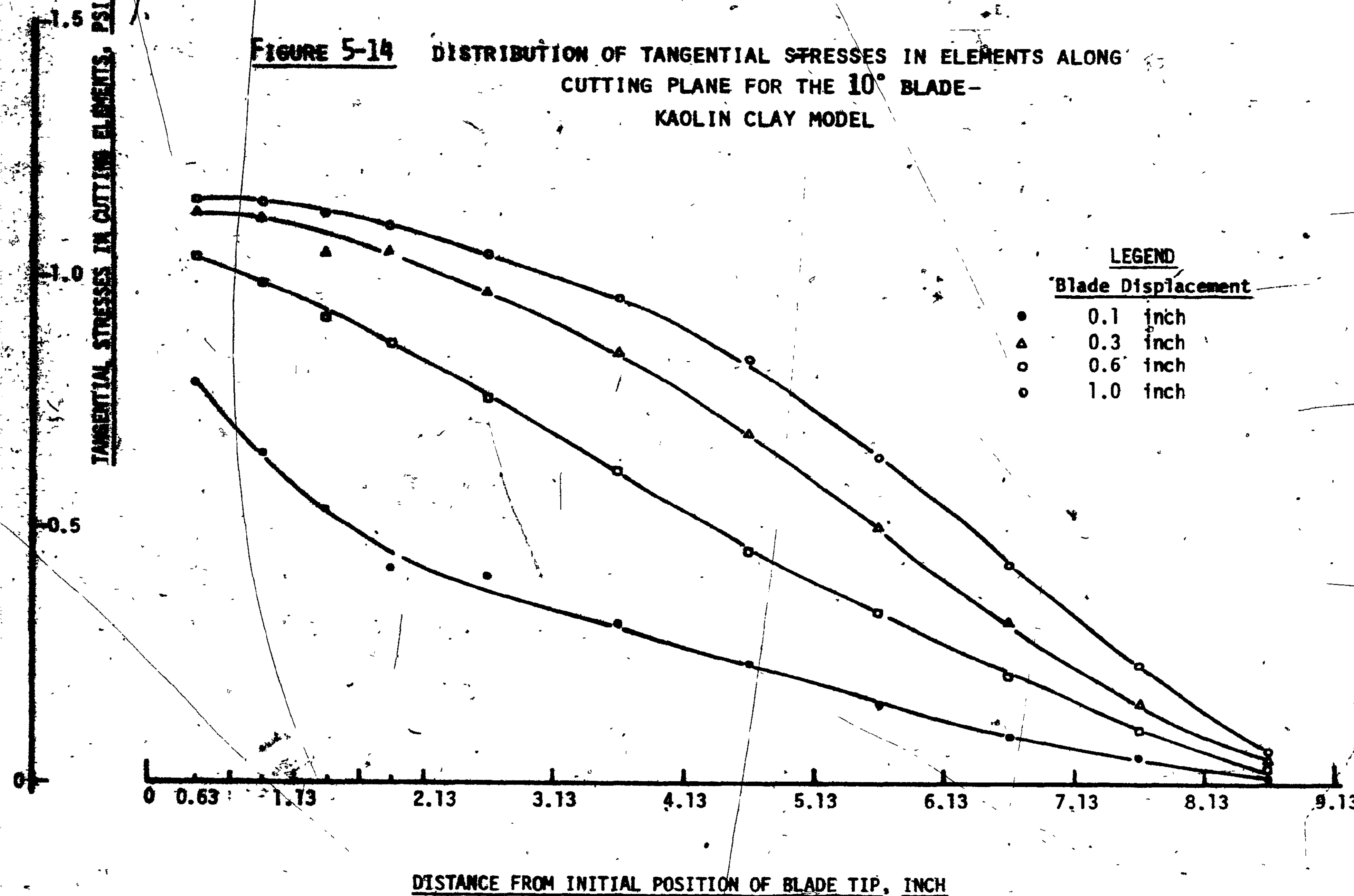

FIGURE 5-15 DISTRIBUTION OF HORIZONTAL DISPLACEMENTS IN ELEMENTS ALONG CUTTING PLANE FOR THE 10° BLADE - KAOLIN CLAY MODEL

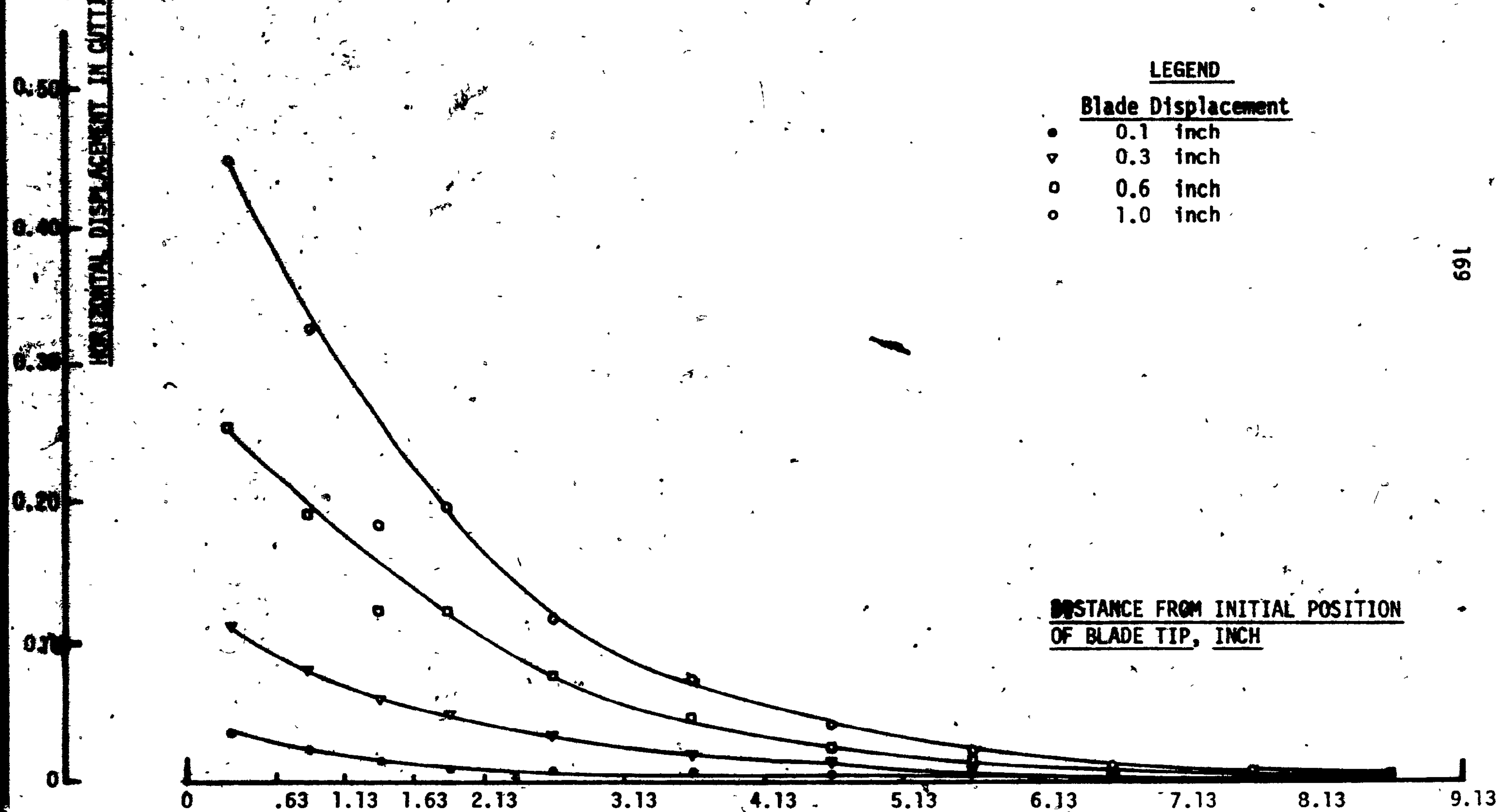

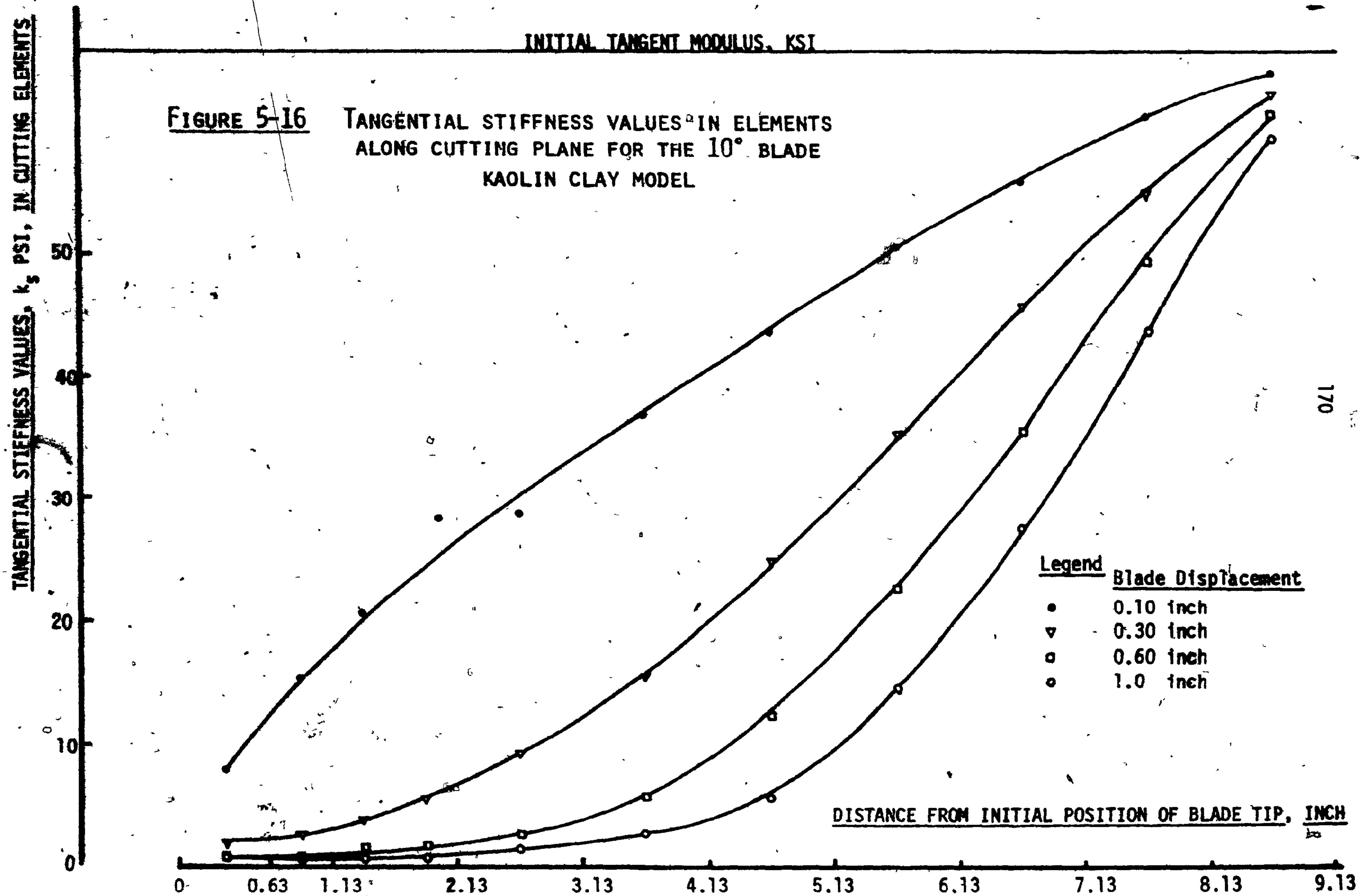

INITIAL TANGENT MODULUS, KSI
FIGURE 5-16 TANGENTIAL STIFFNESS VALUES IN ELEMENTS ALONG CUTTING PLANE FOR THE 10° BLADE KAOLIN CLAY MODEL
TANGENTIAL STIFFNESS VALUES, k_s PSI, IN CUTTING ELEMENTS
0
10
20
30
40
50
Legend
Blade Displacement
0.10 inch
0.30 inch
0.60 inch
1.0 inch
DISTANCE FROM INITIAL POSITION OF BLADE TIP, INCH
0
0.63
1.13
2.13
3.13
4.13
5.13
6.13
7.13
8.13
9.13

FIGURE 5-17 DISTRIBUTION OF TANGENTIAL STRESSES IN ELEMENTS ALONG CUTTING PLANE FOR THE 50° BLADE - KAOLIN CLAY MODEL

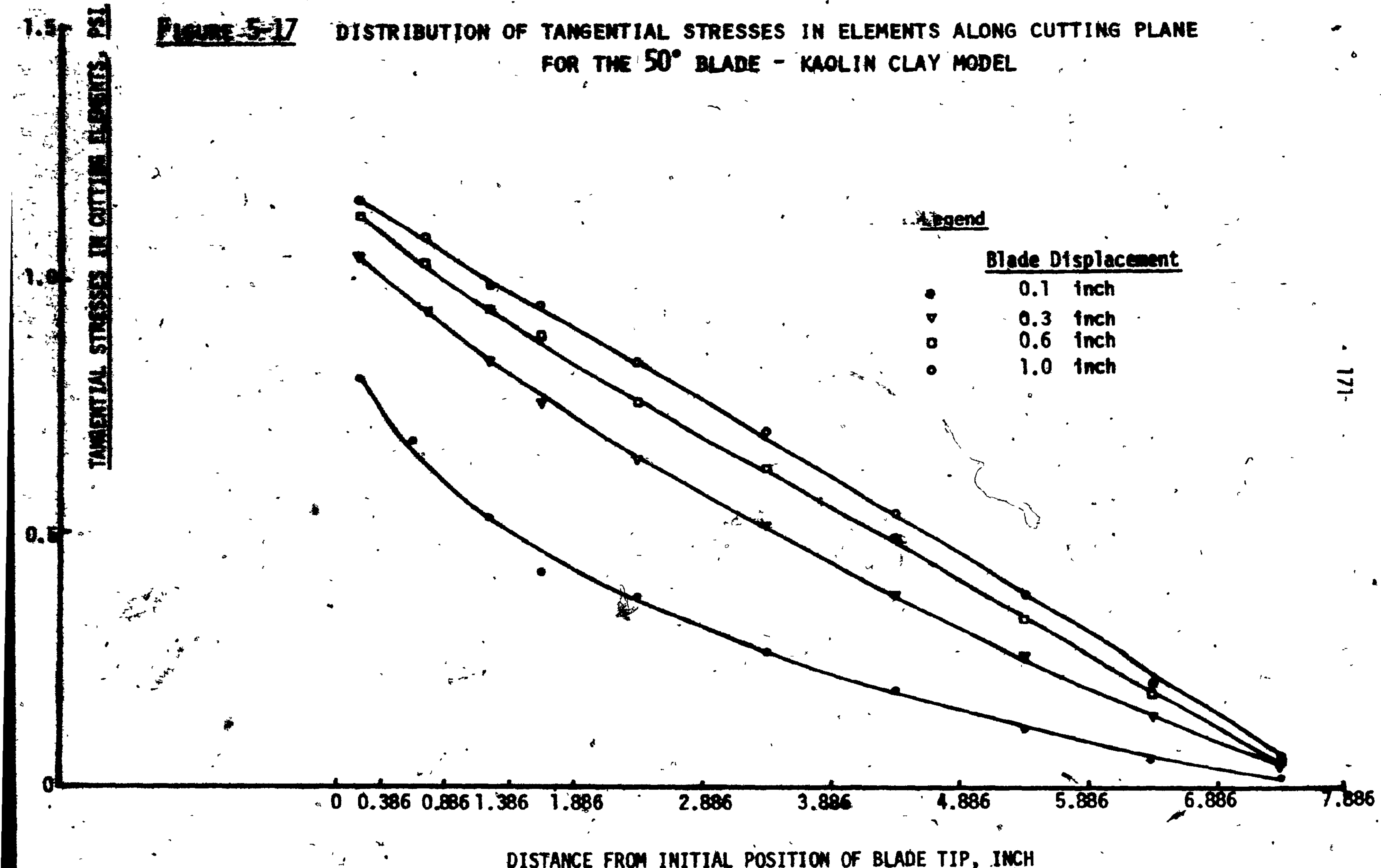

FIGURE 5-18 DISTRIBUTION OF HORIZONTAL DISPLACEMENTS IN ELEMENTS ALONG CUTTING PLANE FOR THE 50° BLADE - KAOLIN CLAY MODEL

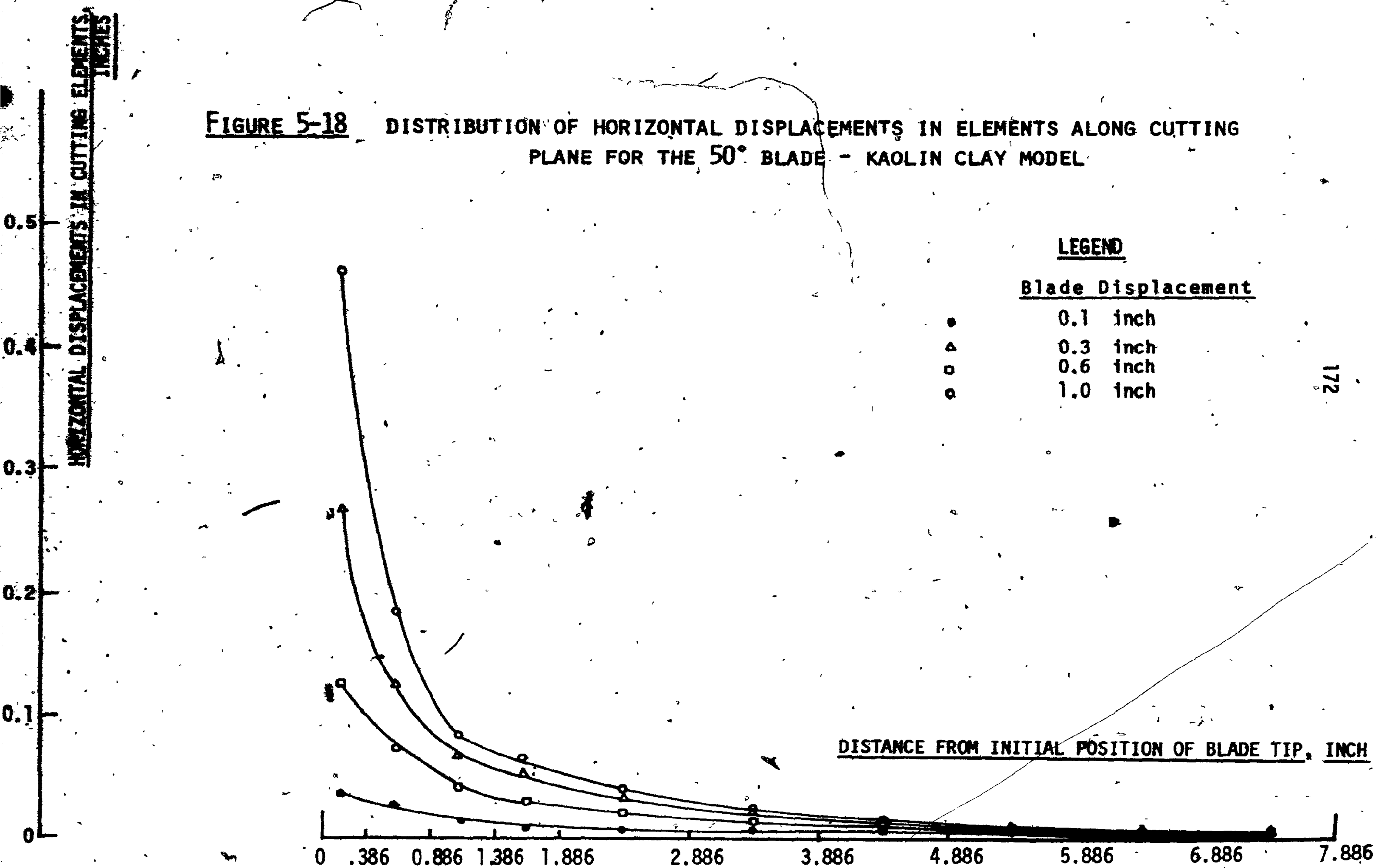

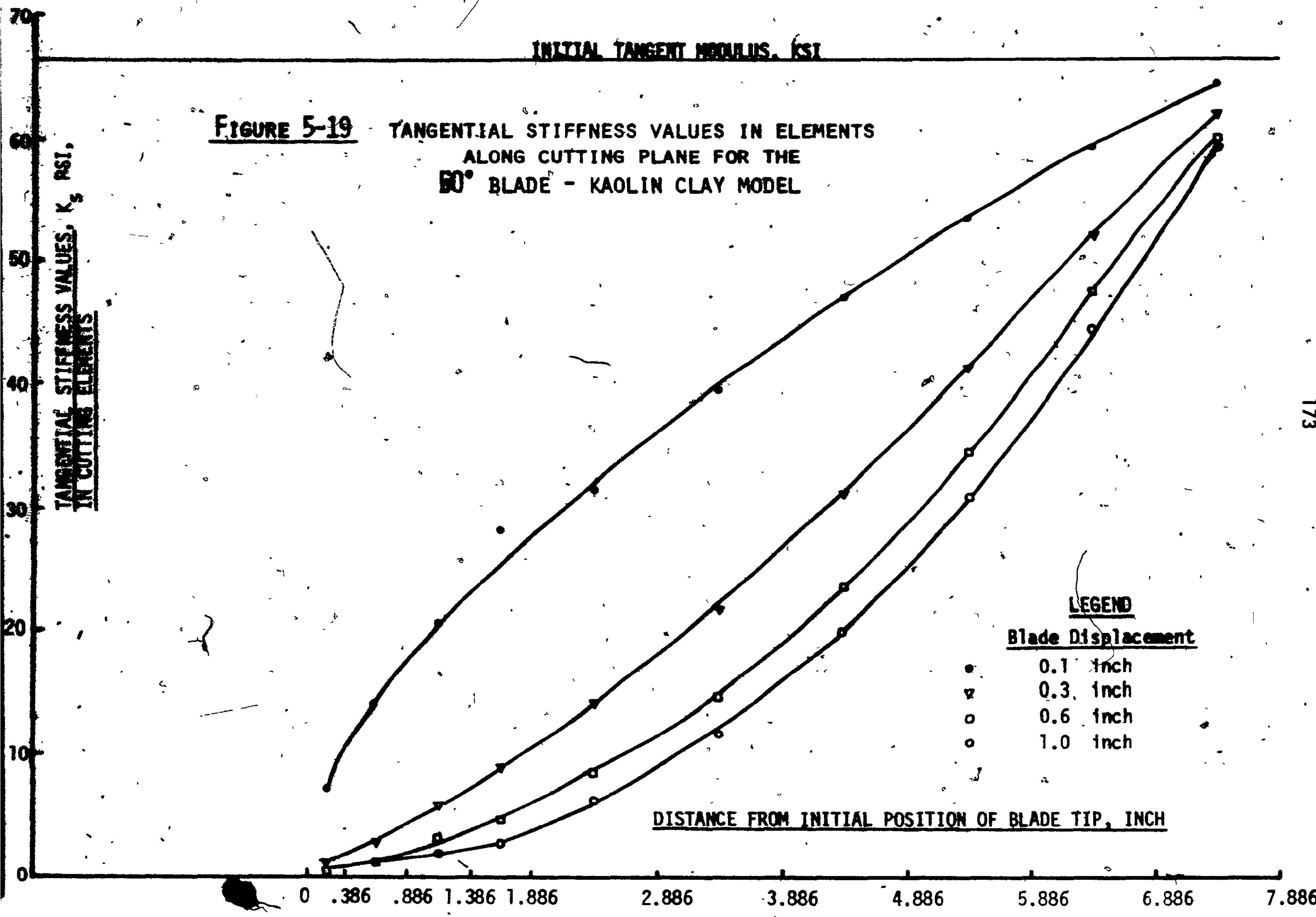

FIGURE 5-19 TANGENTIAL STIFFNESS VALUES IN ELEMENTS ALONG CUTTING PLANE FOR THE 60° BLADE - KAOLIN CLAY MODEL

The results demonstrating the behavior of the interface elements in the finite element analysis of soil cutting are shown in Figs. 5-20 and 5-21. They show the shear displacements and the stresses in the interface elements [inserted between the rigid blades and the clay soil] at blade displacements of 0.1, 0.3, 0.6 and 1.0 inch, respectively. As mentioned previously, the interface elements were assigned properties determined from the direct shear test results of the soil-metal mode, shown in Fig. 4-10. The hyperbolic formulation [Section 2.4.3] was again included to allow the stiffness of these elements to simulate the interface behavior.

It is observed from Figs. 5-20 and 5-21 that the distributions of the tangential relative displacements and stresses along the interface elements are markedly different in the two cases. In both cases the soil moved up the blade surface. Whereas in the case of the 10° inclined blade the tangential displacements and pressures are minimum near the blade tip and increase with distance from the blade tip, the distributions of the tangential displacements and stresses along the 50° inclined interface are shown to be very nearly uniform. In other words, the soil in the case of the 50° inclined blade moved uniformly upward along the blade surface, while in the case of the 10° blade, which penetrated deeper in the soil, the soil near the surface moved upward much more than the soil near the blade tip, creating a situation of variable slip rate along the surface of the blade. These results confirm the observations made by Kostritsyn (1956) who noted that near the surface, soil would rupture or move upward, but at deeper depths the movement was parallel to the direction of travel of the cutter.

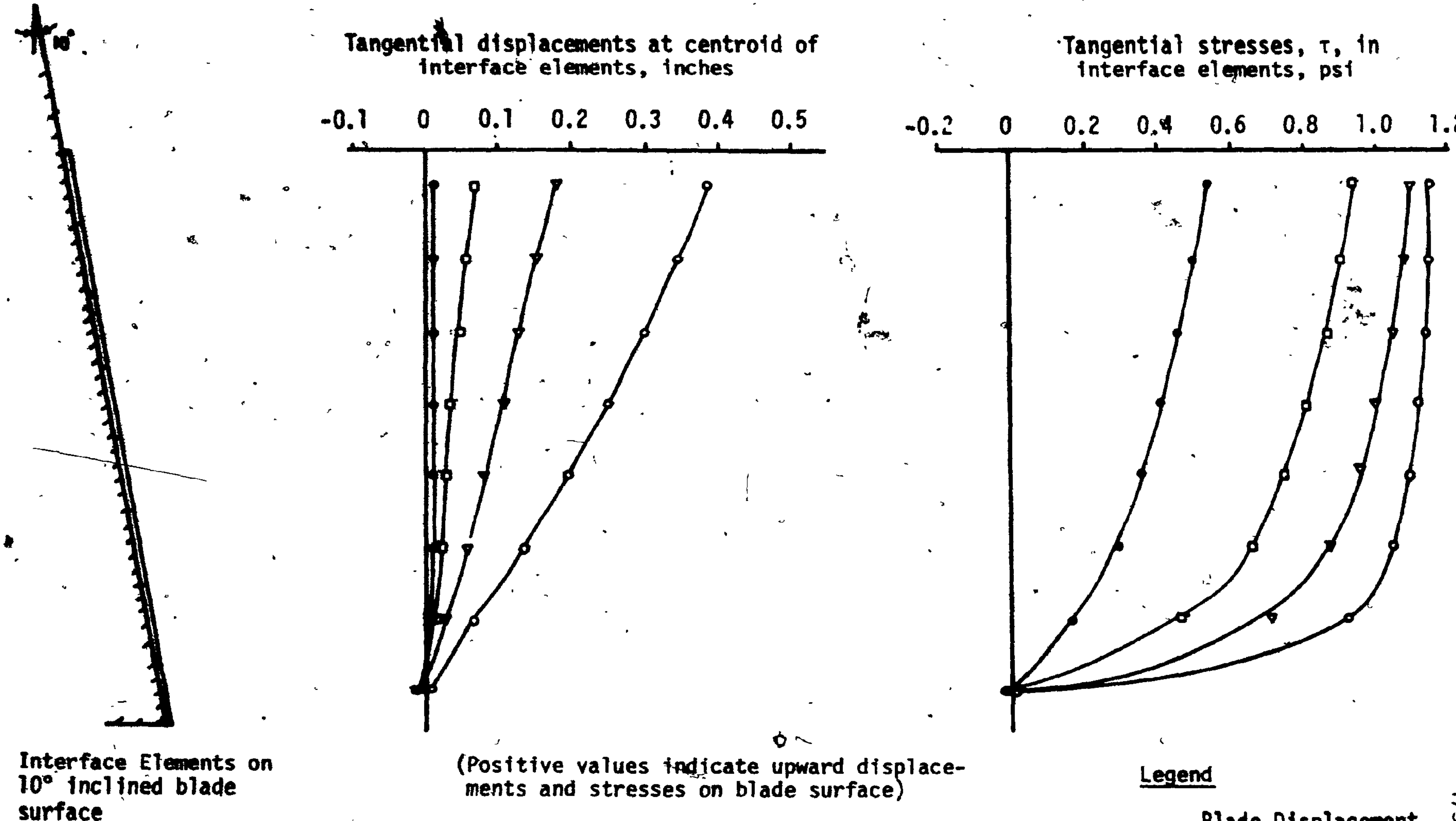

Legend

Blade Displacement

- • 0.1 inch
- ▫ 0.3 inch
- ▿ 0.6 inch
- ○ 1.0 inch

FIGURE 5-20 DISTRIBUTION OF TANGENTIAL STRESSES AND DISPLACEMENTS IN INTERFACE ELEMENTS ON THE 10° BLADE SURFACE

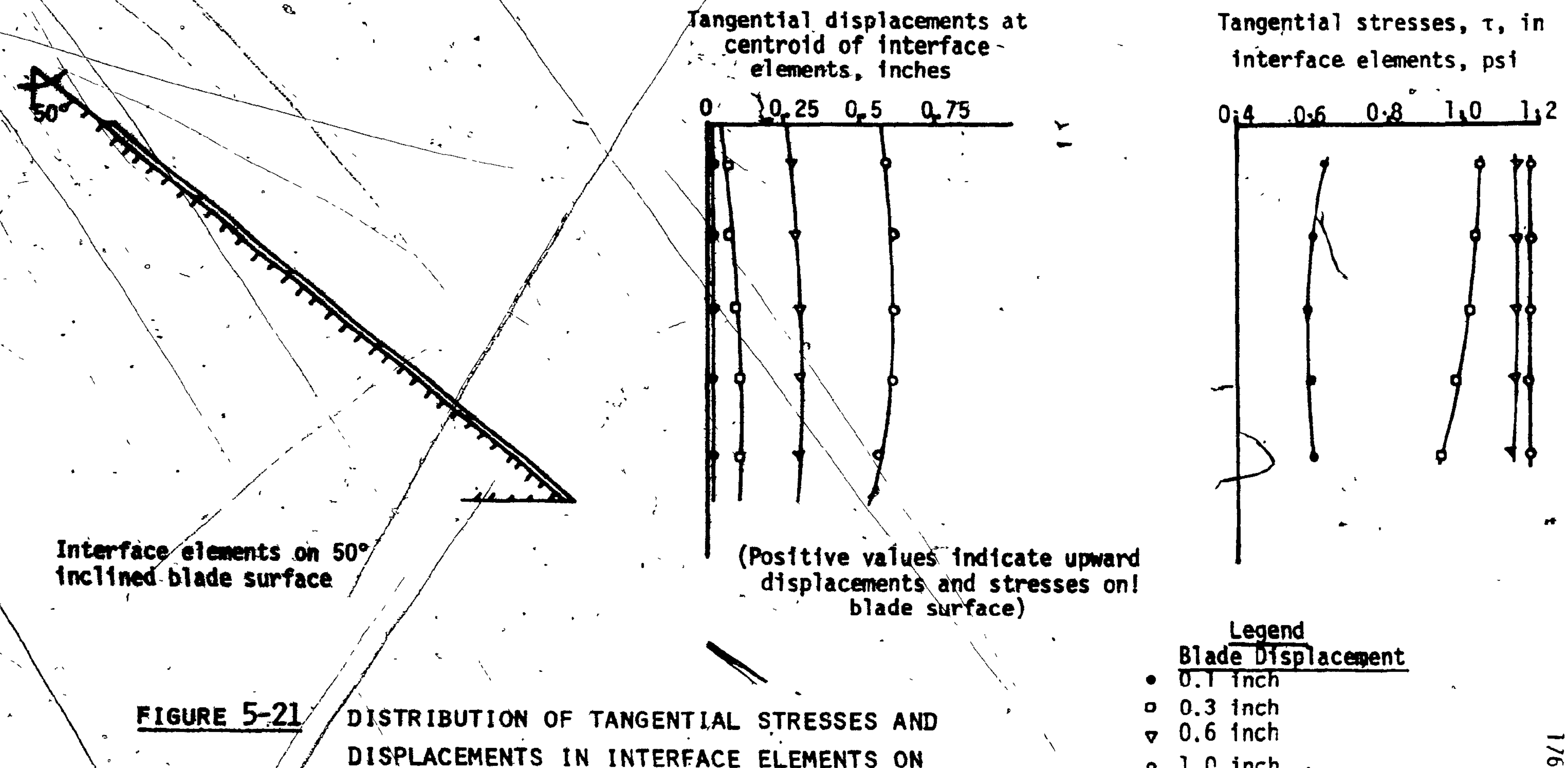

FIGURE 5-21 DISTRIBUTION OF TANGENTIAL STRESSES AND DISPLACEMENTS IN INTERFACE ELEMENTS ON THE 50° BLADE SURFACE

As mentioned earlier, failure zones are located by examining the maximum shear stress induced in each element after each increment. If this stress is equal to or greater than the shear strength of the soil at that location, the modulus value, E, for the element is reduced to a small magnitude indicating failure. Thus, the extent of the failed zone is established on the basis of these elements in which the induced stresses equalled or exceeded the limiting stresses at 20% strain obtained from the stress-strain curves presented in Fig. 4-7.

It must be emphasized, however, that this presentation is not an indication of the establishment of failure or separation surfaces since the criterion of exceeding the shearing strength of the soil is obtained from the plane strain test results where the strength of the soil is taken as the maximum value obtained at 20% strain. In the strength tests, the samples did not fail along distinct planes but exhibited bulging deformation. The failed elements should, therefore, be considered as the elements where failure planes would develop if the soil exhibited failure along shear planes rather than flow.

The development of the failure zones for the 10° and 50° inclined blade idealizations are shown in Figs. 5-22 and 5-23, respectively. The elements failure started in increment No. 7 [0.7 inch of blade displacement] for the 10° blade problem, and in increment No. 5 [0.5 inch of blade displacement] for the 50° blade idealization. The failure patterns show that the failed elements started at the leading edge of the blade and progressed toward the soil surface. The effect of the blade inclination on the shape and progress of the failure zones

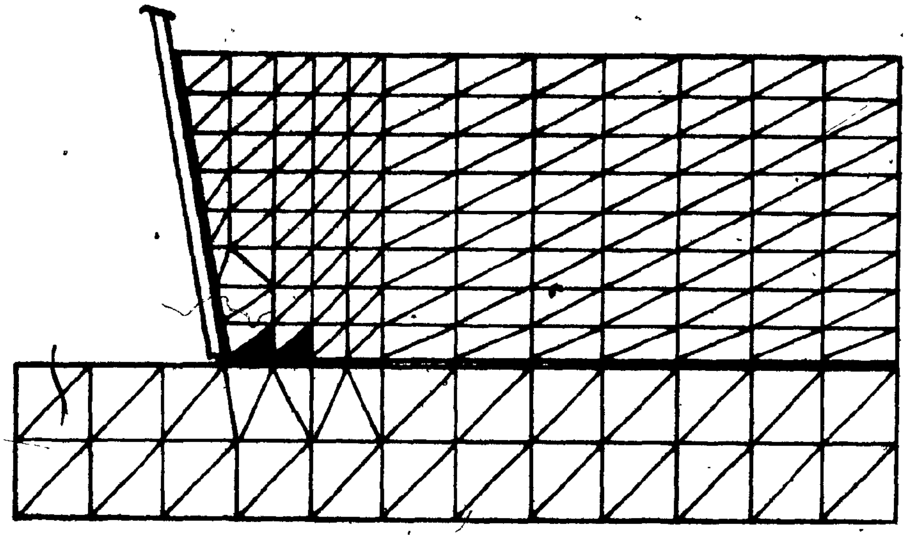

INCREMENT No. 7 - BLADE DISPLACEMENT = 0.70 inch

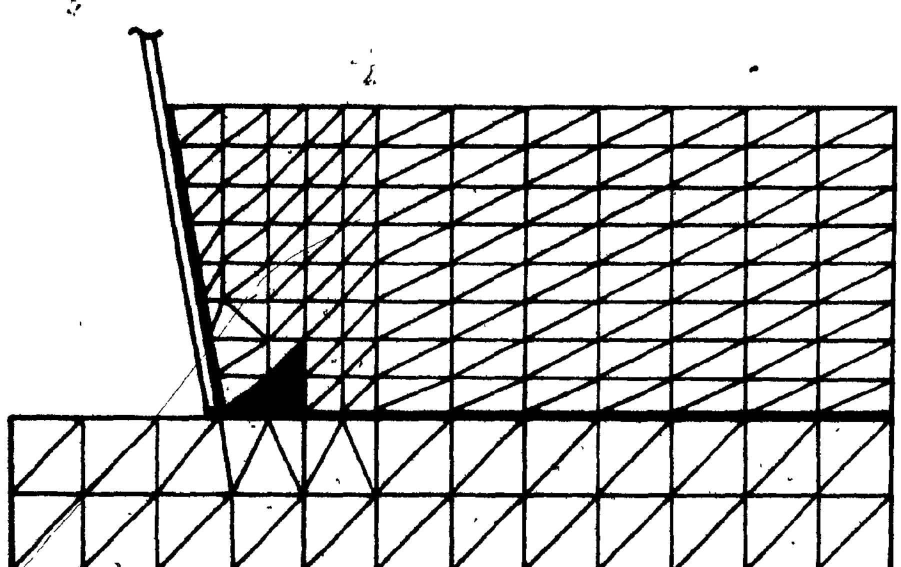

INCREMENT No. 8 - BLADE DISPLACEMENT = 0.80 inch

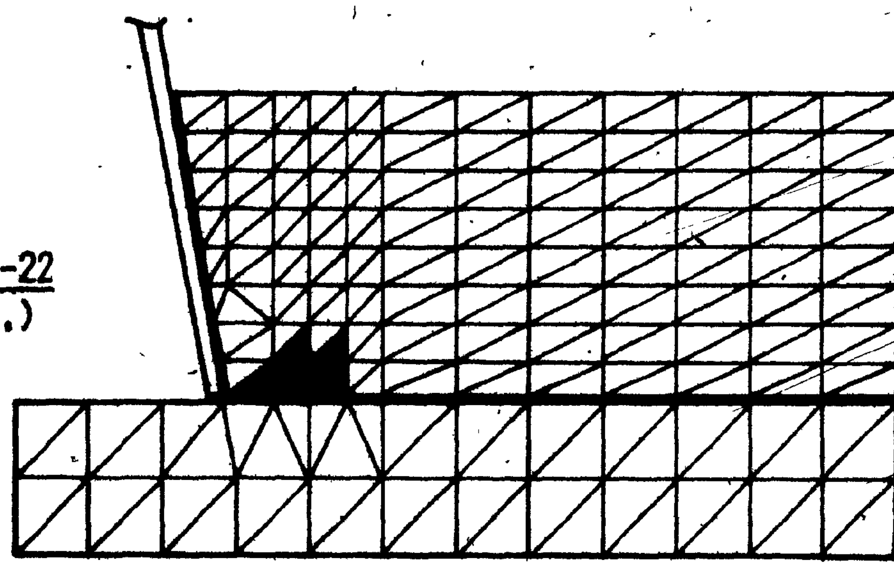

FIGURE 5-22
(CONT'D.)

INCREMENT No. 9 - BLADE DISPLACEMENT = 0.90 inch

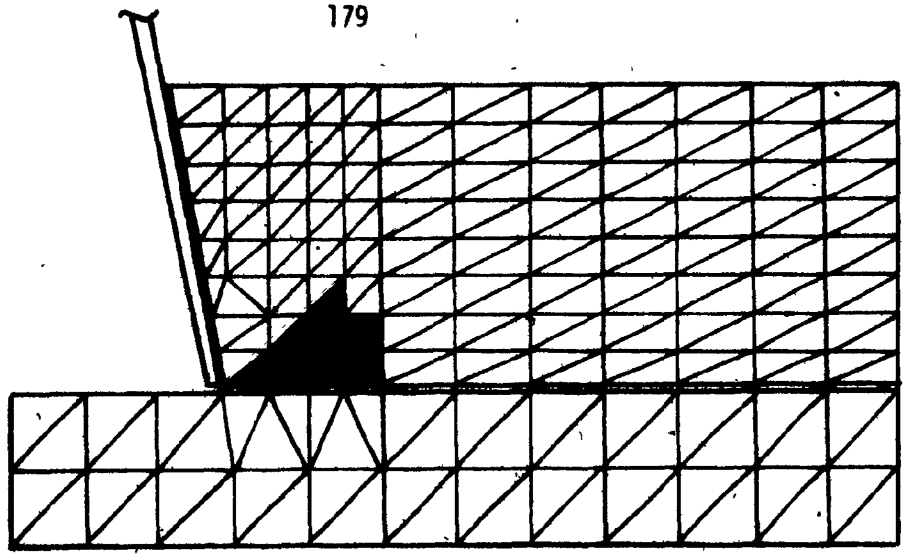

INCREMENT No. 10 -- BLADE DISPLACEMENT = 1.0 inch

FIGURE 5-22 DEVELOPMENT OF FAILURE ZONES FOR THE 10° INCLINED BLADE - KAOLIN CLAY SYSTEM

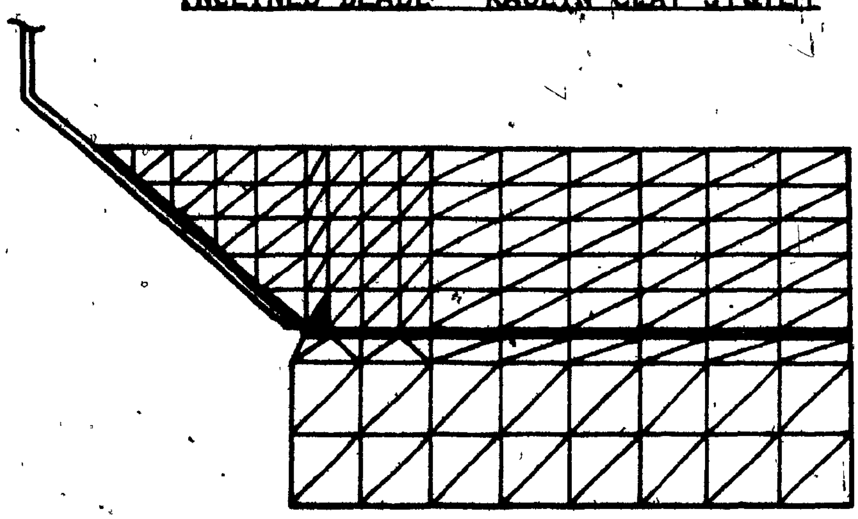

INCREMENT No. 5 - BLADE DISPLACEMENT = 0.50 inch

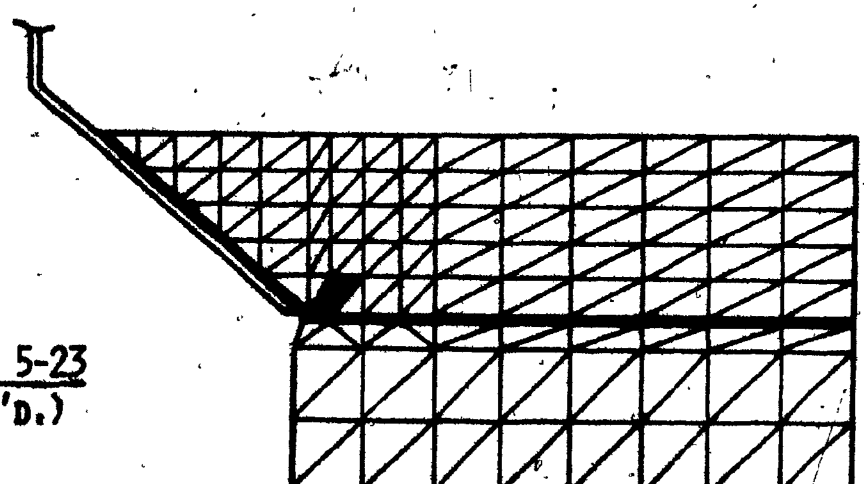

FIGURE 5-23
(CONT'D.)

INCREMENT No. 6 - BLADE DISPLACEMENT = 0.60 inch

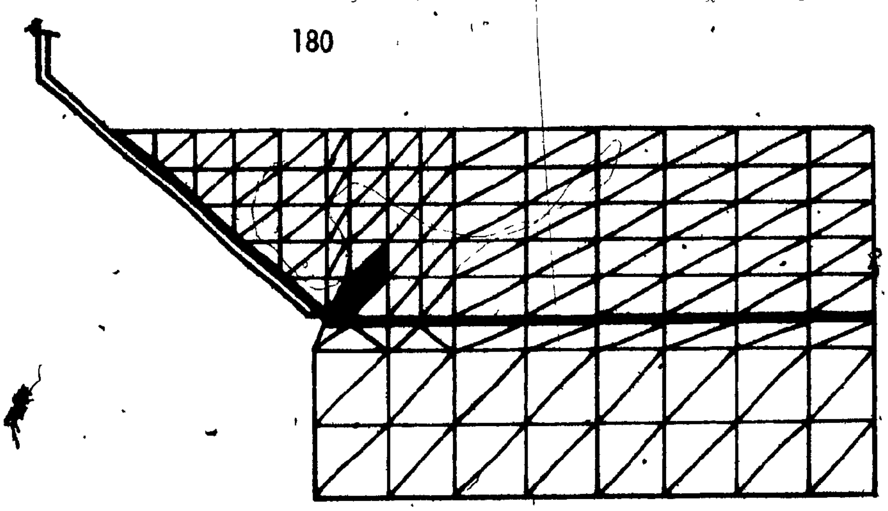

INCREMENT No. 7 - BLADE DISPLACEMENT = 0.70 inch

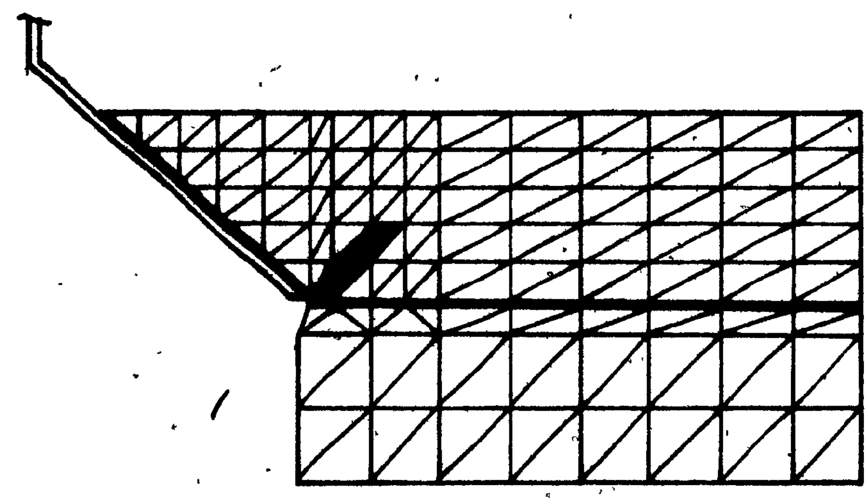

INCREMENT No. 8 - BLADE DISPLACEMENT = 0.80 inch

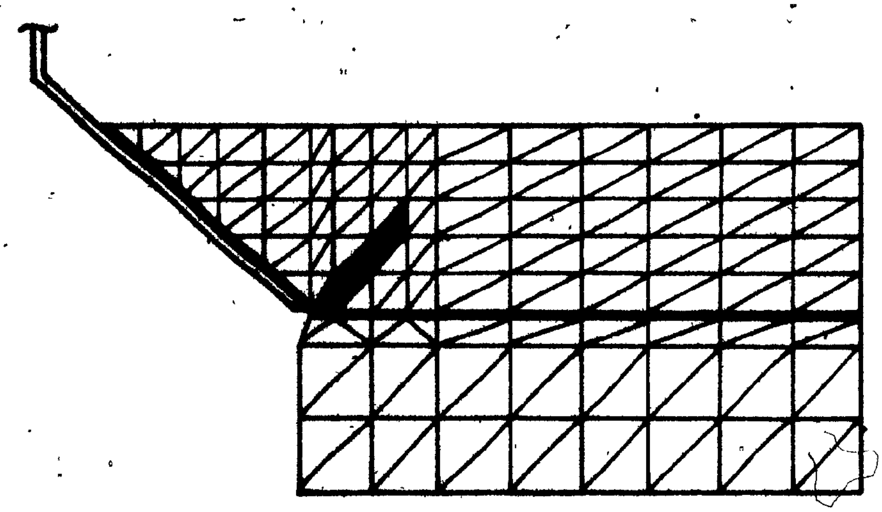

INCREMENT No. 9 - BLADE DISPLACEMENT = 0.90 inch

FIGURE 5-23 (CONT'D) DEVELOPMENT OF FAILURE ZONES FOR THE 50° INCLINED BLADE - KAOLIN CLAY SYSTEM

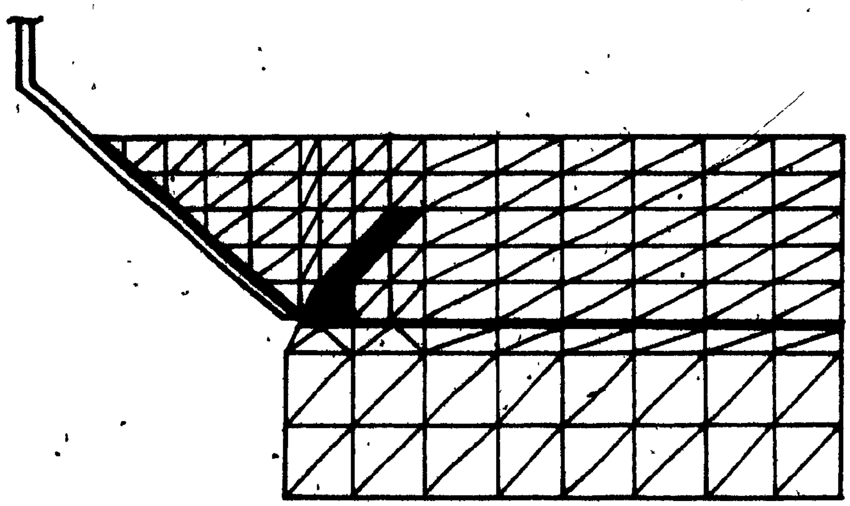

INCREMENT No. 10 - BLADE DISPLACEMENT = 1.0 inch

FIGURE 5-23 DEVELOPMENT OF FAILURE ZONES FOR THE 50° INCLINED BLADE - KAOLIN CLAY SYSTEM is clearly demonstrated in these Figures. While in the 10° blade case the elements are shown to fail in clusters starting at the blade tip and progressing toward the soil surface, the 50° blade figures show single elements failing along a well-defined plane. The correlation of these failure zones and actual experimental observations needs further documentation; however, they appear to be indicative of actual progressive failure.

5.5 NORMAL PRESSURE DISTRIBUTION

Normal pressures on the surface of the blades, as displacements are increased, are shown in Figs. 5-24 and 5-25. Figure 5-24 shows the distributions for the 10° inclined blade at displacements of 0.1, 0.3, 0.6 and 1.0 inch. The normal pressure distributions, in this case, are seen to be uniform over about three-quarters of the blade surface. Near the blade tip, however, the pressure increases to about 145 to 165 per cent of the average pressure over the whole surface. The shape of the distribution curve remains the same throughout the entire loading range. Figure 5-25 shows the normal pressure distributions on the 50° inclined blade at similar displacements. In this case, the normal pressures increase near the tip of the blade to about 200 to 300 per cent of the average pressure over the whole blade surface.

Another look at Figs. 5-24 and 5-25 will show that in the case of the 10° inclined blade, the pressure increases proportionally with increasing blade displacement. However, this is not the case for the 50° blade, as the pressure is shown to increase at a much higher

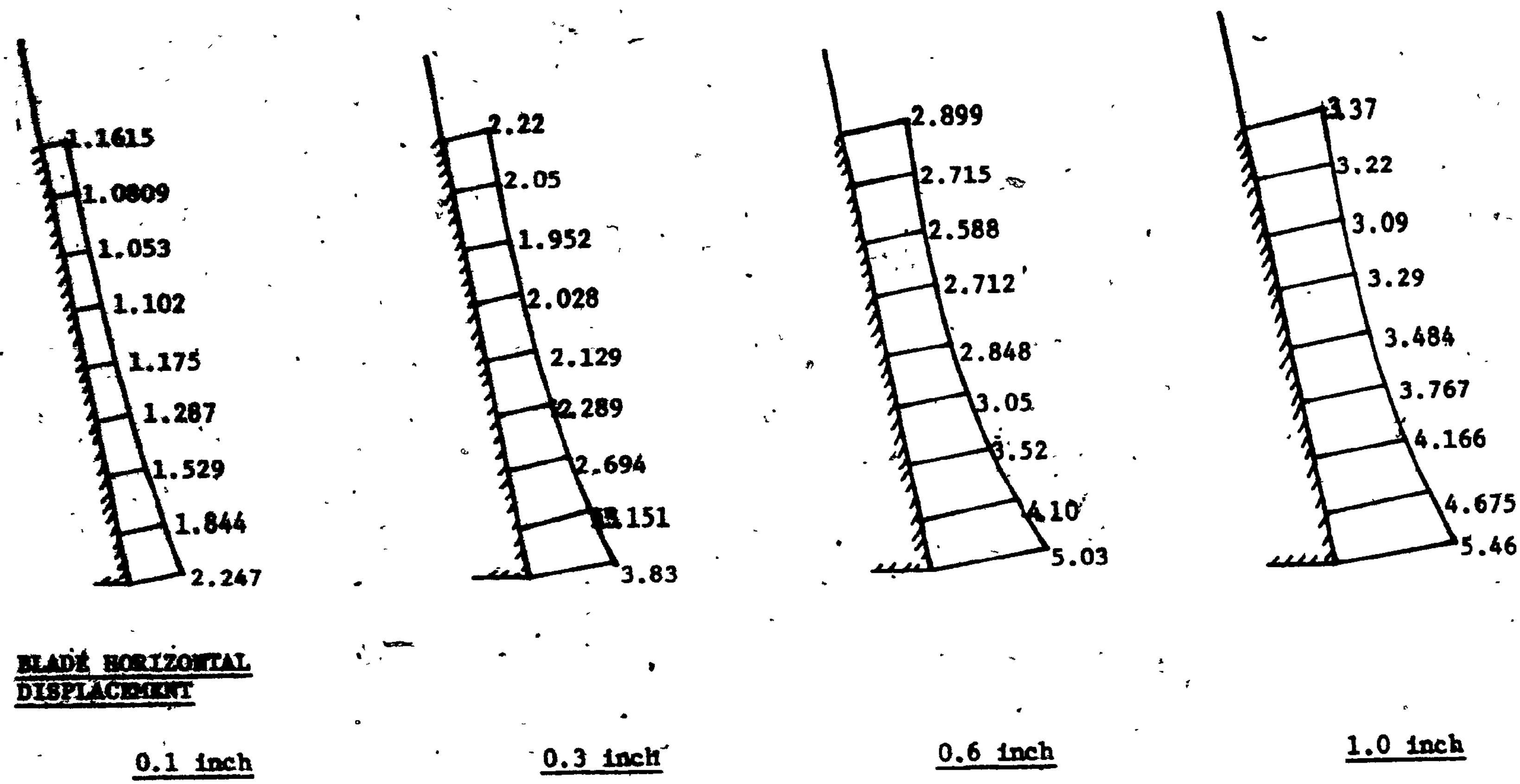

SCALE: 1 inch = 7.2 psi

FIGURE 5-24 NORMAL PRESSURE DISTRIBUTION ON THE 10° INCLINED BLADE

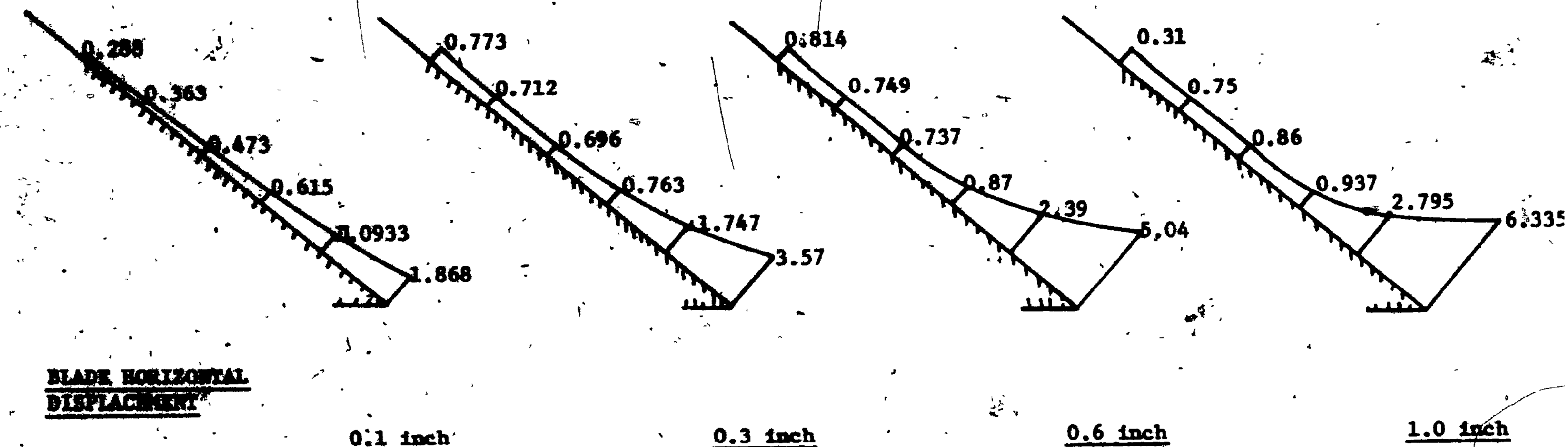

SCALE: 1 inch = 7.2 psi

FIGURE 5-25 NORMAL PRESSURE DISTRIBUTION ON THE 50° INCLINED BLADE rate near the tip than in the middle and upper locations. Furthermore, the data shown indicate that the upper one-half of the 50° blade does not materially add to the draft, while in the case of the 10° blade the whole surface contributes to the developed forces.

In general, the smaller the forces or pressures developed on the cutting tool the better the performance. But the extent of soil manipulation must also be considered because it may alter any conclusions that are based on pressures alone. At the present time, no information is available to indicate what magnitude or distribution of pressure can be considered to be good performance. Certainly, however, criteria could be developed and performance measured in terms of the distribution and magnitude of pressure on the soil-engaging surface of cutting tools, provided that the degree of soil manipulation is taken into consideration.

5.6 COMPARISON OF ANALYSIS WITH EXPERIMENTAL RESULTS

This Section presents comparisons between the soil cutting experimental data reported in Chapter 4, and the finite element analysis presented in the previous Sections of this Chapter. Such comparisons permit a rational assessment of the admissibility and viability of the finite element method as a means of predicting the performance of a cutting tool - the stated aim of the current study [Chapter 1]. In addition, this Section examines the constraints and requirements implied by the proposed analytical technique. The discrepancies between the theoretical model and the physical conditions are also evaluated and their significance discussed.

As mentioned earlier [Chapter 1], the problem at hand is a mixed boundary value problem with the boundary conditions specified in terms of both displacement and stress. In such problems, the stress and velocity fields must be compatible as there is no apparent independence between the two fields. Therefore, it is essential to establish separate correlations of both the stress distribution and the soil deformation with the physical measurements, before the technique is judged to be satisfactory. In the present study, the correlation is done in the following fashion:

1. The calculated blade reactions [both vertical and horizontal] obtained from the finite element solution are compared with the experimentally measured forces. Such correlation is an indication of the extent of similarity between the stress fields.

2. The contours of the nodal displacements obtained from the finite element model proposed are superimposed on the contours obtained from the recorded grid deformation to demonstrate the similarities and discrepancies in the deformation patterns.

3. Finally, as differences in the stress and deformation fields are reflected on the scalar values of the energy field, it is reasoned that the examination of the deformation energy values would provide a rational and expedient means of evaluating and comparing the analytical solution with the values obtained from experiments and experimental analysis.

5.6.1 Comparison of Measured and Calculated Forces

The load-displacement curves as obtained from the finite element analysis based on the proposed model are shown in Fig. 5-26 for the horizontal force and in Fig. 5-27 for the vertical load for both the 10° and 50° inclined blades, respectively. The experimental results are also plotted on the same Figures for comparison.

The agreement between the experimental and the finite element results is very satisfactory in the case of the horizontal forces for the two blade inclinations analyzed. In case of the 50° blade, the difference is about 3 pounds over the whole displacement range analyzed, with the analytical results lying always below the experimental curve. For the 10° blade, the errors are found to be almost negligible up to blade displacement of 0.4 inch, beyond which the analytical and test results diverge, with the predicted results again lying below the experimental values.

The vertical forces computed from the finite element analysis, shown in Fig. 5-27, are seen to be smaller than the measured values. A more complete comparison of the analytical results with those obtained from the measured force-displacement curves is presented in Table 5-1. The comparisons are made in terms of measured and predicted values and are reported at 0.25 inch intervals over a total blade displacement of 1.0 inch. The deviations between the two sets of values, expressed as a percentage of the applicable experimental values, are also indicated.

No analyses are presented here for blade inclinations lying between the 10° and the 50° angles. It was reasoned that these angles

FIGURE 5-26 COMPARISON OF MEASURED AND PREDICTED VALUES OF DEVELOPED HORIZONTAL FORCE ON THE 10° AND 50° INCLINED BLADES (KAOLINITE CLAY)

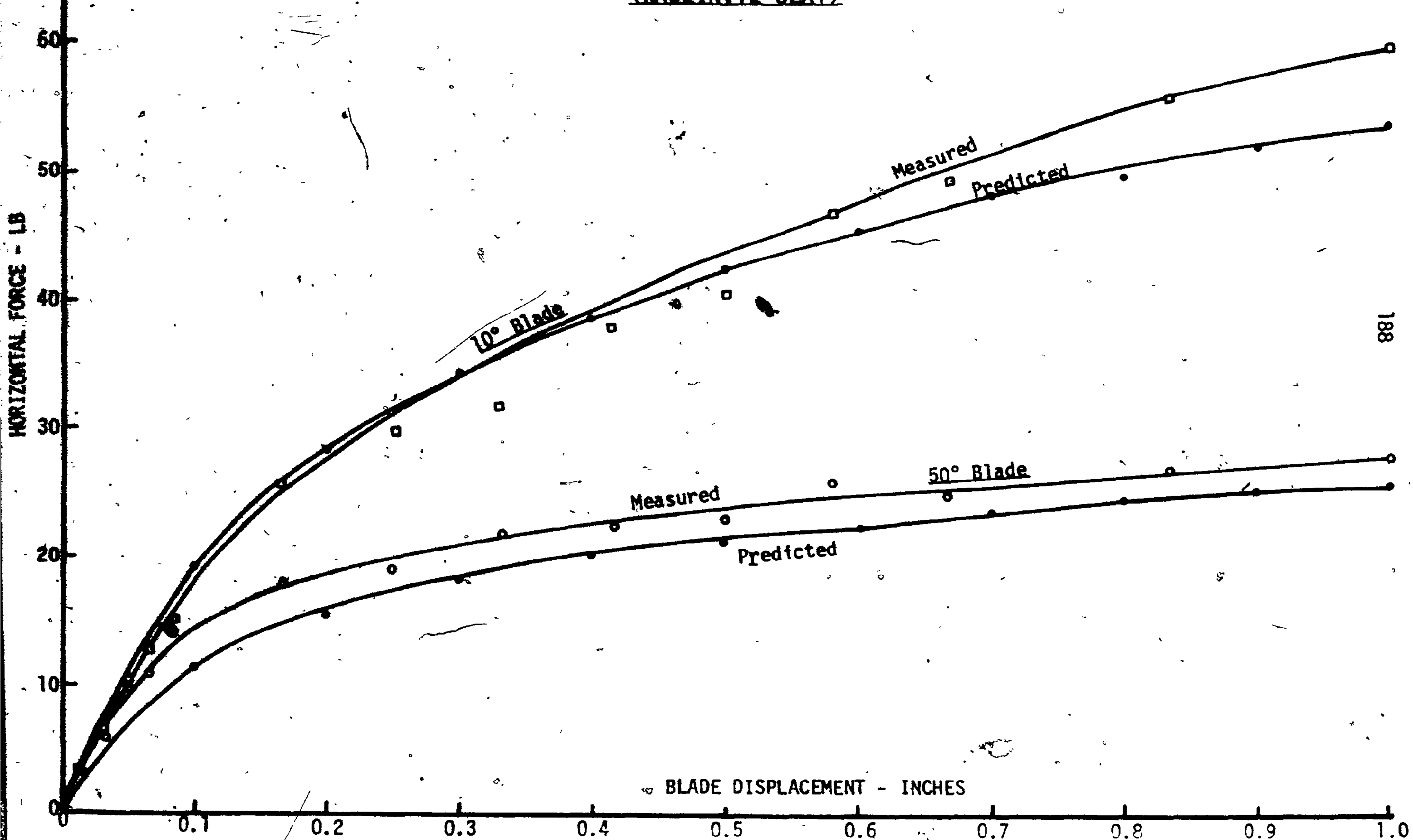

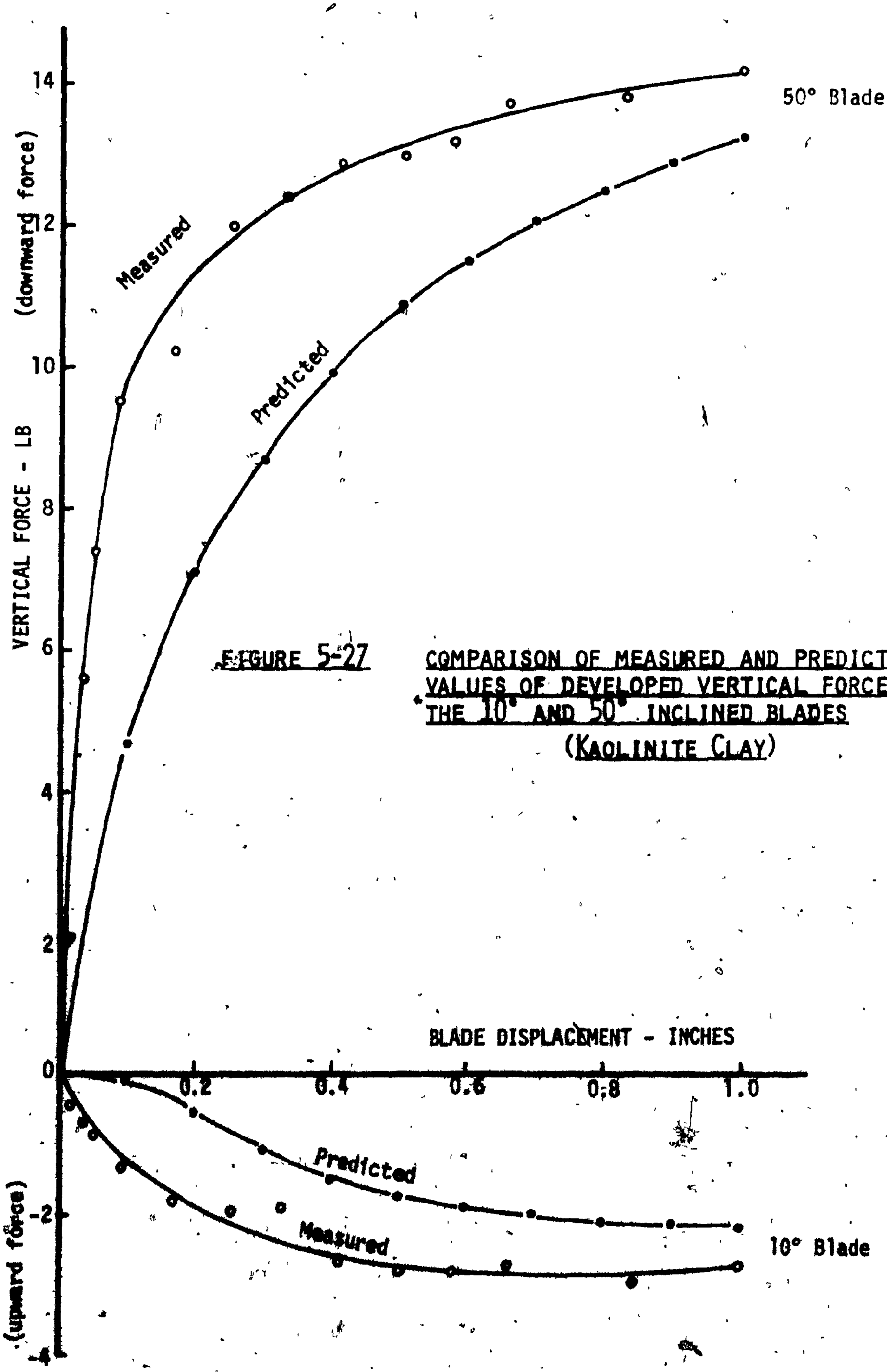

FIGURE 5-27 COMPARISON OF MEASURED AND PREDICTED VALUES OF DEVELOPED VERTICAL FORCE ON THE 10° AND 50° INCLINED BLADES (KAOLINITE CLAY)

TABLE 5-1

COMPARISON OF MEASURED AND PREDICTED VALUES OF DEVELOPED FORCES ON THE 10° AND 50° INCLINED BLADES

Test No.	Angle of Blade with Vertical	Tool Displacement (d) inch	Horizontal Force (lb)			Vertical Force (lb)		
			Measured	Predicted	% Difference	Measured	Predicted	% Difference
27	10°	0.25	29.8	31.6	+ 6.0	-2.13	- 0.8	-62.4
		0.50	40.8	42.46	+ 4.0	-2.75	- 1.75	-36.3
		0.75	52.0	49.5	- 4.8	-2.85	- 2.05	-28.0
		1.00	56.1	54.07	- 3.6	-2.7	- 2.15	-20.3
30	10°	0.25	30.5	31.6	+ 3.6	-1.95	- 0.8	-64.1
		0.50	44.0	42.46	- 3.5	-2.13	- 1.75	-17.8
		0.75	53.5	49.5	- 7.47	-2.25	- 2.05	- 8.9
		1.00	60.0	54.07	- 9.9	-2.30	- 2.15	- 6.5
29	50°	0.25	20.0	17.5	-12.5	9.3	8.1	-12.9
		0.50	24.0	21.25	-11.45	12.2	10.9	-10.7
		0.75	26.0	24.2	- 6.92	13.8	12.3	-10.9
		1.00	28.2	26.07	- 7.55	14.2	13.2	- 7.0
31	50°	0.25	20.5	17.5	-14.6	12.0	8.1	-32.5
		0.50	24.3	21.25	-12.6	13.1	10.9	-16.8
		0.75	26.5	24.2	- 8.7	13.8	12.3	-10.9
		1.00	29.0	26.07	-10.1	14.13	13.2	- 6.6

Notes: (1) Predicted values refer to values obtained from the finite element analysis.

(2) Difference expressed in percentage of measured values.

represent a bound on the verification of the proposed model, and, if the technique is found suitable for these inclinations, it could be assumed that it may be used successfully for any blade inclination within these limits.

Examination of the data in Figs. 5-26 and 5-27 and Table 5-1 indicates that the analytical model provides reasonable estimates of the developed forces on the cutting tools analyzed. This is particularly true of the horizontal forces, in which the average error of estimate is of the order of 8%, while the maximum error is some 15%. For the vertical forces, the values obtained from the theoretical solution are, however, more subject to variation from the experimentally deduced values especially in the case of the 50° inclined blade. Such differences in the vertical forces can be attributed to the effect of the soil deformation behind and below the blades, effect that has not been considered in the finite element idealization.

5.6.2 Comparison of Analytical and Experimental Deformation Fields

It will be recalled that photographic records were made of the deforming grid at 5-second intervals of tool motion. With the aid of an x-y plotter and a process control computer, the coordinate pairs corresponding to each of the plotted points were obtained. The particle displacements, over successive grid positions, were then calculated on the basis of the change of the particle position in the coordinate directions. These calculations were performed by the initial section of program "FIT" Appendix E. A more comprehensive account of these techniques are provided in Appendices B and F.

The experimentally measured displacement fields are plotted in Figs. 5-28 to 5-31 together with the analytical fields obtained from the finite elements nodal displacements, for a tool displacement of 1.0 inch. These deformation fields are presented in terms of horizontal and vertical displacements and are shown for the 10° inclined blade in Figs. 5-28 and 5-29, and for the 50° inclined blade in Figs. 5-30 and 5-31, respectively. As a means of facilitating comparisons, the results are illustrated in contour forms plotted in the undeformed position.

In these Figures, the discontinuity in displacements at the level of the blade tip is clearly demonstrated in the experimental plots. However, a close examination of the horizontal displacement fields reveals that the contours are only discontinuous in the vicinity of the blades, while at a distance they are seen to be continuous above and below the cutting plane. Such behavior implies that the discontinuity propagates with the blade movement. This is not the case in the finite element solution where the discontinuity is assumed to extend all the way to the end boundary. Moreover, the deviation between the experimental and the analytical horizontal displacement fields indicates that the finite element solution underestimates the horizontal displacements in the zone near the soil surface, while it overestimates in the soil mass situated directly above the cutting plane.

Examination of the vertical displacement fields, Figs. 5-29 and 5-31, indicates a significant deviation in the location of the zero

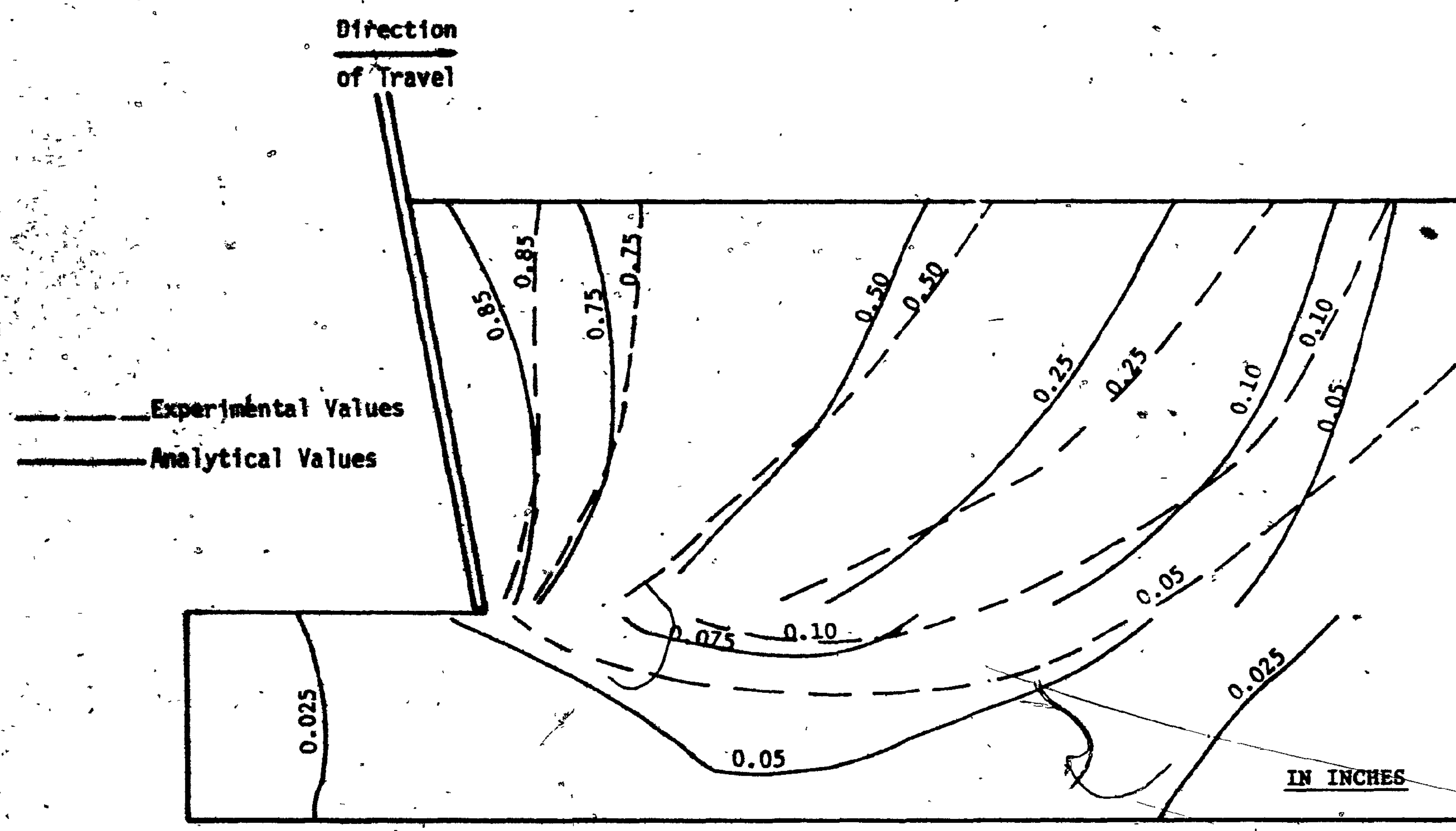

FIGURE 5-28 EXPERIMENTAL AND ANALYTICAL HORIZONTAL DISPLACEMENT FIELDS FOR THE 10° INCLINED BLADE-SOIL SYSTEM

[BLADE DISPLACEMENT = 1.0 INCH]

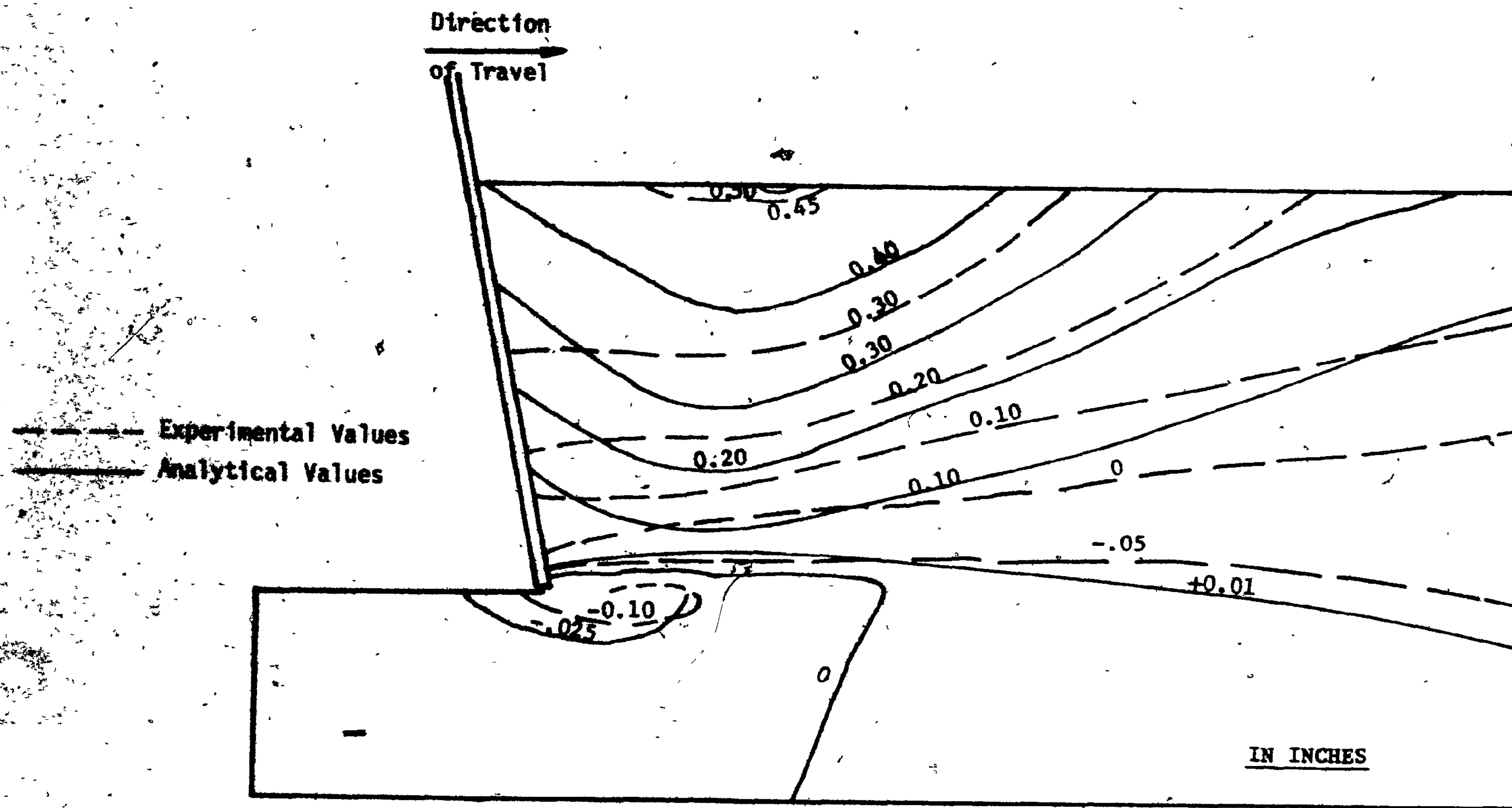

FIGURE 5-29 EXPERIMENTAL AND ANALYTICAL VERTICAL DISPLACEMENT FIELDS FOR THE 10° INCLINED BLADE-SOIL SYSTEM

[BLADE DISPLACEMENT = 1.0 INCH]

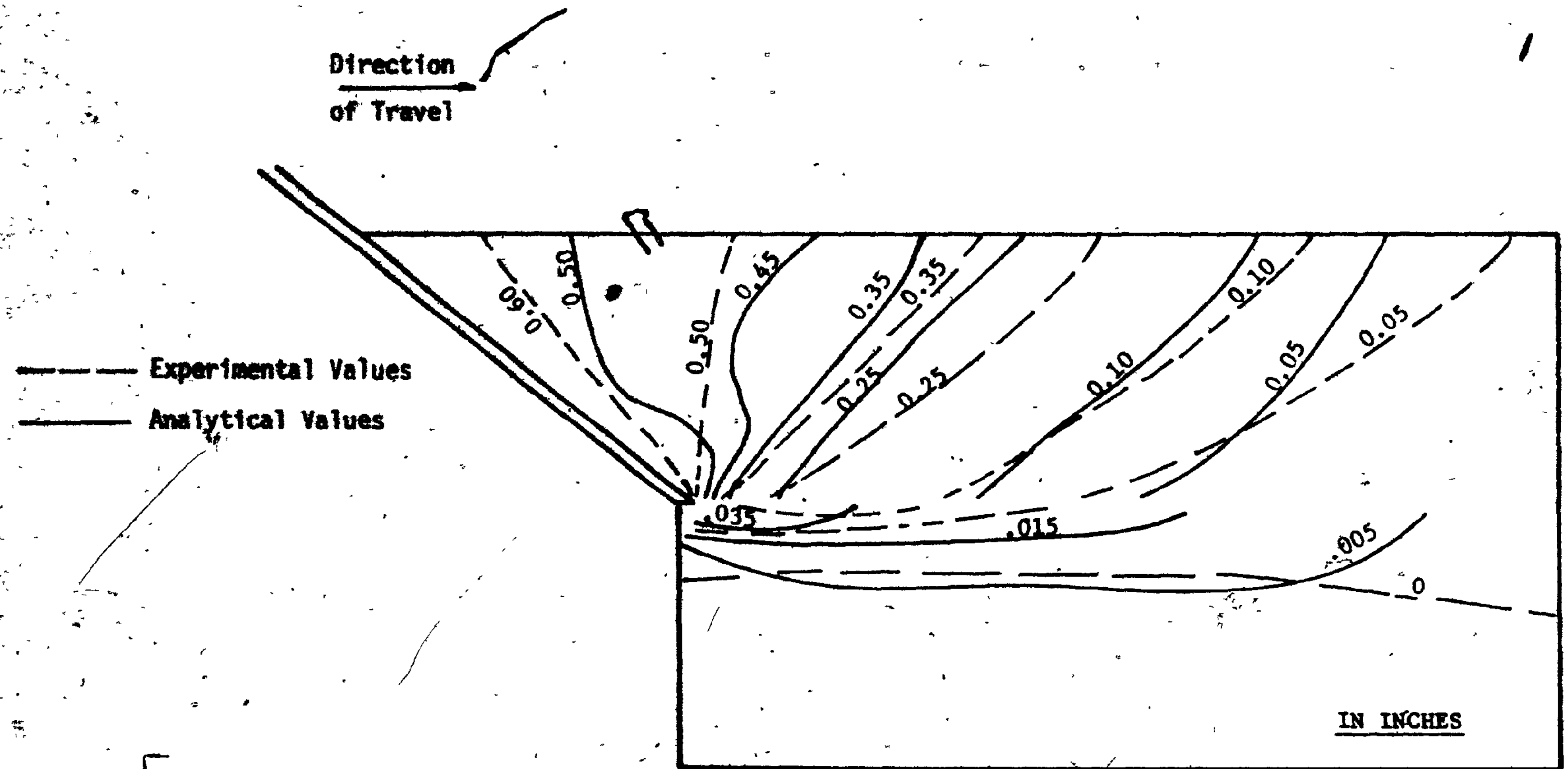

FIGURE 5-30 EXPERIMENTAL AND ANALYTICAL HORIZONTAL DISPLACEMENT FIELDS FOR THE 50° INCLINED BLADE-SOIL SYSTEM

[BLADE DISPLACEMENT = 1.0 INCH]

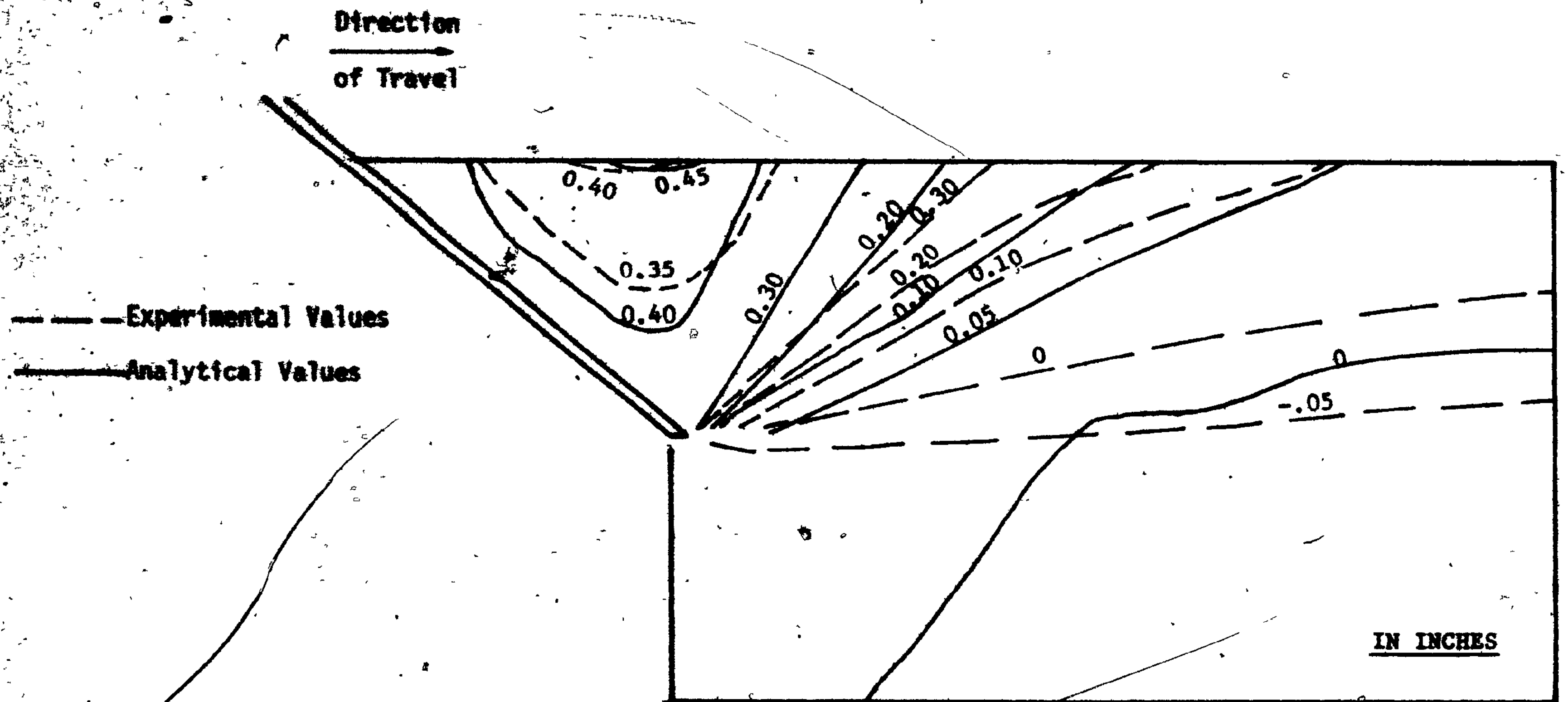

FIGURE 5-31 EXPERIMENTAL AND ANALYTICAL VERTICAL DISPLACEMENT FIELDS FOR THE 50° INCLINED BLADE-SOIL SYSTEM

[BLADE DISPLACEMENT = 1.C INCH]

vertical displacement contour dividing zones of upward and downward movements. It is shown that the experimental zero contour lies above the cutting plane for both the 10° and 50° inclined blades. The corresponding line from the analytical analysis, however, takes a different shape and lies below the experimental one for both cases. Nevertheless, the qualitative agreement between the two fields [experimental and analytical] is seen to be generally satisfactory.

5.6.3 Prediction of Deformation Energy

It has already been noted [Section 4.B.5] that the deformation energy results shown so far have been experimental in nature, in that they were obtained by:

1. the application of the visioplasticity method to the experimentally recorded deformation fields with the assumption that the stress-deformation behavior of the soil can be described by a rigid plastic model. This model in turn demands the following conditions:

   (a) the application of a yield criterion,

   (b) the measurement of a deformation field from experiments and calculations of the resultant strain rate fields within the loaded soil, and

   (c) the selection of plasticity flow rules consistent with the choice of the yield criterion.

2. the integration of the areas under the experimentally measured force-displacement curves.

It will be recalled that the proposed energy budget for the tool-soil system, given as Eq. (4.2), was written as:

$$\int_s F\,ds = D + I$$

$$\text{(Work Input)} = \begin{pmatrix}\text{Deformation}\\ \text{energy loss}\end{pmatrix} + \begin{pmatrix}\text{Interfacial}\\ \text{energy loss}\end{pmatrix}$$

As the system is in a state of dynamic equilibrium such that the input energy is expended completely in producing plastic deformation with no work output and with negligible interfacial energy losses, the above equation can be reduced to:

$$\int_s F\,ds = D$$

Energy models for the analysis and the prediction of tool-soil interaction performance will rely on the ability to measure [or determine] response function performance. So, while the results of integrating the areas under the experimentally measured force-displacement curves can be considered as a measure of the work input, the response function is characterized by the work output or the energy dissipated in the system. The work output is determined by two methods: one by using the visioplasticity method, the other by using the finite element stress and strain fields.

First Method

For a material which follows the von Mises yield criterion, the total work done, and hence the total energy dissipated in plastic deformation under plane-strain conditions was expressed previously by Eq. (4.17), and repeated here for convenience as:

$$D = 2b \int_{t_1}^{t_2} \int_{x_1}^{x_2} \int_{y_1}^{y_2} K \sqrt{I_2}\, dx\, dy\, dt \tag{5.4}$$

Second Method

The deformation energy during a time interval can be evaluated from the finite element solution by the following equation [Desai and Abel (1972)]:

$$D = \int_{v} \int_{t} [\sigma]^T d[\varepsilon] \quad dt\, dv \tag{5.5}$$

where

$[\sigma]$ = element stress matrix.

$d[\varepsilon]$ = element incremental strain matrix.

t = increment duration.

v = element volume.

These two methods are used to calculate the deformation energy of the tool-soil system. The results obtained from their application are shown in Figs. 5-32 and 5-33 for the 10° and 50° inclined blade problems, respectively. Comparisons of these results with those obtained from the integration of the areas under the experimentally

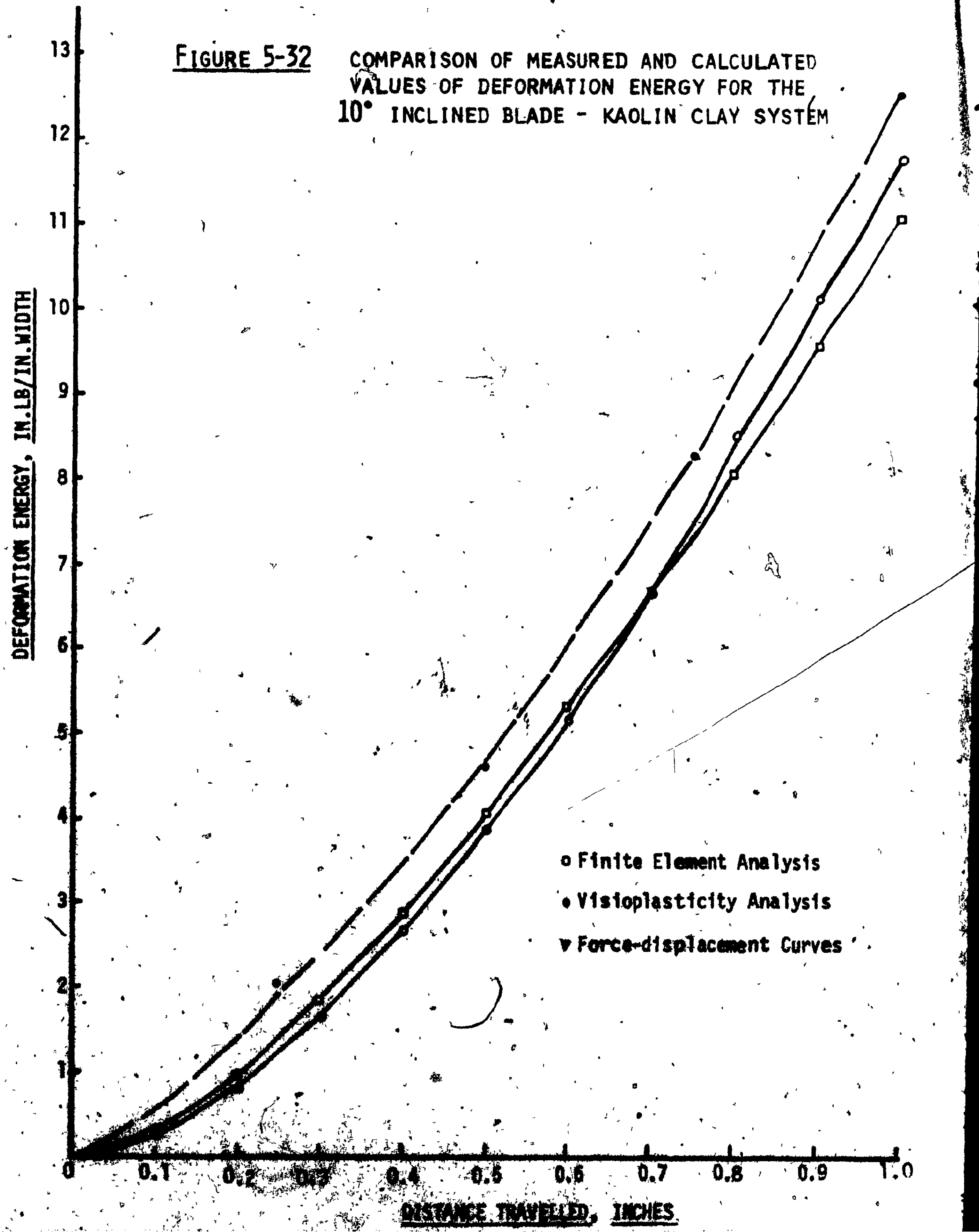

FIGURE 5-32 COMPARISON OF MEASURED AND CALCULATED VALUES OF DEFORMATION ENERGY FOR THE 10° INCLINED BLADE - KAOLIN CLAY SYSTEM

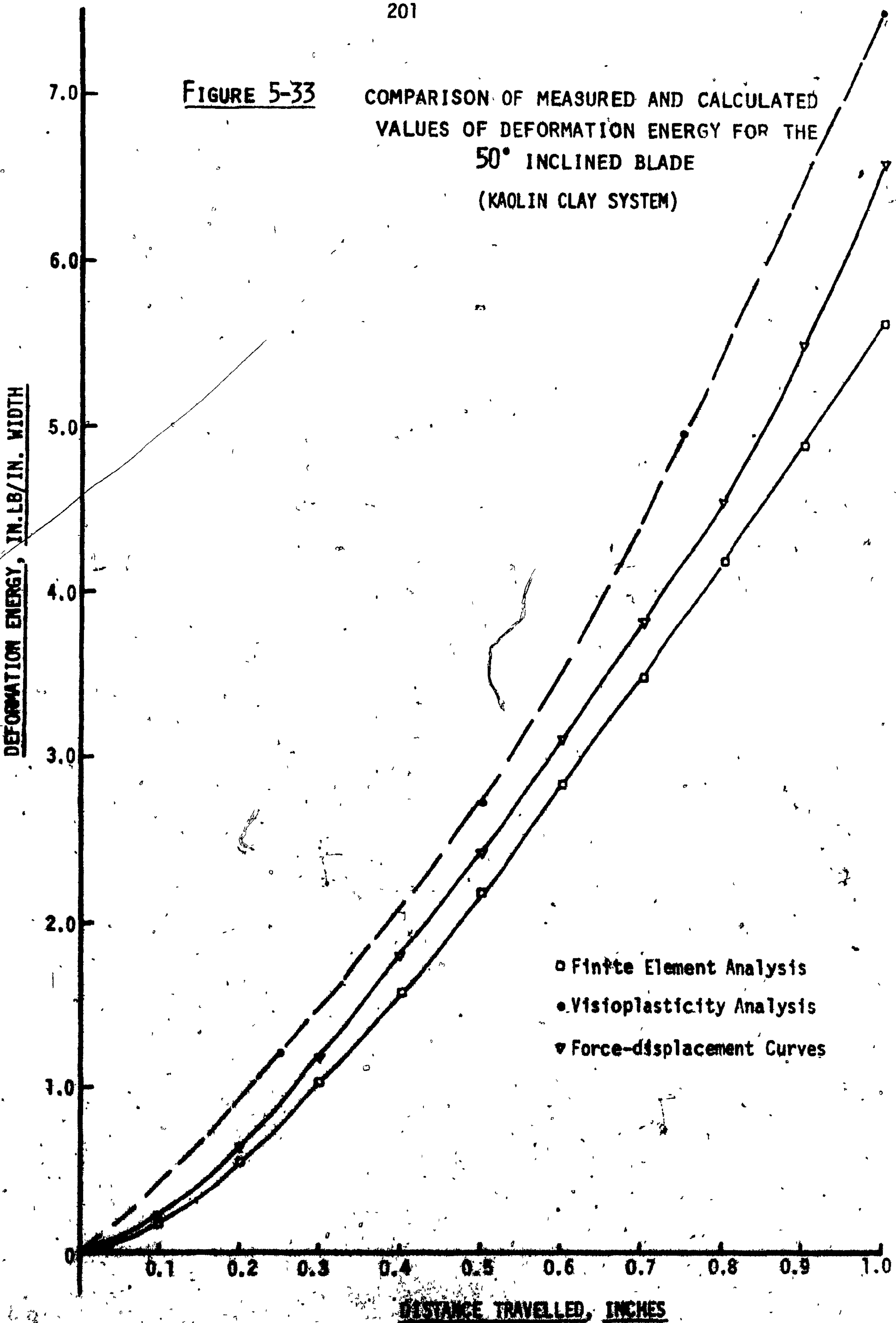
FIGURE 5-33
COMPARISON OF MEASURED AND CALCULATED VALUES OF DEFORMATION ENERGY FOR THE 50° INCLINED BLADE
(KAOLIN CLAY SYSTEM)
DEFORMATION ENERGY, IN.LB/IN. WIDTH
DISTANCE TRAVELLED, INCHES
7.0
6.0
5.0
4.0
3.0
2.0
1.0
0
0.1
0.2
0.3
0.4
0.5
0.6
0.7
0.8
0.9
1.0
Finite Element Analysis
Visioplasticity Analysis
Force-displacement Curves

measured force-displacement curves are also shown. The information is reported in Table 5-2 at 0.25 inch intervals of tool displacement of 1.0 inch. The deviations between the values obtained from the application of the two methods outlined above, expressed as a percentage of the applicable measured input energy, are indicated in Table 5-3.

As pointed out earlier in Section [4.B.5], the visioplasticity method which assumes a rigid plastic model overpredicts the deformation energy, especially in the initial stages of the deformation process. It is reasoned that replacing the work-hardening form of the stress-strain curves shown in Section [4.A.3] by a rigid plastic idealization should be expected to result in the overestimation of the deformation energy, particularly in the present case of gradual load application.

In the finite element analysis of the present problem, the soil was treated as a non-linear-elastic-strain hardening material subject to boundary conditions of an incremental form, thus permitting calculations to be made for the description of the growth of stresses within the loaded soil from initial to final states. A solution of this form should be expected to provide better estimates of the energy dissipated within the soil, subject to the approximations made in the theoretical development. Comparisons of the finite element calculated with the experimentally obtained energy values demonstrate that the developed analytical model provides reasonable prediction of the energy dissipated in the soil. The average error of estimate is of the order of 10%, while the maximum error is 18%.

TABLE 5-2

COMPARISON OF THE DEFORMATION ENERGY VALUES OBTAINED BY VARIOUS METHODS FOR THE 10° AND 50° INCLINED BLADE PROBLEMS

Test No.	Angle of Blade with Vertical	Deformation Energy in.lb/in.width — Tool Displacement: d = 0.25 inch			d = 0.5 inch			d = 0.75 inch			d = 1.0 inch		
		a	b	c	a	b	c	a	b	c	a	b	c
27	10°	1.32	1.95	1.39	3.92	4.60	4.06	7.65	8.35	7.32	12.05	12.62	11.04
30	10°	1.20	2.05		3.86	4.56		7.40	8.25		11.71	12.50	
29	50°	0.92	1.23	0.79	2.436	2.737	2.17	4.3	4.95	3.83	6.57	7.50	5.61
31	50°	0.88	1.17		2.60	2.91		4.1	4.65		6.90	7.55	

Notes:

(1) Columns headed with the letter (a) denote values obtained from the experimental force-displacement curves.

(2) Columns headed with the letter (b) denote calculated values obtained from Eq. (4.17).

(3) Columns headed with the letter (c) denote values obtained from the finite element solution.

TABLE 5-3

ERRORS OF ESTIMATES OF DEFORMATION ENERGY VALUES FOR THE 10° AND 50° INCLINED BLADE PROBLEMS

Test No.	Deformation Energy in.lb/in.width											
	Measured Values	Error of Visio-plasticity	Estimate Finite Element	Measured Values	Error of Visio-plasticity	Estimate Finite Element	Measured Values	Error of Visio-plasticity	Estimate Finite Element	Measured Values	Error of Visio-plasticity	Estimate Finite Element
	d = 0.25 inch			d = 0.5 inch			d = 0.75 inch			d = 1.0 inch		
27	1.32	+ 47.7	+ 5.3	3.92	+ 17.3	+ 3.60	7.65	+ 9.10	- 4.13	12.05	+ 4.7	- 8.40
30	1.20	+ 70.8	+ 15.8	3.86	+ 18.1	+ 5.20	7.40	+ 11.48	- 1.1	11.71	+ 6.7	- 5.70
29	0.92	+ 33.6	- 14.1	2.436	+ 12.3	- 10.75	4.3	+ 15.1	-10.9	6.57	+ 14.1	- 14.6
31	0.83	+ 32.9	- 10.2	2.60	+ 11.92	- 17.4	4.1	+ 13.4	- 6.6	6.90	+ 9.42	- 18.71

Notes:

(1) Errors expressed in percentage of measured values.

(2) Measured values refer to values obtained from the integration of the areas beneath the experimentally measured force-displacement curves.

CHAPTER 6

FINITE ELEMENT ANALYSIS OF SOIL-GROUSER INTERACTION PROBLEM

A solution of the traction problem - that is, obtaining adequate traction at a suitable speed in a practical manner and at a reasonable cost - lies in an understanding of:

1. the manner in which stresses are applied to the soil, and
2. the reaction of the soil to the applied stresses.

Bearing in mind this understanding, which is necessary to deal with an interaction process, a direction of approach may be established.

As previously mentioned [Chapter 4], while soil cutting and traction problems can be considered to be one problem in principle, [both situations requiring analyses of soil stresses and deformations, as well as the evaluation of developed reactions on the cutting or traction devices], the purpose of a traction device is to cause deformation of soil in a certain manner as to develop adequate traction capacity [optimum developed reactions]. To achieve this, it is necessary to change the geometry of the traction tools, or, in other words, the interacting boundary conditions, in order to reach the manner of soil manipulation for the production of adequate traction. The importance of accurate specifications of boundary conditions cannot be overemphasized.

Three illustrative examples are studied in this Chapter to demonstrate the validity of the proposed method. Three grouser geometries were chosen for modelling by the finite element method. These grousers are the plate grouser [R.A.P.G.] with an aspect ratio [h/l] of 0.833, the C.E.W. type (2) grouser, and the S.E.W. grouser, shown to scale in Fig. 3-1, Chapter 3. The reason for the choice of these grousers was based on the fact that they represent different geometries and therefore different boundary conditions.

6.1 MESHES AND BOUNDARIES

The meshes adopted for the three grousers chosen for the finite element analysis are shown in Figs. 6-1, 6-2 and 6-3. The material is again assumed to be nonlinear elastic with constitutive behavior derived from the stress-strain results discussed in Section 4.A.3. The initial modulus of elasticity, E_0, is assumed to be equal to the slope of the initial tangent of the zero confining pressure stress-strain curve shown in Fig. 4-7, and the Poisson's ratio, ν, is kept constant at 0.48 through the entire deformation process.

As mentioned earlier, plane strain condition is assumed in cross-section, and constant strain triangles are employed to represent the soil mass. Some objectives in subdividing the mass by C.S.T. [constant strain triangle] elements are the following:

(a) Small triangles in the areas of most interest.

(b) All triangles approximately equilateral.

(c) Less than 400 total triangles and 200 nodes to keep computer storage requirements down.

(d) No more than six elements incident to any one node to keep computer storage requirements down.

(e) Uniform meshes as to facilitate plotting and interpolation of results.

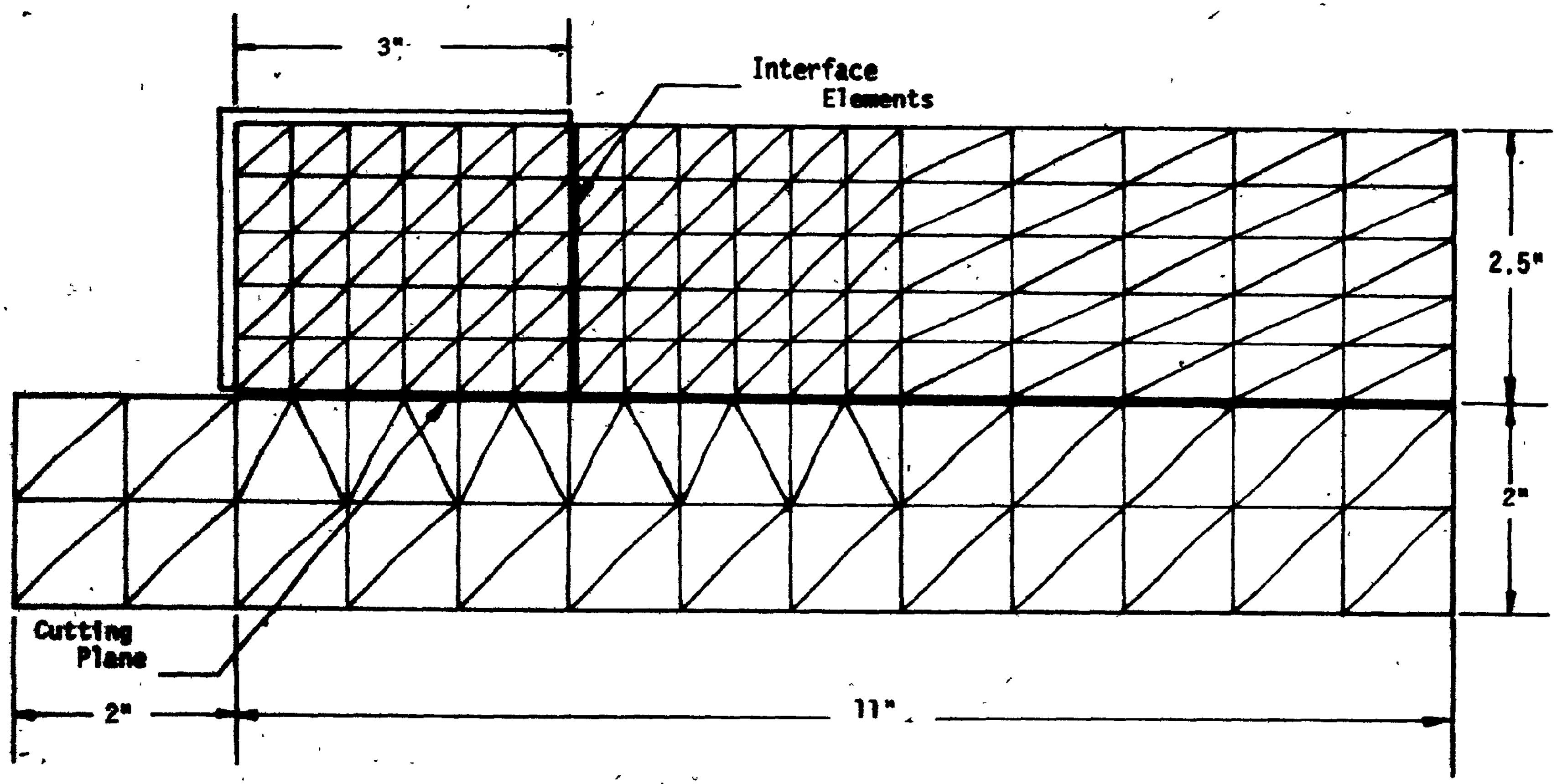

FIGURE 6-1 MESH LAYOUT FOR THE PLATE GROUSER (R.A.P.G.)-SOIL SYSTEM

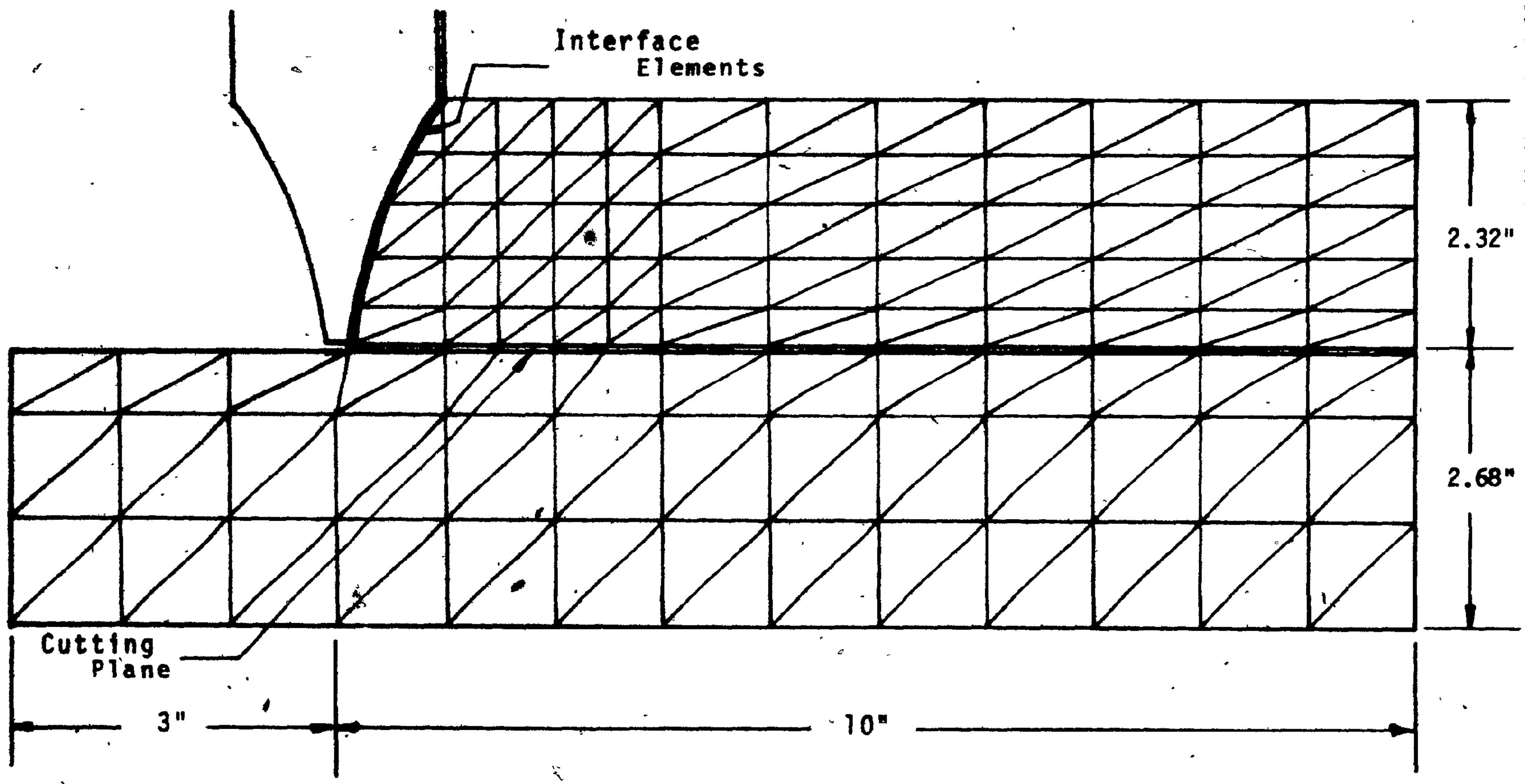

FIGURE 6-2 MESH LAYOUT FOR THE C.E.W. TYPE (2) GROUSER-SOIL SYSTEM

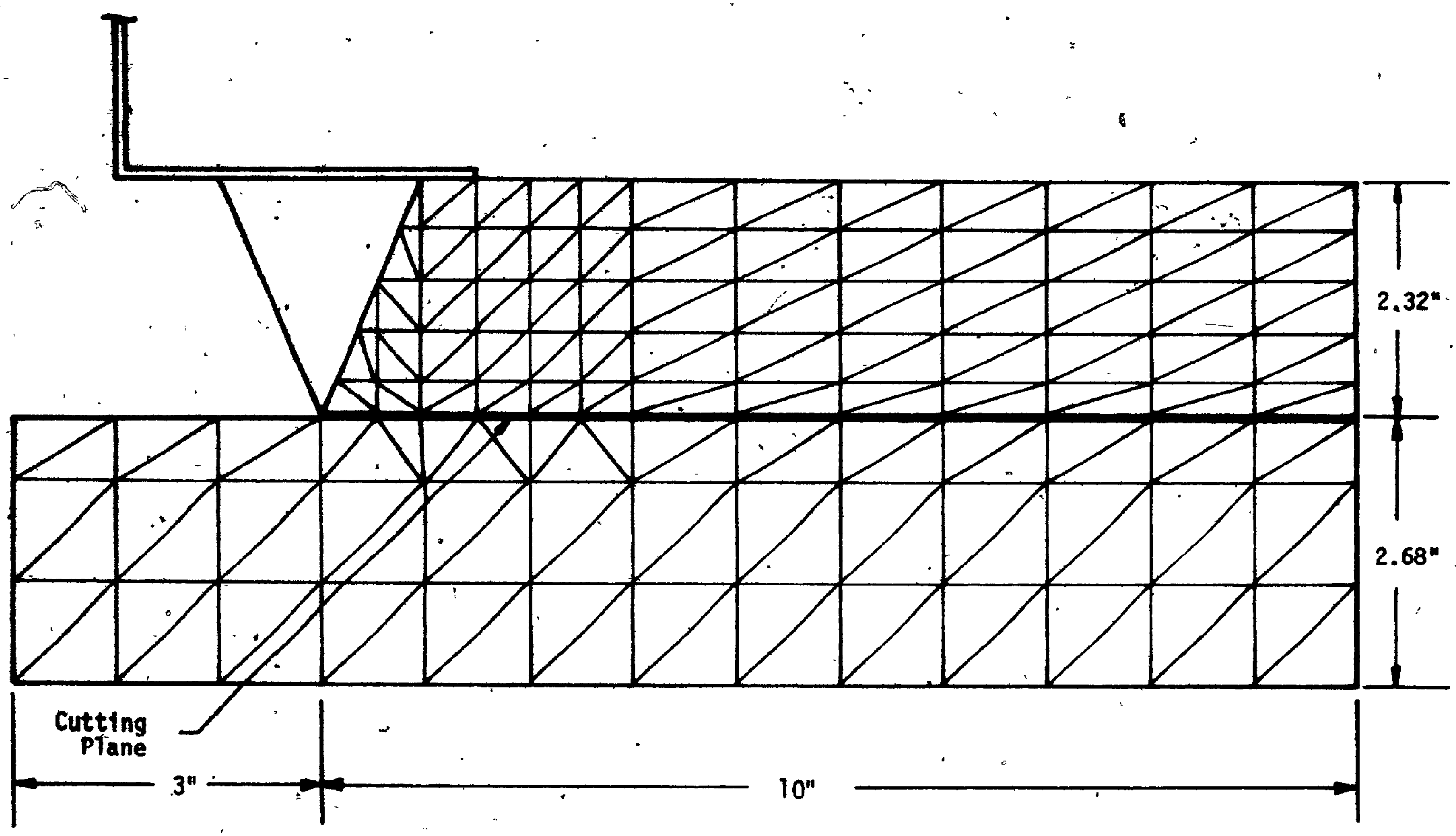

FIGURE 6-3 MESH LAYOUT FOR THE S.E.W. GROUSER-SOIL SYSTEM

In all the idealizations, Figs. 6-1 to 6-3, cutting [joint] elements are placed on the plane where the cutting is anticipated. This cutting plane is assumed to start in all cases at the level of the grouser tip. It is realized that such an assumption can lead to a certain degree of error as the soil is forced to separate on a particular plane having a fixed position and direction. Comparisons with the available experimental deformation fields, as well as the overall performance, are essential before judging the extent of the validity of such an assumption on the solution technique.

Figure 6-1 presents the idealization adopted for the R.A.P.G. with [h/l] ratio of 0.833. As previously mentioned, observations of both the experimental soil displacement and velocity patterns indicated that the soil situated in the rectangle formed by the two sides of the grouser experiences very little displacement relative to the grouser, with virtually no soil slip on the grouser interface. This zone was termed the "dead" zone in Chapter 4 and is presented in Fig. 6-4 as zone 'ABCD'. This no-slip condition eliminated the need for placing interface elements between the soil and the grouser interface. However, it was observed that, while the dead zone does not experience any appreciable slip on the grouser interface, relative displacements [or slip] do occur between the soil in the "dead" zone and the surrounding soil mass. These relative displacements occur on the outer edge of the "dead" zone represented by plane 'BC' in Fig. 6-4. It was found out that in order to account for such a discontinuity in the deformation field, joint [interface] elements must be inserted on the plane 'BC'. Fig. 6-4. A computer analysis performed on the idealization that did not include

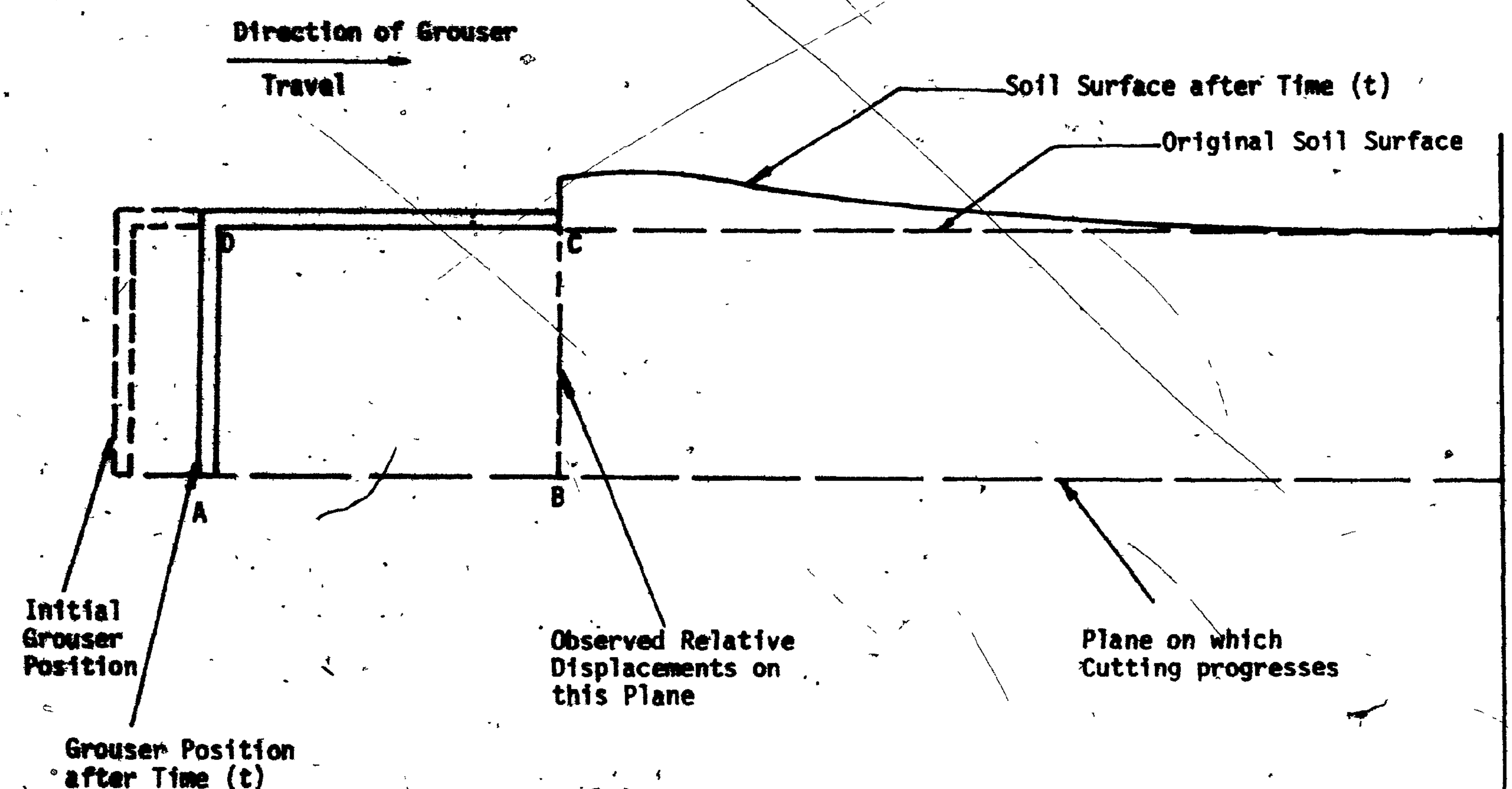

FIGURE 6-4 OBSERVED DEFORMATION PATTERN FOR SOIL SUBJECTED TO PLATE GROUSER (R.A.P.G.) LOADING

such discontinuity showed that both the deformation field and the predicted forces do not correlate with the experimental results.

In Fig. 6-2, the idealization of the C.E.W. type (2) grouser-soil system is shown with interface elements inserted on the grouser-soil interface. In modelling the S.E.W. grouser, Fig. 6-3, it was found that interface elements are not required as the horizontal plate placed on top of the grouser creates a no-slip condition, similar to that observed in the R.A.P.G. case.

The sides and bottom boundary conditions are similar to those adopted in the soil cutting analysis. It is assumed that the side and bottom boundaries are placed on rollers. The horizontal movement is restrained on the sides and the vertical movement is prevented on the bottom. Uniform horizontal displacement is applied to all the nodes on the grousers' surfaces. The displacements are increased in ten equal increments of 0.1 inch each for a total displacement of 1.0 inch.

6.2 DISPLACEMENT AND VELOCITY PATTERNS

The nodal displacement patterns for the R.A.P.G.-soil system are shown in Figs. 6-5 and 6-6 for grouser displacements of 0.5 and 1.0 inch, respectively. From these plots the displacement patterns could be divided into three distinctive zones:

1. The "dead" zone. The material adjacent to the grouser interface is seen to behave as a rigid body with very little deformation. The rigid body zone can be approximately defined as the material occupying the

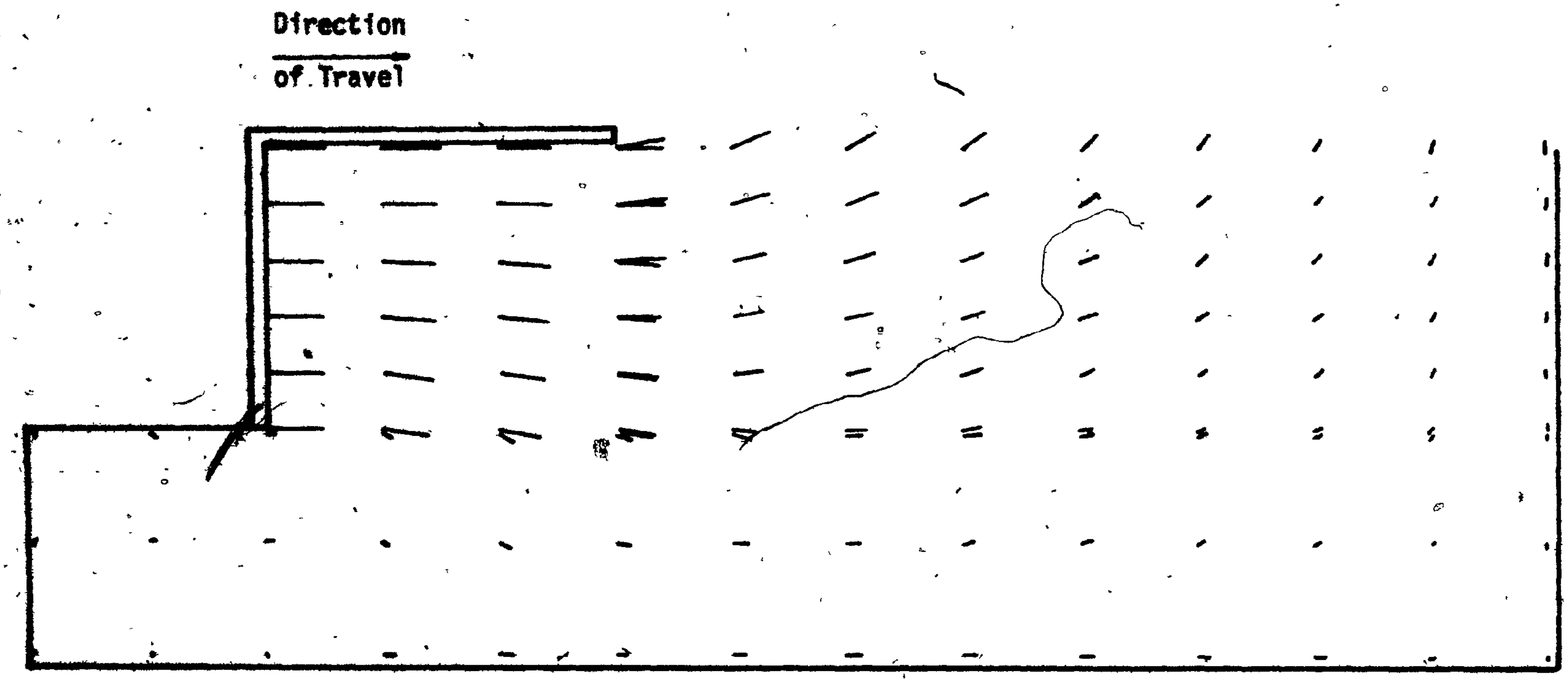

FIGURE 6-5 DISPLACEMENT FIELD FOR THE R.A.G.P.-SOIL SYSTEM

(BLADE DISPLACEMENT = 0.50 INCH)

SCALE : 1 INCH = 0.65 INCH

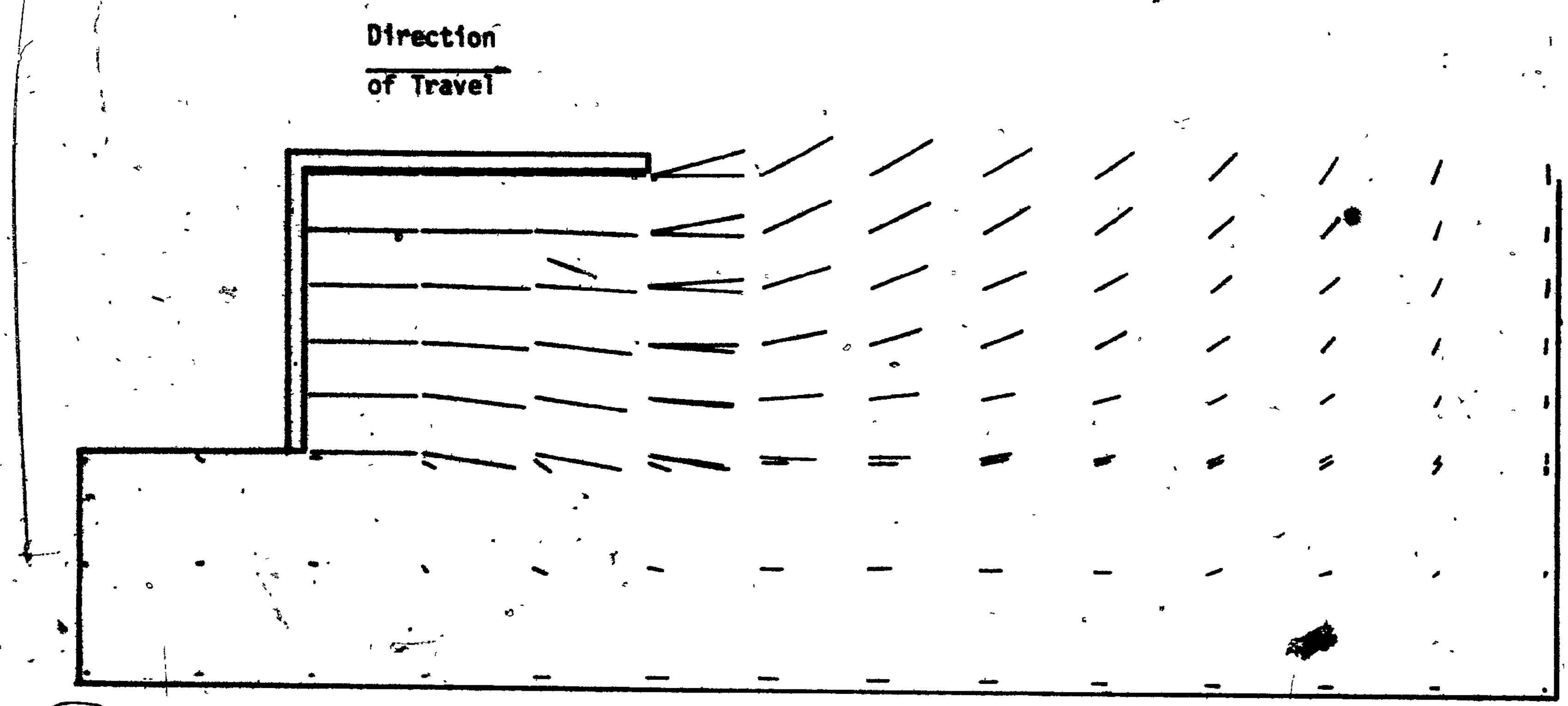

FIGURE 6-6 DISPLACEMENT FIELD FOR THE R.A.G.P.-SOIL SYSTEM

(BLADE DISPLACEMENT = 1.0 INCH)

SCALE : 1 INCH = 0.65 INCH

triangle 'ACD' in Fig. 6-4. In the remainder of the "dead" zone 'ABC' in Fig. 6-4, the nodal displacements indicate compression of material with downward motion.

2. The soil occupying the area above the cutting plane between the "dead" zone and the side boundary. The nodal displacements indicate mostly an upward movement with the exception of the area adjacent to the "dead" zone where the nodes are seen to continue moving downward. The upward motion of the top surface nodes in this zone clearly indicates the gradual formation of surcharge.

3. The soil lying below the cutting plane. This material experiences very little deformation with downward motion below the "dead" zone, and upward displacement for the soil situated on the right.

The general displacement pattern suggests that the soil deformation changes from downward motion in the grouser vicinity to upward motion away from it, and the cutting plane seems to deform accordingly. Also, the effect of the interface elements placed on plane "BC', Fig. 6-4, on the displacement pattern is evident in the nodal displacement plots, Figs. 6-5 and 6-6. In These Figures it is shown that the soil on the righthandside slides upward on this plane [BC], creating a discontinuity in the deformation field which is compatible with experimental observations as will be shown in a later Section.

All of these findings could be confirmed from the plots of the horizontal and vertical nodal points' velocity contours shown in Fig. 6-7. These velocity contours represent the soil velocity during the first increment of deformation [0.1 inch grouser displacement]. It can be also seen that the vertical interface elements create a discontinuity in the horizontal velocity field. This behavior is to be expected since the direction of the velocity vector outside the "dead" zone changes to an upward position resulting in a sudden reduction of the horizontal velocity component. From the vertical velocity plot it is shown that the velocity is downward in the "dead" zone, with the zone confined by the two sides of the grouser experiencing negligible velocity [rigid body zone defined in Fig. 6-4 by area 'ACD'].

The horizontal and vertical velocity contours for the C.E.W. type (2) and the S.E.W. grousers are plotted in Figs. 6-8 and 6-9. From these Figures the following observations could be made:

1. In the case of the C.E.W. type (2) grouser, the horizontal velocity above the cutting plane is shown to decrease with increasing distance from the grouser interface. Below the cutting plane, the soil velocity is in the direction of the grouser motion. The highest velocity occurs in a zone near the grouser tip, with decreasing values behind the grouser and close to the righthandside boundary.
2. From the plots of the vertical velocity field of the C.E.W. type (2)-soil system, Fig. 6-8, it may be seen that a contour of zero vertical velocity intersects the grouser

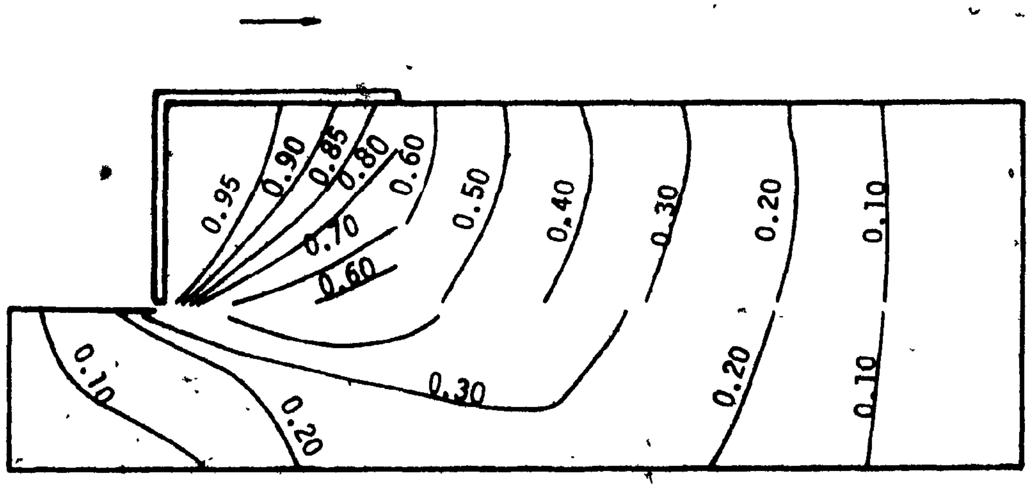

HORIZONTAL VELOCITY FIELD

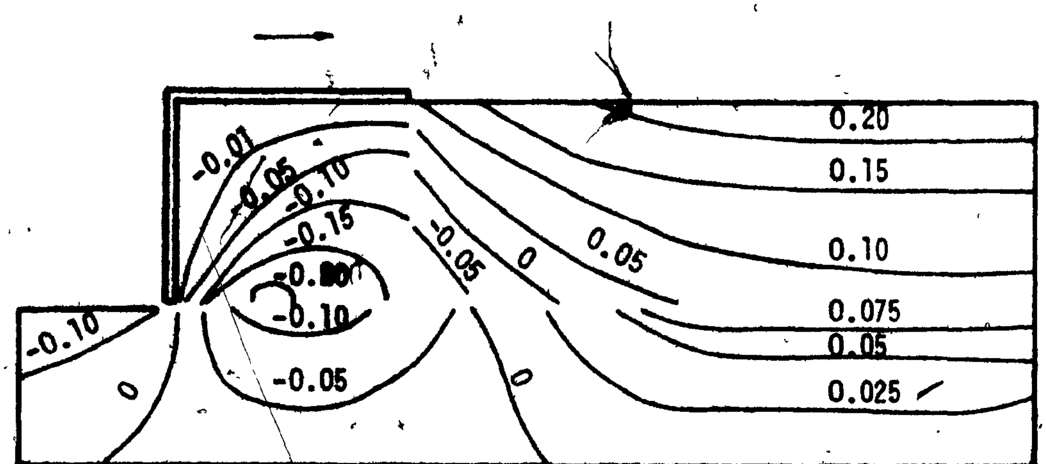

VERTICAL VELOCITY FIELD

FIGURE 6-7 HORIZONTAL AND VERTICAL VELOCITY FIELDS FOR THE PLATE GROUSER (R.A.P.G.) - SOIL SYSTEM DURING THE FIRST DISPLACEMENT INCREMENT OF 0.10 INCH

(Contour Values are in inches/minute)

(Grouser Velocity = 1.0 inch/minute)

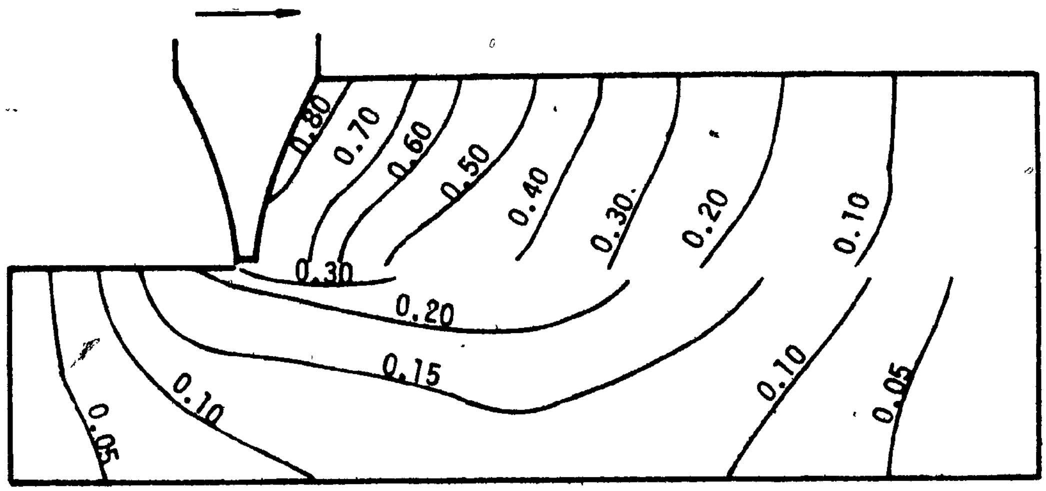

HORIZONTAL VELOCITY FIELD

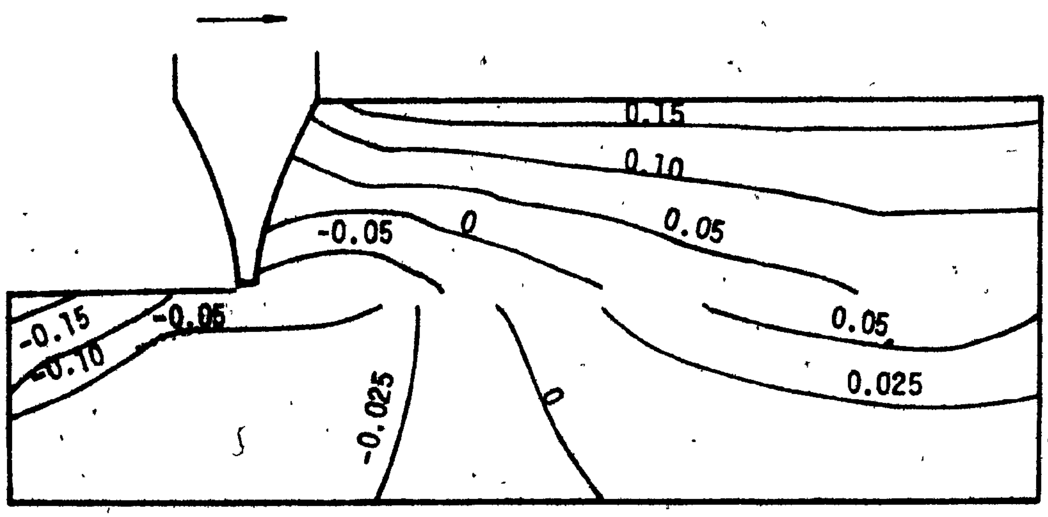

VERTICAL VELOCITY FIELD

FIGURE 6-8 HORIZONTAL AND VERTICAL VELOCITY FIELDS FOR THE C.E.W. TYPE (2) GROUSER - SOIL SYSTEM DURING THE FIRST DISPLACEMENT INCREMENT OF 0.10 INCH

(CONTOUR VALUES ARE IN INCHES/MINUTE)

(GROUSER VELOCITY = 1.0 INCH/MINUTE)

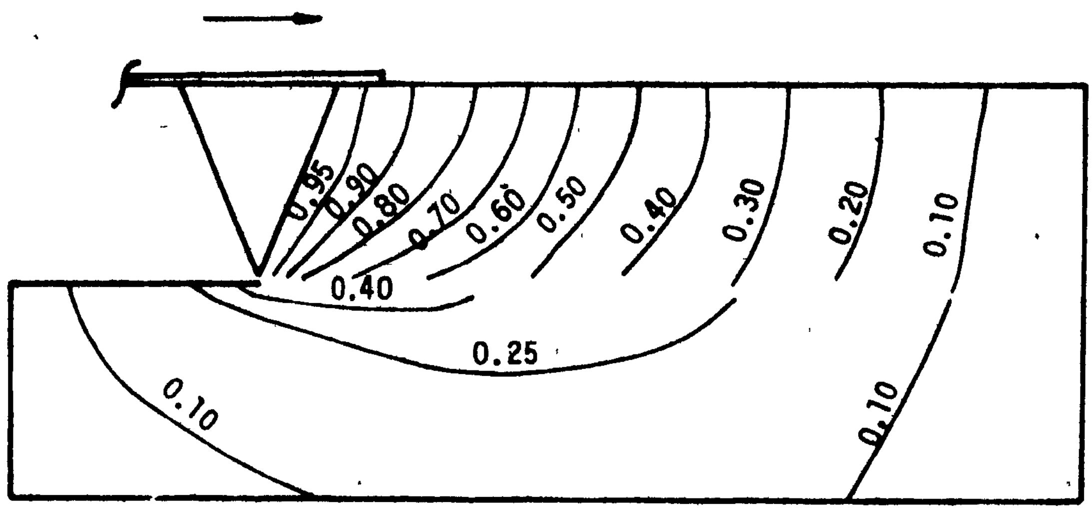

HORIZONTAL VELOCITY FIELD

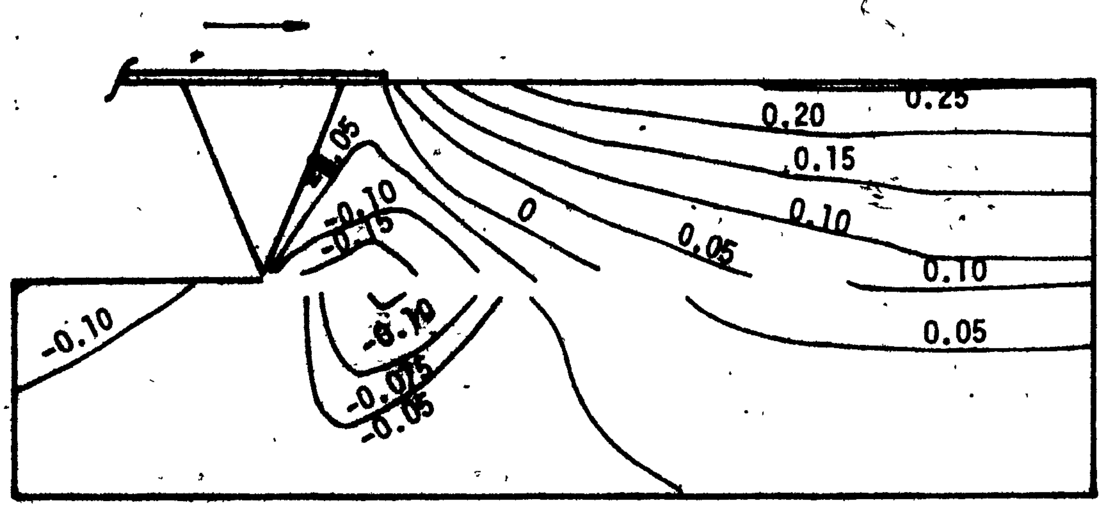

VERTICAL VELOCITY FIELD

FIGURE 6-9 HORIZONTAL AND VERTICAL VELOCITY FIELDS FOR THE S.E.W. GROUSER - SOIL SYSTEM DURING THE FIRST DISPLACEMENT INCREMENT OF 0.10 INCH

(CONTOUR VALUES ARE IN INCHES/MINUTE)
(GROUSER VELOCITY = 1.0 INCH/MINUTE)

interface. Below the cutting plane, this contour is displaced to the right due to the influence of the cutting action. Below and behind these zero vertical velocity contours the material experiences downward motion while above and in front the soil moves upward.

3. The plot of the horizontal velocity of the S.E.W. grouser-soil system, Fig. 6-9, indicates the existence of a small "dead" zone located between the soil-grouser interface and the top horizontal plate. With the exception of this "dead" zone, the x-velocity field for this grouser is similar in pattern to that of the C.E.W. type (2) grouser. However, the horizontal velocity at any specific distance from the soil-grouser interface is found to be lower for the case of the C.E.W. type (2) grouser system, when compared with the values of the S.E.W. field. This is again attributed to the existence of a "dead" zone in the S.E.W. system which creates a rigid body zone, having about the same velocity as the grouser.

4. In the vertical velocity plot of the S.E.W. system, Fig. 6-9, the zero vertical velocity contour is seen to start from the leading edge of the top horizontal plate, creating a larger zone of downward moving soil. Again, all the material below and behind the zero contour moves downward, while above and in front the soil moves upward.

6.3 STRESS ANALYSIS

As was discussed in Section 6.1, it was found from the examination of the experimental displacement fields that there is no need for placing interface elements along the soil-metal interface for the R.A.P.G. system. The interface boundary conditions are assumed as fixed in the x-and y-directions for the nodes connected to the vertical side of the grouser. However, the nodes attached to the horizontal interface are assumed to be fixed only in the vertical direction, but free in the horizontal direction. It was reasoned that these assumptions for the interface conditions would lead to reasonable stress distributions and consequently developed reactions. The distributions of the horizontal, vertical and shear stresses in the soil obtained for the finite element idealization of the R.A.P.G.-soil system shown in Fig. 6-1 are plotted in Figs. 6-10 and 6-11. Figures 6-10 and 6-11 show, respectively, the stress contours for grouser displacement of 0.1 inch and 0.5 inch.

A close look at these plots will reveal the following illustrative points;

1. The largest horizontal compressive stresses occur in the "dead" zone with stress concentrations at the bottom of the vertical interface.
2. In addition to the discontinuity in the horizontal stress field occurring across the cutting plane elements, the vertical interface elements plane [placed on plane 'BC' in Fig. 6-4] produce another discontinuity. Such discontinuity, however, seems to result in no sudden change in the horizontal stress magnitudes.

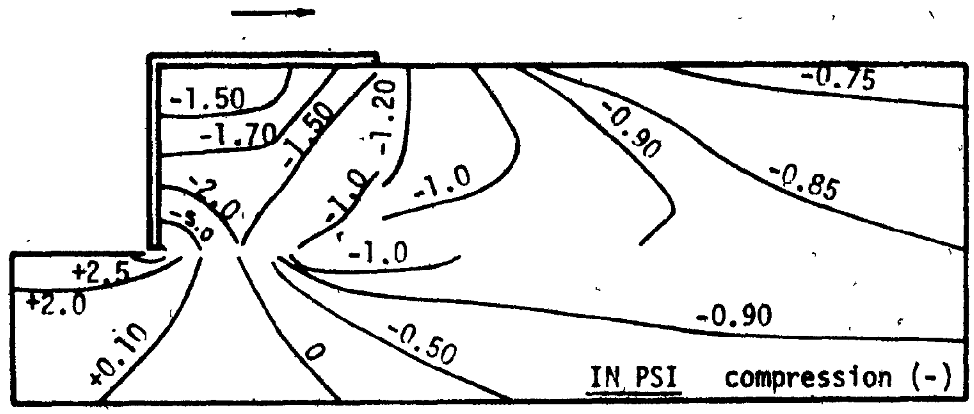

(a) HORIZONTAL STRESS, σ_x

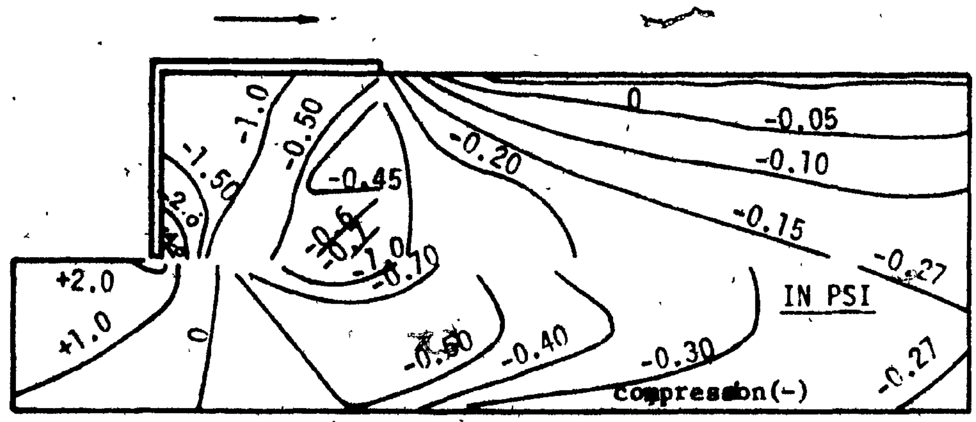

(b) VERTICAL STRESS, σ_y

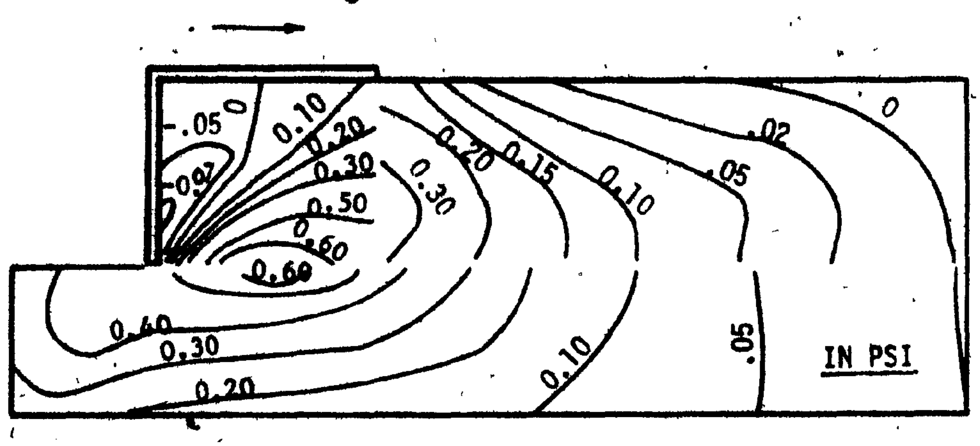

(c) SHEAR STRESS, τ_{xy}

FIGURE 6-10 STRESS FIELDS FOR THE PLATE GROUSER (R.A.P.G.) - SOIL SYSTEM AT 0.10 INCH DISPLACEMENT

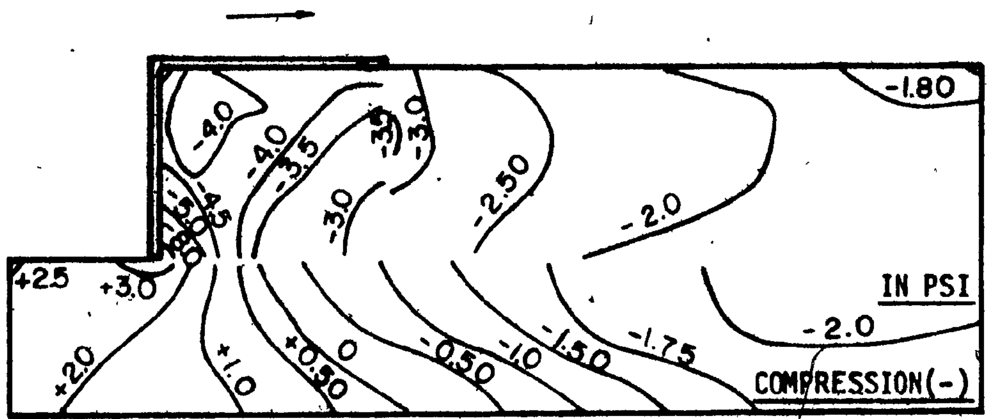

(a) HORIZONTAL STRESS, σ_x

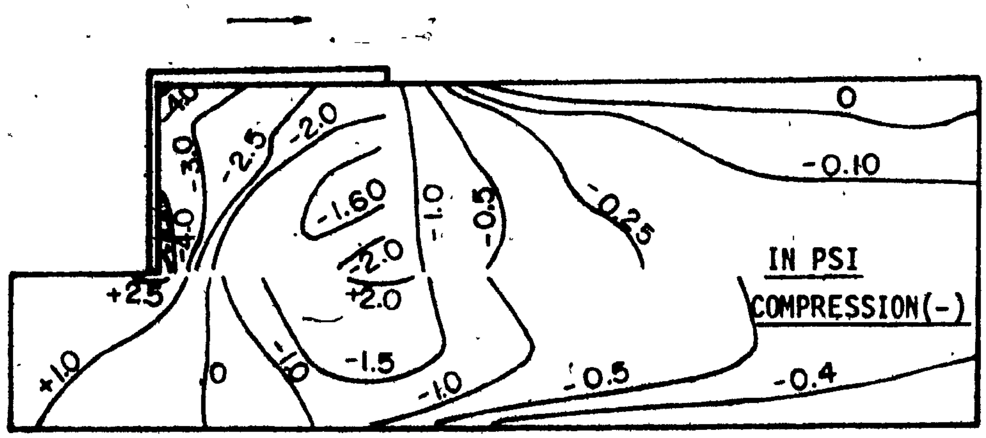

(b) VERTICAL STRESS, σ_y

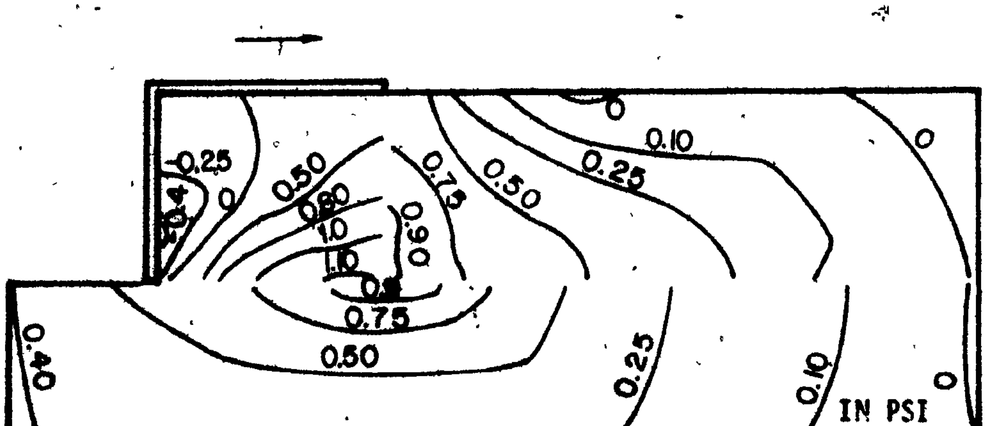

(c) SHEAR STRESS, τ_{xy}

FIGURE 6-11 STRESS FIELDS FOR THE PLATE GROUSER (R.A.P.G.)-SOIL SYSTEM AT 0.5 INCH DISPLACEMENT

3. It is shown that while the horizontal compressive stresses above the cutting plane decrease with increasing distance from the grouser-soil interface, the reverse occurs below the cutting plane. This behavior is attributed to the fact that the material located in the zone directly underneath the grouser is subjected to horizontal tensile stresses. These tensile stresses gradually change into compressive stresses which increase until they reach values similar to the stresses developed above the cutting plane near the right-handside boundary.

4. It is indicated that the material confined by the grouser sides is subjected to very high vertical compressive stresses (σ_y), Figs. 6-10 and 6-11. Outside the "dead" zone the stresses suddenly drop to a little more than half the magnitude. Further, the shape of the contours in the "dead" zone indicates the influence of the grouser sides, while outside it the contours change to a shape similar to what would be expected from a material with a free top surface boundary.

5. An examination of the shear stress plots, indicates that the zone 'ACD' in Fig. 6-4 experiences very little shear distortion. A zero shear stress divide is shown to occur on the boundary of this zone; to its left the material is shearing in a clockwise [positive]

direction, while to its right the shear is negative [anticlockwise direction].

6. The zone of maximum shear stresses initiates at a distance from the grouser toe level in the initial loading stage, Fig. 6-10, and is shown to be moving forward with increasing grouser displacement, Fig. 6-11. From the plots of the failed elements, Fig. 6-16, it will be established that the zone of maximum shear stress moves outside the "dead" zone at larger grouser displacements.

The distributions of σ_x, σ_y, and τ_{xy} stresses for both the C.E.W. type (2) and the S.E.W. grouser-soil systems are presented in Figs. 6-12 to 6-15. Again, the stress contours for these systems are plotted at 0.1 and 0.5 inch of tool displacements. Examination of the horizontal and vertical stresses of the two systems suggests that, with the exception of the zone adjacent to the grouser interface, the horizontal as well as the vertical stress distributions seem to be similar. Moreover, the contours maintain the same general shapes with increasing grouser displacement.

Comparisons of the stress fields in front of both grousers show that the stress values near the toe of the S.E.W. grouser are higher than those occurring in front of the C.E.W. type (2) grouser. The difference in stress magnitudes is attributed to the difference in the grousers' toe geometries. The attack angle [angle between bottom portion of the interface and the cutting plane] of the C.E.W. type (2)

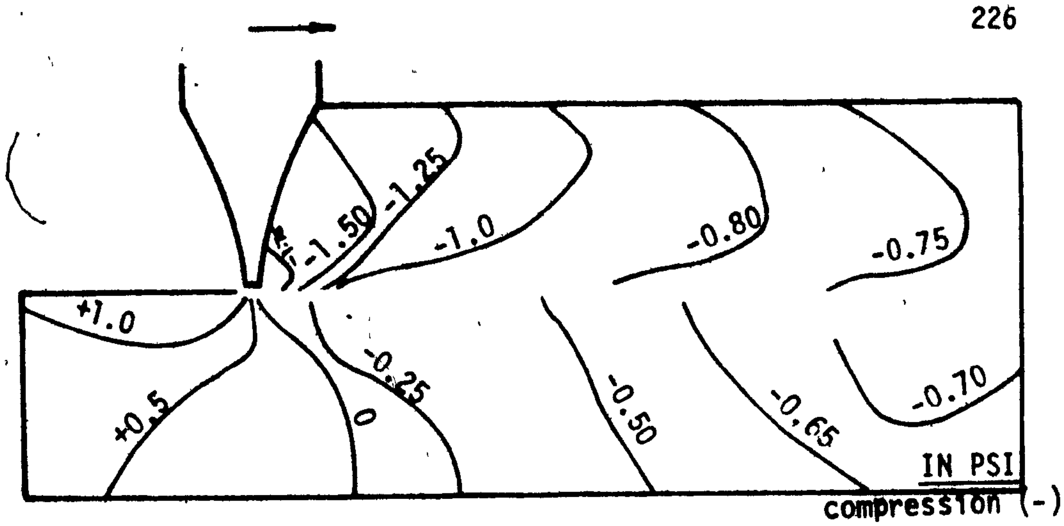

(a) HORIZONTAL STRESS, σ_x

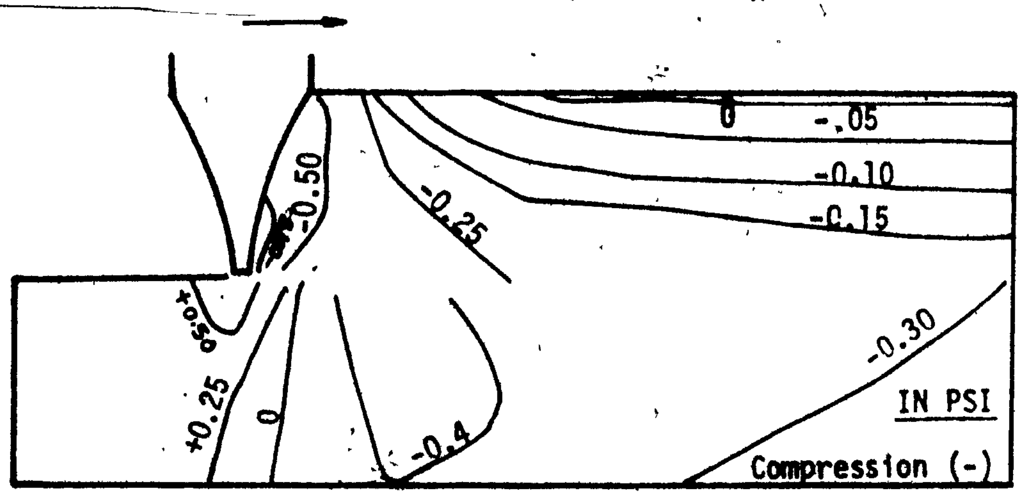

(b) VERTICAL STRESS, σ_y

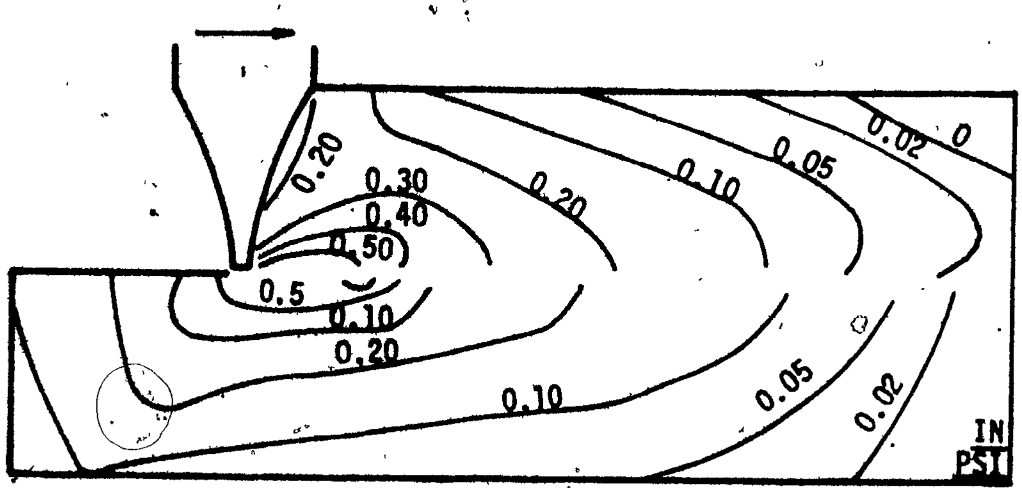

(c) SHEAR STRESS, τ_{xy}

FIGURE 6-12 STRESS FIELDS FOR THE C.E.W. TYPE (2) GROUSER - SOIL SYSTEM AT 0.10 INCH DISPLACEMENT

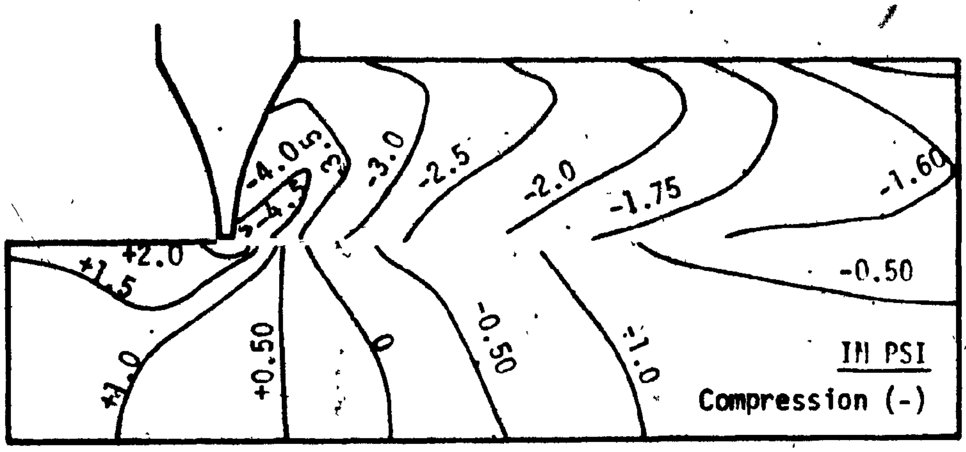

(a) HORIZONTAL STRESS, σ_x

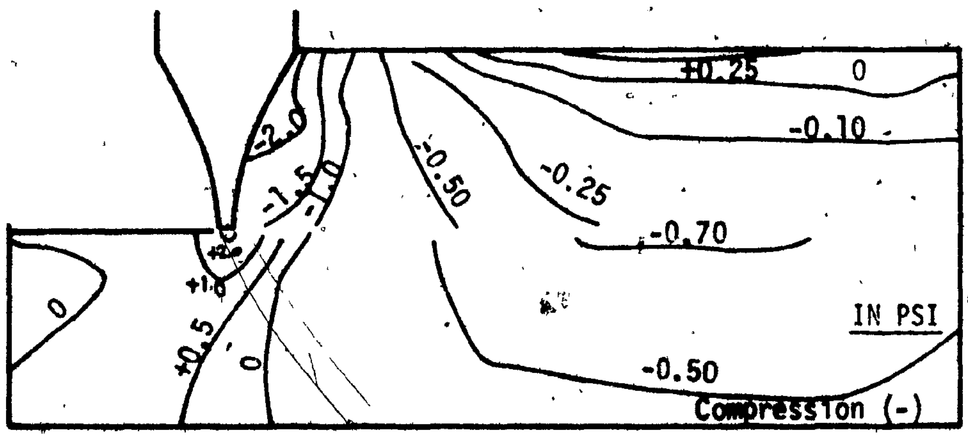

(b) VERTICAL STRESS, σ_y

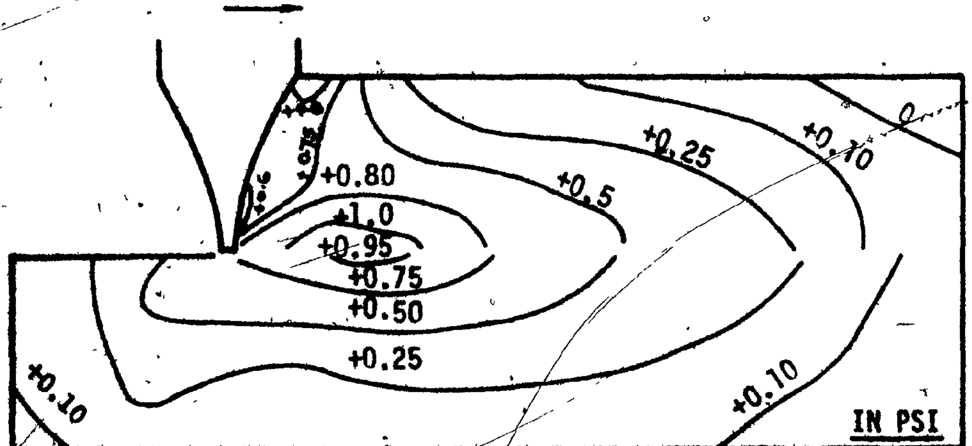

(c) SHEAR STRESS, τ_{xy}

FIGURE 6-13 STRESS FIELDS FOR THE C.E.W. TYPE (2) GROUSER - SOIL SYSTEM AT 0.50 INCH DISPLACEMENT

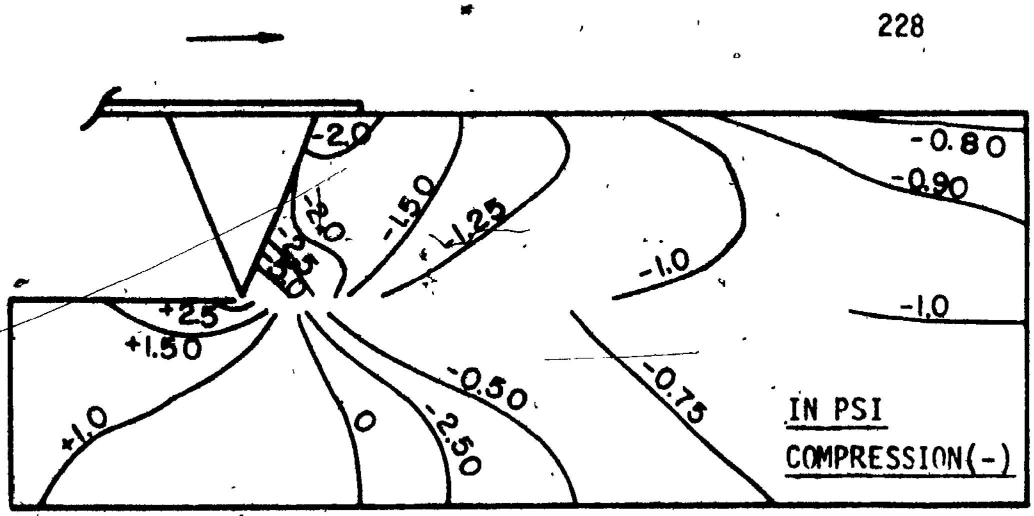

(a) HORIZONTAL STRESS, σ_x

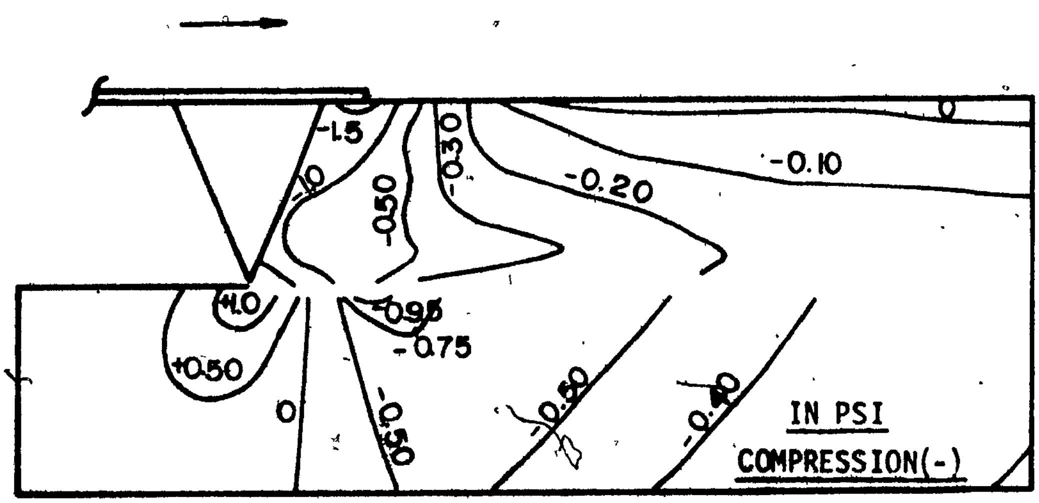

(b) VERTICAL STRESS, σ_y

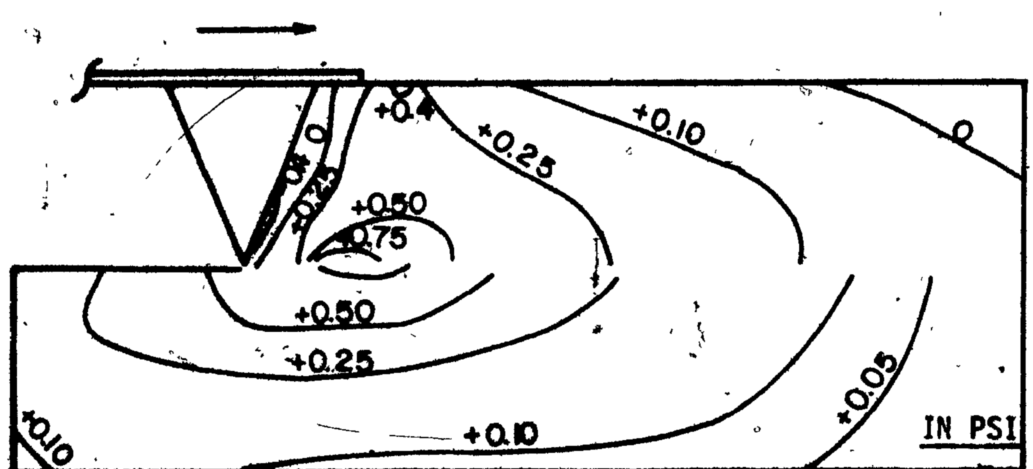

(c) SHEAR STRESS, τ_{xy}

FIGURE 6-14 STRESS FIELDS FOR THE S.E.W. GROUSER-SOIL SYSTEM AT 0.10 INCH DISPLACEMENT

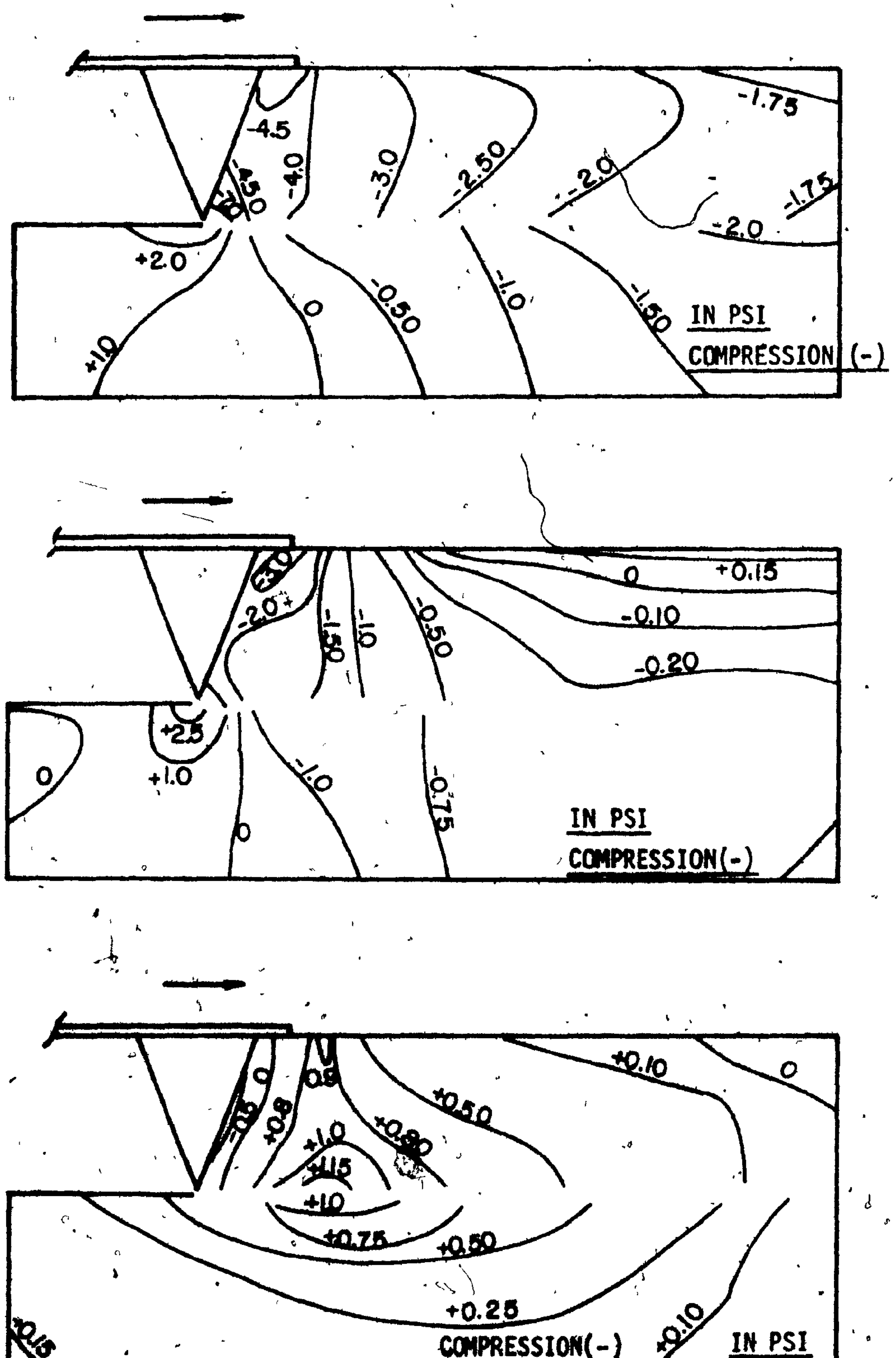

FIGURE 6-15 STRESS FIELDS FOR THE S.E.W. GROUSER-SOIL SYSTEM AT 0.50 INCH DISPLACEMENT

grouser is 90°, while it is only 67.5° for the S.E.W. system, Fig.3-1. Due to this variation, one would expect higher stress concentrations for the acute grouser attack angle. Another dissimilarity is the higher horizontal and vertical stresses developing under the top horizontal plate of the S.E.W. system. These stresses are caused by the confining influence of this plate on the adjacent material.

Finally, the plots of the shear stresses, τ_{xy}, for the S.E.W. system, Figs. 6-14 and 6-15, show a zero shear stress divide which indicates the existence of a small "dead" zone similar to the one observed in the R.A.P.G. stress fields. This zone can be approximately defined by the area located between the grouser interface and the line connecting the grouser toe with the leading edge of the top horizontal plate. Inside this area the material is shown to have negative shear [i.e., clockwise] values - near the grouser interface. No indication of any similar zone is observed in the C.E.W. type (2) grouser stress fields.

The development of the failure zones for the R.A.P.G., the C.E.W. type (2), and the S.E.W. grouser-soil systems is shown in Figs. 6-16, 6-17 and 6-18, respectively. For the R.A.P.G.-soil system, yielding occurs in two different locations, Fig. 6-16. At the toe of the grouser, the adjacent element fails in increment No.8. In subsequent increments, only one additional element is added to this zone. This suggests that this zone represents a localized shear area caused by stress concentrations due to the cutting action. The main failure in the material occurs outside the so-called "dead zone". It is seen that failure starts in two elements just outside the "dead" zone in

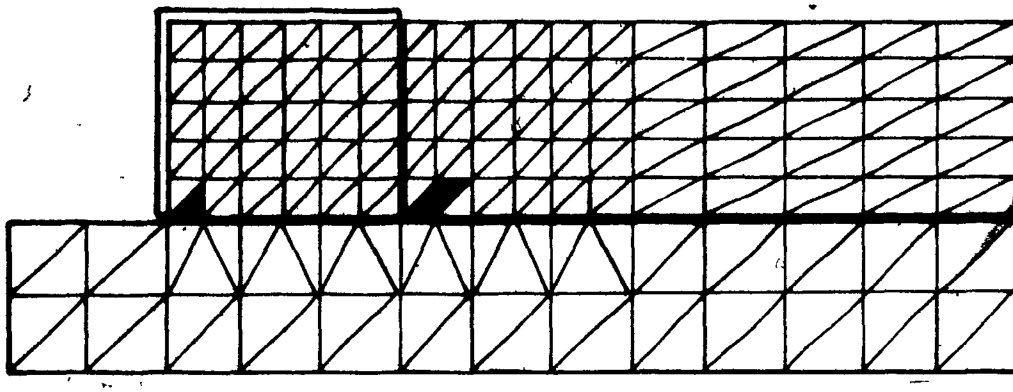

(INCREMENT No. 8 - GROUSER DISPLACEMENT = 0.80 inch)

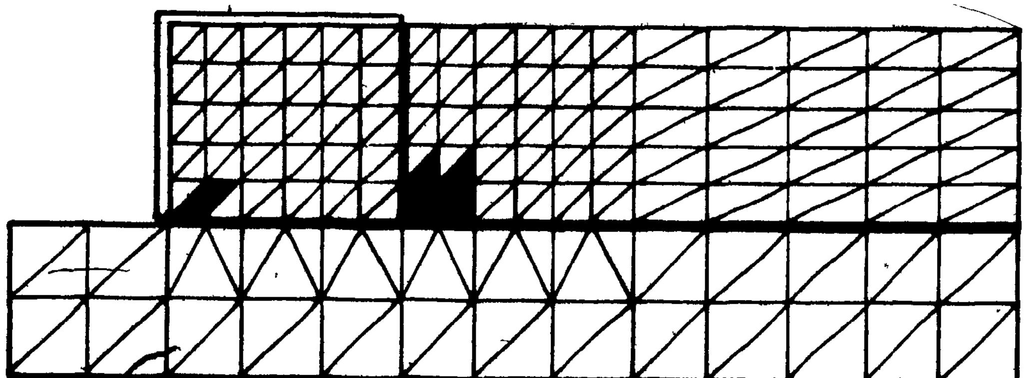

(INCREMENT No. 9 - GROUSER DISPLACEMENT = 0.90 inch)

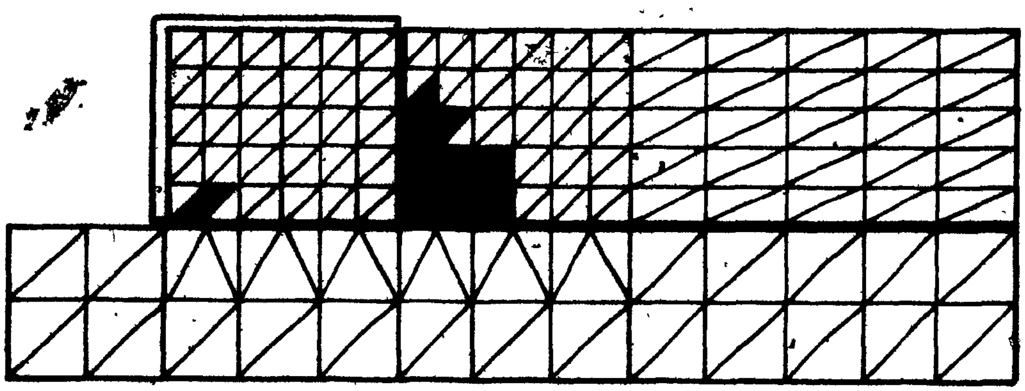

(INCREMENT No. 10 - GROUSER DISPLACEMENT = 1.0 inch)

FIGURE 6-16 DEVELOPMENT OF FAILURE ZONES FOR THE PLATE GROUSER (R.A.P.G.) - KAOLIN CLAY SYSTEM

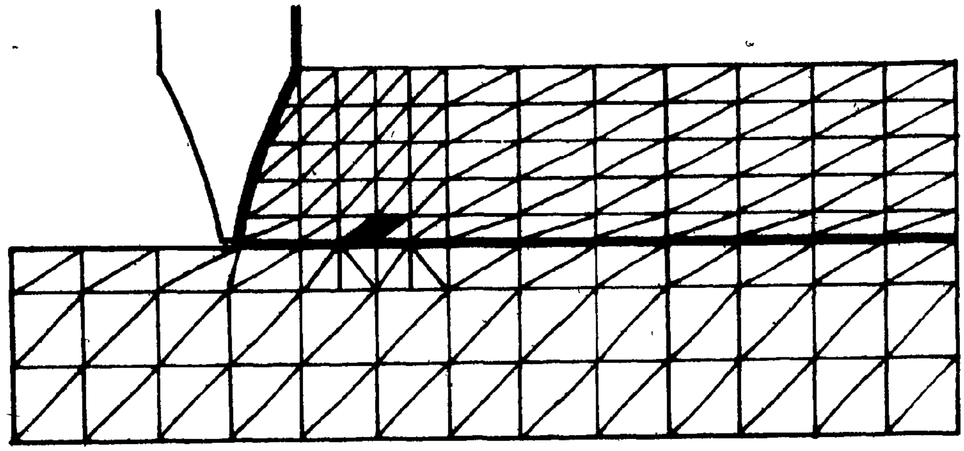

(INCREMENT No. 8 - GROUSER DISPLACEMENT = 0.80 inch)

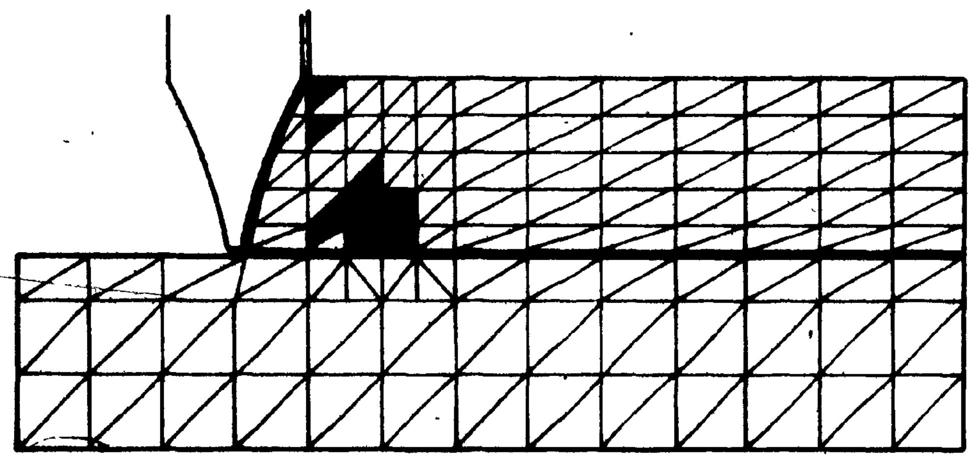

(INCREMENT No. 9 - GROUSER DISPLACEMENT = 0.90 inch)

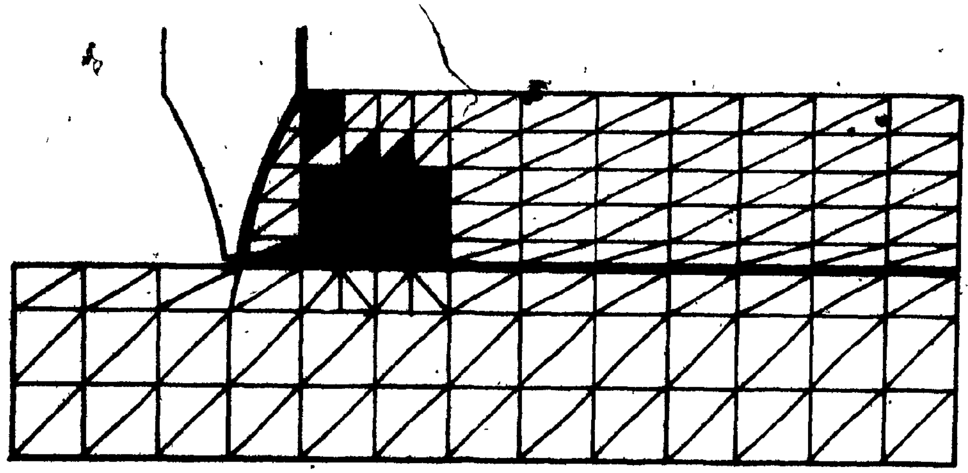

(INCREMENT No. 10 - GROUSER DISPLACEMENT = 1.0 inch)

FIGURE 6-17 DEVELOPMENT OF FAILURE ZONES FOR THE C.E.W. TYPE (2) GROUSER - KAOLIN CLAY SYSTEM

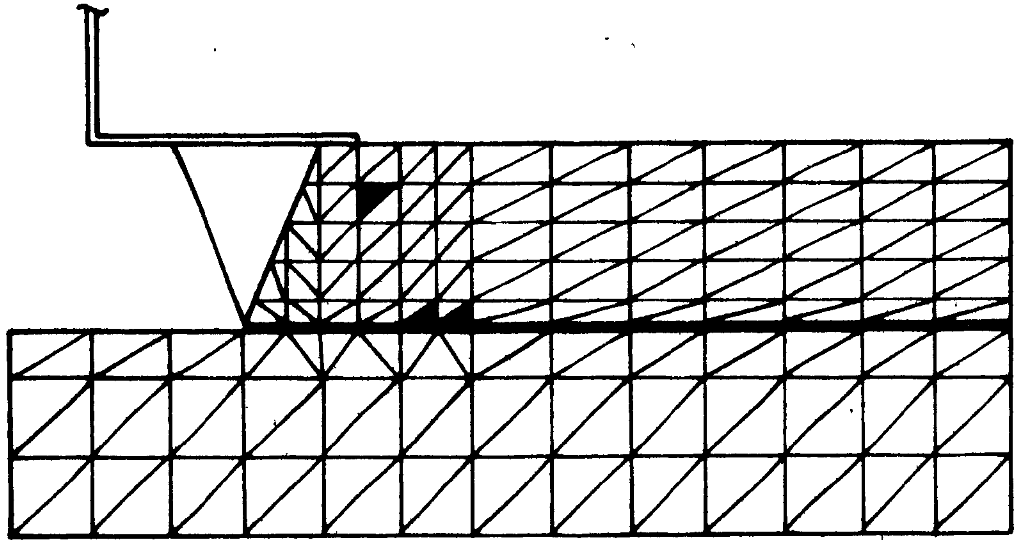

(INCREMENT No. 8 - GROUSER DISPLACEMENT = 0.80 inch)

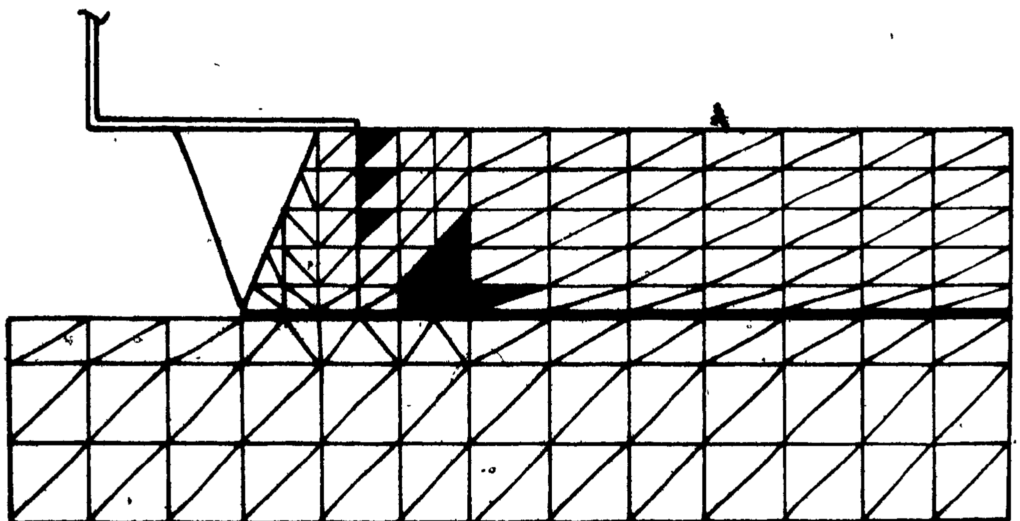

(INCREMENT No. 9 - GROUSER DISPLACEMENT = 0.90 inch)

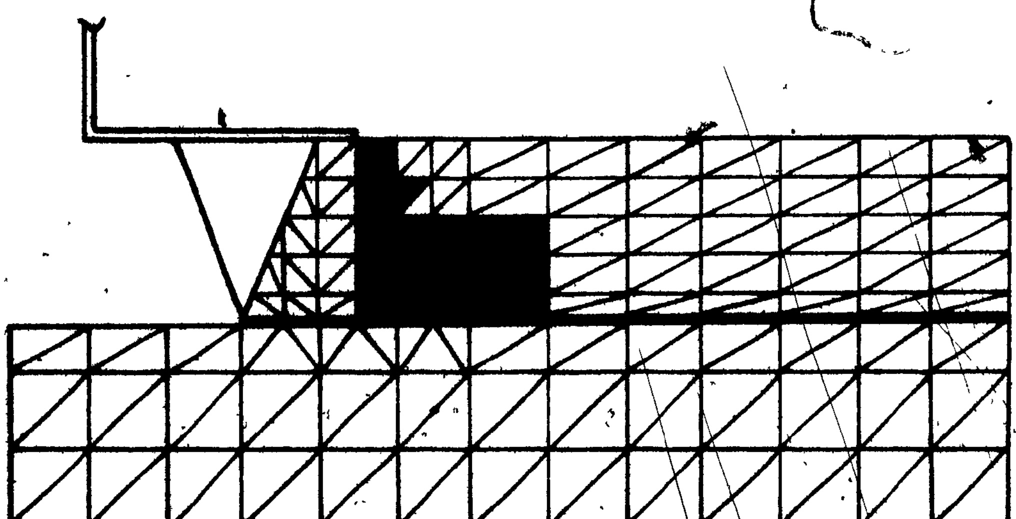

(INCREMENT No. 10 - GROUSER DISPLACEMENT = 1.0 inch)

FIGURE 6-18 DEVELOPMENT OF FAILURE ZONES FOR THE S.E.W. GROUSER - KAOLIN CLAY SYSTEM increment No.8 and then moves upward and forward with increasing grouser displacement. While in the shear stress plots of Figs. 6-10 and 6-11 the region of maximum shear stresses is located within the lower part of the "dead" zone, it is shown to be moving forward with increasing grouser displacement. The actual failure occurs outside this zone starting in increment No.8.

For the C.E.W. type (2) and the S.E.W. system, the failed zones, as shown in Figs. 6-17 and 6-18, do not start at the grousers' toes, but at approximately the same distances where regions of maximum shear stresses occur, [Figs. 6-12 to 6-15]. Of interest is the localized failed areas near the point of intersection of the grouser interface with the free soil surface. Again these zones can be considered as localized areas of maximum shear due to stress concentrations. However, it is seen that in increment No.10 these localized failed areas join with the main failure zones. Another point of interest is the extension of the failure zone back to the grouser toe in the case of the C.E.W. type (2) system, a phenomenon that is not exhibited in the S.E.W. system. This observation substantiates the fact that a small "dead" zone experiencing very little shear distortion exists in front of the S.E.W. grouser.

6.4 CONTACT PRESSURE DISTRIBUTION

The normal pressure distributions on the R.A.P.G.-soil interface are plotted in Fig. 6-19 at grouser displacements of 0.1, 0.3, 0.6 and 1.0 inch. These results are obtained by dividing the reactions developed at the interface nodal points by the areas of influence of each nodal reaction. The plots indicate that the maximum pressure on

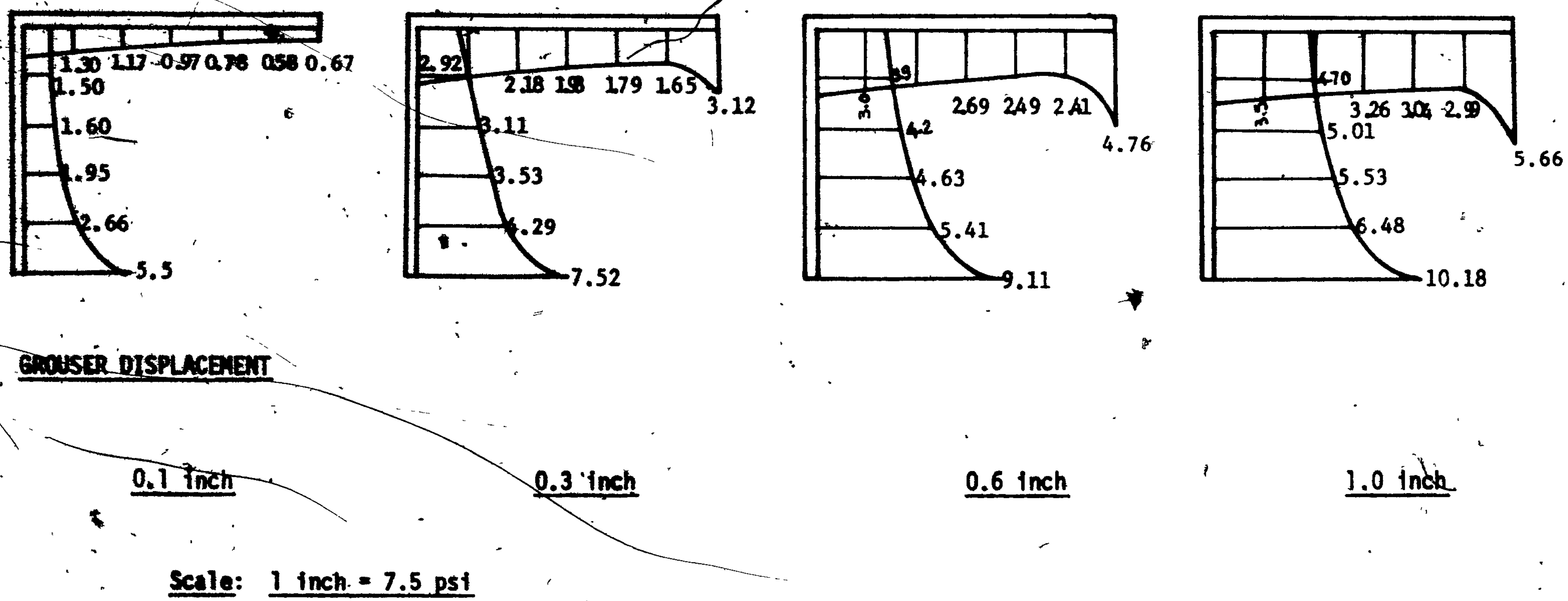

FIGURE 6-19 NORMAL PRESSURE DISTRIBUTION ON THE PLATE GROUSER (R.A.P.G.)

the vertical side of the grouser occurs at the grouser toe where a region of stress concentration develops. At a distance of approximately half an inch above the toe, the normal pressure is found to drop to approximately half the value of the cutting pressure. It is also seen from this Figure that in the initial stages of deformation [0.1 inch grouser displacement] no pressure peak develops on the horizontal interface. However, with increasing grouser displacement a pressure peak starts to form on the leading edge. This behavior is attributed to the formation of a stress concentration zone, below the leading edge, caused by the confining effect of the horizontal interface. No tangential stress distributions are drawn for this grouser for it was assumed that the nodes on the horizontal interface are free to move in the horizontal direction [smooth boundary], resulting in zero tangential stresses on this interface. The values of the tangential stresses on the vertical side were found to be of very small magnitudes.

Figures 6-20 and 6-21 show the normal pressure distributions on the C.E.W. type (2) and the S.E.W. grousers, respectively. The C.E.W. type (2) grouser normal pressure distributions are of parabolic shape with peaks at the toe and at the leading edge. Larger peak values develop on the leading edge, accounting for the appearance of failed elements near this edge before the toe failure commences, Fig. 6-17. The same argument is true for the S.E.W. system, Fig. 6-21, with the exception that the leading edge, in this particular case, is the top horizontal plate.

The corresponding tangential stress distributions on these

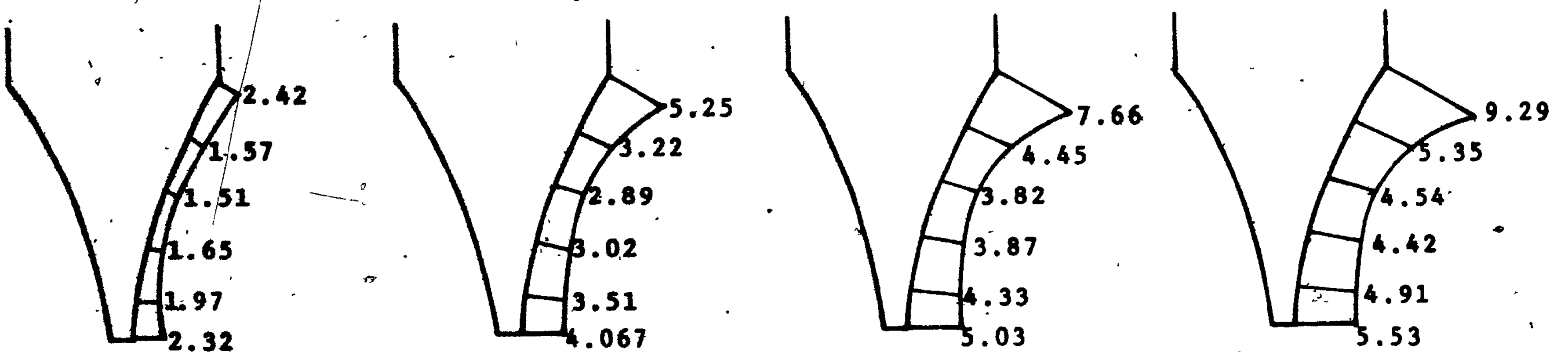

GROUSER DISPLACEMENT

0.1 inch 0.3 inch 0.6 inch 1.0 inch

Scale: 1 inch = 15 psi

FIGURE 6-20 NORMAL PRESSURE DISTRIBUTION ON THE C.E.W. TYPE (2) GROUSER

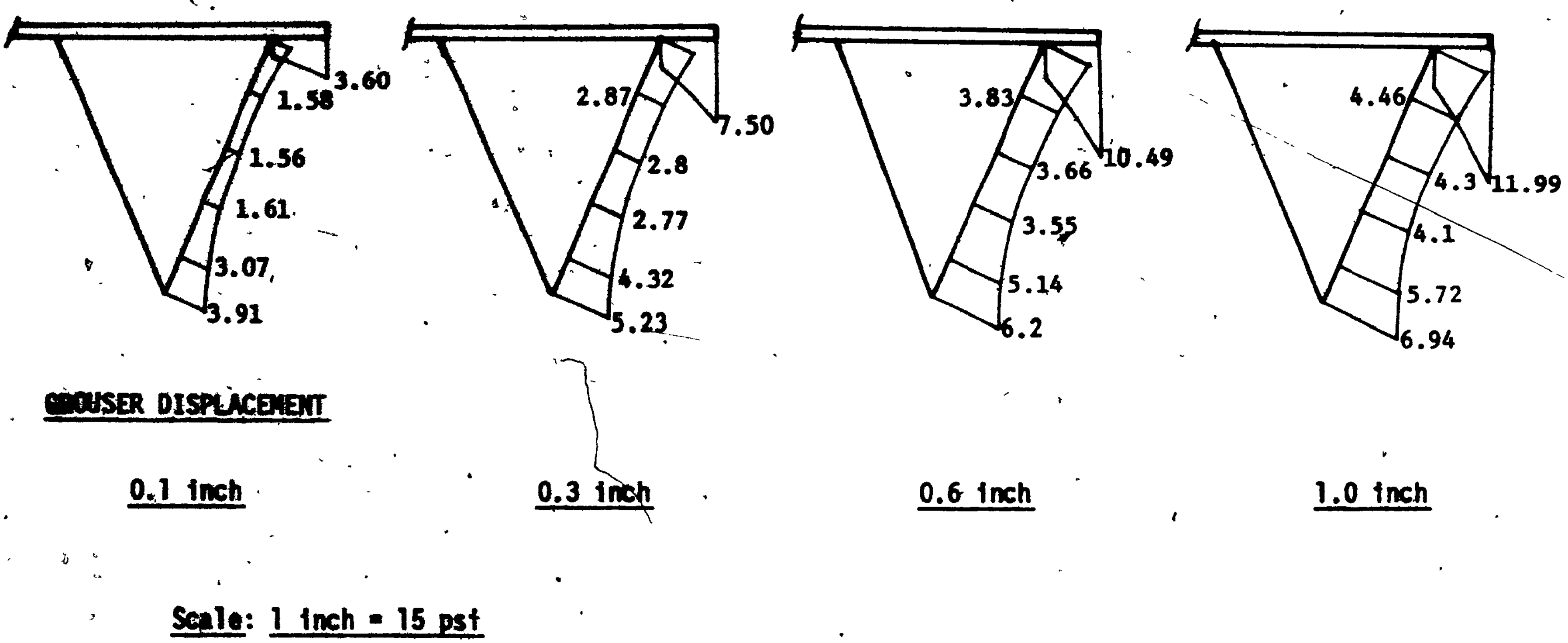

FIGURE 6-21 NORMAL PRESSURE DISTRIBUTION ON THE S.E.W. GROUSER

grousers are plotted in Figs. 6-22 and 6-23. In both systems the shear stress changes direction at a certain point on the soil-grouser interface. But, while the shear direction is negative [anticlockwise] on the bottom half of the C.E.W. type (2) grouser interface, and positive on the top part, the reverse occurs on the S.E.W. grouser interface. As the tangential reactions are obtained from resolving the horizontal and vertical reactions in the tangential direction, the direction of the tangential reaction is expected to depend upon the relative magnitudes of the x- and y-reaction components. The curvature of the C.E.W. type (2) interface results in a continuous variation in the angles made between the x- and y-reactions and the interface. This causes a change in the magnitudes of the tangential components contributed by each of the horizontal and vertical reactions along the curved interface. Moreover, the presence of the top horizontal plate in the S.E.W. system influences the direction of the reaction on the interface nodal points, resulting in a negative [downward] shear along approximately the top two-thirds of the inclined interface.

6.5 COMPARISON OF ANALYSIS WITH EXPERIMENTAL RESULTS

6.5.1 Comparison of Measured and Calculated Forces

The force-displacement relations obtained from the finite element analysis for the various grouser-soil systems are shown in Figs. 6-24 to 6-26, inclusive. The idealizations, assumptions, and the boundary conditions adopted for the analyses of these systems were discussed in Section 6.1. Plotted on the same Figures are typical load-displacement records obtained from the traction series. For the

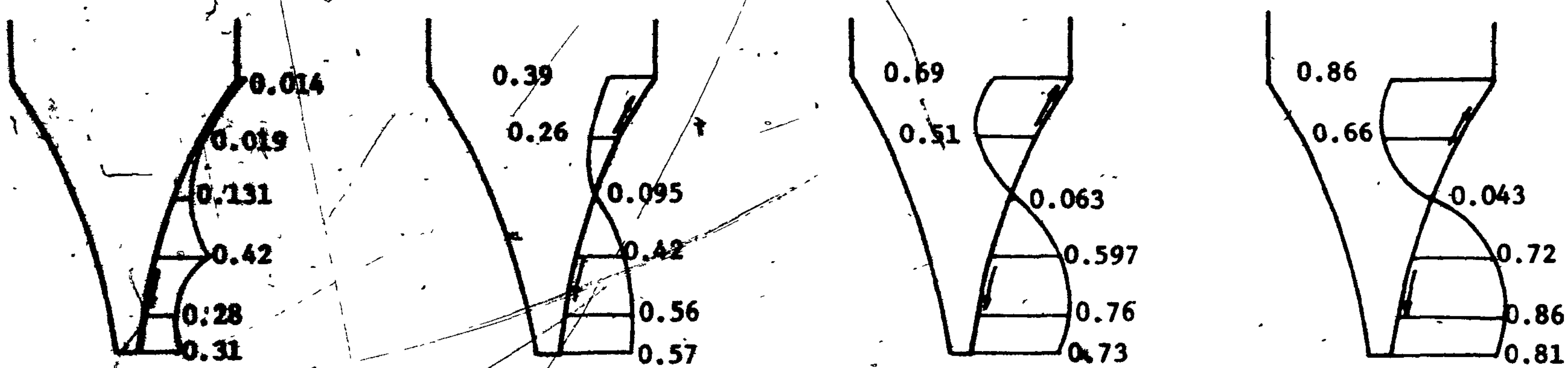

GROUSER DISPLACEMENT

0.1 inch   0.3 inch   0.6 inch   1.0 inch

Scale: 1 inch = 1.5 psi

FIGURE 6-22 TANGENTIAL STRESS DISTRIBUTION ON THE C.E.W. TYPE (2) GROUSER

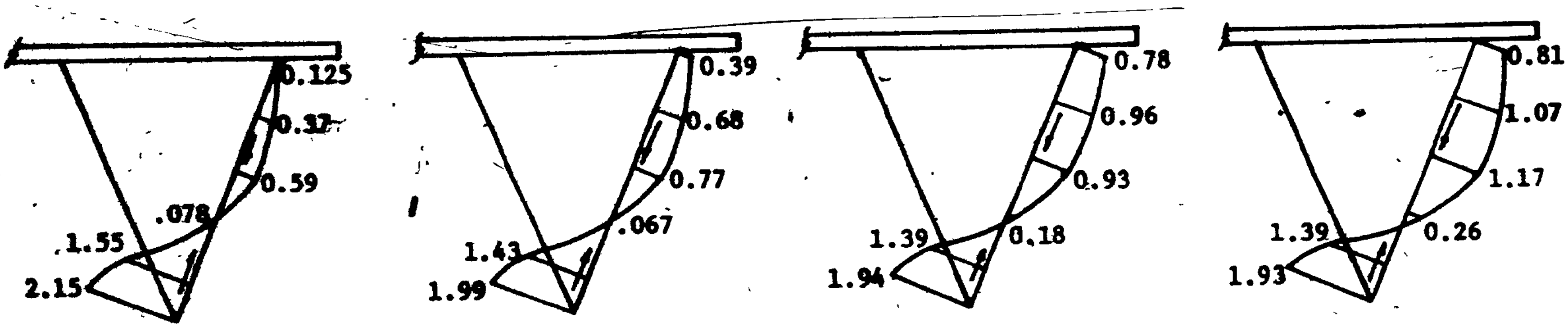

GROUSER DISPLACEMENT

0.1 inch 0.3 inch 0.6 inch 1.0 inch

Scale: 1 inch = 4.0 psi

FIGURE 6-23 TANGENTIAL STRESS DISTRIBUTION ON THE S.E.W. GROUSER

FIGURE 6-24 COMPARISON OF MEASURED AND PREDICTED VALUES OF DEVELOPED HORIZONTAL AND VERTICAL FORCES ON THE PLATE GROUSER (R.A.P.G.) WITH AN ASPECT RATIO H/L = 0.833

(KAOLINITE CLAY)

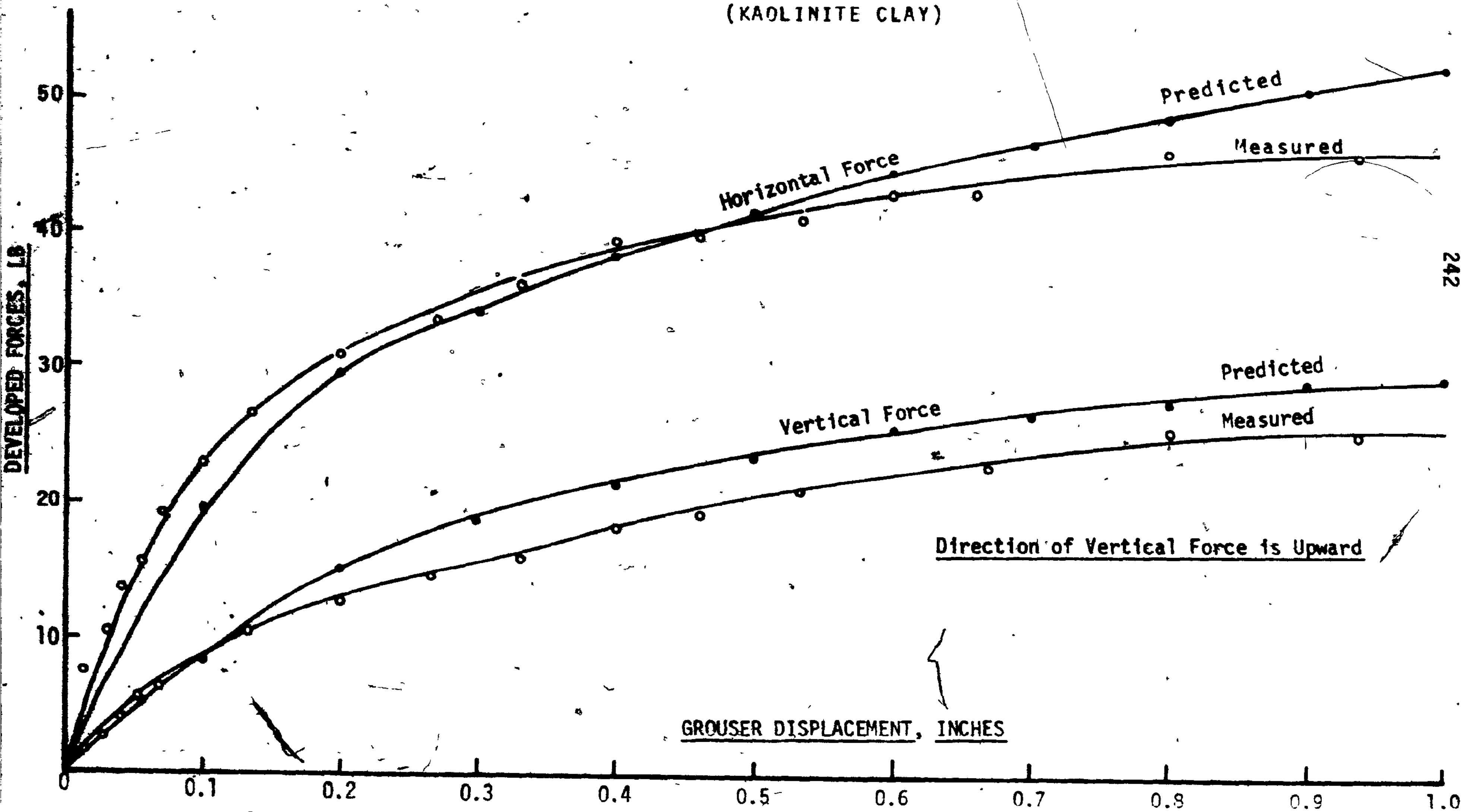

FIGURE 6-25 COMPARISON OF MEASURED AND PREDICTED VALUES OF DEVELOPED HORIZONTAL AND VERTICAL FORCES ON THE C.E.W. TYPE (2) GROUSER

(KAOLINITE CLAY)

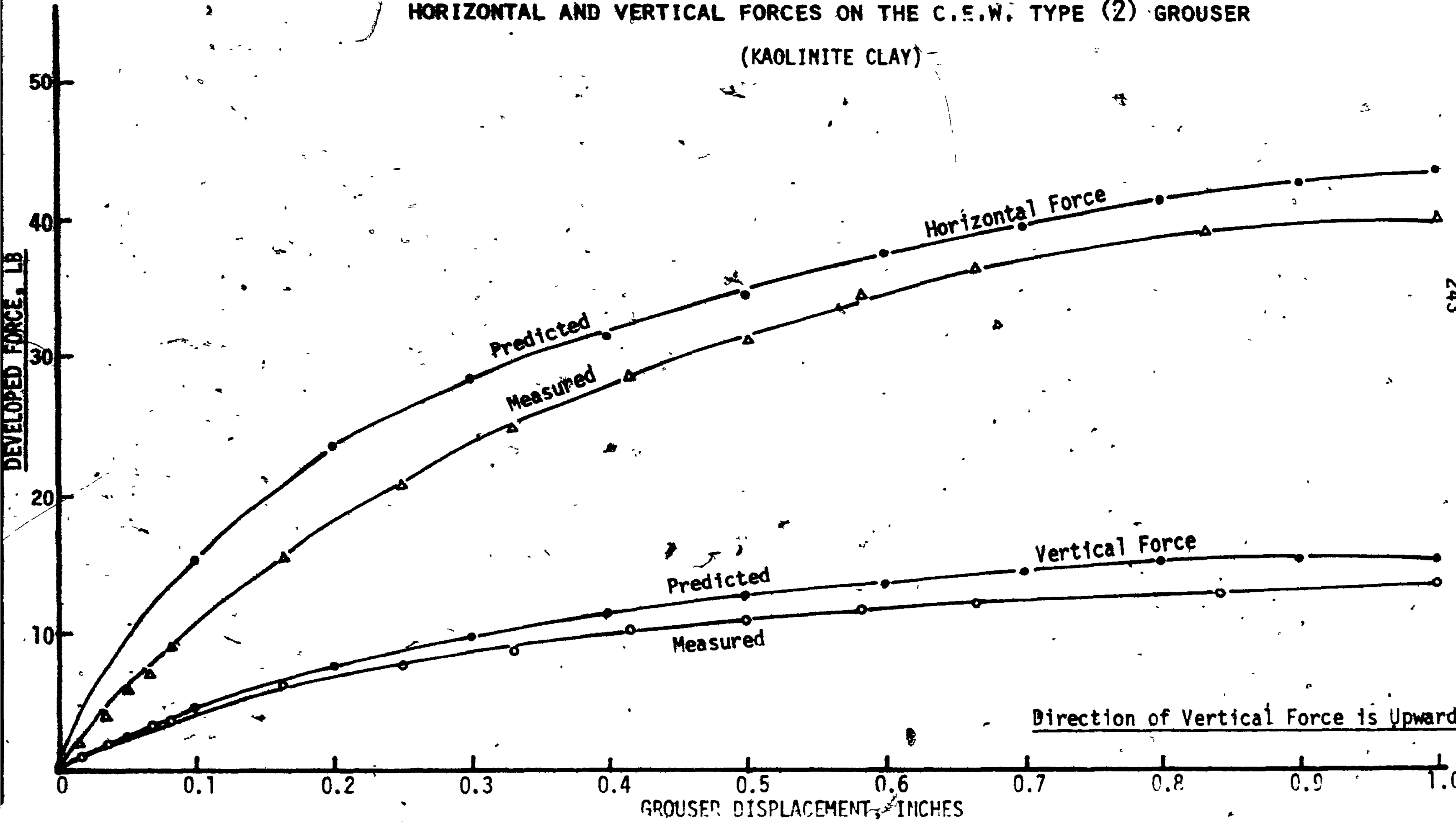

FIGURE 6-26 COMPARISON OF MEASURED AND PREDICTED VALUES OF DEVELOPED HORIZONTAL AND VERTICAL FORCES ON THE S.E.W. GROUSER

(KAOLINITE CLAY)

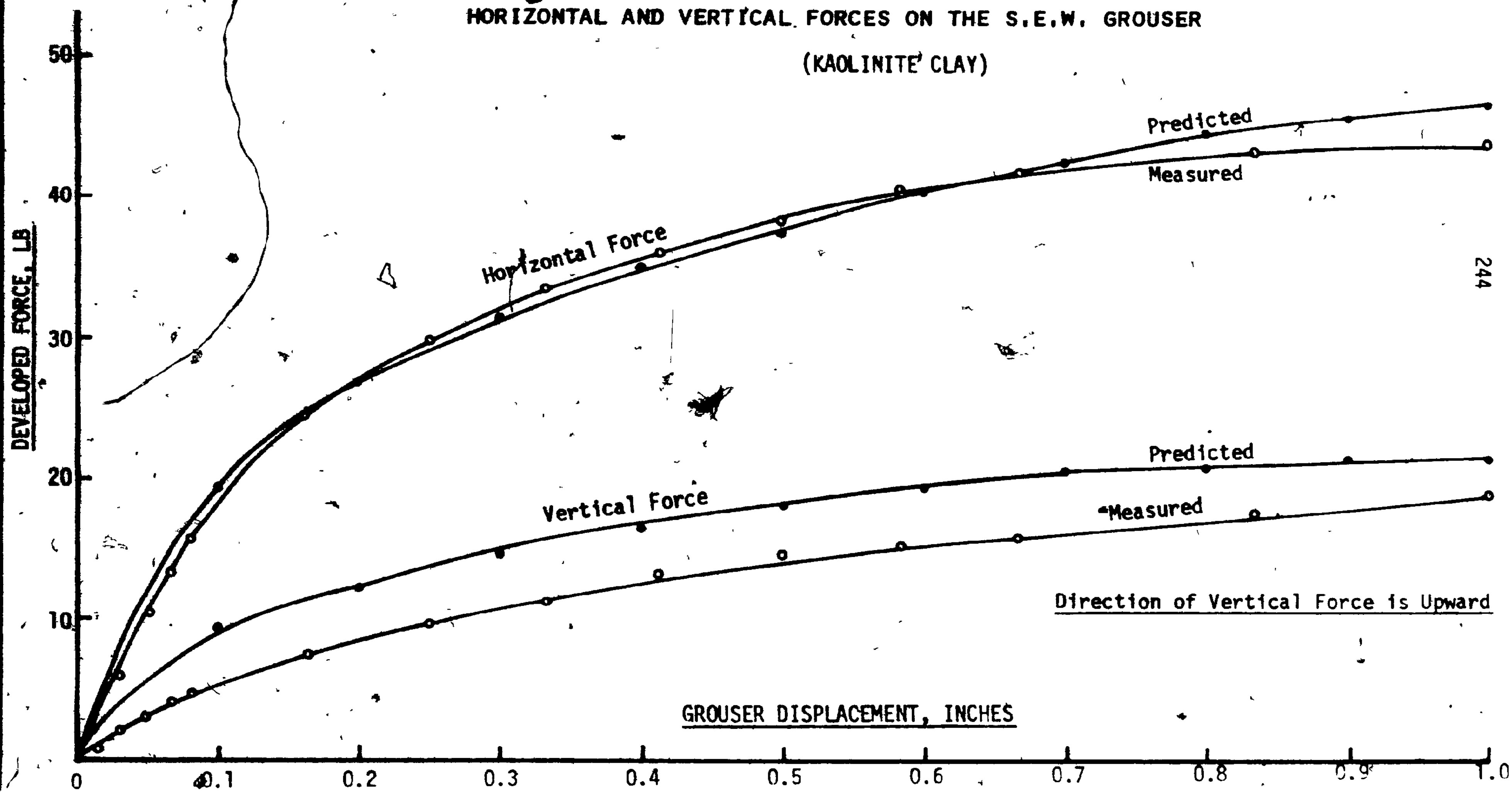

sake of comparison, both the analytical and experimental forces are also reported in Table 6-1 at 0.25 inch intervals over a total grouser displacement of 1.0 inch, together with the difference between the two sets of values expressed as a percentage of the experimental value.

The agreement between the experimental and the finite element results, considering the numerous assumptions made, is generally very satisfactory. The analytical and test results, however, show better agreement in the case of the horizontal forces, for which the percentage difference rarely exceeds 10%. In the case of the vertical forces the average error of estimate is in the order of 20%, while the maximum error is some 40%. It must be noted that the trend of better predictions of horizontal forces was also observed in the soil cutting results, Section 5.6.1.

6.5.2 Comparison of Analytical and Experimental Deformation Fields

Typical deformation fields for the traction test series are shown in Figs. 6-27 to 6-32, plotted at 1.0 inch grouser displacement. The analytical fields obtained from the finite element nodal displacements are also plotted on the same Figures for comparison.

Figures 6-27 and 6-28 illustrate the horizontal and vertical displacement fields for the plate grouser-soil system. From the examination of these Figures the following observations could be made:

1. Generally the correspondence between the analytical and the experimental fields for both the horizontal and vertical displacements is satisfactory. The

TABLE 6-1

COMPARISON OF MEASURED AND PREDICTED VALUES OF DEVELOPED FORCES FOR TRACTION TESTS

TEST No.	GROUSER TYPE	GROUSER DISPLACEMENT (inch)	HORIZONTAL FORCE (lb) Measured	HORIZONTAL FORCE (lb) Predicted	HORIZONTAL FORCE (lb) Difference %	VERTICAL FORCE (lb) Measured	VERTICAL FORCE (lb) Predicted	VERTICAL FORCE (lb) Difference %
34	R.A.P.G. (h/l = 0.833)	0.25	33.5	32.4	- 3.3	13.1	17.20	+ 31.3
		0.50	41.2	41.47	+ 0.6	18.0	23.63	+ 31.3
		0.75	44.5	48.0	+ 7.9	21.8	27.43	+ 25.8
		1.00	47.0	52.5	+ 11.70	25.2	29.43	+ 16.7
33	C.E.W.type(2)	0.25	21.0	26.0	+ 23.8	8.9	7.9	- 11.2
		0.50	32.0	34.88	+ 9.0	11.0	12.71	+ 15.5
		0.75	38.0	40.4	+ 6.3	12.2	14.9	+ 22.1
		1.00	40.0	43.78	+ 8.63	13.6	15.4	+ 13.2
38	C.E.W.type(2)	0.25	23.0	26.0	+ 13.0	8.5	7.9	- 7.0
		0.50	31.0	34.88	+ 12.5	11.7	12.71	+ 8.6
		0.75	37.3	40.4	+ 8.3	13.1	14.9	+ 13.7
		1.00	41.3	43.78	+ 6.0	14.3	15.4	+ 7.7
32	S.E.W.	0.25	30.0	29.0	- 3.3	9.70	13.9	+ 43.2
		0.50	38.8	37.98	- 2.1	14.7	18.2	+ 23.8
		0.75	42.5	43.8	+ 3.0	16.4	20.9	+ 27.4
		1.00	44.0	46.97	+ 6.8	19.0	21.53	+ 13.3
37	S.E.W.	0.25	27.0	29.0	+ 7.4	11.3	13.9	+ 23.0
		0.50	35.0	37.95	+ 8.5	15.9	18.2	+ 14.5
		0.75	41.1	43.8	+ 6.6	18.8	20.9	+ 11.2
		1.00	42.9	46.97	+ 9.4	20.1	21.53	+ 7.1

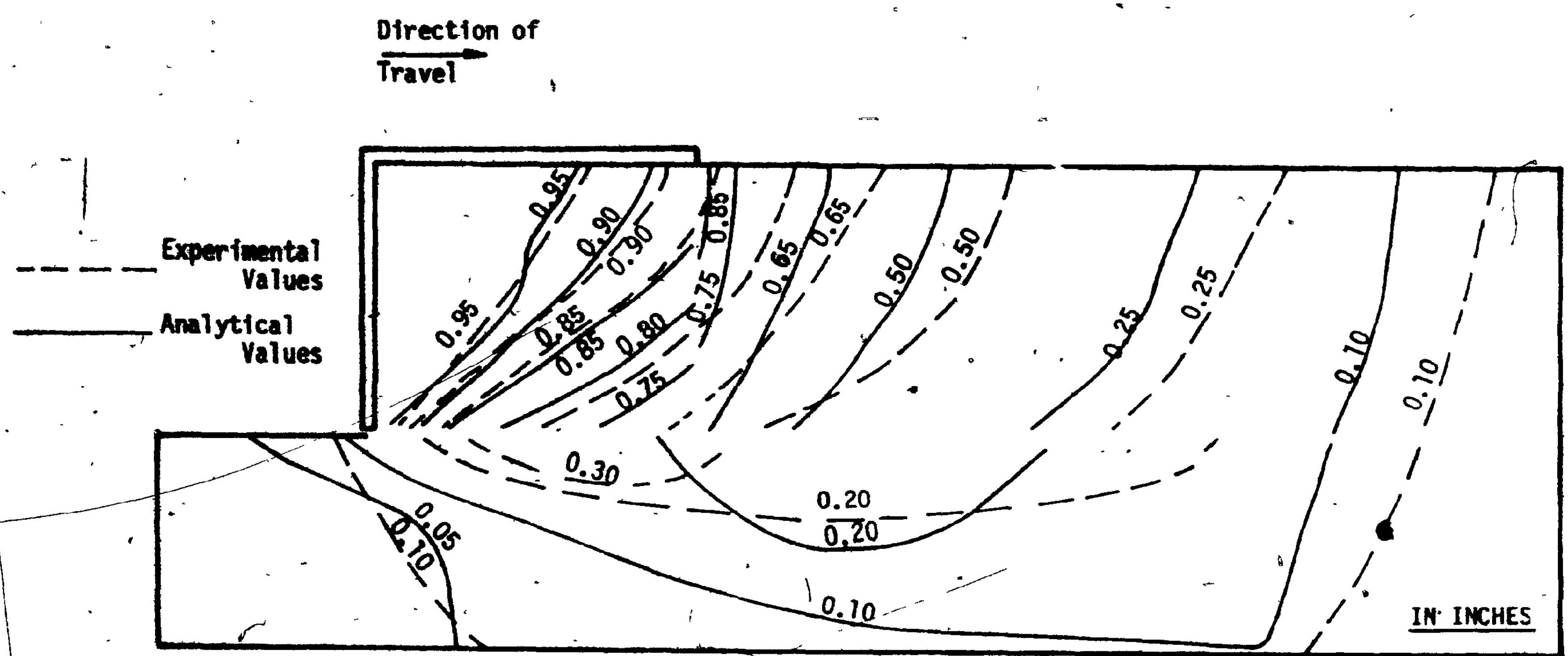

FIGURE 6-27 EXPERIMENTAL AND ANALYTICAL HORIZONTAL DISPLACEMENT FIELDS FOR THE PLATE GROUSER (R.A.P.G.) - SOIL SYSTEM

(GROUSER DISPLACEMENT = 1.0 INCH)

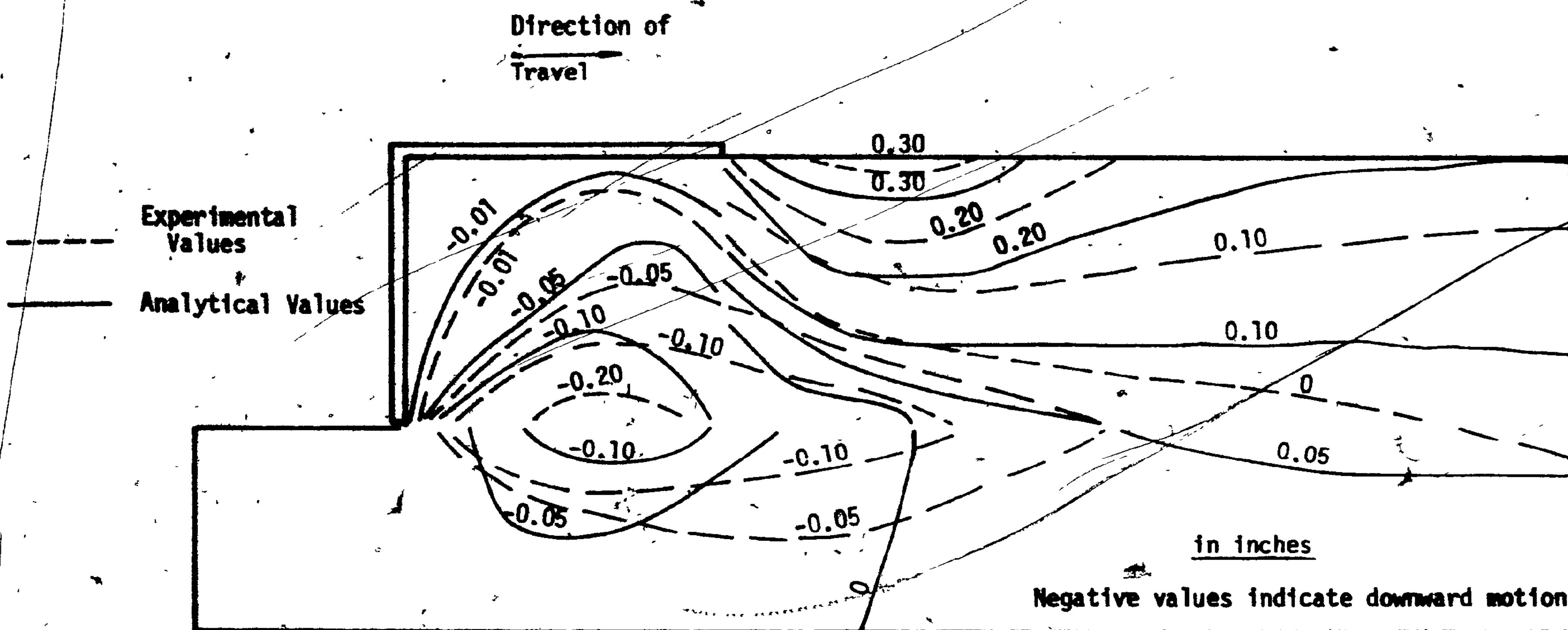

FIGURE 6-28 EXPERIMENTAL AND ANALYTICAL VERTICAL DISPLACEMENT FIELDS FOR THE PLATE GROUSER (R.A.P.G.) - SOIL SYSTEM

(GROUSER DISPLACEMENT = 1.0 INCH)

finite element model, however, is seen to possess more rigidity in the x-direction, and more flexibility in the y-direction, when comparing nodal displacements with those measured during the test series.

2. There appears to be no discontinuity in the measured horizontal displacement fields, Fig. 6-27, across the position of the interface elements placed at the outer edge of the rectangle formed by the two sides of the grouser, line BC, Fig. 6-4. Such discontinuity is shown, however, to occur in the experimental vertical displacement field near the soil surface, Fig. 6-28. Such performance substantiates the reasoning for placing interface elements on this plane.

3. Examination of the experimental vertical displacement field confirms the fact that the soil located below the grouser moves downward, while the soil in front of the grouser moves upward. Such performance corresponds to that obtained from the analytical solution, shown in Figs. 6-5 and 6-6. A significant deviation between the two fields, however, is shown in the location of the zero vertical displacement contour dividing zones of upward and downward movements.

In comparing the computed deformation fields with the measured ones for both the C.E.W. type (2) grouser and the S.E.W. grouser-soil systems, Figs. 6-29 to 6-32, the following points could be made:

1. The computed horizontal deformation fields for the two systems are shown to correspond very closely with the experimentally measured fields, with the finite element results again indicating higher model rigidity than that of the physical system.

2. From the vertical displacement plots, Figs. 6-30 and 6-32, the downward motion of the C.E.W. type (2) system is shown to be localized in a very small region below the toe of the grouser, while in the case of the S.E.W. system the corresponding region is shown to be much larger, signifying the confining effect of the top horizontal plate, Fig. 3-1.

3. The location of the zero vertical displacement contour-line for both systems is again shown to differ when comparing the computed with the measured fields. The measured fields indicate larger zones of downward motion than those obtained from the analytical model. This is believed to be due to the predefinition of the cutting plane discontinuities in the finite element model.

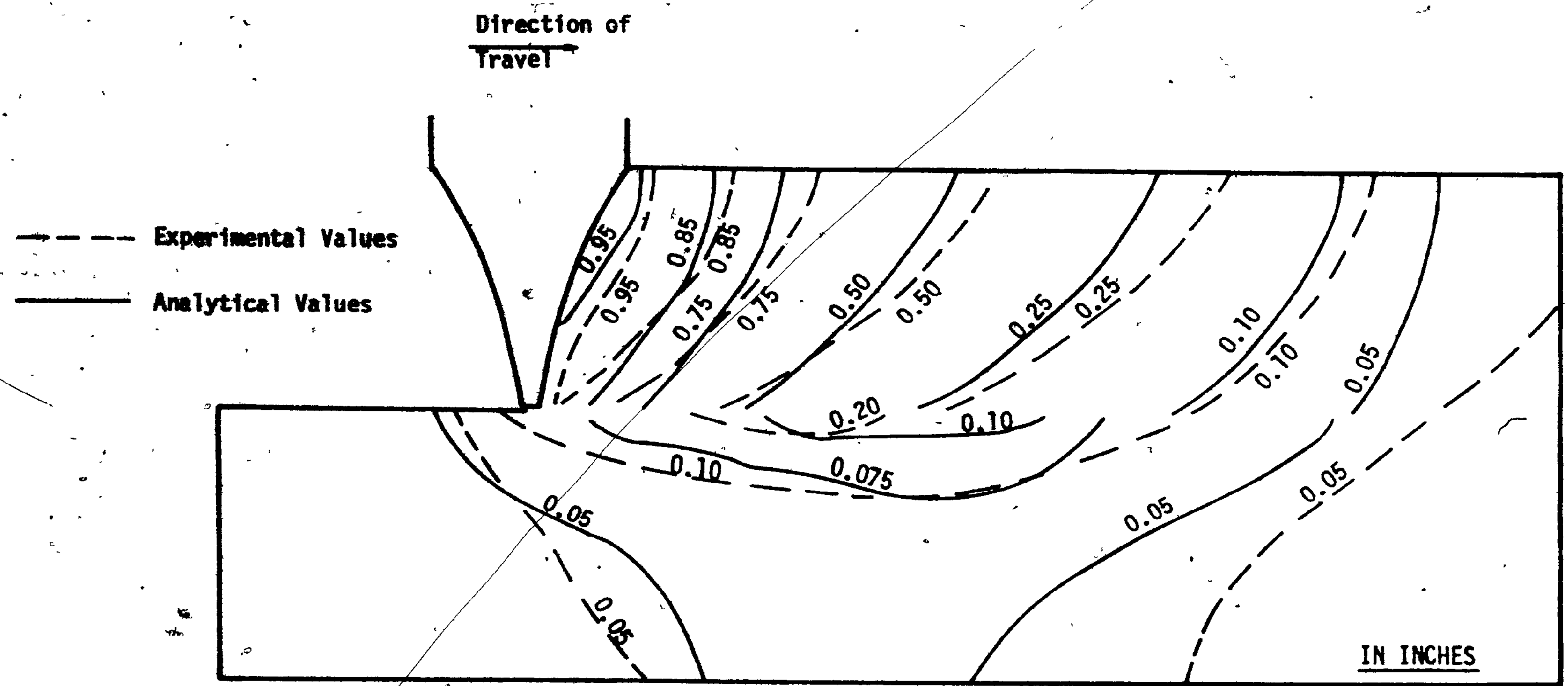

FIGURE 6-29 EXPERIMENTAL AND ANALYTICAL HORIZONTAL DISPLACEMENT FIELDS FOR THE C.E.W. TYPE (2) GROUSER - SOIL SYSTEM

(GROUSER DISPLACEMENT = 1.0 INCH)

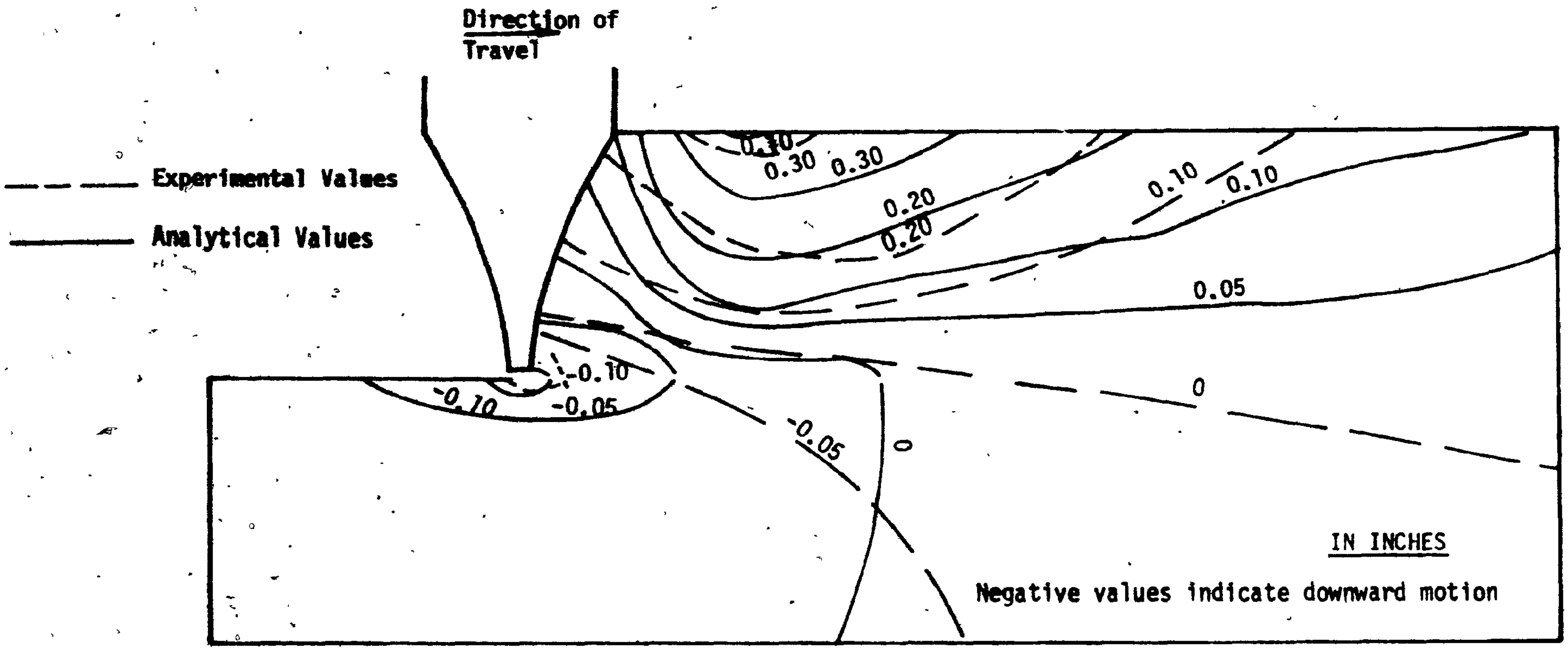

FIGURE 6-30 EXPERIMENTAL AND ANALYTICAL VERTICAL DISPLACEMENT FIELDS FOR THE C.E.W. TYPE (2) GROUSER - SOIL SYSTEM

(GROUSER DISPLACEMENT = 1.0 INCH)

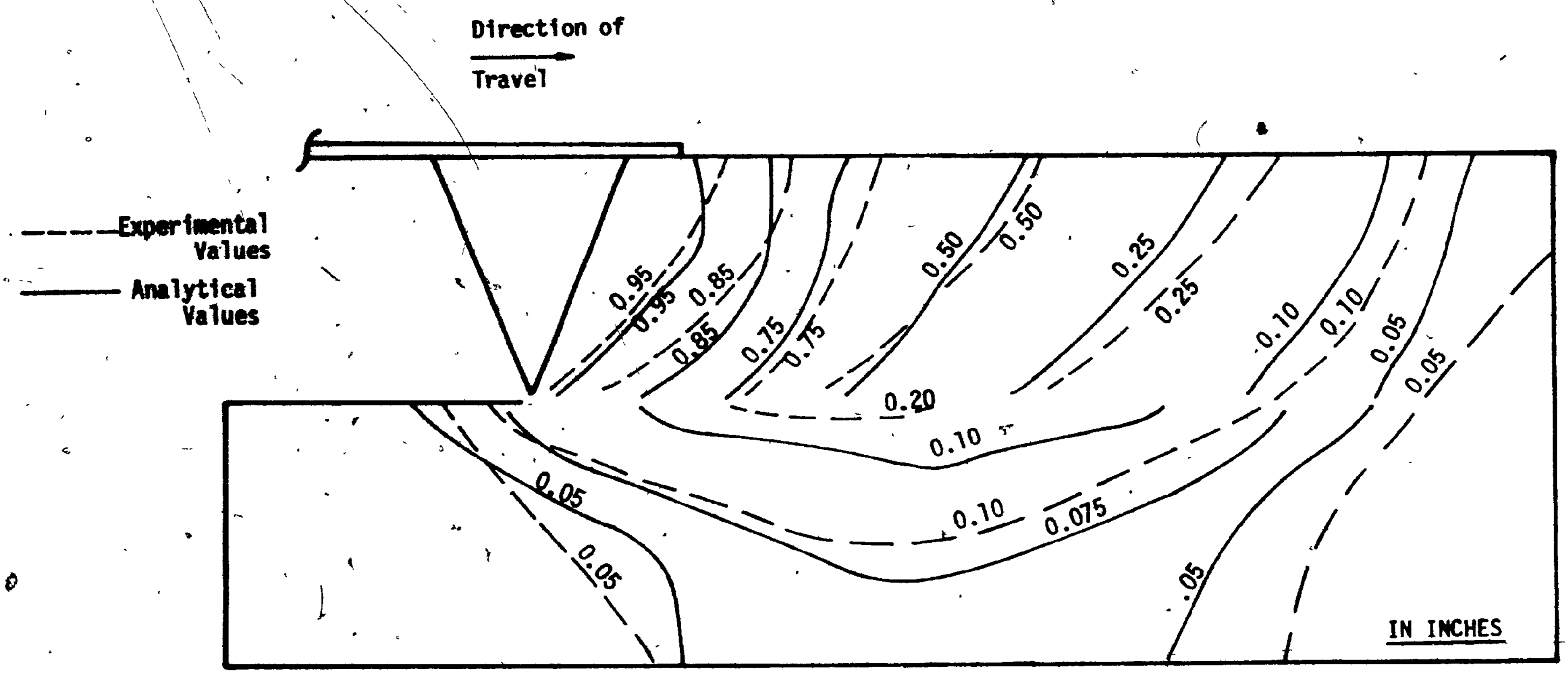

FIGURE 6-31 EXPERIMENTAL AND ANALYTICAL HORIZONTAL DISPLACEMENT FIELDS FOR THE S.E.W. GROUSER - SOIL SYSTEM

(GROUSER DISPLACEMENT = 1.0 INCH)

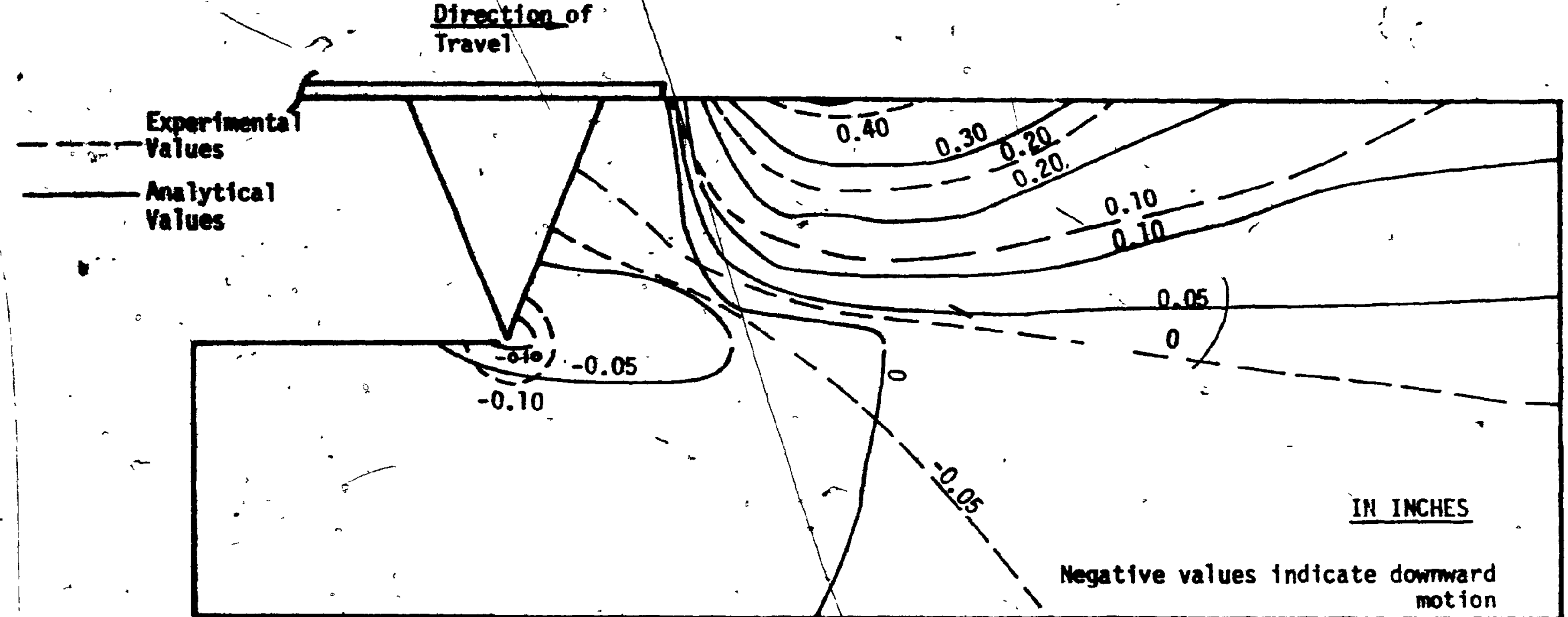

FIGURE 6-32 EXPERIMENTAL AND ANALYTICAL VERTICAL DISPLACEMENT FIELDS FOR THE S.E.W. GROUSER - SOIL SYSTEM

(GROUSER DISPLACEMENT = 1.0 INCH)

6.5.3. Prediction of Deformation Energy

As outlined in Section 5.6.3, the deformation energy of the tool-soil system is obtained by various methods. These methods were classified as follows:

Experimental - by integration of the experimentally measured force-displacement relationships,

Semi-analytical - by application of the visioplasticity method to the experimentally recorded deformation fields,

Theoretical - by calculating the deformation energy of the finite element idealizations proposed in this study.

The results computed using these methods are plotted in Figs. 6-33, 6-34 and 6-35 for the plate (R.A.P.G.), the C.E.W. type (2) and the S.E.W. grouser-soil systems, respectively. In Table 6-2 the energy values are reported at 0.25 inch intervals of tool displacement of 1.0 inch. The deviations between the semi-analytical and theoretical values of deformation energy, expressed as a percentage of the values obtained from the integration of the areas under the measured force-displacement curves, are shown in Table 6-3. It is seen from these results that, as in the case of the soil cutting comparisons, Section 5.6.3, the visioplasticity method overestimates the deformation energy in all cases, while the finite element results show a better correlation with the measured input energy. The reasons given in Section 5.6.3 for the discrepancies between the two predictive methods also apply to the above results.

FIGURE 6-33 COMPARISON OF MEASURED AND CALCULATED VALUES OF DEFORMATION ENERGY FOR THE PLATE GROUSER (R.A.P.G.) (KAOLIN CLAY SYSTEM)

(Grouser Aspect Ratio (h/l) = 0.833)

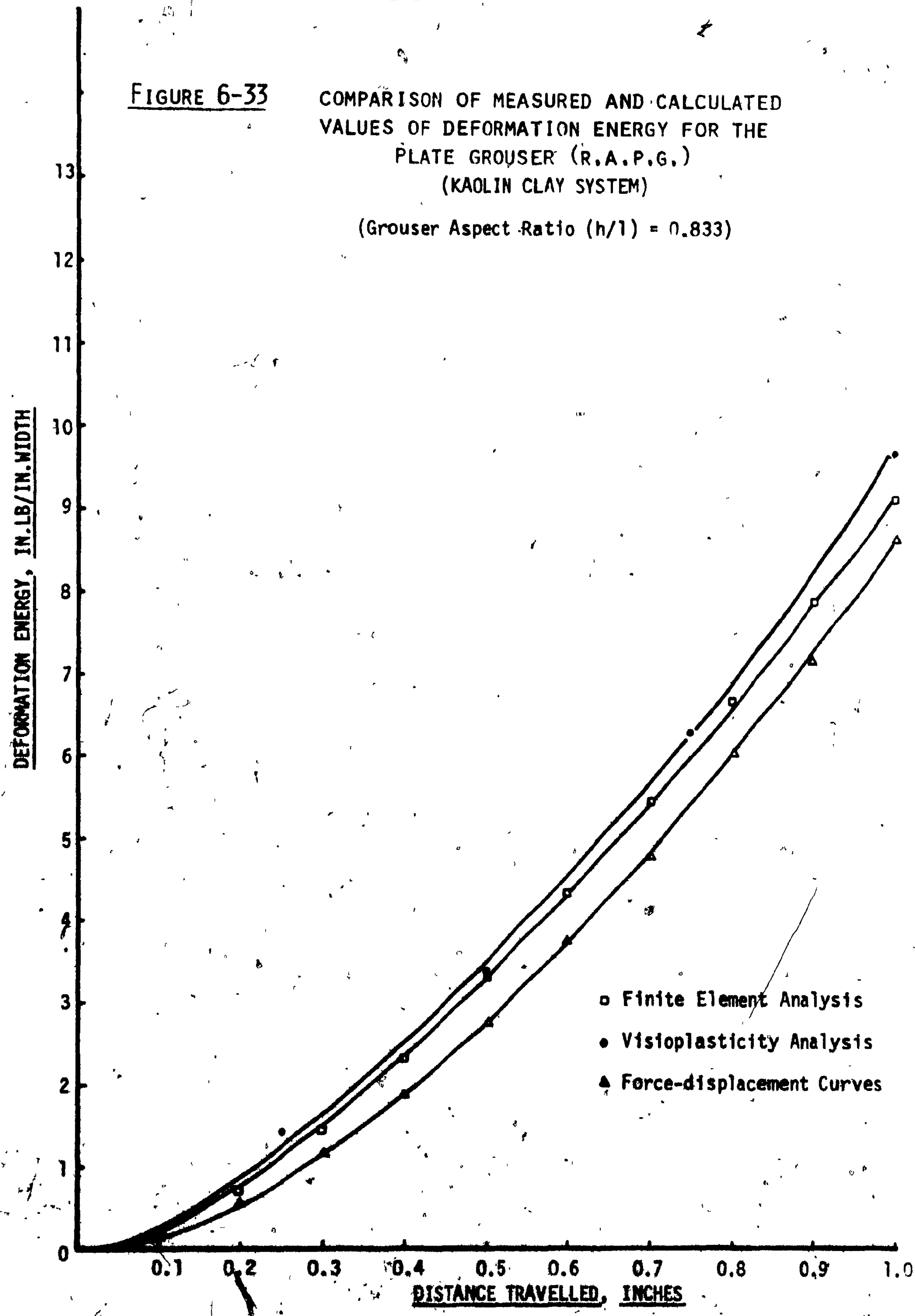

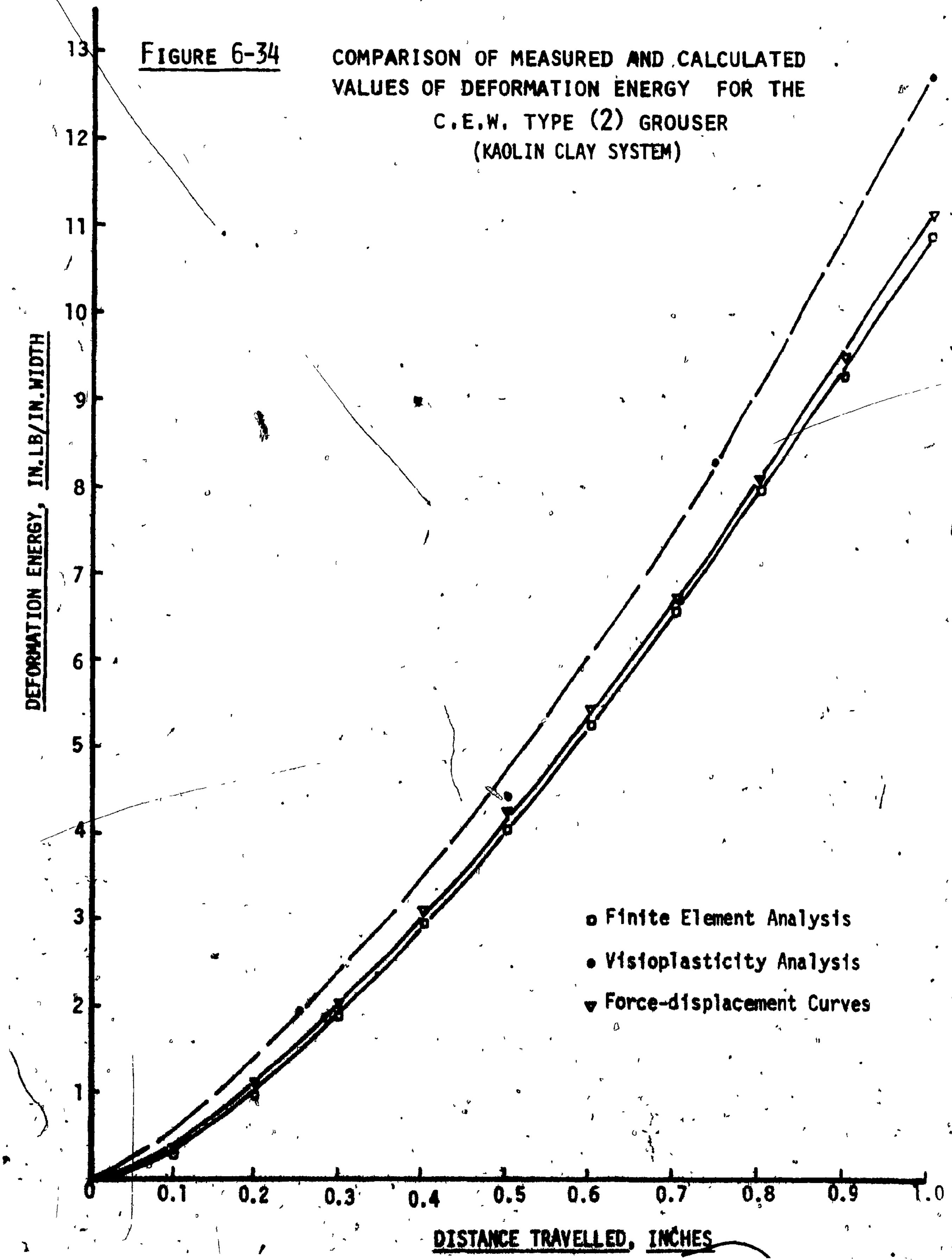
FIGURE 6-34
COMPARISON OF MEASURED AND CALCULATED VALUES OF DEFORMATION ENERGY FOR THE C.E.W. TYPE (2) GROUSER
(KAOLIN CLAY SYSTEM)
DEFORMATION ENERGY, IN.LB/IN.WIDTH
DISTANCE TRAVELLED, INCHES
0
0.1
0.2
0.3
0.4
0.5
0.6
0.7
0.8
0.9
1.0
1
2
3
4
5
6
7
8
9
10
11
12
13
Finite Element Analysis
Visioplasticity Analysis
Force-displacement Curves

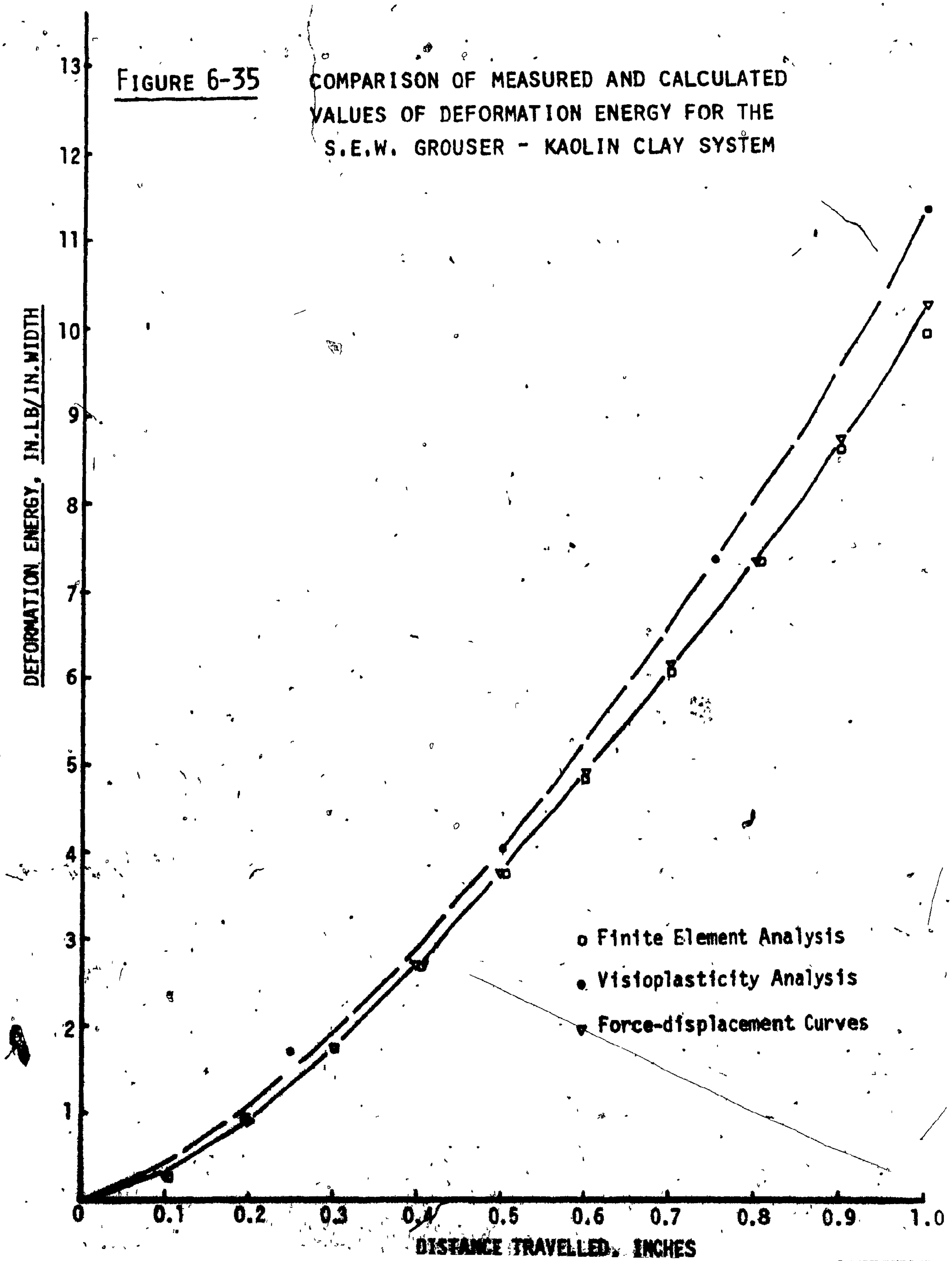

FIGURE 6-35 COMPARISON OF MEASURED AND CALCULATED VALUES OF DEFORMATION ENERGY FOR THE S.E.W. GROUSER - KAOLIN CLAY SYSTEM

TABLE 6-2

COMPARISON OF THE DEFORMATION ENERGY VALUES OBTAINED BY THE VARIOUS METHODS FOR TRACTION TESTS

TEST No.	GROUSER TYPE	DEFORMATION ENERGY IN.LB/IN.WIDTH											
		Tool Displacement d = 0.25 inch			Tool Displacement d = 0.50 inch			Tool Displacement d = 0.75 inch			Tool Displacement d = 1.0 inch		
		a	b	c	a	b	c	a	b	c	a	b	c
34	R.A.P.G. (h/l = 0.833)	1.56	1.90	1.40	4.26	4.445	4.05	7.343	8.255	7.21	11.14	12.70	10.85
33	C.E.W.type(2)	0.821	1.44		2.76	3.36		5.278	6.24		8.57	9.6	
				1.09			3.32			6.01			9.05
38	C.E.W.type(2)	0.95	1.34		3.10	3.4		5.91	6.35		8.70	9.4	
32	S.E.W.	1.31	1.70		3.79	3.97		6.72	7.38		10.29	11.35	
				1.35			3.77			6.70			9.94
37	S.E.W.	1.42	1.79		3.4	3.9		6.51	7.12		10.6	11.71	

Notes:

(1) Columns headed with the letter (a) denote values obtained from the experimental force-displacement curves.

(2) Columns headed with the letter (b) denote calculated values obtained from Equation (4.17).

(3) Columns headed with the letter (c) denote values obtained from the finite element solution.

TABLE 6-3

ERRORS OF ESTIMATES OF DEFORMATION ENERGY VALUES
FOR TRACTION TESTS

TEST No.	DEFORMATION ENERGY IN.LB/IN.WIDTH											
	Measured Values	Error of Estimates		Measured Values	Error of Estimates		Measured Values	Error of Estimates		Measured Values	Error of Estimates	
		Visio-plasticity	F.E.		Visio-plasticity	F.E.		Visio-plasticity	F.E.		Visio-plasticity	F.E.
	d = 0.25 inch			d = 0.5 inch			d = 0.75 inch			d = 1.0 inch		
34	1.56	+22.06	-10.25	4.26	+ 4.34	- 4.95	7.343	+12.41	- 1.8	11.14	+ 14.0	- 2.6
33	0.821	+75.3	+32.7	2.76	+21.7	+20.1	5.278	+18.22	+13.8	8.57	+ 12.0	+ 5.5
38	0.95	+41.0	+14.7	3.10	+ 9.6	+ 6.51	5.91	+ 7.45	+ 1.70	8.70	+ 8.04	+ 4.0
32	1.31	+29.8	+ 3.0	3.79	+ 4.74	- 0.5	6.72	+ 9.82	- .30	10.29	+ 10.3	- 3.4
37	1.42	+26.0	- 4.9	3.4	+14.7	+10.8	6.51	+ 9.37	+ 2.90	10.6	+ 10.4	- 6.2

6.6 ANALYTICAL TECHNIQUE SENSITIVITY TO STRENGTH TESTS LOADING CONDITION

It is recalled that the stress-strain relationships for the soil represented by the continuum elements in the finite element solution were obtained by subjecting prismatic samples to a plane-strain loading condition in a modified triaxial cell [Appendix A]. These tests were performed in order to reproduce as closely as possible the plane strain conditions applicable to the soil cutting and traction experimental boundary conditions adopted in this study. In addition to these tests, an axisymmetric loading condition was applied to cylindrical samples placed in a standard triaxial cell. The main objective for conducting the axisymmetric tests was, as mentioned previously, to verify the fact that the nonexistence of a well-defined failure condition is not a result of the plane strain "True Triaxial" test constraint [Section 4.A.3.].

The application of axisymmetric triaxial loading condition is considered a standard testing procedure, requiring no special devices. This is not the case with the plane strain loading condition which is viewed as a special type of test. Due to this fact, it is of interest to examine the sensitivity of the proposed finite element analysis to the strength test loading condition, as well as its effect on the predicted results. For this purpose the artificial clay-grouser interaction problems were analyzed, employing the input stress-strain curves of both loading conditions. The stress-strain curves obtained from both the axisymmetric and plane strain loading conditions for the artificial clay are shown in Fig. A-6, Appendix A. The artificial clay was chosen for the sensitivity analysis as the performance of this clay is not influenced by the magnitude of the confining pressure, Appendix A, and hence one stress-strain curve is employed for each loading condition. Moreover, such analysis leads to further verification of the validity of the proposed analytical technique when applied to tool interaction with a purely plastic material.

It has been shown in Section 2.4.2 that for a plane strain loading condition of an incompressible material ($\nu = 0.5$), Hooke's Law, Eq. (2.28), gives:

$$E = \frac{3}{4} \frac{\sigma_1 - \sigma_3}{\varepsilon_1}$$

with the term $(\sigma_1 - \sigma_3)/\varepsilon_1$ representing the slope of the secant modulus, (E_T), of the deviator stress, $(\sigma_1 - \sigma_3)$, versus principal strain, ε_1, curve obtained under plane strain loading condition. Equation (2.28) simplifies to:

$$E = \frac{3}{4} E_T \tag{6.1}$$

It should be pointed out here that E represents the elastic modulus of the material which is a material property and should not depend on the loading condition. On the other hand, the modulus E_T, is obtained, in this case, from the stress deviator-principal strain curve resulting from plane strain loading.

In the axisymmetric triaxial compression test,

$\sigma_2 = \sigma_3$ and $\varepsilon_2 = \varepsilon_3$

Applying Hooke's Law for an isotropic, linear, elastic material, in a principal plane, Eq. (2.28) reduces to:

$$\epsilon_1 = \frac{\sigma_1}{E} - \frac{2\nu\sigma_3}{E} = \frac{1}{E}(\sigma_1 - 2\nu\sigma_3) \tag{6.2}$$

$$\epsilon_2 = \epsilon_3 = \frac{\sigma_3}{E} - \frac{\nu}{E}(\sigma_1 + \sigma_3) \tag{6.3}$$

For an incompressible material $\nu = 0.5$, and from Eq. (6.2),

$$E = \frac{\sigma_1 - \sigma_3}{\epsilon_1} \tag{6.4}$$

Also, in an unconfined compression test $\sigma_3 = 0$, and from Eq. (6.2),

$$E = \frac{\sigma_1}{\epsilon_1} \tag{6.5}$$

Equations (6.4) and (6.5) represent the slope E_T of the deviator stress, $(\sigma_1 - \sigma_3)$, versus principal strain, ϵ_1 for the axisymmetric triaxial and unconfined compression curves, respectively. Thus in these two cases,

$$E = E_T \tag{6.6}$$

Employing Eq. (6.1) and Eq. (6.4) together with the appropriate stress-strain curve for the artificial clay, shown in Fig. A-6, Appendix A, the problems of the R.A.P.G., the C.E.W. type (2), and the S.E.W. grousers were analyzed. The idealizations presented in Section 6.1, Figs. 6-1, 6-2 and 6-3, were adopted. The predicted forces, obtained from: (1) the analysis employing the axisymmetric stress-strain curve and Eq. (6.6), (2) the analysis using the plane-strain curve and Eq. (6.1), and (3) the experiments, are plotted as a function of grouser displacement in Figs. 6-36, 6-37 and 6-38 for the three grousers. It can be seen from these Figures that employing the plane strain curve results in lower predicted horizontal and vertical forces when compared with those obtained from the analysis adopting the axisymmetric triaxial curve. This behavior can be explained by the fact that while the plane strain loading condition produces a stress-strain curve exhibiting higher stresses, Fig. A-6, Appendix A, the elastic modulus, E, in the finite element analysis employing the plane strain curve is taken equal to three-quarters that of the curve secant value, E_T, Eq. (6.1). In case of the analysis using the axisymmetric curve, on the other hand, the E values are taken equal to the secant values of the axisymmetric curve, Eq. (6.1). This resulted in slightly lower E values for the plane strain case, and hence lower predicted forces. The difference in E values resulting from the two loading conditions is attributed to the non-uniform and dissimilar distributions of stresses and strains within the cylindrical and prismatic samples due to the effect of the end restraints and side restraints in the case of plane strain loading condition. Finally, it is of interest to note that while both techniques predict horizontal forces which agree closely with the measured values, the vertical forces obtained from the analysis employing the plane strain curve correlate better with the measured vertical forces.

FIGURE 6-36 COMPARISON OF MEASURED AND PREDICTED VALUES OF DEVELOPED HORIZONTAL AND VERTICAL FORCES ON THE R.A.P.G. (H/L = 0.833) IN ARTIFICIAL CLAY

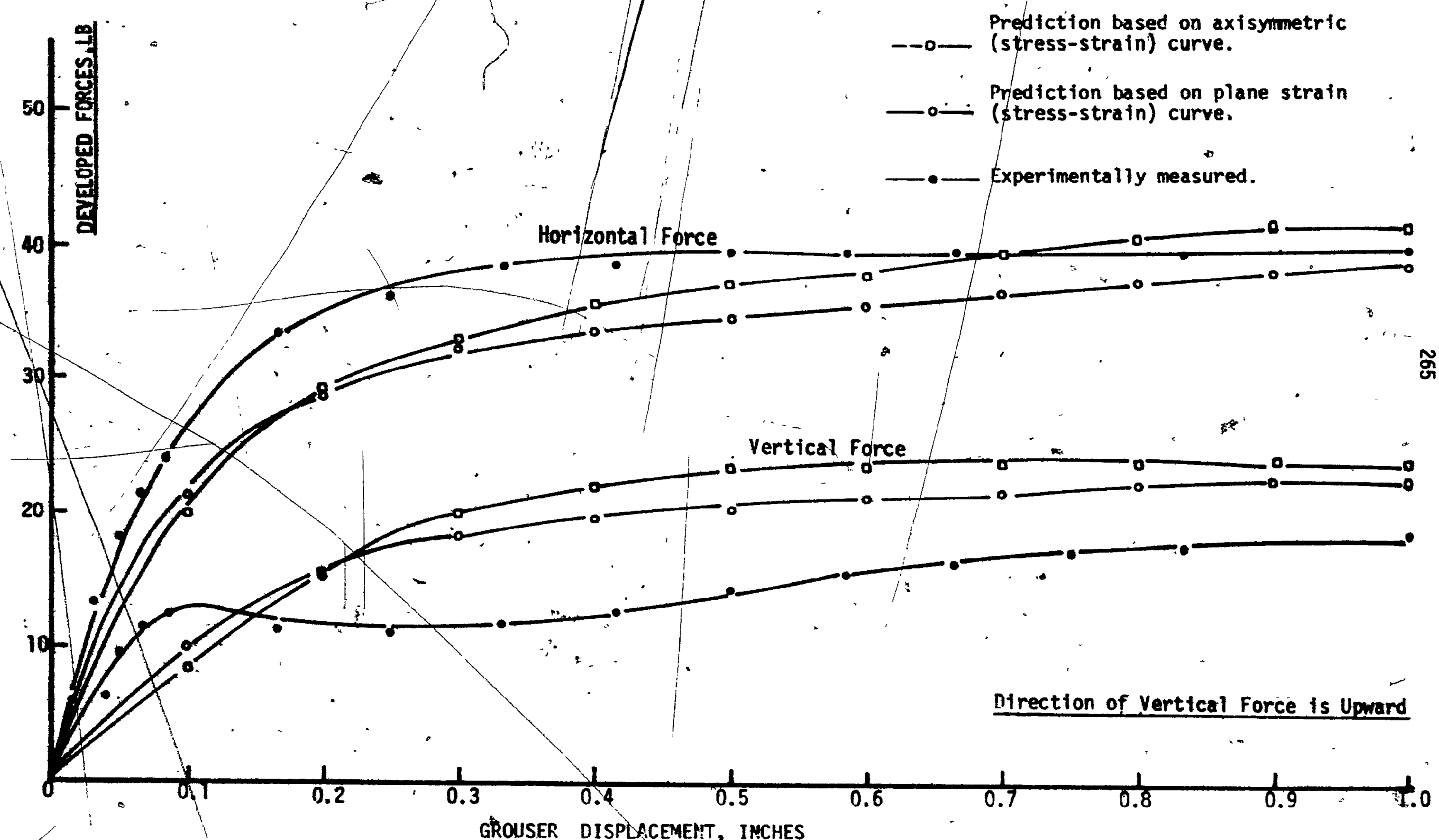

FIGURE 6-37 COMPARISON OF MEASURED AND PREDICTED VALUES OF DEVELOPED HORIZONTAL AND VERTICAL FORCES ON THE C.E.W. TYPE (2) GROUSER IN ARTIFICIAL CLAY

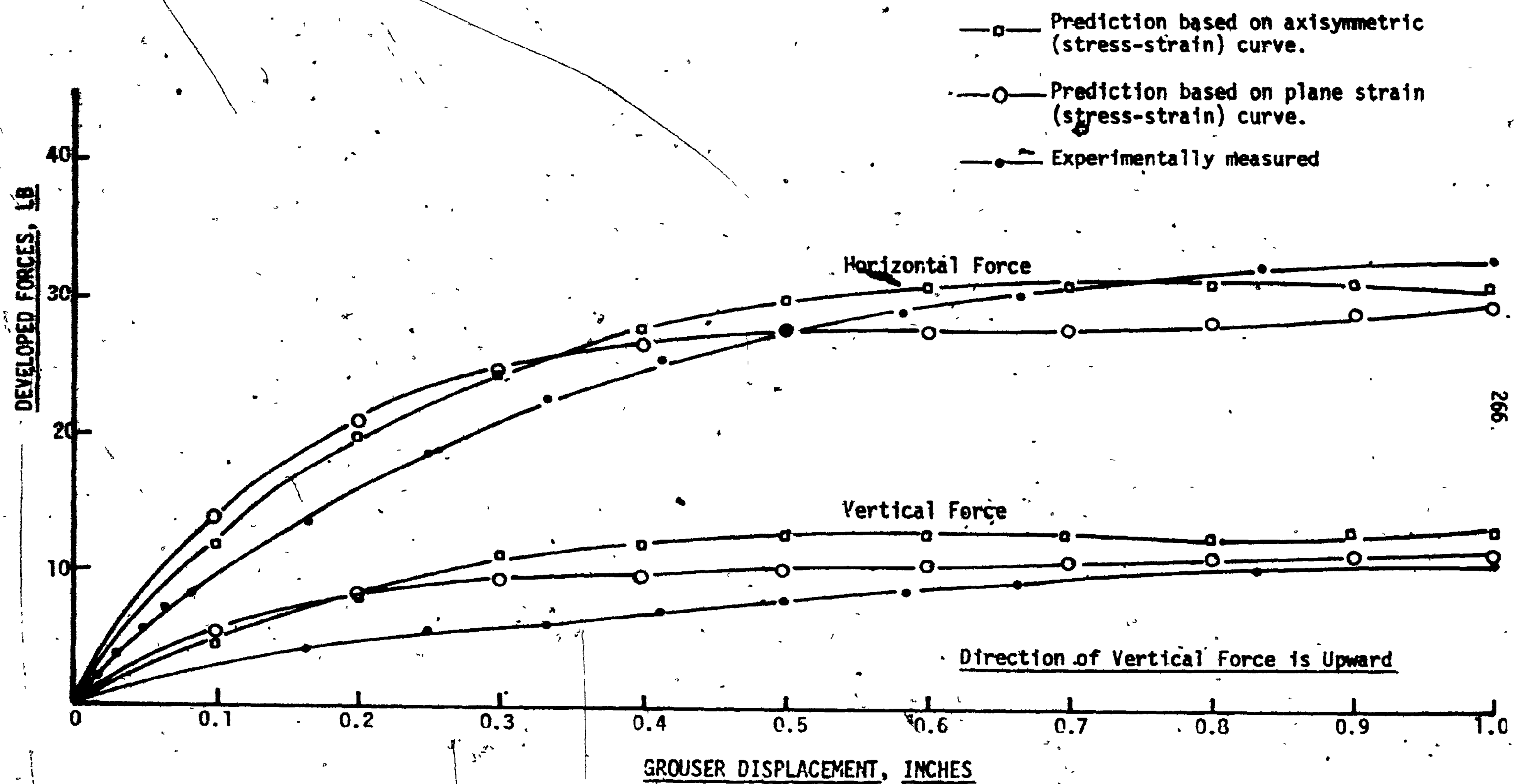

FIGURE 6-38 COMPARISON OF MEASURED AND PREDICTED VALUES OF DEVELOPED HORIZONTAL AND VERTICAL FORCES ON THE S.E.W. GROUSER IN ARTIFICIAL CLAY

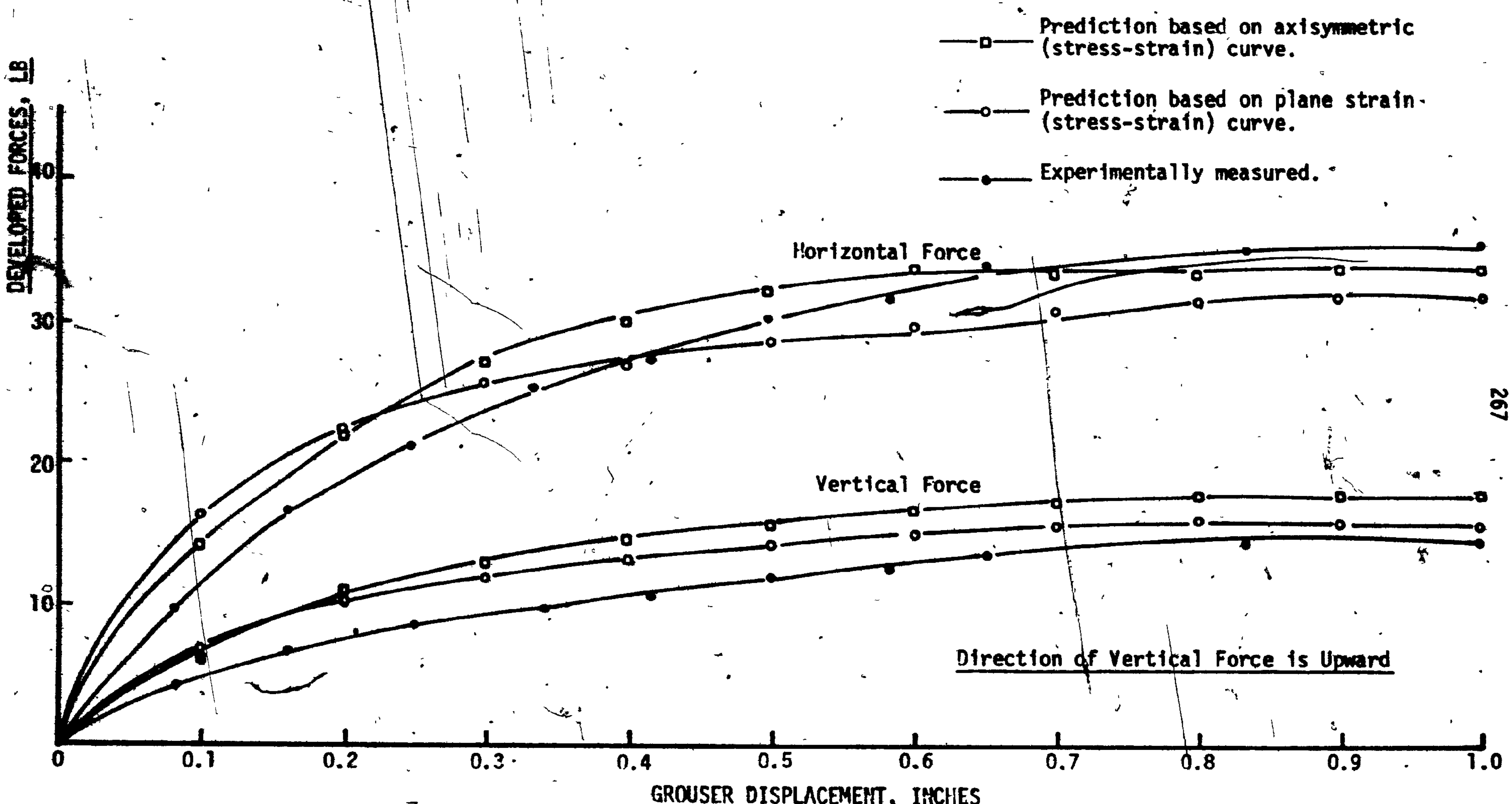

CHAPTER 7

COMPUTER SOLUTION AND COMPARISON WITH ANALYTICAL RESULTS

7.1 INTRODUCTION

In Chapters 5 and 6 the results of the soil cutting and traction experiments, conducted during the course of this study, were compared with the finite element analyses. The agreement was found to be satisfactory. Following from Fig. 4-1, the purpose of this Chapter is to establish the validity of the developed solution technique by presenting a number of verifications of the solution against conventional methods based on closed-form solution schemes.

A typical example of a nonlinear plane-strain problem is the load-deformation characteristics of a long vertical retaining wall with soil mass on one side. The determination of the actual earth pressure on the wall is extremely complicated, because it depends on the relative movement of the wall and the soil. This relative movement mobilizes frictional and/or adhesional forces along the soil-wall interface which affect the earth pressure magnitude and direction. Although many experiments have been carried out on the load-deformation characteristics of walls, there is no widely accepted theory to determine the load-deformation relationship.

While the present study is mainly concerned with the analyses of simple soil cutting and traction problems, the familiar case of two-dimensional soil response encountered in long retaining walls when yielding in a passive sense bears a close parallel to wide cutting blades moving in soil. This is particularly true as the term "passive earth pressure", in the broadest sense, indicates the resistance of a mass of soil against displacement by lateral pressure. Bearing this in mind, the passive earth pressure behind a model retaining wall has been calculated by a nonlinear analysis with differing boundary conditions employing the developed computer program. The results obtained from this analysis are compared in this Chapter with results obtained from the classical theory of earth pressure. The assessment of the admissability and viability of the solution technique is carried out through a parametric study to establish the relative importance of the various features and assumptions implemented in the finite element technique.

The second part of this Chapter is devoted to comparisons of soil cutting and traction analytical and experimental results obtained in this study with results computed from existing theories. The sequence in presentation of results and related discussions for this part is consistent with the earlier separation of the overall problem under study into two principal parts, i.e. soil cutting and traction.

7.2 LOAD-DEFORMATION CHARACTERISTICS FOR A STRIP OF LONG VERTICAL WALL RETAINING CLAY

7.2.1 Background

The case of a simple retaining wall and its interaction with a soil was treated by Coulomb (1776) and Rankine (1857), and the theories developed have continued to be used with remarkable success up to the present time as the most common basis for the design of retaining walls. From these theories the resultant of the earth pressure acting on the wall at some limiting conditions can be obtained, without, however, any information as to the deformation of the wall or earth. In both theories the earth mass is assumed to behave as a rigid-plastic material governed by a Mohr-Coulomb failure criterion, and the structure itself is assumed perfectly rigid.

Only through experimental work such as that of Terzaghi (1932, 1934, and 1936) and more recently Rowe and Peaker (1964), and James and Bransby (1970), an insight was gained into the wall deformations associated with the limit conditions and the dependence of earth pressure on mode of wall deformation. To account for the effect of the mode of wall deformation, more sophisticated limit theories have been developed [Hansen (1953), Drucker (1953), and Sokolovski (1965)] which have application to a much wider class of problems than the simple retaining wall. Elastic solutions have also been derived which can account for the flexibility of the structure [Hetenyi (1964) and Finn (1963)]. In either type of solution however, the material behavior is highly idealized; in the first instance the earth mass is assumed to be a rigid-plastic material governed by a Mohr-Coulomb failure criterion, while in the second it is assumed to be homogenous, isotropic and linearly elastic, regardless of the stress level.

Girijavallabhan and Reese (1968) first demonstrated the successful simulation of a retaining wall problem by finite element techniques. They analyzed two model retaining wall tests in which the wall was forced into first a loose, and then a dense, backfill by pure translation. A nonlinear elastic model was employed for the soil and the interface between the wall, and the backfill was assumed perfectly smooth. Remarkable agreement was obtained when comparing the predicted and observed results.

Morgenstern and Eisenstein (1970) conducted finite element analyses to investigate the effects of the foundation deformations as well as those of excavation on retaining wall behavior. Two problems were analyzed - in the first, the wall was assumed smooth and unmoving, the interface between the soil and the wall smooth, and the soil to be linear elastic. The foundation layer underlying the wall varied from zero thickness to a thickness equal to the height of the wall. Relative to a normal linear k_0 distribution, their analyses showed that the earth pressure near the bottom of the wall was increased and at the top decreased, in some cases going into tension, as the thickness of the foundation layer increased. In the second set of analyses, the wall was allowed to yield in an active and passive sense by 0.0025 of wall height. In this case they noted that the boundary conditions between the foundation layer and the rigid base have a significant effect on the earth pressures, the pressure distribution on the wall becoming nonlinear with a rough boundary for both the active and passive analyses.

Analyses of retaining walls were performed by Clough and Duncan (1971) using the one-dimensional element of Goodman et al. (1968) to simulate the interface between the wall and the backfill. The wall was assumed to be either perfectly rough ($\delta = \phi$), perfectly smooth ($\delta = 0$)

or moderately rough ($\delta = 2/3\ \phi$), and it was displaced by rotation and translation in both the active and passive senses. The minimum active and maximum passive pressures calculated in these analyses were found to be in good agreement with the results of the classical earth pressure theory, and the amount of movement required to reach the full active and full passive conditions were found to be in agreement with the results of the model retaining wall tests performed by Terzaghi (1934).

7.2.2 Finite Element Analysis of the Retaining Wall Problem

(a) Idealization: Several analyses were conducted to evaluate the effectiveness of the analysis procedures described previously, using the rigid wall and backfill shown in Fig. 7-1. Beginning from initial at-rest pressure condition, the wall was moved toward the backfill in a series of increments, adjusting the properties of the elements in accordance with the stresses for each increment to approximate nonlinear behavior [Chapter 2]. The wall was assumed to be either perfectly rough [i.e. no possibility for slip between wall and soil], perfectly smooth [no shear stresses at the interface], or moderately rough [soil-wall adhesion case governed by nonlinear, stress dependent interface behavior]. The moderately rough [soil-wall adhesion] case was simulated in the finite element analysis by inserting interface elements between the soil and the wall, Fig. 7-1. The boundaries were placed on rollers such that horizontal displacements were prevented on the sides and no vertical movement was allowed on the rigid base.

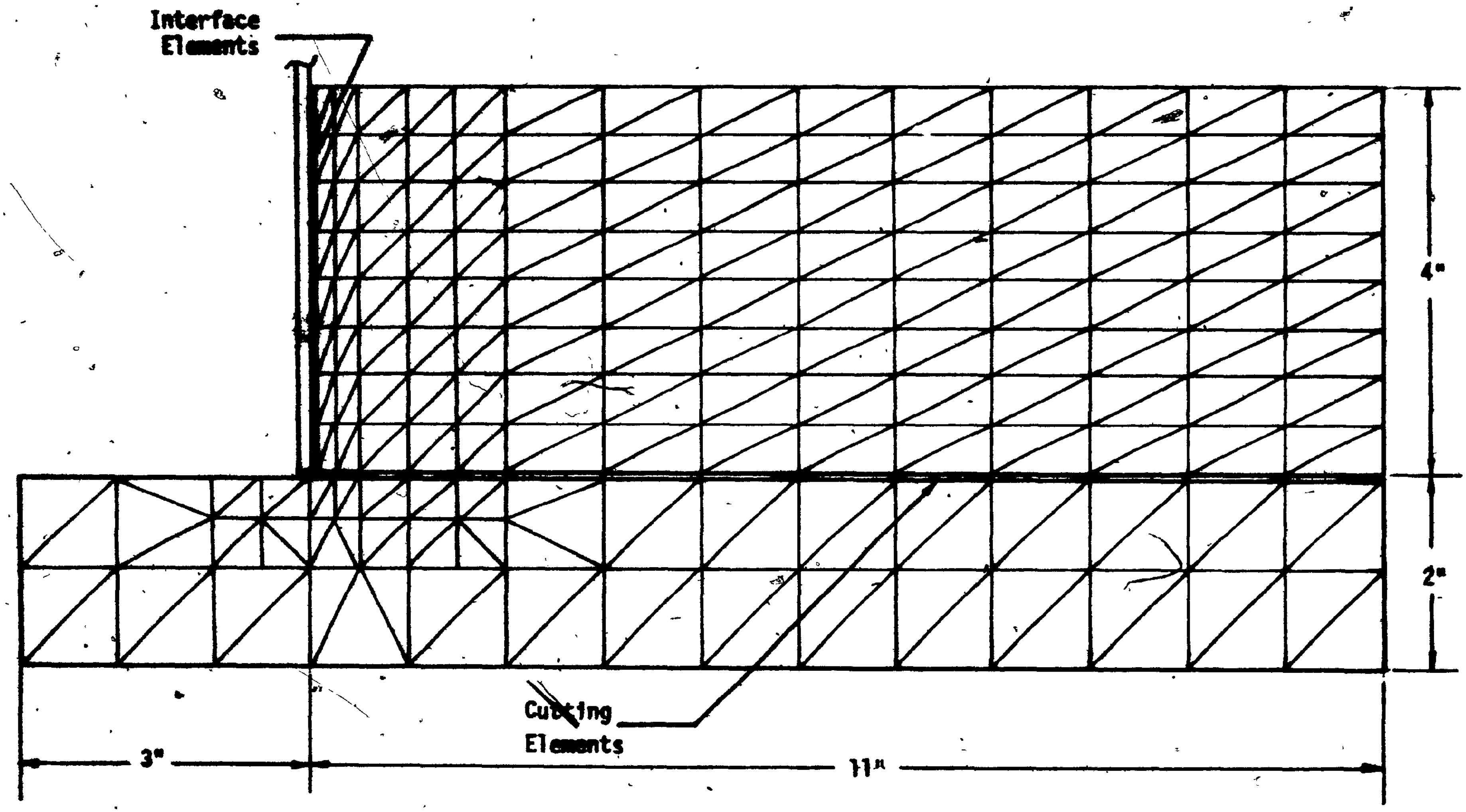

FIGURE 7-1 FINITE ELEMENT IDEALIZATION OF A PROBLEM OF EARTH PRESSURE BEHIND A YIELDING WALL

MODERATELY ROUGH WALL - CUTTING PLANE

To examine the influence of the cutting plane adopted in the finite element idealization on the developed forces and pressure distributions, one of the idealizations analyzed did not include a cutting plane. It should be recalled that these planes were included in the formulation to account for the severe relative displacements at the wall base, especially at large wall deformation.

An incremental-iterative method of nonlinear analysis was utilized to solve the problem. This method of analysis was described in detail in Chapter 2, and used in the soil cutting and traction analyses. The nonlinear plane-strain triaxial stress-strain curves shown in Fig. 4-7 for the kaolinite clay were used in the analysis to represent the constitutive behavior of the constant strain triangular elements. For the interface and cutting elements the hyperbolic relationships of the tangential stress-displacement curves, shown in Fig. 4-13, for the soil-to-soil mode, and in Fig. 4-14 for the soil-to-metal mode, were utilized. The shear strength of the clay was about 1.16 psi, and an initial elastic modulus of 90 psi was adopted. The Poisson's ratio, ν, was kept constant at 0.48 in all the problems. A total wall movement of 0.5 inch was applied in ten equal increments of 0.05 inch each. Three iterations were performed during each increment.

(b) <u>Variables studied:</u> One of the purposes of analyzing the retaining wall problem was to study the influence of the boundary conditions on earth pressure and soil deformation. Knowledge of the boundary conditions is as essential for the reliable estimate of lateral loads and deformations as both the initial conditions and the constitutive relations. These boundary conditions must represent the interaction between the soil and the wall rather than be simple analytical conditions such as "rigid, perfectly rough" or "perfectly smooth" [Clough and Duncan (1971)].

Another purpose of this study is to demonstrate the significance of specifying the boundary conditions at the base of the wall. In view of the marked difference in the soil deformation above and below the level of the wall base, a discontinuity in the finite element idealization must be incorporated at this level in order to account for the relative displacements occurring in the soil media, especially at large wall deformation. Such discontinuity is essential as there is no provision in the oonventional finite element theory for relative displacements to occur between adjacent elements. It will be recalled that the discontinuity behavior as adopted in this study is governed by the soil constitutive shear stress-relative displacement relationship.

The significance of providing such discontinuity can be demonstrated with reference to Morgenstern and Eisenstein (1970) results. Figure 7-2 shows a set of results obtained for conditions of passive pressure where the wall is pushed into an elastic medium by a distance equal to 0.0025 of wall height. It is seen that the passive resistance is increased substantially by the presence of a rough rigid base at the bottom of the excavation. Moreover, the influence of conditions along the rigid base decreases with increasing distance from the bottom of the excavation. Morgenstern and Eisenstein concluded that the boundary conditions between the rigid base and the foundation layer have a significant effect on earth pressures, the pressure distribution on the wall becoming nonlinear with a rough boundary. It is argued here that such

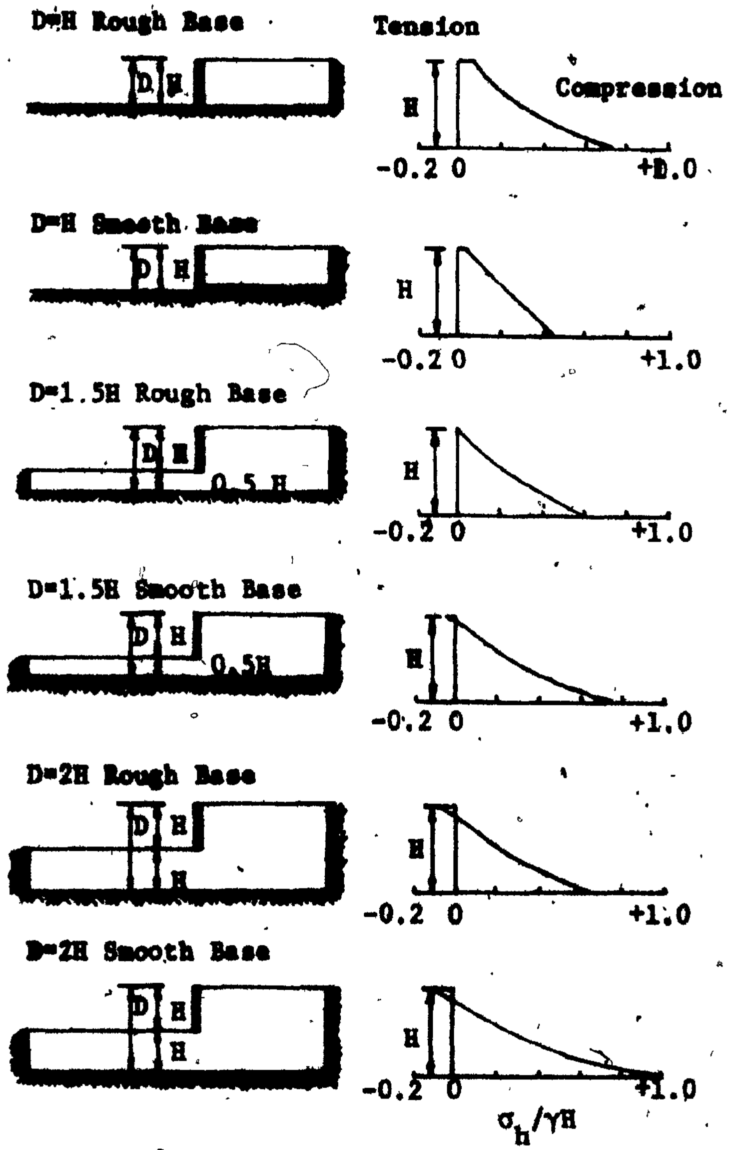

(a) Boundary Conditions Scheme

(b) Distribution of Lateral Pressure along the Wall

FIGURE 7-2 LATERAL PRESSURE DISTRIBUTIONS FOR DIFFERENT BOUNDARY CONDITIONS WHEN THE WALL YIELDS 0.0025 H IN THE PASSIVE SENSE.

(After Morgenstern and Eisenstein, 1970) an effect resulted from inadequacy of the proposed finite element model to deal with relative displacement at the bottom of the excavation. In their model the wall has to drag all the foundation layer as it moves, which results in very high pressures at the base of the wall as shown in their pressure distributions. More appreciation of this point will be gained in the next section with the presentation of results and related discussion.

With this understanding of the problem, four analyses of walls translating in a passive sense were performed. Table 7-1 lists the different schemes employed in the analysis of these problems.

7.2.3. Results and Discussion

(a) Total lateral pressures: The total lateral pressures for a 4.0 inch model retaining wall are plotted in Fig. 7-3 as a function of the wall displacement toward the backfill. Each of the pressure displacement curves is labelled according to the problem boundary conditions adopted [Table 7-1]. On the same Figure the classical passive earth pressure value for a smooth wall is also plotted. According to the Coulomb and the Rankine theories, a soil with no friction ($\phi = 0$) but with cohesion ($C > 0$) will offer resistance to lateral displacements expressed by:

$$P_p = \tfrac{1}{2}\gamma H^2 + 2CH \qquad (7.1)$$

At depth h below the soil surface, the lateral resistance will be

$$P_h = \gamma h + 2C \qquad (7.2)$$

where

TABLE 7-1

CLASSIFICATION OF SCHEMES EMPLOYED IN ANALYSES OF RETAINING WALL PROBLEM

Problem No.	Interface Condition	Cutting Plane	Total No. of Elements	No. of Interface Elements	No. of Cutting Elements	No. of Nodes	Total Wall Displ. Inch	No. of Increments	No. of Iterations	Material Properties
1	Rough	No	302	-	-	178	0.5	10	3	E_o = 90psi
2	Rough	Yes	316	-	14	193	0.5	10	3	ν = 0.48
3	Wall adhesion	Yes	324	8	14	202	0.5	10	3	γ = 100 pcf
4	Smooth	Yes	316	-	14	193	0.5	10	3	C = 1.16 psi
										ϕ = 0

FIGURE 7-3 PRESSURE RESULTANTS ACTING ON WALL CALCULATED FROM THE CLASSICAL EARTH PRESSURE THEORY AND THE FINITE ELEMENT METHOD PLOTTED AS A FUNCTION OF WALL DISPLACEMENT.

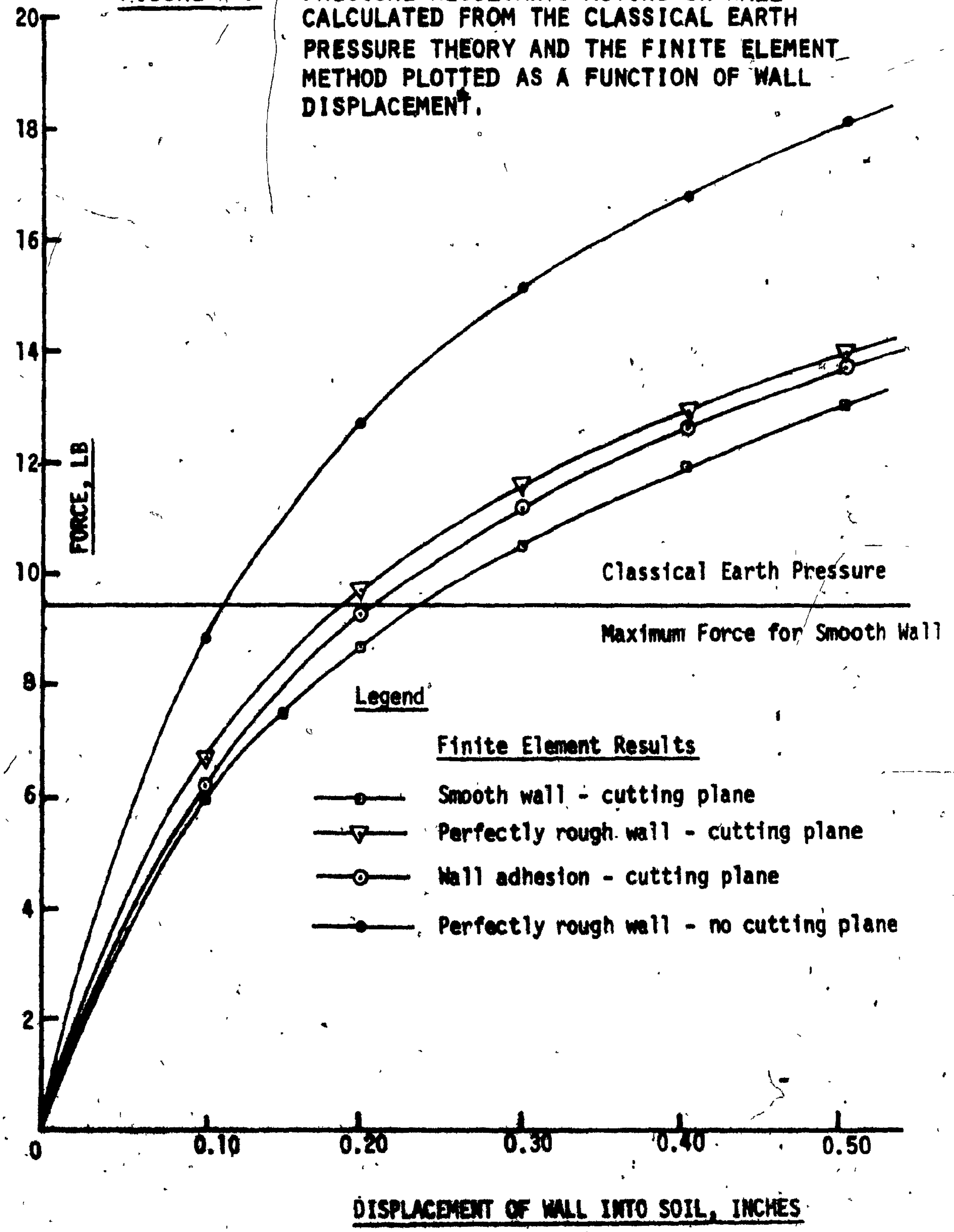

P_p = total lateral pressure on the wall, lb.

γ = soil density, pcf.

H = wall height, feet.

P_h = lateral pressure at depth h below the soil surface, psf.

The data in Fig. 7-3 show that the classical passive earth pressure is reached at different values of wall movement, depending on the boundary conditions assumed. At an inward movement of the wall, Δ, of only 0.11 inch [or at a Δ/H ratio of 0.0275], the perfectly rough wall-no cutting plane model reaches the value predicted by the classical earth pressure theory. For the smooth wall-cutting plane model, the passive condition is reached at the largest wall movement Δ of 0.05875 of wall height. The perfectly rough wall-cutting plane and the wall adhesion-cutting plane models lie in between the above two limits.

Table 7-2 presents a summary of the total lateral pressures calculated by the finite element analyses as a percentage of the classical earth pressure value for a smooth wall. From this Table, and also from Fig. 7-3, the following observations can be made:

1. The effect of the cutting plane is to reduce the total lateral pressure on the wall. The reduction varies from 32.5% for Δ/H of 0.025 to 28.5% for Δ/H of 0.125. Such reduction is caused by the decrease in the magnitude of pressure developing at the bottom of the wall [shown in the pressure distribution diagrams, Figs. 7-4 and 7-5].

TABLE 7-2

SUMMARY OF TOTAL LATERAL PRESSURE WITH WALL MOVEMENT
CALCULATED BY THE FINITE ELEMENT ANALYSES
AS A PERCENTAGE OF CLASSICAL EARTH PRESSURE VALUE FOR A SMOOTH WALL

Problem No.	Boundary Conditions	$\frac{\Delta}{H} = 0.025$*	$\frac{\Delta}{H} = 0.05$	$\frac{\Delta}{H} = 0.075$	$\frac{\Delta}{H} = 0.10$	$\frac{\Delta}{H} = 0.125$
		%	%	%	%	%
1	Perfectly rough wall No cutting plane	94	134.4	159.7	177.8	192
2	Perfectly rough wall Cutting plane	71.4	102.2	121.7	136.2	147.5
3	Wall adhesion (interface element) Cutting plane	64.9	98.6	119.1	133.8	145.4
4	Smooth wall Cutting plane	64.8	92.0	111.4	126.3	137.9

* Δ = Wall movement

H = Total Height of Wall

2. As would be expected, wall translation with full adhesion [perfectly rough case] increases pressure on the back of the wall, while the case of no wall adhesion [smooth] gives the minimum pressure. The wall adhesion [i.e. interface element] model is seen to lie between the two limiting assumptions.

(b) Wall pressure distributions: The lateral earth pressure distributions for the four cases being discussed are shown in Figs. 7-4 to 7-7, inclusive. These pressure distributions are plotted for various amounts of wall translation and each of the pressure-depth curve shown is labelled according to the amount of inward wall movement Δ, as a ratio of wall height, H. In these Figures the lateral passive earth pressure distribution computed from the classical theories of Coulomb and Rankine, Eq. (7.2), is also plotted.

It is of interest to note that a strongly nonlinear distribution arises in the case of a perfectly rough wall with no cutting plane, Fig. 7-4. Such nonlinearity is shown to be due to the development of substantial lateral pressure along the base of the wall. This distribution, when compared with the distribution of the perfectly rough wall-cutting plane model, Fig. 7-5, indicates close similarity for the upper three-quarters of wall height. In the lower quarter of the wall a reduction in pressure of more than 50% resulted when including a cutting plane in the finite element analysis. It is seen that, without taking into consideration the wall interface characteristics, the cutting plane model indicates closer agreement with the classical theory distribution.

FIGURE 7-4 VARIATION OF HORIZONTAL WALL PRESSURE DISTRIBUTIONS WITH RELATIVE WALL MOVEMENT

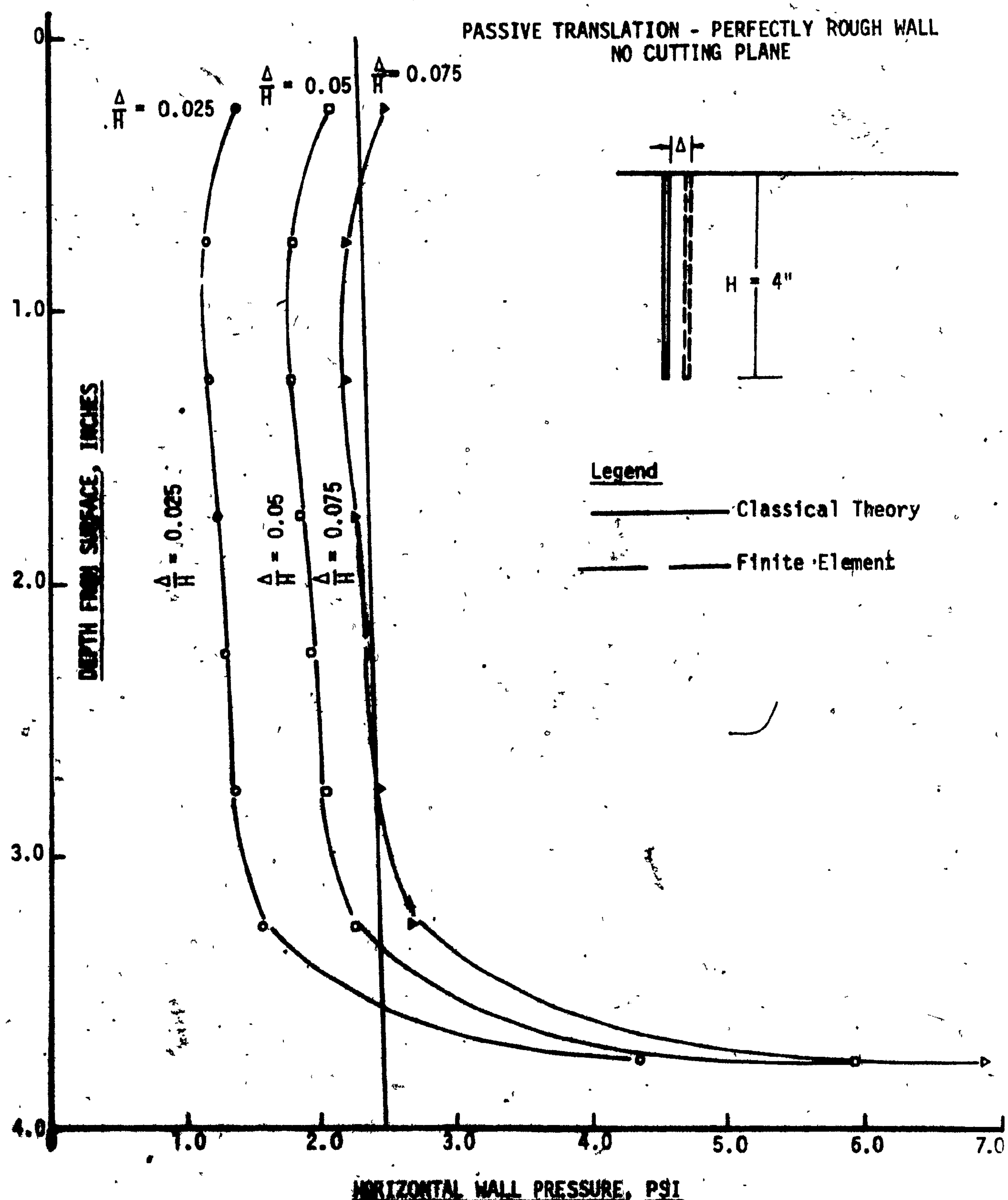

FIGURE 7-5 VARIATION OF HORIZONTAL WALL PRESSURE DISTRIBUTIONS WITH RELATIVE WALL MOVEMENT

PASSIVE TRANSLATION - PERFECTLY ROUGH WALL
CUTTING PLANE

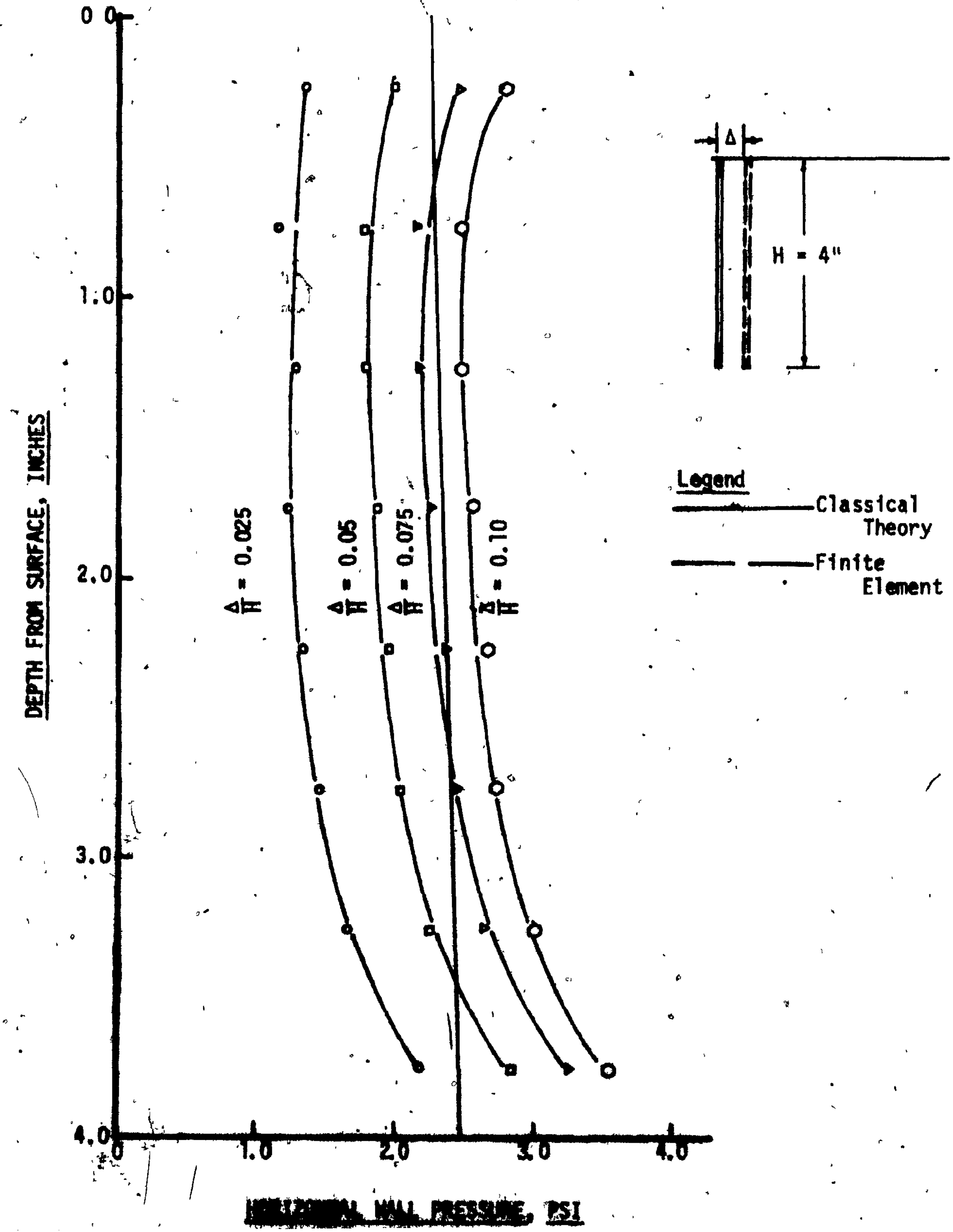

FIGURE 7-6 VARIATION OF HORIZONTAL WALL PRESSURE DISTRIBUTIONS WITH RELATIVE WALL MOVEMENT

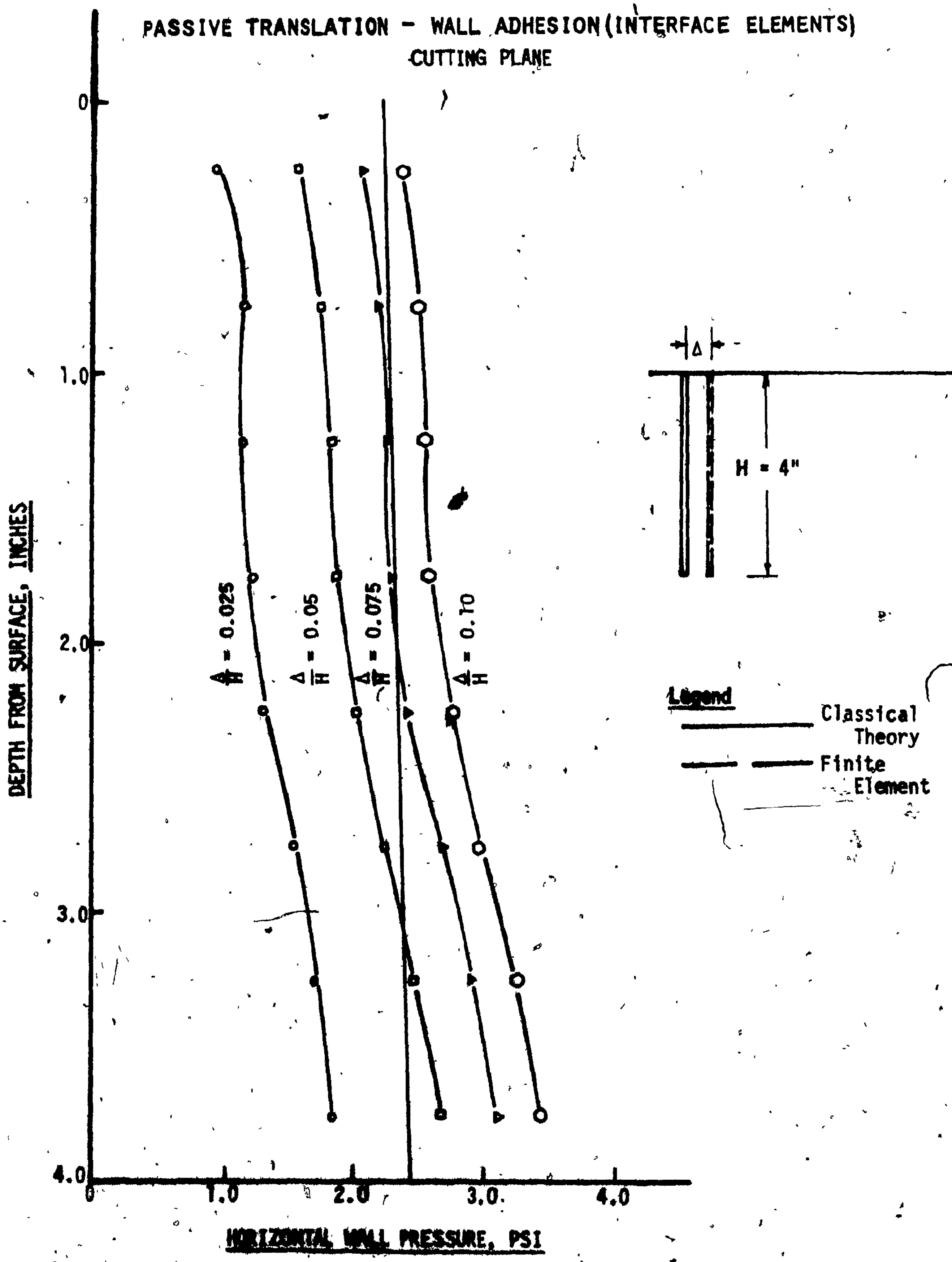

FIGURE 7-7 VARIATION OF HORIZONTAL WALL PRESSURE DISTRIBUTIONS WITH RELATIVE WALL MOVEMENT

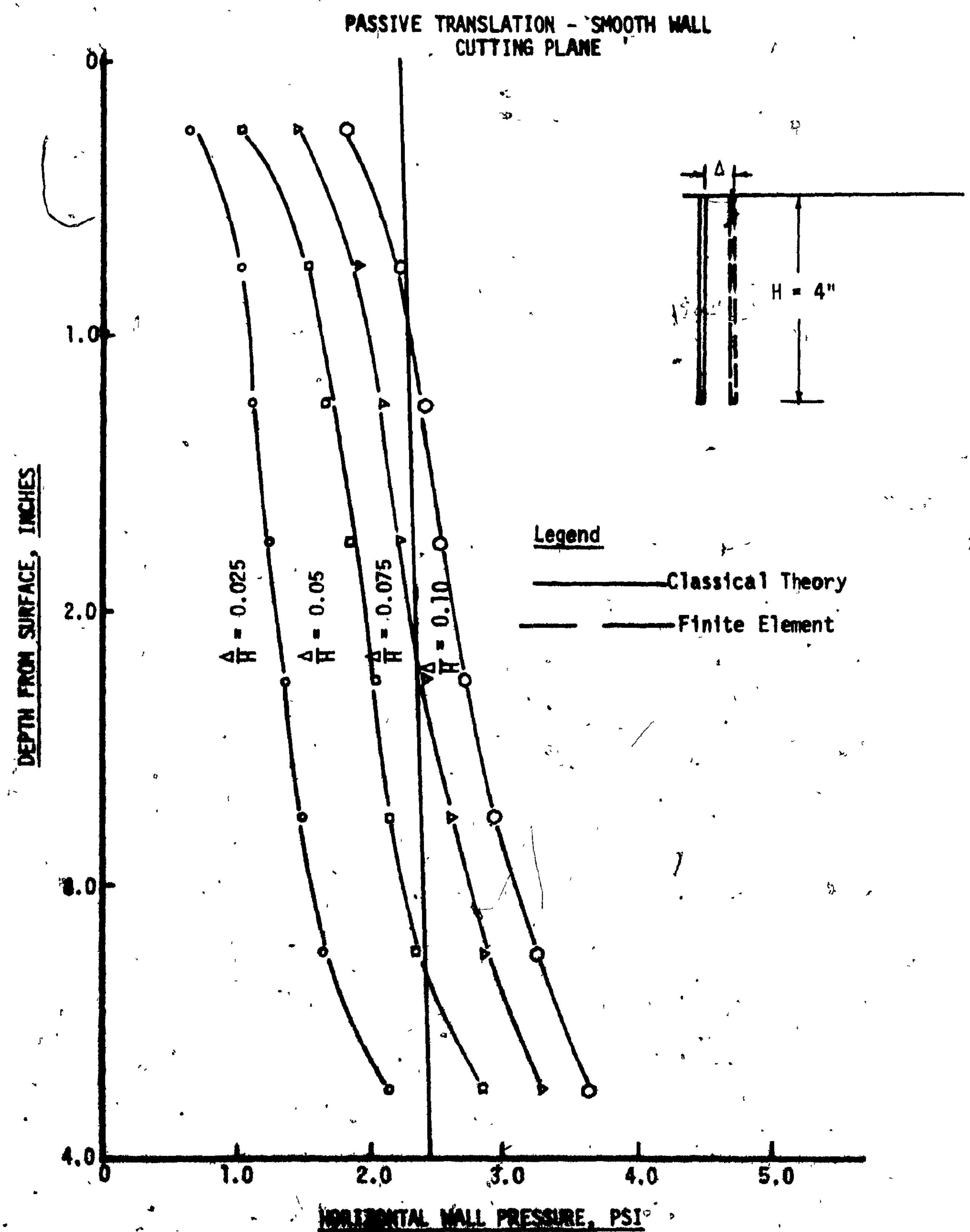

Examination of Figs. 7-5, 7-6 and 7-7, discloses the influence of soil-wall interface characteristics on the shape of the lateral pressure distribution. The main difference between the various shapes is exhibited in the nonlinearity of the diagrams near the soil surface. When the wall is considered perfectly rough the pressure reaches a minimum near the wall mid-height and then increases approaching the soil surface. In the cases of the smooth wall and the wall adhesion models, the pressures are seen to be minimum at the soil surface, with lower values for the smooth wall . Closer agreement between the pressure distribution of the wall adhesion case and the classical distribution is again observed.

The tangential pressure distributions are plotted in Figs. 7-8, 7-9 and 7-10 for the perfectly rough-no cutting plane, perfectly rough-cutting plane and wall adhesion-cutting plane models, respectively. It is seen from these figures that the direction of the tangential pressure is mostly downward except at the base of the wall where it reverses to upward, The existence of a cutting plane is shown to reduce the upward tangential stresses at the wall base. Finally, the wall adhesion model is seen to exhibit very little upward pressure at the wall base, and smaller tangential pressures along the wall.

(c) <u>Stresses in soil</u>: Since the stress distribution may be used as the basis for predicting the locations of the failure zones, it is of interest to compare the influence of the boundary conditions on the distribution of stresses in the soil mass, for the cases studied. Three examples of contours of horizontal, vertical and shear soil stresses

FIGURE 7-8 VARIATION OF TANGENTIAL PRESSURE DISTRIBUTIONS WITH RELATIVE WALL MOVEMENT

PERFECTLY ROUGH WALL - NO CUTTING PLANE MODEL
PASSIVE TRANSLATION

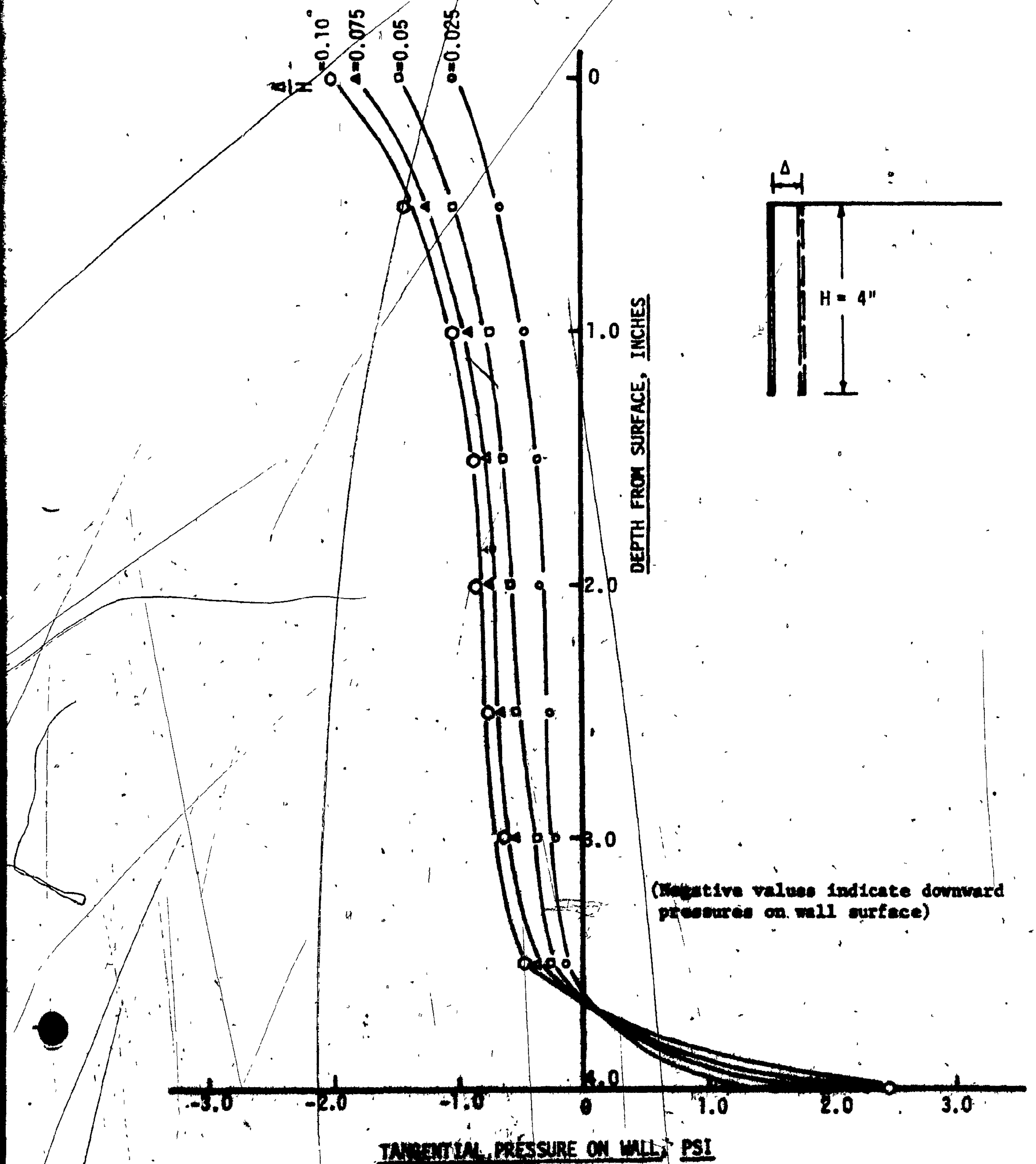

FIGURE 7-9 VARIATION OF TANGENTIAL PRESSURE DISTRIBUTIONS WITH RELATIVE WALL MOVEMENT

PERFECTLY ROUGH WALL-CUTTING PLANE MODEL - PASSIVE TRANSLATION

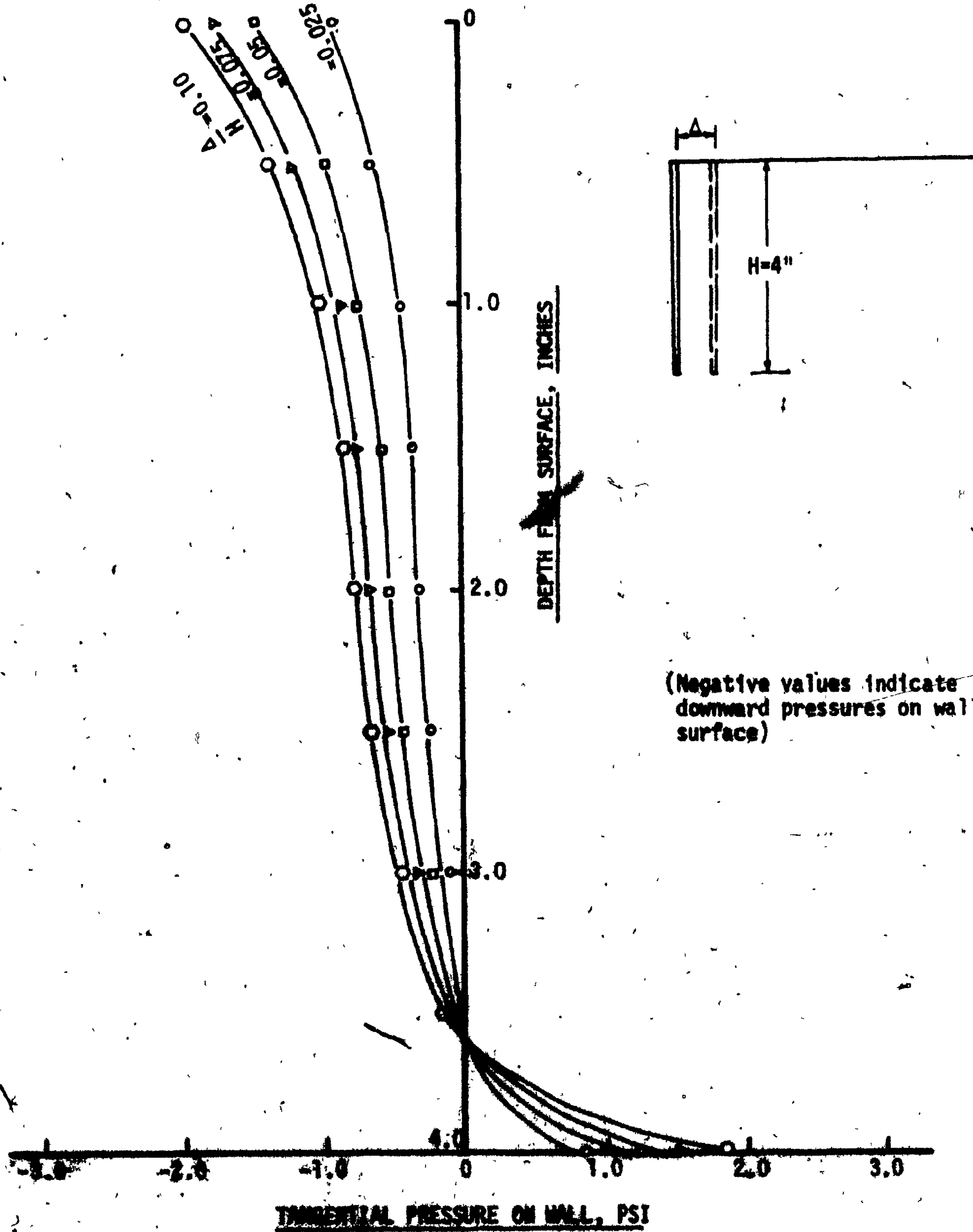

FIGURE 7-10 VARIATION OF TANGENTIAL PRESSURE DISTRIBUTIONS WITH RELATIVE WALL MOVEMENT

WALL ADHESION (INTERFACE ELEMENTS) - CUTTING PLANE MODEL

PASSIVE TRANSLATION

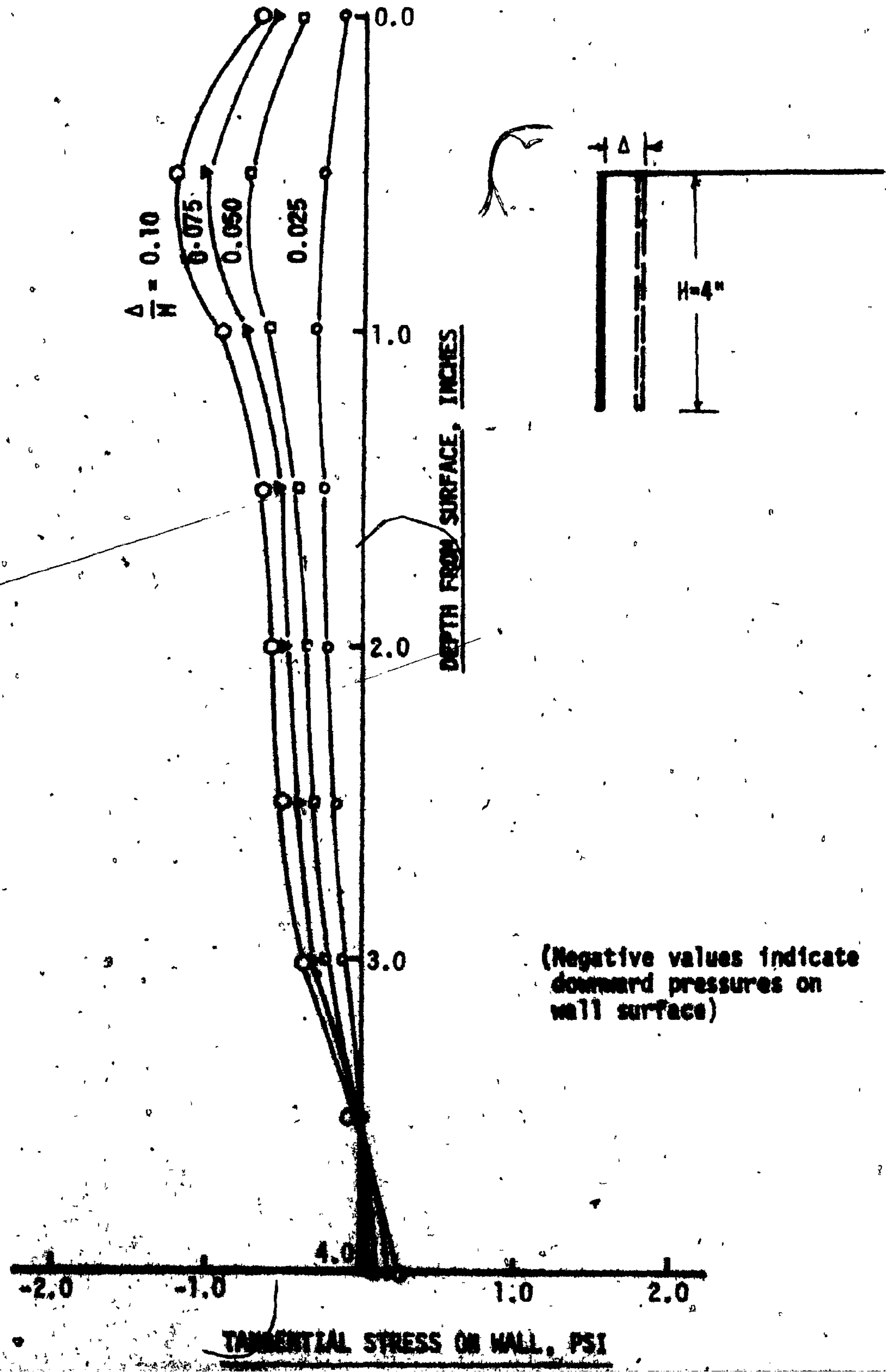

are shown in Figs. 7-11 to 7-13 for the perfectly rough-cutting plane, wall adhesion-cutting plane and smooth-cutting plane models. These examples are all for wall movement, Δ of 0.05 of wall height, and therefore the differences arise from the boundary conditions. It is seen from these Figures that substantial differences exist in the stress distributions for the three cases. The horizontal, vertical and shear stresses developed for the case of perfectly rough wall are shown to be much higher than those developed in front of a smooth wall, with the stresses for the wall adhesion case lying in between. Also, while the contours of the horizontal normal stress, σ_x, seem to maintain the same general shapes for the three cases, the vertical stress, σ_y, distribution for the case of a smooth wall differs from the other two cases. A large zone of the soil in front of the smooth wall experiences zero vertical stresses or very slight tension. This behavior was also observed in case of cutting blades, Section 5.4, at a larger blade displacement of 0.5 inch. It may be recalled that all the cutting blade analyses were performed with interface elements which suggest that the effect of the roughness of the moving element [or the upward tangential stresses] is to retard the formation of zones of vertical tensile stresses.

In case of shear stress distributions, it is seen that the stresses developed in the wall adhesion case are very similar to those existing in front of the perfectly rough wall. Much lower shear stresses are developed when the wall is smooth. It is clear from the above discussion that the effect of soil-wall interface condition is very pronounced on the development of stresses in the soil mass.

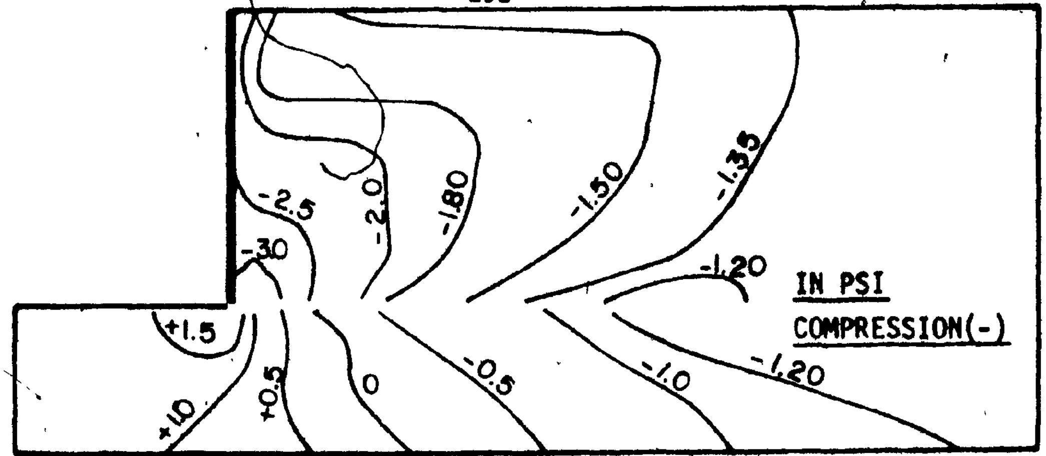

(a) PERFECTLY ROUGH WALL - CUTTING PLANE SCHEME

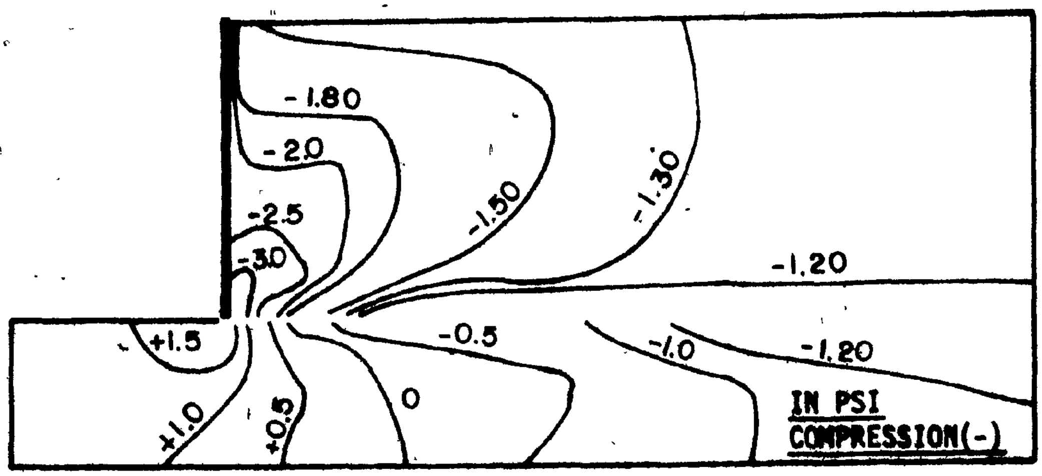

(b) WALL ADHESION (INTERFACE ELEMENTS) - CUTTING PLANE SCHEME

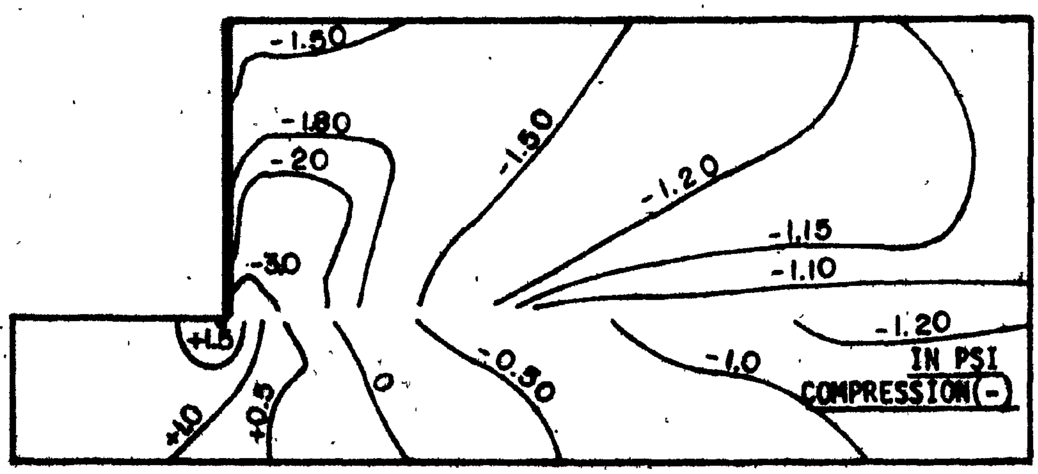

(c) SMOOTH WALL - CUTTING PLANE SCHEME

FIGURE 7-11 HORIZONTAL NORMAL STRESS, σ_x, FIELDS FOR THE VARIOUS SCHEMES EMPLOYED IN THE ANALYSIS OF THE RETAINING WALL PROBLEM

(WALL MOVEMENT Δ = 0.05 H)

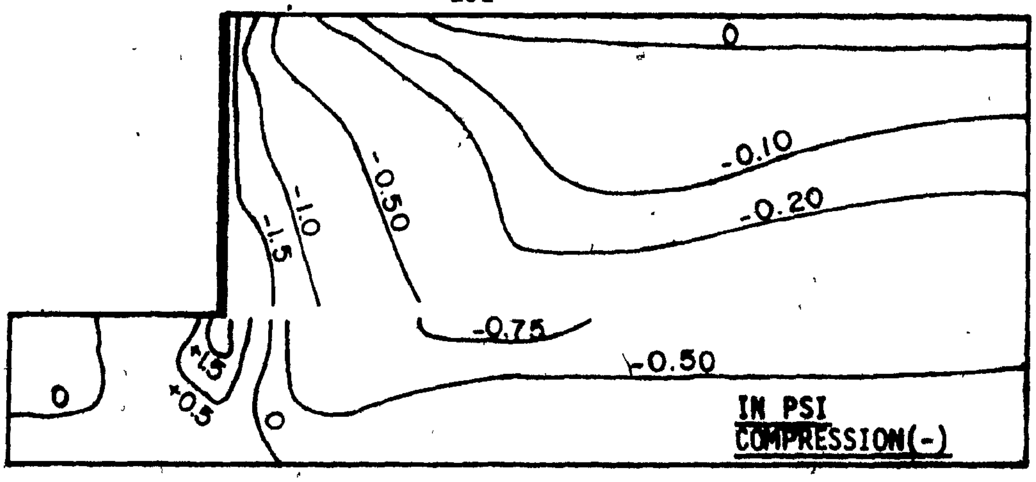

(a) PERFECTLY ROUGH WALL - CUTTING PLANE SCHEME

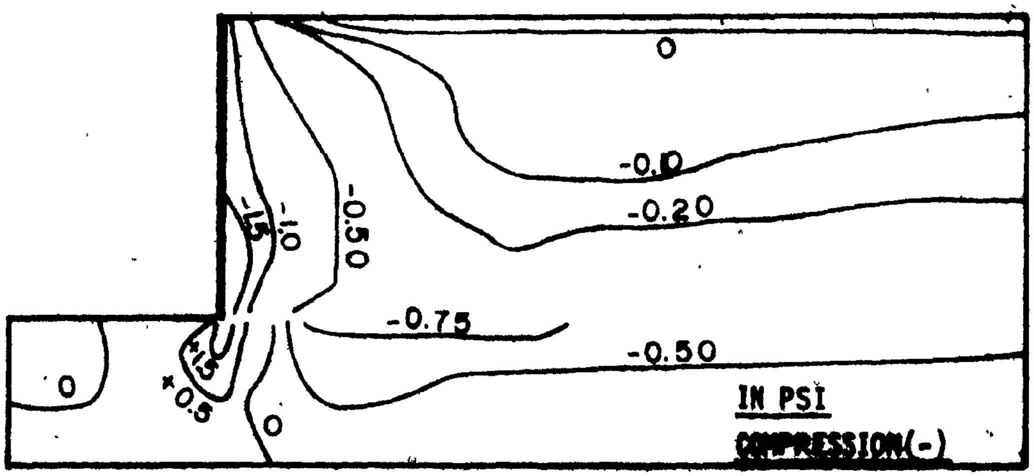

(b) WALL ADHESION (INTERFACE ELEMENTS) - CUTTING PLANE SCHEME

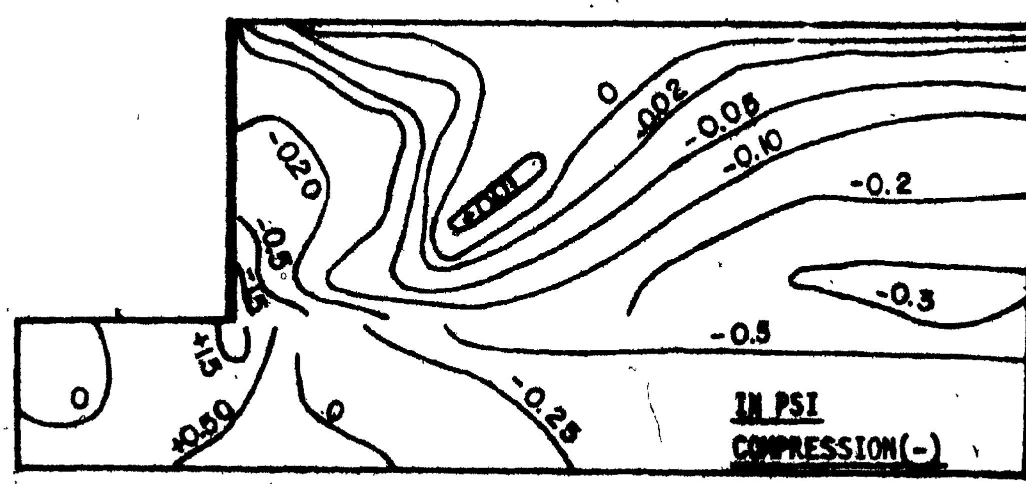

(c) SMOOTH WALL - CUTTING PLANE SCHEME

FIGURE 7-12 VERTICAL NORMAL STRESS, σ_y, FIELDS FOR THE VARIOUS SCHEMES EMPLOYED IN THE ANALYSIS OF THE RETAINING WALL PROBLEM (WALL MOVEMENT Δ = 0.05 H)

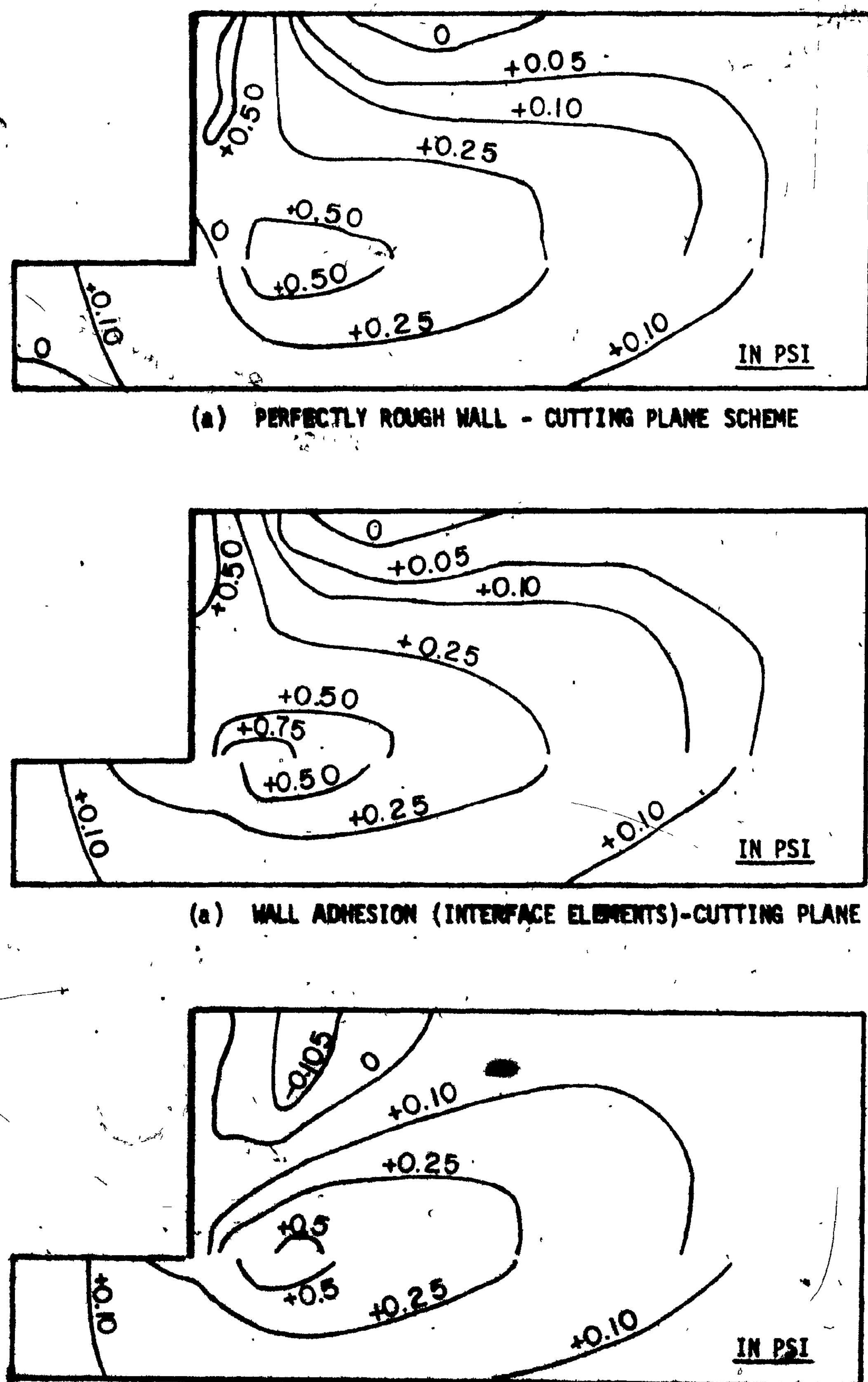

(a) PERFECTLY ROUGH WALL - CUTTING PLANE SCHEME

(a) WALL ADHESION (INTERFACE ELEMENTS)-CUTTING PLANE SCHEME

(c) SMOOTH WALL - CUTTING PLANE SCHEME

FIGURE 7-13 SHEAR STRESS, τ_{xy}, FIELDS FOR THE VARIOUS SCHEMES EMPLOYED IN THE ANALYSIS OF THE RETAINING WALL PROBLEM.
(WALL MOVEMENT Δ = 0.05 H)

7.2.4. Summary

The study described in this Section was performed to obtain comparisons between the finite element results derived from the idealizations and the solution technique developed with a conventional method based on a closed-form solution. To this end a typical example of a nonlinear problem of a long vertical retaining wall with cohesive soils on one side was analyzed. Four schemes were adopted to examine the influence of the soil-wall interface characteristics and the effectiveness of inserting a cutting plane at the base of the excavation. Examination of the results reported in this Section shows that:

(a) The effect of the cutting plane is found to reduce the magnitude of the high pressures developed at the wall base caused by the inadequacy of the conventional finite element idealization to account for the soil relative displacements at the bottom of the excavation.

(b) The soil stress distributions are shown to depend on the soil-wall interface condition. The soil stresses for the case of the perfectly rough wall are shown to be the highest, followed by the soil-wall adhesion case, and then the smooth wall scheme.

(c) With regard to the wall pressure distribution as influenced by the different schemes of soil-wall interface characteristics, it has been shown that the soil-wall adhesion finite element scheme [employing interface elements] provides the closest correspondence to the classical earth pressure distribution.

7.3 SOIL CUTTING PROBLEM - COMPARISONS WITH RESULTS COMPUTED FROM THE PREVIOUS THEORIES OF SOIL CUTTING

The problems of soil cutting have been studied by several investigators [Appendix C]. Most of the theories developed to predict the forces on two-dimensional cutting blades were based on the assumption of a slip surface along which the failure of the soil mass takes place. Osman (1964) has shown that the method due to Ode (1938) for the solution of the plastic equilibrium of the mass of soil within a curved failure boundary yielded accurate correlation with experimental observations in three types of soil [viz. a purely frictional, a purely cohesive, and a C-ϕ type of soil]. A similar investigation carried out by Siemen's et al. (1964), when re-assessed on the soil values worked out by Bailey (1964), also showed that the logarithmic spiral method gave good correlation with experimental observations. Some of the widely used relations are due to Reece (1965) and Hettiaratchi et al. (1966), which also use the analytical solution due to Ode for computing the forces on blades. In this Section, the results obtained from the finite element analysis and the experimental data will be compared with those obtained from Reece and Hettiaratchi et al. methods of computation.

Reece (1965) proposed an equation similar to that of Terzaghi's bearing capacity equation [Terzaghi (1944)], to compute the draft forces on a two-dimensional blade. This equation has the form:

$$F \text{ lb/ft} = 2CbN_c + 2b^2\gamma N_\gamma + 2bqN_q + C_a bN_\alpha \tag{7.3}$$

where

F = force per unit width.

b = a characteristic dimension.

C = cohesion.

γ = soil density.

q = surcharge pressure.

C_a = soil-metal adhesion.

$N_c, N_\gamma, N_q, N_\alpha$ = dimensionless factors depending on shape of soil failure surface.

In Eq. (7.3) the four terms on the righthandside represent the effect of the soil's cohesion, its weight, any surcharging load that is present, and the adhesion that develops between the soil and the blade surface. The N-factors are dimensionless numbers describing the shape of the soil failure surface. They, therefore, depend on the angle of internal friction, ϕ, the angle of wall friction, δ, and the shape of the structure and soil mass involved in the system.

It must be pointed out here that Reece's equation is not based on any rigorous mathematical proof. In addition, the failure zone chosen, as Reece admits, does not even fulfil the conditions of static equilibrium [it results in an impossible stress situation at the actual blade surface], let alone kinematic requirements. The simple four-part equation [Eq.(7.3)] with its dimensionless N-factors are shown to be dependent on the main variables [density γ, cohesion C, adhesion C_a, and surcharge q], leading to a certain degree of error. The magnitudes of error in predicting the forces on cutting blades, employing Reece's equation, were evaluated by Hettiaratchi et al. (1966).

While Eq. (7.3) includes terms for soil-metal adhesion and surcharge effect, Reece (1965) presented charts for the determination of the N_c and N_γ factors only [i.e., soil weight and cohesion effects).

The cohesion value for the kaolinite clay used in this study was found to be 1.16 psi [Fig. A-5, Appendix A]. This value, together with an average value of soil density of 0.060 lb/in^3 was used for the calculation of forces on the blades employing Eq. (7.3), with the soil adhesion and surcharge terms omitted. The computed horizontal and vertical forces are compared with the finite element and experimental results in Fig. 7-14 and Table 7-3. Examination of these results are presented later on in this Section.

An investigation was undertaken by Hettiaratchi et al. (1966) to check the solution of the passive earth pressure problem as proposed by Reece (1965) and to present computed values of his N-factors for the solution of simple two-dimensional soil cutting problems. Briefly, the logarithmic spiral method as used by the authors assumes a composite failure boundary composed of a curved part 'BC' [Fig. 7-15] and a plane section 'CD'. The latter is the last slip plane of the Rankine passive zone 'ACD' which joins up with the failure plane containing the lower edge of the loaded interface. Thus 'CD' and 'AC' make an angle of $(45 - \phi/2)$ with the horizontal free soil surface. The curved part 'BC' is assumed to be part of a logarithmic spiral represented by $r = r_0 e^{\omega \tan\phi}$, where r_0 is the initial radius 'OB' and ω is the spiral angle 'BOC'. The pole O of the spiral is assumed to line on 'CA' or 'CA' produced. Evidently there is an infinite number of possible failure surfaces for a given interface geometry consistent with the location of the pole at

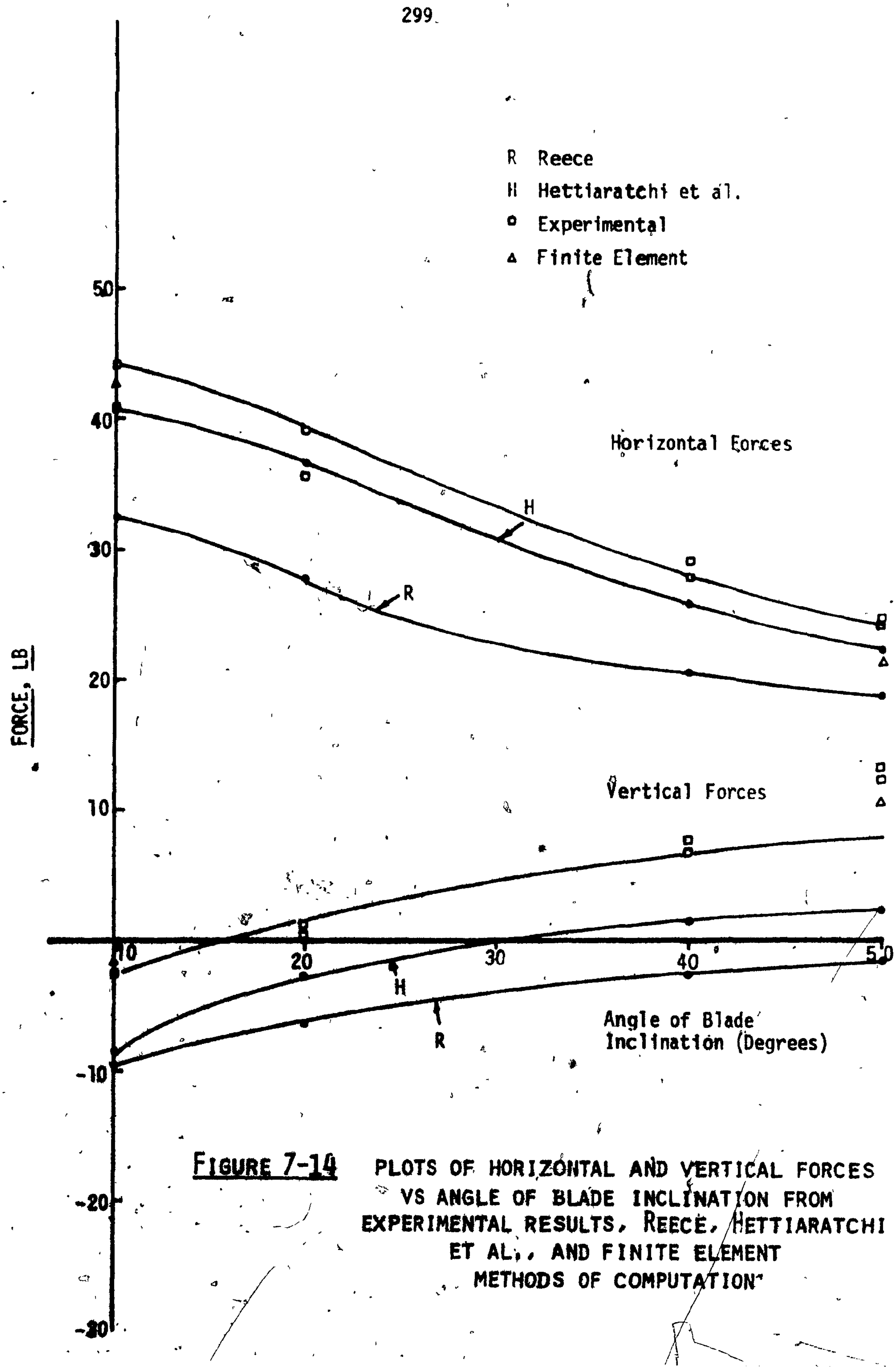

FIGURE 7-14 PLOTS OF HORIZONTAL AND VERTICAL FORCES VS ANGLE OF BLADE INCLINATION FROM EXPERIMENTAL RESULTS, REECE, HETTIARATCHI ET AL., AND FINITE ELEMENT METHODS OF COMPUTATION

TABLE 7-3

COMPARISON OF HORIZONTAL AND VERTICAL FORCES ON SOIL-CUTTING BLADES BY DIFFERENT METHODS

	HORIZONTAL FORCE				VERTICAL FORCE			
	ANGLE OF BLADE INCLINATION-DEGREES				ANGLE OF BLADE INCLINATION-DEGREES			
	10	20	40	50	10	20	40	50
Reece's Equation	32.2	27.8	20.6	18.8	- 9.9	- 6.2	- 2.8	- 1.45
Hettiaratchi et al. Equation	40.6	36.8	25.95	22.05	- 8.45	- 2.94	+ 1.73	+ 2.38
Finite Element at 0.5 inch Displacement	42.46	-	-	21.25	- 1.75	-	-	+10.90
Experiment at 0.5 inch Displacement	40.8 44.0	39.0 35.5	27.8 29.0	24.3 24.0	- 2.13 - 2.75	+ 0.50 + 1.20	+ 7.90 + 7.0	+12.2 +13.1
Finite Element at 1.0 inch Displacement	54.07	-	-	26.07	- 2.15	-	-	+13.2
Experiment at 1.0 inch Displacement	56.1 60.0	49.0 46.4	32.1 36.3	29.0 28.2	- 2.3 - 2.7	+ 1.7 + 4.1	+ 9.3 +12.4	+14.2 +14.13

- Negative values indicate upward forces.

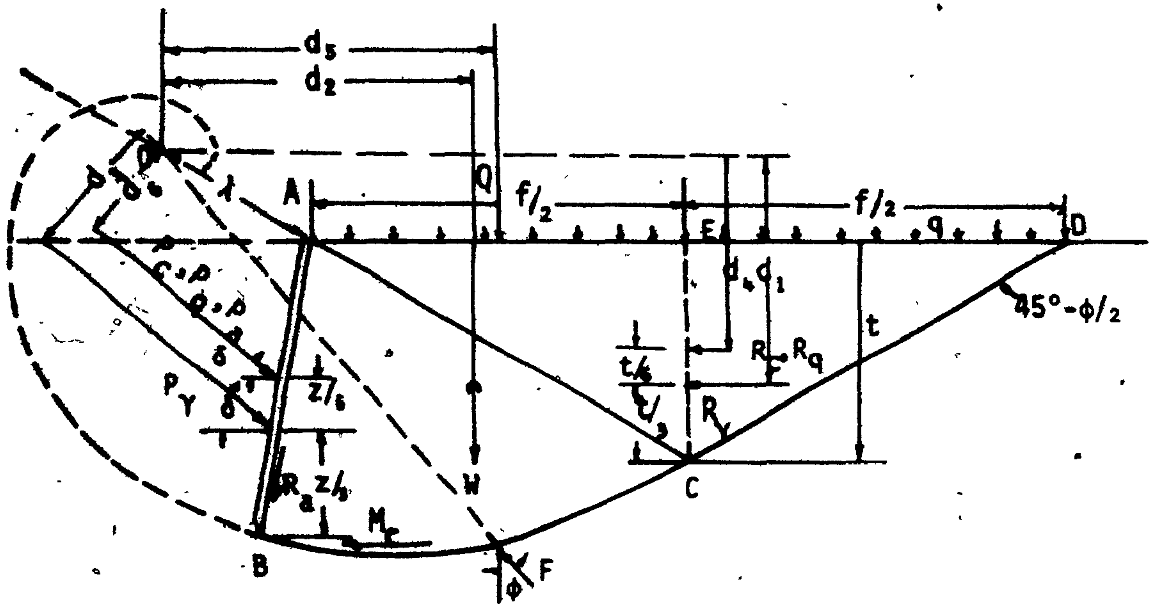

FIGURE 7-15 DETERMINATION OF PASSIVE EARTH PRESSURE BY THE LOGARITHMIC SPIRAL METHOD

[After Hettiaratchi et al. (1966)]

some point on 'CA'. The required failure surface boundary is the one that gives the minimum force on the loaded interface 'AB'. Thus, for any given location of the pole 0 at a distance say λ from A along 'CA', the total soil reaction P on the plane 'AB' can be evaluated by considering the equilibrium of the soil within the segment 'ABCE'. The correct value of P can be found for that value of λ which satisfies the condition $\frac{dP}{d\lambda} = 0$. As the calculation of P for even a single value of λ is extremely tedious, the authors proposed an alternative method. From Fig. 7-15, P is found to be equal to the sum of P_γ, P_c, P_a and P_q, or

$$P = P_\gamma + P_c + P_a + P_q$$

$$= \gamma Z^2 N_\gamma + CZN_c + C_a Z N_\alpha + qZN_q$$

where P_γ, P_c, P_a, P_q are the soil reactions on the interface due to weight, cohesion, adhesion and surcharge, respectively.

The value of N_γ, in the above equation, can be obtained simply by considering a soil with no cohesion, adhesion or surcharge. Thus, the force P acting on a particular interface under these conditions can be computed for arbitrary values of γ and Z over the entire range of variables [ϕ, δ and Z]. Values of N_c can be obtained by calculating fresh values of P taking into account cohesion as well as weight. In a similar manner values of N_α and N_q are obtained. Hettiaratchi et al. (1966) computed the four N-factors for a complete range of values of ϕ for the two extreme values of δ, that is, $\delta = 0$ and $\delta = \phi$, for values of rake angles varying from 45 - ϕ/2 to 135 - ϕ/2. They also produced suitable interpolation formulae and graphs showing the rupture distance as a function of the soil and blade variables.

In applying the method suggested by Hettiaratchi et al. to the problem under study, the following values are used:

Soil properties: $C = 1.16$ psi $\phi = 0$, $\gamma = 0.060$ lb/in^3

Soil-metal values: $\delta = 0$ $C_a = 1.16$ psi

The horizontal and vertical forces computed, using the N-factors presented by Hettiaratchi et al., are plotted in Fig. 7-14 and shown in Table 7-3, as a function of blade inclination angle.

According to the mathematical model of limit equilibrium, the soil is rigid up to the point of failure, whereupon it flows steadily at constant stress. This would result in a definite failure load at zero displacement, which then increases linearly with the displacement as the surcharge builds up. The theory would predict the initial force value. In practice, however, this is not the case. The force-displacement results shown in Figs. 4-2 and 4-3 indicate that the force records reach their maximum values at very considerable values of strain. Moreover, the force records have no peaks, indicating failure at maximum density, nor valleys, signifying reduced resistance offered by the soil after it has failed.

It was thought that a decision as to which point on the force record should be taken could perhaps be made by noting when the first shear plane emerged at the surface. However, as mentioned earlier, the soil tested did not exhibit distinct failure planes.

It must be mentioned here that it is not always possible to obtain information on first peaks in many reported studies for comparison purposes. It is expected that the asymptotic value of the force record may be the one generally used. In that regard, the limit equilibrium approach to the analysis of the problem would in general underestimate the total draft or horizontal force in view of the marked change in the geometry of the deforming soils.

For lack of a more definite criteria to define failure in the experimental force records reported in this study, computed forces using Reece's and Hettiaratchi et al. limiting equilibrium approach are compared with the finite element and experimental forces obtained at 0.5 and 1.0 inch of blade displacements. While such a choice may raise questions, any other failure definition is just as arbitrary. Such inability to correlate between forces developed in a continuous deformation process and forces predicted by the limit equilibrium theorems is due, as pointed out earlier, to the development of the limit equilibrium approach without reference to the stress-strain relations and kinematic considerations.

The analytical methods suggested by Reece (1965) and Hettiaratchi et al. (1966) for computing the theoretical forces may be examined, using the test results obtained from this study as a base for comparison. In Fig. 7-14 and Table 7-3, these comparisons are shown together with the present finite element approach computations for forces acting on the 10° and 50° inclined blades. It is seen that the predicted horizontal forces using Hettiaratchi et al. data show good agreement with the forces obtained from the actual test results as well as the finite element analysis obtained at 0.5 inch of blade displacement. On the other hand, Reece's method is found to underestimate the draft forces.

The divergence between Reece's and Hettiaratchi et al. results can be accounted for by considering the following factors:

1. While Reece presented Eq. (7.3) with the four terms representing the gravitational, cohesive, adhesive and surcharge components of the soil reaction, he only provided data for obtaining N_γ and N_c. Thus, Eq. (7.3) reduces in fact to the following form:

$$P = \gamma Z^2 N_\gamma + CZN_c$$

Whereas the surcharge effect can be considered to be negligible in the present case, eliminating the soil-metal adhesion term leads to a large error, especially when dealing with a purely cohesive soil as in the present investigation. The value of the adhesion term $C_a Z N_\alpha$, with the magnitude of N_α obtained from Hettiaratchi et al. charts, was added to Reece's results. This resulted in a very close agreement with the horizontal forces obtained from Hettiaratchi et al. data for the 10°, and to a certain extent, the 20° inclined blades. However, in case of the 40° and 50° inclined blades appreciable differences remained even after adding the adhesion term to Reece's equation.

2. In the case of a cohesive soil, the largest contribution to the draft force results from the cohesion term CZN_c. The N_c values obtained for the different inclined blades are as follows:

Blade angle with vertical	10°	20°	40°	50°
N_c [Reece]	1.75	1.45	1.00	0.90
N_c [Hettiaratchi et al.]	1.75	1.65	1.45	1.35

It is seen that while the N_c values obtained from the two methods are the same for the 10° blade, Reece's N_c values are smaller than those of Hettiaratchi et al. for the rest of the blade angles. The deviation between the N_c values is seen to increase with the blade inclination. This results in lower values for Reece's cohesion term (CZN_c), and hence smaller predicted forces.

The above two reasons account fully for the difference between the forces predicted by Reece's data and those obtained using Hettiaratchi et al. method of computation.

In comparing the developed forces obtained from the limit equilibrium approach [Reece and Hettiaratchi et al. methods], Table 7-3 lists both the experimental and the finite element results at 0.5 and 1.0 inch of blade displacements. A closer examination of the values in this Table reveals that the forces reported at 0.5 inch of blade displacement are seen to provide a better degree of correspondence with those computed using the limit equilibrium methods. As pointed out earlier in this Section, the limit equilibrium approach assumes that the soil is rigid up to the point of failure. This would result in a definite failure load at zero blade displacement which then increases with displacement as the surcharge builds up. Such an assumption is not realistic especially in the case of a plastic soil where the failure occurs at a very considerable value of strain. Taking this consideration into account, it was decided that the 0.5 inch blade displacement is large enough to produce failure conditions similar to those of the limit equilibrium model, and is small enough not to include the surcharge effect.

From Fig. 7-14 and Table 7-3 it is noted that while both the experimental and theoretical horizontal forces [developed at 0.5 inch of blade displacement] reported in this study do agree with those computed by Hettiaratchi et al. method, it is not the case with regard to the vertical forces. It is perhaps instructive at this point to note that Reece's equation [Eq.(7.3)] computes the total resultant force P per unit width of the interface, Fig. 7-15. This force acts at angle δ with the normal to the interface. If, however, the vertical force is required, it is computed as the resultant of the vertical component of the force P and the appropriate component of the adhesion force R_a Fig. 7-15, which acts upwards along the interface. The adhesion force R_a is equal to:

$$R_a = C_a x l$$

where C_a = adhesion, lb/in.^{2}

l = length of blade, inches.

In the application of the limit equilibrium approach it is assumed that the soil directly in front of the blade is in a state of failure and that the full adhesion value, C_a, is developed along the interface. Harrison (1973) has shown that this is often not so. The adhesion value of the kaolin clay, as measured by the soil-to-metal direct shear test presented in Section 4.A.3, is shown to be lower than the clay strength or the cohesion value, Fig. 4-11. It has also been found that the tangential stress values, or adhesion, on the soil-metal interface increases with increasing displacement reaching maximum values at relative displacements of approximately 0.2 inch, Fig. 4-10. Moreover, the adhesion values are shown to depend on the normal stresses, ranging from 93% of the cohesion value under zero normal load to about 82% for a normal load of 5.0 lb or more, Fig. 4-12. While the adhesive forces should be independent of the normal load, it should be recalled that such dependence was already shown to be due to the change of failure mode along the interface from a soil-to-soil shear under low normal stresses to a soil-to-metal failure when the normal stresses are increased.

Applying all these findings to the problem at hand, it has been made clear from the finite element analysis that the mobilization of the soil adhesion is a function of the relative displacements between the soil and the blade, or, in other words, a function of the blade displacement. Figures 5-20 and 5-21 show that the full value of adhesion is mobilized at a blade displacement of about 1.0 inch. These Figures also show that the mobilization of the soil adhesion is a function of the blade rake angle as the distributions of the tangential stresses are markedly different along the 10° and 50° inclined blade surfaces. Such complex behavior sheds doubt on the validity of Hettiaratchi et al. assumption of constant uniform adhesion along the blade surface, and hence the computed vertical forces.

7.4 SOIL-GROUSER INTERACTION PROBLEM - COMPARISONS WITH RESULTS COMPUTED FROM THE PREVIOUS THEORIES OF SOIL-GROUSER INTERACTION

Most of the research done to date on the grouser-soil interaction problem has been oriented towards investigating the performance of the plate-grousers, either individually or in groups, Appendix C. The intensive research on the interaction of this grouser with soil is mainly due to the wide use of such an element in tracked-vehicles. As warranted as this may be, it is still necessary to examine other grouser geometries and their tractive efforts. It is precisely in this area that there appears to be a great lack of experimental or theoretical research work. Bearing this in mind, the examination and comparison of the traction results will be divided into two parts, those of the wedge grousers [i.e., C.E.W. and S.E.W. grousers], followed by those of the plate-grousers [R.A.P.G.].

a) Wedge Grousers

The wedge grouser-soil interaction process can be considered as a lateral earth pressure problem involving backward raked soil interfaces [i.e., rake angle > 90°]. In other words, the analysis can be performed considering the grousers as cutting elements with their lower edges trailing. Hettiaratchi et al. (1966) pointed out that lateral earth pressure problems involving backward raked soil interfaces [$\alpha > 90°$, Fig. 7-16], have not yet been investigated experimentally, and that therefore the soil failure mode is not known. They postulated that under these conditions the interface "converts" itself by means of soil wedge ['ABG', Fig. 7-16], into a perfectly rough interface 'AG' having a smaller rake angle α'. They proposed that the solution

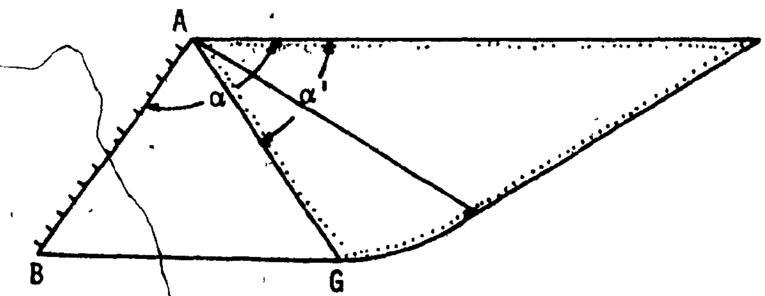

FIGURE 7-16 HETTIARATCHI ET AL. (1966) PROPOSED FAILURE SURFACE FOR LATERAL EARTH PRESSURE AT LARGE RAKE ANGLES

to this problem could be obtained using their method [Section 7.3] in conjunction with an appropriate modification factor. They also stated that suitable modifications and simplifications are required in using their method of solution to deal with problems of curved elements.

Investigating the draft of curved blades, Osman (1964) considered any curved blade to be one of a family of blades of increasing curvature, starting from the straight blade forming the chord between the cutting edge and the soil surface. While realizing that increasing curvature will cause increasing draft because shear strains must occur throughout the soil mass in front of the blade, he postulated that the draft cannot increase beyond that required to cause the soil to flow up the straight line forming the chord across the blade between the cutting edge and the top edge. This is because it is possible for the soil to fill up the curve, transforming the blade into a straight one with the same depth and rake angle, which results in a condition where $\delta = \phi$ and $C_a = C$. Such reasoning enabled Osman to put forward and experimentally verify the hypothesis that the draft of a curved blade must lie between two limits. The lower limit corresponds to a hypothetical plate blade forming the chord across the curved blade and having the friction and adhesion values of the curved blade surface. The upper limit is represented by the same straight blade but with the angle of soil-metal friction increased to ϕ and the adhesion, C_a, to the value of soil cohesion, C.

By considering the wedge grousers to act as cutting elements with backward raked soil interfaces, the predictive methods of Reece (1965) and Hettiaratchi et al. (1966) [Section 7.3] may be used to compute the developed forces on these elements to compare with those reported in this study. For the curved-edge wedge grousers [C.E.W. type (1) and C.E.W. type (2), Fig. 3-1], the hypothesis made by Osman (1964) is adopted to account for the effect of element curvature on the developed forces. It must be pointed out at this stage that these methods will not account for the effect of the horizontal plate, placed on top of the S.E.W. and the C.E.W. type (1) grousers, on the developed forces. The influence of these plates is to change the problem boundary conditions from those similar to a lateral earth pressure problem where soil failure takes place due to a horizontal movement of the soil interface, to a problem combining the effect of lateral pressure with surface bearing capacity. Such change in boundary conditions should be expected to lead to errors in prediction.

In applying the methods of Reece and Hettiaratchi et al. for predicting the forces on the wedge grousers, the following assumptions and approximations are made:

1. The failure boundary is composed of a curved part 'BC' Fig. 7-15, and a plane section 'CD'. The latter is the last slip plane of the Rankine passive zone 'ACD' which joins up with the failure plane containing the lower edge of the loaded interface. This assumption is subject to further experimental evidence.

2. The curved grouser-soil interfaces are idealized by flat surfaces having the same depth and rake angle [Osman (1964)].

3. The soil-metal adhesion is equal to the value of the soil cohesion, and the angle of metal friction $\delta = 0$. According to Osman's hypothesis, such an assumption represents an upper bound on the draft values.

The results computed employing Reece's and Hettiaratchi et al. methods, with the adoption of the above approximations, are shown in Table 7-4 for the three wedge grousers analyzed in this study, together with the finite element results and the experimental measurements obtained at 0.5 inch of grouser displacement. The reasons for the choice of the 0.5 inch grouser displacement criterion for comparison with the limit equilibrium results were discussed earlier in Section 7.3.

Examination of the results in Table 7-4 shows that, as in the case of soil cutting discussed in Section 7.3, Reece's method predicts smaller forces than those computed from Hettiaratchi et al. data. The lower values obtained from Reece's analysis are again attributed to the omission of the soil-metal adhesion term, $C_a bN_\alpha$, and to lower values of the cohesion term, CZN_c, Eq. (7.3). It is also observed that Reece and Hettiaratchi et al. methods of computations, with the adoption of Osman's hypothesis, give the same forces for both the S.E.W. and the C.E.W. type (1) grouser-soil systems. The same forces on both systems resulted since, by adopting Osman's hypothesis, the C.E.W. type (1) grouser, when idealized by a flat surface, will have the geometry of the S.E.W. grouser. Moreover, even with the assumption of the metal-soil adhesion value equal to the soil cohesion, which is supposed to give an upper bound on the measured forces, the computed horizontal force for the C.E.W. type (1) grouser is shown to be less than the measured one. Obviously, these results are in contradiction with Osman's hypothesis in that the increase of element surface curvature increases the soil-metal contact area, and consequently the strains and stresses developed in the soil, which should lead to larger computed draft forces. It is only in case the soil-metal adhesion value is considerably less than the soil cohesion would such a hypothesis lead

TABLE 7-4

COMPARISON OF HORIZONTAL AND VERTICAL FORCES ON WEDGE GROUSERS BY DIFFERENT METHODS

	HORIZONTAL FORCE			VERTICAL FORCE		
	GROUSER TYPE			GROUSER TYPE		
	S.E.W.	C.E.W. Type (1)	C.E.W. Type (2)	S.E.W.	C.E.W. Type (1)	C.E.W. Type (2)
Reece's Equation	24.92	24.92	23.19	-22.91	-22.91	-22.61
Hettiaratchi et al. Method	33.42	33.42	32.04	-26.43	-26.43	-25.86
Finite Element at 0.5 inch Displacement	37.98	-	34.88	-18.2	-	-12.71
Experiment at 0.5 inch Displacement	35.0 38.8	40.0 39.0	31.0 32.0	-15.9 -14.7	-16.5 -17.2	-11.0 -11.70

- Negative values indicate upward forces.

to an upper bound on the draft forces.

Comparing the developed forces computed by the various methods, with all the above points taken into consideration, it is seen that the horizontal forces predicted by Hettiaratchi et al. method show a fairly good degree of correspondence with the experimentally measured horizontal forces. However, the method is shown to overestimate the vertical forces. The reasons for such divergence were previously discussed in Section 7.3 and can be summarized, with regard to the traction results, in the following points:

1. While the methods of limit equilibrium assume full mobilization of the soil-metal adhesion forces, it has been shown that the mobilization of adhesion is a function of the relative displacement between the soil and the metal interface, Section 7.3.

2. It has been shown from the finite element analysis, Fig. 6-22 and 6-23, that the shear stresses on the soil-metal interfaces change direction at a certain point on the interface. This finding is in contradiction with the limit equilibrium models proposed by Reece and Hettiaratchi et al. in which the adhesion force is assumed constant and acting upwards along the interface.

Finally, in general it is observed that the agreement between the finite element and the experimental results is very satisfactory for the two soil-grouser systems analyzed by the finite element method.

b) Plate Grousers

Regarding the developed forces on the plate grousers, results computed from Bekker's equations [Bekker (1960)] are compared with both the theoretically computed and the measured values in Table 7-5. In the Bekker equations [Eqs. (1.1) and (1.2) in Chapter 1 and also in Appendix C], the horizontal and vertical forces, H and W, are not expressed explicitly in terms of system parameters but are rather proportional to an angle θ defined by:

$$\theta = \arctan H/W$$

where

$$H = b(\eta_c lc + \gamma\eta_q lz + \gamma\eta_\gamma l^2) \sin\theta$$

$$W = b(\eta_c lc + \gamma\eta_q lz + \gamma\eta_\gamma l^2) \cos\theta$$

It is seen that H and W are dependent on such dimensionless trafficability factors as η_q, η_c, and η_γ, all of which in themselves are dependent on ϕ, θ and the ratio of l/h, (Fig. 7-2).

In view of the above considerations, the two equations for H and W do not permit a direct determination of these forces but instead, must be solved by an iterative process, see Appendix C. In the case of a grouser moving at a constant elevation, an estimate for either H or W must be made to arrive at an estimate for θ. The experimentally measured values of the vertical forces obtained at 0.5 inch of grouser displacement were substituted in Bekker's equations, and the corresponding horizontal forces were computed. The results of these computations are shown in Table 7-5, and it is seen that the deviation between Bekker's and the experimentally measured values is of the order of 6% for grouser aspect ratio h/l of 0.5 and about 18% for grouser with an aspect ratio (h/l) of 0.833.

Harrison (1973) developed a theory that predicts the passive pressure on a rough two-dimensional interface with one edge in the soil surface. The theory is based on slip line fields including wedges of soil that are in equilibrium, not failing, but in a stress state of incipient failure. The slip line fields vary with the interface angle α and the angle of internal shearing resistance ϕ, and are a function of the direction of motion of the interface θ. The detailed mathematical expressions for the horizontal and vertical forces acting on a plate grouser are given in Appendix C. Forces computed from Harrison's equations [Eq. (C.3), Appendix C], are compared in Table 7-5 with both the finite element and the experimentally measured forces obtained at 0.5 inch of grouser displacement. From this Table, it is shown that Harrison's results deviate appreciably from the measured values. It is interesting to note that when examining Harrison's results for the case of constant grouser elevation [i.e. $\theta = 0$], large discrepancies are found between the measured and the theoretically calculated forces. These discrepancies are reported in both the loam and clay series, while in the sand series good correlations are obtained. This behavior suggests that Harrison's hypothesis of the existence of a wedge-shaped zone of soil fixed to the interface, forming pseudo interface along which actual failure occurred, is not valid for the case of constant elevation tests in cohesive soils.

TABLE 7-5

COMPARISON OF HORIZONTAL AND VERTICAL FORCES
ON RIGHT ANGLE PLATE GROUSERS BY DIFFERENT METHODS

	Grouser Aspect Ratio h/l = 0.5		Grouser Aspect Ratio h/l = 0.833	
	Horizontal Force	Vertical Force	Horizontal Force	Vertical Force
Harrison's Equation	48.62	- 81.16	58.57	- 64.0
Bekker's Equation	35.60	-	49.84	-
Finite Element at 0.5 inch Displacement	-	-	41.47	- 23.63
Experiment at 0.50 inch Displacement	33.2 34.1	- 13.9 - 14.3	41.20 43.0	- 18.0 - 19.2

- Negative Values Indicate Upward Forces

CHAPTER 8

SUMMARY AND CONCLUSIONS

8.1 SUMMARY

The primary goal of the problem examined in this study was to look into the possibility of providing a rational analytical means for predicting the performance of a number of cutting and traction tools, using parameters that describe the soil response due to interaction with the tool. The review of past work revealed the need for an analytical technique that can be efficiently employed in predicting both the stress distribution and the soil deformation resulting from a cutting or a traction tool loading, by taking into consideration the nonlinear behavior of soil and the effect of large deformation due to implement movement.

The field of research was shown to be extensive and of many dimensions. The scope of the study was therefore limited to verifying the validity and applicability of the suggested analytical model [finite element model] to the analysis of the problem of simplified cutting and traction elements interacting with a nearly-saturated kaolinite and an artificial-oil based clays under plane-strain conditions. The purpose of the experimental program was, therefore, to provide data on the interaction process which could be compared with the analytical results. The experimental investigation was divided into cutting tests and traction tests. In the former phase a series of flat blades with different angles of inclination were moved through the soil. On the other hand, the traction study was concerned with the influence of grouser geometries on the developed forces. Both phases of the study were performed at specified constant speed and constant depth of cut.

An analytical model was developed using the finite element method to provide a theoretical solution to the soil cutting and traction problems. The developed model takes into account the effect of the progressive cutting of the soil at the tool tip, with the possible development of failure zones wherever the shear strength of the soil is exceeded. The solution provides detailed stress and deformation fields within the loaded soil, and contact stresses at the soil-tool interface for various tool positions. Consequently, a relatively complete description of the load-deformation behavior as the tool advances in the soil was obtained.

The main features of the finite element model adopted in this study can be summarized as follows:

a) <u>Idealization</u>

1. The model incorporates two discontinuities. A cutting plane discontinuity positioned at the level of the tool tip representing the action of the cutting element, where severe relative displacements and separation of soil blocks take place. The second discontinuity is a soil-tool interface discontinuity representing the relative displacements occuring between the soil and the tool surface.

2. The soil mass is modelled by plane-strain continuum elements representing a region in which plastic deformations take place with possibilities of localized or shear failures.

b) Boundary Conditions

The boundary conditions for the analytical model can be either specified pressure, specified displacement, or both. Thus, the model is capable of handling mixed boundary value problems. Moreover, relative displacements occurring across a thin discontinuity are included in the formulation to account for different degrees of interfacial slip.

c) Nonlinear Analysis

In the model developed, the stress-strain relations obtained from laboratory tests are used in the analysis to predict the load-deformation behavior of the soil. The tabular [direct digital] form is used to incorporate the constitutive law into the finite element model. The solution is obtained by the incremental method of analysis improved by iterating a few times in each increment of loading.

The application of energy conservation principles to soil cutting and soil traction problems provided a technique for a check on the finite element solution. Application of the visioplasticity method to the experimentally recorded deformation fields, with the assumption that the stress-deformation behavior of the soil could be described by a rigid plastic model, enabled the calculations of the deformation energy fields of the loaded soils. These energy values were compared to those obtained from the finite element model.

The applicability of the proposed solution technique was further examined in order to assess the significance of the implied conditions and requirements. The examinations were conducted by:

- Firstly, applying the solution technique to the familiar problem of a long retaining wall, yielding in a passive sense. This constituted a parametric study to establish the relative importance of the various features and assumptions implemented in the finite element technique. The results were compared with the conventional solution. A summary and findings of this study are presented in Section 7.2.4, Chapter 7.
- Secondly, comparing the soil cutting and traction [analytical and experimental] results presented in this Thesis with results computed from existing theories.

8.2 CONTRIBUTION

This study contributes to the field mainly by having shown that the soil cutting and traction problems can be dealt with through an analytical approach which has the objective of deriving statically possible stresses compatible with kinematically possible strains while, at the same time, satisfying some average boundary conditions, even though numerous assumptions and approximations needed to be made, especially regarding the mathematical modelling of the deforming medium.

Specific contributions are:

1. The development of an analytical technique for the determination of the soil stress and deformation fields as well as contact stresses on the soil-tool interface, thus providing a relatively complete description of the load-deformation behavior as the tool advances in the soil.

2. The successful application of the method of finite element to the study of soil cutting and traction, and the verification of correspondence between measured and computed values.

3. The successful application of the principle of energy conservation to the cutting and traction element-soil systems. The developed solution, using the method of visioplasticity, provides reasonably good predictions of the experimentally measured energy components.

To the author's knowledge, the above has not been available in past published work and, in the author's opinion, contributes to the field of soil-machine interaction analysis.

8.3 CONCLUSIONS

On a long term basis, the present study may be looked upon as a step in the direction of an improved method for soil machine-interaction analysis. In its immediate application, the proposed method may contribute to a systematic study of cutting and traction elements travelling in clays by a rational scanning of all pertinent parameters. Eventually, it could be attempted to rationalize the deformation patterns and stress fields in terms of significant soil and tool parameters, and hence establish a complete and unified theory for cutting and traction in clay soils.

The following is a short summary of the conclusions arrived at in this study concerning the soil cutting and traction problems:

A. Soil Cutting Problem

Regarding the soil cutting developed forces it was found that:

1. The agreement between the experimentally measured and the finite element calculated forces is very satisfactory in the case of the horizontal forces for both the blade inclinations analyzed; the average error of estimate is of the order of 8%, while the maximum error is some 15%. With regard to the vertical forces, the values obtained from the analytical solution are, however, more subject to variation. The differences in the vertical forces can be attributed to the effect of the soil deformation behind and below the blades which has not been considered in the finite element idealization.

Regarding the deformation fields it was found that:

1. The discontinuity in displacement at the level of the blade tip [on the cutting plane] is clearly demonstrated from the experimental plots. However, the experimental horizontal displacement fields reveal that the displacement contours are only discontinuous in the vicinity of the blade while at a distance they are shown to be continuous above and below the assumed cutting plane. Such behavior implies that the discontinuity in displacement propagates with the blade movement.

2. Examination of the experimental and the analytical horizontal displacement fields indicates that the finite element solution underestimates the horizontal displacements in the zone near the soil surface, while it overestimates in the soil mass situated directly above the cutting plane.

3. In the vertical displacement fields a deviation between the experimental and analytical fields was observed in the location of the zero vertical displacement contour dividing zones of upward and downward movements.

4. The qualitative agreement between the experimental and the analytical deformation fields, taking all the above points into consideration, is found to be very satisfactory.

Regarding the deformation energy fields it was found that:

The visioplasticity method as applied in this study, with the assumption of a rigid plastic model, overpredicts the deformation energy calculated from the integration of the experimentally measured load-deformation relationship, especially in the initial stages of the deformation process. On the other hand, the finite element model developed in this Thesis, which treats the soil as a non-linear strain-hardening material subject to boundary conditions of an incremental form, provides better estimates of the energy dissipated within the soil. The finite element average error of estimate, compared to the experimentally obtained energy values, is of the order of 10%. The maximum deviation is about 18%.

Comparison with results computed from the previous theories of soil cutting indicated that:

1. The predicted horizontal forces using Hettiaratchi et al. (1966) data show good agreement with the forces obtained from the test results as well as from the finite element analysis at 0.5 inch of blade displacement. On the other hand, Reece's method is found to underestimate the draft forces.

2. The vertical forces [experimental and analytical] deviate significantly from those computed from Hettiaratchi et al. method. This deviation is attributed to the fact that the mobilization of the soil-blade adhesion is a function of:

i) the relative displacements between the soil and the blade, or in other words, a function of blade displacement, and

ii) the blade rake angle. The distributions of the tangential stresses are markedly different along the 10° and 50° inclined blade surfaces. This finding is in contrast to Hettiaratchi et al. and Reece's assumption of constant uniform adhesion along the blade surface.

B. Soil-Grouser Interaction Problem

Regarding the developed forces on the various grousers it was found that:

1. Concerning the measured developed forces on the various grousers employed in this study, the plate grouser [R.A.P.G.] with an aspect ratio h/l of 0.833 was found to develop the highest horizontal as well as vertical forces when compared to the wedge grousers. This is attributed to the soil deformation behavior in front of the plate grouser where a rigid zone, similar to the "dead" zone postulated by Terzaghi (1948) for bearing capacity, was observed. The compression in this zone extends the region of influence of the grouser, resulting in larger developed forces. In the wedge grouser experiments, very small or no rigid zones were observed, and the regions of influence of such grousers were found to be smaller than those of the plate grouser [R.A.P.G.].

2. The agreement between the experimentally measured and the finite element calculated forces, considering the assumptions made, is generally very satisfactory. The analytical and test results, however, show better agreement in the case of the horizontal forces, for which the percentage difference rarely exceeds 10%. In the case of the vertical forces, the average error or estimate is of the order of 20%, while the maximum error is some 40%.

Regarding the deformation fields it was found that:

Generally the correspondence between the analytical and the experimental deformation fields for both the horizontal and vertical displacements is judged to be satisfactory. The finite element model, however, is found to possess more regidity in the x-direction and more flexibility in the y-direction, when comparing displacements with those measured.

Regarding the deformation energy fields it was found that:

As in the case of the soil cutting comparisons, the visioplasticity method overestimates the deformation energy in all cases, while the finite element results show a better correlation with the measured input energy.

<u>Comparison with results computed from the previous theories of soil-grouser interaction indicated that:</u>

1. By considering the wedge grousers to act as cutting elements with backward raked soil interfaces, the predictive methods of Reece (1965) and Hettiaratchi et al. (1966), together with the hypothesis put forward by Osman (1964) to account for the effect of element curvature, could be used to compute the developed forces on these elements.

2. The horizontal forces predicted by Hettiaratchi et al. method of computation show a fairly good degree of correspondence with the measured forces for the wedge grousers. With regard to the vertical forces, a significant deviation is obtained between the calculated and the measured values. The deviation is attributed to the facts that:

   i) The mobilization of adhesion is a function of the relative displacement between the soil and the metal interface.

   ii) The shear stresses on the soil-metal interfaces change direction at a certain point on the interface.

3. When comparing the developed forces on the plate grouser [R.A.P.G.] with Bekker's equations, the deviation between Bekker's and the experimentally measured values is found to be of the order of 6% for grouser aspect ratio [h/l] of 0.5 and about 18% for the grouser with a ratio [h/l] of 0.833.

4. Forces computed from Harrison's equations (1973) deviate considerably from those measured or computed. However, when examining Harrison's results for the case of constant grouser elevations, large discrepancies were also found between his measured and his calculated values. This sheds doubt on the validity of his hypothesis for the case of grousers tested under constant elevation condition in cohesive soils.

APPENDIX A

SECTION A

EXPERIMENTAL CONSIDERATIONS

A.1 DESCRIPTION OF THE TEST FACILITY

A.1.1 Apparatus

As constructed, the apparatus consisted of a tool plate rigidly attached to a carriage which allowed it to translate both horizontally and vertically but which permitted no angular rotation, Fig. A-1 and Plate A-1.

The carriage itself was mounted on roller bearings which travelled in polished guide rails. The rails were machined to a tolerance of 0.003 inches, and as a consequence the frictional resistance of the system was reduced to a minimum, the force required to overcome this resistance being typically of the order of two per cent to four per cent of the total measured horizontal force.

The drive mechanism of the apparatus consisted of a threaded shaft which was, in effect, a worm gear. This was driven by a 1/2-horsepower varying speed electric motor and a V-belt pulley assembly through a system of gears.

The carriage and tool assembly were mounted on a frame in such a position that it was directly above a soil bin whose dimensions were 22 1/2 ins. x 4 ins. in planform and which usually accommodated a

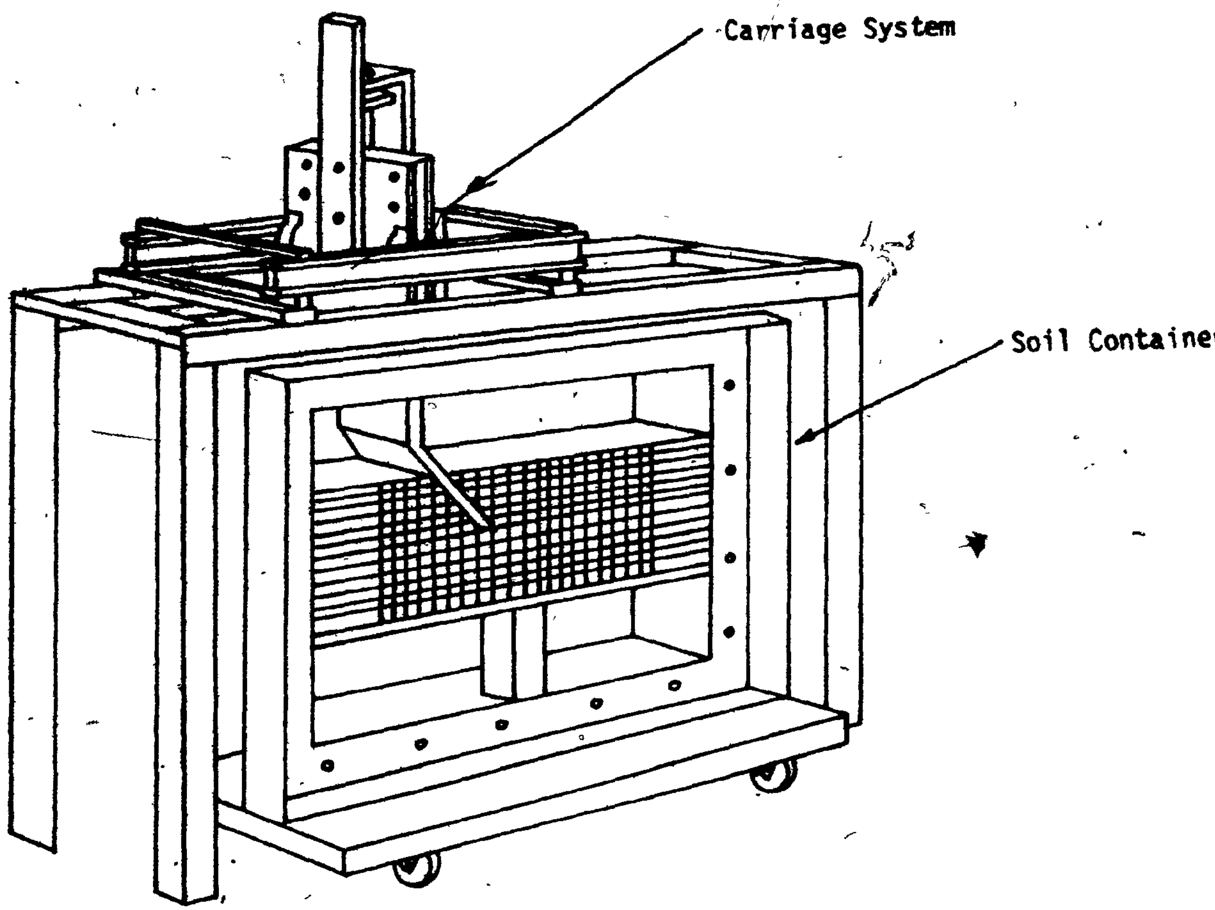

FIGURE A-1 ISOMETRIC VIEW OF TEST EQUIPMENT

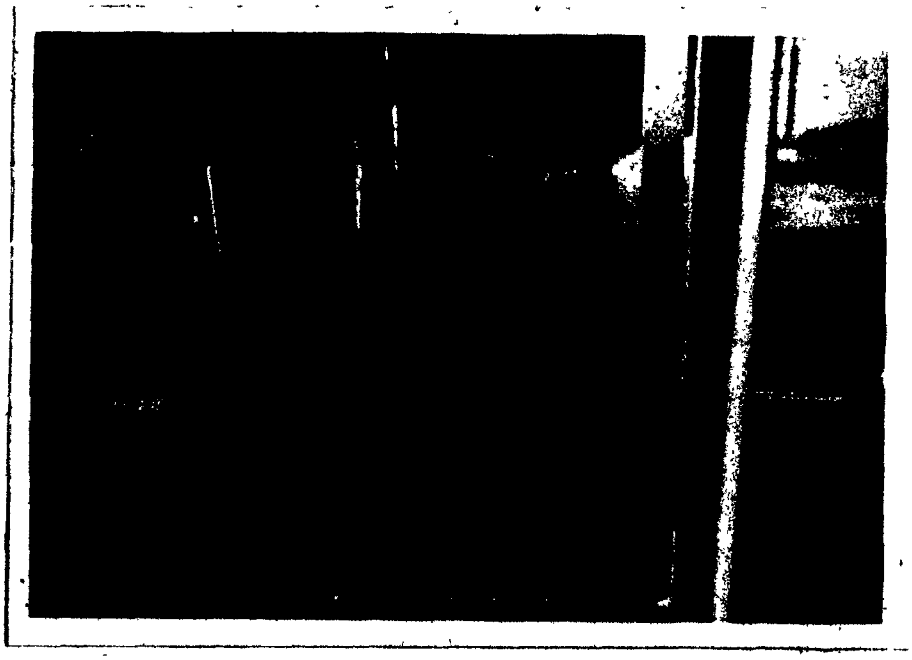

PLATE A 1 THE CARRIAGE SYSTEM

depth of clay of the order of nine inches. The bin was equipped with removable lucite side walls and was mounted on castors to facilitate its removal from under the carriage. The carriage and bin are shown in Fig. A-1.

A.1.2 Measuring and Recording Devices

All forces and displacements were measured by means of electrical transducers. The horizontal and vertical force transducers were of 0-100 lb capacity, and were manufactured by the Dynisco Division of the Abex Corporation. They were both excited by a 6-volt direct current voltage and had a full range sensitivity of the order of 3.5 mv/volt of excitation.

The horizontal displacement transducer was of the linear displacement type, utilizing a moving core in an electro-magnetic field. This transducer also required a 6-volt direct current excitation signal and had a maximum stroke of 1.5 inches.

The output of the transducers were fed into a 6-channel Sanborn Series 850 Recording System. The signals from the force transducers were fed into series 850-1800 preamplifiers with a sensitivity range of 0-100 mv/cm of deflection, while the displacement transducer signal was fed into series 850-1300 preamplifier with sensitivity range of 0-50 volts/cm in ten steps.

A 35 mm Pentax type SV Camera with Kodak Plus-X Panachromatic film was used to record grid distortions.

A.2 SAMPLE PREPARATION

The soil was prepared for placement in the soil bin by the following steps:

Soil Mixing [in the case of the natural kaolinite clay]. Dry kaolinite in powder form [stored in approximately 50-pound bags] was deposited in 50-pound lifts forming approximately two inch deep layer in a batching reservoir. Each lift was sprinkled with sufficient water to bring the soil to the desired water content. The water was allowed to soak in and the next lift was added. The wet soil was allowed to stand in the batching bin for seven days. At the end of this period the soil was mechanically mixed to improve homogeneity.

Soil Placing The removable side of the bin was first taken off and the inner surfaces of the remaining open box were coated with vaseline. Remoulded kaolinite of water content of 52.5% ± 1.0% was manually deposited in small lumps, tamped and rolled in one inch lifts. When the sample thickness was a little over the thickness of the bin, the excess was trimmed off with a wire saw and the surface smoothed over with a trowel.

Grid Placing Once the soil sample had been prepared, the selected tool [cutting blade or grouser] was embedded in the clay at a specified location. The various grousers employed during the course of this investigation are shown in Plates A-2 to A-4, inclusive. A grid network of one-half-inch squares was then made on the soil surface with a black pen and a

PLATE A-2 THE C.E.W. TYPE (2) GROUSER

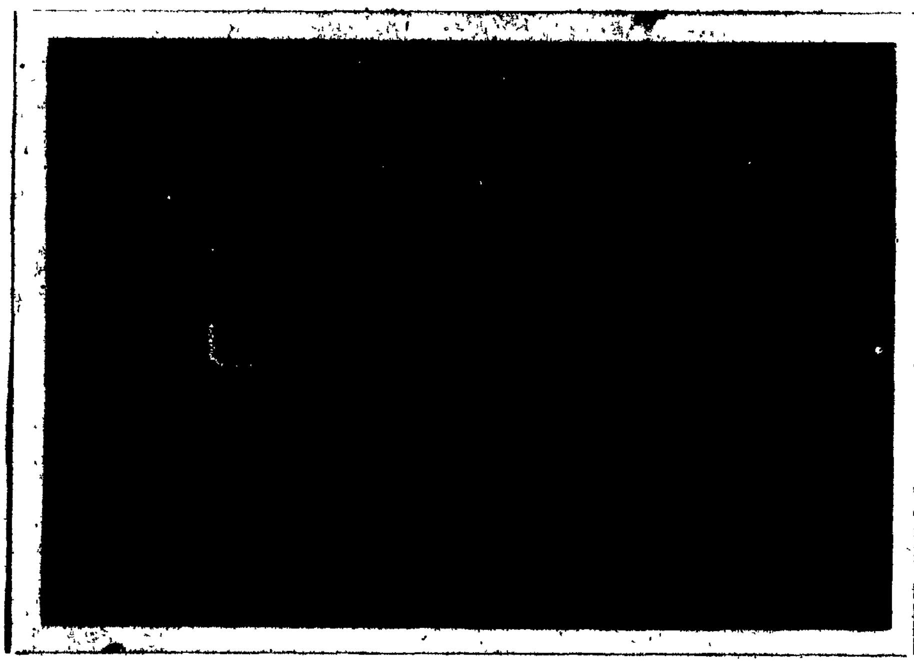

PLATE A-3 THE C.E.W. TYPE (1) GROUSER (LEFT)
AND THE S.E.W. GROUSER (RIGHT)

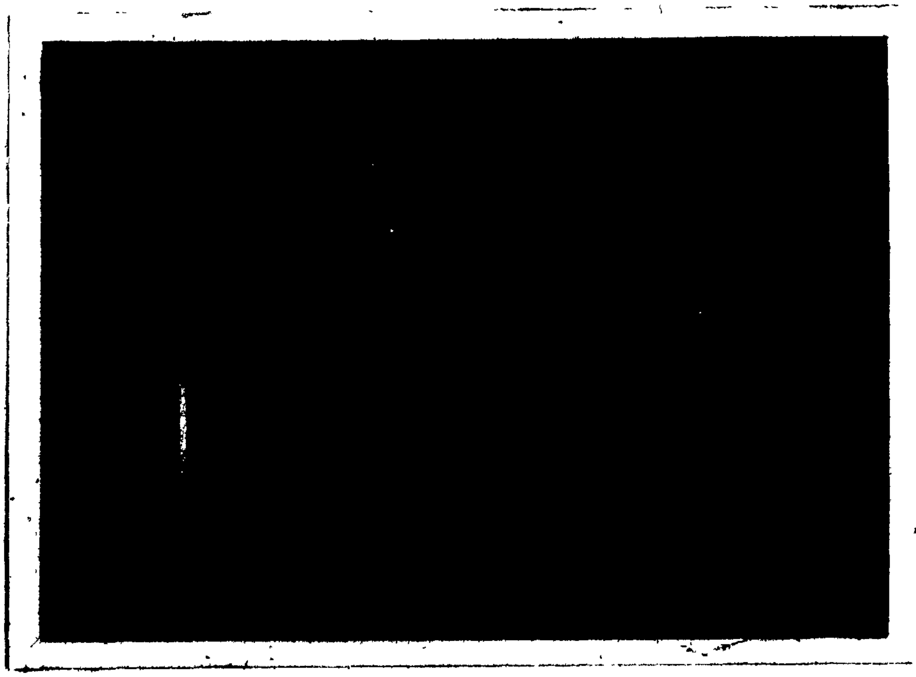

PLATE A-4   RIGHT ANGLE PLATE GROUSERS (R.A.P.G.) with (h/l) RATIOS of 0.833 (LEFT) and 0.5 (RIGHT) plotted lucite sheet. This was done by first placing the plotted lucite sheet in one direction and drawing lines in the slots. The lucite sheet was then turned 90 degrees, and the procedure was repeated until a grid of one-half-inch squares resulted. The bin lucite front was then lubricated with vaseline and placed on the soil surface, and the aluminum frame bolted back on.

A.3 TESTING PROCEDURE

Once the soil sample had been prepared, it was placed under the carriage and the tool was attached to the carriage system by a nut-and-bolt system. Care was taken not to disturb the sample during this operation.

At this point, the tool speed desired [generally 1.0 inch/minute] was preset on the motor control box. An initial photograph of the undeformed grid was taken and the carriage was then set in motion. During the course of the test, further photographs of the deforming grid were taken at five-second intervals. A photographic record of a soil cutting test is shown in Plate A-5.

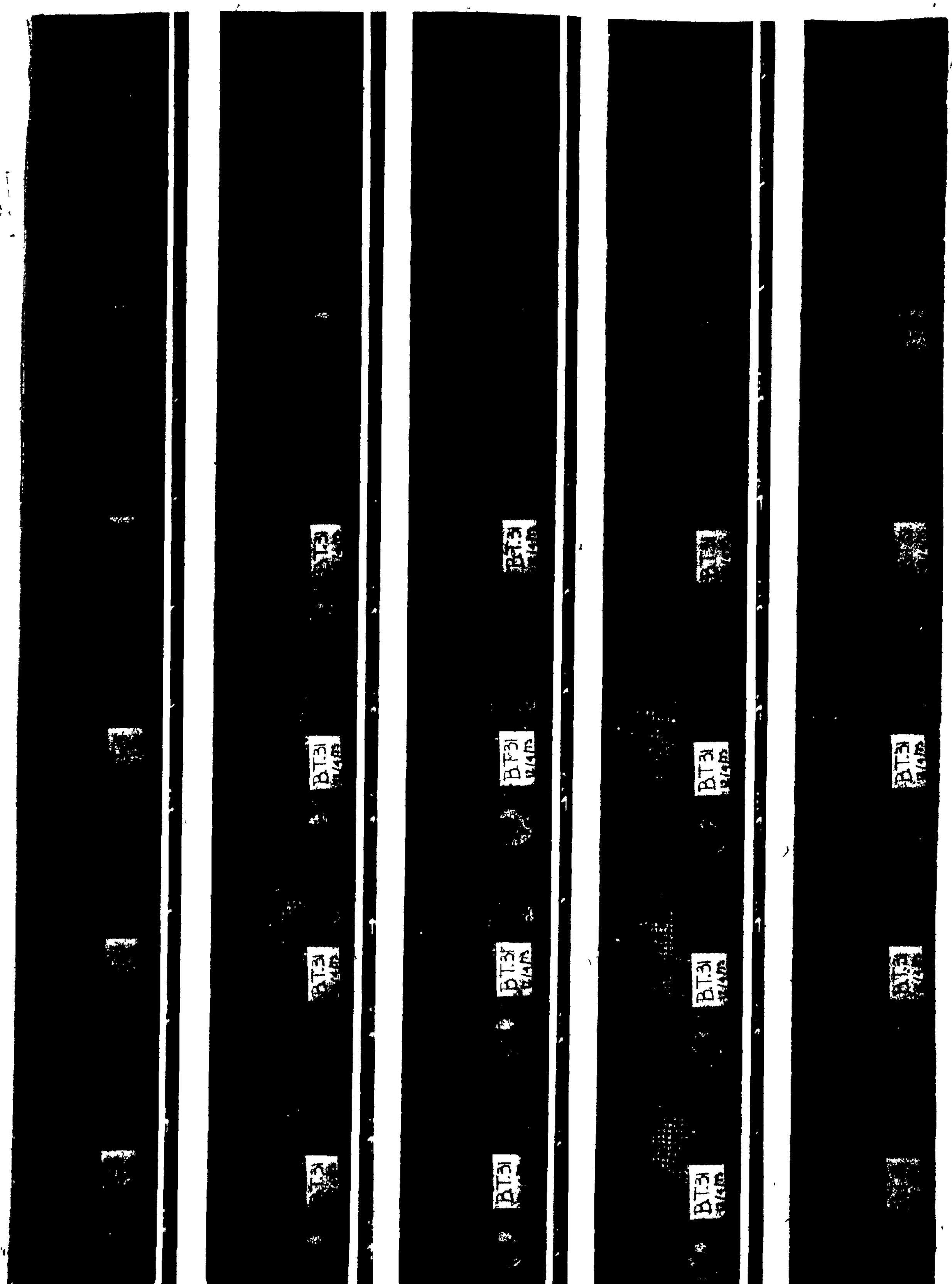

PLATE A-5 PHOTOGRAPHIC RECORD OF A SOIL CUTTING TEST

SECTION B

SOIL PROPERTIES

The natural clay used in both phases of the experimental study [i.e. cutting and traction tests] was an "English China Clay" formerly designated "S-187" and now known as "Lee Moor SPS". The predominant clay mineral constituent was kaolinite, as shown by the chemical analysis of samples. The complete chemical analysis, by weight, as provided by the supplier, is given as:

SiO_2	47.39%
Al_2O_3	37.94%
Fe_2O_3	0.36%
TiO_2	0.05%
MgO	0.18%
CaO	0.32%
k_2O	1.17%
Na_2O	0.07%
Loss on ignition	13.02%

An X-ray diffraction revealed that the clay was primarily kaolinite [approximately 93% by weight] with some illite [about 7%].

The soil was in part donated by, and in part purchased from Domtar Fine Papers Ltd. and was found to have the following engineering properties, as determined from laboratory tests:

Liquid limit	54.5%
Plastic limit	37.5%
Specific gravity	2.62
Particle size distribution	74% finer than 2 microns

A complete grain size distribution is shown in Fig. A-2.

The artificial clay employed during the investigation was "Plasticine" [trade name] as manufactured by Harbutts Ltd. of England. Although the manufacturer's specifications stated that the material was temperature insensitive, such did not prove to be the case with regard to stress-strain performance. For this reason all the tests were conducted within a temperature range of 70°-75°F. A small amount [about 3% by weight] of petroleum jelly was added to the clay to reduce its strength.

The static stress-strain curves of the artificial clay are shown in Fig. A-6. The particle size distribution of the solid residue reported by Japp (1967) is shown in Fig. A-3. Japp found that approximately 20% by weight is of clay size fraction. An X-ray diffraction study revealed that no clay minerals were present, and that the solid phase was primarily quartz.

At a loading velocity of 1.0 inch/minute, triaxial tests were conducted on confined and unconfined specimens. The results of these tests revealed that the performance of the artificial clay is not influenced by the magnitude of the confining pressure and hence a $\phi = 0$ analysis is valid [Japp (1967)].

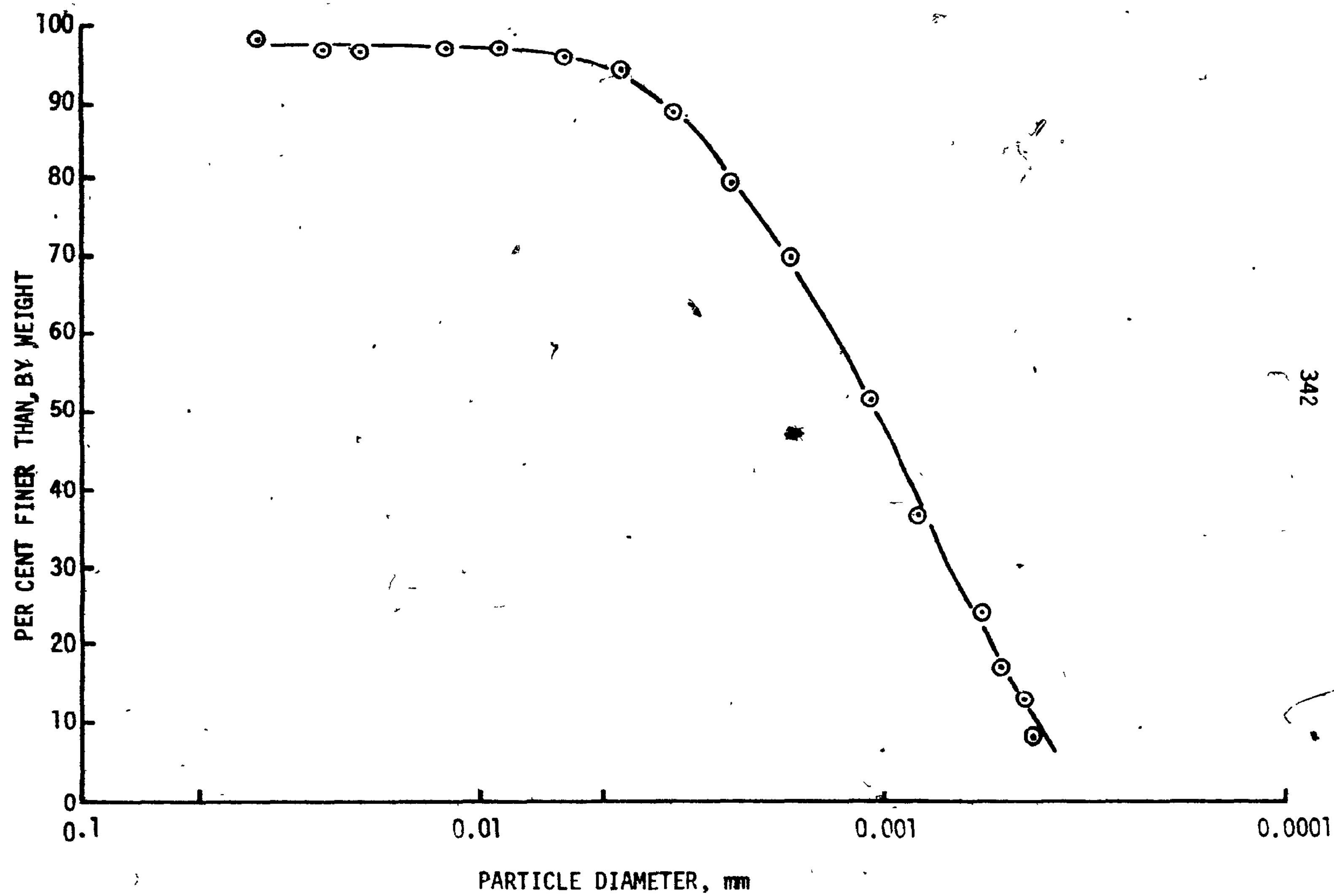

FIGURE A-2 GRAIN SIZE DISTRIBUTION FOR S-187 CLAY

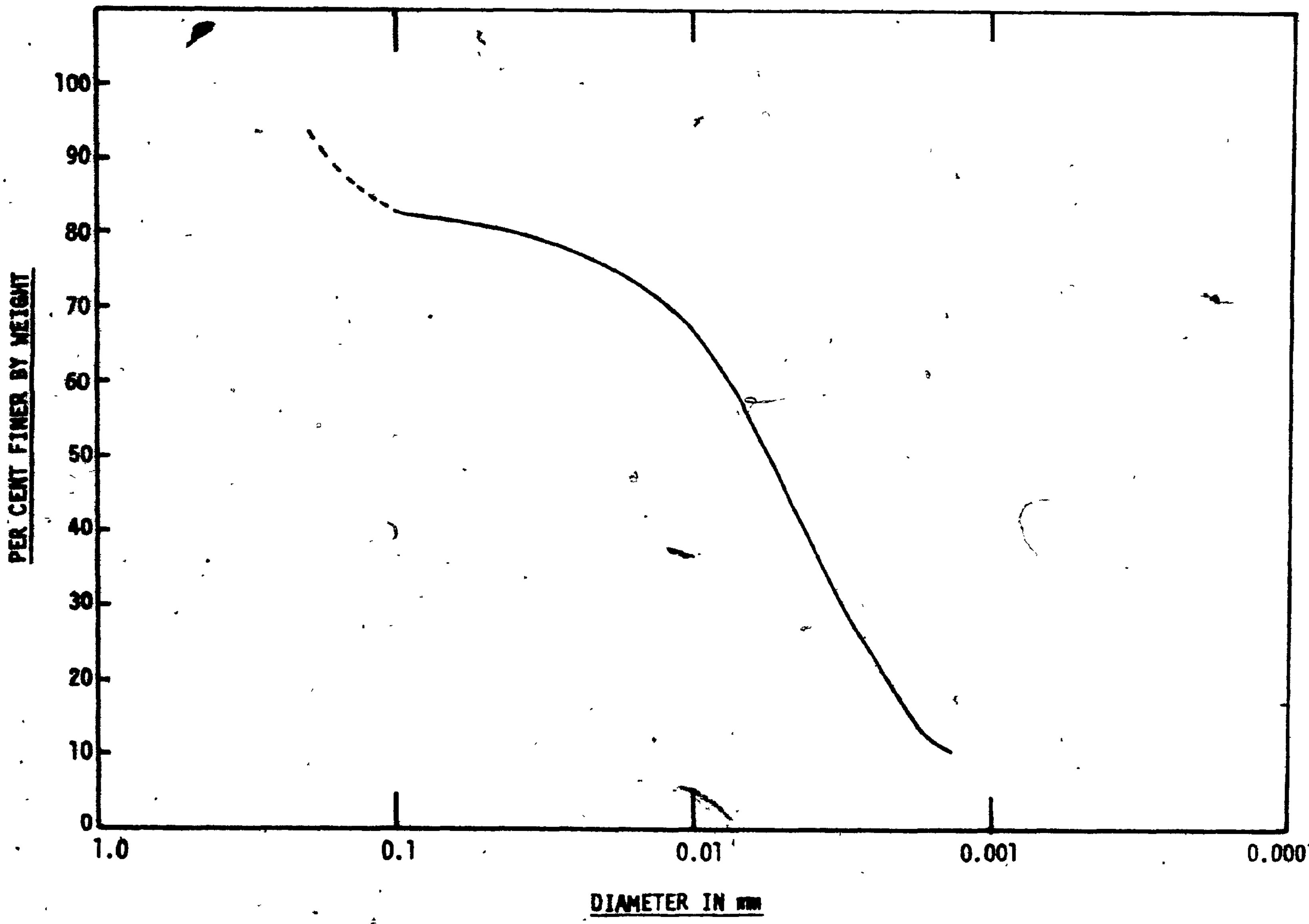

FIGURE A-3 GRAIN SIZE DISTRIBUTION FOR THE ARTIFICIAL OIL-BASED (PLASTICINE) CLAY (After Japp (1967)

SECTION C

SHEAR STRENGTH TESTS

"True Triaxial" tests were performed under plane strain conditions in order to reproduce as closely as possible the assumed conditions existing in the cutting and traction tests. In this case, prismatic samples [2 ins. x 1 1/2 ins. x 4 1/4 ins.] of both artificial clay and nearly saturated remoulded [kaolinite] clay were prepared in a similar manner to the compacted samples used in the cutting and traction tests. The prepared sample was placed in a modified triaxial chamber between two polished brass plates [see Fig. A-4]. The distance between the plates was adjusted so that no material deformation of the sample, normal to the plates, was permitted. The samples were then placed in a testing machine and axial loads applied. The tests were performed at three different cell pressures [0, 2.5 and 5.0 psi] and at axial loading velocities of 0.1, 0.5 and 1.0 ins/min. The results of the tests on the kaolinite clay have previously been shown as Fig. 4-7.

Similar tests were performed on cylindrical samples. These samples were 1.40 ins. in diameter and 3 1/8 ins. in length. Axi-symmetric tests were performed in order to verify that the nonexistence of a well-defined failure conditions, i.e. no strain softening behavior, is not a result of the plane strain, "True Triaxial", test restraints. The results have been included in Fig. 4-8 for the natural kaolinite clay and in Fig. A-6 for the artificial clay employed during the initial stages of the experimental programme. Figure A-5 shows the effect of

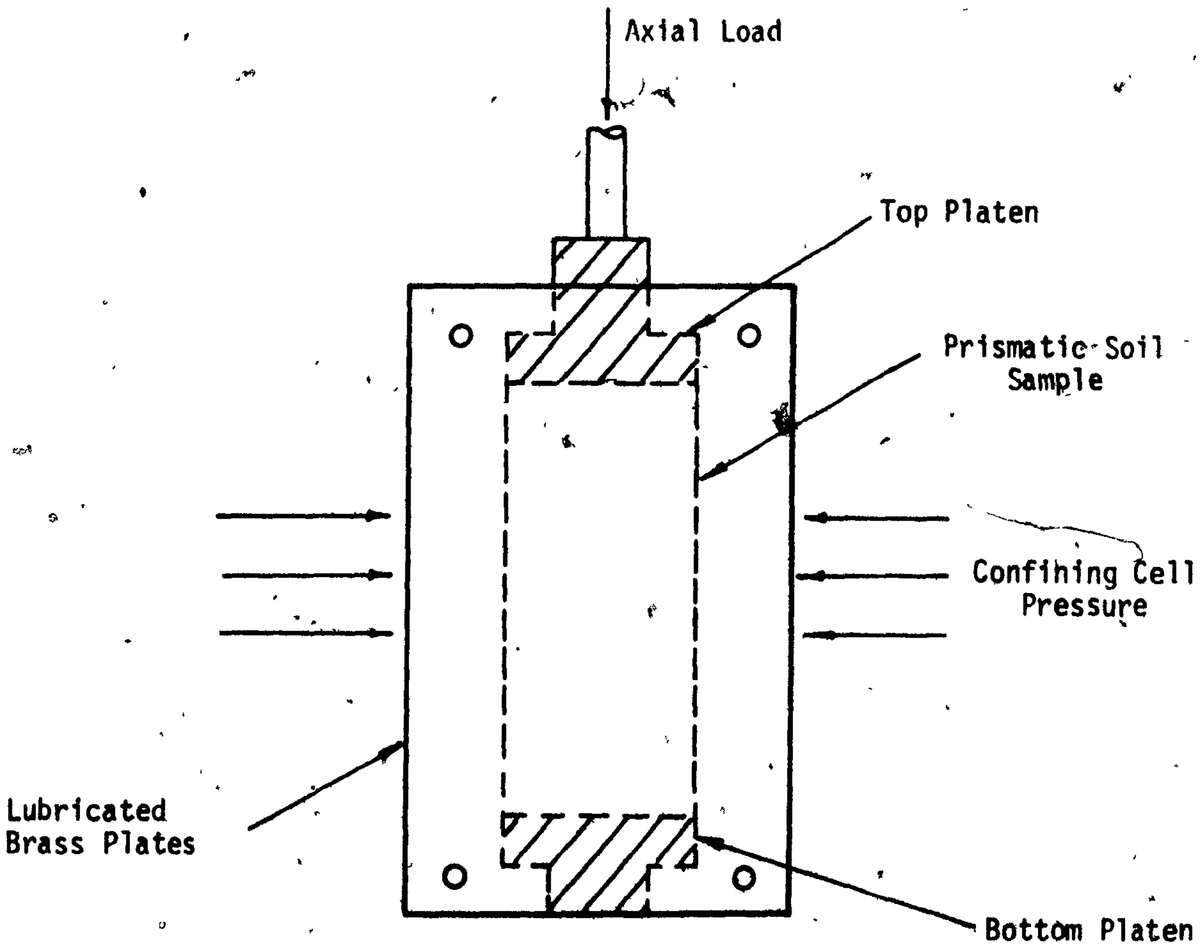

FIGURE A-4 SCHEMATIC REPRESENTATION OF PLANE STRAIN TRIAXIAL TEST the loading rate on the shear strength values for the kaolinite clay.

Finally, direct shear tests were performed on the compacted soil in both the soil-to-soil and the soil-to-metal modes. Samples were cut from clay compacted in the test bin and these were trimmed and tested, Section 4.A.3. The direct shear test results are shown in Fig. 4-9 for the soil-to-soil mode and in Fig. 4-10 for the soil-to-metal mode.

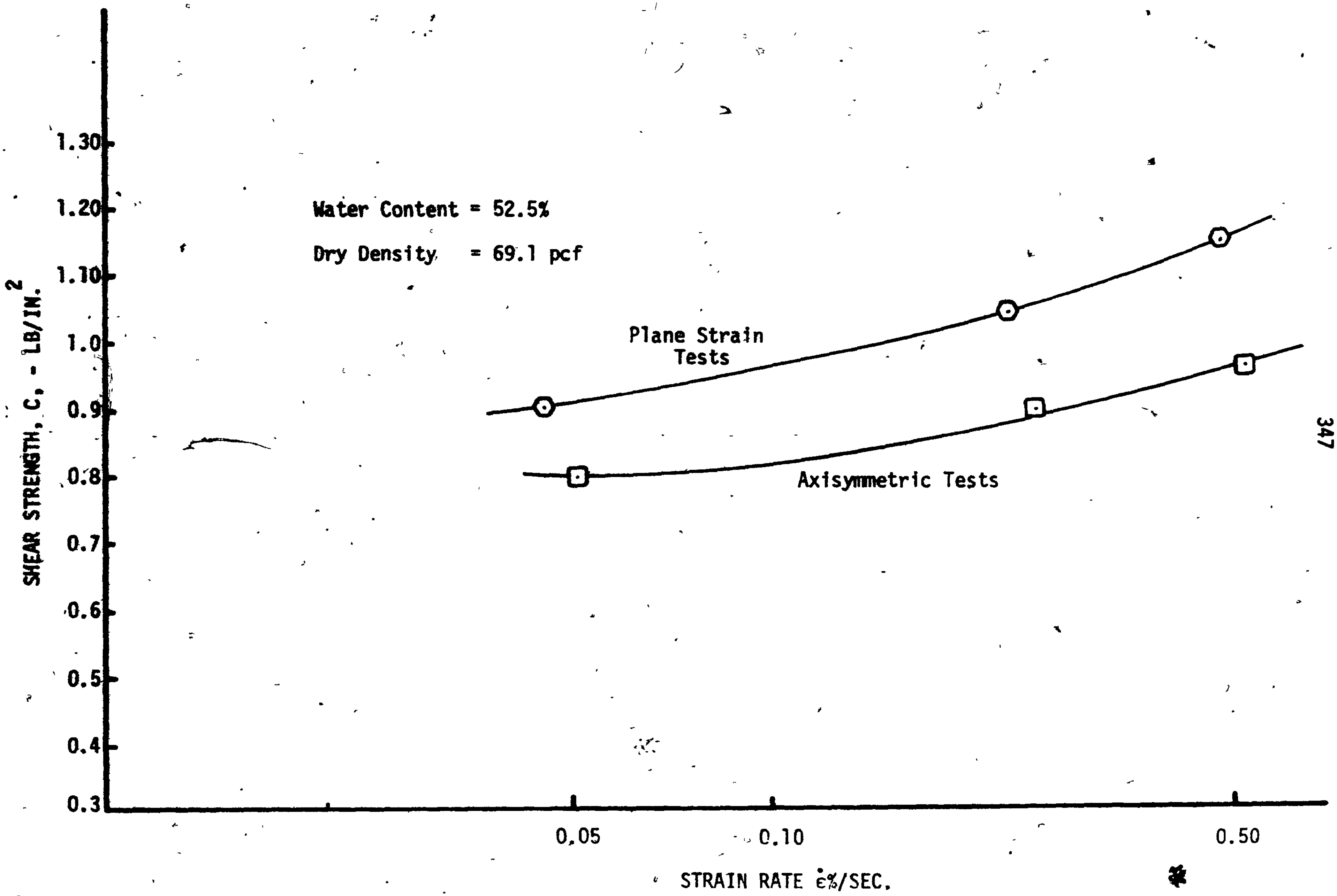

FIGURE A-5 . PLOTS OF SHEAR STRENGTH OF S-187 ENGLISH (KAOLINITE) CLAY VS STRAIN RATE

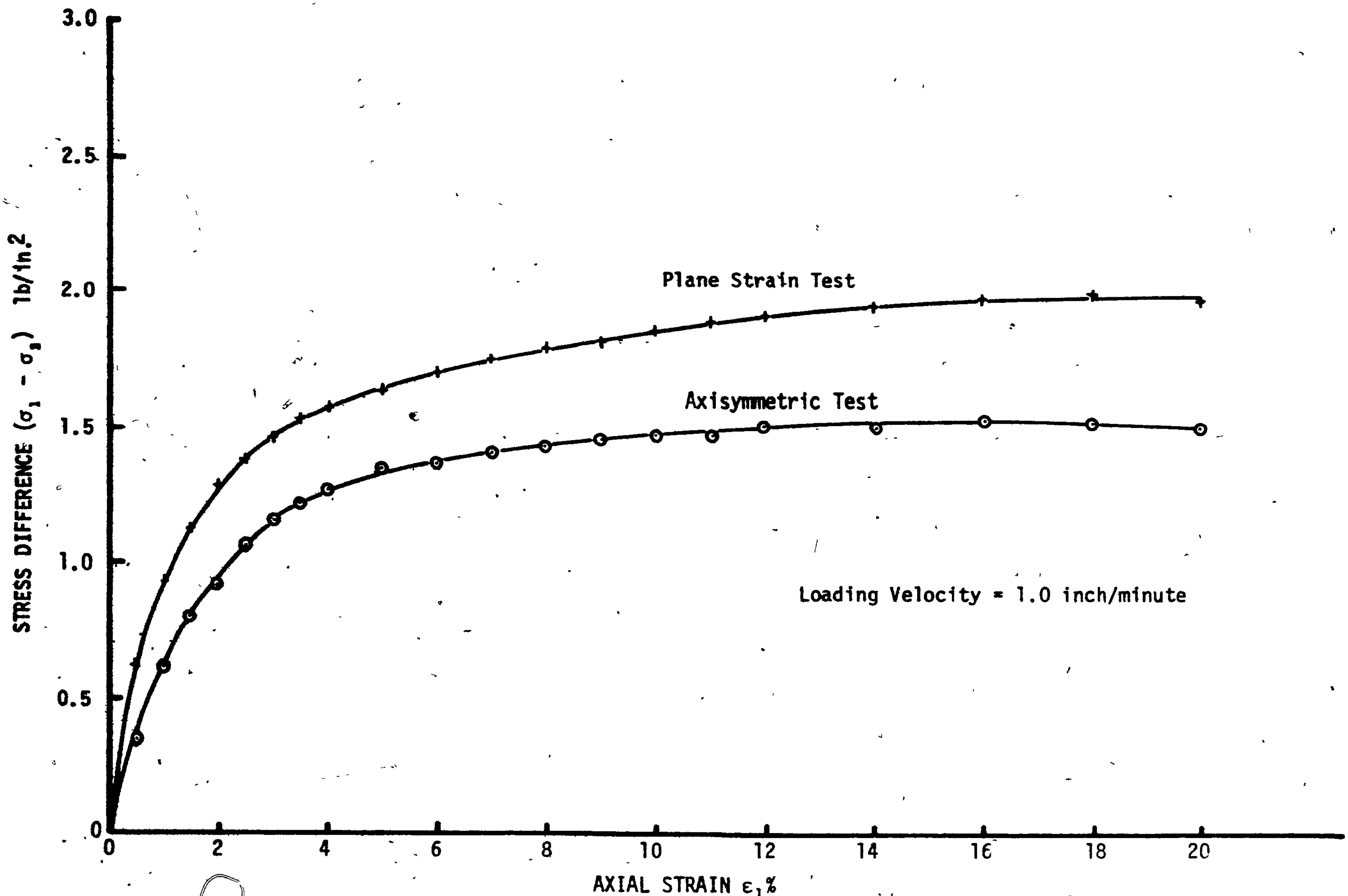

FIGURE A-6 - TYPICAL STRESS-STRAIN CURVES FOR ARTIFICIAL CLAY

SECTION D

ARTIFICIAL CLAY CUTTING AND TRACTION TEST RESULTS

FIGURE A-7 HORIZONTAL FORCE VS DISTANCE TRAVELLED FOR DIFFERENT BLADE INCLINATIONS
(ARTIFICIAL CLAY)

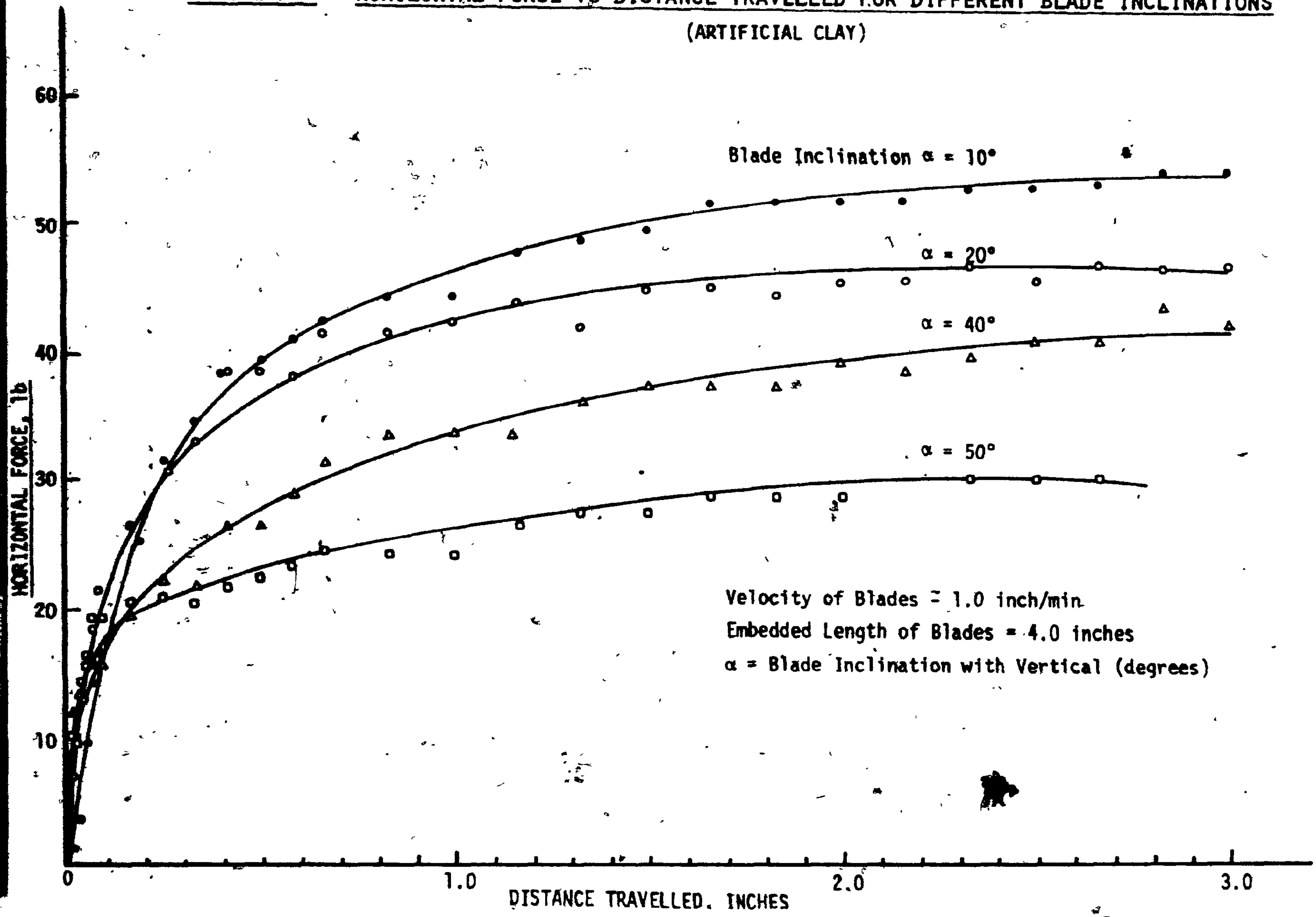

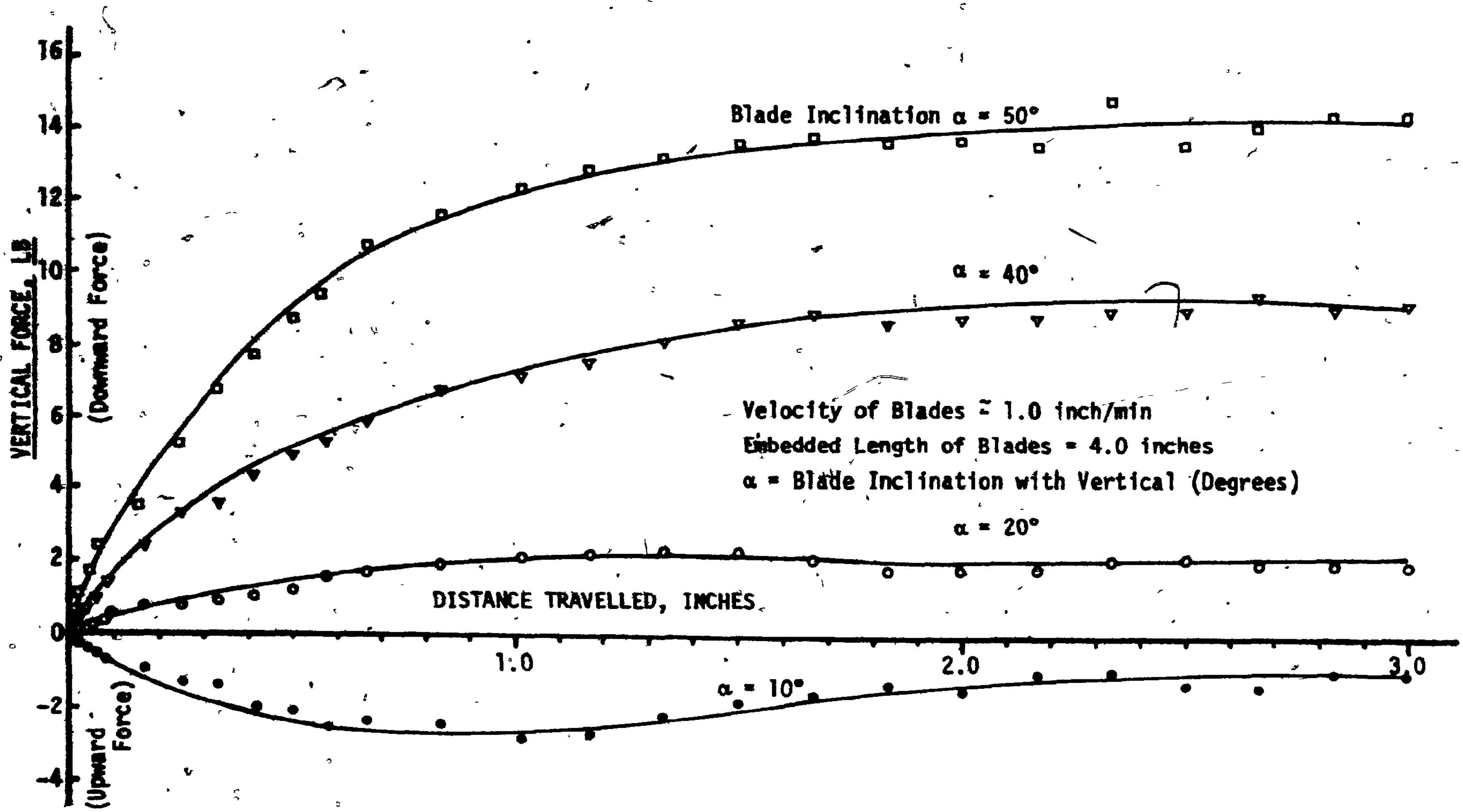

FIGURE A-8 VERTICAL FORCE VS DISTANCE TRAVELLED FOR DIFFERENT BLADE INCLINATIONS

(ARTIFICIAL CLAY)

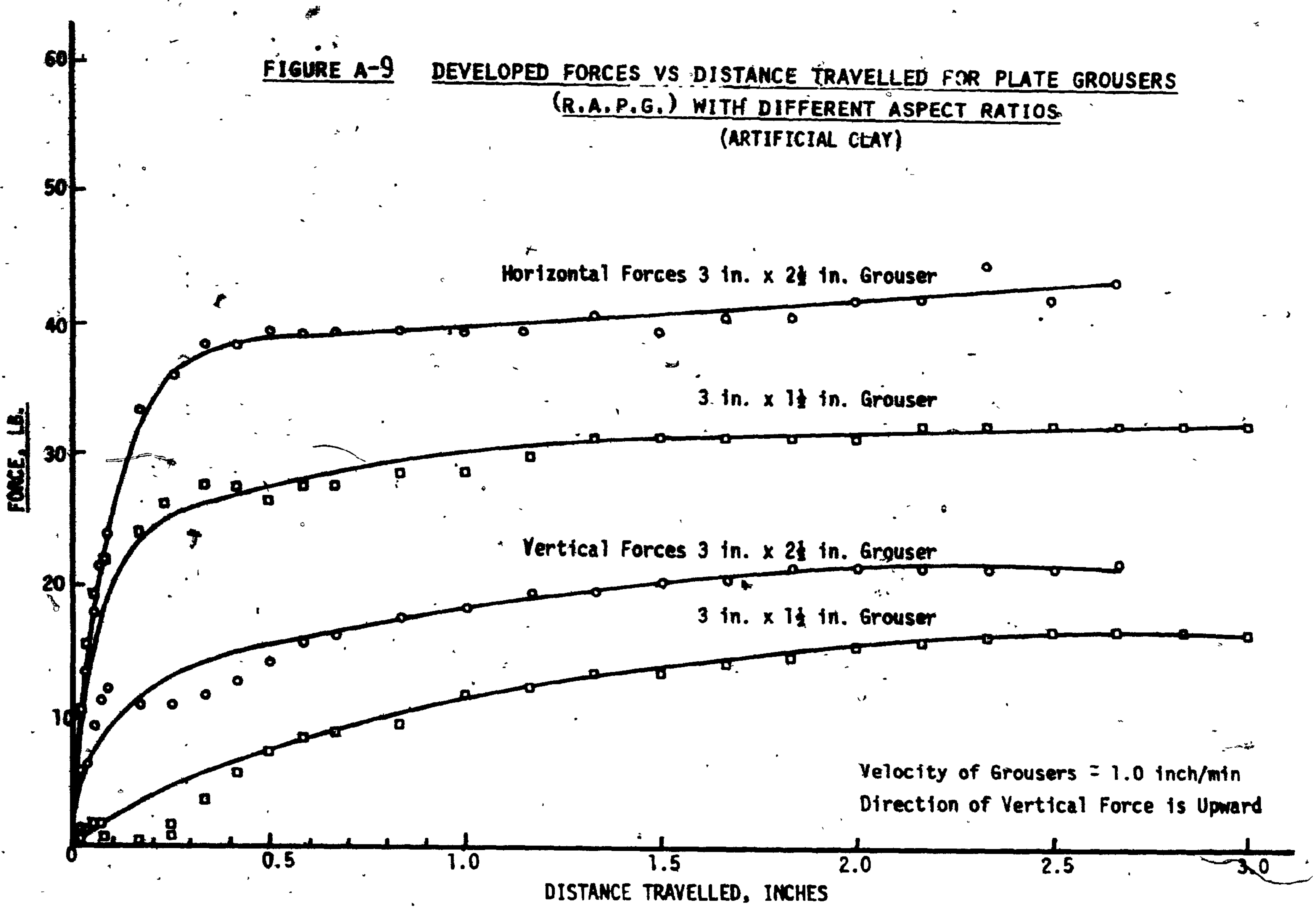
FIGURE A-9 DEVELOPED FORCES VS DISTANCE TRAVELLED FOR PLATE GROUSERS (R.A.P.G.) WITH DIFFERENT ASPECT RATIOS
(ARTIFICIAL CLAY)
Horizontal Forces 3 in. x 2½ in. Grouser
3 in. x 1½ in. Grouser
Vertical Forces 3 in. x 2½ in. Grouser
3 in. x 1½ in. Grouser
Velocity of Grousers = 1.0 inch/min
Direction of Vertical Force is Upward
FORCE, LB.
60
50
40
30
20
10
0
0.5
1.0
1.5
2.0
2.5
3.0
DISTANCE TRAVELLED, INCHES

FIGURE A-10 - DEVELOPED FORCES VS DISTANCE TRAVELLED FOR WEDGE GROUSERS

(ARTIFICIAL CLAY)

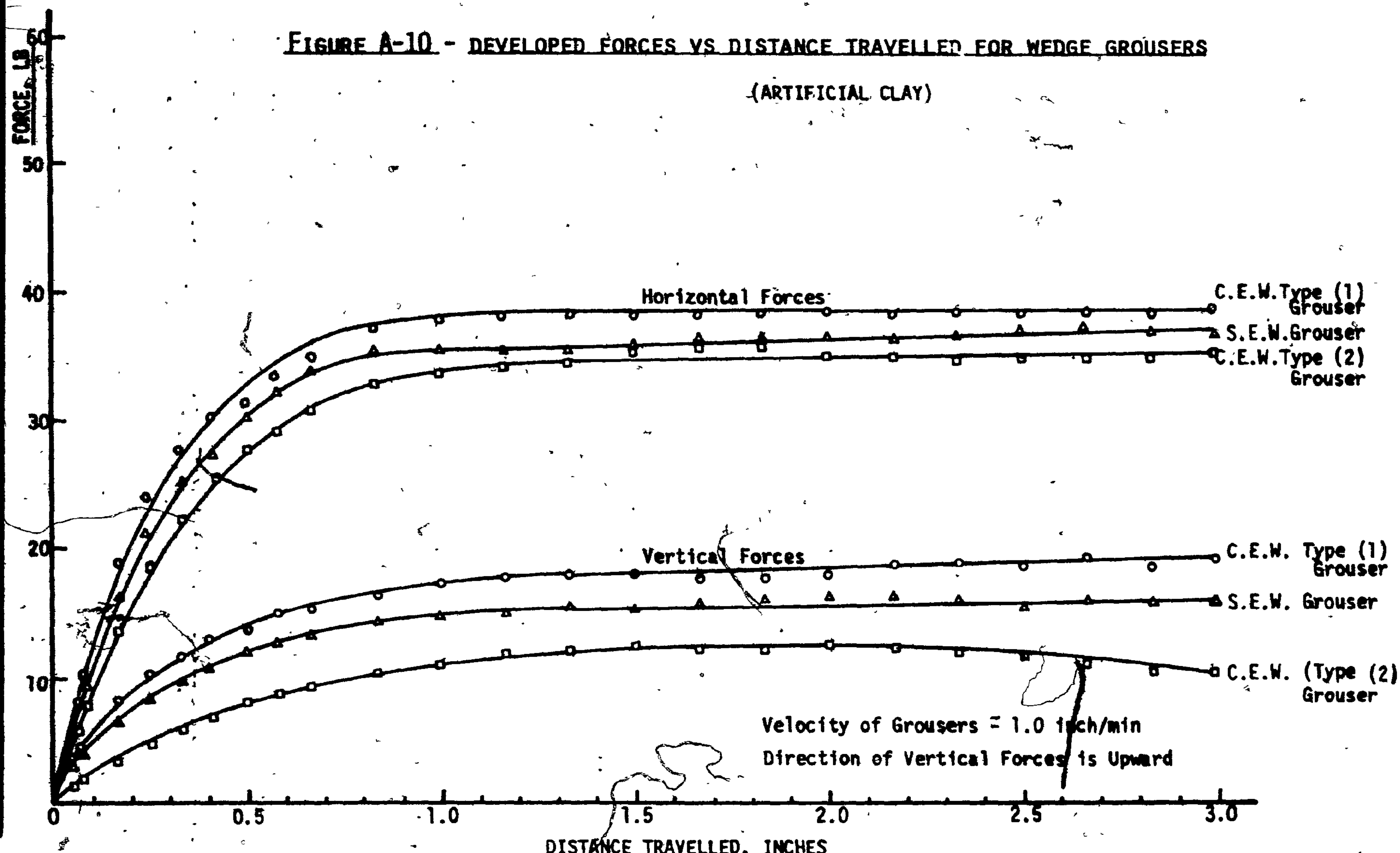

353

APPENDIX B

DATA REDUCTION TECHNIQUES

The basic steps adopted for data reduction of the soil cutting and traction experiments are described in this Appendix. The techniques were described briefly in Chapter 4 [Section 4-B-2]. The method adopted in this study is similar to those previously reported by Chen (1972) and by Sylvestre-Williams (1973). A flow chart of the various steps followed in the reduction of experimental data, shown as Fig. 4-17, is given in Fig. B-1. In a chronological order these steps are:

Plotting of successive grid nodes.

Transfer of grid coordinate locations to Process Control Computer.

Grid adjustments.

Calculations of displacement and velocity components.

Calculations of strain rates and effective strain rates.

Estimation of volume changes.

Calculation of power of deformation.

These steps are discussed in detail in subsequent sections of this Appendix.

B.1 PLOTTING OF SUCCESSIVE GRID NODES

Selected frames from the photographic record of the grid nodes were projected and the grid displacement patterns at successive time intervals, together with the tool [blade or grouser] positions at these times, were plotted on paper [Fig. 4-16]. The grid nodes were taken

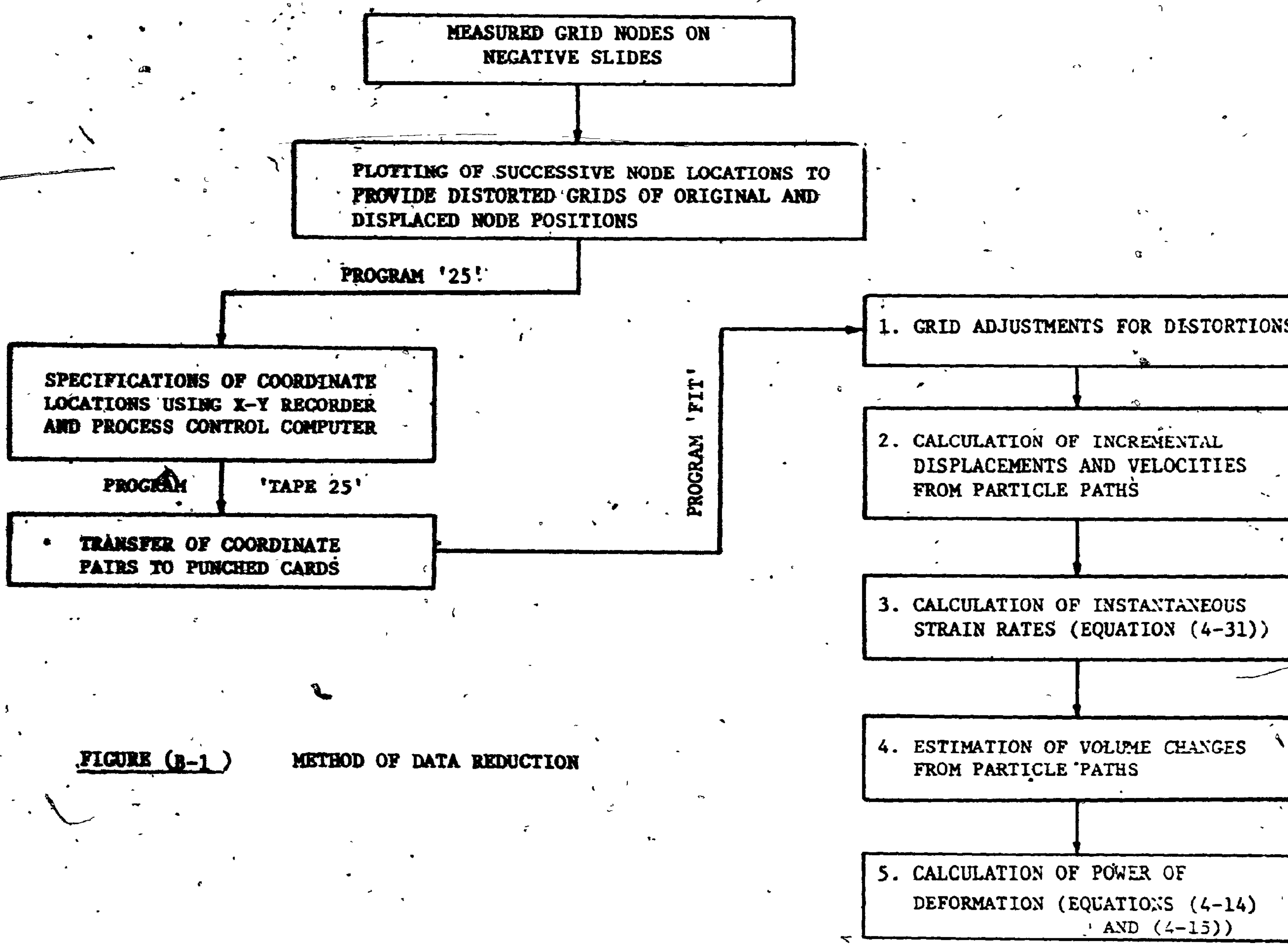

FIGURE (B-1) METHOD OF DATA REDUCTION

as the points of intersection of the horizontal and vertical lines. The plotted field for each image consisted of a network of ten horizontal points spaced at one inch intervals by 14 vertical points spaced at one-half inch intervals. This resulted in a rectangular network having a size of nine inches by six and one-half inches with the top lefthand-side point taken as the closest node to the point of tool intersection with the original soil surface. As pointed out earlier, five image positions were recorded, representing respectively the initial position plus four subsequent positions at 0.25, 0.50, 0.75 and 1.0 inch tool displacement. These five images were then superposed on each other to provide a detailed description of the nodal displacement trajectories over a tool horizontal displacement of 1.0 inch.

B.2 TRANSFER OF GRID COORDINATE LOCATIONS TO PROCESS CONTROL COMPUTER

The plotted grid images were placed on a Moseley Autograph Model 2D-2AM-X-Y recorder which was connected to a Canadian General Electric Process Control Computer, model GEPAC 4020. The plotted images paper was fixed in position on the X-Y recorder and the carriage needle moved manually, by adjusting two potentiometers to each node location. The grid points were then plotted row by row, image by image. The voltages corresponding to the horizontal and vertical coordinates of each location were input to an integrating digital voltmeter which fed into the computer logic circuits. By means of programme [25] shown in Appendix E, the input voltages produced by the X-Y recorder were converted into coordinate values [X and Y] in centimeters. The resulting coordinate values were then temporarily stored on a magnetic disc, from which they were transferred to an IBM Magnetic Tape at the end of each test plot. The coordinate values stored on the magnetic tape were then transferred to punched cards by means of programme "TAPE 25" shown in Appendix E.

B.3 GRID ADJUSTMENTS

As can be seen from Fig. 4-16, the undeformed grid is usually in a slightly distorted state. The distortion is due in part to the manual grid placing technique and soil heterogeneity, but it is mainly caused by the preparation and manipulation of the clay sample after the grid is placed. In order to ensure a regular interval between adjacent grid nodes which greatly facilitates the calculation of velocity and strain rate components, the initial undeformed and subsequently deformed plotted grids were subjected to approximate geometrical adjustments shown in Fig. B-2. The method adopted by Windisch (1969) consists of the specification of arbitrarily defined grid coordinates to provide an adjusted undeformed grid of regular horizontal and vertical lines. This new network corresponds as closely as possible to the initial undeformed grid. Utilizing the following notation, the procedure is detailed below.

XI, YI = original undeformed coordinates

XIA, YIA = adjusted undeformed coordinates

XX, YY = original deformed coordinates

XXA, YYA = adjusted deformed coordinates

The adjustment to the abscissa of an undeformed grid point [I, J] is given as:

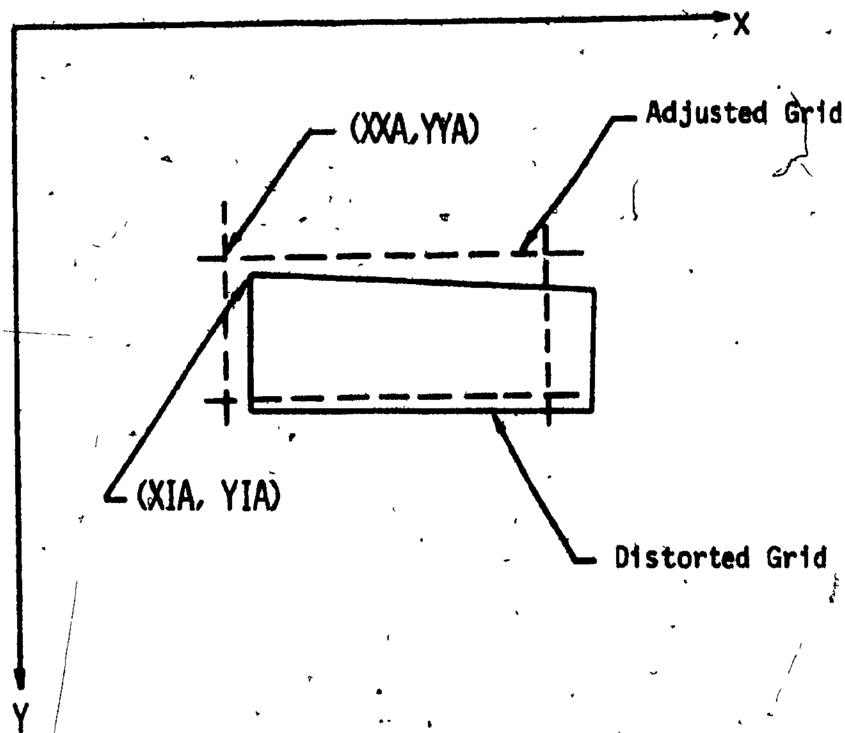

FIGURE B-2 GRID ADJUSTMENT

$$D_1 = XIA(I,J) - XI(I,J)$$

This value is then applied as a first adjustment to the corresponding grid point abscissa. The rate of adjustment along row J is:

$$C_1 = \left| \frac{XIA\ (I+1,J) + XI\ (I,J) - XIA\ (I,J) - XI\ (I+1,J)}{XI\ (I+1,\ J) - XI\ (I,J)} \right|$$

If the constant, C_1, is regarded as being a gradient along row J between adjacent points, a second adjustment can be made to the abscissa of the deformed grid point, viz:

$$D_2 = [XX\ (I,J,JS) - XI\ (I,J)]\ C_1$$

Here JS represents the image at 0.25, 0.50, 0.75 and 1.0 inch tool displacement, and corresponds to the indices two, three, four and five.

The adjustment of any given grid point will, by necessity, depend on the location of adjacent undeformed grid points in the following row. Hence, the rate of adjustment of the abscissa along row J+1 can be expressed as:

$$C_2 = \frac{XIA\ (I+1,\ J+1) - XI\ (I+1,\ J+1) - XIA\ (I,J+1) + XI\ (I,J+1)}{XI\ (I+1,\ J+1) - XI\ (I,\ J+1)}$$

From this, a further adjustment is made to the deformed coordinate, of magnitude:

$$D_2^1 = [XX\ (I,\ J+1,\ JS) - XI\ (I,\ J+1)]\ C_2$$

A third correction is the result of adjustments in the ordinate direction of the grid point, viz:

$$D_3 = (D_2^1 - D_1)\ \frac{YY\ (I,\ J,\ JS) - YI\ (I,\ J)}{YI\ (I,\ J+1) - YI\ (I,\ J)}$$

The final adjusted abscissa value of the deformed grid point (I,J,JS) is then given as:

$$XXA\ (I,J,JS) = XX\ (I,J,JS) + D_1 + D_2 + D_3 \qquad \text{(B-1)}$$

Similar adjustments are performed on the plotted ordinate values of the grid nodes.

The above calculations, given by Eq. (B-1) and by an analogous equation for the ordinate values, are performed by the first part of the Computer programme "FIT" given in Appendix E. It should be noted that in this computer routine, the following substitutions of symbols are made:

$$XI\ (I,J) = XX\ (I,J,1)$$

$$YI\ (I,J) = YY\ (I,J,1)$$

$$XIA\ (I,J) = XXA\ (I,J,1)$$

$$YIA\ (I,J) = YYA\ (I,J,1)$$

B.4 VELOCITY CALCULATIONS

The particle valocities, over successive grid positions, were calculated on the basis of the time rate of change of the particle position in the coordinate directions. The velocity components are given as:

$$U_{IJK} = \frac{XXA\ (I,J,\ k+1) - XXA\ (I,J,k)}{TT}$$

$$V_{IJK} = \frac{YYA\ (I,J,\ k+1) - YYA\ (I,J,k)}{TT} \qquad \text{(B-2)}$$

where

I,J = column and row indices, respectively

XXA, YYA = adjusted coordinates

k = image number

U,V = velocity components in the x- and y- coordinate directions, respectively

TT = time interval between successive images.

B.5 STRAIN RATE COMPONENTS

The strain rate components were calculated by the application of Eq. (4-4) repeated as:

$$\dot{\varepsilon}_x = \frac{\partial u}{\partial x}$$

$$\dot{\varepsilon}_y = \frac{\partial v}{\partial y} \qquad \text{(B-3)}$$

$$\dot{\varepsilon}_{xy} = \tfrac{1}{2}\left(\frac{\partial u}{\partial y} + \frac{\partial v}{\partial x}\right)$$

However, in the actual calculation, carried out by the digital programme "FIT" shown in Appendix E, the strain rate components were determined to be the average value of the quantities calculated for adjacent rows or columns. Thus, Eqs. (B-3) are written as:

$$(\dot{\varepsilon}_x)_{XN,YN} = \frac{\frac{1}{2}\,U\,(I+1,\,J,k) - U\,(I,J,k)}{XXA\,(I+1,J,k) - XXA\,(I,J,k)} + \qquad \text{(B-4)}$$

$$\frac{\frac{1}{2}\,U\,(I+1,J+1,\,k) - U\,(I,\,J+1,\,k)}{XXA\,(I+1,\,J+1,k) - XXA\,(I,J+1,k)}$$

where

$(\dot{\varepsilon}_x)_{XN,YN}$ = $\dot{\varepsilon}_x$ at the point (XN,YN) located at the center of area of the quadrilateral formed by the points (I,J,k), (I+1,J,k), (I+1, J+1, k) and (I, J+1, k).

I,J = column and row numbers, respectively

k = image number

U = particle velocity in the x-direction

XXA = adjusted abscissa value of particle coordinates

Similar equations were used to determine the values of the other strain rate components.

The effective strain rate $\bar{\dot{\varepsilon}}$ was obtained from the calculated strain rate components, viz:

$$\bar{\dot{\varepsilon}} = \frac{2}{3}\left[(\dot{\varepsilon}_x)^2 + (\dot{\varepsilon}_y)^2 - \dot{\varepsilon}_x\dot{\varepsilon}_y + \frac{3}{4}(\dot{\gamma}_{xy})^2\right]^{\frac{1}{2}} \qquad \text{(B.5)}$$

B.6 VOLUME CHANGE CALCULATIONS

The method by which the permanent volume changes were estimated has been described in detail in Section 4.B.3. The results of these calculations, performed by programme "FIT" in Appendix E, have been presented as Table 4-3. In summary, however, the method makes use of the principle of the conservation of mass [Fung (1965)], applied to the elemental areas within the deforming field. If reference is made to Fig. B-3, it will be seen that the application of this principle results in:

$$\rho_1 A_1 = \rho_2 A_2 = \rho_3 A_3$$

for plane strain deformation. These equations may be rewritten as:

$$\frac{\rho_i}{\rho_j} = \frac{A_j}{A_i} \qquad \text{(B.6)}$$

where

ρ_i = mass density or specific mass of the ith elemental area.

A_i = area of the ith element.

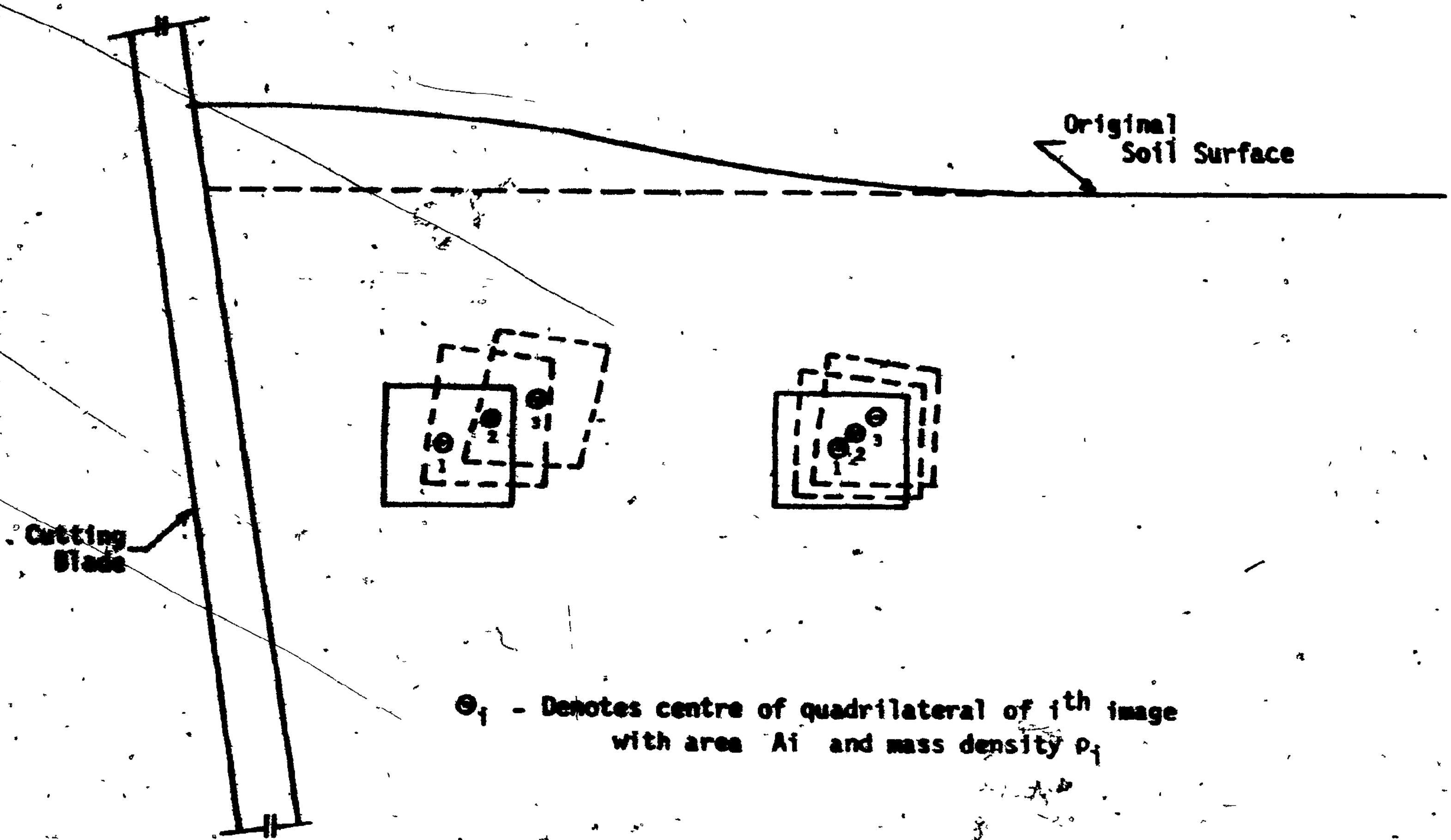

FIGURE B-3 CALCULATION OF DENSITIES AT SUCCESSIVE IMAGE POSITIONS FOR A CUTTING BLADE

Machine computation of the areas, carried out by programme "FIT", permitted a comparison of the mass densities of the deforming soil through successive grid positions. Estimates of the volume changes were thus obtained.

B.7 CALCULATION OF POWER OF DEFORMATION AND TOTAL DEFORMATION ENERGY

The power of deformation at the coordinate location [XN, YN] is obtained from the application of Eq. (4.16) repeated as:

$$\dot{W} = 2k\sqrt{I_2}$$

to form the product:

$$PD = \dot{W} \times A \tag{B.7}$$

where

PD = power of deformation at coordinate location [XN,YN].

A = area of quadrilateral surrounding the point [XN,YN].

$k^2 = J_2$ = second invariant of the stress deviation.

I_2 = second invariant of the strain rate tensor.

The summation of the values of PD calculated at the various points given by [XN, YN], is carried out by means of Simpson's rule [Hildebrand (1965)] to yield the total energy dissipated in the plastic deformation of the soil.

APPENDIX C

REVIEW OF PREVIOUS WORK

A. INVESTIGATIONS ON SOIL CUTTING

During the early part of the century [1918 to 1939], researchers in the United Kingdom and the U.S.A. apparently confined their work to the investigation of the draft of tillage implements. They could not, however, isolate the relevant soil parameters from their work because of the very large number of inter-related factors considered. For example, "no clear distinction was made between a directly involved soil property like cohesion and a characteristic such as colloidal content, which is only relevant insofar as it affects cohesion" [Hettiaratchi (1965)]. Consequently, it was impossible for them to conclude that a theoretical analysis in terms of classical soil mechanics was possible.

An important and noticeable feature of all recent work in the field of soil cutting is the application of the theories of classical soil mechanics to greatly simplified soil working tools. It was felt by most researchers that once these problems were understood, it would not be unreasonable to extend the study to more complex and realistic problems.

Basically, the foundation of this work was laid by Coulomb, and the following factors were involved:

a) Soil parameters such as cohesion, internal friction, density.

b) Soil-metal properties such as soil-metal friction and adhesion.

c) Assumptions that the soil was rigid and incompressible. Forces were evaluated by studying the static equilibrium of an assumed failure surface which was chosen to satisfy the limiting stress condition of a Coulomb material.

Payne (1956) first confined his investigations to vertical tines. He classified narrow tines as those having a shape factor [depth/width ratio] greater than unity, and blades as those with shape factors less than 0.5. Although he analyzed the forces of his proposed complicated failure pattern in front of a narrow tine, he did not produce a solution in a readily usable form. Furthermore, the very complicated expression he derived for the force on the tine was for an arbitrary failure surface; also such an expression "has to be further subjected to trial computations required in a minimizing process for conformity with the requirements of a minimum value postulate before the final value is obtained." [Hettiaratchi (1965)]. Payne's work was later extended by Payne and Tanner (1959), and by Tanner (1960) to cover the behavior of narrow tines over a wide range of rake angles. Experimental observations were in good agreement with the complex failure shape proposed by Payne.

Osman (1964) analyzed very thoroughly the wide blade cutting problem. In his investigations, Osman used wide blades with varying rake angles. By using wide blades, he simplified the stress-field to a simple two-dimensional one, and his experimental work was carried out on dry sand, stiff clay, and a C-ϕ type of soil. He attempted to check two theories for passive pressure:

a) Coulomb's solution for a granular material, and

b) Ode's logarithmic spiral method.

He concluded that Coulomb's wedge solution was only good for smooth blades of small rake angles working in cohesionless soils, and showed that Ohde's solution could accurately predict the forces required to cut a wide range of soils.

It has been pointed out by Osman that the usefulness of his analysis is limited, in that it is a function of a large number of variables and it is necessary to have access to a computer to solve for each individual case. With a view to overcoming this difficulty, Osman made use of dimensional analysis and was able to write the following equation:

$$D/_{\gamma z^2} = f\left(\frac{c}{\gamma z}, \delta, \phi, \frac{Ca}{\gamma z}, \alpha, h/_z\right)$$

where

$D/_{\gamma z^2}$ = ratio of draft to gravity forces

$C/_{\gamma z}$ = ratio of cohesive to gravity forces

δ = soil to metal frictional angle

ϕ = angle of internal friction

$\frac{Ca}{\gamma z}$ = ratio of adhesive to gravity forces

α = rake angle, degrees

h = height of surcharge, inches, and

z = blade depth, inches.

α and $h/_z$ describe the geometry of the blade and the surcharge.

Osman presented charts that would enable the calculation of draft forces to be made for a range of soil types of practical interest.

Siemens and his colleagues (1964) conducted similar investigations but with fewer experimental variables, and they used a combination of Ode's retaining wall theory and a "free body" theory to compute theoretical loads on the blade. There was, however, poor agreement between predicted and experimental observations, the former being higher in value than the latter. This seemed to cast doubt on the validity of the Ohde logarithmic spiral solution. Subsequent measurements of soil parameters revealed that too high a value of cohesion had been used in the original computation. Predicted forces utilizing the revised value for cohesion showed good agreement with experimental results.

Selig and Nelson (1964) conducted qualitative investigations into the mode of failure of three types of soil under the action of flat blades, and, generally, their observations supported the idea that the failure geometry was in accordance with the postulated logarithmic spiral solution for retaining walls.

Reece (1965) proposed that the cutting force acting on a blade could be expressed by means of the following equation:

$$D = \gamma z^2 N_\gamma + CzN_c + C_a ZN_\alpha + qzN_q$$

where

D = cutting force per unit width of blade and N_γ, N_c, N_a, N_q are dimensionless numbers representing the boundary conditions of the failure surface and functions of ϕ, δ, blade geometry and failure boundary.

q' = the weight of the uniformly distributed surcharge due to piled-up soil.

Reece's equation is not only simple but it also applies to the computation of the force required to produce failure of the soil beneath any form of loading structure with a two-dimensional failure pattern.

However, as pointed out by Hettiaratchi (1965), this equation is not absolutely correct. Hettiaratchi et al. (1966) computed the four N factors for a complete range of values of ϕ for the two extreme values of wall friction δ, that is, $\delta = 0$ and $\delta = \phi$, for values of rake angle varying from $(45° - \phi/_2)$ to $(135° - \phi/_2)$. They also produced suitable interpolation formulae and graphs showing the rupture distance as a function of the soil and blade variables.

O'Callaghan and Farrelly (1964) derived a simplified expression for the draft per unit width on the basis that two distinct regimes of deformation occur in vertical and horizontal planes. This expression appeared to give good correlation for cohesive soils but failed in cohesionless soils.

Hettiaratchi and Reece (1967) attempted to provide a useful solution which would enable certain symmetrical three-dimensional soil failure problems to be analyzed rapidly by the use of charts describing the failure geometry, together with some simple trigonometrical factors.

Certain simplifying assumptions were made and their limitations pointed out. However, more experimental support was needed as pointed out by the authors.

Elijah and Weber (1968) conducted experiments using model and full-scale flat blades in artificial and field soils to determine the soil failure patterns and the distribution of normal and tangential pressures on the blade surface. These blades were designed so that the cutting edges were separated from the blade surface. In this work, four distinct failure patterns were identified. They were designated as "shear plane", "flow", "bending" and "tensile" failures. Elijah and Weber pointed out that there was a need for definition of new soil parameters in order to predict when these patterns will occur and what tool forces are involved. They found that the pressure distribution on the blade surface varied with the location on the blade and with the type of soil. Reasonably good agreement was obtained when the pressures were integrated and used to predict the total cutting force acting on the blade for the various soils.

Reece (1969) pointed out that while the methods of classical soil mechanics can solve the problem of wide cutting blade, time has come to make use of the theory of plasticity, with a proper description of the relation between stress and strain, in developing soil machine mechanics.

Wismer and Forth (1969) and Wismer and Luth (1970) derived prediction equations for the draft and vertical forces on blades operating in both sand and saturated clay. These equations were developed by application of dimensional analysis and nonlinear curve fitting to experimental results for a wide range of blade sizes, angles, and operating speeds. In these experiments cone penetrometer measurements were made to determine the properties of the soil, and the soil strength was expressed in terms of the cone index of a standard cone instead of the more conventional terms of cohesion and angle of internal friction. For this reason, no quantitative comparisons with other investigations can be made since the relationship between the cone index and the conventional strength parameters depends on the soil type.

Yong et al. (1969) and Yong and Chen (1970) employed the principle of limit equilibrium where the stability of the soil mass is controlled or affected by the moving blade. The development of the solution technique was based on the following assumptions:

1] The stressed soil in front of the blade is divided into two regions: Region I being the radial shear zone and Region II the simple passive Rankine zone, Fig. 2-2-A.

2] The soil mass is incompressible and is assumed to obey the Mohr-Coulomb yield function.

With the use of a similarity solution technique, the equations of equilibrium, and the Mohr-Coulomb yield condition, they were able to predict the forces on cutting blades in both cohesionless and C-ϕ soils.

Yong and Chen (1970) showed that for conditions where limit equilibrium in the soil is approached, and for the purposes of predicting first failure in the soil under the action of a moving blade, the analytical technique developed, utilizing the method of characteristics for solution, gave a good correspondence between computed and measured values. Moreover, comparisons with reported values from other studies showed the applicability of the method to the solution of the problem.

B. INVESTIGATIONS ON SOIL-GROUSER INTERACTION

The first systematic attempt to provide a basis from which reliable predictions of vehicle behavior could be made was carried out by Micklethwait (1944). Based on his experimental work, Micklethwait proposed an equation expressing the maximum tractive effort of a tracked vehicle in cohesive soils of the form:

$$H = blc + W \tan \phi$$

where

H = gross tractive effort in lb

b = track width in inches

l = track length in inches

c = cohesion in psi

W = vehicle weight in lb

This equation is very rarely used at the present time, but was the basis of vehicular design until Bekker (1956, 1960) examined the problem of soil-grouser interaction from a theoretical point of view. Bekker considered that Micklethwait's equation was incomplete in that several parameters were not taken into account. As a result, a pair of equations were proposed, the first of which described the horizontal thrust developed by a grouser in terms of track geometry, vehicular weight and the rate of slip. This equation was developed for use with the conventional linked track, where a condition referred to as "grip failure" results, Fig. C-1. This condition occurs at very high values of the ratio of horizontal to vertical forces ($H/_W$) and rupture occurs along interface ab with the forces acting as shown. The relationship between H and W for this case is given as:

$$H = W\frac{h + S\tan\phi}{S - h\tan\phi} + \frac{C(h^2 + S^2)}{S - h\tan\phi} \qquad \text{(C-1)}$$

The second of these equations was applicable to a spaced link track, a system which is analogous to a series of isolated grousers moving through a soil. The condition of failure in this case was referred to as "ground failure". This equation expressed the horizontal thrust in terms of the grouser geometry and soil parameters, and was based on the assumption that the grouser plate could be approximated by a strip footing inclined to the horizontal at an angle given by:

$$\theta = \text{arc tan } (H/_W)$$

where

H = horizontal thrust developed by grouser

W = applied vertical load

As a consequence of this assumption, the development of the equation follows the methods proposed by Terzaghi (1944) in that dimensionless constants analogous to bearing capacity factors were used. The equations and the force diagram have already been given in Chapter 1 as Eqs. (1.1) and (1.2) and Fig. 1-2 respectively, and were examined in Section 7-4 . The resultant force $2P_p$, Fig. 1-2, is given by Bekker as:

$$2P_p = b(n_c l_c + \gamma n_q l z + \gamma n_\gamma l^2) \qquad \text{(C-2)}$$

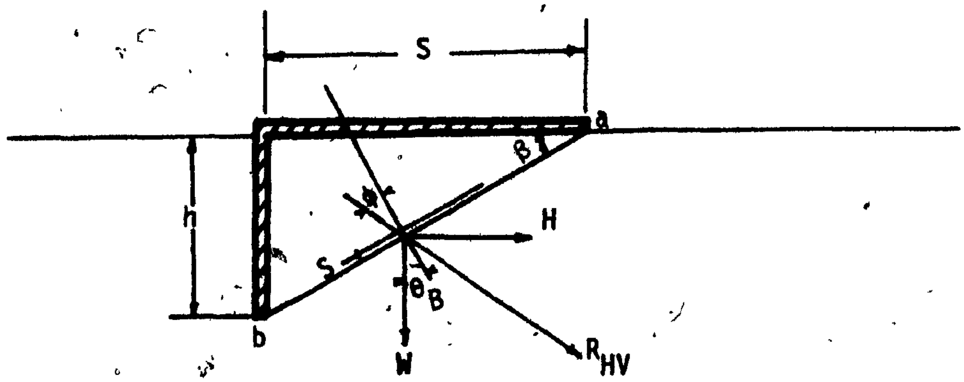

FIGURE C-1 FORCE DIAGRAM OF THE GRIP FAILURE

[After BEKKER (1960)]

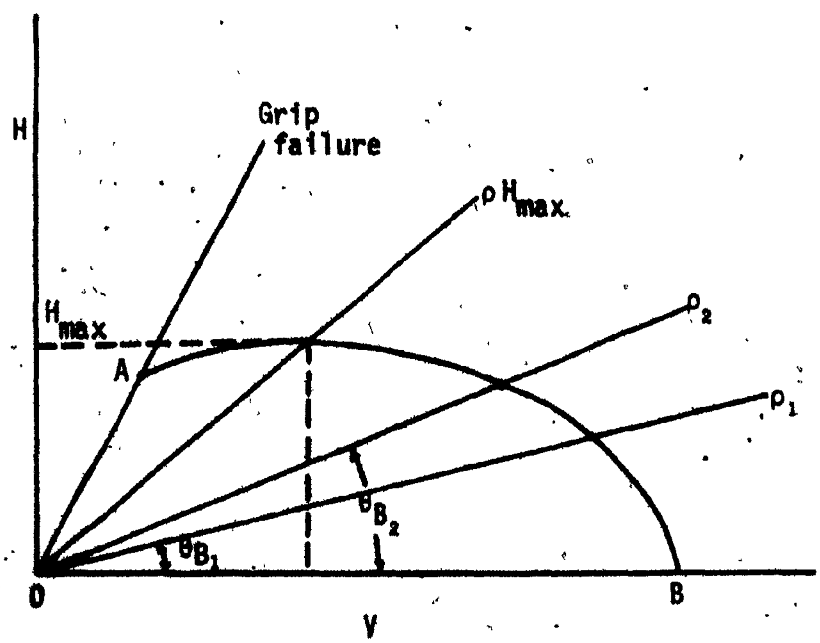

FIGURE C-2 BEKKER TRAFFICABILITY CURVE

[After BEKKER (1960)]

Equation (C-2) is used to plot a trafficability curve, Fig. C-2. The curve from point A to point B is generated by plotting polar coordinates of $2P_p$ at θ over cartesian coordinates of H and W. Point A is determined by the intersection of Eqs. (C-1) and (C-2), and point B is the ultimate bearing capacity under vertical load. From the trafficability curve one may obtain the optimum values of W and H for any given W/H ratio and for the plate grouser and soil strength parameters used.

Harrison (1973) pointed out two main objections to the approach proposed by Bekker. The failure pattern chosen is not compatible with the properties of a rigid Coulomb material, and the forces assumed to act on planes within the pattern are not reasonable. Nevertheless, the investigations carried out by Bekker represent an ambitious attempt to supply solutions to some of the problems associated with the soil-vehicle interaction process. Unfortunately, there appears to be a lack of firm experimental support of these theories reported in the readily accessible literature.

Haythornthwaite (1961) considered the problem of a grouser being driven through a soil possessing both cohesion and friction. In his analysis, Haythornthwaite utilized the methods of limit plasticity developed by Drucker and Prager (1952). With the assumptions of:

a) a soil possessing both cohesion and friction,

b) the Coulomb yield criterion,

$$\tau = C + \sigma \tan \phi$$

describing the stress conditions at failure, and

c) a weightless, perfectly plastic model for the soil, a statically admissible stress distribution was postulated by means of which a lower bound solution was obtained. An upper bound solution was then inferred by calculating the dissipated energy along an assumed failure surface. Examples of upper and lower bound conditions as described by Haythornthwaite are shown in Figs. C-3a and C-3b respectively. A numerical solution to these assumed conditions is shown in Fig. 3-3c. In this approach through sophisication of the stress and flow pattern, the lower bound is maximized and the upper bound is minimized until the curves shown in Fig. C-3c coincide. A more sophisticated upper bound model chosen by Haythornthwaite is presented in Fig. C-3d.

The solutions arrived at by Haythornthwaite are severely restrictive. The calculation of the dissipation energy function for the upper bound was based on the failure hypothesis proposed by Drucker and Prager (1952) and is only valid for a material possessing cohesion. For a non-cohesive material, the dissipation energy and hence the upper bound is zero. In addition, as a consequence of the assumption of a perfectly plastic material, the solution will only be valid for soils which possess a very small angle of internal friction, ϕ, since . . . "a material is only plastic to the extent that it is not frictional." [Drucker (1961)].

A main objection to the application of the limit analysis theorems as stated by Harrison (1973) is "The degree of probability that the two bounds can be made to coincide within a reasonable number of assumed flow and stress options. The intuition required to cause the upper and lower bound solutions to converge would conceivably require a considerable number of solutions or a knowledge of the stress-strain

$$P^U/C = \frac{h \cos \phi}{\cos^2(\pi/4 + \phi/2 + \alpha/2)}$$

$$P^L/C = 2L \sin \alpha \tan(\pi/4 + \phi/2)$$

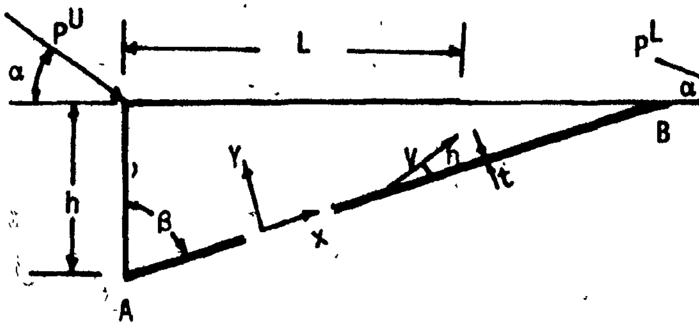

(A) FIRST UPPER BOUND FLOW PATTERN

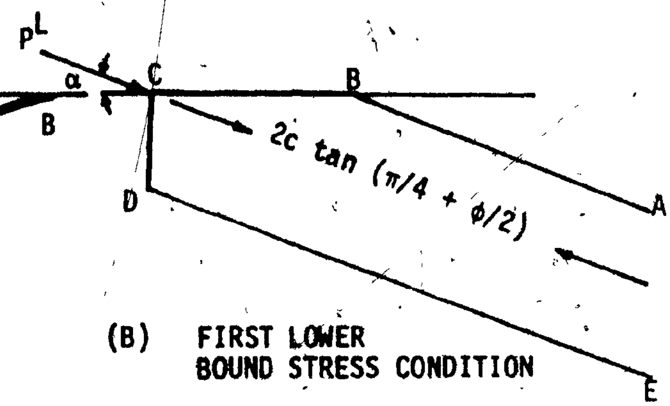

(B) FIRST LOWER BOUND STRESS CONDITION

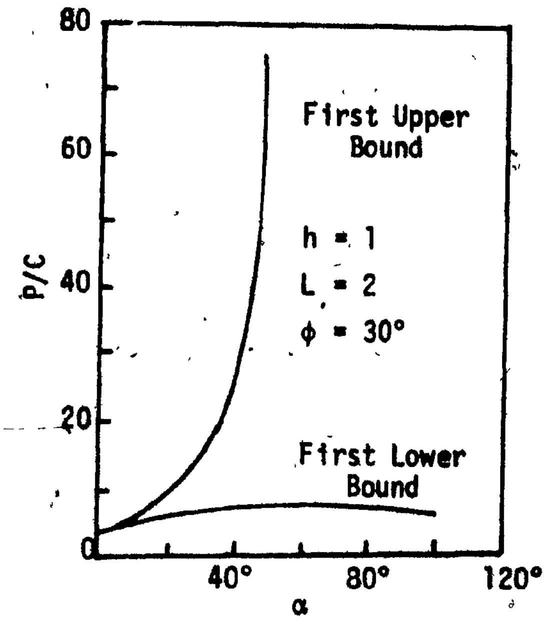

(C) NUMERICAL SOLUTION OF FIRST UPPER AND LOWER BOUND EXAMPLES

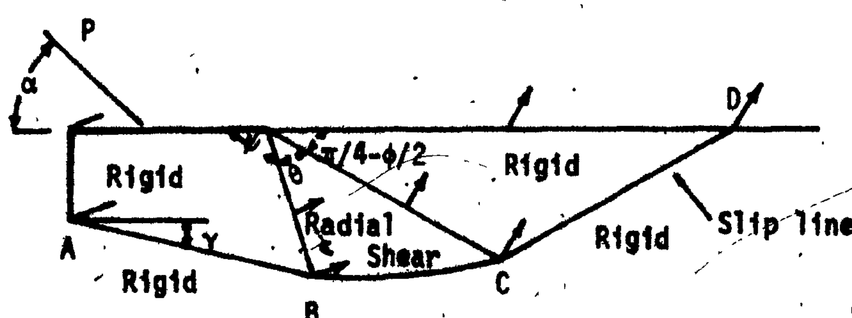

(D) UPPER BOUND FLOW PATTERN

FIGURE C-3

[After HAYTHORNTHWAITE (1961)]

behavior of soils uncommon to the ordinary researcher."

The limit equilibrium approach has been successfully used by Yong and Sylvestre-Williams (1969). The analytical model adopted is shown in Fig. C-4. The following assumptions were made:

1] Admissibility of the Mohr-Coulomb failure criteria.

2] Rigidity of block ABCD.

3] Full failure development in the entire mass defined by zone CDE.

4] Insignificant volume change in zone ABCED.

In analyzing such a model, a similar approach to that of Yong et al. (1969) and Yong and Chen (1970), [a similarity solution technique together with the method of characteristics] was followed. Integration of the stresses over the length of CD [Fig. C-4] provided the forces on the grouser. Confirmation between analytical model prediction and physical performance was obtained, for grousers moving at controlled depth or under constant vertical loads in sand, by:

a) matching physical failure surface due to grouser action with theoretically computed failure characteristic, and

b) matching computed forces with physical values.

Comparing their results with those computed from Bekker's equations [e.g. Eq. (1.1) and (1.2) in Chapter 1] showed little agreement.

Harrison (1973), on consideration of the discrepancies between experimentally observed slip line fields and those predicted by the theory, came to the conclusion that these discrepancies were, to a large extent, due to the existence of a wedge-shaped zone of soil fixed to the interface,

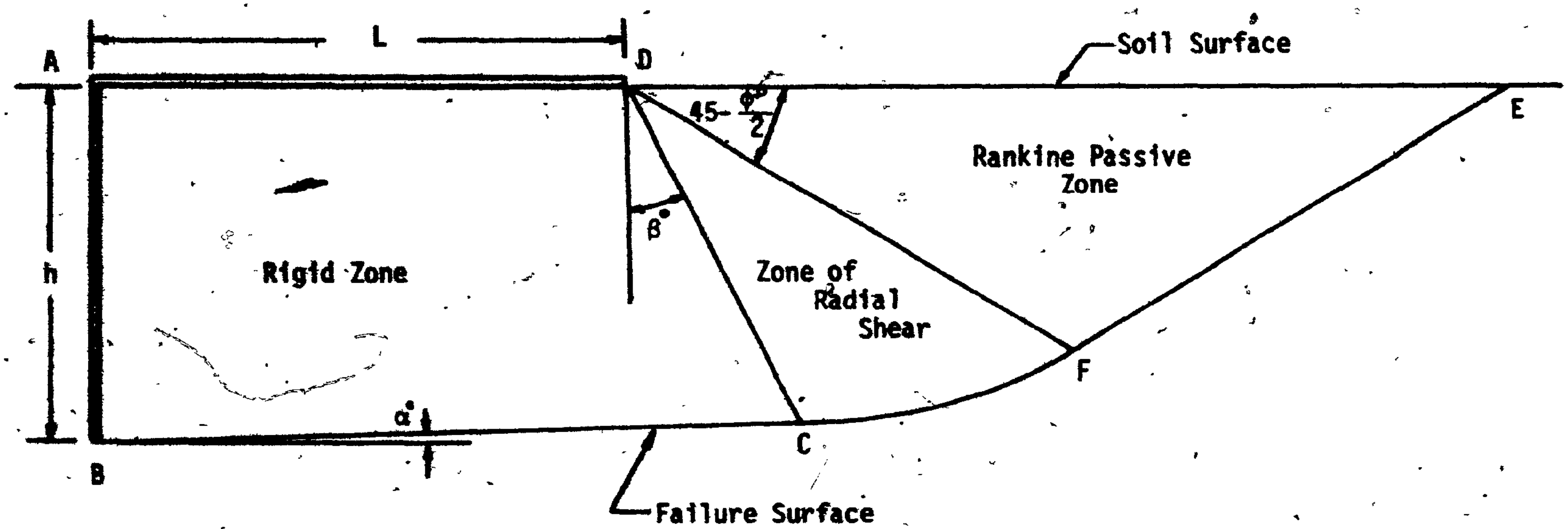

FIGURE C-4 ANALYTICAL MODEL ADOPTED BY YONG AND SYLVESTRE-WILLIAMS (1969) FOR SOIL-GROUSER PROBLEM forming a pseudo-interface along which actual failure occurs. He postulated that the interface shear zone transformed itself into a wedge if the direction of motion of the lower edge of the interface was at a smaller angle to the horizontal than the slip line at that point. Considering Fig. C-5a, a wedge will form if the interface is driven forward at an angle smaller than θ_c, where $\theta_c = 90 + \phi - \beta$, Fig. C-5b; otherwise the normal slip line will apply.

Having made this postulate, Harrison analyzed the plate-grouser problem using a combination of Ohde's retaining wall theory and a "free body" theory to compute the loads on the grouser. The mathematical solution is based on the relationship between the horizontal force H, the vertical force V, and the direction of plate-grouser movement θ, for a given set of soil strength parameters, and a given plate-grouser configuration. The solution requires that either V or θ be known. The horizontal and vertical forces are given by Harrison as:

$$
\begin{aligned}
H &= \tfrac{1}{2}\gamma S^2 k_\gamma \sin(\beta-\Delta) + CS[k_c \sin(\beta-\Delta) + \tan\Delta \cot\phi] \\
V &= \tfrac{1}{2}\gamma S^2 [k_\gamma \cos(\beta-\Delta) - \tan\beta] + CS[k_c \cos(\beta-\Delta) \\
&\quad - \tan\beta \tan\Delta \cot\phi]
\end{aligned}
\qquad \text{(C-3)}
$$

where

$$
k_\gamma = \frac{\sin^2(\beta+\theta)}{\cos^2\beta \sin(\beta+\theta-\phi-\Delta)} \left\{ \frac{1}{8\sin^2\phi + 1} \left| e^{3\omega \tan\phi} \left(\frac{2\sin\phi(1+2\sin\phi)}{\cos\psi}\right) + 3\tan\phi \sin(\theta-\phi) + \cos(\theta-\phi) \right| - \frac{\sin(\theta-\phi)\cos(\beta+\theta-\phi)}{\sin(\beta+\theta)\cos\phi} \right\}
$$

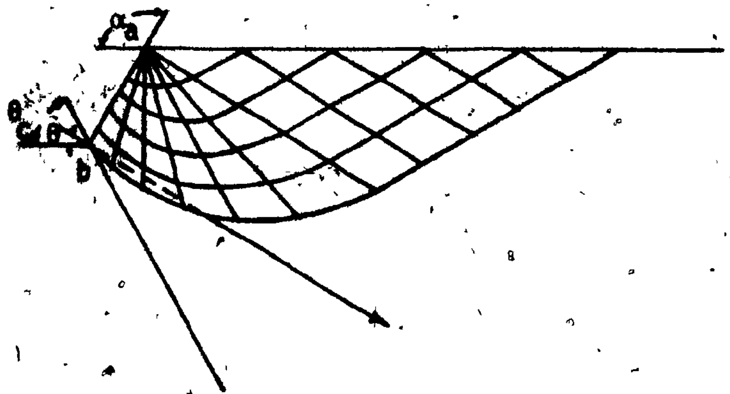

(A)

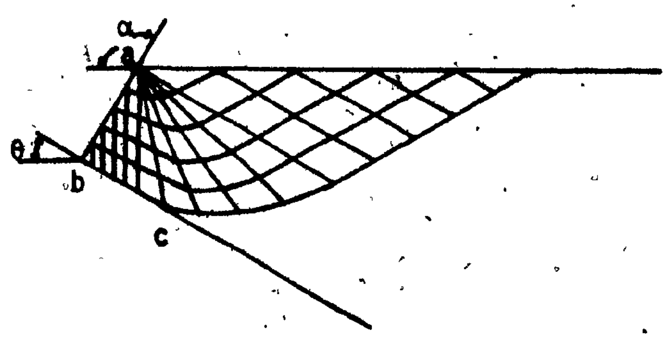

(B)

FIGURE C-5A CONDITIONS OF WEDGE FORMATION

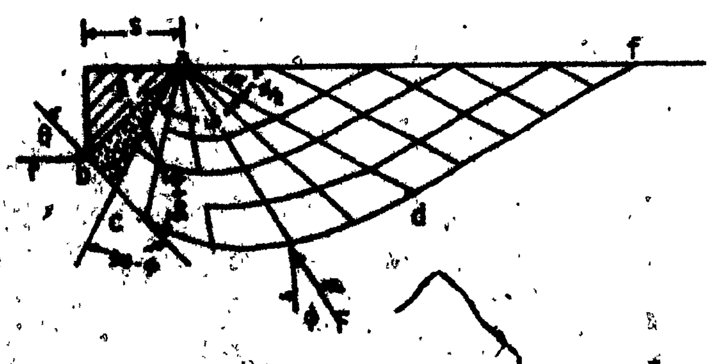

(C)

FIGURE C-5B SOIL WEDGE AND SLIPLINE FIELD
WHEN $\theta_c > \theta > -\alpha > -\beta$

[After HARRISON (1973)]

$$k_c = \frac{1}{\cos\beta \sin(\beta+\theta-\phi-\Delta)} \left\{ \left| \frac{e^{2\omega \tan\phi}-1}{\sin\phi} + e^{2\omega\tan\phi} \right| \right.$$

$$\left. \sin(\beta+\theta) + \cos(\beta+\theta-\phi)[1 + \cot\phi \tan\Delta] \right\}$$

$$\Delta = \text{arc tan} \frac{\sin\theta^1 \sin\phi}{1 + \cos\theta^1 \sin\phi}$$

$$\theta^1 = 2(\beta+\theta) - (90+\phi)$$

$$\omega = \epsilon+\theta = 45-\phi/2+\theta$$

= angle between specified radii of log spiral

ψ = angle $45+\phi/2$ degrees

β = characteristic angle of a plate-grouser [degrees], Fig. C-5c.

θ = instantaneous direction of plate-grouser movement with the horizontal at soil failure [degrees]

S = plate length in inches

γ = soil bulk density, lb/in^3.

C = apparent cohesion, psi

ϕ = angle of soil shearing resistance [degrees].

Harrison conducted experiments on quite large grousers driven into a saturated clay, a dry sand and an intermediate loam. The experimental observations verified the postulated slip line fields. Moreover, there was fairly good agreement between the predicted forces and the experimentally measured ones, with the exception of the case of a horizontally moving grouser [i.e. $\theta = 0$] driven in loam and clay where the difference between the predicted and the measured values was very significant.

Investigating the problem of traction from a macroscopic point of view, a great deal of work has been done in recent years by the U.S. Army at the Waterways Experimental Station in Vicksburg and at the OTAC at the Detroit arsenal. Studies on the trafficability of soils by both wheeled and tracked vehicles have been carried out by W.E.S., and a great deal of work has been done on the problem of soil wheel interaction. In the course of their research, W.E.S. have proposed formulae for the determination of a dimensionless Mobility Index based on the determination of the cone penetration resistance of the soil in question. The Mobility Index is an indication of the ability of the soil to allow fifty passes of the vehicle under consideration without that vehicle being stuck. Some attempts at correlating the theories proposed by Bekker and the trafficability theories proposed by W.E.S. have been made by trafficability research teams of the Israeli Army [trafficability research team 1961] while Seia (1961) has provided a theoretical solution to Bekker's tractive effort-slip relationship.

It must be pointed out that most of the research done to date on the tracked vehicle-soil interaction problem has been oriented towards the provision of "go/no-go" criteria for given vehicles in given soils. As warranted as this may be, it is still necessary to understand the fundamental interaction process, and it is precisely in this area that there appears to be a great lack of experimemtal or theoretical research effort. In addition, reviewing the available literature it is evident that very little work has been done in investigating the interaction of grousers other than that of the plate-grouser with soil. As the problem of traction is related to the interaction of stress between the ground and the loading area, and the motion resistance depends on the relation between stresses and strains, studies of the effect of grouser geometries on the loaded soil may lead to a grouser shape that produces a rather significant improvement in traction.

APPENDIX D

SOLUTION OF LINEAR EQUATIONS BY DIRECT GAUSSIAN ELIMINATION METHOD

The equilibrium equations for a continuum system may be written in the following form:

$$A_{11}X_1 + A_{12}X_2 + A_{13}X_3 + \ldots\ldots\ldots + A_{1N}X_N = B_1 \qquad \text{(D-1a)}$$

$$A_{21}X_1 + A_{22}X_2 + A_{23}X_3 + \ldots\ldots\ldots + A_{2N}X_N = B_2 \qquad \text{(D-1b)}$$

$$A_{31}X_1 + A_{32}X_2 + A_{33}X_3 + \ldots\ldots\ldots + A_{3N}X_N = B_3 \qquad \text{(D-1c)}$$

$$\ldots\ldots\ldots\ldots\ldots\ldots\ldots\ldots\ldots\ldots\ldots\ldots$$

$$A_{N1}X_1 + A_{N2}X_2 + A_{N3}X_3 + \ldots\ldots + A_{NN}X_N = B_N \qquad (\ldots\ldots)$$

or symbolically:

$$[A][X] = [B] \qquad \text{(D-1)}$$

where

[A] = the stiffness matrix

[X] = the unknown displacements

[B] = the applied loads.

GAUSSIAN ELIMINATION METHOD

The first step in the solution of the above set of equations is to solve Eq. (D-1a) for X_1, or

$$X_1 = B_1/A_{11} - (A_{12}/A_{11})X_2 - (A_{13}/A_{11})X_3 \ldots\ldots(A_{1N}/A_{11})X_N \qquad \text{(D-2)}$$

If Eq. (D-2) is substituted into Eqs. (D-1b, c, . . . N) a modified set of N-1 equations is determined.

$$A^1_{22}X_2 + A^1_{23}X_3 + \ldots\ldots\ldots\ldots + A^1_{2N}X_N = B^1_2 \qquad \text{(D-3a)}$$

$$A^1_{32}X_2 + A^1_{33}X_3 + \ldots\ldots\ldots\ldots + A^1_{3N}X_N = B^1_3 \qquad \text{(D-3b)}$$

$$\ldots\ldots\ldots\ldots\ldots\ldots\ldots\ldots\ldots\ldots$$

$$A^1_{N2}X_2 + A^1_{N3}X_3 + \ldots\ldots\ldots\ldots + A^1_{NN}X_N = B^1_N$$

where

$$A^1_{ij} = A_{ij} - A_{i1}A_{1j}/A_{11} \qquad i, j = 2, \ldots\ldots, N \qquad \text{(D-4a)}$$

$$B^1_i = B_i - A_{i1}B_1/A_{11} \qquad i = 2, \ldots\ldots, N \qquad \text{(D-4b)}$$

A similar procedure is used to eliminate X_2 from Eq. (D-3), etc.

A general algorithm for the elimination of X_n may be written as:

$$X_n^* = (B_n^{n-1}/A_{nn}^{n-1}) - \sum (A_{nj}^{n-1}/A_{nn}^{n-1})X_j \qquad j = n+1, \ldots, N \qquad \text{(D-5)}$$

$$A_{ij}^n = A_{ij}^{n-1} - A_{in}^{n-1}\,(A_{nj}^{n-1}/A_{nn}^{n-1}) \qquad i,j = n+1, \ldots, N \qquad \text{(D-6)}$$

$$B_i^n = B_i^{n-1} - A_{in}^{n-1}\,(B_n^{n-1}/A_{nn}^{n-1}) \qquad i = n+1, \ldots, N \qquad \text{(D-7)}$$

Equations (D-5), (D-6), and (D-7) may be rewritten in compact form:

$$X_n = D_n - \sum H_{nj}X_j \qquad j = n+1, \ldots, N \qquad \text{(D-8)}$$

$$A_{ij}^n = A_{ij}^{n-1} - A_{in}^{n-1}\,H_{nj} \qquad i,j = n+1, \ldots, N \qquad \text{(D-9)}$$

$$B_i^n = B_i^{n-1} - A_{in}^{n-1}\,D_n \qquad i = n+1, \ldots, N \qquad \text{(D-10)}$$

where

$$D_n = B_n^{n-1}/A_{nn}^{n-1}$$

$$H_{nj} = A_{nj}^{n-1}/A_{nn}^{n-1}$$

After the above procedure is applied N-1 times, the original set of equations is reduced to the following single equation:

$$A_{NN}^{N-1} X_N = B_N^{N-1}$$

which is solved directly for X_N

$$X_N = B_N^{N-1}/A_{NN}^{N-1}$$

In terms of the previous notations, this is:

$$X_N = D_N$$

The remaining unknowns are determined in reverse order by the repeated application of Eq. (D-8).

SIMPLIFICATION FOR BANDED MATRICES

For many situations it is possible to place the stiffness matrix in a "band" form which results in the concentration of the elements of the stiffness matrix along the main diagonal. Therefore, the following simplifications in the general algorithm [Eqs.(D-8), (D-9) and (D-10)] are possible:

$$X_n = D_n - \sum H_{nj} X_j \qquad j = n+1, \ldots, n+M-1 \qquad \text{(D-12)}$$

$$A_{ij}^{n} = A_{ij}^{n-1} - A_{in}^{n-1} H_{nj} \qquad i,j = n+1, \ldots, n+M-1 \qquad \text{(D-13)}$$

$$B_i^{n} = B_i^{n-1} - A_{in}^{n-1} D_n \qquad i = n+1, \ldots, n+M-1 \qquad \text{(D-14)}$$

where M = the band width of the matrix.

The number of numerical operations can further be reduced by recognizing that the reduced matrix at any stage of procedure is symmetric. Accordingly, Eq. (D-13) may be replaced by the following equation:

$$A_{ij}^{n} = A_{ij}^{n-1} - A_{in}^{n-1} H_{nj} \qquad \begin{array}{l} i = n+1, \ldots, n+M-1 \\ j = i, \ldots, n+M-1 \end{array} \qquad \text{(D-15)}$$

Since

$$A_{ji}^{n} = A_{ij}^{n}$$

The number of numerical operations required for the solution of a band matrix is proportional to NM^2 as compared to N^3 which is required for the solution of a full matrix. Also, the computer storage required by the band matrix procedure is NM as compared to N^2 required by a set of N arbitrary equations. Equation (D-15) is utilized in Subroutine "SOLVE" of programme "MAIN", Appendix E, to solve for the unknown finite elements nodal displacements.

APPENDIX E

SECTION A

COMPUTER PROGRAMS - MAIN SERIES

During the course of the present study, several computer programs were developed to solve general nonlinear plane-strain problems occurring in soil mechanics. The programs were grouped under a series named "MAIN" and were based on Zienkiewicz's program (1971). All the programs can handle nonlinear material properties, and the different methods used to perform the nonlinear analysis and idealize the continuum usually classified the type of the program.

"MAIN 1" and "MAIN 2" [Figs. E-1 and E-2] use an incremental-iterative method without predictions [Chapter 2] to solve nonlinear problems in clay. "MAIN 1" is a general routine developed to handle problems with no discontinuities in the deformation field, the joint analysis was incorporated in "MAIN 2" to handle such problems. The programs were written in the Fortran language for use on the IBM 360/75 computer. A brief outline of the working of the "MAIN 2" program is given here. A listing of the program, together with general flow charts for the various routines are included. A number of comment cards are added in the listing for better understanding of the mechanics of the program.

The computer time required for a problem usually depends on the number of elements and nodal points used in the idealization of the problem, the number of increments and iterations [Table E-1].

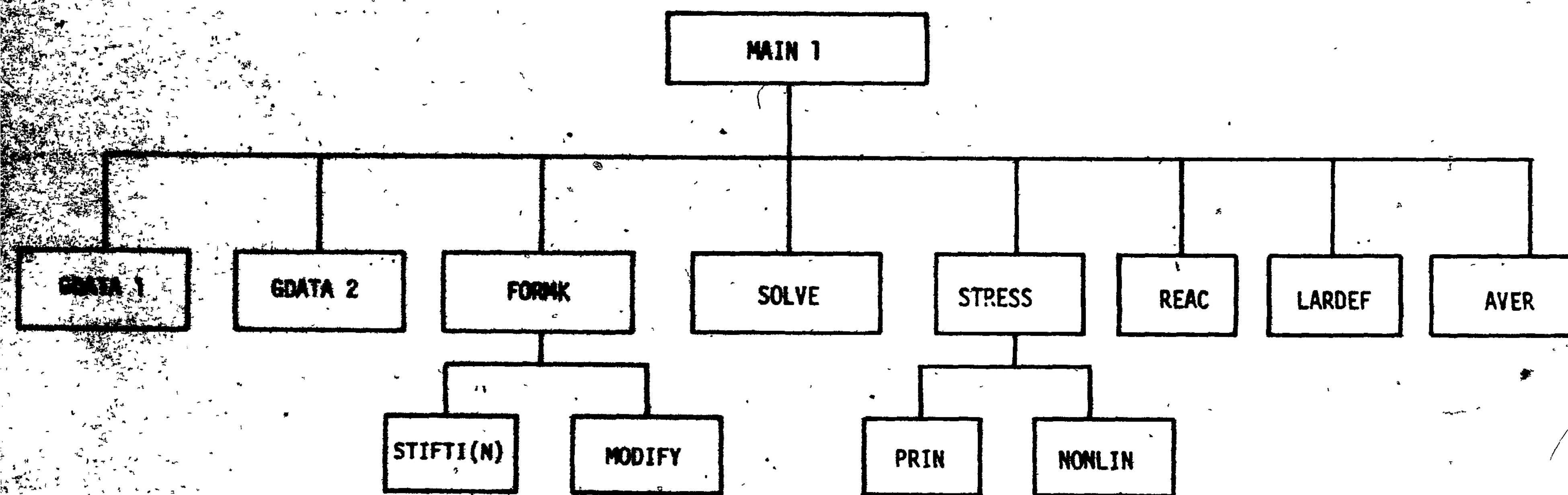

FIG. E-1 - MAIN 1 SUBPROGRAM LINKAGE

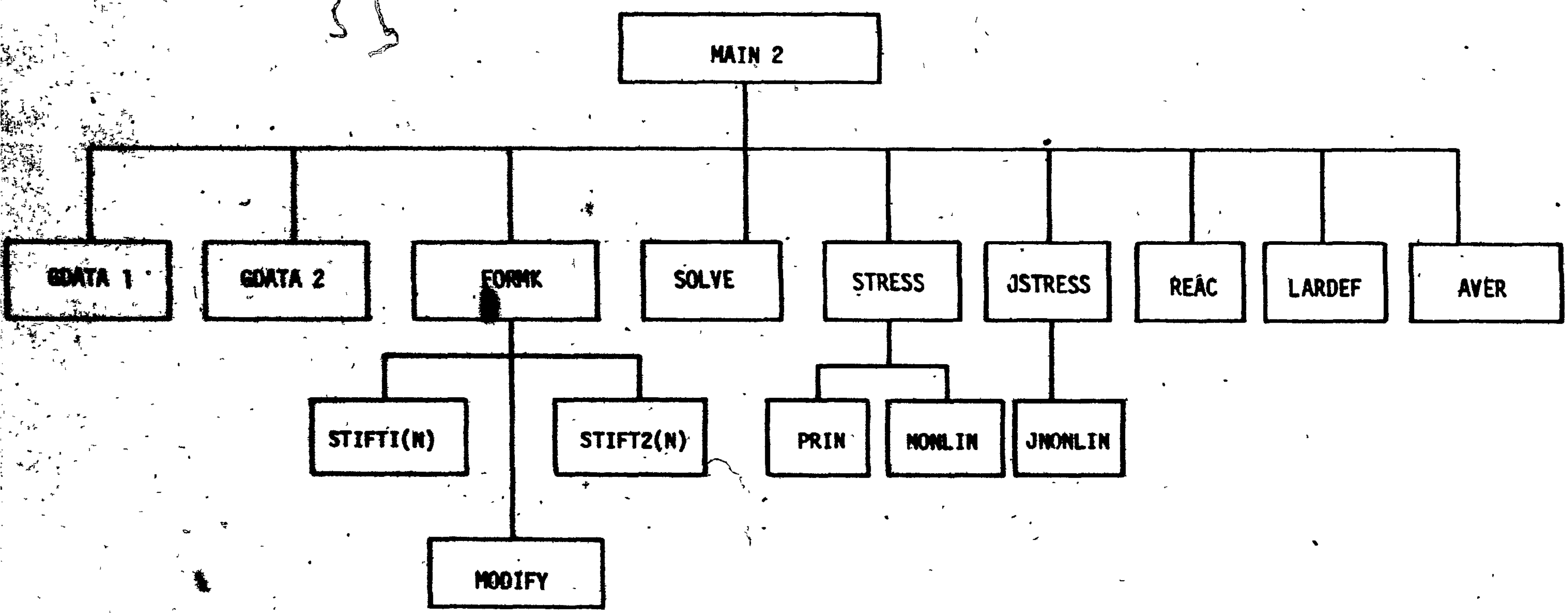

FIG. E-2 - MAIN 2 SUBPROGRAM LINKAGE

PROBLEM NUMBER	PROBLEM DESCRIPTION	No. OF CST ELEMENTS	No. OF JOINT ELEMENTS	No. OF NODES	BAND WIDTH	No. OF INCREMENTS	No. OF ITERATIONS WITHIN EACH INCREMENT	COMPUTER TIME* (Minutes)
1	Cutting blade-10° with vertical	237	29	176	78	10	3	9.10
2	Cutting blade - 50° with vertical	175	24	136	74	10	3	7.10
3	R.A.P.G. - h/ℓ = 0.833	228	17	156	44	10	3	7.33
4	R.A.P.G. - h/ℓ = 0.833	228	22	162	44	10	3	7.45
5	S.E.W. Grouser	205	13	139	38	10	3	5.30
6	C.E.W. Grouser	199	18	144	36	10	3	5.45
7	Retaining wall-Rough Interface-No cutting plane	302	-	178	58	10	3	9.25
8	Retaining wall-Rough Interface-cutting plane	302	14	193	58	10	3	10.0
9	Retaining wall-Interface elements-cutting plane	302	22	202	58	10	3	10.75

* Does not include compilation time of 40 seconds.

TABLE E-1

COMPUTER TIME

A.1 GENERAL OUTLINE OF PROGRAM "MAIN 2"

The "MAIN 2" program consists of several subroutines and a brief description of the subroutines is given below.

Main Program - "MAIN 2"

This is the main driver routine of the program. It calls two subroutines to handle the input data and calls several others to execute the problem. This routine initializes all nodal and element arrays, and specifies the size of the loading increment. All output with the exception of the reactions are printed out in the subroutines.

Subroutines "GDATA 1" and "GDATA 2"

Since this program deals with nonlinear material properties, it was found most appropriate to provide two data input routines. Subroutine "GDATA 1" reads the basic data, which are:

1) Junction Coordinates and element characteristics.
2) Initial material properties for each element type.
3) Boundary conditions.
4) Number of increments, and number of iterations in every increment required for execution of the problem.

Subroutine "GDATA 2" incorporates the nonlinear stress-strain data into the program. As mentioned earlier, the stress-strain laws derived from laboratory tests are used directly in a digital form. Several points on the stress-strain curve are selected as input to this routine in the form of number pairs. The first half of this routine reads the selected input points on the stress difference $(\sigma_1 - \sigma_3)$ vs axial strain (ε_1) curve for each confining pressure. The second half reads data for the joint elements nonlinear properties. The input data, in this case, are the hyperbolic coefficients (a) and (b), Eq. (2.32) for each normal pressure.

Subroutine "STIFT 1(N)" and "STIFT 2(N)"

The purpose of these two routines is to create the element stiffness coefficients appropriate to the problem. They have all necessary data transmitted to them through common storage and passes the element stiffness matrix back to the calling routine "FORMK". The element stiffness matrix is generated using the constitutive relations of the material and the geometry of the element. Subroutine "STIFT 1(N)" computes the stiffness matrix for a joint element [cutting or interface element]. In case the element is of the constant strain triangle type, subroutine "STIFT 2(N)" is called to generate the stiffness matrix.

Subroutines "FORMK" and "MODIFY"

The "FORMK" routine assembles the total stiffness matrix for the entire continuum using the direct stiffness method. Because of the bonded form of the resulting total stiffness matrix, only the main diagonal elements and the lower triangle elements are stored in a rectangular matrix with a width of half the band, [Zienkiewicz (1971)].

The "FORMK" routine also generates the total nodal force vector. The applied nodal forces are added directly, while the total stiffness matrix is modified for the applied displacement conditions [Chapter 2] using subroutine "MODIFY". The body forces due to gravity are also added in this routine.

Subroutine "SOLVE"

This routine uses Gaussian elimination method [Appendix D] and solves for the unknown displacements from the set of stiffness equations generated in "FORMK".

Subroutine "STRESS" and "JSTRES"

These routines compute the stresses and strains at the center of each element using the nodal displacements obtained from "SOLVE". Subroutine "STRESS" is called for the determination of stresses and strains in the "CST" elements. The routine also computes the principal stresses and principal strains in each "CST" element. Moreover, it calls subroutine "NONLIN(N)" to update the "CST" elements' elastic properties.

Subroutine "JSTRES" is used for the computations of the average incremental shear and normal stresses across the joint elements and the accumulative corresponding values. This routine calls subroutine "JNONL(N)" for updating the stiffness values of the joint elements to be used in the subsequent increments.

Subroutines "NONLIN(N)" and "JNONL(N)"

The nonlinear analysis is performed in these subroutines. In "NONLIN(N)" routine, values of E and ν are computed for each element from the nonlinear stress-strain curves depending on the state of strain and confining pressure in each element. This nonlinear routine can handle several nonlinear curves for any number of different materials by suitably altering the dimension statements.

Subroutine "JNONL(N)" interpolates for shear stiffness values (k_s) from the hyperbolic shear stress-relative displacement relationships. Values of the coefficients (a) and (b), Eq. (2.32), are computed for each cutting or interface element depending on the state of shear displacement and the normal pressure in the element. Again this routine can handle several nonlinear curves for any number of different joint behaviors by suitably altering the dimension statements.

Subroutine "REAC"

The reactions at certain nodal points resulting from specifying displacement boundary conditions for these nodes are determined in this routine. The reactions at the desired node are obtained by multiplying the nodal displacement vector of the element by the stiffness values of the particular node. The reactions obtained for any particular increment are then added to the cumulative values obtained in previous increments to obtain total reactions.

Subroutine "AVER"

In this subroutine output results are averaged at the nodes. The stresses, the strains, and the strain rates of all the elements connected to a node are summed and divided by the number of elements.

Subroutine "LARDEF"

After each increment, the element nodal coordinates are updated. This is done in subroutine "LARDEF" by adding the nodal displacements to the element nodal coordinates to obtain new coordinates for the next increment [Chapter 2]. In addition, the velocity components of the nodal points are determined together with elements strain-rate components and their principal values and directions. The "LARDEF" routine also computes the incremental deformation energy and power of deformation and adds them to previously obtained values for determination of total deformation energy and power of deformation.

Subroutine "PRIN"

This routine evaluates the principal stresses [or strains] from the known nodal values.

A.2 FLOW CHARTS

PROGRAM MAIN 2

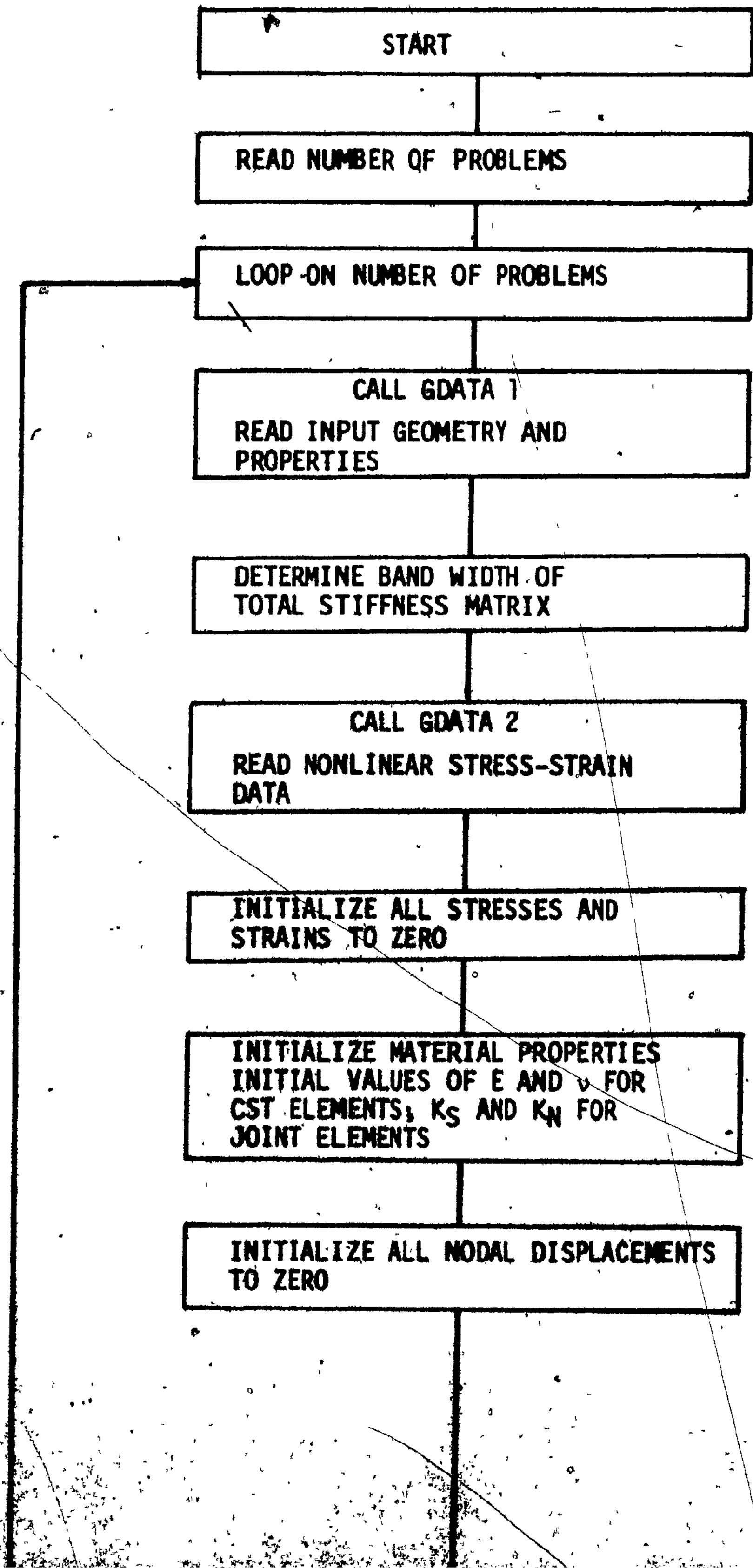

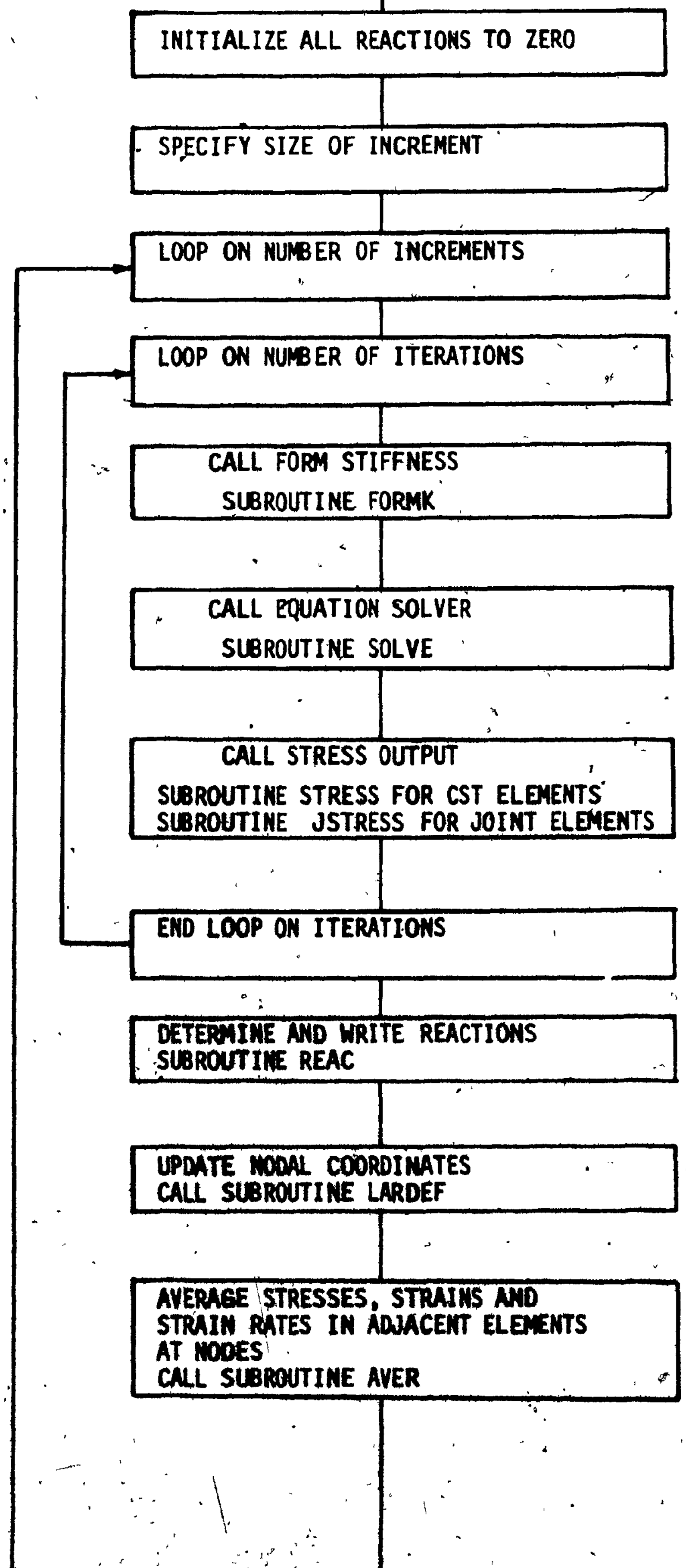
INITIALIZE ALL REACTIONS TO ZERO
SPECIFY SIZE OF INCREMENT
LOOP ON NUMBER OF INCREMENTS
LOOP ON NUMBER OF ITERATIONS
CALL FORM STIFFNESS
SUBROUTINE FORMK
CALL EQUATION SOLVER
SUBROUTINE SOLVE
CALL STRESS OUTPUT
SUBROUTINE STRESS FOR CST ELEMENTS
SUBROUTINE JSTRESS FOR JOINT ELEMENTS
END LOOP ON ITERATIONS
DETERMINE AND WRITE REACTIONS
SUBROUTINE REAC
UPDATE NODAL COORDINATES
CALL SUBROUTINE LARDEF
AVERAGE STRESSES, STRAINS AND
STRAIN RATES IN ADJACENT ELEMENTS
AT NODES
CALL SUBROUTINE AVER

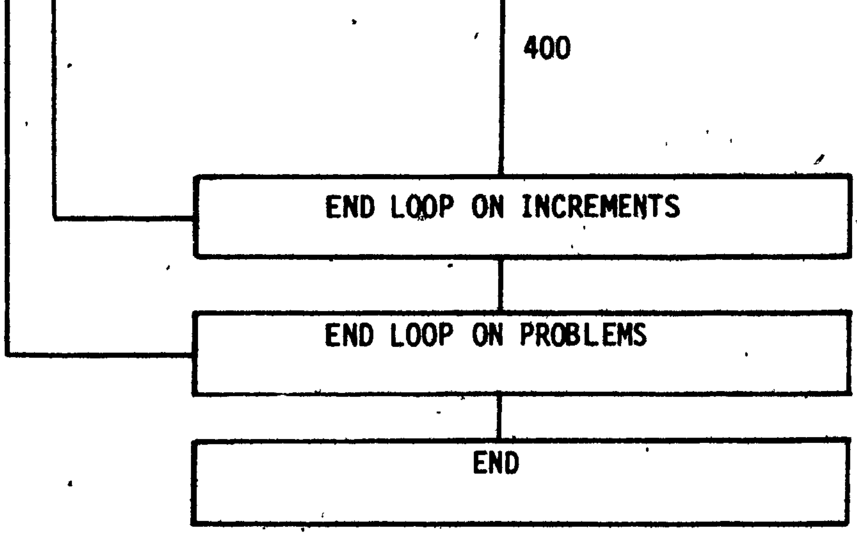
400
END LOOP ON INCREMENTS
END LOOP ON PROBLEMS
END

SUBROUTINE GDATA 1

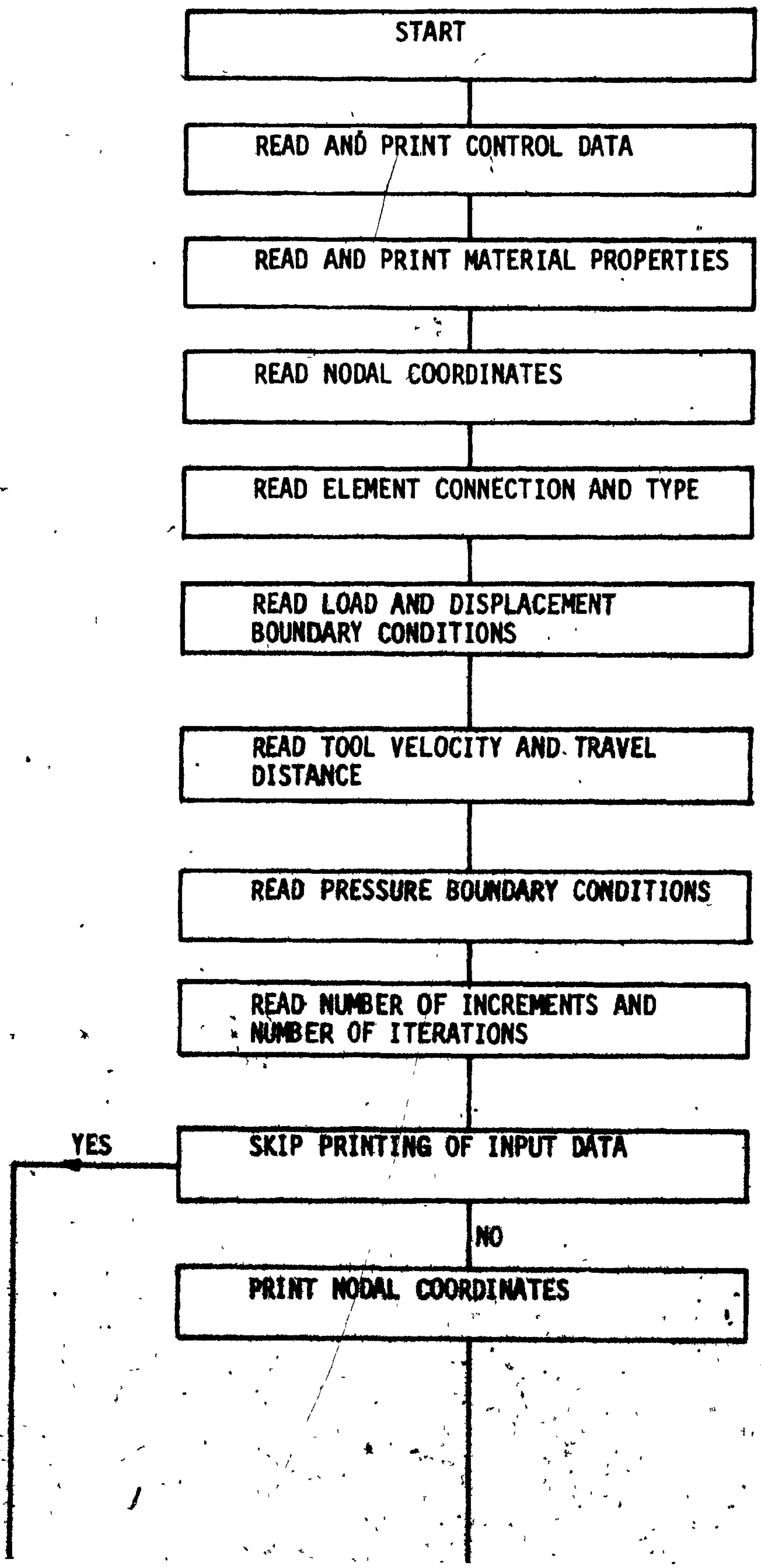

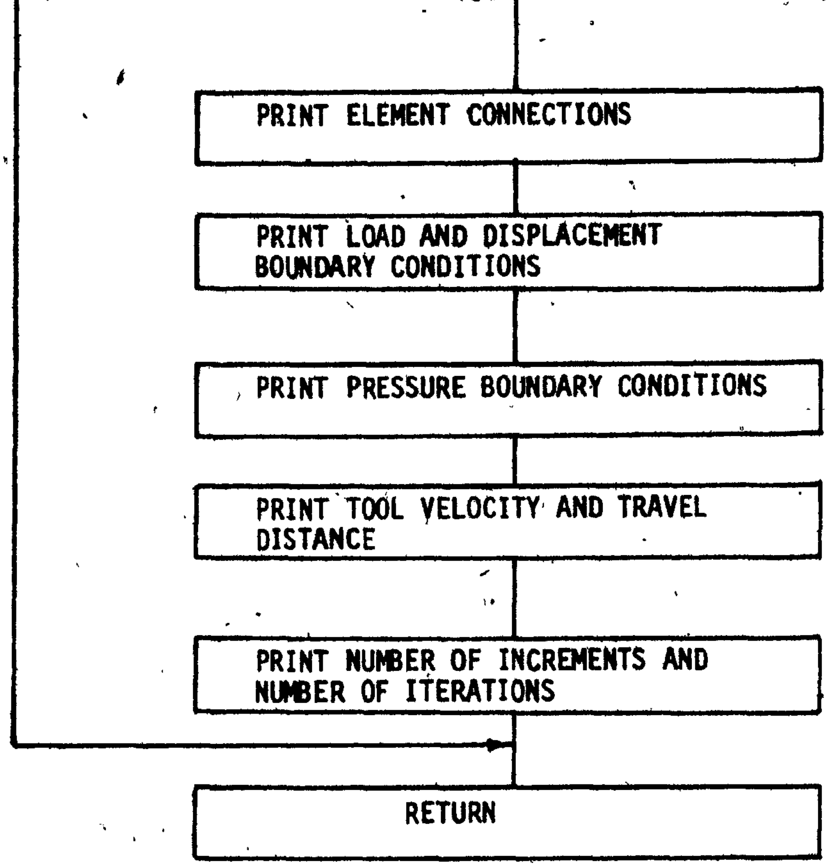
PRINT ELEMENT CONNECTIONS
PRINT LOAD AND DISPLACEMENT BOUNDARY CONDITIONS
PRINT PRESSURE BOUNDARY CONDITIONS
PRINT TOOL VELOCITY AND TRAVEL DISTANCE
PRINT NUMBER OF INCREMENTS AND NUMBER OF ITERATIONS
RETURN

SUBROUTINE GDATA 2

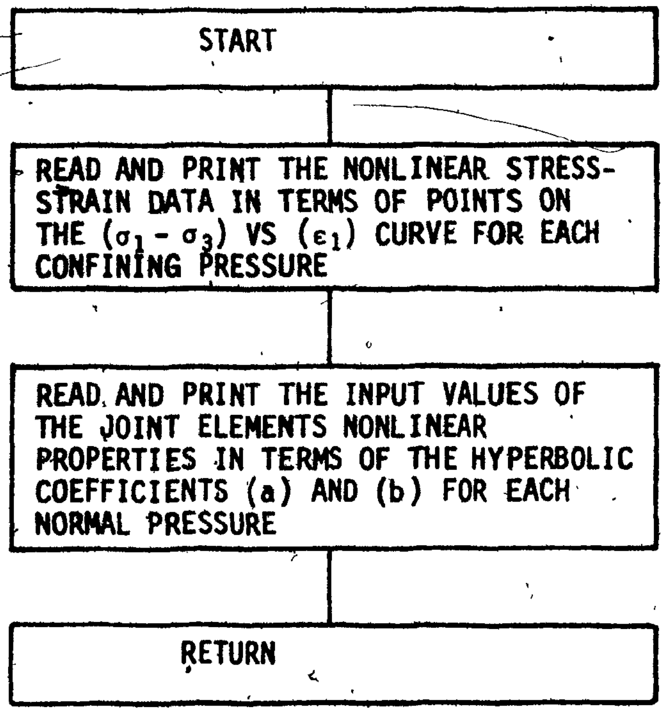

SUBROUTINE FORMK

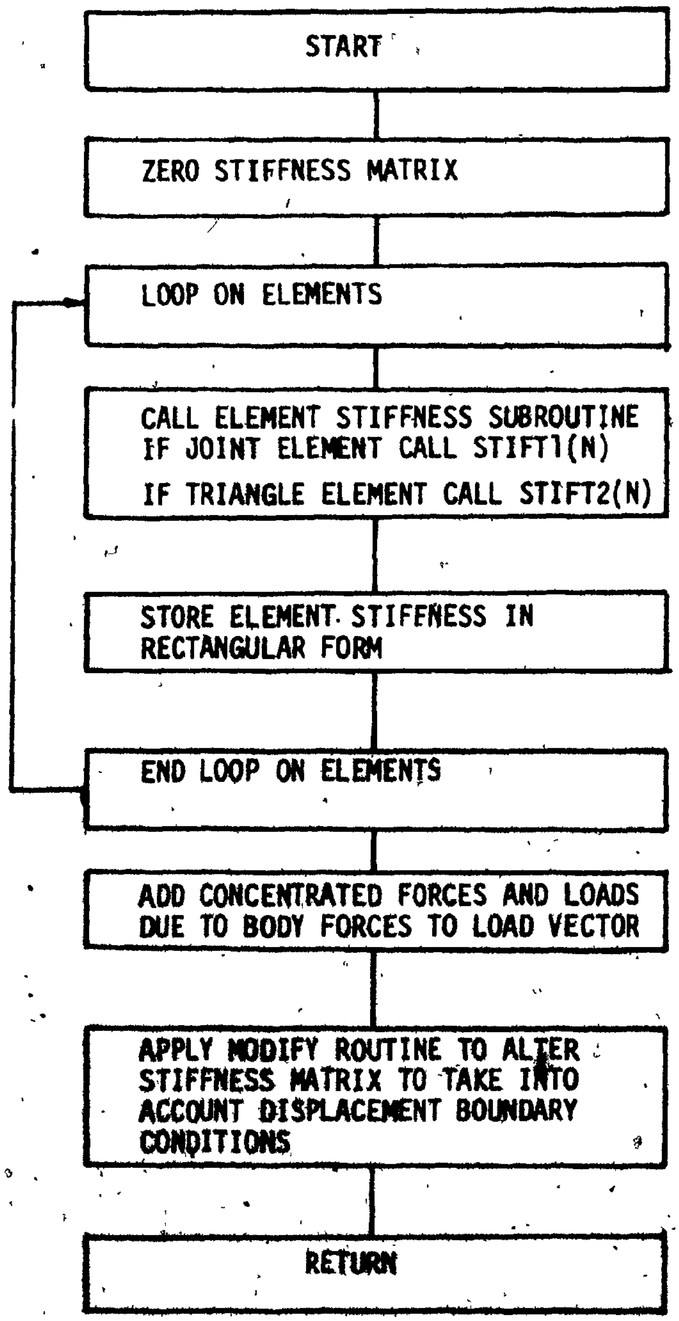

SUBROUTINE STIFT1(N)

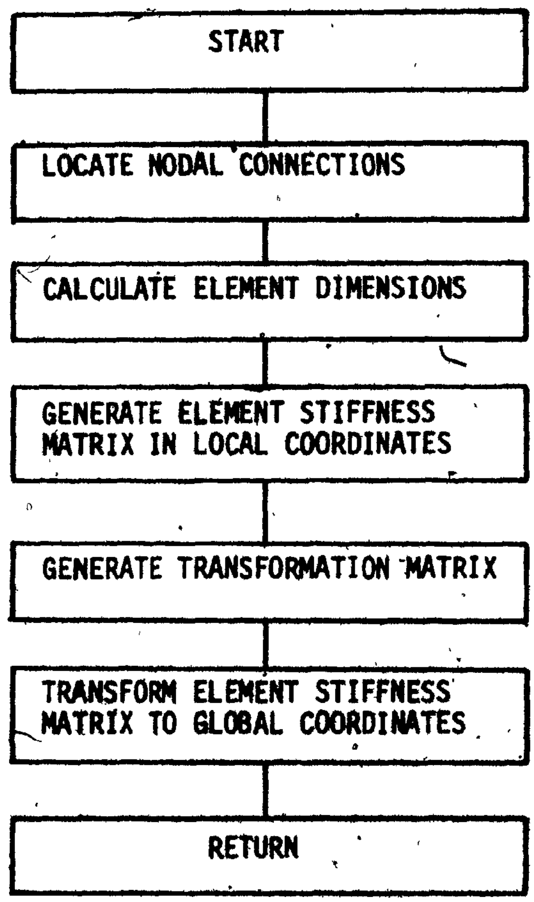

SUBROUTINE STIFT2(N)

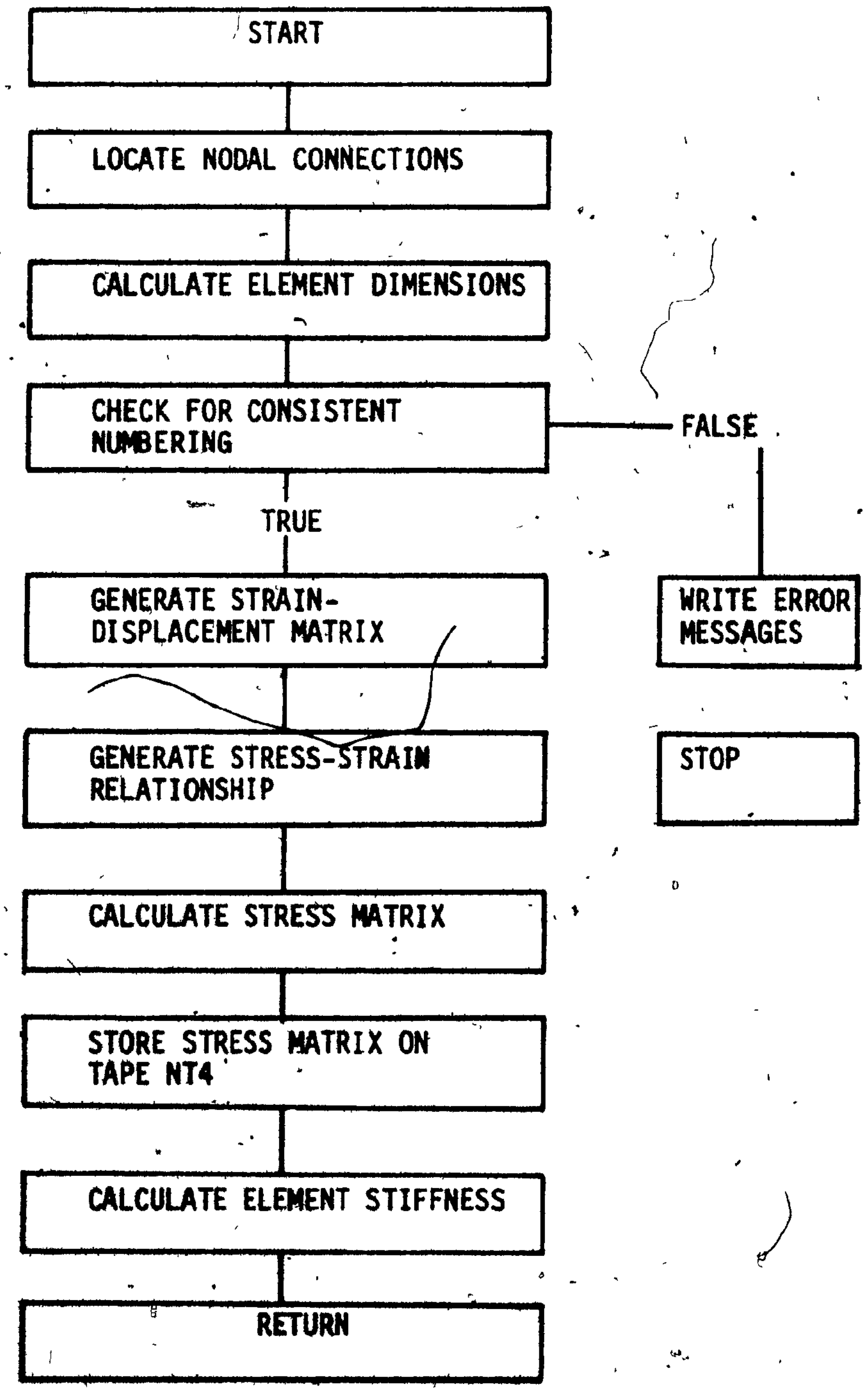

SUBROUTINE MODIFY

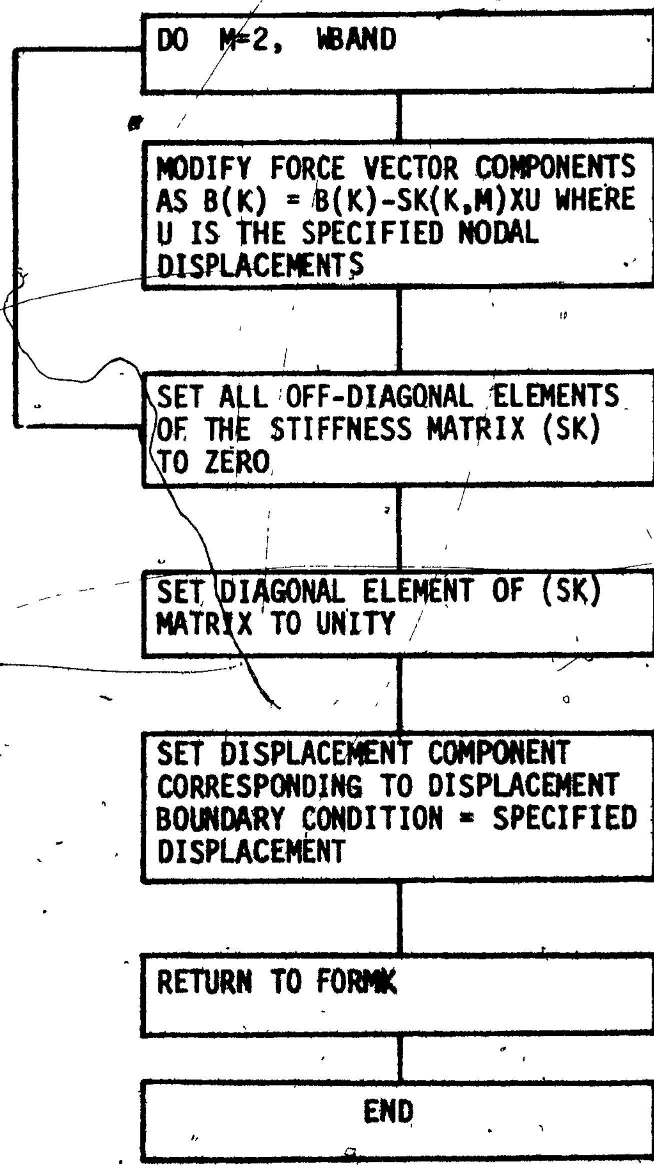

SUBROUTINE SOLVE

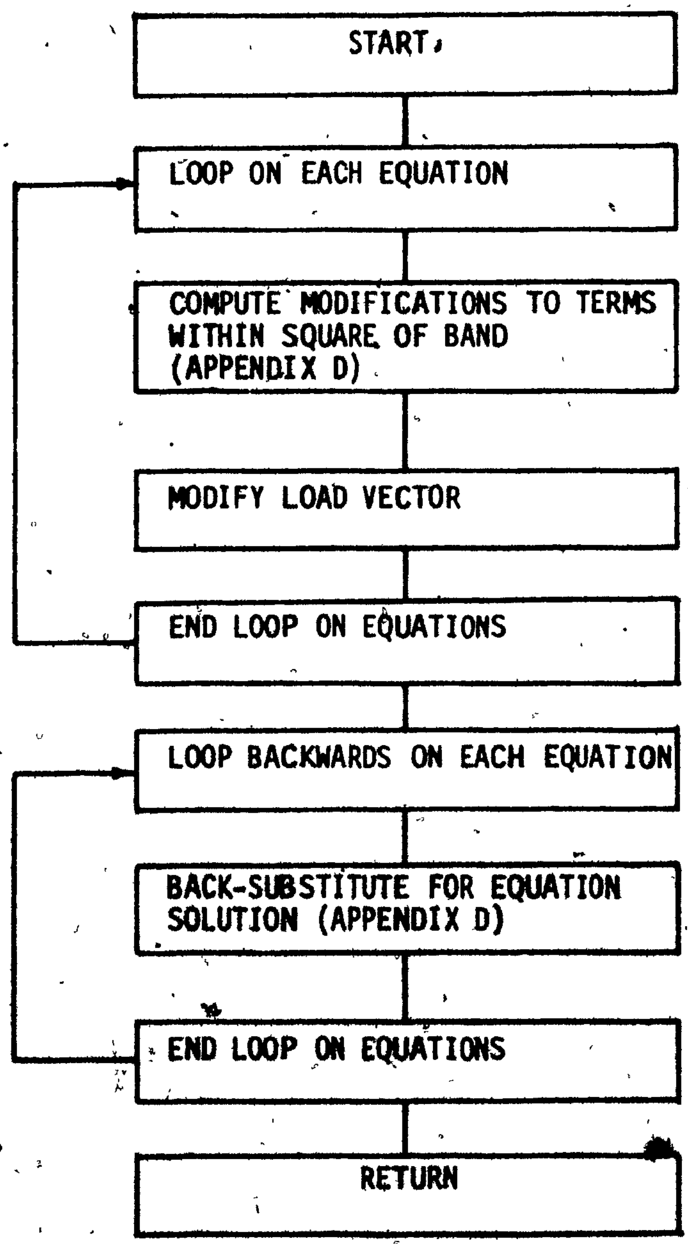

SUBROUTINE STRESS

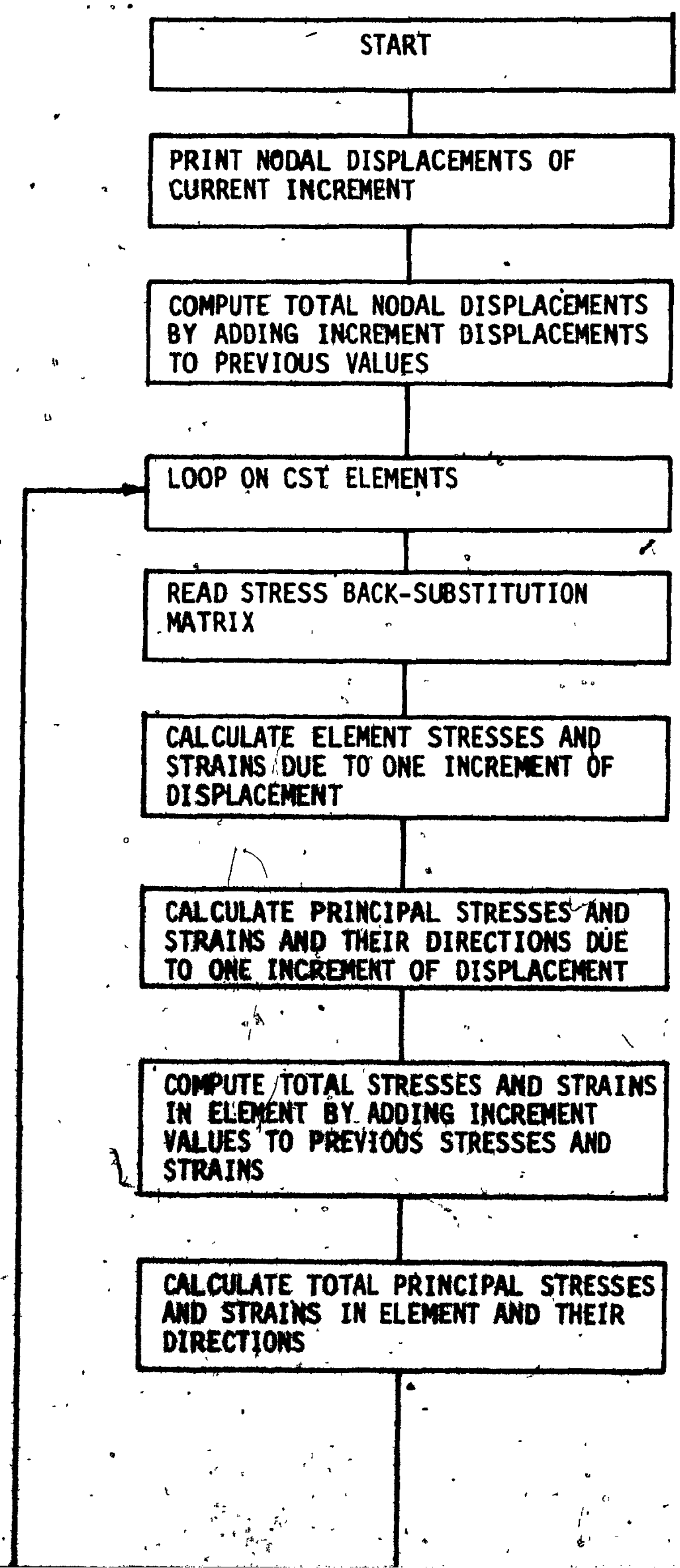

CALCULATE ELASTIC MODULUS IN ELEMENT FROM INCREMENTAL STRESSES AND STRAINS

CALL SUBROUTINE NONLIN(N)

PRINT ELEMENT CONFINING PRESSURE, THE ELASTIC MODULUS OBTAINED FROM THE INPUT STRESS-STRAIN DATA, AND THE ELASTIC MODULUS CALCULATED FROM INCREMENTAL STRESSES AND STRAINS

END LOOP ON CST ELEMENTS

RETURN

SUBROUTINE JSTRES

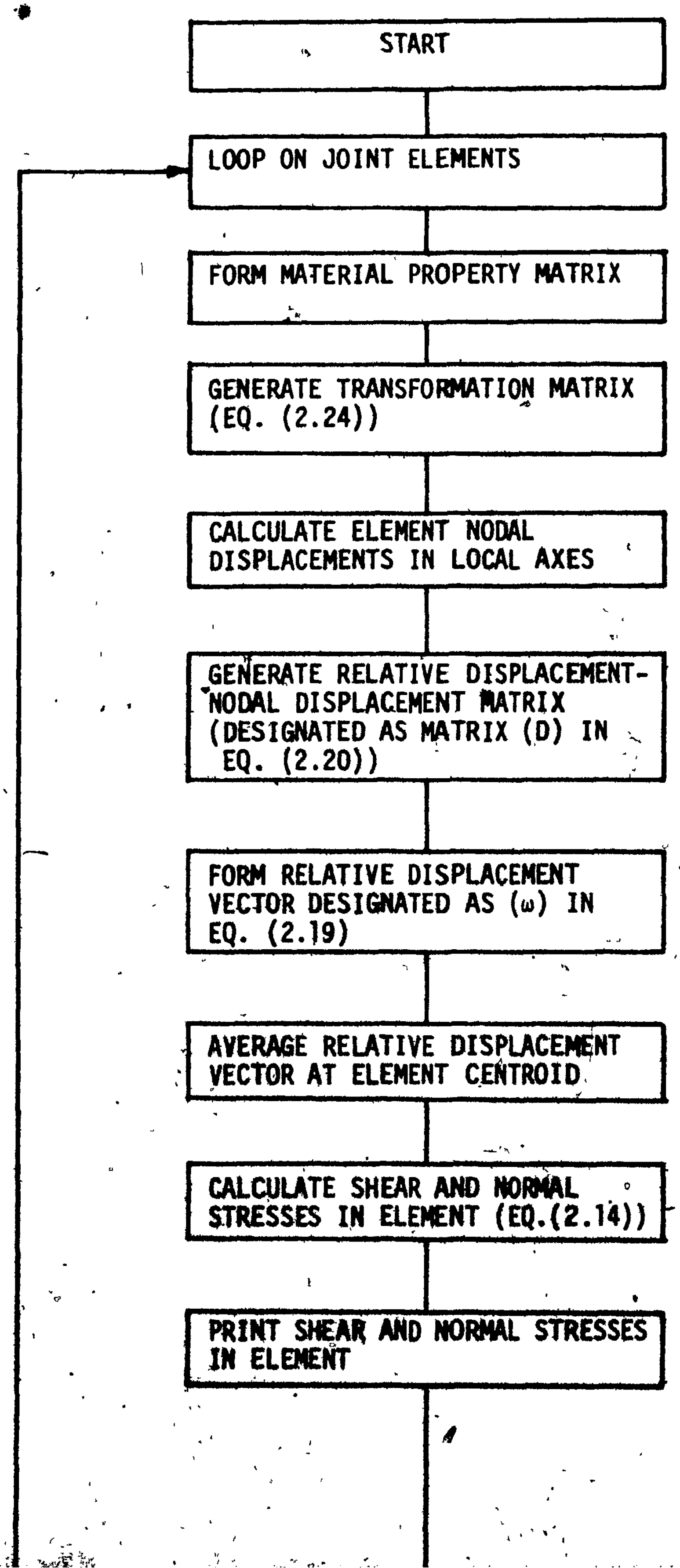

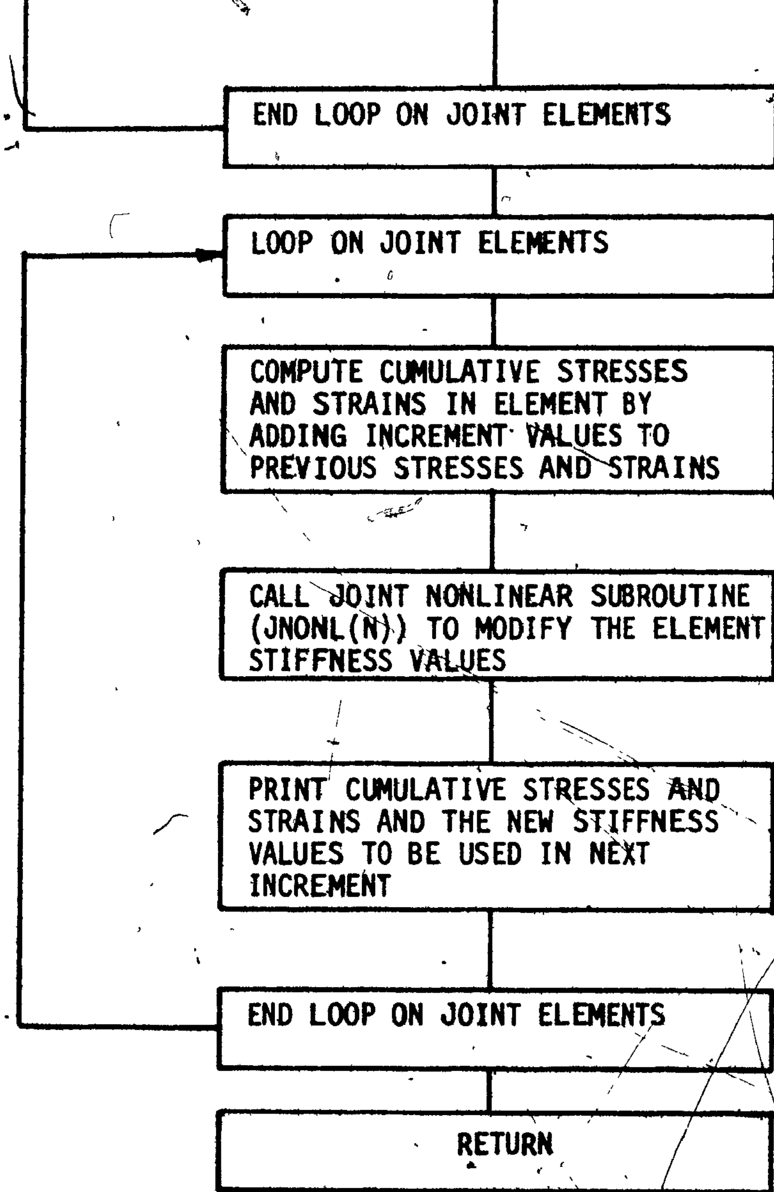
END LOOP ON JOINT ELEMENTS
LOOP ON JOINT ELEMENTS
COMPUTE CUMULATIVE STRESSES AND STRAINS IN ELEMENT BY ADDING INCREMENT VALUES TO PREVIOUS STRESSES AND STRAINS
CALL JOINT NONLINEAR SUBROUTINE (JNONL(N)) TO MODIFY THE ELEMENT STIFFNESS VALUES
PRINT CUMULATIVE STRESSES AND STRAINS AND THE NEW STIFFNESS VALUES TO BE USED IN NEXT INCREMENT
END LOOP ON JOINT ELEMENTS
RETURN

SUBROUTINE REAC

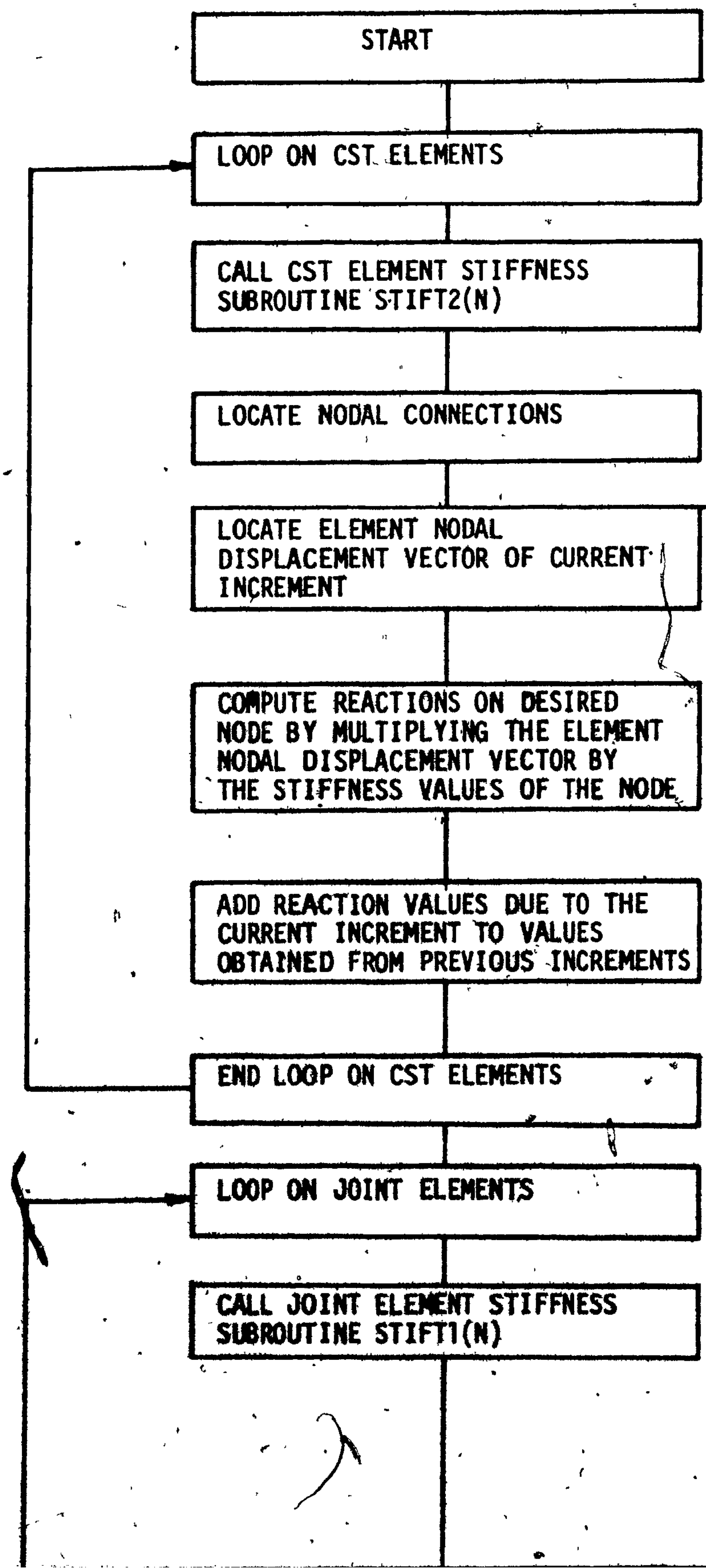

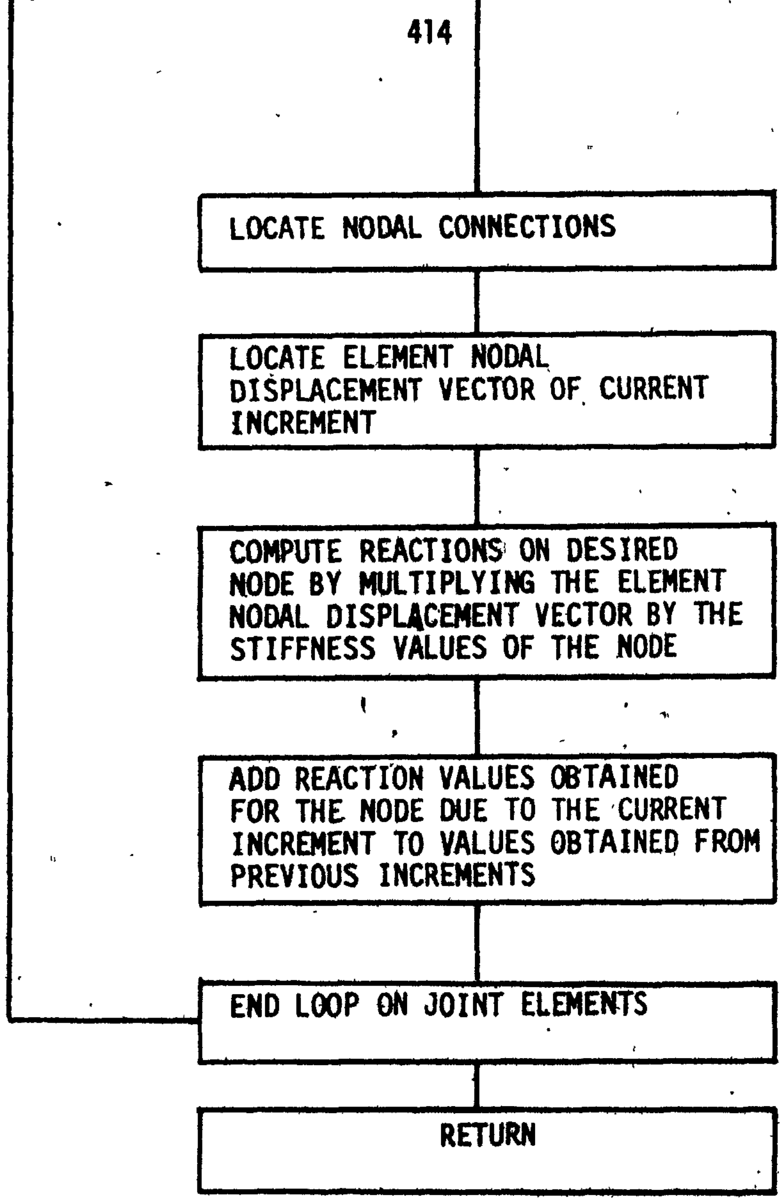
LOCATE NODAL CONNECTIONS
LOCATE ELEMENT NODAL DISPLACEMENT VECTOR OF CURRENT INCREMENT
COMPUTE REACTIONS ON DESIRED NODE BY MULTIPLYING THE ELEMENT NODAL DISPLACEMENT VECTOR BY THE STIFFNESS VALUES OF THE NODE
ADD REACTION VALUES OBTAINED FOR THE NODE DUE TO THE CURRENT INCREMENT TO VALUES OBTAINED FROM PREVIOUS INCREMENTS
END LOOP ON JOINT ELEMENTS
RETURN

SUBROUTINE LARDEF

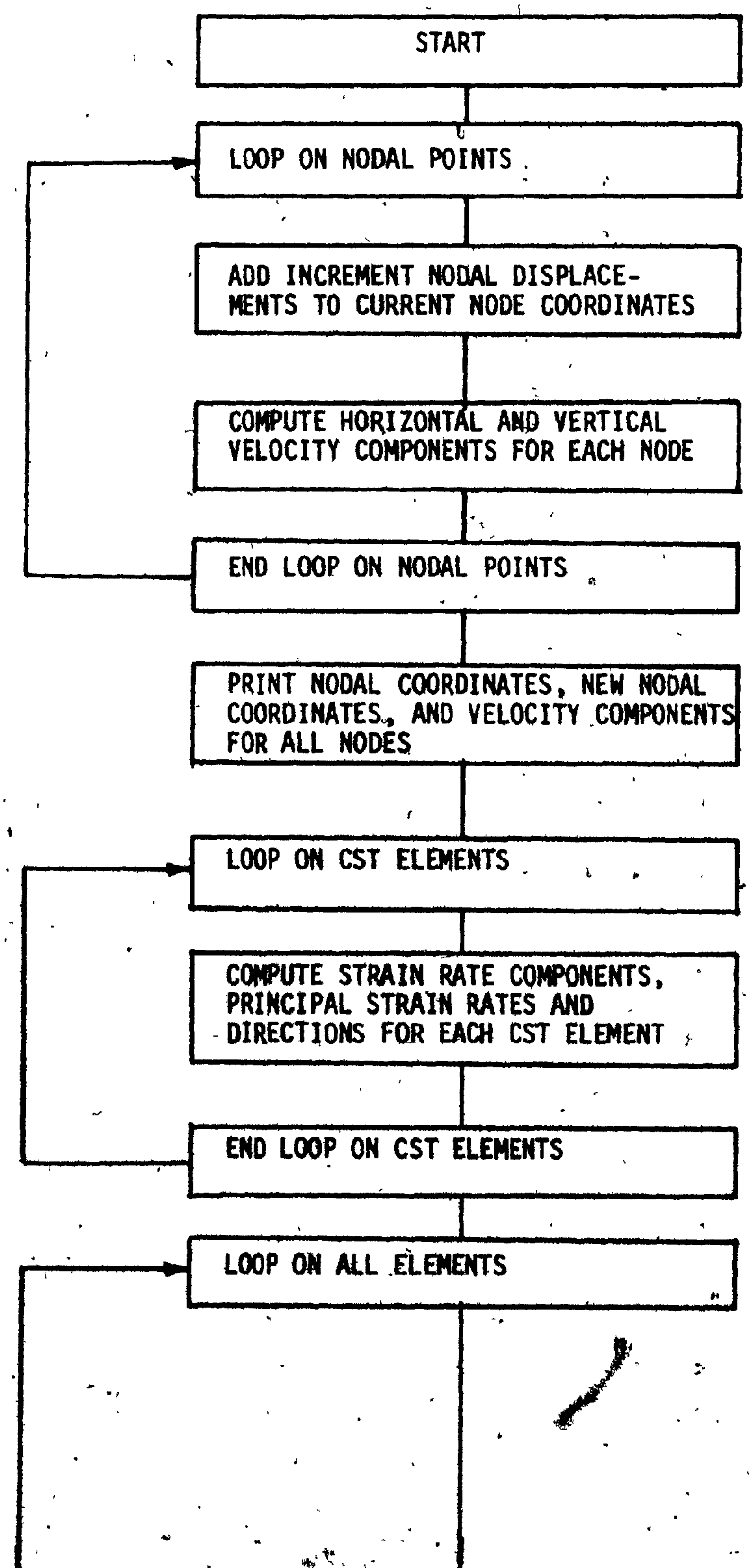

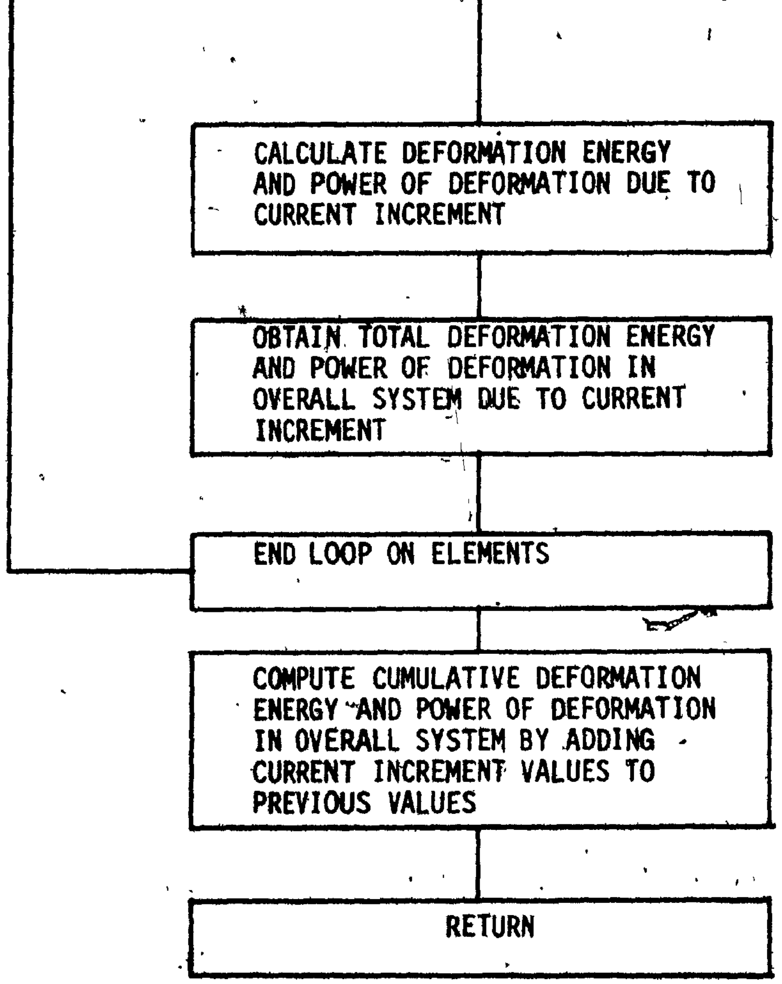
CALCULATE DEFORMATION ENERGY AND POWER OF DEFORMATION DUE TO CURRENT INCREMENT
OBTAIN TOTAL DEFORMATION ENERGY AND POWER OF DEFORMATION IN OVERALL SYSTEM DUE TO CURRENT INCREMENT
END LOOP ON ELEMENTS
COMPUTE CUMULATIVE DEFORMATION ENERGY AND POWER OF DEFORMATION IN OVERALL SYSTEM BY ADDING CURRENT INCREMENT VALUES TO PREVIOUS VALUES
RETURN

SUBROUTINE NONLIN(N)

START

COMPUTE CONFINING PRESSURE IN ELEMENT

FIND MAXIMUM PRINCIPAL STRAIN (ε_1) IN ELEMENT

DETERMINE TWO ADJOINING CONFINING PRESSURE DEPENDENT CURVES DEPENDING ON THE CONFINEMENT OF THE ELEMENT

INTERPOLATE FOR STRESS DIFFERENCE ($\sigma_1 - \sigma_3$) CORRESPONDING TO (ε_1)

COMPUTE (E) VALUE FOR ELEMENT FOR THE NEXT LOAD INCREMENT

RETURN

SUBROUTINE JNONL(N)

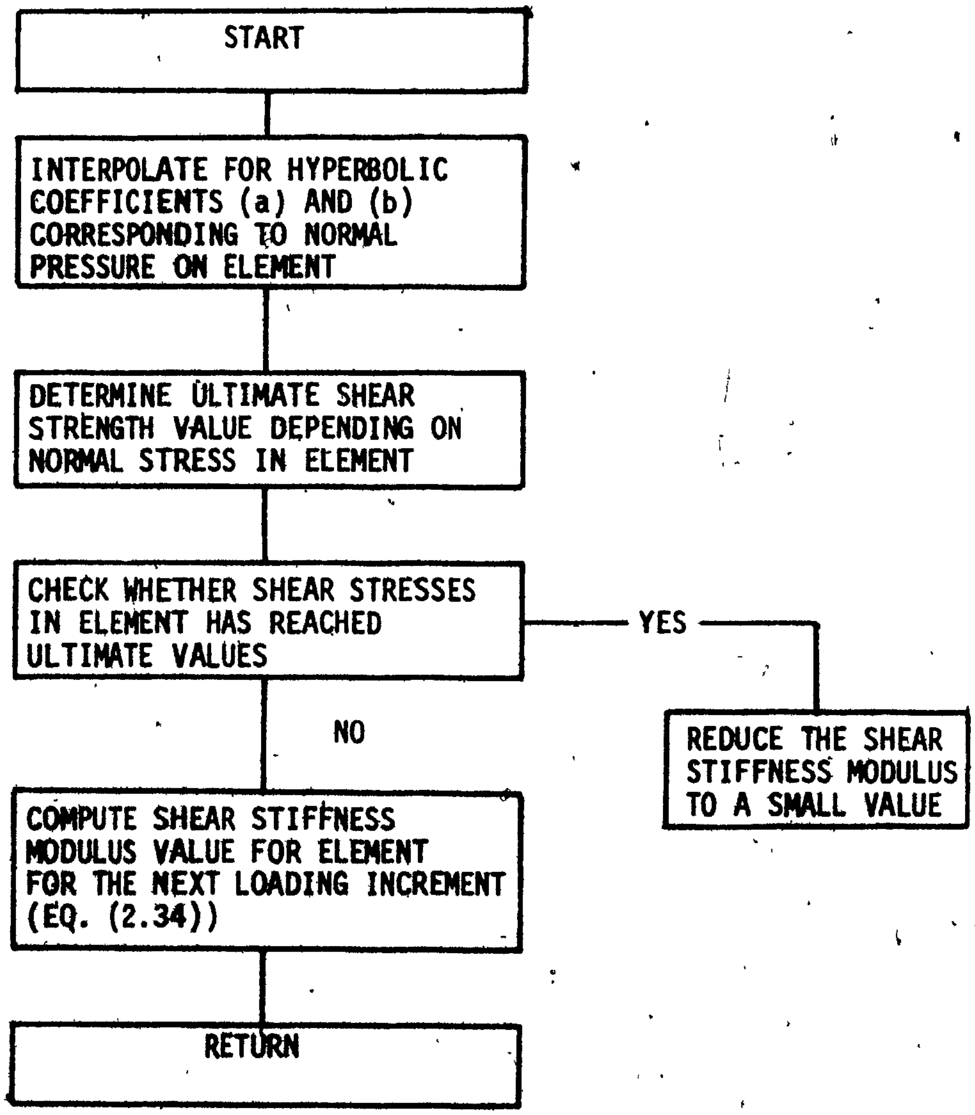

SUBROUTINE AVER

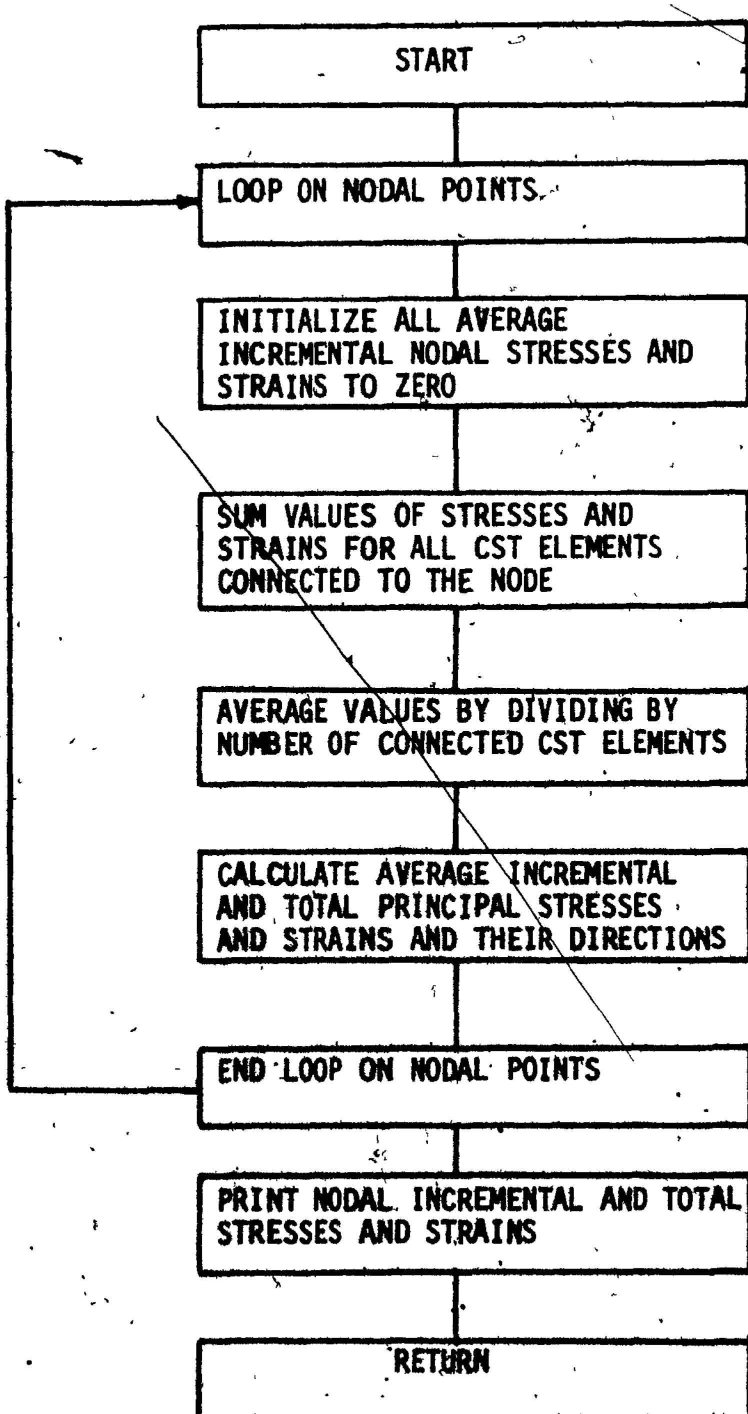

A.3 IDENTIFIERS USED IN THE "MAIN 2" PROGRAM

Symbols and arrays appearing in the various routines of the program are listed below in the order in which they appear.

COMMON BLOCK/CONTR/

TITLE	:	Word title array.
NP	:	Number of nodal points.
NE	:	Number of elements.
NB	:	Number of restrained boundary nodes.
NDF	:	Number of degrees of freedom per node.
NCN	:	Maximum number of nodes per element.
NLD	:	Number of load cases.
NMAT	:	Number of element material types.
NSZF	:	Number of equations in the system.
LI	:	Load case counter.
NT4	:	Logical storage device numbers.
NT5	:	Logical storage device numbers.
NOPC	:	Number of boundary pressure cards.
NCMAT	:	Number of "CST" element material types.

COMMON BLOCK/DATA

CORD	:	Nodal point coordinate array.
NOP	:	Element connection array.
IMAT	:	Element material type array.
NBC	:	Restrained boundary node numbers.
CODE	:	Code for various boundary conditions, = 0.0 specified load in both X and Y directions = 1.0 specified displacement in X-direction, load in Y-direction.

= 2.0 specified load in X-direction, displacement in Y-direction.

= 3.0 specified displacement in both X and Y directions.

UX	:	X-force or displacement at the nodal point.
UY	:	Y-force or displacement at the nodal point.
IBC	:	Nodal point I for the boundary pressure.
JBC	:	Nodal point J for the boundary pressure.
PRE	:	Boundary pressure between I and J.
T	:	Element thickness array.
XDEN	:	Body forces in X-direction.
YDEN	:	Body forces in Y-direction.
ORX	:	X-coordinate of element centroid.
ORY	:	Y-coordinate of element centroid.
PRCORD	:	Nodal point coordinate at previous increment.

COMMON BLOCK/ANAL/

NOINC	:	Number of increments.
KOUNT	:	Counter for number of increments.
NTEST	:	Alphanumeric identifier of type of problem. = 0 for linear problem. = 1 for nonlinear problem.
LTEST	:	Alphanumeric input to specify whether problem is linear or nonlinear.
NOITER	:	Number of iterations.
NITER	:	Counter for number of iterations executed.
VEL	:	Tool velocity.
THD	:	Tool total horizontal displacement.

COMMON BLOCK/STIFF/

ESTIFM	:	Stress-strain matrix, later used for element stiffness matrix.
A	:	Strain-displacement matrix.
B	:	Stress back-substitution matrix.
SK	:	Rectangular matrix for equations.
AREA	:	Area of element.
C	:	Initially contains nodal force vector for the total stiffness matrix, but displacement solution vector replaces it.
R	:	Vector of element nodal displacements.
H	:	Nodal displacement vector of joint elements in local coordinates.
WBAND	:	Band width of the stiffness matrix.
D	:	Nodal force vector for the total stiffness matrix; replaces vector C before modifying for displacement boundary conditions.
AR	:	Nodal reaction array.

COMMON BLOCK/STRES/

DISTO	:	Total nodal displacement vector.
SIGTO	:	Total element stress vector.
STRTO	:	Total element strain vector.
SMAXTO	:	Total maximum principal stress.
SMINTO	:	Total minimum principal stress.
ANGTO	:	Clockwise angle from vertical to line of action of total maximum principal stress.

EANGTO : Clockwise angle from vertical to line of action of total maximum principal strain.

EMAXTO : Total maximum principal strain.

EMINTO : Total minimum principal strain.

FORCE : Vector of element incremental stresses.

STR : Vector of element incremental strains.

PSIGTO : Total element stress vector at previous increment.

PSTRTO : Total element strain vector at previous increment.

PDISTO : Total nodal displacement vector at previous increment.

COMMON BLOCK/NONL/

NCUR : Vector of numbers of nonlinear curves input for each material.

CPR : Confining pressure for a nonlinear curve.

NPTS : Number of points on each nonlinear curve.

EG : Stress coordinate of the nonlinear curve for data.

GAM : Strain coordinate of the nonlinear curve for data.

EY : Stress coordinate of the nonlinear curve.
= EG X AXMUL1

GAMOC : Strain coordinate of the nonlinear curve.
= GAM X AXMUL2

PRESTR : Principal strain at previous increment.

PREDEV : Principal stress difference ($\sigma_1 - \sigma_3$) at previous increment.

CONPRE : Element confining pressure.

COMMON BLOCK /DEF/

DX	:	X-displacement of nodal point for a loading increment.
DY	:	Y-displacement of nodal point for a loading increment.
VX	:	Horizontal velocity of nodal point for a loading increment.
VY	:	Vertical velocity of nodal point for a loading increment.
EPSX	:	Horizontal strain rate for a loading increment.
EPSY	:	Vertical strain rate for a loading increment.
GAMXY	:	Shear strain rate for a loading increment.
EPSI 1	:	Major principal strain rate for a loading increment.
EPSI 2	:	Minor principal strain rate for a loading increment.
PSI	:	Clockwise angle from vertical to line of action of major principal strain rate.
CSUMPD	:	Total deformation energy.
CSUMPW	:	Total power of deformation.

COMMON BLOCK /ELAS/

E	:	Starting modulus of elasticity for the material.
ENU	:	Poisson's ratio for the material.
EE	:	Array of values of E modified for nonlinear analysis.
EC	:	Array of values of E determined from stresses and strains calculated in increment.
DKSIJ	:	Starting tangential stiffness value for cutting joint elements.
DKNIJ	:	Starting normal stiffness value for cutting joint elements.
DKSII	:	Starting tangential stiffness value for interface joint elements.

DKNII	:	Starting normal stiffness value for interface joint elements.

COMMON BLOCK/JOINT/

T 1	:	Joint element transformation matrix from local element axes to global axes.
BL	:	Working matrix for the transformation process.
AL	:	Element length.
ANG(N)	:	Angle element N making with horizontal.
DKS(N)	:	Tangential stiffness coefficient for element N.
DKN(N)	:	Normal stiffness coefficient for element N.
SD	:	A diagonal material property matrix expressing the joint stiffness per unit length in the normal and tangential directions.
W(N,1) W(N,2)	:	Incremental shear and normal displacements for element N, respectively.
P(N,1) P(N,2)	:	Incremental shear and normal stresses for element N, respectively.
V(N,1) V(N,2)	:	Average incremental shear and normal displacements for element N, respectively.
AVP(N,1) AVP(N,2)	:	Average incremental shear and normal stresses for element N, respectively.
CV(N,1) CV(N,2)	:	Cumulative average shear and normal displacements for element N, respectively.
CAVP(N,1) CAVP(N,2)	:	Cumulative average shear and normal stresses for element N, respectively.

PCV(N,1)	:	) Working vectors for
PCV(N,2)	:	) the summation process.
PCAVP(N,1)	:	) Working vestors for
PCAVP(N,2)	:	) the summation process
B1	:	Relative element displacement-nodal displacement matrix. [Designated as matrix D in Eq. (2.20)].

COMMON BLOCK/JNONL/

NVAL	:	Vector of numbers of nonlinear curves input for each joint material.
CNP	:	Array of normal pressures for nonlinear curves.
AH	:	Hyperbolic coefficient (a) array.
BH	:	Hyperbolic coefficient (b) array.

COMMON BLOCK /AVRG/

AVSMAX	:	Average incremental maximum principal stress.
AVSMIN	:	Average incremental minimum principal stress.
AVANG	:	Clockwise angle from vertical to line of action of incremental maximum principal stress.
AVTMX	:	Average total maximum principal stress.
AVTMN	:	Average total minimum principal stress.
AVTANG	:	Clockwise angle from vertical to line of action of average total maximum principal stress.
AVSMX	:	Average incremental maximum principal strain.
AVSMN	:	Average incremental minimum principal strain.
AVSANG	:	Clockwise angle from vertical to line of action of average incremental maximum principal strain.
AVSTMX	:	Average total maximum principal strain.

AVSTMN : Average total minimum principal strains.

AVSTAN : Clockwise angle from vertical to line of action of average total maximum principal strain.

AVPSI 1 : Average incremental maximum principal strain rate.

AVPSI 2 : Average incremental minimum principal strain rate.

AVPSI : Clockwise angle from vertical to line of action of average incremental maximum principal strain rate.

VARIABLE DEFINITIONS

PROGRAM MAIN

NPROB : Number of problems.

NPR : Counter on number of problems.

SUBROUTINE GDATA 1

I 1 : Control for print of input data.

BANGLE : Angle of cutting blade [only in case of soil-cutting analysis] with vertical.

SUBROUTINE GDATA 2

TMAT : Type of material.

AXMUL1 : Multiplier for the stress coordinate of the non-linear curve.

AXMUL2 : Multiplier for the strain coordinate of the non-linear curve.

SUBROUTINE STIFT 1(N)

I, J, K, L : Element connections, later used as loop counters.

SUBROUTINE STIFT 2(N)

I, J, K : Element connections, later used as loop counters.

AJ,BJ,AK,BK : Local coordinates of triangles.

SUBROUTINE FORMK

NROWB :)
NCOLB :) Variables defining location of element stiffness matrix.
NCOL :)

SUBROUTINE SOLVE

N : Equation counter for elimination and back-substitution.

G : Working variable for the elimination process.

SUBROUTINE STRESS

DIS : Vector of displacement.
EQUIVALENCE statement allows array DSIS(2,200) to be used for the solution vector C(400).

SMAX : Maximum principal stress for element N.

SMIN : Minimum principal stress for element N.

ANG : Clockwise angle from vertical to line of action of maximum principal stress for element N.

EMAX : Maximum principal strain for element N.

EMIN : Minimum principal strain for element N.

EANG : Clockwise angle from vertical to line of action of maximum principal strain for element N.

SUBROUTINE REAC

J1,J2,K1, :) Element horizontal and vertical reaction
K2,L1,L2 :) directions corresponding to nodes.

U : Vector of element nodal displacements.

SUBROUTINE LARDEF

SUMPW : Incremental deformation energy for the entire continuum.

SUMPD : Incremental power of deformation for the entire continuum.

DUP : Working variable for calculation of deformation energy for element N.

DUPV : Incremental deformation energy for element N.

PDOF : Incremental power of deformation for element N.

SUBROUTINE AVER

SFORCE : Working variable for summation of incremental stresses in elements connected at node, later used for average incremental stresses at node.

SSIGTO : Working variable for summation of total stresses in elements connected at node, later used for average total stresses at node.

SSTRTO : Working variable for summation of total strains in elements connected at node, later used for average total strains at node.

SSTR : Working variable for summation of incremental strains in elements connected at node, later used for average incremental strains at node.

SESPSX :
SEPSY :
SGAMXY : Working variables for summation of incremental horizontal, vertical and shear strain rates, respectively, in elements connected at node, later used for average incremental values at node.

NOEL	:	Counter for number of elements attached to node.

SUBROUTINE NONLIN

EPRE	:	E-value of an element at previous increment
PRSTTO	:	Principal strain (ε_b).
NC	:	Nonlinear curve number.
BOTSTR	:	Intermediate values in interpolation for stress difference ($\sigma_1 - \sigma_3$) corresponding to strain, ε_i.
TOPSTR	:	
STRNEW	:	
DZNOM	:	
FUMER	:	

SUBROUTINE JNONL

TOWM	:	Ultimate strength of joint material employing the hyperbolic formulation.
NV	:	Nonlinear curve number.
AHI	:	Interpolated (a) and (b) coefficients, Eq. (2.33).
BHI	:	

A.4 LISTING OF PROGRAM "MAIN-2L"

```
FORTRAN IV G LEVEL  21                 MAIN                DATE = 73195          04/43/41              PAGE 0001

              C      *******************************************************************************
              C      *******************************************************************************
              C                     M A I N - 2L
              C      *******************************************************************************
              C      *******************************************************************************
              C                     NOTE THAT ALL THE RESULTS ARE IN TERMS OF UNIT WIDTH
              C
              C                     PROGRAM CAPACITY
              C       NUMBER OF NONLINEAR MATERIALS                                         =3
              C       NUMBER OF NONLINEAR CONTINUUM MATERIALS                               =1
              C       TOTAL NUMBER OF ELEMENTS                                              =450
              C       NUMBER OF TRIANGULAR ELEMENTS                                         =400
              C       NUMBER OF JOINT ELEMENTS                                              =50
              C       NUMBER OF NODAL POINTS                                                =200
              C       NUMBER OF SPECIFIED BOUNDARY CONDITIONS(LOAD OR DISPLACEMENTS)        =50
              C       NUMBER OF SPECIFIED PRESSURE BOUNDARY CONDITIONS                      =10
              C       NUMBER OF NONLINEAR CURVES FOR EACH CONTINUUM MATERIAL                =10
              C       NUMBER OF POINTS ON EACH NONLINEAR CONTINUUM CURVE                    =50
              C       NUMBER OF NONLINEAR CURVES FOR EACH JOINT MATERIAL                    =10
              C       BAND WIDTH                                                            =80
              C       CONTROL MAIN PROGRAM
 0001                 COMMON/CONTR/TITLE(12),NP,NE,NB,NDF,NCN,NLD,NMAT,NSZF,LI,NT4,NT5
                     1,NOPC,NCMAT
 0002                 COMMON/DATA/CORD(200,2),NOP(450,4),IMAT(450),NBC(50),CODE(200),UX
                     1(200),UY(200),IBC(10),JBC(10),PRE(10),T(450),XDEN,YDEN,ORX(450),
                     2ORY(450),PRCORD(200,2)
 0003                 COMMON/ANAL/NOINC,KOUNT,NTEST,LTEST,NITER,NOITER,VEL,THO
 0004                 COMMON/STIFF/ESTIFM(12,12),A(3,6),B(3,6),SK(400,80),AREA(450),
                     1C(400),R(8),H(8),WBAND,D(400),AR(400)
 0005                 COMMON/STRES/DISTO(2,200),SIGTO(450,4),STRTO(450,3),SMAXTO(450),
                     1SMINTO(450),ANGTO(450),EANGTO(450),EMAXTO(450),EMINTO(450),FORCE
                     1(450,4),STR(450,3),PSIGTO(450,4),PSTRTO(450,3),POISTO(2,200)
 0006                 COMMON/NONL/NCUR(2),CPN(2,10),NPTS(2,10),EG(50),GAM(50),
                     1EY(2,10,50),GAMOC(2,10,50),PRESTR(450),PRSDEV(450),CONPRE(450)
 0007                 COMMON/DEF/DX(200),DY(200),VX(200),VY(200),EPSX(450),EPSY(450),
                     1GAMXY(450),EPSI1(450),EPSI2(450),PSI(450),CSUMPO,CSUMPW
 0008                 COMMON/ELAS/E,ENU,EE(450),EC(450),DKSEJ,DKNIJ,DKSII,DKNII
 0009                 COMMON/JOINT/T1(8,8),BL(8,8),AL(450),ANG(450),DKS(450),DKN(450),SD
                     1(2,2),W(450,2),P(450,2),V(450,2),AVP(450,2),CV(450,2),CAVP(450,2),
                     2PCV(450,2),PCAVP(450,2),BI(8,8)
 0010                 COMMON/JNONL/NVAL(2),CNP(2,10),AM(2,10),BM(2,10)
 0011                 COMMON/AVRG/AVSMAX(200),AVSMIN(200),AVANG(200),AVTMX(200),
                     1AVTMN(200),AVTANG(200),AVSMX(200),AVSMN(200),AVSANG(200),
                     2AVSTMX(200),AVSTMN(200),AVSTAN(200),AVPSI1(200),AVPSI2(200),
                     3AVPSI(200)
 0012                 INTEGER WBAND
              C
              C                     INITALIZE TAPE NO.
              C                     AND NUMBER OF CORNER NODE MAX.
 0013                 NT4=11
 0014                 NT5=12
 0015                 READ(5,1) NPROB
              C                     LOOP ON NO. OF PROBLENS
 0016                 DO 405 NPR=1,NPROB
```

```
FORTRAN IV G LEVEL  21              MAIN            DATE = 73195         04/43/41              PAGE 0002

                C                  READ INPUT GEOMETRY AND PROP.
 0017                 READ(5,100) NTEST
 0018             100 FORMAT(I5)
 0019                 LTEST=0
 0020                 CALL GDATA1
 0021                 NSZF=NP*NDF
                C                  DETERMINATION OF BAND WIDTH
                C                  FIND LARGEST DIFFERENCE IN NODAL NUMBERS
                C                  IN ANY ELEMENT
 0022                 JJ=0
 0023                 DO 350 N=1,NE
 0024                 DO 350 I=1,4
 0025                 DO 360 L=1,4
 0026                 KK=IABS(NOP(N,I)-NOP(N,L))
 0027                 IF(KK-JJ) 360,360,365
 0028             365 JJ=KK
 0029             360 CONTINUE
 0030             350 CONTINUE
                C                  COMPUTE BAND WIDTH AS 2*JJ+NO. OF DEGREES
                C                  OF FREEDOM
 0031                 WBAND=2*JJ+2
 0032                 WRITE(6,12) WBAND
                C                  READ NONLINEAR STRESS-STRAIN VALUES
 0033                 IF(NTEST.EQ.LTEST) GO TO 300
 0034                 CALL GDATA2
                C                  INITIALIZE ALL STRESSES AND STRAINS
 0035             300 DO 200 N=1,NE
 0036                 IF(IMAT(N).EQ.3) GO TO 104
 0037                 IF(NOP(N,3).NE.NOP(N,4)) GO TO 101
 0038                 DO 500 I=1,4
 0039             500 SIGTO(N,I)=0.0
 0040                 DO 301 I=1,3
 0041             301 STRTO(N,I)=0.0
 0042                 SMAXTO(N)=0.0
 0043                 SMINTO(N)=0.0
 0044                 EMAXTO(N)=0.0
 0045                 EMINTO(N)=0.0
 0046                 PRESTR(N)=0.0
 0047                 PREDEV(N)=0.0
 0048                 CONPRE(N)=0.0
 0049                 EE(N)=E
                C                  INITIALIZE JOINT STRESS-STRAIN PROPERTIES
 0050                 GO TO 20C
 0051             101 DKN(N)=DKNIJ
 0052                 DKS(N)=DKSIJ
 0053                 GO TO 105
 0054             104 DKN(N)=DKNII
 0055                 DKS(N)=DKSII
 0056             105 DO 102 I=1,2
 0057                 CV(N,I)=0.0
 0058             102 CAVP(N,I)=0.0
 0059             200 CONTINUE
 0060                 CSUMPD=0.0
 C061                 CSUMPW=0.C
```

```
FORTRAN IV G LEVEL  21                MAIN              DATE = 73195        04/43/41          PAGE 0003
                C                     INITIALIZE ALL NODAL DISPLACEMENTS TO ZERO
 0062                 DO 600 M=1,NP
 0063                 DO 600 J=1,2
 0064             600 DISTO(J,M)=0.0
                C                     INITIALIZE ALL REACTIONS TO ZERO
 0065                 DO 437 J=1,NB
 0066                 M=NBC(J)
 0067                 N=2*M-1
 0068                 L=2*M
 0069                 AR(N)=0.0
 0070                 AR(L)=0.0
 0071             437 CONTINUE
                C                     INCREMENTAL LOADS AND DISPLACEMENTS
 0072                 DO 800 K=1,NB
 0073                 NN=NBC(K)
 0074                 UX(NN)=UX(NN)/NOINC
 0075                 UY(NN)=UY(NN)/NOINC
 0076             800 CONTINUE
 0077                 IF (NOPC.EQ.0) GO TO 711
 0078                 DO 710 LI=1,NOPC
 0079             710 PRE(LI)=PRE(LI)/NOINC
 0080             711 CONTINUE
                C                     LOOP ON NO. OF INCREMENTS
 0081                 KOUNT=1
 0082                 DO 700 IK=1,NOINC
 0083                 DO 714 L=1,NOITER
 0084                 NITER=L
 0085                 REWIND NT4
 0086                 REWIND NT5
                C                     FORM STIFFNESS MATRIX THEN SOLVE
                C                     SIMULTANEOUS EQUATIONS
 0087                 CALL FORMK
 0088                 CALL SOLVE
                C                     CALCULATE STRESSES
 0089                 CALL STRESS
 0090                 CALL JSTRES
                C                     ITERATE ON ELASTIC MODULUS
 0091                 IF(NTEST.EQ.LTEST) GO TO 713
 0092             714 CONTINUE
                C                     DETERMINATION OF REACTIONS
 0093                 IF(NITER.NE.NOITER) GO TO 440
 0094                 DO 438 L=1,NB
 0095                 M=NBC(L)
 0096                 DO 901 NI=1,NE
 0097                 IF(NOP(NI,3).NE.NOP(NI,4)) GO TO 706
 0098                 NCN=3
 0099                 GO TO 707
 0100             706 NCN=4
 0101             707 DO 901 I=1,NCN
 0102                 IF(NOP(NI,I)-M) 901,705,901
 0103             705 N=NI
 0104                 J=I
 0105                 IF(CODE(M)) 438,438,422
 0106             422 CALL REAC(J,M,N)
```

```
FORTRAN IV G LEVEL  21                MAIN               DATE = 73195          04/13/41              PAGE 0004

 0107            901 CONTINUE
 0108            430 CONTINUE
 0109            440 CONTINUE
               C                  WRITE REACTIONS
 0110                IF(NITER.NE.NOITER) GO TO 441
 0111                WRITE(6,203)
 0112                DO 439 K=1,NB
 0113                M=NBC(K)
 0114                N=2*M-1
 0115                L=2*M
               C                  ADD BODY FORCES TO FIRST INCREMENT
 0116                IF(CODE(M).NE.1.) GO TO 501
 0117                AR(N)=AR(N)-D(N)
 0118                GO TO 503
 0119            501 IF(CODE(M).EQ.2.) GO TO 502
 0120                AR(N)=AR(N)-D(N)
 0121            502 AR(L)=AR(L)-D(L)
 0122            503 CONTINUE
 0123                WRITE(6,201) M,AR(N),AR(L)
 0124            439 CONTINUE
 0125            441 CONTINUE
               C                  CHANGE ELEMENT COORDINATES
 0126            713 IF(NOINC.EQ.1) GO TO 712
 0127                CALL LARDEF
               C                  AVERAGE STRESSES , STRAINS AND STRAIN RATES IN ADJACENT
               C                  ELEMENTS
 0128                CALL AVER
 0129                KOUNT=KOUNT+1
 0130            700 CONTINUE
 0131            712 CONTINUE
 0132            400 CONTINUE
 0133              1 FORMAT(9I5)
 0134             12 FORMAT('0',1X,'BAND WIDTH=',I5)
 0135            201 FORMAT(I5,2F15.6)
 0136            203 FORMAT('1',5X,'TABLE 11- REACTIONS'//
                    1                          10X,'X-REACTIONS',10X,'Y-REACTIONS')
 0137                STOP
 0138                END

  *OPTIONS IN EFFECT*  ID,EBCDIC,SOURCE,NOLIST,NODECK,LOAD,NOMAP
  *OPTIONS IN EFFECT*  NAME = MAIN    , LINECNT =       56
  *STATISTICS*    SOURCE STATEMENTS =       138,PROGRAM SIZE =      3212
  *STATISTICS*  NO DIAGNOSTICS GENERATED
```

```
FORTRAN IV G LEVEL  21                 GDATA1              DATE = 73195          04/43/41              PAGE 0001

 0001                SUBROUTINE GDATA1
 0002                COMMON/CONTR/TITLE(12).NP.NE.NB.NDF.NCN.NLD.NMAT.NSZF.LI.NT4.NT5
                    1.NCPC.NCMAT
 0003                COMMON/DATA/CORD(200.2).NOP(450.4).IMAT(450).NBC(50).CODE(200).UX
                    1(200).UY(200).IBC(10).JBC(10),PHE(10).T(450).XDEN.YDEN.DRX(450).
                    2DRY(450).PRCORD(200.2)
 0004                COMMON/ANAL/NOINC.KOUNT.NTEST.LTEST.NITER.NOITER.VEL.THO
 0005                COMMON/STIFF/ESTIFM(12.12).A(3.6).B(3.6).SK(400.80).AREA(450).
                    1C(400).R(8).H(8).WBAND.D(400).AR(400)
 0006                COMMON/ELAS/E.ENU.EE(450).EC(450).DKSIJ.DKNIJ.DKSII.DKNII
 0007                INTEGER WBAND
              C
              C                    READ AND PRINT TITLE AND CONTROL
 0008                READ(5.7) TITLE
 0009                WRITE(6.100) TITLE
 0010                READ(5.1) NP.NE.NB.NDF.NMAT.NCMAT.NOPC.XDEN.YDEN.II
 0011                WRITE(6.9)
 0012                WRITE(6.10) NP.NE.NB.NDF.NMAT.NCMAT.NOPC.XDEN.YDEN.II
              C                    READ AND PRINT MATERIAL DATA
 0013                READ(5.8) E.ENU.DKSIJ.DKNIJ.DKSII.DKNII
 0014                WRITE(6.108)
 0015                WRITE(6.8)E.ENU.DKSIJ.DKNIJ.DKSII.DKNII
              C                    READ NODAL POINT DATA
 0016                READ(5.2)(N.(CORD(N.M).M=1.2).L=1.NP)
              C                    READ ELEMENT DATA
 0017                READ(5.3)(N.(NOP(N.M).M=1.4).IMAT(N).T(N).L=1.NE)
              C                    READ BOUNDARY DATA
              C      CODE=0.0.SPECIFIED LOAD IN X AND Y DIRECTIONS
              C      CODE=1.0.SPECIFIED DISPLACEMENT IN X DIRECTION- LOAD IN Y DIRECTION
              C      CODE=2.0.SPECIFIED LOAD IN X DIRECTION- DISPLACEMENT IN Y DIRECTION
              C      CODE=3.0.SPECIFIED DISPLACEMENT IN X AND Y DIRECTIONS,
 0018                READ(5.12) (NBC(I).I=1.NB)
 0019                DO 800 K=1.NB
 0020                NN=NBC(K)
 0021            800 READ(5.13) CODE(NN).UX(NN).UY(NN)
              C                    READ BLADE VELOCITY AND HORIZONTAL TRAVEL DISTANCE
 0022                READ(5.8) THO.VEL.BANGLE
              C                    READ PRESSURE BOUNDARY CONDITIONS
 0023                IF(NOPC.EQ.0) GO TO 110
 0024                DO 490 L=1.NOPC
 0025                READ(5.118) IBC(L).JBC(L).PHE(L)
 0026            490 CONTINUE
              C                    READ NO. OF INCREMENTS AND NO. OF ITERATIONS
 0027            110 READ(5.4) NOINC.NOITER
 0028            480 IF(II.NE.0) GO TO 500
              C                    PRINT INPUT DATA
 0029                WRITE(6.102)
 0030                WRITE(6.2) (N.(CORD(N.M).M=1.2).N=1.NP)
 0031                WRITE(6.103)
 0032                WRITE(6.3) (N.(NOP(N.M).M=1.4).IMAT(N).T(N).N=1.NE)
 0033                WRITE(6.104)
 0034                DO 900 K=1.NB
 0035                NN=NBC(K)
 0036            900 WRITE(6.11)NN.CODE(NN).UX(NN).UY(NN)
```

```
FORTRAN IV G LEVEL  21              GDATA1              DATE = 73195          04/43/41               PAGE 0002

                IF(NOPC.EQ.0) GO TO 113
                WRITE(6,475)
                WRITE(6,510) (IBC(L),JBC(L),PRE(L),L=1,NOPC)
            113 CONTINUE
                WRITE(6,111) THD,VEL,DANGLE
            111 FORMAT(//,1X,'TRAVEL DISTANCE=',F10.2,3X,'INCH'/1X,'BLADE VELOCITY
               1 =',F10.2,3X,'INCH/MINUTE'/1X,'BLADE ANGLE WITH HORIZONTAL=',F10.
               2,3X,'DEGREES')
                IF(NTEST.EQ.LTEST) GO TO 300
                WRITE(6,301)
                GO TO 112
            300 WRITE(6,303)
            301 FORMAT(//,1X,'NONLINEAR ANALYSIS'//)
            303 FORMAT(//,1X,'LINEAR ANALYSIS'//)
            112 WRITE(6,105) NOINC,NOITER
            800 CONTINUE
              1 FORMAT(7I5,2F10.3,I5)
              2 FORMAT(I10,2F10.3)
              3 FORMAT(6I5,F10.3)
              4 FORMAT(2I5)
              7 FORMAT(12A6)
              8 FORMAT(2F10.2,4E15.7)
              9 FORMAT(5X,'NP',6X,'NE',6X,'NB',5X,'NOF',5X,'NMAT',3X,'NCMAT',4X,
               1'NOPC',6X,'DENSITY'/60X,'X',9X,'Y')
             10 FORMAT(7I8,2F10.3,I5)
            100 FORMAT('1',5X,12A4//5X,'TABLE I - INPUT GEOMETRY AND PROPERTIES'//
               1)
            102 FORMAT(1X,'NODAL POINTS  ')
            103 FORMAT(1X,'ELEMENTS      ')
            104 FORMAT(1X,'BOUNDARY CONDITIONS ')
            105 FORMAT(1X,'NO. OF INCREMENTS=',I5/1X,'NO. OF ITERATIONS=',I5)
            108 FORMAT(1H0,'MATERIAL PROPERTIES ')
            116 FORMAT(2I5,E10.3)
            475 FORMAT('0',2X,'PRESSURE BOUNDARY CONDITIONS',//,16X,'I',3X,'J',
               12X,'PRESSURE')
             11 FORMAT(I5,F10.3,2E15.7)
            510 FORMAT(5X,2I5,E10.3)
             12 FORMAT(15I5)
             13 FORMAT(F10.3,2E15.7)
                RETURN
                END

 *OPTIONS IN EFFECT*  ID,EBCDIC,SOURCE,NOLIST,NODECK,LOAD,NOMAP
 *OPTIONS IN EFFECT*  NAME = GDATA1  , LINECNT =       56
 *STATISTICS*    SOURCE STATEMENTS =       72,PROGRAM SIZE =      2960
 *STATISTICS*  NO DIAGNOSTICS GENERATED
```

```
FORTRAN IV G LEVEL  21              GDATA2            DATE = 73195        04/43/41            PAGE 0001

              SUBROUTINE GDATA2
              COMMON/CONTR/TITLE(12),NP,NE,NB,NDF,NCN,NLD,NMAT,NSZF,LI,NT4,NTS
             1,NOPC,NCMAT
              COMMON/NONL/NCUR(2),CPR(2,10),NPTS(2,10),EG(50),GAM(50),
             1EV(2,10,50),GAMOC(2,10,50),PRESTR(450),PREDEV(450),COMPRE(450)
              COMMON/JNONL/NVAL(2),CNP(2,10),AM(2,10),BM(2,10)
C
C                      DATA FOR NONLINEAR MATERIAL PROPERTIES
C
C                      THE INPUT CURVE FOR EACH CONFINING PRESSURE IS
C                      (SIGMA1-SIGMA3) VS EPSILON1
C
C                      START READING NON-LINEAR INPUT DATA
C
              WRITE(6,66)
              READ(5,95) THAT
C                  NCURV IS THE NUMBER OF NONLINEAR CURVES INPUT
              READ(5,100) (NCUR(I),I=1,NCMAT)
              DO 3000 I=1,NCMAT
              NCURV=NCUR(I)
              IF (NCURV) 304,304,310
          304 WRITE(6,452)
              STOP
          310 DO 330 NC=1,NCURV
              READ(5,110) CPR(I,NC),AXMUL1,AXMUL2,NPTS(I,NC)
              WRITE (6,459) NC,CPR(I,NC),NPTS(I,NC)
              NPT=NPTS(I,NC)
              READ(5,120) (EG(LP),LP=1,NPT)
              READ(5,120) (GAM(LP),LP=1,NPT)
              WRITE(6,465)
              DO 330 LP=1,NPT
              EV(I,NC,LP)=EG(LP)*AXMUL1
              GAMOC(I,NC,LP)=GAM(LP)*AXMUL2
              WRITE(6,472) EV(I,NC,LP),GAMOC(I,NC,LP)
          330 CONTINUE
         3000 CONTINUE
C                      DATA FOR JOINT NONLINEAR PROPERTIES
C                      THE INPUT VALUES FOR EACH NORMAL PRESSURE
C                      ARE HYPERBOLIC COEFFICIENTS A AND B
              IF(NMAT.EQ.NCMAT) GO TO 601
              NL=NCMAT+1
              READ(5,100) (NVAL(I),I=NL,NMAT)
              WRITE(6,67)
              DO 600 I=NL,NMAT
              NVALUE=NVAL(I)
              IF(NVALUE)603,603,604
          603 WRITE(6,609)
              STOP
          604 WRITE(6,607)
              DO 605 NV=1,NVALUE
              READ(5,606) CNP(I,NV),AM(I,NV),BM(I,NV)
              WRITE(6,608) NV,CNP(I,NV),AM(I,NV),BM(I,NV)
          605 CONTINUE
          600 CONTINUE
```

```
FORTRAN IV G LEVEL  21              GDATA2           DATE = 73195          04/43/41              PAGE 0002

      401 CONTINUE
      609 FORMAT(5X,'ERROR IN NVALUE CARD')
      606 FORMAT(3F10.3)
      607 FORMAT(2X,'NUM.    NORMAL PRESS.    A-VALUE    B-VALUE')
      608 FORMAT(2X,I5,3(F10.3,5X))
      100 FORMAT(5I5)
       67 FORMAT(//,5X,'TABLE 3 - JOINT NONLINEAR CURVES'///)
       75 FORMAT(A4)
      452 FORMAT(5X,'ERROR IN NCURVE CARD')
      110 FORMAT(3E10.3,I5)
      459 FORMAT(10X,' NUM.        CONF. PRESS.        NUM. OF POINTS',/
         19X,I5,10X,E10.3,8X,I5)
      465 FORMAT(4X,' DEV. STRESS',3X,'AXIAL STRAIN')
      472 FORMAT(5X,E10.3,5X,E10.3)
       66 FORMAT('1',5X,'TABLE 2 - NONLINEAR CURVES',//)
      120 FORMAT(10F7.3)
          RETURN
          END

 *OPTIONS IN EFFECT*  ID,EBCDIC,SOURCE,NOLIST,NODECK,LOAD,NOMAP
 *OPTIONS IN EFFECT*  NAME = GDATA2  , LINECNT =       56
 *STATISTICS*    SOURCE STATEMENTS =        57,PROGRAM SIZE =      1828
 *STATISTICS*  NO DIAGNOSTICS GENERATED
```


-7434333

```
FORTRAN IV G LEVEL  21              STIFT1              DATE = 73195          04/43/41                    PAGE 0001

0001           SUBROUTINE STIFT1(N)
          C                      J O I N T   E L E M E N T
0002           COMMON/CONTR/TITLE(12),NP,NE,NB,NDF,NCN,NLD,NMAT,NSZF,LI,NT4,NTS
              1,NOPC,NCMAT
0003           COMMON/DATA/CORD(200,2),NOP(450,4),IMAT(450),NBC(50),CODE(200),UX
              1(200),UY(200),IBC(10),JBC(10),PRE(10),T(450),XDEN,YDEN,ORX(450),
              2ORY(450),PRCORD(200,2)
0004           COMMON/STIFF/ESTIFM(12,12),A(3,6),W(3,6),SK(400,80),AREA(450),
              1C(400),R(8),H(8),MBAND,D(400),AR(400)
0005           COMMON/ JOINT/T1(8,8),DL(6,8),AL(450),ANG(450),DKS(450),DKN(450),SD
              1(2,2),W(450,2),P(450,2),V(450,2),AVP(450,2),CV(450,2),CAVP(450,2),
              2PCV(450,2),PCAVP(450,2),B1(8,8)
0006           I=NOP(N,1)
0007           J=NOP(N,2)
0008           K=NOP(N,3)
0009           L=NOP(N,4)
0010           IF(CORD(I,1).EQ.CORD(J,1)) GO TO 11
0011           ANG(N)=ATAN((CORD(J,2)-CORD(I,2))/(CORD(J,1)-CORD(I,1)))
0012           GO TO 12
0013        11 ANG(N)=90.0/57.29578
0014        12 CONTINUE
0015           AL(N)=SQRT((CORD(J,2)-CORD(I,2))**2+(CORD(J,1)-CORD(I,1))**2)
0016           ORX(N)=(CORD(I,1)+CORD(J,1)+CORD(K,1)+CORD(L,1))/4.
0017           ORY(N)=(CORD(I,2)+CORD(J,2)+CORD(K,2)+CORD(L,2))/4.
          C                      JOINT ELEMENT
          C                      SUBROUTINE STIFF JOINT
          C                      ESTIFM IS STIFFNESS MATRIX
0018           DO 3 I=1,8
0019           DO 3 J=1,8
0020         3 ESTIFM(I,J)=0.0
0021           ESTIFM(1,1)=DKS(N)*AL(N)/3.0
0022           ESTIFM(1,3)=ESTIFM(1,1)/2.0
0023           ESTIFM(1,5)=-ESTIFM(1,3)
0024           ESTIFM(1,7)=-ESTIFM(1,1)
0025           ESTIFM(2,2)=DKN(N)*AL(N)/3.0
0026           ESTIFM(2,4)=ESTIFM(2,2)/2.0
0027           ESTIFM(2,6)=-ESTIFM(2,4)
0028           ESTIFM(2,8)=-ESTIFM(2,2)
0029           ESTIFM(3,3)=ESTIFM(1,1)
0030           ESTIFM(3,5)=-ESTIFM(1,1)
0031           ESTIFM(3,7)=-ESTIFM(1,1)/2.0
0032           ESTIFM(4,4)=ESTIFM(2,2)
0033           ESTIFM(4,6)=-ESTIFM(2,2)
0034           ESTIFM(4,8)=-ESTIFM(2,2)/2.0
0035           ESTIFM(5,5)=ESTIFM(1,1)
0036           ESTIFM(5,7)=ESTIFM(1,1)/2.0
0037           ESTIFM(6,6)=ESTIFM(2,2)
0038           ESTIFM(6,8)=ESTIFM(2,2)/2.0
0039           ESTIFM(7,7)=ESTIFM(1,1)
0040           ESTIFM(8,8)=ESTIFM(2,2)
0041           DO 4 K=1,7
0042           K1=K+1
0043           DO 4 J=K1,8
0044         4 ESTIFM(J,K)=ESTIFM(K,J)
```

```
FORTRAN IV G LEVEL  21              STIFT1            DATE = 73195         04/43/41             PAGE 0002
          C                 DETERMINE TRANSFORMATION MATRIX
                  E=COS(ANG(N))
                  S=SIN(ANG(N))
                  DO 5 I=1,8
                  DO 5 J=1,8
                5 T1(I,J)=0.0
                  DO 6 I=1,8
                  J=I
                6 T1(I,J)=C
                  DO 7 I=1,7,2
                  J=I+1
                7 T1(I,J)=S
                  DO 8 I=2,8,2
                  J=I-1
                8 T1(I,J)=-S
          C                 TRANSFORM STIFFNESS MATRIX TO GLOBAL AXES
                  DO 9 I=1,8
                  DO 9 J=1,8
                  BL(I,J)=0.0
                  DO 9 L=1,8
                9 BL(I,J)=BL(I,J)+ESTIFM(I,L)*T1(L,J)
                  DO 10 I=1,8
                  DO 10 J=1,8
                  ESTIFM(I,J)=0.0
                  DO 10 L=1,8
               10 ESTIFM(I,J)=ESTIFM(I,J)+BL(L,I)*T1(L,J)
                  RETURN
                  END

  *OPTIONS IN EFFECT*  ID,EBCDIC,SOURCE,NOLIST,NODECK,LOAD,NOMAP
  *OPTIONS IN EFFECT*  NAME = STIFT1  , LINECNT =       56
  *STATISTICS*    SOURCE STATEMENTS =       70,PROGRAM SIZE =      2340
  *STATISTICS*  NO DIAGNOSTICS GENERATED
```

```
0001            SUBROUTINE STIFT2(N)
0002            COMMON/CONTR/TITLE(12),NP,NE,NB,NDF,NCN,NLD,NMAT,NSZF,LI,NT4,NTS
               1,NOPC,NCMAT
0003            COMMON/DATA/CORD(200,2),NOP(450,4),IMAT(450),NBC(50),CODE(200),UX
               1(200),UY(200),IBC(10),JBC(10),PRE(10),T(450),XDEN,YDEN,ORX(450),
               2ORY(450),PRCOND(200,2)
0004            COMMON/STIFF/ESTIFM(12,12),A(3,6),B(3,6),SK(400,80),AREA(450),
               1C(400),H(8),H(8),WBAND,D(400),AR(400)
0005            COMMON/ELAS/E,ENU,EE(450),EC(450),DKSIJ,DKNIJ,DKSII,DKNII
0006            INTEGER WBAND
          C                   DETERMINE ELEMENT CONNECTIONS
0007            I=NOP(N,1)
0008            J=NOP(N,2)
0009            K=NOP(N,3)
0010            ORX(N)=(CORD(I,1)+CORD(J,1)+CORD(K,1))*0.333333
0011            ORY(N)=(CORD(I,2)+CORD(J,2)+CORD(K,2))*0.333333
          C                   SET UP LOCAL COORDINATE SYSTEM
0012            AJ=CORD(J,1)-CORD(I,1)
0013            AK=CORD(K,1)-CORD(I,1)
0014            BJ=CORD(J,2)-CORD(I,2)
0015            BK=CORD(K,2)-CORD(I,2)
0016            AREA(N)=(AJ*BK-AK*BJ)/2.
0017            IF(AREA(N).LE.0.) GO TO 220
                              FORM STRAIN DISP. MATRIX
          C                   AND SAVE ON TAPE
0018            A(1,1)=BJ-BK
0019            A(1,2)=0.
0020            A(1,3)=BK
0021            A(1,4)=0.
0022            A(1,5)=-BJ
0023            A(1,6)=0.
0024            A(2,1)=0.
0025            A(2,2)=AK-AJ
0026            A(2,3)=0.
0027            A(2,4)=-AK
0028            A(2,5)=0.
0029            A(2,6)=AJ
0030            A(3,1)=AK-AJ
0031            A(3,2)=BJ-BK
0032            A(3,3)=-AK
0033            A(3,4)=BK
0034            A(3,5)=AJ
0035            A(3,6)=-BJ
0036            WRITE(NTS) N,((A(I,J),J=1,6),I=1,3)
          C                   FORM STRESS STAIN MATRIX
0037            COMM=EE(N)/((1.+ENU)*(1.-ENU*2.)*AREA(N))
0038            ESTIFM(1,1)=COMM*(1.-ENU)
0039            ESTIFM(1,2)=COMM*ENU
0040            ESTIFM(1,3)=0.
0041            ESTIFM(2,1)=ESTIFM(1,2)
0042            ESTIFM(2,2)=ESTIFM(1,1)
0043            ESTIFM(2,3)=0.
0044            ESTIFM(3,1)=0.
0045            ESTIFM(3,2)=0.
```

```
FORTRAN IV G LEVEL  21                STIFT2            DATE = 73195          04/43/41               PAGE 0002

 0046               ESTIFM(3,3)=EE(N)/(2.*(1.+ENU)*AREA(N))
              C                        B IS THE STRESS BACKSUBSTITUTION
              C                        MATRIX AND IS SAVED ON TAPE
 0047               DO 205 I=1,3
 0048               DO 205 J=1,6
 0049               B(I,J)=0.
 0050               DO 205 K=1,3
 0051           205 B(I,J)=B(I,J)+ESTIFM(I,K)/2.*A(K,J)
 0052               WRITE(NT4) N,((B(I,J),J=1,6),I=1,3)
              C                        ESTIFM IS STIFFNESS MATRIX
 0053               DO 210 I=1,6
 0054               DO 210 J=1,6
 0055               ESTIFM(I,J)=0.
 0056               DO 210 K=1,3
 0057           210 ESTIFM(I,J)=ESTIFM(I,J)+B(K,I)/2.*A(K,J)
 0058               RETURN
              C                        ERROR EXIT FOR BAD CONNECTIONS
 0059           220 WRITE(6,100) N
 0063           100 FORMAT('ZERO OR NEGATIVE AREA ELEMENT NO',I4/'EXECUTION TERMINATED
                   1')
 0061               STOP
 0062               END

 *OPTIONS IN EFFECT*  ID,EBCDIC,SOURCE,NOLIST,NODECK,LOAD,NOMAP
 *OPTIONS IN EFFECT*  NAME = STIFT2  , LINECNT =       56
 *STATISTICS*    SOURCE STATEMENTS =       62,PROGRAM SIZE =      1966
 *STATISTICS*  NO DIAGNOSTICS GENERATED
```

```
                 SUBROUTINE FORMK
           C                          FORMS STIFFNESS MATRIX
                 COMMON/CONTR/TITLE(12),NP,NE,NB,NDF,NCN,NLD,NMAT,NSZF,LI,NT4,NTS
                1,NOPC,NCMAT
                 COMMON/DATA/CORD(200,2),NOP(450,4),IMAT(450),NBC(50),CODE(200),UX
                1(200),UY(200),IHC(10),JUC(10),PRE(10),T(450),XDEN,YDEN,ORX(450),
                2ORY(450),PRCORD(200,2)
                 COMMON/ANAL/NOINC,KOUNT,NTEST,LTEST,NITER,NOITER,VEL,TMD
                 COMMON/STIFF/ESTIFM(12,12),A(3,6),B(3,6),SK(400,80),AREA(450),
                1C(400),R(8),M(8),MBAND,D(400),AM(400)
                 DIMENSION XE(3,2)
                 INTEGER MBAND
           C                          ZERO STIFFNESS MATRIX
                 DO 300 N=1,NSZF
                 C(N)=0.0
                 D(N)=0.0
                 DO 300 M=1,MBAND
             300 SK(N,M)=0.
           C                          SCAN ELEMENTS
                 DO 400 N=1,NE
                 IF(NOP(N,3).EQ.NOP(N,4)) GO TO 100
                 CALL STIFT1(N)
                 GO TO 101
             100 CALL STIFT2(N)
             101 CONTINUE
           C                          RETURNS ESTIFM AS STIFFNESS MATRIX
           C
           C                          STORE ESTIFM IN SK
           C                          FIRST ROWS
                 IF(NOP(N,3).EQ.NOP(N,4)) GO TO 307
                 NCN=4
                 GO TO 308
             307 NCN=3
             308 DO 360 JJ=1,NCN
                 NROWB=(NOP(N,JJ)-1)*NDF
                 IF(NROWB)360,305,305
             305 DO 350 J=1,NDF
                 NROWB=NROWB+1
                 I=(JJ-1)*NDF+J
           C                          THEN COLUMNS
                 DO330 KK=1,NCN
                 NCOLB=(NOP(N,KK)-1)*NDF
                 DO 320 K=1,NDF
                 L = (KK-1)*NDF + K
                 NCOL = NCOLB + K + 1 -NROWB
           C                          SKIP STORING IF BELOW BAND
                 IF(NCOL)320,320,310
             310 SK(NROWB,NCOL)=SK(NROWB,NCOL)+ESTIFM(I,L)
             320 CONTINUE
             330 CONTINUE
             350 CONTINUE
             360 CONTINUE
             400 CONTINUE
           C                          ADDITION OF CONCENTRATED FORCES
```

```
FORTRAN IV G LEVEL  21            FORMK            DATE = 73195          04/43/41            PAGE 0002

          DO 297 I=1,NB
          N=NBC(I)
          K=2*N
          IF(CODE(N)-1.) 295,295,296
      296 IF(CODE(N).EQ.2.) GO TO 301
      298 IF(CODE(N)-3.) 425,297,425
      295 C(K)=C(K)+UY(N)
          IF(CODE(N).NE.0.0) GO TO 297
      301 C(K-1)=C(K-1)+UX(N)
          GO TO 297
      425 WRITE(6,426) N
          STOP
      297 CONTINUE
      426 FORMAT(5X,'ERROR IN CODE NUMBER-NODE-EXECUTION TERMINATED',I4)
C                        NORMAL PRESSURE BOUNDARY CONDITION
          IF(NOPC) 306,306,250
      250 DO 302 L=1,NOPC
          I=IBC(L)
          J=JBC(L)
          PP=PRE(L)/2.0
          DX=(CORD(I,2)-CORD(J,2))*PP
          DY=(CORD(J,1)-CORD(I,1))*PP
          II=2*I
          SINA=0.0
          COSA=1.0
          C(II-1)=C(II-1)+(COSA*DX+SINA*DY)
          C(II)=C(II)-(SINA*DX-COSA*DY)
          JJ=2*J
          C(JJ-1)=C(JJ-1)+(COSA*DX+SINA*DY)
          C(JJ)=C(JJ)-(SINA*DX-COSA*DY)
      302 CONTINUE
      306 CONTINUE
C                        CALCULATION OF LOADS DUE TO BODY FORCES
          IF(KOUNT.GT.1) GO TO 30
          IF(XDEN) 880,882,880
      882 IF(YDEN) 880,30,880
      880 DO 20 II=1,NE
          IF(NOP(II,3).NE.NOP(II,4)) GO TO 20
          DO 85 I=1,3
          JJ=NOP(II,I)
          XE(I,1)=CORD(JJ,1)
       85 XE(I,2)=CORD(JJ,2)
          VOL=0.166667      *(XE(2,1)*(XE(3,2)-XE(1,2))+XE(1,1)*(XE(2,2)-
         1XE(3,2))+XE(3,1)*(XE(1,2)-XE(2,2)))
          UT=VOL*XDEN
          VT=VOL*YDEN
          DO 86 I=1,3
          JJ=NOP(II,I)
          C(2*JJ-1)=C(2*JJ-1)+UT
       86 C(2*JJ)=C(2*JJ)+VT
       20 CONTINUE
       30 CONTINUE
C                        TRANSFER LOAD VECTOR TO D
          DO 601 I=1,NSZF
```

```
FORTRAN IV G LEVEL  21              FORMK              DATE = 73195          04/43/41          PAGE 0003

                 D(I)=C(I)
             601 CONTINUE
         C          DISPLACEMENT BOUNDARY CONDITIONS
                 DO 401 J=1,NB
                 M=NBC(J)
                 U=UX(M)
                 M=2*M-1
                 IF(CODE(M)) 401,401,311
             311 IF(CODE(M)-1.0) 401,325,331
             331 IF(CODE(M).EQ.2.) GO TO 336
                 IF(CODE(M)-3.) 401,340,401
             325 CALL MODIFY(SK,C,NSZF,WBAND,M,U)
                 GO TO 401
             340 CALL MODIFY(SK,C,NSZF,WBAND,M,U)
             336 U=UY(M)
                 M=M+1
                 CALL MODIFY(SK,C,NSZF,WBAND,M,U)
             401 CONTINUE
                 RETURN
                 END

 *OPTIONS IN EFFECT*  ID,EBCDIC,SOURCE,NOLIST,NODECK,LOAD,NOMAP
 *OPTIONS IN EFFECT*  NAME = FORMK    , LINECNT =       56
 *STATISTICS*    SOURCE STATEMENTS =      109,PROGRAM SIZE =      3028
 *STATISTICS*  NO DIAGNOSTICS GENERATED
```

```
FORTRAN IV G LEVEL  21              MODIFY          DATE = 73195          04/43/41            PAGE 0001

                    SUBROUTINE MODIFY(SK,B,NUEQ,WBAND,N,U)
                    DIMENSION SK(400,80),B(400)
                    INTEGER WBAND
C                             SUBROUTINE MODIFY MODIFIES THE STIFFNESS MATRIX
C                             SO AS TO ACCOUNT FOR THE SPECIFIED DISPLACEMENTS
                    DO 240 M=2,WBAND
                    K=N-M+1
                    IF(K) 210,210,220
               220  B(K)=B(K)-SK(K,M)*U
                    SK(K,M)=0.0
               210  K=N+M-1
                    IF(NUEQ-K) 240,230,230
               230  B(K)=B(K)-SK(N,M)*U
                    SK(N,M)=0.0
               240  CONTINUE
                    SK(N,1)=1.0
                    B(N)=U
                    RETURN
                    END

 *OPTIONS IN EFFECT*  ID,EBCDIC,SOURCE,NOLIST,NODECK,LOAD,NOMAP
 *OPTIONS IN EFFECT*  NAME = MODIFY  , LINECNT =       56
 *STATISTICS*    SOURCE STATEMENTS =       17,PROGRAM SIZE =       706
 *STATISTICS*  NO DIAGNOSTICS GENERATED
```

```
FORTRAN IV G LEVEL  21                  SOLVE              DATE = 73195        04/43/41              PAGE 0001

 0001                   SUBROUTINE SOLVE
               C           SPECFICATION STATMENTS
 0002                   COMMON/CONTR/TITLE(12),NP,NE,NB,NDF,NCN,NLD,NMAT,NSZF,LI,NT4,NT5
                       1,NDPC,NCMAT
 0003                   COMMON/STIFF/ESTIFM(12,12),A(3,6),B(3,6),SK(400,80),AREA(450),
                       1C(400),R(8),H(8),WBAND,D(400),AN(400)
 0004                   INTEGER WBAND
               C                             REDUCE MATRIX
 0005                   DO 300 N = 1,NSZF
 0006                   I = N
 0007                   DO 290 L=2,WBAND
 0008                   I = I + 1
 0009                   IF(SK(N,L))240,290,240
 0010             240 G =SK(N,L)/SK(N,1)
 0011                   J = 0
 0012                   DO 270 K=L,WBAND
 0013                   J = J + 1
 0014                   IF(SK(N,K))260,270,260
 0015             260 SK(I,J)=SK(I,J) - G*SK(N,K)
 0016             270 CONTINUE
 0017             280 SK(N,L) = G
               C                      AND LOAD VECTOR
               C                      FOR EACH EQUATION
 0018                   C(I)=C(I)-G*C(N)
 0019             290 CONTINUE
 0020             300 C(N)=C(N)/SK(N,1)
               C                      BACK-SUBSTITUTION
 0021                   N=NSZF
 0022             350 N = N - 1
 0023                   IF(N)500,500,360
 0024             360 L = N
 0025                   DO 400 K=2,WBAND
 0026                   L = L + 1
 0027                   IF(SK(N,K))370,400,370
 0028             370 C(N)=C(N)-SK(N,K)*C(L)
 0029             400 CONTINUE
 0030                   GO TO 350
               C
 0031             500 CONTINUE
 0032                   RETURN
 0033                   END

 *OPTIONS IN EFFECT*  ID,EBCDIC,SOURCE,NOLIST,NODECK,LOAD,NOMAP
 *OPTIONS IN EFFECT*  NAME = SOLVE    , LINECNT =       56
 *STATISTICS*    SOURCE STATEMENTS =        33,PROGRAM SIZE =       932
 *STATISTICS*  NO DIAGNOSTICS GENERATED
```

```
FORTRAN IV G LEVEL  21                 STRESS               DATE = 73195          04/43/41                    PAGE 0001

 0001                SUBROUTINE STRESS
 0002                COMMON/CONTR/TITLE(12),NP,NE,NB,NDF,NCN,NLD,NMAT,NSZF,LI,NT4,NT5
                    1,NOPC,NCMAT
 0003                COMMON/DATA/CORD(200,2),NOP(450,4),IMAT(450),NBC(50),CODE(200),UX
                    1(200),UY(200),IBC(10),JBC(10),PRE(10),T(450),XDEN,YDEN,ORX(450),
                    2ORY(450),PRCORD(200,2)
 0004                COMMON/ANAL/NOINC,KOUNT,NTEST,LTEST,NITER,NOITER,VEL,THO
 0005                COMMON/STIFF/ESTIFM(12,12),A(3,6),B(3,6),SK(400,80),AREA(450),
                    1C(400),R(8),H(8),MBAND,D(400),AR(400)
 0006                COMMON/STRES/DISTO(2,200),SIGTO(450,4),STRTO(450,3),SMAXTO(450),
                    1SMINTO(450),ANGTO(450),EANGTO(450),EMAXTO(450),EMINTO(450),FORCE
                    1(450,4),STR(450,3),PSIGTO(450,4),PSTRTO(450,3),PDISTO(2,200)
 0007                COMMON/NONL/NCUR(2),CMR(2,10),NPTS(2,10),EG(50),GAN(50),
                    1EV(2,10,50),GAMDC(2,10,50),PRESTR(450),PREDEV(450),COMPRE(450)
 0008                COMMON/ELAS/E,ENU,EE(450),EC(450),DKSIJ,DKNIJ,DKSII,DKNII
 0009                DIMENSION DIS(2,200)
 0010                EQUIVALENCE(DIS,C)
 0011                INTEGER MBAND
 0012                REWIND NT4
 0013                REWIND NT5
             C                    PRINT DISPLACEMENTS
 0014                IF(NITER.NE.NOITER) GO TO 902
 0015                WRITE(6,100) KOUNT
 0016                WRITE(6,117)(N,(DIS(J,N),J=1,NDF),N=1,NP)
 0017           902  CONTINUE
             C                    NODAL DISPLACEMENTS DUE TO EACH INCREMENT ARE
             C                    CUMULATIVELY ADDED TO THOSE EXISTING BEFORE
 0018                IF(NITER.NE.1) GO TO 601
 0019                DO 280 N=1,NP
 0020                DO 280 J=1,2
 0021                PDISTO(J,N)=DISTO(J,N)
 0022           280  DISTO(J,N)=DISTO(J,N)+DIS(J,N)
 0023           601  DO 602 N=1,NP
 0024                DO 602 J=1,2
 0025           602  DISTO(J,N)=PDISTO(J,N)+DIS(J,N)
 0026                IF(NITER.NE.NOITER) GO TO 903
 0027                WRITE(6,112)
 0028                WRITE(6,117) (N,(DISTO(J,N),J=1,2),N=1,NP)
 0029           903  CONTINUE
             C                    CALCULATE ELEMENT FORCES
             C                    CALCULATE ELEMENT STRAINS
 0030                DO 200 NC=1,NE
 0031                IF(NOP(NC,3).NE.NOP(NC,4)) GO TO 200
 0032                READ(NT4) N,((B(I,J),J=1,6),I=1,3)
 0033                READ(NT5) N,((A(I,J),J=1,6),I=1,3)
 0034                DO 260 I=1,3
 0035                N=NOP(N,I)
 0036                IF(N.EQ.0)GO TO 260
 0037                K = (I - 1)*NDF
 0038                DO 240 J =1,NDF
 0039                IJ = J + K
 0040           240  R(IJ) = DIS(J,N)
 0041           260  CONTINUE
 0042                IA = K + NDF
```


7434343

```
      DO 500 I=1,4
  500 FORCE(N,I)=0.
      DO 300 I = 1,3
      STR(N,I)=0.
      DO 300 J = 1,IA
      STR(N,I)=STR(N,I)+(A(I,J)*R(J))/(2.*AREA(N))
  300 FORCE(N,I) = FORCE(N,I) + B(I,J)*R(J)
      FORCE(N,4)=FORCE(N,4)+ENU*(FORCE(N,1)+FORCE(N,2))
  400 CONTINUE
C                     CALCULATE PRINCIPAL STRESSES
C                     AND DIRECTIONS
      DO 600 N = 1,NE
      IF(NOP(N,3).NE.NOP(N,4)) GO TO 600
  250 G = (FORCE(N,1)+ FORCE(N,2))/2.
      Q=SQRT(((FORCE(N,2)-FORCE(N,1))/2.)**2+ FORCE(N,3)**2)
      SMAX=G+Q
      SMIN=G-Q
      IF(FORCE(N,2).EQ.SMIN)GO TO 700
      ANG=57.29578*ATAN(FORCE(N,3)/(FORCE(N,2)-SMIN))
      GO TO 210
  700 ANG = 90.
  210 CONTINUE
  600 CONTINUE
C                     CALCULATE PRINCIPAL STRAINS
C                     AND DIRECTIONS
      DO 800 N=1,NE
      IF(NOP(N,3).NE.NOP(N,4)) GO TO 800
      E=(STR(N,1)+STR(N,2))/2.
      F=SQRT(((STR(N,2)-STR(N,1))/2.)**2+(STR(N,3)/2.)**2)
      EMAX=E+F
      EMIN=E-F
      IF(STR(N,2).EQ.EMIN) GO TO 900
      EANG=57.29578*ATAN((STR(N,3)/2.)/(STR(N,2)-EMIN))
      GO TO 220
  900 EANG=90.
  220 CONTINUE
  800 CONTINUE
C                     CUMULATIVE STRESSES AND STRAINS
      IF(NITER.NE.1) GO TO 802
      DO 801 N=1,NE
      IF(NOP(N,3).NE.NOP(N,4)) GO TO 801
      DO 290 I=1,3
      PSTRTO(N,I)=STRTO(N,I)
  290 STRTO(N,I)=STRTO(N,I)+STR(N,I)
      DO 304 I=1,4
      PSIGTO(N,I)=SIGTO(N,I)
  304 SIGTO(N,I)=SIGTO(N,I)+FORCE(N,I)
  801 CONTINUE
      GO TO 806
  802 DO 807 N=1,NE
      IF(NOP(N,3).NE.NOP(N,4)) GO TO 807
      DO 803 I=1,3
  803 STRTO(N,I)=PSTRTO(N,I)+STR(N,I)
      DO 805 I=1,4
```

```
FORTRAN IV G LEVEL  21              STRESS              DATE = 73195          04/43/41              PAGE 0003

          805 SIGTO(N,I)=PSIGTO(N,I)+FORCE( N,I)
          807 CONTINUE
          806 CONTINUE
C                   TOTAL PRINCIPAL STRESSES AND STRAINS AND DIRECTIONS
              DO 301 N=1,NE
              IF(NOP(N,3).NE.NOP(N,4)) GO TO 301
              C1=(SIGTO(N,1)+SIGTO(N,2))/2.
              D1=SQRT(((SIGTO(N,2)-SIGTO(N,1))/2.)**2+SIGTO(N,3)**2)
              SMAXTO(N)=C1+D1
              SMINTO(N)=C1-D1
              IF(SIGTO(N,2).EQ.SMINTO(N)) GO TO 701
              ANGTO(N)=57.29578*ATAN(SIGTO(N,3)/(SIGTO(N,2)-SMINTO(N)))
              GO TO 702
          701 ANGTO(N)=90.0
          702 CONTINUE
              E1=(STRTO(N,1)+STRTO(N,2))/2.
              F1=SQRT(((STRTO(N,2)-STRTO(N,1))/2.)**2+(STRTO(N,3)/2.)**2)
              EMAXTO(N)=E1+F1
              EMINTO(N)=E1-F1
              IF(STRTO(N,2).EQ.EMINTO(N)) GO TO 703
              EANGTO(N)=57.29578*ATAN((STRTO(N,3)/2.)/(STRTO(N,2)-EMINTO(N)))
              GO TO 704
          703 EANGTO(N)=90.0
          704 CONTINUE
          301 CONTINUE
C                   CALL SUBROUTINE NONLIN
              IF(NTEST.EQ.LTEST) GO TO 307
              DO 305 N=1,NE
              IF(NOP(N,3).NE.NOP(N,4)) GO TO 305
              IF(STR(N,1).EQ.0.) GO TO 937
              EC(N)=(FORCE(N,1)-ENU*(FORCE(N,2)+FORCE(N,4)))/STR(N,1)
              GO TO 938
          937 IF(STR(N,2).EQ.0.) GO TO 940
              EC(N)=(FORCE(N,2)-ENU*(FORCE(N,1)+FORCE(N,4)))/STR(N,2)
              GO TO 938
          940 EC(N)=EE(N)
          938 CONTINUE
              CALL NONLIN(N)
          305 CONTINUE
          307 CONTINUE
C                   WRITE INTERPOLATED STRESS DIFFERENCE VALUES
C                   CORRESPONDING TO EPSILON1
              IF(NTEST.EQ. LTEST) GO TO 1003
              IF(NITER.NE.NUITER) GO TO 1003
              WRITE(6,1000)
              DO 1001 N=1,NE
              IF(NOP(N,3).NE.NOP(N,4)) GO TO 1003
         1001 WRITE(6,1002) N,CONDRE(N),EE(N),PRESTR(N),PREDEV(N),EC(N)
         1003 CONTINUE
C                   FORMATS
          100 FORMAT('1',10X,'INCREMENT NO.',I5//
             15X,'TABLE 4 - DISPLACEMENT INCREMENT'/
             27X,'NODE',6X,'X-DISPLACEMENT',3X,'Y-DISPLACEMENT')
          117 FORMAT(I10,2F16.5)
```

```
FORTRAN IV G LEVEL  21                  STRESS              DATE = 73195          04/43/41                 PAGE 0004

 0130          112 FORMAT(///,5X,'TABLE 5 - TOTAL DISPLACEMENT'/
                   1                                                  7X,'NODE',6X,'X-DISPLACEMENT',
                   23X,'Y-DISPLACEMENT')
 0140         1000 FORMAT('0',5X,'TABLE 6 - INTERPOLATED VALUES'//
                   1'      ELEMENT     CONF. PRESS.          MODULUS        PRIN. STRAIN
                   2 DEV. STRESS         MODULUS'/
                   3'                                        TANGENT
                   4                     CHECK')
 0141         1002 FORMAT     (5X,I4,8X,F10.5,5X,F10.3,6X,F10.6,6X,F10.4,6X,F10.3)
 0142              RETURN
 0143              END

 *OPTIONS IN EFFECT*  ID,EBCDIC,SOURCE,NOLIST,NODECK,LOAD,NOMAP
 *OPTIONS IN EFFECT*  NAME = STRESS  , LINECNT =       56
 *STATISTICS*    SOURCE STATEMENTS =      143,PROGRAM SIZE =      4880
 *STATISTICS*  NO DIAGNOSTICS GENERATED
```

```
FORTRAN IV G LEVEL  21              JSTRES              DATE = 73195         04/43/41              PAGE 0001

0001                SUBROUTINE JSTRES
             C                    J O I N T   E L E M E N T
             C      SUBROUTINE JOINT STRESS
0002                COMMON/CONTR/TITLE(12),NP,NE,NB,NDF,NCN,NLD,NMAT,NSZF,LI,NT4,NTS
                   1,NOPC,NCMAT
0003                COMMON/DATA/CORD(200,2),NOP(450,4),IMAT(450),NBC(50),CODE(200),UX
                   1(200),UY(200),IBC(10),JBC(10),PRE(10),T(450),XDEN,YDEN,ORX(450),
                   2ORY(450),PRCORD(200,2)
0004                COMMON/ANAL/NOINC,KOUNT,NTEST,LTEST,NITER,NOITER,VEL,THD
0005                COMMON/STIFF/ESTIFM(12,12),A(3,6),B(3,6),SK(400,80),AREA(450),
                   1C(400),R(8),H(8),NBAND,D(400),AR(400)
0006                COMMON/JOINT/TI(8,8),BL(8,8),AL(450),ANG(450),DKS(450),DKN(450),SD
                   1(2,2),W(450,2),P(450,2),V(450,2),AVP(450,2),CV(450,2),CAVP(450,2),
                   2PCV(450,2),PCAVP(450,2),BI(8,8)
0007                DIMENSION DIS(2,300)
0008                EQUIVALENCE (DIS,C)
0009                IF(NITER.NE.NOITER) GO TO 201
0010                WRITE(6,6000)
0011                WRITE(6,604)
0012            201 CONTINUE
0013                DO 301 N=1,NE
0014                IF(NOP(N,3).EQ.NOP(N,4)) GO TO 301
             C                    FORM STRESS-STRAIN MATRIX
0015                DO 1 I=1,2
0016                DO 1 J=1,2
0017              1 SD(I,J)=0.0
0018                SD(1,1)=DKS(N)
0019                SD(2,2)=DKN(N)
0020                DO 7 I=1,2
0021              7 V(N,I)=0.0
             C                    DETERMINE TRANSFORMATION MATRIX
0022                C=COS(ANG(N))
0023                S=SIN(ANG(N))
0024                DO 13 I=1,8
0025                DO 13 J=1,8
0026             13 TI(I,J)=0.0
0027                DO 14 I=1,8
0028                J=I
0029             14 TI(I,J)=C
0030                DO 15 I=1,7,2
0031                J=I+1
0032             15 TI(I,J)=S
0033                DO 16 I=2,8,2
0034                J=I-1
0035             16 TI(I,J)=-S
             C                    ELEMENT NODAL DISPLACEMENTS
0036                DO 260 I=1,4
0037                M=NOP(N,I)
0038                IF(M.EQ.0) GO TO 260
0039                K=(I-1)*NDF
0040                DO 240 J=1,NDF
0041                IJ=J+K
0042            240 R(IJ)=DIS(J,M)
0043            260 CONTINUE
```

```
FORTRAN IV G LEVEL  21              JSTRES            DATE = 73195          04/43/41             PAGE 0002
      C                DISPLACEMENTS WITH RESPECT TO ELEMENT LOCAL AXES
            DO 12 I=1,8
            H(I)=0.0
            DO 12 IJ=1,8
         12 H(I)=H(I)+T1(I,IJ)*R(IJ)
            X=-AL(N)/2.
            DO 1000 IX=1,2
      C                FORM STRAIN-DISPLACEMENT MATRIX
            F=1.-2.*X/AL(N)
            G=1.+2.*X/AL(N)
            DO 2 I=1,2
            DO 2 J=1,8
          2 B1(I,J)=0.0
            B1(1,1)=-F/2.
            B1(1,3)=-G/2.
            B1(1,5)=G/2.
            B1(1,7)=F/2.
            B1(2,2)=-F/2.
            B1(2,4)=-G/2.
            B1(2,6)=G/2.
            B1(2,8)=F/2.
      C                FORM RELATIVE  DISPLACEMENT VECTOR
            DO 3 I=1,2
            W(N,I)=0.0
            DO 3 J=1,8
          3 W(N,I)=W(N,I)+B1(I,J)*H(J)
      C                AVERAGE RELATIVE DISPLACEMENT
            DO 11 I=1,2
         11 V(N,I)=V(N,I)+W(N,I)
      C                FIND SHEAR AND NORMAL STRESSES
            DO 4 I=1,2
            P(N,I)=0.0
            DO 4 J=1,2
          4 P(N,I)=P(N,I)+SD(I,J)*W(N,J)
            IF(NITER.NE.NOITER) GO TO 1000
       1000 X=X+AL(N)
      C                FIND AVERAGE SHEAR AND NORMAL STRESSES ACROSS
      C                THE ELEMENT
            DO 10 I=1,2
         10 V(N,I)=V(N,I)/2.
            DO 6 I=1,2
            AVP(N,I)=0.0
            DO 6 J=1,2
          6 AVP(N,I)=AVP(N,I)+SD(I,J)*V(N,J)
            ANG(N)=ANG(N)*(360./(2.0*3.141593))
            IF(NITER.NE.NOITER) GO TO 301
            WRITE(6,6000) N,ANG(N),AL(N),ORX(N),ORY(N),V(N,1),V(N,2),AVP(N,1),
           1AVP(N,2)
        301 CONTINUE
      C                CUMMULATIVE AVERAGE STRESSES AND DISPLACEMENTS
            IF(NITER.NE.NOITER) GO TO 302
            WRITE(6,5000)
            WRITE(6,605)
        302 CONTINUE
```

```
FORTRAN IV G LEVEL  21                 JSTRES              DATE = 73195          04/43/41                PAGE 0003

0089              DO 2000 N=1,NE
0090              IF(NOP(N,3).EQ.NOP(N,4)) GO TO 2000
0091              IF(NITER.NE.1) GO TO 601
0092              DO 9 I=1,2
0093              PCV(N,I)=CV(N,I)
0094              PCAVP(N,I)=CAVP(N,I)
0095              CV(N,I)=CV(N,I)+V(N,I)
0096            9 CAVP(N,I)=CAVP(N,I)+AVP(N,I)
0097          601 DO 17 I=1,2
0098              CV(N,I)=PCV(N,I)+V(N,I)
0099           17 CAVP(N,I)=PCAVP(N,I)+AVP(N,I)
        C                           CALL JOINT NONLINEAR SUBROUTINE
0100              IF(NTEST.EQ.LTEST) GO TO 2080
0101              CALL JNONLN(N)
0102              IF(NITER.NE.NOITERS GO TO 2080
0103              WRITE(6,303) N,CV(N,1),CV(N,2),CAVP(N,1),CAVP(N,2),DKS(N),DKN(N)
0104         4000 FORMAT('0',I5,4(F10.3),2F15.7,2F14.6)
0105          300 FORMAT('0',I5,4F15.7,F15.7,E15.5)
0106         2080 CONTINUE
0107         6000 FORMAT('1',5X,'TABLE 9- STRESSES AND DISPLACEMENTS IN JOINT ELEMEN
                 1TS'/)
0108         5000 FORMAT(//,5X,'TABLE 10 - CUMMULATIVE STRESSES AND DISPLACEMENTS IN
                 1 JOINT ELEMENTS'/),
0109          604 FORMAT('0',5X,'N',4X,'ANGLE',4X,'LENGTH',6X,'CENTROID',12X,'AVERAG
                 1E DISPLACEMENT',13X,'AVERAGE STRESS'/32X,'X',9X,'Y',9X,'SHEAR',9X,
                 2'NORMAL',10X,'SHEAR',7X,'NORMAL')
0110          605 FORMAT('0',4X,'N',5X,'CUMMULATIVE DISPLACEMENTS',4X,'CUMMULATIVE S
                 1TRESSES',10X,'STIFFNESS VALUES'/12X,'SHEAR',10X,'NORMAL',9X,'SHEAR
                 2',10X,'NORMAL',8X,'SHEAR',11X,'NORMAL')
0111              RETURN
0112              END

*OPTIONS IN EFFECT*  ID,EBCDIC,SOURCE,NOLIST,NODECK,LOAD,NOMAP
*OPTIONS IN EFFECT*  NAME = JSTRES  , LINECNT =       56
*STATISTICS*     SOURCE STATEMENTS =      112,PROGRAM SIZE =      3728
*STATISTICS*  NO DIAGNOSTICS GENERATED
```

```
FORTRAN IV G LEVEL  21                REAC              DATE = 73195           04/43/41              PAGE 0001

              SUBROUTINE REAC(J,M,R)
              COMMON/CONTR/TITLE(12),NP,NE,NB,NDF,NCN,NLD,NMAT,NSZF,LI,NT4,NTS
             1,NOPC,NCPAT
              COMMON/DATA/CORD(200,2),NOP(450,4),IMAT(450),NBC(50),CODE(200),UX
             1(200),UY(200),IDC(10),JBC(10),PRE(10),T(450),XDEN,YDEN,ORX(450),
             2ORY(450),PRCORD(200,2)
              COMMON/STIFF/ESTIFM(12,12),A(3,6),B(3,6),SK(400,80),AREA(450),
             1C(400),R(8),H(8),WBAND,D(400),AR(400)
              DIMENSION U(8)
              INTEGER WBAND
C                       RECALCULATE STIFFNESS MATRIX FOR ELEMENT N
              IF(NOP(N,3).NE.NOP(N,4)) GO TO 504
              CALL STIFT2(N)
              J1=2*NOP(N,1)-1
              J2=2*NOP(N,1)
              K1=2*NOP(N,2)-1
              K2=2*NOP(N,2)
              L1=2*NOP(N,3)-1
              L2=2*NOP(N,3)
              U(1)=C(J1)
              U(2)=C(J2)
              U(3)=C(K1)
              U(4)=C(K2)
              U(5)=C(L1)
              U(6)=C(L2)
              IF(CODE(M).NE.1.) GO TO 501
              I=2*J-1
              K=2*NOP(N,J)-1
              SUM=0.0
              DO 425 L=1,6
        425   SUM=SUM+ESTIFM(I,L)*U(L)
              AR(K)=AR(K)+SUM
              GO TO 503
        501   IF(CODE(M).EQ.2.) GO TO 502
              I=2*J-1
              K=2*NOP(N,J)-1
              SUM=0.0
              DO 426 L=1,6
        426   SUM=SUM+ESTIFM(I,L)*U(L)
              AR(K)=AR(K)+SUM
        502   I=2*J
              K=2*NOP(N,J)
              SUM=0.0
              DO 427 L=1,6
        427   SUM=SUM+ESTIFM(I,L)*U(L)
              AR(K)=AR(K)+SUM
        503   CONTINUE
              GO TO 3
        504   CALL STIFT1(N)
              I1=2*NOP(N,1)-1
              I2=2*NOP(N,1)
              J1=2*NOP(N,2)-1
              J2=2*NOP(N,2)
              K1=2*NOP(N,3)-1
```

```
FORTRAN IV G LEVEL  21            REAC            DATE = 73195          04/43/41          PAGE 0002
        K2=2*NOP(N,3)
        L1=2*NOP(N,4)-1
        L2=2*NOP(N,4)
        U(1)=C(I1)
        U(2)=C(I2)
        U(3)=C(J1)
        U(4)=C(J2)
        U(5)=C(K1)
        U(6)=C(K2)
        U(7)=C(L1)
        U(8)=C(L2)
        IF(CODE(M).NE.1.) GO TO 1
        I=2*J-1
        K=2*NOP(N,J)-1
        SUM=0.0
        DO 2 L=1,8
      2 SUM=SUM+ESTIFM(I,L)*U(L)
        AR(K)=AR(K)+SUM
        GO TO 3
      1 IF(CODE(M).EQ.2.) GO TO 4
        I=2*J-1
        K=2*NOP(N,J)-1
        SUM=0.0
        DO 5 L=1,8
      5 SUM=SUM+ESTIFM(I,L)*U(L)
        AR(K)=AR(K)+SUM
      4 I=2*J
        K=2*NOP(N,J)
        SUM=0.0
        DO 6 L=1,8
      6 SUM=SUM+ESTIFM(I,L)*U(L)
        AR(K)=AR(K)+SUM
      3 CONTINUE
        RETURN
        END
*OPTIONS IN EFFECT*  ID,EBCDIC,SOURCE,NOLIST,NODECK,LOAD,NOMAP
*OPTIONS IN EFFECT*  NAME = REAC     , LINECNT =       56
*STATISTICS*    SOURCE STATEMENTS =       84,PROGRAM SIZE =      2328
*STATISTICS*  NO DIAGNOSTICS GENERATED
```


7734351

```
0001            SUBROUTINE LARDEF
0002            COMMON/CONTR/TITLE(12),NP,NE,NB,NDF,NCN,NLD,NMAT,NSZF,LI,NT4,NTS
               1,NOPC,NCMAT
0003            COMMON/DATA/CORD(200,2),NOP(450,4),IMAT(450),NBC(50),CODE(200),UX
               1(200),UY(200),IBC(10),JBC(10),PRE(10),T(450),XDEN,YDEN,ORX(450),
               2ORY(450),PRCORD(200,2)
0004            COMMON/ANAL/NOINC,KOUNT,NTEST,LTEST,NITER,NOITER,VEL,THO
0005            COMMON/STIFF/ESTIFM(12,12),A(3,6),B(3,6),SK(400,80),AREA(450),
               1C(400),R(8),H(8),MBAND,D(400),AR(400)
0006            COMMON/STRES/DISTO(2,200),SIGTO(450,4),STRTO(450,3),SMAXTO(450),
               1SMINTO(450),ANGTO(450),GANGTO(450),EMAXTO(450),EMINTO(450),FORCE
               1(450,4),STR(450,3),PSIGTO(450,4),PSTRTO(450,3),PDISTO(2,200)
0007            COMMON/DEF/DX(200),DY(200),VX(200),VY(200),EPSX(450),EPSY(450),
               1GAMXY(450),EPSI1(450),EPSI2(450),PSI(450),CSUMPO,CSUMPW
0008            COMMON/JOINT/TI(8,8),BL(8,8),AL(450),ANG(450),[illegible]KS(450),DKN(450),SD
               1(2,2),W(450,2),P(450,2),V(450,2),AVP(450,2),CV(450,2),CAVP(450,2),
               2PCV(450,2),PCAVP(450,2),BI(8,8)
0009            DIMENSION DIS(2,200)
0010            EQUIVALENCE (DIS,C)
          C                     REPLACE ELEMENT COORDINATES WITH NEW COORDINATES
0011            DO 100 N=1,NP
0012            PRCORD(N,1)=CORD(N,1)
0013            PRCORD(N,2)=CORD(N,2)
0014            CORD(N,1)=CORD(N,1)+DIS(1,N)
0015            CORD(N,2)=CORD(N,2)+DIS(2,N)
0016        100 CONTINUE
          C                     COMPUTATION OF VELOCITY COMPONENTS
0017            TT=(THO/NOINC)/VEL
0018            J=KOUNT
0019            DO 200 N=1,NP
0020            DX(N)=DIS(1,N)
0021            DY(N)=DIS(2,N)
0022            VX(N)=DX(N)/TT
0023            VY(N)=DY(N)/TT
0024        200 CONTINUE
0025            WRITE(6,1)
0026            WRITE([illegible]2) (N,PRCORD(N,1),PRCORD(N,2),CORD(N,1),CORD(N,2),VX(N),
               1VY(N),N=1,NP)
          C                     COMPUTATION OF STRAIN RATES AND DIRECTION OF PRINCIPAL
          C                     STRAIN RATE IN CONTINUUM ELEMENTS
0027            DO 300 N=[illegible],NE
0028            IF(NOP(N,3).NE.NOP(N,4)) GO TO 300
0029            EPSX(N)=STR(N,1)/TT
0030            EPSY(N)=STR(N,2)/TT
0031            GAMXY(N)=STR(N,3)/TT
0032            E=(EPSX(N)+EPSY(N))/2.
0033            F=SQRT(((EPSY(N)-EPSX(N))/2.)**2+(GAMXY(N)/2.)**2)
0034            EPSI1(N)=E+F
0035            EPSI2(N)=E-F
0036            IF(EPSY(N).EQ.EPSI2(N)) GO TO 301
0037            PSI(N)=57.29578*ATAN((GAMXY(N)/2.)/(EPSY(N)-EPSI2(N)))
0038            GO TO 300
0039        301 PSI(N)=90.0
0040        300 CONTINUE
```

```
FORTRAN IV G LEVEL  21                 LARDEF             DATE = 73195          04/43/41              PAGE 0002
                C                   PLASTIC WORK OF DEFORMATION AND POWER OF DEFORMATION
 0041                 SUMPW=0.0
 0042                 SUMPD=0.0
 0043                 DO 121 IK=1,NE
 0044                 IF(NOP(IK,3).NE.NOP(IK,4)) GO TO 123
 0045                 IF(KOUNT.EQ.1) GO TO 101
 0046                 DUP=0.5*(SIGTO(IK,1)+PSIGTO(IK,1))*STR(IK,1)+0.5*(SIGTO(IK,2)+PSIG
                     1TO(IK,2))*STR(IK,2)+0.5*(SIGTO(IK,3)+PSIGTO(IK,3))*STR(IK,3)
 0047                 GO TO 102
 0048             101 DUP=0.5*(SIGTO(IK,1)*STR(IK,1)+SIGTO(IK,2)*STR(IK,2)+SIGTO(IK,3)*
                     1STR(IK,3))
 0049             102 CONTINUE
 0050                 DUPV=DUP*AREA(IK)
 0051                 PDOF=DUPV/TT
 0052                 GO TO 124
 0053             123 DUP=CAVP(IK,1)*V(IK,1)+CAVP(IK,2)*V(IK,2)
 0054                 DUPV=DUP*AL(IK)
 0055                 PDOF=DUPV/TT
                C                   TOTAL INCREMENTAL PLASTIC WORK AND POWER OF DEFORMATION
 0056             124 SUMPW=SUMPW+DUPV
 0057                 SUMPD=SUMPD+PDOF
 0058             121 CONTINUE
                C                   CUMULATIVE PLASTIC WORK AND POWER OF DEFORMATION
 0059                 CSUMPW=CSUMPW+SUMPW
 0060                 CSUMPD=CSUMPD+SUMPD
 0061                 WRITE(6,122) KOUNT,SUMPW,SUMPD,CSUMPW,CSUMPD
 0062               1 FORMAT('1',5X,'TABLE 12- VELOCITY AND NEW CO-ORDINATES'//
                     1            8X,'NODE',3X,'X-CORD',8X,'Y-CORD',8X,'N-X-CORD',5X,
                     2'N-Y-CORD',5X,'X-VELOCITY',5X,'Y-VELOCITY',)
 0063               2 FORMAT    (7X,I3,5X,F10.7,3X,F10.7,3X,F10.7,3X,F10.7,3X,F12.7,3X,
                     1F12.7)
 0064             122 FORMAT('1',5X,'TABLE 14 - PLASTIC WORK AND POWER OF DEFORMATION'//
                     1            15X,'INCREMENT NO.',I5//15X,'TOTAL INCREMENTAL PLASTIC
                     1WORK=',F20.9/15X,'TOTAL INCREMENTAL POWER OF DEFORMATION=',F20.9/
                     115X,'CUMULATIVE PLASTIC WORK=',F20.9/15X,'CUMULATIVE POWER OF DEFO
                     2RMATION=',F20.9)
 0065                 RETURN
 0066                 END

   *OPTIONS IN EFFECT*  ID,EBCDIC,SOURCE,NOLIST,NODECK,LOAD,NOMAP
   *OPTIONS IN EFFECT*  NAME = LARDEF  , LINECNT =       56
   *STATISTICS*    SOURCE STATEMENTS =        66,PROGRAM SIZE =       2260
   *STATISTICS*  NO DIAGNOSTICS GENERATED
```

```
FORTRAN IV G LEVEL  21              AVER              DATE = 73195        04/43/41              PAGE 0001

 0001            SUBROUTINE AVER
           C                     THIS SUBROUTINE AVERAGE STRESSES , STRAINS AND STRAIN RATES
           C                     AT NODAL POINTS AND THEN PROCEEDS TO CALCULATE PRINCIPAL
           C                     VALUES AND DIRECTIONS
 0002            COMMON/CONTR/TITLE(12),NP,NE,NB,NDF,NCN,NLD,NMAT,NSZF,LI,NT4,NTS
                1,NOPC,NCMAT
 0003            COMMON/DATA/CORD(200,2),NOP(450,4),IMAT(450),NBC(50),CODE(200),UX
                1(200),UY(200),IBC(10),JBC(10),PRE(10),T(450),XDEN,YDEN,DRX(450),
                2DRY(450),PRCORD(200,2)
 0004            COMMON/STRES/DISTO(2,200),SIGTO(450,4),STRTO(450,3),SMAXTO(450),
                1SMINTO(450),ANGTO(450),EANGTO(450),EMAXTO(450),EMINTO(450),FORCE
                1(450,4),STR(450,3),PSIGTO(450,4),PSTRTO(450,3),PDISTO(2,200)
 0005            COMMON/DEF/DX(200),DY(200),VX(200),VY(200),EPSX(450),EPSY(450),
                1GAMXY(450),EPSI1(450),EPSI2(450),PSI(450),CSUMPO,CSUMP
 0006            COMMON/AVRG/AVSMAX(200),AVSMIN(200),AVANG(200),AVTMX(200),
                1AVTMN(200),AVTANG(200),AVSMX(200),AVSMN(200),AVSANG(200),
                2AVSTMX(200),AVSTMN(200),AVSTAN(200),AVPSI1(200),AVPSI2(200),
                3AVPSI(200)
 0007            DIMENSION SFORCE(200,4),SSIGTO(200,4),SSTRTO(200,3),SSTR(200,3),
                1SEPSX(200),SEPSY(200),SGAMXY(200)
 0008            DO 100 L=1,NP
           C                       INITIALIZATION
 0009            DO 800 I=1,4
 0010            SFORCE(L,I)=0.0
 0011        800 SSIGTO(L,I)=0.0
 0012            DO 900 I=1,3
 0013            SSTR(L,I)=0.0
 0014        900 SSTRTO(L,I)=0.0
 0015            SEPSX(L)=0.0
 0016            SEPSY(L)=0.0
 0017            SGAMXY(L)=0.0
 0018        100 CONTINUE
           C                     VALUES FOR ADJACENT ELEMENTS
 0019            NOEL=0
 0020            DO 400 NI=1,NE
 0021            IF(NOP(NI,3).NE.NOP(NI,4)) GO TO 400
 0022            DO 400 I=1,3
 0023            IF(NOP(NI,I)-L) 400,300,400
 0024        300 N=NI
 0025            NOEL=NOEL+1
 0026            DO 500 J=1,4
 0027            SFORCE(L,J)=SFORCE(L,J)+FORCE(N,J)
 0028        500 SSIGTO(L,J)=SSIGTO(L,J)+SIGTO(N,J)
 0029            DO 501 J=1,3
 0030            SSTR(L,J)=SSTR(L,J)+STR(N,J)
 0031        501 SSTRTO(L,J)=SSTRTO(L,J)+STRTO(N,J)
 0032            SEPSX(L)=SEPSX(L)+EPSX(N)
 0033            SEPSY(L)=SEPSY(L)+EPSY(N)
 0034            SGAMXY(L)=SGAMXY(L)+GAMXY(N)
 0035        400 CONTINUE
 0036            IF(NOEL.EQ.0) GO TO 663
 0037            GO TO 664
 0038        663 NOEL=1
           C                     AVERAGE VALUES BY DIVIDING BY NUMBER OF ATTACHED ELEMENTS
```

```
0039      664 DO 600 J=1,4
0040          SFORCE(L,J)=SFORCE(L,J)/NOEL
0041      600 SSIGTO(L,J)=SSIGTO(L,J)/NOEL
0042          DO 601 J=1,3
0043          SSTR(L,J)=SSTR(L,J)/NOEL
0044      601 SSTRTO(L,J)=SSTRTO(L,J)/NOEL
0045          SEPSX(L)=SEPSX(L)/NOEL
0046          SEPSY(L)=SEPSY(L)/NOEL
0047          SGAMXY(L)=SGAMXY(L)/NOEL
        C                     CALCULATE PRINCIPAL VALUES AND DIRECTIONS
0048          CALL PRIN(L,SFORCE,AVSMAX,AVSMIN,AVANG)
0049          CALL PRIN(L,SSIGTO,AVTMX,AVTMN,AVTANG)
0050          CALL PRIN(L,SSTR,AVSMX,AVSMN,AVSANG)
0051          CALL PRIN(L,SSTRTO,AVSTMX,AVSTMN,AVSTAN)
0052          E=(SEPSX(L)+SEPSY(L))/2.
0053          F=SQRT(((SEPSY(L)-SEPSX(L))/2.)**2+(SGAMXY(L)/2.)**2)
0054          AVPSI1(L)=E+F
0055          AVPSI2(L)=E-F
0056          IF(SEPSY(L).EQ.AVPSI2(L)) GO TO 307
0057          AVPSI(L)=57.29578*ATAN((SGAMXY(L)/2.)/(SEPSY(L)-AVPSI2(L)))
0058          GO TO 308
0059      307 AVPSI(L)=90.0
0060      308 CONTINUE
0061      100 CONTINUE
        C                     WRITE CALCULATED VALUES
0062          WRITE(6,101)
0063          WRITE(6,102) (L,(CORD(L,J),J=1,2),(SFORCE(L,I),I=1,4),AVSMAX(L),
             1AVSMIN(L),AVANG(L),L=1,NP)
0064          WRITE(6,202)
0065          WRITE(6,103)(L,(CORD(L,J),J=1,2),(SSTR(L,I),I=1,3),AVSMX(L),
             1AVSMN(L),AVSANG(L),L=1,NP)
0066          WRITE(6,114)
0067          WRITE(6,306)
0068          WRITE(6,102) (L,(CORD(L,J),J=1,2),(SSIGTO(L,I),I=1,4),AVTMX(L),
             1AVTMN(L),AVTANG(L),L=1,NP)
0069          WRITE(6,115)
0070          WRITE(6,202)
0071          WRITE(6,103)(L,(CORD(L,J),J=1,2),(SSTRTO(L,I),I=1,3),AVSTMX(L),
             1AVSTMN(L),AVSTAN(L),L=1,NP)
0072          WRITE(6,5)
0073          WRITE(6,3)
0074          WRITE(6,104)(L,SEPSX(L),SEPSY(L),SGAMXY(L),AVPSI1(L),AVPSI2(L),
             1AVPSI(L),L=1,NP)
0075      101 FORMAT('1',5X,'TABLE 6 - INCREMENT STRESS AND STRAIN'//
             15X,'STRESS INCREMENT'/
             1'   NODE      X       Y        X-STRESS           Y-STRESS       XY-STRESS
             2       Z-STRESS        MAX-STRESS        MIN-STRESS     ANGLE')
0076      202 FORMAT('0',5X,'STRAIN INCREMENT'/
             1                '    NODE       X    Y      X-STRAIN          Y-STRAIN       X
             1Y-STRAIN        MAX-STRAIN        MIN-STRAIN        ANGLE')
0077      306 FORMAT('0',5X,'TABLE 7 - TOTAL STRESS AND STRAIN'//
             1'   NODE      X       Y        X-STRESS           Y-STRESS       XY-STRESS
             2       Z-STRESS        MAX-STRESS        MIN-STRESS     ANGLE')
0078      115 FORMAT(///,1X,'TOTAL STRAINS')
```

```
FORTRAN IV G LEVEL  21                    AVER                 DATE = 73195          04/43/41               PAGE 0083

 0079          114 FORMAT('0',1X,'TOTAL STRESSES')
 0080            5 FORMAT('0',5X,'TABLE 13 - STRAIN RATES'//)
 0081            3 FORMAT(1H0,'   NODE            X-STRAIN R     Y-STRAIN R               X
                  1Y-STRAIN R      MAX-STRAIN R  MIN-STRAIN R  ANGLE')
 0082          102 FORMAT(I5,5X,2F6.2,6F15.6,F12.3)
 0083          103 FORMAT(I5,5X,2F6.2,5F15.9,F12.3)
 0084          104 FORMAT(I10,5F17.6,F12.3)
 0085              RETURN
 0086              END

 *OPTIONS IN EFFECT*  ID,EBCDIC,SOURCE,NOLIST,NODECK,LOAD,NOMAP
 *OPTIONS IN EFFECT*  NAME = AVER     , LINECNT =        56
 *STATISTICS*    SOURCE STATEMENTS =        86,PROGRAM SIZE =     17956
 *STATISTICS*  NO DIAGNOSTICS GENERATED
```

```
FORTRAN IV G LEVEL  21                PRIN              DATE = 73195          04/43/41           PAGE 0001

                  SUBROUTINE PRIN (N,A,AMAXP,AMINP,ANGP)
                  DIMENSION A(200,4),AMAXP(200),AMINP(200),ANGP(200)
                  B=(A(N,1)+A(N,2))/2.
                  C=SQRT(((A(N,2)-A(N,1))/2.)**2+A(N,3)**2)
                  AMAXP(N)=B+C
                  AMINP(N)=B-C
                  IF(A(N,2).EQ.AMINP(N)) GO TO 701
                  ANGP(N)=57.29578*ATAN(A(N,3)/(A(N,2)-AMINP(N)))
                  GO TO 702
              701 ANGP(N)=90.0
              702 CONTINUE
                  RETURN
                  END

 *OPTIONS IN EFFECT*  ID,EBCDIC,SOURCE,NOLIST,NODECK,LOAD,NOMAP
 *OPTIONS IN EFFECT*  NAME = PRIN    , LINECNT =        56
 *STATISTICS*    SOURCE STATEMENTS =       13,PROGRAM SIZE =       752
 *STATISTICS*  NO DIAGNOSTICS GENERATED
```

```
FORTRAN IV G LEVEL  21              NONLIN            DATE = 73195          04/43/41              PAGE 0001

 0001            SUBROUTINE NONLIN(N)
 0002            COMMON/CONTR/TITLE(12),NP,NE,NB,NOF,NCN,NLD,NMAT,NSZF,LI,NT4,NTS
                1,NOPC,NCMAT
 0003            COMMON/DATA/CORD(200,2),NOP(450,4),IMAT(450),NBC(50),CODE(200),UX
                1(200),UY(200),IAC(10),JBC(10),PRE(10),T(450),XDEN,YDEN,ORX(450),
                2ORY(450),PRCORD(200,2)
 0004            COMMON/ANAL/NOINC,KOUNT,NTEST,LTEST,NITER,NOITER,VEL,THD
 0005            COMMON/STRES/DISTO(2,200),SIGTO(450,4),STRTO(450,3),SMAXTO(450),
                1SMINTO(450),ANGTO(450),EANGTO(450),EMAXTO(450),EMINTO(450),FORCE
                1(450,4),STR(450,3),PSIGTO(450,4),PSTRTO(450,3),PDISTO(2,200)
 0006            COMMON/NONL/NCUR(2),CPR(2,10),NPTS(2,10),EG(50),GAM(50),
                1EY(2,10,50),GAMOC(2,10,50),PRESTR(450),PREDEV(450),CONPRE(450)
 0007            COMMON/ELAS/E,ENU,EE(450),EC(450),DKSIJ,DKNIJ,DKSII,DKNII
           C                NON-LINEAR ANALYSIS
           C                NONLIN IS A ROUTINE THAT INTERPOLATES FOR
           C                STRESSES FROM KNOWN VALUES OF STRAIN
           C
           C                USES (SIGMA1-SIGMA3) .VS. EPSILON1 CURVES
           C
           C                COMPUTE CONFINING PRESSURE IN ELEMENT
 0008            IF(SMAXTO(N).NE.0.) GO TO 601
 0009            IF(SMINTO(N).EQ.0.) GO TO 392
 0010        601 CONTINUE
 0011            IF(ABS(SMAXTO(N)).GT.ABS(SMINTO(N))) GO TO 291
 0012            CONPRE(N)=(SMAXTO(N)+SIGTO(N,4))/2.
 0013            GO TO 292
 0014        291 CONPRE(N)=(SMINTO(N)+SIGTO(N,4))/2.
 0015        292 EPRE=EE(N)
 0016            IF(ABS(EMAXTO(N)).GT.ABS(EMINTO(N))) GO TO 351
 0017            PRSTTO=ABS(EMINTO(N))
 0018            GO TO 352
 0019        351 PRSTTO=ABS(EMAXTO(N))
 0020        352 CONTINUE
           C                DETERMINE TWO ADJOINING CONFINING PRESSURE DEPENDENT
           C                CURVES DEPENDING ON THE CONFINEMENT OF THE ELEMENT
 0021            I=IMAT(N)
 0022            NCURV=NCUR(I)
 0023            IF(NCURV-1) 359,300,310
 0024        300 NC=1
 0025            GO TO 325
 0026        310 DO 340 NC=1,NCURV
 0027            IF(CPR(I,NC)-ABS(CONPRE(N))) 340,325,325
 0028        340 CONTINUE
 0029        325 NPT=NPTS(I,NC)
           C                DETERMINE TWO ADJOINING STRAIN COORDINATES DEPENDING
           C                ON THE MAJOR PRINCIPAL STRAIN OF THE ELEMENT
 0030            DO 355 LP=1,NPT
 0031            IF(GAMOC(I,NC,LP)-ABS(PRSTTO)) 355,350,350
 0032        355 CONTINUE
 0033            EE(N)=0.5
 0034            IF(NITER.NE.NOITER) GO TO 392
 0035            PRESTR(N)=PRSTTO
 0036            PREDEV(N)=EY(I,NC,NPT)
 0037            GO TO 392
```

```
                 C                       INTERPOLATE FOR STRESS DIFFERENCE VALUE
                 C                       CORRESPONDING TO EPSILONI
 0038              350 DENOM=GAMOC(I,NC,LP)-GAMOC(I,NC,LP-1)
 0039                  FUMER=(GAMOC(I,NC,LP)-PRSTTO)*(EY(I,NC,LP-1)-EY(I,NC,LP))
 0040                  TOPSTR=EY(I,NC,LP)+FUMER/DENOM
                 C                       IF ONLY ONE STRESS-STRAIN CURVE IS GIVEN
 0041                  IF(NCURV-1) 359,360,365
 0042              359 WRITE(6,452)
 0043              452 FORMAT(5X,'ERROR IN NCURVE CARD')
 0044              360 EE(N)=ABS(TOPSTR-PREDEV(N))/ABS(PRSTTO-PRESTR(N))
 0045                  IF(NITER.NE.NOITER) GO TO 392
 0046                  PRESTR(N)=PRSTTO
 0047                  PREDEV(N)=TOPSTR
 0048                  GO TO 392
                 C                       IF MORE THAN ONE STRESS-STRAIN CURVE IS GIVEN
 0049              365 IF(ABS(CONPRE(N))-0.0) 375,370,375
 0050              375 IF(ABS(CONPRE(N))-CPR(I,NC)) 380,370,385
 0051              380 NC=NC-1
 0052                  BOTSTR=TOPSTR
 0053                  GO TO 325
 0054              370 EE(N)=ABS(TOPSTR-PREDEV(N))/ABS(PRSTTO-PRESTR(N))
 0055                  IF(NITER.NE.NOITER) GO TO 392
 0056                  PRESTR(N)=PRSTTO
 0057                  PREDEV(N)=TOPSTR
 0058                  GO TO 392
 0059              385 STRNEW=TOPSTR+(ABS(CONPRE(N))-CPR(I,NC))/(CPR(I,NC+1)-CPR(I,NC))*
                      1(BOTSTR-TOPSTR)
 0060                  EE(N)=ABS(STRNEW-PREDEV(N))/ABS(PRSTTO-PRESTR(N))
 0061                  IF(NITER.NE.NOITER) GO TO 392
 0062                  PRESTR(N)=PRSTTO
 0063                  PREDEV(N)=STRNEW
 0064              392 CONTINUE
 0065                  RETURN
 0066                  END

 *OPTIONS IN EFFECT*  ID,EBCDIC,SOURCE,NOLIST,NODECK,LOAD,NOMAP
 *OPTIONS IN EFFECT*  NAME = NONLIN  , LINECNT =       56
 *STATISTICS*     SOURCE STATEMENTS =        66,PROGRAM SIZE =      2308
 *STATISTICS*  NO DIAGNOSTICS GENERATED
```

```
0001              SUBROUTINE JNONLN(N)
0002              COMMON/DATA/CORD(200,2),NOP(450,4),IMAT(450),NBC(50),CODE(200),UX
                 1(200),UY(200),IBC(10),JBC(10),PRE(10),T(450),XDEN,YDEN,DRX(450),
                 2DRY(450),PRCORD(200,2)
0003              COMMON/JOINT/TI(8,8),DL(8,8),AL(450),ANG(450),DKS(450),DKN(450),SD
                 1(2,2),W(450,2),P(450,2),V(450,2),AVP(450,2),CV(450,2),CAVP(450,2),
                 2PCV(450,2),PCAVP(450,2),B1(8,8)
0004              COMMON/JNONL/NVAL(2),CNP(2,10),AH(2,10),BH(2,10)
           C                    JOINT NONLINEAR ANALYSIS
           C                    JNONLIN IS A ROUTINE THAT INTERPOLATES FOR SHEAR
           C                    STIFFNESS MODULUS FROM HYPERBOLIC STRESS-STRAIN CURVES
           C                    DETERMINE TWO ADJOINING NORMAL PRESSURE DEPENDENT
           C                    CURVES DEPENDING ON THE NORMAL PRESSURE ON THE ELEMENT
0005              I=IMAT(N)
0006              NVALUE=NVAL(I)
0007              IF(NVALUE-1) 359,300,310
0008          359 WRITE(6,452)
0009          452 FORMAT(5X,'ERROR IN NVALUE CARD')
0010          300 TOWM=1./BH(I,1)
0011              IF(CAVP(N,1)-TOWM) 350,350,355
0012          355 CONTINUE
0013              DKS(N)=0.5
0014              GO TO 392
0015          350 NV=1
0016              DKS(N)=((1.-ABS(CAVP(N,1))*BH(I,1))**2)/AH(I,1)
0017              GO TO 392
0018          310 DO 340 NV=1,NVALUE
0019              IF(CNP(I,NV)-CAVP(N,2)) 340,325,325
0020          340 CONTINUE
           C                    INTERPOLATE FOR A AND B VALUES CORRESPONDING TO NORMAL
           C                    PRESSURE - LINEAR INTERPOLATION
0021          325 AHI=AH(I,NV)-(AH(I,NV)-AH(I,NV-1))*(CNP(I,NV)-CAVP(N,2))/
                 1(CNP(I,NV)-CNP(I,NV-1))
0022              BHI=BH(I,NV)-(BH(I,NV)-BH(I,NV-1))*(CNP(I,NV)-CAVP(N,2))/
                 1(CNP(I,NV)-CNP(I,NV-1))
0023              TOWM=1./BHI
0024              IF(CAVP(N,1)-TOWM) 360,360,365
0025          365 CONTINUE
0026              DKS(N)=0.5
0027              GO TU 392
0028          360 DKS(N)=((1.-ABS(CAVP(N,1))*BHI)**2)/AHI
0029          392 CONTINUE
0030              RETURN
0031              END

 *OPTIONS IN EFFECT*  ID,EBCDIC,SOURCE,NOLIST,NODECK,LOAD,NOMAP
 *OPTIONS IN EFFECT*  NAME = JNONLN  , LINECNT =       56
 *STATISTICS*    SOURCE STATEMENTS =      31,PROGRAM SIZE =      1490
 *STATISTICS*  NO DIAGNOSTICS GENERATED

 *STATISTICS*  NO DIAGNOSTICS THIS STEP 2
```

SECTION (B)

B.1 LISTING OF PROGRAM "FIT"

```
FORTRAN IV G LEVEL  21                MAIN              DATE = 73191          00/03/13              PAGE 0001

            DIMENSION XX(10,14,5),YY(10,14,5),XXA(10,14,5),YYA(10,14,5)
            DIMENSION X(5),Y(5),WT(5),COF(4),XF(1),YF(1)
            DIMENSION XT(5),YT(5),XFIT(10,14,5),YFIT(10,14,5)
            DIMENSION DX(10,14,4),DY(10,14,4),UX(10,14,4),VY(10,14,4)
            DIMENSION PG(9,13,4),PDTOT(9,13)
            DIMENSION AREA(9,13,5),AREAM(9,13,4),PDA(9,13,4)
            DIMENSION ESTR(9,13,4),EST(9,13)
            DIMENSION PDT(13,4),PDTO(4)
            DIMENSION ESTT(13)
            REAL I2
            REAL I3
      C     RAX1
      C     UNDEFORMED AND DEFORMED COORDINATES
      C
            READ(5,316) NOT
        316 FORMAT(I2)
            DC 318 II=1,NOT
            READ(5,100)VXC,VYC,D,TEST,NO
        100 FORMAT(3F8.3,A4,I2)
            WRITE(6,7)TEST,NO
          7 FORMAT('1',///////////////////////////,53X,'TEST NO. ',A4,I2/' ',53
           1X,'===============')
            DO 20 JS=1,5
            DC 20 JC=1,14
         20 READ(5,15) (XX(I,JC,JS),I=1,10),(YY(I,JC,JS),I=1,10)
         15 FORMAT(10F8.3/10F8.3)
            DC 242 JS=1,5
            DO 30 JC=1,14
            DO 30 I=1,10
            XX(I,JC,JS)=(XX(I,JC,JS)-VXC)/2.54
         30 YY(I,JC,JS)=(YY(I,JC,JS)-D)/2.54
            IF(JS-1) 240,238,240
        238 WRITE(6,239)
        239 FORMAT(1H1,27HUNDEFORMED GRID COORDINATES/1H ,27H=================
           1==========/1H0)
            GO TO 245
        240 WRITE(6,241)
        241 FORMAT(1H1,25HDEFORMED GRID COORDINATES/1H ,25H===================
           1======/1H0)
        245 DO 242 JC=1,14
            WRITE(6,243)JC,(XX(IC,JC,JS),IC=1,10)
        243 FORMAT(1H ,3HROW,I3,3X,1HX,10F7.3)
            WRITE(6,244) (YY(IC,JC,JS),IC=1,10)
        244 FORMAT(1H ,8X,1HY,10F7.3)
        242 CONTINUE
      C
      C     RAX 2
      C     ADJUSTED DEFORMED AND UNDEFORMED GRID COORDINATES
      C
       5000 JS=1
            DO 25 JC=1,14
            E=0.0
            DO 25 IC=1,10
            XXA(IC,JC,JS)=E
```

```
   25 E=E+1.
C
      DO 28 IC=1,10
      DO 28 JC=1,14
   28 YYA(IC,JC,JS)=FLOAT(JC-1)*0.5+YY(1,1,1)
      JS1=JS+1
      DO 290 K=1,4
  200 DO 210 JC=1,12
      JC2=JC+2
  201 DO 210 IC=1,9
      IC1=IC+1
      D1=XXA(IC,JC,JS)-XX(IC,JC,JS)
      D2=XXA(IC1,JC,JS)-XX(IC1,JC,JS)-XXA(IC,JC,JS)+XX(IC,JC,JS)
      D3=XX(IC1,JC,JS)-XX(IC,JC,JS)
      IF(D3-0.) 203,202,203
  202 D4=0.
      GO TO 204
  203 D4=(XX(IC,JC,JS1)-XX(IC,JC,JS))/D3
  204 D5=XXA(IC1,JC2,JS)-XX(IC1,JC2,JS)-XXA(IC,JC2,JS)+XX(IC,JC2,JS)
      D6=XX(IC1,JC2,JS)-XX(IC,JC2,JS)
      IF(D7-0.) 206,205,206
  205 D7=0.
      GO TO 207
  206 D7=(XX(IC,JC,JS1)-XX(IC,JC,JS))/D6
  207 D8=YY(IC,JC2,JS)-YY(IC,JC,JS)
      IF(D8-0.) 209,208,209
  208 D9=0.
      GO TO 210
  209 D9=(YY(IC,JC,JS1)-YY(IC,JC,JS))/D8
  210 XXA(IC,JC,JS1)=XX(IC,JC,JS1)+D1+D2*D4+(D5*D7-D2*D4)*D9
C
  220 DO 229 JC=1,12
      JC2=JC+2
      DO 229 IC=1,9
      IC1=IC+1
      D1=YYA(IC,JC,JS)-YY(IC,JC,JS)
      D2=YYA(IC,JC2,JS)-YY(IC,JC2,JS)-YYA(IC,JC,JS)+YY(IC,JC,JS)
      D3=YY(IC,JC2,JS)-YY(IC,JC,JS)
      IF(D3-0.) 222,221,222
  221 D4=0.
      GO TO 223
  222 D4=(YY(IC,JC,JS1)-YY(IC,JC,JS))/D3
  223 D5=YYA(IC1,JC2,JS)-YY(IC1,JC2,JS)-YYA(IC1,JC,JS)+YY(IC1,JC2,JS)
      D6=YY(IC1,JC2,JS)-YY(IC1,JC,JS)
      IF(D6-0.) 225,224,225
  224 D7=0.
      GO TO 226
  225 D7=(YY(IC,JC,JS1)-YY(IC,JC,JS))/D6
  226 D8=XX(IC1,JC,JS)-XX(IC,JC,JS)
      IF(D8-0.) 228,227,228
  227 D9=0.
      GO TO 229
  228 D9=(XX(IC,JC,JS1)-XX(IC,JC,JS))/D8
  229 YYA(IC,JC,JS1)=YY(IC,JC,JS1)+D1+D2*D4+(D5*D7-D2*D4)*D9
```

```
C
      IC=10
      DO 230 JC=1,14
      XXA(IC,JC,JS1)=XX(IC,JC,JS1)+XXA(IC,JC,JS)-XX(IC,JC,JS)
  230 YYA(IC,JC,JS1)=YY(IC,JC,JS1)+YYA(IC,JC,JS)-YY(IC,JC,JS)
      DO 232 JC=13,14
      DO 232 IC=1,10
      XXA(IC,JC,JS1)=XX(IC,JC,JS1)+XXA(IC,JC,JS)-XX(IC,JC,JS)
  232 YYA(IC,JC,JS1)=YY(IC,JC,JS1)+YYA(IC,JC,JS)-YY(IC,JC,JS)
  290 JS1=JS1+1
      JS=1
      WRITE(6,901)
  901 FORMAT(1H1,36HADJUSTED UNDEFORMED GRID COORDINATES/1H ,25H---------
     1----------------/1H0)
      DO 902 JC=1,14
      WRITE(6,903)JC,(XXA(IC,JC,JS),IC=1,10)
  903 FORMAT(1H ,3HROW,I3,3X,1HX,10F7.3)
      WRITE(6,904)(YYA(IC,JC,JS),IC=1,10)
  904 FORMAT(1H ,8X,1HY,10F7.3)
  902 CONTINUE
C
      DO 916 JS=2,5
      WRITE(6,911)
  911 FORMAT(1H1,34HADJUSTED DEFORMED GRID COORDINATES/1H ,25H----------
     1---------------/1H0)
      WRITE(6,912)JS
  912 FORMAT(1H ,10X,8HIMAGE NO,I3)
      DO 916 JC=1,14
      WRITE(6,914)JC,(XXA(IC,JC,JS),IC=1,10)
  914 FORMAT(1H ,3HROW,I3,3X,1HX,10F7.3)
      WRITE(6,915)(YYA(IC,JC,JS),IC=1,10)
  915 FORMAT(1H ,8X,1HY,10F7.3)
  916 CONTINUE
C
C
C     COMPUTATION OF VELOCITY COMPONENTS
C
      READ(5,301)TT
  301 FORMAT(F7.3)
      TT=TT/60.
      WRITE(6,305)
  305 FORMAT(1H1,'VELOCITY COMPONENTS CALCULATED FROM FITTED COORDINATES
     *')
      DO 311 JS=1,4
      JS1=JS+1
      IF(JS-1) 308,306,308
  306 WRITE(6,307) JS,JS1
  307 FORMAT(1H0,'IMAGE',I2,'-',I2)
      GO TO 312
  308 WRITE(6,309) JS,JS1
  309 FORMAT(1H1,'IMAGE',I2,'-',I2//)
  312 DO 311 JC=1,14
      DO 313 I=1,10
      DX(I,JC,JS)=XXA (I,JC,JS1)-XXA (I,JC,JS)
```

470

```
FORTRAN IV G LEVEL  21                MAIN                DATE = 73191          00/03/13                PAGE 0004

0142            DY(I,JC,JS1)=YYA (I,JC,JS1)-YYA (I,JC,JS)
0143            UX(I,JC,JS)=DX(I,JC,JS)/TT
0144        313 VY(I,JC,JS)=DY(I,JC,JS)/TT
0145            WRITE(6,315) JC,(DX(I,JC,JS),I=1,10),(DY(I,JC,JS),I=1,10)
0146            WRITE(6,310) JC,(UX(I,JC,JS),I=1,10),(VY(I,JC,JS),I=1,10)
0147        315 FORMAT(1H ,'ROW',I3,5X,'DX',3X,10F8.3/1H ,11X,' DY',3X,10F8.3)
0148        310 FORMAT(1H ,'ROW',I3,5X,'UX',3X,10F8.3/1H ,11X,' VY',3X,10F8.3)
0149        311 CONTINUE
      C
      C         COMPUTATION OF STRAIN RATES AND DIRECTION OF PRINCIPAL STRAIN RATE
      C
0150            WRITE(6,320)
0151        320 FORMAT(1H1,'STRAIN RATES AND DIRECTION OF PRINCIPAL STRAIN RATE')
0152            DO 330 JS=1,4
0153            IF(JS-1) 323,321,323
0154        321 WRITE(6,322)JS
0155        322 FORMAT(1H0,'SET',I2,/1H ,9X,'XN',18X,'YN',17X,'EPSX',16X,'EPSY',15
               *X,'EPSXY',15X,'PSI',17X,'PD'/1H ,9X,'--',18X,'--',17X,'----',16X,'
               *----',15X,'-----',15X,'---',17X,'--')
0156            GO TO 325
0157        323 WRITE(6,324)JS
0158        324 FORMAT(1H1,'SET',I2,/1H ,9X,'XN',18X,'YN',17X,'EPSX',16X,'EPSY',15
               *X,'EPSXY',15X,'PSI',17X,'PD'/1H ,9X,'--',18X,'--',17X,'----',16X,'
               *----',15X,'-----',15X,'---',17X,'--')
0159        325 JS1=JS+1
0160            DO 330 JC=1,13
0161            JC1=JC+1
0162            WRITE(6,326)JC1
0163        326 FORMAT(1H0,'ROW',I2)
0164            DO 330 I=1,9
0165            I1=I+1
0166            EPSX=0.50*((UX(I1,JC,JS)-UX(I,JC,JS))/(XXA (I1,JC,JS)-XXA (I,JC,JS
               1))+(UX(I1,JC1,JS)-UX(I,JC1,JS))/(XXA (I1,JC1,JS)-XXA (I,JC1,JS)))
0167            EPSY=0.50*((VY(I,JC1,JS)-VY(I,JC,JS))/(YYA (I,JC1,JS)-YYA (I,JC,JS
               1))+(VY(I1,JC1,JS)-VY(I1,JC,JS))/(YYA (I1,JC1,JS)-YYA (I1,JC,JS)))
0168            EPSXY=0.25*((UX(I,JC1,JS)-UX(I,JC,JS))/(YYA (I,JC1,JS)-YYA (I,JC,
               1JS))+(UX(I1,JC1,JS)-UX(I1,JC,JS))/(YYA (I1,JC1,JS)-YYA (I1,JC,JS))
               *+(VY(I1,JC,JS)-VY(I,JC,JS))/(XXA (I1,JC,JS)-XXA (I,JC,JS))+(VY(I1,
               *JC1,JS)-VY(I,JC1,JS))/(XXA (I1,JC1,JS)-XXA (I,JC1,JS)))
0169            XN=(XXA (I,JC,JS)+XXA (I,JC1,JS)+YYA (I1,JC1,JS)+XXA (I1,JC,JS))/4
               *.
0170            YN=(YYA (I,JC,JS)+YYA (I,JC1,JS)+YYA (I1,JC1,JS)+YYA (I1,JC,JS))/4
               *.
0171            IF(ABS(EPSX-EPSY).LE.0.0001) GO TO 331
0172            F=2.*EPSXY/(EPSX-EPSY)
0173            PSI=0.5*ATAN(F)
0174            PSI=(PSI*360.)/(2.*3.14159)
0175            GO TO 332
0176        331 IF(EPSXY-0.0) 334,335,336
0177        334 PSI=135.
0178        335 PSI=0.
0179        336 PSI=45.
      C
      C         COMPUTATION OF POWER OF DEFORMATION AT (XN,YN)
```

```
                 C
 0180              332 RX=1.
 0181                  I2=(ABS(EPSX)**2.+ABS(EPSY)**2.)/2.+(ABS(EPSXY)**2.)
 0182                  I3=(ABS(EPSX)**2.+ABS(EPSY)**2.+2.*(ABS(EPSXY)**2.))
 0183                  ESTR(I,JC,JS)=SQRT(0.66667)*SQRT(I3)
 0184                  PD(I,JC,JS)=2.*RK*SQRT(I2)
 0185                  WRITE(6,328) XN,YN,EPSX,EPSY,EPSXY,PSI,PD(I,JC,JS)
 0186              328 FORMAT(1H ,F14.3,5F20.3,F16.3)
 0187              330 CONTINUE
                 C
                 C     AREA COMPUTATION
                 C
 0188                  WRITE(6,630)
 0189              630 FORMAT(1H1,10X,'MEAN AREAS')
 0190                  DO 602 JC=1,13
 0191                  DO 601 I=1,9
 0192                  DO 600 JS=1,5
 0193                  AREA(I,JC,JS)=(ABS((XXA (I,JC+1,JS)-XXA (I,JC,JS))*(YYA (I+1,JC+1,
                      1JS)-YYA (I,JC,JS))-(XXA (I+1,JC+1,JS)-XXA (I,JC,JS))*(YYA (I,JC+1,
                      1JS)-YYA (I,JC,JS)))+ABS((XXA (I+1,JC,JS)-XXA (I,JC,JS))*(YYA (I+1,
                      1JC+1,JS)-YYA (I,JC,JS))-(XXA (I+1,JC+1,JS)-XXA (I,JC,JS))*(YYA (I+
                      1,JC,JS)-YYA (I,JC,JS))))/2.
 0194              600 CONTINUE
 0195                  DO 604 JS=1,4
 0196              604 AREAM(I,JC,JS)=(AREA(I,JC,JS)+AREA(I,JC,JS+1))/2.
 0197              601 CONTINUE
 0198                  KI=POD(JC,4)
 0199                  IF(KI.NE.1) KI=0
 0200                  WRITE(6,605)KI,JC
 0201              605 FORMAT(//I1,'ROW',I3)
 0202                  DO 606 I=1,9
 0203              606 WRITE(6,607)(AREAM(I,JC,JS),JS=1,4)
 0204              607 FORMAT(1H ,4F10.4)
 0205              602 CONTINUE
                 C
                 C     COMPUTATION OF TOTAL POWER OF DEFORMATION
                 C
 0206                  WRITE(6,514)
 0207              514 FORMAT(1H1,'TOTAL POWER OF DEFORMATION')
 0208                  DO 623 JC=1,13
 0209                  DO 622 I=1,9
 0210                  DO 622 JS=1,4
 0211                  PDA(I,JC,JS)=PD(I,JC,JS)*AREAM(I,JC,JS)
 0212              622 CONTINUE
 0213                  KJ=MOD(JC,4)
 0214                  IF(KJ.NE.1) KJ=0
 0215                  WRITE(6,608)KJ,JC
 0216              608 FORMAT(//I1,'ROW',I3)
 0217                  DO 609 I=1,9
 0218              609 WRITE(6,610)(PDA(I,JC,JS),JS=1,4)
 0219              610 FORMAT(1H ,4F10.4)
 0220              623 CONTINUE
 0221                  DO 62 JS=1,4
 0222                  DO 61 JC=1,13
```

```
0223            PDT(JC,JS)=0.0
0224            DO 61 I=1,9
0225         61 PDT(JC,JS)=PDT(JC,JS)+PDA(I,JC,JS)
0226            PCTO(JS)=0.0
0227            DO 63 JC=1,13
0228         63 POTO(JS)=POTO(JS)+PDT(JC,JS)
0229         62 CONTINUE
0230            WRITE(6,64) (POTO(JS),JS=1,4)
0231         64 FORMAT(1H0,'INCREMENTAL ENERGIES'/4F10.4)
0232            JS=1
0233            JS1=2
0234            JS2=3
0235            JS3=4
0236            DO 525 JC=1,13
0237            DO 525 I=1,9
0238        525 PDTOT(I,JC)=(TT/3.)*(PDA(I,JC,JS)*4.+PDA(I,JC,JS1)*2.+PDA(I,JC,JS2
               1)*4.+PDA(I,JC,JS3))
0239            DO 518 JC=1,13
0240            KK=MOD(JC,4)
0241            IF(KK.NE.1) KK=0
0242            WRITE(6,521) KK,JC
0243        521 FORMAT(//I1,'ROW',I3)
0244        523 DO 518 I=1,9
0245        518 WRITE(6,526) I,PDTOT(I,JC)
0246        526 FORMAT(1H ,'POINT',I3,F20.3)
          C     COMPUTATION OF EFFECTIVE STRAINS AT (XN,YN)
0247            WRITE(6,400)
0248        400 FORMAT(1H1,'EFFECTIVE STRAINS')
0249            JS=1
0250            JS2=2
0251            JS3=3
0252            JS4=4
0253            DC 402 JC=1,13
0254            DO 402 I=1,9
0255        402 EST(I,JC)=(TT/3.)*(ESTR(I,JC,JS)*4.+ESTR(I,JC,JS2)*2.+ESTR(I,JC,JS
               13)*4.+ESTR(I,JC,JS4))
0256            DO 403 JC=1,13
0257        403 WRITE(6,404) JC,(EST(I,JC),I=1,9)
0258        404 FORMAT(1H ,'ROW',I3,9F10.5)
0259            DO 1006 J=1,13
0260            ESTT(J)=0.0
0261            DO 1005 I=1,9
0262       1005 ESTT(J)=ESTT(J)+EST(I,J)
0263       1006 CONTINUE
0264            SUM=0.0
0265            DO 1008 J=1,13
0266       1008 SUM=SUM+ESTT(J)
0267            WRITE(6,1007) (ESTT(J),J=1,13),SUM
0268       1007 FORMAT(1H0,48X,'SUM OF EFFECTIVE STRAINS'/1H0,13F9.5/1H0,F15.5)
0269        318 CCNTINUE
0270            STOP
0271            END
```

OPTIONS IN EFFECT ID,BCD,SOURCE,NOLIST,NODECK,LOAD,NOMAP

B.2 LISTING OF PROGRAM "25"

SAT. 23 FEB. 1974   10:47:37   PAGE 0001

```
JOB,START=10322
JOB,REMOVE,25
JOB,COMPILE,25,NOLIST
C
C
C       WHEN THE PROGRAM IS STARTED .  THE USER IS GIVEN THE OPTION
C       OF STARTING A NEW RUN OR CONTINUING AN OLD RUN
C
C       THE PROGRAM IS FAIL-SAFE.  DATA IS WRITTEN TO DISC AFTER
C       EVERY POINT ENTRY.
C
C       A BUTTON PUSH WITH SW17 UP MEASURES A COORDINATE PAIR
C       IF SW16 IS NOT DOWN THAT PAIR IS PRINTED
C
C       A BUTTON PUSH WITH SW17 DOWN GIVES THE USER 4 OPTIONS
C
C       NOP..  IGNORES THE BUTTON PUSH
C       FINI ... TRIGGERS THE CALCULATIONS AND REPORT
C       STOP     STOPS THE PROGRAM ALLOWING THE USER TO CONTINUE
C                AT A LATER TIME
C       BACK... ALLOWS THE USER TO BACKSPACE   IT CALLS FOR THE
C               NEW INDICES  I,J  FOR  VW(I,J)  AND  VW(I+1,J)
C               I  MUST BE AN ODD NUMBER
C
C
C       THE PROGRAM RINGS THE I/O DEVICE BELL AFTER EACH 10 POINTS
C
C
        LOGICAL ISSW
        DIMENSION J(10),W(196,5),VW(196,5),RES(3)
        DIMENSION XC(7,14,5),YC(7,14,5)
        DATA IBELL /001603407/
        IP=IXTX
        IR=IXKY
        CALL ACI
        NU=IXSY
C
 1100   CALL MISTYP(IP,16,16HNEW RUN=0,CONT=1)
        K=IREPLY(IR,10,I)
        GO TO (1110,1100,1100,9999),I
C
 1110   IF(K.NE.0)  GO TO 1130
C
        DO 1120 JD=1,5
       DO 1120 ID =1,196
        W(ID,JD)=0
 1120   VW(ID,JD)=0
C
        ID=-1
        JD=1
```

```
C
      GO TO 7000
C
      ENTER PAL
*1130 SPB DTRC02
      LDA XFERIN
      SPB DELC30
*
      LEAVE PAL
C
 1200 WRITE(IP,1) ID,JD,VW(ID,JD),VW(ID+1,JD)
    1 FORMAT(1X,10HLAST POINT,2I4,2F10.4)
      GO TO 2100
C
 2000 IF(.NOT.ISSW(17)) GO TO 3000
 2100 CALL MSGTYP(IP,26,26HNCP=0,FIN=1,STOP=2,BACK=3)
      K=IREPLY(IR,10,I)
      GO TO (2110,2100,2100,9999),I
 2110 IF(K.EQ.0) GO TO 7000
      IF(K.EQ.1) GO TO 9000
      IF(K.EQ.2) GO TO 9999
      IF(K.NE.3) GO TO 2100
C
 2200 CALL MSGTYP(IP,7,7HENTER I)
      ID=IREPLY(IR,10,I)
      GO TO (2210,2200,2200,9999),I
 2210 IF((ID.LT.1).OR.(ID.GT.196)) GO TO 2200
C
 2220 CALL MSGTYP(IP,7,7HENTER J)
      JD=IREPLY(IR,10,I)
      GO TO (2230,2220,2220,9999),I
 2230 IF((JD.LT.1).OR.(JD.GT.5)) GO TO 2220
C
      ID=ID-2
      IF(ID.GT.0) GO TO 1200
      ID=1
      JD=JD-1
      GO TO 1200
C
 3000 ID=ID+2
      IF(ID.LE.196) GO TO 3050
      ID=1
      JD=JD+1
 3050 IF(JD.LE.5) GO TO 3100
      CALL MSGTYP(IP,11,11H 450 POINTS)
      GO TO 7000
C
 3100 CALL SOLVE(SOLN,RES)
      VW(ID,JD)=RES(1)
      VW(ID+1,JD)=RES(2)
```

SAT. 23 FEB. 1974 10:48:28 PAGE 0003

```
      IF( NOT ISSW(14)) WRITE(IP,2)  ID,JE,RES(1),RES(2)
    2 FORMAT(1X,2I4,2F10.4)
     K = MOD(ID,14)
      IF(K.EQ.13)  CALL MSGTYP(IP,1,IEELL)
C
      ENTER PAL
*
      SPB DTRCO2
      LDY XFR
      SPB DELC3O
*
*
#7000 LDX NU,5
      LDX IR,6
      LDX IP,7
      SPB AC4
      LDA PRIONO
      IAI
      STA XNTPOO
      SPB FIXCOZ
      SPB OFFCO1
      PRO 0,0,0,*+1,0
      LDZ
      STA XNTPOO
      PAI
      SPB AC3
      BRU #2000
      LEAVE PAL
C
 9000 CONTINUE
      IP2=7
     JS = 1
      A = 8.156/(VW(43,JS) - VW(15,JS))
     B = 8.28/(VW(100,JS) - VW(72,JS))
     READ(IR,21)J4
   21 FORMAT(A2)
     DO 202 JS=1,5
     DO 202 I = 1,195,2
      W(I,JS)=VW(I,JS)*A
  202 CONTINUE
     DO 203 JS=1,5
     DO 203 I=2,196,2
      W(I,JS)=VW(I,JS)*B
  203 CONTINUE
     WRITE(IP2,47)J4
   47 FORMAT(////////1H ,10X,19HPLOTTED COORDINATES,20X,7HTEST NO,1X,A
    13)
  140 JS=1
  143 JC=1
     IM=C
```


1600194

SAT, 23 FEB. 1974 10:48:51 PAGE 0004

```
  144 IC=1
  145 I =IM + (IC*2)-1
      I1=I+1
      XC(IC,JC,JS)=W(I,JS)
      YC(IC,JC,JS)=W(I1,JS)
      IC=IC+1
      IF(IC- 7) 145,145,146
  146 IM=IM+14
      JC=JC+1
      IF(JC-14) 144,144,147
  147 JS=JS+1
      IF(JS-5)143,143,150
  150 IF(ISSW(12))GO TO 205
  160 DO 205 JS=1,5
      WRITE(IP2,175)JS
  175 FORMAT(1H0,50X,8HIMAGE NO.I2,1H0,50X,12H------------)
      DO 190 JC=1,14
      WRITE(IP2,180)JC,(XC(IC,JC,JS),IC=1,7 )
  180 FORMAT(1H0,3HROW,I3,3X,1HX,7 F7 3)
      WRITE(IP2,185)(YC(IC,JC,JS),IC=1,7)
  185 FORMAT(/1H ,6X,1HY,7 F7.3)
  190 CONTINUE
  205 CONTINUE
C
       ENTER PAL
       SPB DTRC02
       LDX XFER
       SPB DELC20
       LEAVE PAL
C
 9999  CALL AC2
       STOP
C
       ENTER PAL
BLKAD  EQL /1=23000
BUF    EQL /2000
*
XFR    DEL 1,BLKAD
       FOR 0,BUF
       DEL 0,VW
XFERIN DEL 0,BLKAD
       FOR 0,BUF
       DEL 0,VW
XFER   DEL 1,BLKAD
       FOR 0,BUF
       DEL 0 W
W      BSS 220
       CON D,-1
       CON D,1
       BSS 42
```

SAT. 23 FEB. 1974 10:49:15 PAGE 0005

```
VW      BSS 980
ID      BSS 1
JD      BSS 1
        BSS 42
SCWD    CON 0,00336007
        CON 0,00336010
        CON D,-1
DELC30  LIB
AC3     LIB
AC4     LIB
        LEAVE PAL
        END
JOB,RELEASE,25
JOB,LJV
025,10322
JOB,END
```

B.3 LISTING OF PROGRAM "TAPE 25"

```
FORTRAN IV G LEVEL  21                MAIN                DATE = 73148         17/43/22             PAGE 0001

            DIMENSION BUF(1400)
            J=1
        101 READ(8,3,END=999,ERR=998)
          3 FORMAT(64A3)
            READ(8,1,END=999,ERR=998) BUF
          1 FORMAT((8(64A3)))
            DO 100 I=1,1400
        100 BUF(I)=AEGPAC(BUF(I))
            N=1
         27 NN=N+19
            WRITE(6,2)(BUF(I),I=N,NN,2)
            WRITE(7,2)(BUF(I),I=N,NN,2)
            M=N+1
            MM=NN+1
            WRITE(6,2)(BUF(I),I=M,MM,2)
            WRITE(7,2)(BUF(I),I=M,MM,2)
          2 FORMAT(10F8.3)
            WRITE(6,4)
          4 FORMAT(1H0)
            N=N+20
            IF(N-1391) 27,27,28
         28 CONTINUE
            J=J+1
        999 IF(J.LE.4) GO TO 101
            STOP
        998 STOP 1
            END

 *OPTIONS IN EFFECT*  ID,EBCDIC,SOURCE,NOLIST,NODECK,LOAD,NOMAP
 *OPTIONS IN EFFECT*  NAME = MAIN    , LINECNT =       56
 *STATISTICS*    SOURCE STATEMENTS =        27,PROGRAM SIZE =      6574
 *STATISVICS*  NO DIAGNOSTICS GENERATED
```

```
FORTRAN IV G LEVEL  21              AEGPAC            DATE = 73149          17/43/22              PAGE 0001

0001              FUNCTION AEGPAC(N)
            C
            C  CONVERTS 24 BIT GEPAC FLOATING POINT TO 32 BIT IBM FLOATING POINT
            C  THE RETURNED VARIABLE IS REAL
            C
0002              DATA L17/131072/
0003              DATA L24/16777216/
0004              DATA L26/67108864/
0005              DATA L30/1073741824/
            C
0006              IF(N)  1,2,2
0007            1 NEG=1
0008              N=(N+L30*2)/256
0009              GO TO 3
0010            2 NEG=0
0011              N=N/256
0012            3 M17=N/L17
            C
0013              I=1+4**MOD(M17+3,4)
0014              J=((MOD(M17,64)+32)*L26)/L26
0015              IF(J.GT.0)  J=J+3
0016              J=(J/4)*L24+MOD(N,L17)*I+L30
0017              CALL SUNDE(X,J)
0018              IF(NEG.EQ.1)  X=-X
0019              AEGPAC=X
0020              RETURN
0021              END

 *OPTIONS IN EFFECT*  ID,EBCDIC,SOURCE,NOLIST,NODECK,LOAD,NOMAP
 *OPTIONS IN EFFECT*  NAME = AEGPAC  , LINECNT =       56
 *STATISTICS*    SOURCE STATEMENTS =       21,PROGRAM SIZE =       768
 *STATISTICS*  NO DIAGNOSTICS GENERATED
```

```
FORTRAN IV G LEVEL  21                SWMDE              DATE = 73148          17/43/22              PAGE 0001

 0001              SUBROUTINE SWMDE(I,J)
             C
             C  THIS SUBROUTINE IS USED TO DEFFAT THE IMPLICIT CHANGE OF MODE
             C  IN THE STATEMENT      N=J
             C
 0002              I=J
 0003              RETURN
 0004              END

 *OPTIONS IN EFFECT*  ID,EBCDIC,SOURCE,NOLIST,NODECK,LOAD,NOMAP
 *OPTIONS IN EFFECT*  NAME = SWMDE   , LINECNT =       56
 *STATISTICS*    SOURCE STATEMENTS =        4,PROGRAM SIZE =       302
 *STATISTICS*  NO DIAGNOSTICS GENERATED

 *STATISTICS*  NO DIAGNOSTICS THIS STEP 2
```

BIBLIOGRAPHY

Abbott, M. B. (1966). An Introduction to the Method of Characteristics, Thames and Hudson, London.

Anderson, H. W. and Dodd, J. S. (1966). "Finite Element Method Applied to Rock Mechanics", Proceedings, 1st Congress, Int. Soc. for Rock Mechanics, Lisbon.

Bailey, A. (1964). "Preliminary Experiments with a Method of Simulating a Soil with Controllable Shear Strength", Paper No. 64-113, Presented at the 1964 Annual Meeting of the American Society of Agricultural Engineers, Chicago, Illinois.

Bekker, M. G. (1956). The Theory of Land Locomotion, University of Michigan Press, Ann Arbor.

Bekker, M. G. (1960). Off-the-Road Locomotion, University of Michigan Press, Ann Arbor.

Bekker, M. G. (1969) Introduction to Terrain-Vehicle Systems, University of Michigan Press, Ann Arbor.

Bishop, A. W. and Henkel, D. J. (1957). The Measurement of Soil Properties in the Triaxial Test, Edward Arnold, London, 2nd Edition.

Chen, C. K. (1972). "Wedge and Cone Indentation", Thesis submitted for the Degree of Doctor of Philosophy, McGill University, Montreal.

Clough, G. W. and Duncan, J. M. (1971). "Finite Element Analysis of Retaining Wall Behaviour", Journal of the Soil Mechanics and Foundations Division, Proceedings of the American Society of Civil Engineers, Vol. 97, No. SM12

Clough, R. W. and Woodward, R. J. (1967). "Analysis of Embankment Stresses and Deformations", Journal of the Soil Mechanics and Foundations Division, American Society of Civil Engineers, Vol. 93, No. SM4.

Coulomb, C. A. (1776). "Esai sur une Application des Regles des Maximis et Minimis a Quelques Problemes de Statique", Memoires Academique Royale des Sciences, Vol. 7, Paris.

Desai, C. S. (1972). "Overview, Trends and Projections: Theory and Application of the Finite Element Method in Geotechnical Engineering, State-of-the-Art", Proceedings of the Symposium on the Application of the Finite Element Method in Geotechnical Engineering, Vicksburg, Mississippi.

Desai, C. S. and Abel, J. F. (1972). Introduction to the Finite Element Method, Van Nostrand Reinhold Company, New York.

Drucker, D. C. (1953). "Limit Analysis of Two- and Three-Dimensional Soil Mechanics Problems", Journal Mechanics and Physics of Solids, Vol.1, pp. 217-226.

Drucker, D. C. (1961). "On Stress-Strain Relations for Soils and Load Carrying Capacity", Proceedings, 1st Int. Conf. on the Mech. of Soil-Vehicle Systems, Turin, Italy, p.15.

Drucker, D. C. and Prager, W. (1952). "Soil Mechanics and Plastic Analysis or Limit Design", Quarterly of Appl. Math, Vol.10.

Duncan, J. M. and Goodman, R. E. (1968). "Finite Element Analysis of Slopes in Jointed Rocks", Contract Report No. S-68-3, U.S. Army Engineer Waterways Experiment Station, Vicksburg, Mississippi.

Duncan, J. M. and Goodman, R. E. (1968). "Finite Element Analysis of Slopes in Jointed Rocks", Contract Report No. S-68-3, U.S. Army Engineer Waterways Experiment Station, Vicksburg, Mississippi.

Eligah, D. L. and Weber, J. A. (1968). "Soil Failure and Pressure Patterns for Flat Cutting Blades", Paper No. 68-655, Presented at the 1968 Winter Meeting of the American Society of Agricultural Engineers, Chicago, Illinois.

Finn, W. D. L. (1963). "Boundary Value Problems of Soil Mechanics", Journal of the Soil Mechanics and Foundation Division, American Society of Civil Engineers, Vol. 89, No.SM5, pp. 39-72.

Fox, L. (1965). An Introduction to Numerical Linear Algebra, Oxford University Press, New York, N.Y.

Freitag, D. R. (1965). "Wheels on Soft Soil : An Analysis of Existing Data", Tech. Report No. 3-670 U.S. Army Engineering Waterways Station, Vicksburg, Mississippi.

Freitag, D. R. (1965a). "The Design of Off-Road Vehicle Test Beds. Waterways Experiment Station Mobility Index System", Paper presented to the Fifth Meeting, Quadripartite Standing Working Group on Ground Mobility, U.S. Army Engineers Waterways Experiment Station, Vicksburg, Mississippi.

Freitag, D. R. (1965b). "A Mathematical Model for Predicting Cross-Country Mobility. Single-Pass Criteria for Soft Soil Performance (Preliminary)", Paper presented to the Fifth Meeting, Quadripartite Standing Working Group on Ground Mobility, U.S. Army Engineers Waterways Experiment Station, Vicksburg, Mississippi.

Freitag, D. R. (1968). "Penetration Tests for Soil Measurement"; Transactions of the American Society of Agricultural Engineers, p.750.

Fung, Y. C. (1965). Foundations of Solid Mechanics, Prentice Hall, New Jersey.

Gill, R. W. and Vanden Berg, B. E. (1967). Soil Mechanics in Tillage and Traction, Agricultural Research Service, United States Department of Agriculture, Agriculture Handbook No. 316.

Girijavallabhan, C. V. (1967). "Application of the Finite Element Method to Problems in Soil and Rock Mechanics", Thesis submitted for the Degree of Doctor of Philosophy, University of Texas at Austin, Texas.

Girijavallabhan, C. V. and Reese, L. C. (1968). "Finite Element Method Applied to some Problems in Soil Mechanics", Journal of the Soil Mechanics and Foundations Division, American Society of Civil Engineers, Vol. 94, No. SM2.

Goodman, R. E., Taylor, R. L. and Brekke, T. L. (1968). "A Model for the Mechanics of Jointed Rock", Journal of Soil Mechanics and Foundation Division, American Society of Civil Engineers, Vol. 94, No. SM3.

Hansen, J. B. (1953). Earth Pressure Calculation, The Danish Technical Press, The Institution of Danish Civil Engineers, Copenhagen.

Harrison, W. L. (1973a). "Soil Failure under Inclined Loads - I", Journal of Terramechanics, Vol. 9, No. 4, pp. 41-63.

Harrison, W. L. (1973b). "Soil Failure under Inclined Loads - II", Journal of Terramechanics, Vol. 10, No. 1, pp. 11-50.

Haythornthwaite, R. M. (1961). "Methods of Plasticity in Land Locomotion Studies", Proceedings, 1st Int. Conf. on the Mechanics of Soil-Vehicle Systems, Turin.

Haythornthwaite, R. M. (1963). "The Kinematics of Soils". Progress in Applied Mechanics, Prager Anniversary Volume, Macmillan, New York, p. 253.

Hetenyi, M. (1964). Beams on Elastic Foundations, University of Michigan Press, Ann Arbor, Michigan, 7th Edition.

Hettiaratchi, D. R. P. (1965). "The Present State of the Theory of Soil Cutting", Journal of Terramechanics, Vol. 2 pp. 63-76.

Hettiaratchi, D. R. P., Witney, B. D. and Reece, A. R. (1966). "The Calculation of Passive Pressure in Two-Dimensional Soil Failure", Journal of Agricultural Engineering Research, Vol. 11, No.2.

Hettiaratchi, D. R. P. and Reece, A. R. (1967). "Symmetrical Three-Dimensional Soil Failure", Journal of Terramechanics, Vol. 4, No. 3, p.45.

Heuze, F. E. and Goodman, R. E. (1971). "Numerical Analyses of Deformability Tests in Jointed Rock" - Joint Perturbation" and "No Tension Finite Element Solutions", Journal of Rock Mechanics, Vol. 3, pp.13-24.

Hilderbrand, F. B. (1965). Methods of Applied Mathematics, Prentice Hall Inc., New Jersey, 2nd Edition.

Hill, R. (1950). The Mathematical Theory of Plasticity, Oxford University Press, London.

James, R. G. and Bransby, P. L. (1970). "Experimental and Theoretical Investigations of a Passive Earth Pressure Problem", Geotechnique, Vol. 20, No. 1, pp. 17-37.

Japp, R. D. (1967). "An Investigation of the Dynamic Behaviour of Inelastic Materials", Thesis submitted for the Degree of Doctor of Philosophy, McGill University, Montreal.

Kostritsyn, A. K. (1956). "[Cutting of a Cohesive Medium with Knives and Cones.] Vsesoiuzz. Akad. Sel'skokh. Oziaistvennykh Nank. Zeml. Mekh, Sborn. Trudov. (Leningrad) 3:247-290 [National Institute Agricultural Engineers, Eng. Translation 58].

McCormick, C. W. (1963). "Plane Stress Analysis", Journal of the Structural Engineering Division, American Society of Civil Engineers, Vol. 89.

Mendelson, A. (1968). Plasticity: Theory and Application, The Macmillan Co. N. Y.

Micklethwait, E. W. E. (1944). Soil Mechanics in Relation to Fighting Vehicles, Military College of Science, Chobham Lane, Chertsey, England.

Morgenstern, N. R. and Eisenstein, A. (1970). "Methods of Estimating Lateral Loads and Deformations", Proceedings, 1970 Specialty Conference on Lateral Stresses in the Ground and Design of Earth Retaining Structures, Cornell University, pp. 51-102.

Ngo, D. and Scordelis, A. C. (1967). "Finite Element Analysis of Reinforced Concrete Beams", Journal of the American Concrete Institute, Vol. 69.

Nilson, A. H. (1968). "Nonlinear Analysis of Reinforced Concrete by the Finite Element Method", Journal of American Concrete Institute, Vol. 65, No. 9.

O'Callaghan, J. R. and Farrelly, K. M. (1964). "Cleavage of Soil by Tined Implements", Journal of Agricultural Engineering Research, Vol. 9, No. 3.

Ohde, J. (1938). "Zur Theorie des Erddrukes Unter Besonderer Berücksichtigung der Erddruckverteilung" (Theory of Soil Pressure with Particular Reference to its Distribution)", Bautechnik, Vol. 16.

Olson, D. J. and Weber, A. J. (1966). "Effect of Speed on Soil Failure Patterns in Front of Model Tillage Tools", Transactions of the Society of Automotive Engineers, Vol. 74, No. 4, pp. 298-310.

Osman, M. S. (1964). "The Mechanics of Soil Cutting Blades", Journal of Agricultural Engineering Research, Vol. 9, No. 4.

Payne, P. C. J. (1956). "The Relationship between the Mechanical Properties of Soil and the Performance of Simple Cultivation Implements", Journal of Agricultural Engineering Research, Vol. 1, No. 1.

Payne, P. C. J. and Tanner, D. W. (1959). "The Relationship between Rake Angle and the Performance of Simple Cultivation Elements", Journal of Agricultural Engineering Research, Vol. 4, No. 4.

Rankine, W. J. (1857). "On the Stability of Loose Earth", Transactions, Royal Society, London, Vol. 147.

Reece, A. R. (1965). "The Fundamental Equation of Earth Moving Mechanics", Symp. of Earthmoving Machines, Inst. of Mechanical Engineers.

Reece, A. R. (1969), "Machines and Soils", Journal of Terramechanics, Vol. 6, No. 3, pp. 9-19.

Rowe, P. W. and Peaker, K. (1965). "Passive Earth Pressure Measurements", Geotechnique, Vol. XV, No. 1, pp. 57-78.

Rowe, R. J. and Barnes, K. K. (1961). "Influence of Speed on Elements of Draft of a Tillage Tool", American Society of Agricultural Engineers Trans., Vol. 4, No. 1, pp. 55-57.

Seia, A. D. (1961). "On the Slip and Tractive Effort", Proceedings, 1st Int. Conf. on the Mechanics of Soil-Vehicle Systems, Turin, Italy, p. 587.

Selig, E. T. and Nelson, R. D. (1964). "Observations of Soil Cutting with Blades", Journal of Terramechanics, Vol. 1, No. 3.

Siemens, J. C. (1963). "Mechanics of Soil under the Influence of Model Tillage Tools", Thesis submitted for the Degree of Doctor of Philosophy, University of Illinois Library, Urbana, Illinois.

Siemens, J. C., Weber, J. A. and Thornburn, T. H. (1964). "Mechanics of Soils under the Influence of Model Tillage Tools", American Society of Agricultural Engineers, Annual Meeting.

Söhne, W. (1956). "Einige Grudlagen für eine Landtechnische Bodenmechanik, (Some Basic Consideration of Soil Mechanics as Applied to Agricultural Engineering)", Grudlagen der Landtechnik, Vol. 7, Translation 53, Library, National Institute of Agricultural Engineers, Silsoe, England.

Sokolvski, V. V. (1960). Statics of Soil Media, Butterworths, London.

Sylvestre-Williams, R. (1973). "Indentation and Trafficability Studies on Clay", Thesis submitted for the Degree of Doctor of Philosophy, McGill University, Montreal.

Tanner, D. W. (1960). "Further Work on the Relationship between Rake Angle and the Performance of Simple Cultivation Implements", Journal of Agricultural Engineering Research, Vol. 5, No. 3.

Terzaghi, K. (1932). "Record Earth-Pressure Testing Machine", Engineering News Record, Vol. 109, pp. 365-369.

Terzaghi, K. (1934). "Large Retaining Wall Tests, I. Pressure of Dry Sand", Engineering News Record, Vol. 111, pp. 136-140.

Terzaghi, K. (1936). "A Fundamental Fallacy in Earth Pressure Computations", Journal of the Boston Society of Civil Engineers, Vol. 23, p. 71.

Terzaghi, K. (1944). Theoretical Soil Mechanics, John Wiley and Sons, New York.

Thomsen, E. G., Yang, C. T. and Kobayashi, S. (1965). "Mechanics of Plastic Deformation in Metal Processing, The Macmillan Co., New York.

Trafficability Research Team, (1961). "A Suggested Empirical Combination between the Bekker and the Vicksburg Methods in Trafficability Analyses of Deep Loose Sands", Proceedings, 1st Int. Conf. on the Mechanics of Soil-Vehicle Systems, Turin, Italy, p. 837.

Windisch, E. J. (1969). "Study of Towed Wheel-Soil Interaction", Thesis submitted for the Degree of Doctor of Philosophy, McGill University, Montreal.

Windisch, E. J. and Yong, R. N. (1970). "The Determination of Soil Strain-Rate Behaviour beneath a Moving Wheel", Journal of Terramechanics, Vol. 7, No. 1, p.55.

Wismer, R. N. and Forth, M. W. (1969). "Soil Dynamics Research at Deere Co.", 3rd Int. Conf. of the Society for Terrain Vehicle Systems, Vol. 3.

Wismer, R. D. and Luth, H. J. (1970). "Performance of Plane Soil Cutting Blades in Clay", Paper No. 70-120, Presented at the 1970 Annual Meeting of the American Society of Agricultural Engineers, Minneapolis, Minnesota.

Yang, C. T. and Thomsen, E. G. (1953). "Plastic Flow in a Lead Extrusion", Transaction of the American Society of Mechanical Engineers, Vol. 75, No. 4, p. 575.

Yong, R. N. (1972). "Analytical Predictive Requirements for Physical Performance of Mobility", Paper No. 72-616, Presented at the 1972 Winter Meeting, American Society of Agricultural Engineers, Chicago, Illinois.

Yong, R. N., Boyd, C. W. and Webb, G. L. (1967). "Experimental Study of Behaviour of Sand under Moving Rigid Wheels", Report No. D. Phys. R.(G.) Misc. 27, Defence Research Board, Canada.

Yong, R. N. and Chen, C. K. (1970). "Analytical and Experimental Studies of Soil Cutting", Paper No. 70-676, Presented at the 1970 Winter Meeting of the American Society of Agricultural Engineers, Chicago, Illinois.

Yong, R. N., Chen, C. K. and Sullivan, R. J. (1969). "Application of Limit Analysis to Soil Cutting", Proceedings, 3rd. Int. Conf. of the Society for Terrain Vehicle Systems, Vol. 2.

Yong, R. N. and Sylvestre-Williams, R. (1969). "Analysis and Prediction of Grouser Thrust on Sand", Soil Mechanics Series No. 26, McGill University, Report to Defence Research Establishment, Ottawa, (Geophysics).

Yong, R. N. and Warkentin, B. P. (1966). Introduction to Soil Behaviour, Macmillan Co., New York.

Yong, R. N. and Webb, G. L. (1969). "Energy Dissipation and Drawbar Pull Prediction in Soil Wheel Interaction", Proceedings, 3rd. Int. Conf. of the Society for Terrain Vehicle Systems Vol.1, Essen, Germany.

Yong, R. N. and Windisch, E. J. (1970). "Determination of Wheel Contact Stress from Measured Instantaneous Soil Deformation", Journal of Terramechanics, Vol. 7, Nos. 3 and 4, pp. 57-67.

Zienkiewicz, O. C. (1971). "The Finite Element Method in Engineering Science", 2nd Edition, McGraw-Hill Co., London.

Zienkiewicz, O. C., Best, B., Dullage, C. and Stagg, K. G. (1970). "Analysis of Nonlinear Problems in Rock Mechanics with Particular Reference to Jointed Rock Systems", Proceedings, 2nd. Int. Congress on Rock Mechanics, Belgrade.